

# **Spatial Diversity in MIMO Communication Systems with Distributed or Co-located Antennas**

## **Dissertation**

zur Erlangung des akademischen Grades  
Doktor der Ingenieurwissenschaften (Dr.-Ing.)  
der Technischen Fakultät  
der Christian-Albrechts-Universität zu Kiel

vorgelegt von

**Jan Mietzner**

Kiel 2007

Jan Mietzner, *Spatial Diversity in MIMO Communication Systems with Distributed  
or Co-located Antennas*

Tag der Einreichung: 02. Oktober 2006

Tag der Disputation: 13. Dezember 2006

Dekan: Prof. Dr. rer. nat. Manfred Schimmler

Berichterstatter: Prof. Dr.-Ing. Peter Adam Höher  
Dr.-Ing. habil. Wolfgang H. Gerstacker  
Prof. Dr. Lajos Hanzo

# Preface

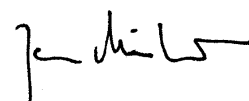
This thesis was developed during my work as a research and teaching assistant at the Information and Coding Theory Lab (ICT), Faculty of Engineering, Christian-Albrechts University of Kiel (CAU), Germany.

First of all, I would like to thank my advisor Prof. Dr. Peter Adam Höher for his enduring support and interest in my work. The working environment in Kiel was very enjoyable, which is largely his credit. In times of scarce financial resources he enabled me to visit numerous international conferences, which was a great experience.

Next, I would like to thank Dr. Wolfgang Gerstacker from the University of Erlangen-Nuremberg, Germany, and Prof. Dr. Lajos Hanzo from the University of Southampton, U.K., for evaluating this work. I am indeed very happy that Prof. Höher was able to win them for this task. The various interesting discussions, especially with Dr. Gerstacker, were very helpful. Also many thanks to Prof. Dr. Manfred Schimmler, the dean of the Faculty of Engineering, and to Prof. Dr. Ludger Klinkenbusch, for setting up a prompt date for the thesis defence.

I would like to thank my former colleagues of the ICT and the Institute for Circuit and System Theory for the pleasant time in Kiel and many technical as well as non-technical discussions. Moreover, I would like to thank Dr. Xiao-Ming Chen (Thomson, Hanover, Germany) and Prof. Dr. Badri-Höher (FHWT University of Applied Sciences, Vechta-Diepholz-Oldenburg, Germany) for providing parts of the software used for this work. Many thanks also to our former students Jan Eick, Malte Kautza, and Ravisankar Natarajan for their valuable contributions. Finally, many thanks to Justus Fricke (ICT), Dr. David Haley (Cohda Wireless, Kent Town, Australia), James Howarth (Macquarie University, Sydney, Australia), and my former office mate Prof. Dr. Ingmar Land (Aalborg University, Denmark) for proof-reading parts of the manuscript.

Last but not least, I would like to thank my wife Annika Mietzner, who has accompanied and encouraged me throughout my complete Ph.D. studies, and my parents Günter and Ursula Mietzner for their continuous support.



Vancouver, March 2007



# Abstract

**T**HE USE OF multiple antennas in wireless communication systems has gained much attention during the last decade. It was shown that multiple-antenna systems, called multiple-input multiple-output (MIMO) systems, offer huge advantages over single-antenna systems, both with regard to capacity and error performance.

Typically, quite restrictive assumptions are made in the literature on MIMO systems concerning the spacing of the individual antenna elements. On the one hand, it is typically assumed that the antenna elements at the transmitter and the receiver are co-located, i.e., they belong to some sort of antenna array. On the other hand, it is often assumed that the antenna spacings are sufficiently large, so as to justify the assumption of independent fading on the individual transmission links. From numerous publications it is known that spatially correlated links caused by insufficient antenna spacings lead to a loss in capacity and error performance. In the first part of the thesis, it is shown that this is also the case when the individual transmit or receive antennas are spatially distributed on a large scale. Possible applications include simulcast networks, reach-back links for wireless sensors, as well as wireless networks with cooperating relays. Specifically, it is proven that any spatially correlated MIMO system can be transformed into an equivalent (with regard to the resulting capacity distribution) spatially distributed MIMO system, and vice versa. Moreover, the asymptotic equivalence with regard to the pairwise error probability of space-time codes is proven. Correspondingly, MIMO systems with distributed antennas and MIMO systems with co-located antennas can be treated in a single, unifying framework.

This fact is utilized in the second part of the thesis, where appropriate transmit power allocation strategies are developed for MIMO systems with distributed or co-located transmit antennas. In particular, fading scenarios are taken into account that occur especially in distributed MIMO systems. Focus is on power allocation schemes that require solely statistical channel knowledge at the transmitter side, which can easily be acquired in practical systems. By means of analytical results, it is shown that significant performance gains in comparison to equal power allocation are achieved.

The third part of the thesis focuses on two problems that are of particular interest for MIMO systems with distributed transmit antennas. First, due to the distributed nature of the system, independent local oscillators are employed for up-converting the individual transmitted signals. This causes frequency offsets between the transmission links, which results in time-varying channel impulse responses. The impact of frequency offsets on the performance of different space-time coding techniques is analyzed, and possible counter measures are considered. Second, if the transmit antennas are spaced very far apart and no

timing advance techniques are employed, significantly different propagation delays occur that lead to intersymbol interference effects. To this end, suitable space-time coding and equalization techniques are identified, so as to maintain a diversity advantage in comparison to a single-antenna system.

**Keywords:** Wireless communications, MIMO systems, space-time codes, spatial fading correlation, distributed antennas, performance analysis, transmit power allocation, equalization, frequency offset. ★

# Kurzfassung

**M**OBILFUNKSYSTEME mit mehreren Sende- und Empfangsantennen, sog. Multiple-Input Multiple-Output- (MIMO-) Systeme, haben in den letzten zehn Jahren großes Interesse geweckt. Wie vielfach gezeigt wurde, bieten MIMO-Systeme hinsichtlich höherer Datenraten und geringerer Fehlerraten beachtliche Vorteile gegenüber Mobilfunksystemen mit nur einer Sende- und Empfangsantenne.

Typischerweise werden in der Literatur über MIMO-Systeme relativ strenge Annahmen bezüglich der Abstände der einzelnen Antennenelemente getroffen: Auf der einen Seite nimmt man normalerweise an, dass die Sende- und Empfangsantennen Teil eines Antennen-Arrays sind (“co-located antennas”). Auf der anderen Seite wird häufig angenommen, dass die Antennenabstände hinreichend groß sind, so dass man von statistisch unabhängigen Fadingprozessen auf den einzelnen Übertragungslinks ausgehen kann. Aus zahlreichen Publikationen ist bekannt, dass räumliche Korrelationseffekte – verursacht durch unzureichende Antennenabstände – zu Verlusten hinsichtlich der erreichbaren Daten- und Fehlerraten führen. Im ersten Teil der Arbeit wird gezeigt, dass dies ebenso der Fall ist, wenn die einzelnen Sende- oder Empfangsantennen räumlich verteilt sind (auf einer großen Skala). Mögliche Anwendungen sind zum Beispiel sog. Gleichwellennetze für Rundfunkanwendungen, drahtlose Sensornetze sowie Mobilfunknetze mit kooperierenden Zwischenstationen. Insbesondere wird gezeigt, dass (hinsichtlich verschiedener Performance-Kriterien) jedes räumlich korrelierte MIMO-System in ein äquivalentes räumlich verteiltes MIMO-System überführt werden kann und umgekehrt. Demzufolge können MIMO-Systeme mit verteilten Antennen und MIMO-Systeme mit korrelierten Antennen in einem gemeinsamen theoretischen Rahmen behandelt werden.

Diese Tatsache wird im zweiten Teil der Arbeit ausgenutzt, in dem geeignete Strategien zur Verteilung der Sendeleistung auf die einzelnen (korrelierten oder verteilten) Sendeantennen entwickelt werden. Insbesondere wird auf Fading-Szenarien eingegangen, die speziell in verteilten MIMO-Systemen auftreten können. Die betrachteten Techniken benötigen ausschließlich statistische Kanalkennntnis auf der Sendeseite, welche in praktischen Systemen leicht zur Verfügung gestellt werden kann. Mit Hilfe analytischer Ergebnisse wird gezeigt, dass durch eine geeignete Verteilung der Sendeleistung deutliche Gewinne erzielt werden können.

Der dritte Teil der Arbeit befasst sich schließlich mit zwei Problemen, die insbesondere für MIMO-Systeme mit verteilten Sendeantennen von Interesse sind. Zum einen werden aufgrund der räumlichen Trennung der Sendeantennen unabhängige Frequenzoszillatoren zur Aufwärtsmischung der zu übertragenden Signale verwendet. Dies führt zu Frequenzversätzen und somit zu zeitvarianten Kanalimpulsantworten. Der Einfluss

solcher Effekte auf die Leistungsfähigkeit verschiedener MIMO-Übertragungstechniken wird analysiert, und mögliche Gegenmaßnahmen werden vorgeschlagen. Zum anderen, wenn die Sendeantennen räumlich sehr weit getrennt sind und keinerlei Techniken zur Signallaufzeitkompensation verwendet werden, treten deutliche Unterschiede zwischen den einzelnen Ausbreitungsverzögerungen auf, welche zu Intersymbol-Interferenz-Effekten führen. Dementsprechend werden geeignete Sender- und Empfängertechniken identifiziert, die einen Diversitätsgewinn im Vergleich zu einem Einantennensystem aufrecht erhalten.

**Stichwörter:** Mobilfunkkommunikation, MIMO-Systeme, Space-Time-Codes, räumliche Korrelation, verteilte Antennen, Performance-Analyse, Sendeleistungsverteilung, Entzerrung, Frequenzversatz. ★



# Contents

|          |  |           |
|----------|--|-----------|
| <b>1</b> | <b>Introduction and Overview</b>                                 | <b>1</b>  |
| 1.1      | Benefits of Multiple Antennas . . . . .                          | 2         |
| 1.2      | Distributed and Co-located MIMO Systems . . . . .                | 5         |
| 1.3      | Scope and Aim of the Thesis . . . . .                            | 7         |
| 1.4      | Main Contributions . . . . .                                     | 8         |
| 1.5      | Thesis Outline . . . . .   | 8         |
| <b>2</b> | <b>Wireless Systems with Multiple Antennas</b>                   | <b>11</b> |
| 2.1      | An Overview of MIMO Systems . . . . .                            | 12        |
| 2.1.1    | Spatial Multiplexing Techniques . . . . .                        | 12        |
| 2.1.2    | Spatial Diversity Techniques . . . . .                           | 18        |
| 2.1.3    | Smart Antennas and Beamforming Techniques . . . . .              | 28        |
| 2.1.4    | Other Classifications of Multiple-Antenna Techniques . . . . .   | 31        |
| 2.1.5    | Focus of the Thesis . . . . .                                    | 33        |
| 2.2      | System and Channel Model . . . . .                               | 33        |
| 2.2.1    | Statistical Multipath Signal Propagation Model . . . . .         | 34        |
| 2.2.2    | Statistical Discrete-Time Channel Model . . . . .                | 37        |
| 2.2.3    | Analysis of the Statistical Properties . . . . .                 | 43        |
| 2.2.4    | Other Types of Fading . . . . .                                  | 49        |
| 2.3      | Details of Some Space-Time Coding Schemes . . . . .              | 50        |
| 2.3.1    | Orthogonal Space-Time Block Codes . . . . .                      | 50        |
| 2.3.2    | Quasi-Orthogonal Space-Time Block Codes . . . . .                | 61        |
| 2.3.3    | Time-Reversal Space-Time Block Code . . . . .                    | 62        |
| 2.3.4    | Delay Diversity and Space-Time Trellis Codes . . . . .           | 64        |
| 2.4      | Chapter Summary . . . . .  | 68        |
| <b>3</b> | <b>Distributed and Co-located MIMO Systems</b>                   | <b>69</b> |
| 3.1      | Examples of Distributed MIMO Systems . . . . .                   | 70        |
| 3.2      | Equivalence of Distributed and Co-located MIMO Systems . . . . . | 73        |
| 3.2.1    | System Model for Co-located MIMO Systems . . . . .               | 74        |
| 3.2.2    | System Model for Distributed MIMO Systems . . . . .              | 75        |
| 3.2.3    | Capacity Distribution of MIMO Systems . . . . .                  | 76        |
| 3.2.4    | Pairwise Error Probability of Space-Time Codes . . . . .         | 85        |
| 3.2.5    | Error Rates of Orthogonal Space-Time Block Codes . . . . .       | 88        |
| 3.2.6    | A Simple Performance Measure . . . . .                           | 98        |

|          |   |            |
|----------|---|------------|
| 3.3      | Generalization to other Channel Models . . . . .                  | 101        |
| 3.3.1    | Generalized Fading Models . . . . .                               | 101        |
| 3.3.2    | Generalized Spatial Correlation Models . . . . .                  | 108        |
| 3.4      | Benefits of Macroscopic Diversity . . . . .                       | 109        |
| 3.4.1    | Discussion of Previous Results . . . . .                          | 110        |
| 3.4.2    | System Model with Macroscopic Diversity . . . . .                 | 110        |
| 3.4.3    | Influence of Line-of-Sight Signal Components . . . . .            | 113        |
| 3.4.4    | Influence of Shadowing . . . . .                                  | 116        |
| 3.5      | Chapter Summary . . . . .   | 119        |
|          | Appendix 1 . . . . .  | 121        |
|          | Appendix 2 . . . . .  | 121        |
| <b>4</b> | <b>Optimal Transmitter and Receiver Strategies</b>                | <b>123</b> |
| 4.1      | Optimal Transmit Power Allocation Schemes . . . . .               | 124        |
| 4.1.1    | System Model with Statistical Transmit Power Allocation . . . . . | 124        |
| 4.1.2    | Benefits with Regard to Ergodic Capacity . . . . .                | 128        |
| 4.1.3    | Combination with Outer Space-Time Code . . . . .                  | 131        |
| 4.1.4    | Impact of Estimation Errors . . . . .                             | 141        |
| 4.2      | Use of Statistical Channel Knowledge at the Receiver . . . . .    | 143        |
| 4.2.1    | System Model with Reduced-Dimension Receiver . . . . .            | 143        |
| 4.2.2    | Impact of Estimation Errors . . . . .                             | 146        |
| 4.3      | Chapter Summary . . . . .   | 147        |
|          | Appendix 1 . . . . .  | 148        |
|          | Appendix 2 . . . . .  | 149        |
|          | Appendix 3 . . . . .  | 149        |
| <b>5</b> | <b>Unsynchronized Distributed MIMO Systems</b>                    | <b>151</b> |
| 5.1      | Imperfect Carrier-Frequency Synchronization . . . . .             | 152        |
| 5.1.1    | System Model with Carrier-Frequency Offsets . . . . .             | 152        |
| 5.1.2    | Performance Loss of Orthogonal Space-Time Block Codes . . . . .   | 154        |
| 5.1.3    | Performance Loss of Other Space-Time Coding Schemes . . . . .     | 159        |
| 5.2      | Imperfect Timing Synchronization . . . . .                        | 162        |
| 5.2.1    | System Model with Propagation Delay Differences . . . . .         | 162        |
| 5.2.2    | Performance of Alamouti's Transmit Diversity Scheme . . . . .     | 165        |
| 5.2.3    | Rake Receiver Bound for Frequency-Selective Fading . . . . .      | 170        |
| 5.2.4    | Use of the Time-Reversal Space-Time Block Code . . . . .          | 172        |
| 5.2.5    | Performance and Optimization of Delay Diversity . . . . .         | 174        |
| 5.3      | Chapter Summary . . . . .   | 177        |
|          | Appendix . . . . .  | 178        |
| <b>6</b> | <b>Summary and Conclusions</b>                                    | <b>181</b> |
| <b>A</b> | <b>Acronyms and Abbreviations</b>                                 | <b>185</b> |
| <b>B</b> | <b>Notation</b>   | <b>189</b> |

|          |  |            |
|----------|--|------------|
| <b>C</b> | <b>Mathematical Definitions</b>                          | <b>199</b> |
| C.1      | Special Functions . . . . .                              | 199        |
| C.2      | Important Statistical Distributions . . . . .            | 201        |
| C.3      | Moments of a Statistical Distribution . . . . .          | 205        |
| C.4      | Entropy and Mutual Information . . . . .                 | 208        |
| C.5      | Important Theorems . . . . .                             | 209        |
| <b>D</b> | <b>Matrix Calculus</b>                                   | <b>211</b> |
| D.1      | Vector and Matrix Norms . . . . .                        | 211        |
| D.2      | Special Matrix Products . . . . .                        | 211        |
| D.3      | Orthogonal Matrices . . . . .                            | 212        |
| D.4      | Unitary Matrix Transforms . . . . .                      | 213        |
| D.5      | Eigenvalue and Singular-Value Decomposition . . . . .    | 215        |
| D.6      | Covariance and Correlation Matrices . . . . .            | 216        |
| <b>E</b> | <b>Convex Optimization</b>                               | <b>219</b> |
| E.1      | Optimization Problems and Strong Duality . . . . .       | 219        |
| E.2      | Convex Optimization Problems . . . . .                   | 220        |
| <b>F</b> | <b>Channel Modeling</b>                                  | <b>223</b> |
| F.1      | Physical Perspective on Multipath Propagation . . . . .  | 223        |
| F.2      | Statistical Multipath Propagation Model . . . . .        | 226        |
| F.3      | Calculation of Antenna Correlations . . . . .            | 230        |
| F.4      | Numerical Examples . . . . .                             | 233        |
| F.5      | Further Remarks . . . . .                                | 236        |
| <b>G</b> | <b>Capacity of Static MIMO Channels</b>                  | <b>239</b> |
| G.1      | Generic Capacity Result . . . . .                        | 239        |
| G.2      | Specific Capacity Results . . . . .                      | 241        |
| <b>H</b> | <b>Considerations for Distributed MIMO Systems</b>       | <b>245</b> |
| H.1      | Illustration of the Unitary Matrix Transforms . . . . .  | 245        |
| H.2      | Virtual Antenna Arrays for Cellular Systems . . . . .    | 248        |
| <b>I</b> | <b>Error Performance of MRC Systems</b>                  | <b>255</b> |
| I.1      | PDF of the Instantaneous Signal-to-Noise Ratio . . . . . | 255        |
| I.2      | Symbol and Bit Error Probability . . . . .               | 257        |
| <b>J</b> | <b>Space-Time Coding in the Presence of ISI</b>          | <b>261</b> |
| J.1      | Channel Estimation for MIMO Systems . . . . .            | 261        |
| J.2      | Trellis-Based Equalization for STBCs . . . . .           | 264        |
| J.3      | Performance Analysis Based on Distance Spectra . . . . . | 269        |
| <b>K</b> | <b>Own Publications Related to the Thesis</b>            | <b>277</b> |
|          | <b>Bibliography</b>                                      | <b>281</b> |



# Chapter 1

## Introduction and Overview

**H**OW IS IT possible to build high-speed, high-quality wireless communication systems? Since Shannon's 1948 landmark paper [Sha48], this has become a central question for researchers and manufacturers in the field of digital communications. It deals with two key requirements for modern wireless systems: High bit rates and small error rates. The disruptive characteristics of wireless channels, however, make it challenging to accomplish both of these objectives at the same time.

Wireless communication has emerged as one of the largest sectors of the telecommunications industry. During the last fifteen years, it has evolved from a niche business to one of the most promising areas for growth [RABT02]. Traditionally, wireless applications were voice-centric and demanded only moderate bit rates. Most high-bit-rate applications such as file transfer or video streaming were wireline applications. Since then, there has been a shift to wireless multimedia applications, which is reflected in the convergence of wireless networks and the Internet [Oli99, Goo00]. For example, cell phones with integrated digital cameras are ubiquitous already today. One can take a photo, send it to a friend – and make a phone call, of course. In order to guarantee a certain quality of service, however, not only high bit rates are required, but also a good error performance.

There are several ways to increase the bit rate of a digital communication system. For example, one can choose a shorter symbol duration  $T$ . However, this implies that a larger fraction of the frequency spectrum will be occupied, since the required system bandwidth is determined by the symbol rate  $1/T$ . In wireless communications, such a bandwidth expansion is typically undesired, because frequency spectrum has become a valuable resource.<sup>1</sup> Moreover, wireless channels are typically characterized by multipath signal propagation caused by reflections, scattering, and diffraction [Jak74, Ste94, Rap96]. A shorter symbol duration can therefore cause an increased degree of intersymbol interference (i.e., interference between subsequent data symbols), which may lead to a loss in error performance. As an alternative to a shorter symbol duration, one can employ a multicarrier approach [HMCK03] and multiplex data symbols onto multiple narrow subbands, therefore circumventing the problem of intersymbol interference. But still, the increased bandwidth requirement remains. Another method to enhance the bit rate of

---

<sup>1</sup>In August 2000, the German government auctioned 145 MHz of frequency spectrum for the Universal Mobile Telecommunication System (UMTS) – for the incredible amount of more than 50bn Euros.

a digital communication system is to use higher-order modulation schemes transmitting more than one bit per data symbol [BB99,Pro01], which results in a higher bit rate without bandwidth expansion. However, given the same average transmit power per bit, the error performance will again deteriorate. Finally, one can employ sophisticated source-coding techniques [CT91,Mac03], in order to compress the information sequence before transmission. However, an excessive compression rate will cause signal distortions [CT91, Ch. 13]. In fact, efficient quasi-lossless source-coding algorithms for voice and multimedia data are already employed today [Spa94,Sik05].

The error rate of a digital communication system can be improved by the principle of channel coding [LC83,Bos99]. Prior to transmission, redundancy is added to the information bits in a structured way, enabling error detection and error correction at the receiver. Due to the added redundancy, however, channel coding reduces the effective bit rate. Altogether, the above examples illustrate that, given a fixed bandwidth, there is a trade-off between the bit rate (bandwidth efficiency) and the error rate (power efficiency) of digital wireless communication systems. Conventional (single-antenna) techniques aiming at an optimal wireless system performance either operate in the time domain or in the frequency domain. However, when utilizing multiple antennas, the previously unused *spatial* domain can be exploited.

## 1.1 Benefits of Multiple Antennas for Wireless Communications

The great potential of using multiple antennas for wireless communications has only become apparent during the last decade. At the end of the 1990s, multiple-antenna techniques were shown to provide a novel means to achieve both higher bit rates and smaller error rates. Correspondingly, they constitute an important technology for modern wireless communications [LFV01,PGNB04]. The benefits of multiple antennas for wireless communication systems are summarized in Fig. 1.1. In the sequel, they are characterized in more detail.

### Higher Bit Rates with Spatial Multiplexing

Spatial multiplexing techniques simultaneously transmit independent information sequences, often called layers, over multiple antennas. Using  $M$  transmit antennas, the overall bit rate compared to a single-antenna system is thus enhanced by a factor of  $M$  without requiring extra bandwidth or extra transmission power.<sup>2</sup> Channel coding is often employed, in order to guarantee a certain error performance. Since the layers are superimposed during transmission, they have to be separated at the receiver using an interference-cancellation type of algorithm (typically in conjunction with multiple receive antennas). A well-known spatial multiplexing scheme is the Bell-Labs Layered Space-Time

---

<sup>2</sup>In other words, compared to a single-antenna system the transmit power per transmit antenna can be lowered by a factor of  $1/M$ .

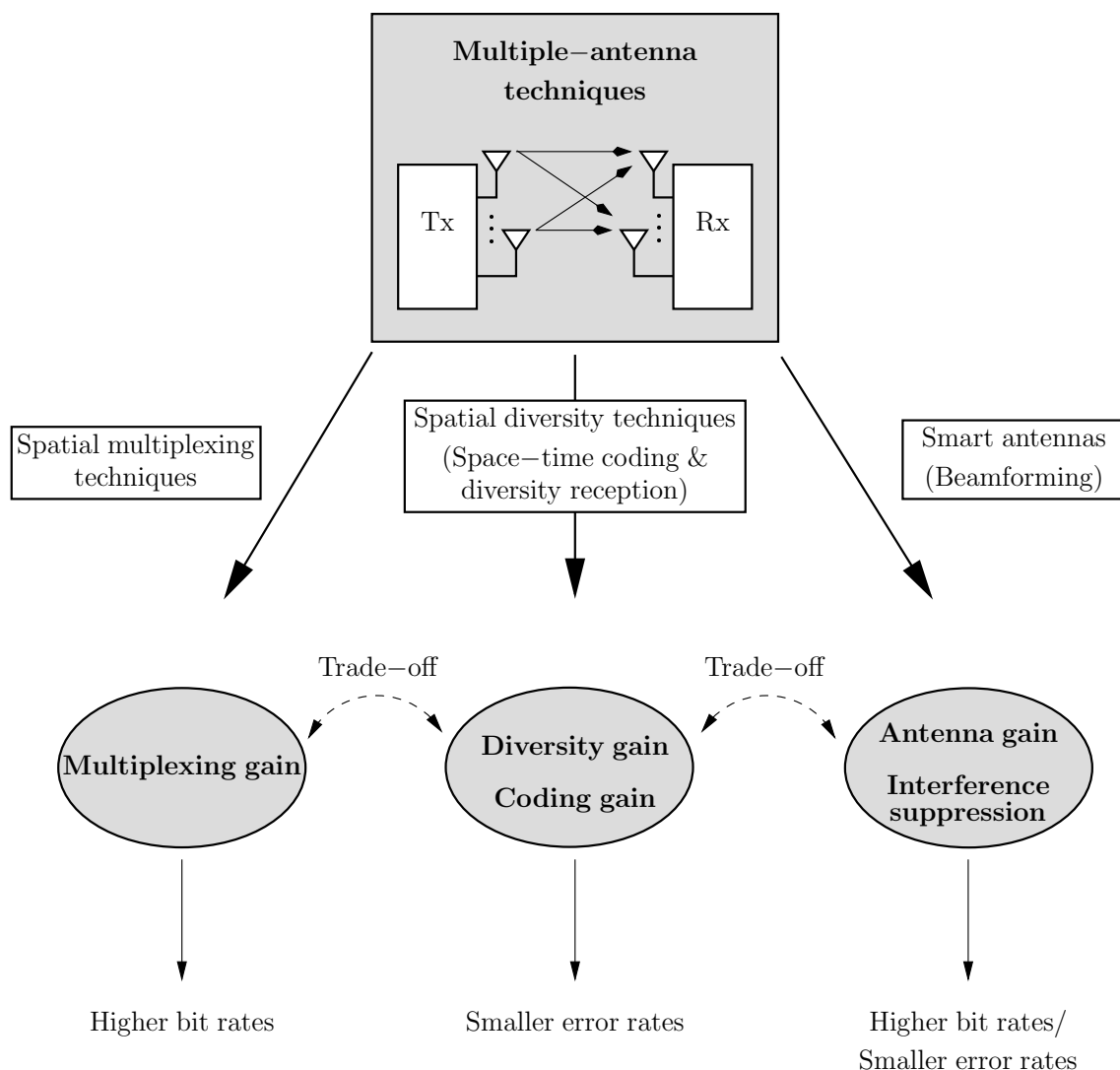


Figure 1.1: Benefits of multiple-antenna techniques for wireless communications.

Architecture (BLAST) [Fos96]. The achieved gain in terms of bit rate (in comparison to a single-antenna system) is called multiplexing gain in the literature.

### Smaller Error Rates through Spatial Diversity

Similar to channel coding, multiple antennas can also be used to improve the error rate of a system, by transmitting or receiving redundant signals representing the same information sequence. By means of two-dimensional coding in time and space, commonly referred to as space-time coding, the information sequence is spread out over multiple transmit antennas. At the receiver, an appropriate combining of the redundant signals has to be performed. Optionally, multiple receive antennas can be used, in order to further improve the error performance (diversity reception). The advantage over conventional channel coding is that redundancy can be accommodated in the spatial domain, rather than in the time

domain. Correspondingly, a coding gain (and thus an improved error performance) can be achieved without lowering the effective bit rate compared to single-antenna transmission. Additionally, a spatial diversity gain is achieved which also contributes to an improved error performance.<sup>3</sup> Although the major goal of spatial diversity techniques is to improve error performance (or, equivalently, to reduce the transmit power required to achieve a certain error performance), they can also be used to increase the bit rate of a system, when employed in conjunction with an adaptive modulation/channel coding scheme [CEGH02].<sup>4</sup> Well-known spatial diversity techniques for systems with multiple transmit antennas are, for example, Alamouti's transmit diversity scheme [Ala98] as well as space-time trellis codes [TSC98] invented by Tarokh, Seshadri, and Calderbank. For systems, where multiple antennas are available only at the receiver, there are well-established linear diversity combining techniques dating back to the 1950's [Bre59].

### Improved Signal-to-Noise Ratios with Smart Antennas

In addition to higher bit rates and smaller error rates, multiple-antenna techniques can also be utilized to improve the signal-to-noise ratio (SNR) at the receiver and to suppress co-channel interferers in a multiuser scenario. This is achieved by means of adaptive antenna arrays [Hay85, Com88, Gab92], also called smart antennas or software antennas in the literature. Using beamforming techniques, the beam patterns of the transmit and receive antenna array can be steered in certain desired directions, whereas undesired directions (e.g., directions of significant interferers) can be suppressed. Beamforming can be interpreted as linear filtering in the spatial domain. The SNR gains achieved by beamforming are often called antenna gains or array gains. Beamforming techniques can also be beneficial in scenarios with strong spatial fading correlations due to insufficient antenna spacings. The concept of antenna arrays with adaptive beam patterns is not new and has its origins in the field of radar (e.g., for target tracking) and aerospace technology. However, intensive research on smart antennas for wireless communication systems started only in the 1990's.

### Focus of the Thesis

The above families of multiple-antenna techniques are, in fact, quite different. Spatial multiplexing is closely related to the field of multiuser communications. Space-time coding is more in the field of modulation and channel coding, and beamforming techniques belong more in the area of signal processing and filtering. There are also composite transmission schemes that aim at a combination of the different gains mentioned above. However, given a fixed number of transmit and receive antennas, there are certain trade-offs between multiplexing gains, diversity gains, and SNR gains [ZT03]. In this thesis, the main focus will be on spatial diversity techniques, i.e., on space-time coding and diversity reception techniques.

---

<sup>3</sup>If the antenna spacings at transmitter and receiver are sufficiently large, the individual transmission links can be regarded as statistically independent. Correspondingly, the probability that all links are degraded at the same time is significantly smaller than for a single link.

<sup>4</sup>Adaptive modulation and channel coding schemes are employed in most state-of-the-art wireless communication systems.



## 1.2 Distributed and Co-located MIMO Systems

As we have seen, the benefits of multiple-antenna systems, often called multiple-input multiple-output (MIMO) systems in the literature, are manifold. The new insights into the benefits of multiple-antenna techniques at the end of 1990s fueled tremendous interest both in academia and industry. To date, more than 100 groups are working in the field in Europe alone [KWBR04], and there is an enormous number of yearly publications.<sup>5</sup> Although the period of intensive research activities has been quite short, multiple-antenna techniques are already entering standards [DGI+02] for third-generation (3G) and fourth-generation (4G) wireless communication systems, e.g. [E03, I04b]. Interestingly, the authors of [AFLP03] predict that multiple-antenna techniques will become crucial for system operators to secure the financial viability of their business.

In most publications on spatial diversity and spatial multiplexing techniques, quite stringent assumptions are made about the spacings of the individual transmit and receive antenna elements, see Fig. 1.2. On the one hand, one typically assumes that the individual antenna elements are *co-located*, i.e., they belong to some type of antenna array, cf. Fig. 1.2 a). On the other hand, it is often assumed that the antenna spacings are sufficiently large, so as to justify the assumption of statistically independent links.

In many practical scenarios, sufficient antenna spacings cannot be guaranteed (cf. Fig. 1.2 b)), which causes correlations between the individual transmission links [OAA04].<sup>6</sup> Mobile terminals, for example, are typically characterized by a small size, mainly due to design issues. An appropriate separation of the antenna elements is therefore difficult. However, correlation effects do also occur at the base stations of cellular networks. This is because a base station is typically surrounded by only a small number of local scatterers, which causes a small angular spread of the transmitted and received signals [GSS+03]. Due to this, generous antenna spacings of several wave lengths are typically required, in order to accomplish small correlations between the individual links.

In order to shift the limits of wireless communications, new and unconventional concepts are required. One idea that has recently gained considerable interest is the concept of cooperative wireless networks [NHH04]. In such networks, multiple network nodes cooperate and, for example, share their antennas by using a distributed space-time coding scheme or a distributed diversity reception scheme. By this means, a virtual antenna array is established, cf. Fig. 1.2 c). The cooperating nodes, possibly equipped with only a single antenna, can thus enjoy some of the benefits offered by (conventional) MIMO systems with co-located antennas. Cooperative wireless networks can be viewed as a mixture of hierarchical and ad-hoc networks [DASC04]. Current wireless networks are typically characterized by an inflexible hierarchical structure, where communication is mainly controlled by a central network node, e.g., a base station. By allowing some amount of cooperation between individual network nodes, elements of an ad-hoc network are introduced. Cooperation can, for example, be performed between multiple base stations with inter-

---

<sup>5</sup>A search with IEEE Xplore<sup>®</sup> for papers in the general field of multiple-antenna communication systems yielded a total number of more than 14,700 documents.

<sup>6</sup>The notion of insufficient antenna spacings is relative, because antenna correlation effects are not only governed by the geometry of the antenna array and the employed carrier wavelength, but also by the richness of scattering from the physical environment (see Chapter 2 for further details).

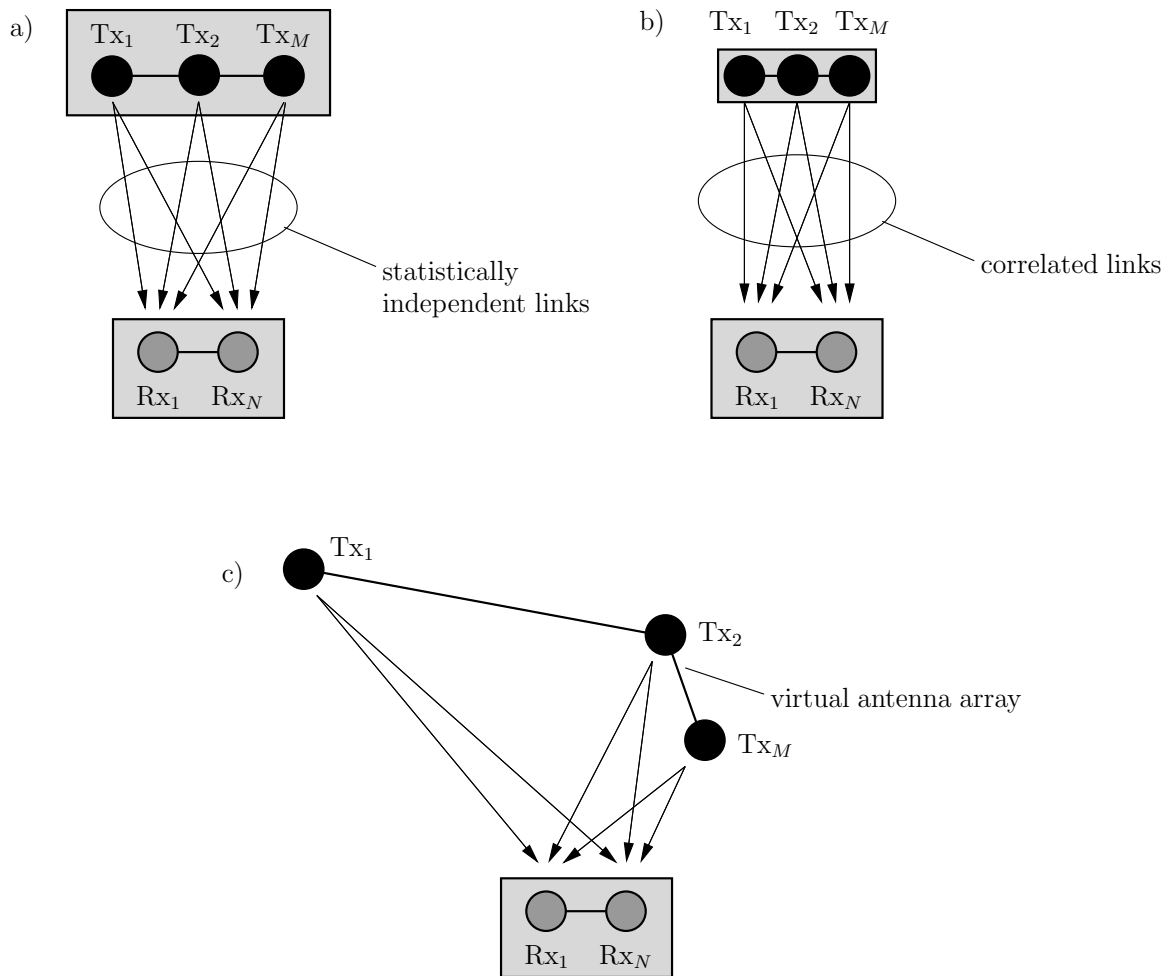


Figure 1.2: Multiple-antenna systems with different antenna spacings (for the example of  $M=3$  transmit and  $N=2$  receive antennas): a) MIMO system with co-located antennas and statistically independent links b) MIMO system with correlated transmit antennas c) Distributed MIMO system with virtual antenna array at the transmitter side.

secting coverage areas. An example are so-called simulcast networks [Wit91] employed for broadcasting or paging applications. Another example for cooperation between fixed network nodes are reach-back links for wireless sensors, where data measured by wireless sensors are collected by multiple distributed receiving nodes and are then processed in a joint fashion. Cooperation can also be performed between mobile terminals. An example are relay-assisted networks [PWS+04] where mobile terminals mutually relay their transmitted or received signals.

## 1.3 Scope and Aim of the Thesis

The focus of this thesis is on spatial diversity aspects in MIMO systems with distributed and co-located antennas. While for co-located MIMO systems, a good portion of work has already been done (concerning performance analysis and the design of efficient transmitter and receiver concepts), the literature on similar results for distributed systems is comparatively sparse.

As will be shown in this thesis, distributed and co-located MIMO systems have more in common than is obvious at a first glance. Within certain limits, a unified view of both types of multiple-antenna systems offers new opportunities for performance analysis as well as for transmitter and receiver design. On the other hand, specific effects arise in distributed systems that typically do not occur in MIMO systems with co-located antennas. For example, in a distributed MIMO system the individual transmission links

- can have different statistics, for example due to shadowing effects, or due to line-of-sight components that occur between some of the transmit-receive antenna pairs
- are typically characterized by different average path losses (due to different link lengths) and thus by different average received SNRs
- can exhibit non-negligible relative signal delays if the individual transmitting (or receiving) nodes are spaced far apart
- can be subject to frequency offsets, due to independent local oscillators employed at the individual transmitting or receiving nodes.

Since the above effects typically occur only in distributed MIMO systems, they are usually not addressed in the standard literature on space-time coding/diversity reception techniques. On the other hand, they are also neglected in most publications on cooperative wireless networks, where focus is usually rather on algorithms and protocols that manage the interaction between the individual network nodes. The aim of this thesis is to

- provide methods for physical-layer performance analysis of distributed MIMO systems
- provide new performance results that are not available in the standard literature on space-time coding and diversity reception techniques
- shed light on the above effects occurring in distributed MIMO systems and thus provide more realistic results for link-level and system-level simulations
- develop appropriate transmitter and receiver strategies and identify suitable space-time coding techniques.

The main contributions of the thesis are highlighted in the following section.

## 1.4 Main Contributions

After a detailed overview concerning the available literature on MIMO systems, a statistical discrete-time MIMO channel model is derived in a transparent fashion, so as to provide the theoretical basis for the remainder of the thesis. As a novel contribution, a rigorous analysis of the resulting statistical properties is presented.

Based on the discrete-time channel model, it is shown that MIMO systems with co-located antennas and MIMO systems with distributed antennas can be treated in a single, unifying framework. It is proven that any spatially correlated MIMO system can be transformed into an (asymptotically) equivalent distributed MIMO system, and vice versa (with regard to different performance criteria). Specifically, a unitary matrix transform is presented, which associates a given distributed MIMO system with an equivalent co-located MIMO system. Utilizing these results, appropriate transmit power allocation strategies are developed for MIMO systems with distributed or co-located antennas. In particular, fading scenarios are taken into account that occur especially in distributed MIMO systems. Focus is on schemes that require solely statistical channel knowledge at the transmitter side, which can easily be acquired in practical systems. By means of analytical results, it is shown that significant performance gains in comparison to equal power allocation are achieved. Moreover, the impact of estimation errors concerning the transmitter correlation matrix is studied.

Finally, the impact of frequency offsets and non-negligible relative signal delays on the performance of distributed MIMO systems is analyzed, and possible counter measures are discussed. Specifically, suitable space-time coding and equalization techniques are identified, so as to maintain a diversity advantage over a single-antenna system.

Parts of this thesis were published as journal papers or refereed conference papers or have recently been accepted for publication: [MKH03, MHS03a, MHS03b, MHS03c, MH04a, MEH04a, MEH04b, MH04b, MTH04, MBH05, MH05, MBLH05, MH06b, MHKX06a, MBLH06, MHKX06b, MH06c]. Another related publication can be found in [FSMH05].

## 1.5 Thesis Outline

The thesis is organized as follows: **Chapter 2** starts with the literature overview on MIMO systems. Following this, the system model is introduced and the statistical discrete-time MIMO channel model is derived. Moreover, a simple and statistically accurate method for simulating block-fading MIMO channels is stated. Finally, some space-time coding schemes that are of special interest in this thesis are described in detail.

The equivalence proofs for co-located and distributed MIMO systems are presented in **Chapter 3**. First, the capacity distribution of coded MIMO systems is considered. Following this, the pairwise error probability of space-time coded MIMO systems is addressed. Finally, the error rates of so-called orthogonal space-time block codes (OSTBCs) [TJC99a, TJC99b], such as Alamouti's transmit diversity scheme [Ala98], are studied. In addition to this, a simple performance measure originally proposed for co-located MIMO systems is discussed and the equivalent measure for distributed systems is derived. To conclude the chapter, the benefits of macroscopic spatial diversity gains (due

to shadowing effects) in distributed MIMO systems are investigated.

The transmit power allocation strategies for co-located and distributed MIMO systems are developed in **Chapter 4**. First, the benefits with regard to ergodic capacity are considered (compared to equal power allocation). Then, statistical power allocation strategies are combined with an outer orthogonal space-time block code. In particular, a simple power allocation strategy is proposed, which provides a near-optimum performance over a wide range of signal-to-noise ratios. After considering the impact of estimation errors concerning the transmitter correlation matrix, the use of statistical channel knowledge at the receiver side is investigated, so as to provide an optimal trade-off between performance and receiver complexity. It is shown that there is a strong relation to the statistical transmit power allocation schemes. Specifically, the impact of estimation errors concerning the receiver correlation matrix can be analyzed along the same lines as for the transmitter side.

Finally, the issue of frequency offsets and non-negligible relative signal delays in distributed MIMO systems is treated in **Chapter 5**. With regard to frequency offsets, the orthogonality loss resulting for orthogonal space-time block codes is studied, and improved receiver concepts are proposed. For Alamouti's transmit diversity scheme, a blind frequency-offset estimation technique is proposed that is applicable for phase-shift-keying signal constellations. With regard to relative signal delays, the use of Alamouti's transmit diversity scheme in conjunction with a trellis-based equalization/detection algorithm at the receiver is considered. As novel contributions, the distance properties of Alamouti's transmit diversity scheme in the presence of intersymbol interference are discussed, and an optimization of the delay diversity scheme [Wit93, SW93] based on the so-called Rake Receiver Bound is presented.

A summary of the thesis and conclusions are given in **Chapter 6**, and possible directions for future work are highlighted. In addition to this, conclusions are also offered at the end of each chapter, along with a summary of the most important results.

Additional material can be found in the appendix, as a supplement to the main chapters. Acronyms and abbreviations used throughout this thesis are listed in **Appendix A**. The mathematical notations and conventions are introduced in **Appendix B**, and a list of mathematical symbols is provided. Mathematical definitions and theorems that are of interest here are stated in **Appendix C** and **Appendix D**, where the latter focuses on the matrix calculus used throughout the thesis. **Appendix E** provides a brief survey of convex optimization, a mathematical tool that is frequently used within this thesis. **Appendix F** offers supplementary material on channel modeling. Additional definitions are stated, important assumptions are discussed, and the calculation of antenna correlations is illustrated, along with some numerical examples. **Appendix G** summarizes the most important results concerning the capacity of static MIMO channels, which serve as a basis for evaluating the capacity distributions of MIMO fading channels. **Appendix H** presents specific considerations for distributed MIMO systems. In particular, properties of virtual antenna arrays for cellular radio systems are discussed. **Appendix I** addresses performance evaluation for maximum-ratio-combining systems, which serves as a theoretical basis for evaluating both the error performance of orthogonal space-time block codes and the Rake Receiver Bound for frequency-selective MIMO fading channels. Finally,

**Appendix J** provides additional material on space-time coding in the presence of inter-symbol interference. In particular, the issue of channel estimation is briefly addressed, a trellis-based equalization/detection algorithm for space-time block codes is presented, and performance evaluation based on distance spectra is discussed. In addition to the above appendices, supplementary material to Chapter 3, Chapter 4, and Chapter 5 has been included at the very end of the corresponding chapter. A complete list of own publications related to the thesis has been included in **Appendix K**.

## Chapter 2

# Wireless Communication Systems with Multiple Antennas

**I**NTENSIVE research on multiple-antenna systems for wireless communications, often called multiple-input multiple-output (MIMO) systems, started less than ten years ago. The great interest was mainly fueled by the seminal works of Telatar [Tel99], Foschini and Gans [Fos96, FG98], Alamouti [Ala98], and Tarokh, Seshadri, and Calderbank [TSC98] at the end of the 1990's. On the one hand, the theoretical results in [FG98, Tel99] promised significantly higher bit rates compared to single-antenna systems. Specifically, it was shown that the (ergodic or outage) capacity of a MIMO system with  $M$  transmit and  $N$  receive antennas, i.e., the maximum bit rate at which error-free transmission is theoretically possible [CT91], grows (approximately) linearly with the minimum of  $M$  and  $N$ . On the other hand, the work in [Fos96, Ala98, TSC98] suggested design rules for practical systems. In [Fos96] a spatial multiplexing scheme, coined Bell-Labs Layered Space-Time Architecture (BLAST), was introduced that accomplished bit rates approaching those promised by theory (at non-zero error rates). In [Ala98], a simple transmit diversity scheme for systems with two transmit antennas was proposed, and in [TSC98] design criteria for so-called space-time trellis codes were derived, which are two-dimensional coding schemes for systems with multiple transmit antennas.<sup>1</sup> The invention of space-time trellis codes was like an ignition spark. With an enormous amount of yearly publications, the field of MIMO systems started to evolve rapidly. To date, there are numerous papers on the performance limits of MIMO systems, and an abundance of transmitter and receiver concepts has been proposed.

Section 2.1 provides an overview of this exciting research field. Following this, the available multiple-antenna techniques are categorized, and the focus of the thesis is highlighted. Although the list of references is not intended to be exhaustive, the cited papers will serve as a good starting point for further reading. In addition to this, there are several books on multiple-antenna techniques, e.g. [HLY02, PNG03, VY03, LS03, KBB+04, BT04a, Jaf05]. Moreover, the following tutorial-style articles can be recommended, all of which have quite a different focus: [PP97, Win98, Koh98, SGGP99, LP99, Pon99, NSC00, Chr00, LFV01, LH02,

---

<sup>1</sup>Space-time codes have the primary goal to improve the error performance of a system. An increased capacity is typically not accomplished.



ML02, AFS+02, STT+02, GSS+03, PGNB04, DASC04, SBM+04, AH04, MH04a, HSdW04, LH04b, SPSH04, SN04, PSY+04, Yan05, ZLZ+05, SS06]. In Section 2.2, the system model is introduced, which constitutes the theoretical basis throughout this thesis. Starting from a physical perspective on multipath signal propagation, a statistical discrete-time MIMO channel model is derived in a transparent fashion. As a novel contribution, a rigorous analysis of the resulting statistical properties is presented, and a simple and statistically accurate method for simulating block-fading MIMO channels is stated. Finally, Section 2.3 provides a closer look on certain multiple-antenna techniques that are of particular interest within the scope of this thesis. A summary of the chapter is provided in Section 2.4.

## 2.1 An Overview of MIMO Systems

Three types of fundamental gains can be obtained by using multiple antennas in a wireless communication system [GSS+03, PGNB04]: A multiplexing gain, a diversity gain, and an antenna gain (cf. Fig. 1.1). Spatial multiplexing techniques such as BLAST [Fos96] predominantly aim at a multiplexing gain, i.e., at increased bit rates compared to a single-antenna system. In contrast to this, spatial diversity techniques such as space-time codes [TSC98, Ala98] and diversity reception techniques [Bre59] aim at a (coding and) diversity gain, i.e., at smaller error rates. Finally, smart antennas and beamforming techniques [Gab92] aim at an antenna gain compared to a single-antenna system, i.e., at an improved signal-to-noise ratio (SNR) or an improved signal-to-interference-plus-noise ratio (SINR). While spatial multiplexing is closely related to the field of multiuser communications, space-time coding is more in the area of modulation and channel coding, while beamforming belongs more in the field of signal processing and filtering.

A strict distinction between these three types of multiple-antenna techniques is sometimes difficult, since often a combination of the above gains is achieved. For example, spatial multiplexing techniques can also accomplish a diversity gain, e.g., if an optimum receiver in the sense of maximum-likelihood (ML) detection is employed [Pro01, Ch. 14.7]. Similarly, spatial diversity techniques can also be used to increase the bit rate of a system, when employed in conjunction with an adaptive modulation/channel coding scheme [PSY+04].<sup>2</sup> In addition to these examples, there are also composite transmission schemes that aim at a good trade-off between higher bit rates and smaller error rates [PSY+04]. In the sequel, an overview of spatial multiplexing, spatial diversity, and smart antenna techniques is provided. More details about certain transmitter and receiver structures are presented in Section 2.3 (with focus on spatial diversity techniques).

### 2.1.1 Spatial Multiplexing Techniques

The fact that the capacity of a MIMO system with  $M$  transmit and  $N$  receive antennas grows (approximately) linearly with the minimum of  $M$  and  $N$  (without requiring extra

---

<sup>2</sup>If the error rate accomplished by means of spatial diversity is smaller than desired, one can switch to a higher-order modulation scheme or to a channel coding scheme with less redundancy [CEGH02]. By this means, it is possible to trade error performance for a higher effective bit rate.



bandwidth or extra transmission power) [Fos96,FG98,Tel99] was an intriguing result. For single-antenna systems it was well known that given a fixed bandwidth, capacity can only be increased logarithmically, namely by increasing the transmit power. In [Fos96], the theoretical capacity results for MIMO systems were complemented by the proposal of the BLAST scheme, which was shown to achieve bit rates approaching 90% of the outage capacity. Similar to the theoretical capacity results, the bit rates of the BLAST scheme were characterized by a linear growth when increasing the number of antenna elements. The first real-time BLAST demonstrator [GFVW99] was equipped with  $M=8$  transmit and  $N=12$  receive antennas. In a rich-scattering indoor environment, it accomplished bit rates as high as 40 bit/s per Hertz bandwidth (corresponding to about 30% of the outage capacity). Wireless spectral efficiencies of this magnitude were unprecedented and cannot be achieved by any single-antenna system.

### Transmitter and Receiver Structure

The idea of spatial multiplexing was first published in [PK92]. The basic principle of all spatial multiplexing schemes is as follows. At the transmitter, the information bit sequence is split into  $M$  sub-sequences (demultiplexing), that are modulated and transmitted simultaneously over the transmit antennas using the same frequency band. At the receiver, the transmitted sequences are separated by employing an interference-cancellation type of algorithm. The basic structure of a spatial multiplexing scheme is illustrated in Fig. 2.1.

In the case of frequency-flat fading, there are several options for the detection algorithm at the receiver, which are characterized by different trade-offs between performance and complexity. A low-complexity choice is to use a linear receiver, e.g., based on the zero-forcing (ZF) or the minimum-mean-squared-error (MMSE) criterion [BTT02,PGNB04]. However, the error performance is typically poor, especially when the ZF approach is used [GSS+03] (unless a favorable channel is given or the number of receive antennas significantly exceeds the number of transmit antennas). Moreover, at least as many receive antennas as transmit antennas are required ( $N \geq M$ ), otherwise the system is inherently rank-deficient. If the number of receive antennas exceeds the number of transmit antennas, a spatial diversity gain is accomplished [Pro01, Ch. 14.7].

The optimum receiver in the sense of the maximum-likelihood (ML) criterion performs a brute-force search over all possible combinations of transmitted bits and selects the most likely one (based on the received signals). The ML detector achieves full spatial diversity with regard to the number of receive antennas [Pro01, Ch. 14.7] irrespective of the number of transmit antennas used. In principle, the use of multiple receive antennas is optional. Yet, substantial performance improvements compared to a single-antenna system are only achieved when multiple receive antennas are employed. The major drawback of the ML detector is its complexity. It grows exponentially with the number of transmit antennas and the number of bits per symbol of the employed modulation scheme. Due to this, the complexity of the ML detector is often prohibitive in a practical system. However, it can be reduced by means of more advanced detection concepts, such as sphere decoding [FP85,VB99,DCB00,AEVZ02].

For the BLAST scheme, an alternative detection strategy known as nulling and canceling was proposed. The BLAST detector was originally designed for frequency-flat fading

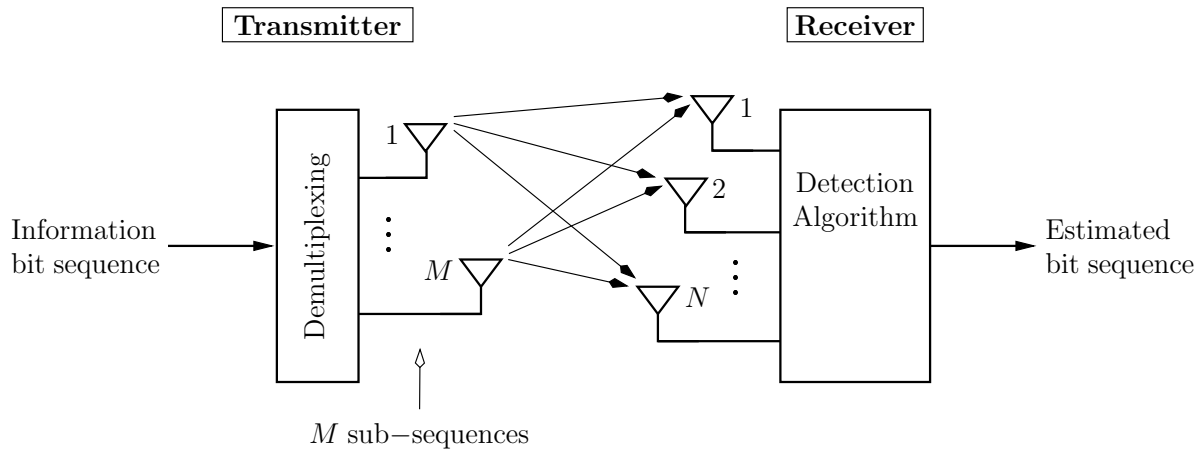


Figure 2.1: Basic principle of spatial multiplexing.

channels and provides a good trade-off between complexity and performance. In contrast to the ML detector, the estimation of the  $M$  sub-sequences, called layers in the terminology of BLAST, is not performed jointly, but successively layer by layer. Starting from the result of the linear ZF receiver (nulling step) [GFVW99, FGVW99] or the linear MMSE receiver [BBPS00, BMY01a], the BLAST detector first selects the layer with the largest SNR and estimates the transmitted bits of that layer, while treating all other layers as interference. Then, the influence of the detected layer is subtracted from the received signals (canceling step). Based on the modified received signals, nulling is performed once again, and the layer with the second largest SNR is selected. This procedure is repeated, until the bits of all  $M$  layers are detected. This detection order is indeed optimal, as shown in [WFGV98]. Due to the nulling operations, the number of receive antennas must at least be equal to the number of transmit antennas (as in the case of the linear receivers), otherwise the overall error performance degrades significantly [SH02].<sup>3</sup> The error performance resulting for the individual layers is typically different. In fact, it depends on the overall received SNR, which layer is best. In the case of a low SNR, error propagation effects from previously detected layers dominate. Correspondingly, the layer detected first has the best performance. At the same time, layers that are detected later have a larger diversity advantage, because less interfering signals have to be nulled. Therefore, in the high SNR regime, where the effect of error propagation is negligible, the layer detected last offers the best performance [BMY01b, WK03]. A rigorous performance analysis of the BLAST detector was, for example, presented in [LG04].

The BLAST detection algorithm is very similar to successive interference cancellation (SIC), which was originally proposed for multiuser detection in code-division-multiple-access (CDMA) systems [Ver93]. Complexity-reduced versions of the BLAST detector were, for example, proposed in [Has00, WBR+01, ZB02, XZH+02, BHC03, Cho04a, ZLC04, WB05, CKLL05]. Variations of the BLAST detector with an improved error performance were suggested in [CCC00, BBPS00, BMY01b, BdE01, FW03, JWMC03, SZDZ03, WBKK03,

<sup>3</sup>Note that this is a crucial requirement when a simple receiver is desired.

BLS06]. An interesting approach to improve the performance of the BLAST scheme was presented in [YW02, WBKK04, Wue05]. Prior to the BLAST detection algorithm, the given MIMO system is transformed into an equivalent system with a better conditioned channel matrix, based on a so-called lattice reduction [LLL82, SE94]. The performance of the BLAST detector is significantly improved by this means and approaches that of the ML detector, while the additional complexity due to the lattice reduction is rather small.

### Channel Coding

In order to guarantee a certain error performance for spatial multiplexing schemes, channel coding techniques are usually required. Most spatial multiplexing schemes employ a channel coding structure that is composed of one-dimensional encoders and decoders operating solely in the time domain [FCG+03]. This is in contrast to space-time coding techniques [TSC98, Ala98], where two-dimensional coding is performed in time and space, i.e., across the individual transmit antennas. In principle, three different types of channel coding schemes can be used in conjunction with spatial multiplexing: Horizontal coding, vertical coding, or a combination of both. Horizontal coding means that channel encoding is performed after the demultiplexer (cf. Fig. 2.1), i.e., separately for each of the  $M$  layers. The assignment between the encoded layers and the transmit antennas remains fixed, i.e., all code bits associated with a certain information bit are transmitted over the same antenna. At the receiver, channel decoding can thus be performed individually for each layer (after applying one of the above receiver structures). In the case of vertical coding, however, channel encoding is performed before the demultiplexer, and the encoded bits are spread among the individual transmit antennas. Compared to horizontal coding, vertical coding thus offers an additional spatial diversity gain. However, the drawback of vertical coding is an increased detector complexity, because at the receiver all layers have to be decoded jointly [PGNB04].

For the BLAST scheme, a combination of horizontal and vertical encoding was proposed, called ‘diagonal’ coding [Fos96]. Correspondingly, the original BLAST scheme is also known as Diagonal BLAST (D-BLAST). As in horizontal coding, channel encoding is performed separately for each layer. Subsequently, a spatial block interleaver is employed. For a certain time period, the assignment between the encoded layers and the transmit antennas remains fixed, and is then changed in a modulo- $M$  fashion. Thus, the overall coding scheme has a diagonal structure in time and space. In principle, diagonal coding offers the same spatial diversity advantage as vertical coding, while retaining the smaller receiver complexity of horizontal coding. A comparative performance study of horizontal, vertical, and diagonal coding was presented in [FCG+03]. Improved channel coding schemes for the BLAST scheme were, for example, proposed in [Gor03, MW03]. The first BLAST demonstrator [GFVW99], coined Vertical BLAST (V-BLAST), was in fact realized without any channel coding scheme.

### Channels with Intersymbol Interference

All of the above receiver concepts were designed for frequency-flat fading channels, i.e., for channels without intersymbol interference (ISI). However, depending on the delay spread of the physical channel (due to multipath signal propagation), the employed transmit and receive filter, and the symbol duration, this assumption might not be

valid in a practical system. If no counter measures are employed, ISI can cause significant performance degradations (see, for example, [BLM02] where the BLAST scheme was studied in the presence of ISI). One approach to circumvent the problem of ISI is to use a multicarrier transmission scheme and multiplex data symbols onto parallel narrow sub-bands that are quasi-flat. Transmission schemes developed for frequency-flat fading channels can then be applied within each sub-band. A popular multicarrier scheme is orthogonal frequency-division multiplexing (OFDM) [HMCK03] which uses an inverse fast Fourier transform (IFFT) at the transmitter and a fast Fourier transform (FFT) at the receiver, making it simple to implement. Specifically, it is straightforward to combine OFDM with multiple antennas (MIMO-OFDM)<sup>4</sup> [RC98, BGP02, SBM+04]. Combinations of (improved) BLAST schemes with OFDM were, for example, considered in [BLM01, PFN+01, BCBR01, Kad03, Soh03, LC05, KYIG05, LLL06, WK06].

Alternatively, one can also use a single-carrier approach and employ suitable techniques for mitigating ISI. Generally, there are two main classes of techniques, namely transmitter-sided predistortion and receiver-sided equalization techniques. Predistortion techniques require channel knowledge at the transmitter, e.g., based on feedback information from the receiver. Predistortion for frequency-selective MIMO channels is a rather new research topic, and not much work has yet been reported [DWLR01, KWZ02, FSH04, CM04].

In contrast to this, there are many equalization schemes for MIMO systems, most of which are generalizations of existing techniques for single-antenna systems. For example, a low-complexity option is to use a linear equalizer (LE) or a decision-feedback equalizer (DFE) [DH89] in time domain. In the case of a single-antenna system, these equalizers are usually realized by means of finite-impulse-response (FIR) filters with real-valued or complex-valued filter coefficients. Generalized linear and decision-feedback equalizers for MIMO systems (MIMO-LEs/DFEs) can be obtained by replacing the scalar filter coefficients by appropriate matrix filter coefficients [ASC97, AS00, WK03]. An alternative to time-domain equalization is frequency-domain equalization (FDE) [FABE02], which is quite similar to OFDM. The major difference is that the FFT and the IFFT are both performed at the receiver. This allows for equalization in the frequency domain by leveling the quasi-flat sub-bands. Like OFDM, FDE can readily be combined with multiple antennas. For example, a combination of BLAST with FDE was considered in [KDFB04].

A high complexity option for mitigating ISI at the receiver is to perform an optimal sequence or symbol-by-symbol estimation, e.g., by means of a trellis-based equalizer. For example, maximum-likelihood sequence estimation (MLSE) can be performed by means of a vector version of the well-known Viterbi algorithm [For72], see [van76]. Alternatively, a generalized version of the Bahl-Cocke-Jelinek-Raviv (BCJR) algorithm [BCJR74] can be used to perform symbol-by-symbol maximum a-posteriori (MAP) detection. The complexity of MLSE and symbol-by-symbol MAP detection grows exponentially with the number of transmit antennas and the number of bits per modulation symbol. Additionally, it grows exponentially with the effective memory length of the channel. In principle, the use of multiple receive antennas is again optional. Similar to the case without ISI, the complexity of MLSE can be reduced significantly by means of the sphere decoding

---

<sup>4</sup>OFDM is also known as discrete multitone (DMT) and MIMO-OFDM as discrete matrix multitone (DMMT).

approach [VH02b].

Finally, direct generalizations of the BLAST detection algorithm to ISI channels were, for example, proposed in [LP02, ZM03]. In essence, the nulling operation is replaced by a set of generalized decision-feedback equalizers for MIMO systems. An iterative extension of [LP02] was proposed in [WK03, Wue05].<sup>5</sup> A combination of MIMO-LEs with the BLAST detection algorithm was considered in [VJU03].

### Alternative Transmitter and Receiver Concepts

More recently, an alternative receiver concept has been proposed for spatial multiplexing systems without ISI [PPWL04], which is based on the concept of probabilistic data association (PDA). PDA has its origins in target tracking and has been adopted in many different areas, for example, in multiuser communication systems based on CDMA [LPWH01]. The key idea is to use an iterative receiver, which detects the individual layers (or, in a multiuser system, the bit sequences of the individual users) by regarding the other, interfering layers as Gaussian noise (Gaussian assumption). Within each iteration, the mean and the variance of the assumed Gaussian noise is adjusted by exploiting knowledge about already detected bits. When a sufficiently large number of layers is used (and a modulation scheme with moderate cardinality) the Gaussian assumption fits well, and a near-optimum error performance is achieved.<sup>6</sup> The principle of the PDA detector can also be applied for mitigating ISI. PDA-based equalizers for MIMO systems were, for example, presented in [LT04]. Further stochastic detection algorithms for spatial multiplexing systems without ISI were proposed in [HZD05]. These are based on the concept of particle filtering [DKZ+03] and achieve near-ML performance at a reasonable complexity.

There are many connections between spatial multiplexing schemes and multiuser communication systems. Hence the idea to adopt multiple-access techniques for spatial multiplexing is quite obvious. For example, one could use orthogonal spreading codes (also called signature sequences) to separate the individual layers, just as in a direct-sequence (DS) CDMA system. However, if perfect mutual orthogonality between all layers is desired, the maximum possible bit rate is the same as in a single-antenna system, i.e., the advantage of using multiple transmit antennas is sacrificed. On the other hand, relaxing the strict orthogonality constraint causes additional noise within the system (overloaded system). Yet, the use of spreading codes can be beneficial in the case of a bad channel, so as to allow for a separation between a few critical layers [MP00a] (possibly, at the expense of a moderate loss in bit rate).

A promising alternative to DS-CDMA is interleave-division multiple access (IDMA) [PLWL06]. In contrast to a DS-CDMA system, the orthogonality constraint is completely dropped in IDMA, and hence no spreading code design is required. The individual users or layers are separated solely on the basis of different, quasi-random interleaver patterns. At the transmitter, the information bits are first encoded using a simple (low-rate) repetition code. Alternatively, a more advanced low-rate channel code may be used [YPW05].

<sup>5</sup>A similar extension of the original BLAST detection algorithm for frequency-flat fading was earlier suggested in [BMY01b].

<sup>6</sup>As shown in [FSMH05], four layers are already sufficient to achieve near-ML performance with quaternary modulation and an outer rate-1/2 turbo code.



Afterwards, the coded bits (called chips) are permuted using a layer-specific quasi-random block interleaver over multiple code words. In order to separate the individual layers at the receiver, the powerful turbo principle is used [BGT93]. The iterative IDMA receiver uses a Gaussian assumption for the interference stemming from other layers (similar to the PDA detector) and is thus able to efficiently separate the individual layers, even in the case of a significantly overloaded system. In [WLP03, WP06], the idea of IDMA was transferred to (single-user) multiple-antenna systems. The ST-IDM scheme in [WLP03] offers an overall bit rate of 1 bit per channel use and is therefore rather a space-time coding scheme. However, by overloading the system the overall bit rate can be increased, so that a multiplexing gain is achieved [WP06].<sup>7</sup> The scheme in [WP06], coined multilayer ST-IDM, has two major advantages when compared to a conventional BLAST system. First, the number of receive antennas can be smaller than the number of transmit antennas, which is particularly attractive for the downlink of a cellular system, where a simple mobile receiver is desired. Even with a single receive antenna, an overall transmission rate up to 4 bits per channel use can be achieved with an error performance close to the capacity limit [WP06]. Second, the multilayer ST-IDM scheme is inherently robust to ISI, making it suitable for a large range of wireless applications.

An alternative approach for spatial multiplexing with less receive antennas than transmit antennas was proposed in [EPP06]. It is based on group MAP detection and is applicable for channels without ISI. In [SH02, SH03b] a spatial multiplexing scheme called Turbo-BLAST was proposed, which is similar to the multilayer ST-IDM scheme. It also uses quasi-random interleaving in conjunction with an iterative receiver structure, so as to separate the individual layers. As in multilayer ST-IDM, the number of receive antennas can be smaller than the number of transmit antennas. Moreover, a generalization of Turbo-BLAST to frequency-selective MIMO channels is straightforward.

Spatial multiplexing in the presence of ISI with less receive than transmit antennas can also be performed using a complexity-reduced version of joint detection, e.g., starting from the trellis-based vector Viterbi algorithm [van76]. For example, a (space-time) channel shortening filter can be employed prior to the vector Viterbi algorithm, in order to reduce the effective memory length of the MIMO channel, e.g. [Al-01a, WK03, BHKX05].<sup>8</sup> A similar receiver structure has previously been applied in the related field of (single-antenna) co-channel interference (CCI) cancellation [HBXK05].

### 2.1.2 Spatial Diversity Techniques

In contrast to spatial multiplexing techniques, where the main objective is to provide higher bit rates compared to a single-antenna system, spatial diversity techniques pre-

<sup>7</sup>In order to accomplish a good error performance, an optimized transmit power allocation strategy is required, however.

<sup>8</sup>Alternatively, a generalized version of a delayed-decision feedback sequence estimator (DDFSE) [DH89] can be used, in conjunction with a (generalized) prefilter for an overall minimum-phase channel impulse response [GT04]. However, for this approach the number of receive antennas must be greater than or equal to the number of transmit antennas. For the channel shortening approach, at least an MMSE solution can be found when the number of transmit antennas exceeds the number of receive antennas, while a ZF solution does in general not exist.

dominantly aim at an improved error performance. This is accomplished on the basis of a diversity gain and a coding gain. Indirectly, spatial diversity techniques can also be used to enhance bit rates, when employed in conjunction with an adaptive modulation/channel coding scheme [PSY+04].

There are two types of spatial diversity, referred to as macroscopic and microscopic diversity. Macroscopic (large-scale) diversity is associated with shadowing effects in wireless communication scenarios, due to major obstacles between transmitter and receiver (such as walls or large buildings). Macroscopic diversity can be gained if there are multiple transmit or receive antennas, that are separated on a large scale (cf. Fig. 1.2 c)). In this case, the probability that all links are simultaneously obstructed is smaller than for a single link. Microscopic (small-scale) diversity is available in rich-scattering environments, where constructive and non-constructive superposition of scattered signal components at the receiver causes a fading signal amplitude (multipath fading) [Jak74]. Microscopic spatial diversity can be gained by employing multiple co-located antennas. Typically, antenna spacings of just a few wavelengths are sufficient, in order to obtain links that fade more or less independently.<sup>9</sup> Similar to macroscopic diversity, the diversity gains are due to the fact that the probability of all links being simultaneously in a deep fade decreases with the number of antennas used. An excellent survey of the value of spatial diversity for wireless communication systems can be found in [DASC04].

The idea to utilize macroscopic diversity in wireless communication systems is not new. It dates back to the 1970's [Gra79]. Even more so, the use of multiple receive antennas for gaining microscopic diversity (diversity reception) has been well established since the 1950's, e.g. [Bre59]. However, it took until the 1990's before transmit diversity techniques were developed.

### Diversity Reception

Diversity reception techniques are applied in systems with a single transmit antenna and multiple receive antennas. They perform a (linear) combining of the individual received signals, in order to provide a microscopic diversity gain. In the case of frequency-flat fading, the optimum combining strategy in terms of maximizing the SNR at the combiner output is maximum ratio combining (MRC) [Bre59], which requires perfect channel knowledge at the receiver. Several suboptimal combining strategies have been proposed in the literature, such as equal gain combining (EGC), where the received signals are co-phased and added up, or selection diversity (SD), where the received signal with the maximum instantaneous SNR is selected, whereas all other received signals are discarded [Bre59]. All three combining techniques achieve full diversity with regard to the number of receive antennas [EKM96]. Optimal combining techniques for frequency-selective fading channels were, for example, considered in [BS92].

### Transmit Diversity and Space-Time Codes

The main idea of transmit diversity is to provide a diversity or coding gain by sending *redundant* signals over multiple transmit antennas (in contrast to spatial multiplexing,

---

<sup>9</sup>Due to this, the term microscopic diversity was chosen for this type of spatial diversity. This does not imply that the associated performance gains are small. In fact, they can be quite substantial.

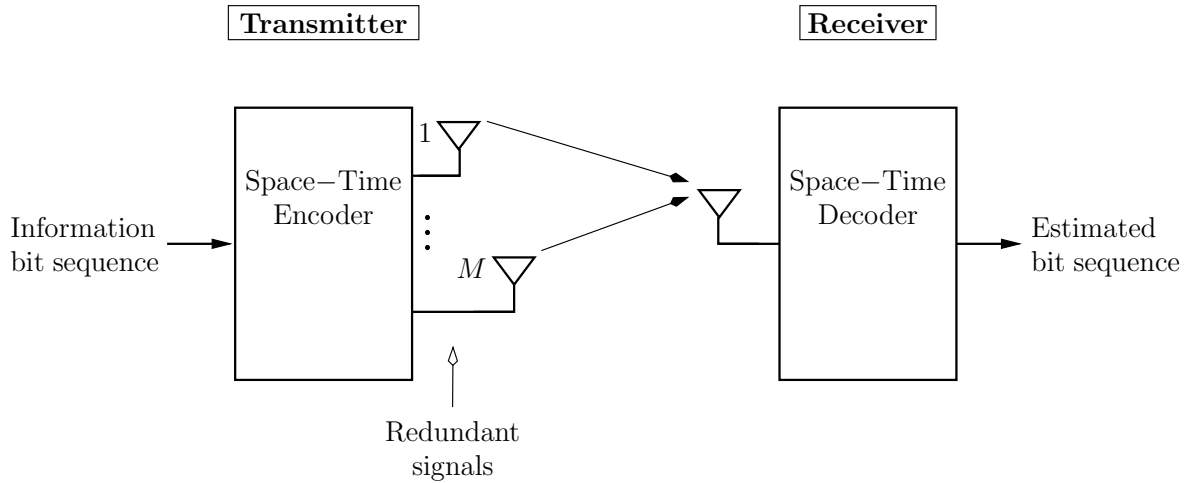


Figure 2.2: Basic principle of space-time coding.

where independent bit sequences are transmitted). To allow for coherent detection at the receiver, an adequate preprocessing of the signals is performed prior to transmission, typically without channel knowledge at the transmitter. With transmit diversity, multiple antennas are only required at the transmitter, whereas multiple receive antennas are optional. However, they can be utilized to further improve performance. In cellular networks, for example, the predominant fraction of the overall data traffic typically occurs in the downlink.<sup>10</sup> In order to enhance the crucial downlink it is therefore very attractive to employ transmit diversity techniques, because then multiple antennas are required only at the base station. With regard to cost, size, and weight of mobile terminals this is a major advantage over diversity reception techniques.

An early beginning of transmit diversity schemes was made with two papers that independently proposed a simple technique called delay diversity [Wit91, Wit93, SW93].<sup>11</sup> Further early publications on transmit diversity were presented in [DS97, KF97]. However, the value of transmit diversity was only recognized in 1998, when Alamouti proposed a simple technique for two transmit antennas [Ala98]. In the same year, Tarokh, Seshadri, and Calderbank invented space-time trellis codes (STTCs) [TSC98], which are two-dimensional coding schemes for systems with multiple transmit antennas. While delay diversity and Alamouti's transmit diversity scheme provide solely a diversity gain (more precisely, full diversity with regard to the number of transmit and receive antennas), STTCs yield both a diversity gain and a coding gain.

Within the scope of this thesis, we will use the generic term *space-time coding scheme* for all transmitter-sided spatial diversity techniques, irrespective of the presence of any additional coding gain. The basic structure of a space-time coding scheme is illustrated in Fig. 2.2. The preprocessing of the redundant transmission signals is performed by the

<sup>10</sup>Comparatively large amounts of data may be downloaded from the base station to a single mobile terminal, whereas in the uplink typically little data traffic is required to initiate the download.

<sup>11</sup>Prior to this, there were already publications on transmit diversity schemes using different modulation parameters at the individual transmit antennas ('modulation diversity'), e.g., [Ada79, HO80, OMH84].



space-time encoder, which depends very much on the specific scheme under consideration. At the receiver, the corresponding detection/decoding process is carried out by the space-time decoder.<sup>12</sup> In the delay diversity scheme [Wit93,SW93], for example, identical signals are transmitted via the individual antennas, using different delays. This causes artificial ISI, which can be resolved at the receiver by means of standard equalization techniques available for single-antenna systems. In contrast to this, Alamouti's transmit diversity scheme [Ala98] performs an orthogonal space-time transmission, which allows for ML detection at the receiver by means of simple (widely) linear processing.

STTCs [TSC98,TNSC99b] may be interpreted as a generalization of trellis-coded modulation [Ung82,Ung87] to multiple transmit antennas. Optimum decoding in the sense of MLSE can be performed using the Viterbi algorithm [For72]. Based on simulation results, it was shown in [TSC98] that STTCs offer an excellent performance that is within 2-3 dB of the outage capacity limit. However, this performance comes at the expense of a comparatively high decoding complexity. Motivated by the simple receiver structure of [Ala98], orthogonal space-time block codes (OSTBCs) were introduced in [TJC99a,TJC99b], which constitute a generalization of Alamouti's scheme to more than two transmit antennas. OSTBCs are designed to achieve full diversity with regard to the number of transmit and receive antennas. In contrast to STTCs, OSTBCs do not offer any additional coding gain.

A closer look at the transmitter and receiver structures of the above space-time coding schemes is provided in Section 2.3.

### Optimized STTCs and OSTBCs

In [TSC98,TNSC99b], general design criteria were derived for STTCs that guarantee a maximum diversity advantage and allow for an optimization of the coding gain (both for high SNR values). These design criteria depend on the number of transmit and receive antennas as well as on the cardinality of the employed modulation scheme. Unfortunately, 'good' STTCs cannot be constructed analytically, but have to be found by means of a computer search. An efficient design procedure for STTCs, which is based on simple lower and upper bounds on the coding gain, was presented in [Blu02]. In [TSC98,TNSC99b], some examples of optimized STTCs were stated, for certain modulation schemes and certain numbers of transmit antennas.<sup>13</sup> Further examples of optimized STTCs, sometimes based on (slightly) modified design criteria, can be found in [BBH00,CYV01,FVY01,IMYL01,TC01,WCWC01,CVYL02,SL02a,Blu02,AHR+03,YCVF03,ANH+04,LC04,LVTZ04]. A tight bound on the error performance of STTCs was, for example, presented in [SD03].

OSTBCs are based on the mathematical theory of (generalized) orthogonal designs [Hur98,Rad22], which dates back to the 1890s. Orthogonal designs are a special class of orthogonal matrices. Examples of generalized orthogonal designs will be presented in Section 2.3.1, where the structure of OSTBCs is discussed in more detail. In general, the use of OSTBCs causes a rate loss when compared to an uncoded single-antenna system. For the case of a real-valued modulation scheme, full-rate (and delay-optimal) OSTBCs for sys-

<sup>12</sup>All space-time coding schemes discussed in the sequel were designed for frequency-flat fading.

<sup>13</sup>The STTCs constructed in [TSC98,TNSC99b] provide the best trade-off between data rate, diversity advantage, and trellis complexity. Specifically, the codes do not cause any rate loss compared to an uncoded single-antenna system.

tems with two to eight transmit antennas could be established in [TJC99a] (partly based on generalized orthogonal designs). Given a complex-valued modulation scheme, however, the only full-rate OSTBC is Alamouti's transmit diversity scheme [Ala98] for two transmit antennas [LX03]. In [TJC99a] it was shown that half-rate OSTBCs for complex-valued modulation schemes can be constructed for any number of transmit antennas. However, to find OSTBCs with higher rates (and moderate decoding delay) is, in general, not a trivial task. A systematic design method for high-rate OSTBCs was presented in [SXL04], for complex-valued modulation schemes and arbitrary numbers of transmit antennas. Examples of optimized OSTBCs for different numbers of transmit antennas can, for example, be found in [TJC99a, TJC99b, TH00, GS01, SX03, LH03a, Lia03a, Lia03b, TSW+04, LFX05]. A performance analysis of OSTBCs based on channel capacity, the overall received SNR, the average symbol error rate, and the average pairwise error probability can be found in [SP00], [GS01], [SL02d], and [GG05], respectively.

### Other Families of Space-Time Codes

Since the advent of STTCs and OSTBCs in 1998/99, various other families of space-time codes have been proposed in the literature. In [TH02] the family of square-matrix embeddable STBCs was introduced, which includes some of the OSTBCs proposed in [TJC99a, TJC99b] as special cases. Similar to OSTBCs, square-matrix embeddable STBCs allow for ML detection at the receiver by means of (generalized) linear processing. A family of non-orthogonal full-rate linear STBCs, called diagonal algebraic STBCs, was constructed in [DAB02, DB03]. Diagonal algebraic STBCs provide full transmit diversity and allow for efficient ML detection by means of the sphere decoding approach. Another non-orthogonal full-rate STBC for two transmit antennas, constructed based on number theory, was presented in [DTB02]. For more than one receive antenna, this STBC provides an improved coding gain compared to Alamouti's transmit diversity scheme [Ala98]. In [XWG03], STBCs based on linear constellation precoding were proposed, which provide full rate and full diversity for any number of transmit antennas and perform superior to OSTBCs. For decoding, a sphere decoding approach as well as suboptimal alternatives were considered in [XWG03]. An alternative idea for constructing full-rate STBCs for complex modulation schemes and more than two transmit antennas was pursued in [Jaf01, SP03, PF03, BI03, SP04, SX04b, DG05, YGT05]. Here the strict constraint of perfect orthogonality was relaxed in favor of a higher data rate. The resulting STBCs are therefore referred to as quasi-orthogonal STBCs. Due to the relaxed orthogonality constraint, however, quasi-orthogonal STBCs typically offer reduced diversity gains compared to OSTBCs. (Examples for quasi-orthogonal STBCs will be discussed in Section 2.3.2.) In addition to the above examples, many other families of STBCs can be found in the literature, some of which are presented in [HMR+00, ED03, San03, LGB03, LSB04, CLP05, XL05, SJ05, LV05b, DV05a, LL05b, Lu05, MK06, SAB06, Lu06, NMN06].

In [HYVC02, GN03], recursive STTCs were considered. For example, in [HYVC02] the parallel concatenation of two identical recursive STTCs was studied. Here the encoder structure was inspired by the original turbo code [BGT93] invented by Berrou, Glavieux, and Thitimajshima in 1993. (Turbo codes are among the most powerful channel codes for additive-white-Gaussian-noise channels.) Recursive STTCs are, for example, well suited

for a serial concatenation with an outer channel code (using an iterative detector at the receiver) [GN03]. In [JS03], the family of super-orthogonal STTCs was introduced and was later extended in [SWX05] to a larger set of modulation schemes. Super-orthogonal STTCs constitute a systematic combination of OSTBCs with the concept of set partitioning [Ung82, Ung87], and offer full rate for two transmit antennas. Moreover, they allow for a trade-off between rate and coding gain. In [JH05a], the concept of super-orthogonal STTCs was extended using quasi-orthogonal STBCs as building blocks. By this means, a full-rate super-quasi-orthogonal STTC for four transmit antennas was constructed. In [TC04a], another class of STTCs called diagonal block space-time codes was proposed. These STTCs are characterized by a special encoder structure (a non-binary block code followed by a diagonal space-time transmission scheme), which allows for a systematic design procedure. Further families of STTCs were, for example, presented in [Ion03, KW03, LVZT06, KW06, SSPH06].

All of the above space-time coding schemes were designed for systems employing *linear* modulation schemes, such as phase-shift-keying (PSK) modulation or quadrature amplitude modulation (QAM). Non-linear continuous-phase modulation schemes are attractive for practical systems, because they offer a compact spectrum and a constant signal envelope, which allows for power-efficient transmitters with inexpensive amplifiers. Motivated by this fact, space-time coding schemes for continuous-phase-modulation systems were, for example, investigated in [ZF02, ZF03, WSX03, WX04, Cav05, BA05a, PHK05, WWX05, CL05, BA05b, PV05b, SSL05a, AR06, XPL06, HC06].

### High-Rate Space-Time Transmission Schemes

As indicated above, “conventional” space-time codes such as STTCs and (O)STBCs offer at most the same data rate as an uncoded single-antenna system. Correspondingly, their main objective is to improve error performance, by providing a spatial diversity advantage and/or a coding gain. In contrast to this, several high-rate space-time transmission schemes with a normalized rate greater than one have been proposed in the literature. These build a bridge between space-time coding and spatial multiplexing techniques.

Some of these transmission schemes explicitly combine ideas of certain space-time codes and the BLAST scheme. For example, high-rate space-time codes that are linear in space and time, so-called linear dispersion codes, were proposed in [HH02b]. Linear dispersion codes provide a flexible trade-off between space-time coding and spatial multiplexing. At the transmitter, the information bit sequence is first split into multiple parallel sub-sequences, similar to a spatial multiplexing technique. Then, linear combinations (in time and in space) of these sub-sequences are simultaneously transmitted. Due to the linear structure of the scheme, detection is very similar to spatial multiplexing schemes, i.e., in principle, any of the receiver structures discussed in Section 2.1.1 can be used. At the same time, linear dispersion codes offer a major advantage over spatial multiplexing systems such as the BLAST scheme. They can handle any configuration of transmit and receive antennas, i.e., they do not require a certain minimum number of receive antennas. Moreover, in comparison to an uncoded V-BLAST system they may accomplish an additional coding gain. Further high-rate space-time transmission schemes that combine ideas of space-time coding and the BLAST scheme can, for example, be found in [TNSC99a,

BBPS00, WTS01, EH01, PV01, El 02a, OANA02, WYL02, SF03a, SF03b, TC04b, ZD05].

A completely different approach to construct high-rate space-time transmission schemes for MIMO systems is to take channel codes, which are known to provide an excellent performance in single-antenna systems, and to generalize them to the case of multiple antennas. For example, the design of repeat-accumulate (RA) codes [DJM98] for MIMO systems was considered in [tK03, YW05b]. As shown in [tK03], RA codes designed for MIMO systems are superior to parallel concatenated codes (PCCs) [BGT93] designed for MIMO systems. The design of low-density parity-check (LDPC) codes [Gal62] for MIMO systems was, for example, considered in [HB03, LYW04, WL04, tKA04, WOCV04, HSM05]. LDPC codes designed for MIMO systems achieve a similar performance as RA codes [tKA04]. Like PCCs, RA codes and LDPC codes can be decoded in an iterative fashion [Lan04, Ch. 3.6], which offers a near-optimum performance at a moderate receiver complexity. In particular, given a certain target SNR value for which convergence of the iterative receiver is desired, the codes can be optimized such that they operate closely to the corresponding capacity limit. This optimization can, for example, be performed by means of the EXIT chart method [ten01], which is widely used, in order to design turbo- and turbo-like transmission schemes. Another class of high-rate space-time transmission schemes, which fits into the framework of iterative detection, are the schemes based on IDMA [WLP03, WP06] discussed in Section 2.1.1.

A rather new branch of work has originated from a paper published by Zheng and Tse in 2003 [ZT03] (see also [TV05, Ch. 9]). In this paper, it was shown that for any space-time transmission scheme there is a fundamental trade-off between diversity gain and multiplexing gain. In this context, the multiplexing gain was defined as the asymptotic slope of the achieved rate as a function of the (logarithmized) SNR.<sup>14</sup> According to this definition, an adaptive space-time transmission scheme is required, in order to achieve a multiplexing gain greater than zero, because the scheme must be able to scale the transmission rate with growing SNR. Such an adaptive space-time transmission scheme might, for example, be constructed using an STTC or an OSTBC in conjunction with a series of symbol alphabets with growing cardinalities. In fact, for  $M=2$  transmit antennas and  $N=1$  receive antenna it was shown in [ZT03] that Alamouti's transmit diversity scheme [Ala98] achieves the optimal diversity-multiplexing trade-off (however, not for  $N>1$  receive antennas). Other space-time transmission schemes that achieve or approach the optimal diversity-multiplexing trade-off (for certain numbers of antennas and certain block lengths) were proposed in [YW03, ECD04, SRK04a, SRK04b, TV04a, WX05, MS05, BRV05, SDL05, KR05, EKL05, ZLW05, DV05b, TV06, VR06].

Further high-rate space-time transmission schemes not mentioned above can, for example, be found in [SB02, SRS03, WLWX04, LK05, LGW05].

## Outer Channel Codes

In order to further improve the performance of space-time coded MIMO systems, the space-time encoder can be concatenated with an outer channel encoder. This is of partic-

<sup>14</sup>This definition of the multiplexing gain is very similar to the widely-used definition of diversity order. The diversity order achieved by a space-time transmission scheme is typically defined as the (negative) slope of the frame or bit error rate at high SNRs (in a log-log plot).

ular interest for OSTBCs, which offer only a diversity gain, but no built-in coding gain.

An excellent survey of such concatenated space-time transmission schemes can be found in [LH02]. The main focus of [LH02] is on OSTBCs as inner space-time codes concatenated with different outer channel coding schemes, such as convolutional codes [Eli55], turbo codes [BGT93], and (turbo) trellis-coded modulation [Ung82,Ung87], among others. Examples of concatenated schemes with inner STTCs are also considered. In all cases, the receiver structure considered in [LH02] consists of an inner soft-input soft-output (SiSo) space-time decoder (based on the symbol-by-symbol MAP criterion) followed by an outer channel decoder. Alternatively, a turbo-type receiver structure can be employed, where a SiSo space-time decoder and a SiSo channel decoder exchange soft information in an iterative fashion.<sup>15</sup> A good overview of iterative receiver structures for concatenated space-time transmission schemes can be found in [HSdW04].

Further examples of space-time coded MIMO systems with outer channel codes (and iterative or non-iterative receiver structures) can be found in [ATP98,YS99,SHP01,BHS01,GL02,GN03,PSL03,DC04,HH04].

### Channels with Intersymbol Interference

All of the above space-time coding schemes were designed for frequency-flat fading, i.e., for channels without ISI. However, as discussed in Section 2.1.1, this assumption might not be valid in a practical system. If no counter measures are employed, ISI can cause a substantial performance loss, compromising the achieved diversity and coding gains. For example, OSTBCs lose their orthogonal property in the presence of ISI, which leads to significant self-interference [MHS03a]. Similarly, STTCs suffer from decreased coding gains if ISI is neglected at the receiver (while the diversity advantage is still maintained) [GL00]. Similar to the case of spatial multiplexing schemes, there are basically three different options to design space-time coding schemes for MIMO channels with ISI. First, one might use a space-time code originally designed for channels without ISI and mitigate the effects of ISI at the receiver using appropriate equalization techniques. Alternatively, one might employ the space-time code in conjunction with a multicarrier scheme (e.g. OFDM), so as to circumvent the problem of ISI. Finally, one might refine or generalize existing space-time codes such that they are suited for ISI channels.

Equalization concepts for OSTBCs were, for example, proposed in [CC99,CB00,ANC01,AI-01b,BHS01,LYL01,AFS+02,AI-02,MHS03a,Cho04b,GOS+04,MH04a,DW05,PV05a] (with focus on Alamouti's transmit diversity scheme [Ala98]). Joint equalization and detection concepts for STTCs in the presence of ISI were presented in [BN99,NS00,SHP01,YYH01,YA02,AFS+02,AI-02,BA02,SC06]. The combination of STBCs with MIMO-OFDM was, for example, considered in [MP00b,LGBS01,SZG02,LWL02,LM03,MMPL03,PGNB04,SKKY04,YC04,RZC04,MPM04,PSY+04,Yan05,LCL05c,YJP+05,KHP05,WI05,TLB05,LT05,SLSL05,WSW+06,DWC06,LK06,AA06]. MIMO-OFDM systems employing STTCs were considered in [ATNS98,NSC00,BLWY01,RG02,LM06,SC06]. In addition to the spatial and the temporal dimension, MIMO-OFDM systems offer a third dimension, namely the frequency domain. Correspondingly, an interesting alternative to

<sup>15</sup>This idea can also be adopted for BLAST-like systems with vertical coding (cf. Section 2.1.1) and interleaving. In this case, the inner space-time decoder is replaced by a soft demapper [Ton00].



space-time coding in MIMO-OFDM systems is to perform two-dimensional coding in space and frequency (i.e., across the individual carriers) or three-dimensional coding in space, time, and frequency. Depending on the properties of the wireless channel, space-frequency (SF) codes or space-time-frequency (STF) codes may offer larger diversity gains than pure space-time coding [PGNB04]. Moreover, SF codes may offer certain implementation advantages over space-time coding techniques [Yan05]. SF codes for MIMO-OFDM systems were considered in [RC98, BP00b, LW00, BBP03, Bau03, EHL+03, SSOL03, GL03a, SSL05b, SR05, RW05, DT05, CPD06, ED06, LL06]. Several of these SF codes were constructed using existing STBCs or STTCs as building blocks. Design and performance criteria for STF codes were, for example, presented in [TJL01, MWW02, SO02b, LXG02, FMS05, SSL05c, WYP+05, SSOL06, SSL06, HSL06, ZXC07].

Finally, several papers proposed generalizations or refinements of existing space-time coding techniques, so as to enable their use for MIMO channels with ISI. For example, optimized versions of delay diversity for ISI channels were suggested in [GSP01, MHS03a, MH04a, HSG05, YSG06]. Similarly, optimized or generalized STTCs for MIMO channels with ISI were proposed in [LFT01, MWC03, AWS03, QB04, DR05]. An interesting generalization of Alamouti's transmit diversity scheme [Ala98] to ISI channels, which is based on a time-reversal (TR) block-encoding structure, was presented in [LP00]. Similar to Alamouti's transmit diversity scheme, simple (widely) linear processing is employed at the receiver, which enables subsequent equalization by means of standard algorithms designed for single-antenna systems (cf. Section 2.3.3 for further details). An extension to more than two transmit antennas is also possible [SL01, JGS06]. A similar transmit diversity scheme for two transmit antennas was also considered in [ZG01, ZG03b]. Special receiver structures for the TR-STBC were, for example, studied in [ZHC01, NM02, SCG04]. Moreover, an alternative STBC design for ISI channels was presented in [SGL04].

### Differential and Non-coherent Space-Time Transmission Schemes

The space-time coding techniques discussed above require some form of channel knowledge at the receiver. In contrast to this, so-called differential/non-coherent space-time transmission schemes do not require any channel knowledge and are thus of particular interest for practical MIMO systems. Differential space-time transmission techniques can be interpreted as an extension of differential single-antenna schemes, e.g., based on differential phase-shift-keying (DPSK) modulation, to multiple antennas. Purely non-coherent transmission schemes do not employ a differential encoder at the transmitter side. One of the first differential space-time transmission schemes was proposed in [TJ00]. It is based on Alamouti's transmit diversity scheme [Ala98] and can be employed in systems with two transmit antennas. Shortly afterwards, two alternative differential schemes were presented in [Hug00] and [HS00], and a purely non-coherent scheme was presented in [HM00]. These schemes can be employed for any number of transmit and receive antennas. Since then, a considerable number of differential space-time transmission/reception schemes has been proposed in the literature, e.g. [SHHS01, WM02, Xia02, HH02a, LX02, LS02, SPS02, SL02b, SL02c, TC03, LSF03, ED03, CV03, LLKZ03, SG03, SPS03a, SPS03b, LLK03, Al03, SNK04, Bau04, CH04, LZC04, LLK04, SX04a, SWSX04, WWX04, SNK05, HSL05, PHK05, LX05b, WWM05, JH05c, PV05b, CZA06, CG06, DB06, WW06, GHL06, CS06, YGT06, Tao06,

ZJ06, Ngu07]. Similar to the case of a single-antenna system, differential space-time transmission schemes with conventional differential detection at the receiver lead to a performance loss of about 3 dB, when compared to coherent reception. This performance loss can, for example, be compensated by employing a multiple-symbol or a decision-feedback differential detection scheme at the receiver [SL02c].

All of the above differential/non-coherent space-time transmission schemes were designed for frequency-flat fading channels. In comparison, little work has been done, in order to design corresponding schemes for ISI channels. One option is again to combine the above differential space-time transmission schemes with MIMO-OFDM, see for example [DASC02]. As an alternative, novel differential/non-coherent schemes for MIMO-OFDM were proposed in [Li03a, Li05, MTL05, BB05, Bau06, LL06, HSL06] employing coding in time, space, and frequency. Another option is to use space-time coding techniques suitable for ISI channels as building blocks. For example, differential schemes that are based on the TR-STBC [LP00] for two transmit antennas were considered in [DASC02, Al-03, Che05]. Further differential space-time transmission schemes for ISI channels can be found in [ZI03, ASB+05].

### Practical Issues

The space-time transmission schemes proposed in the literature are often based on somewhat idealized assumptions [MH04a]. For example, many schemes are designed for MIMO channels without ISI, as discussed above. Block fading is another common assumption, where the channel is presumed to be invariant over the duration of a complete data block. This assumption is questionable if transmitter or receiver move at high speeds, or if there is a significant carrier frequency offset (CFO) between the local oscillators at transmitter and receiver (employed for up- and down-conversion of the transmitted/received signals). Concerning the recovery of the transmitted data symbols, many space-time transmission schemes require accurate channel knowledge at the receiver, which is critical in the case of low SNRs or a rapidly varying channel. Furthermore, one often assumes that the individual transmission links between the transmit and receive antennas are statistically independent. However, due to insufficient antenna spacings or a lack of scattering from the physical environment, the links may be correlated (cf. Section 1.2).<sup>16</sup> Finally, another important issue is that the performance gains actually achieved in a practical MIMO system might be smaller than promised in theory, because implementing an optimal transmitter/receiver strategy might be too complex so that one has to resort to suboptimal solutions. For example, the impact of a reduced-state trellis-based equalizer on the performance of the delay diversity scheme [Wit93, SW93] was considered in [MHS03a].

Several papers study the impact of the above effects on the performance of different space-time transmission schemes. For example, the influence of a time-varying channel and non-perfect channel knowledge on the performance of OSTBCs was investigated in [SBF01, LWL02, AN02, GL03c, ML03, HF03b, MHS03a, TJJG03, SSL04, VLB04, WW04, Ohn04, LCL05c, KHP05, JZP05, DU05].<sup>17</sup> Similar investigations for STTCs, as well as

<sup>16</sup>This issue will be discussed in detail in Section 2.2.

<sup>17</sup>Many of these papers focus on Alamouti's transmit diversity scheme [Ala98].

improved design criteria, were presented in [TSC98, NTSC98, FVY01, WCWC01, SL02a, GW02a, RG02, MJSW02, SL02e, Mue02b, SO02a, YCVF03, ANH+04, DSL04, LC04]. The impact of frequency offsets on the performance of STBCs and STTCs was investigated in [NTSC98, LMG02, VVL03, AB03, MMPL03, MEH04a, MEH04b, SKKY04, MPM04, HC04, YKH+04, AKB05]. Finally, the impact of spatial correlation effects on the performance of STBCs and STTCs was considered in [NTSC98, BP00a, Ale01, GW02b, SBV02, El 02b, VA03, GL03b, JS04b, QB04, YSL04, WSFY04, UG04, LAK04, FMSL04, MH04a, LFWS04, PSY+04, XK05, HSN05]. Further studies concerning practical aspects of MIMO systems can be found in [PP97, PN98, CH99, NSC00, AFS+02, STT+02, VB02, GSS+03, DASC04, SBM+04, Yan05].

### 2.1.3 Smart Antennas and Beamforming Techniques

The potential advantages of using multiple antennas are not limited to increased data rates and improved error rates. They can also be utilized, in order to improve the signal-to-noise ratio (SNR) at the receiver and to suppress co-channel interference (CCI) in a multiuser scenario, i.e., to improve the signal-to-interference-plus-noise ratio (SINR) at the receiver. Both goals can be achieved by means of beamforming techniques [Hay85, Com88].

#### Beamforming

Beamforming can be interpreted as linear filtering in the spatial domain [God97]. Consider an antenna array with  $N$  antenna elements and directional antenna pattern, which receives a radio-frequency (RF) signal from a certain direction. Due to the geometry of the antenna array, the impinging RF signal reaches the individual antenna elements at different time instants, which causes phase shifts between the individual received signals. However, if the underlying complex baseband signal is assumed to be a narrowband signal, it will not change during these small time differences. If the direction of the impinging signal is known, the phase differences of the RF signals can be compensated by means of phase shifters or delay elements, before the received signals are added up [God97]. For example, coaxial cables of different lengths can be used. As a result, the overall antenna pattern of the phased array will exhibit a maximum in the direction of the impinging signal. This principle is called conventional beamforming in the literature.

If only the phases of the received signals are manipulated, the shape of the overall antenna pattern remains unchanged, and solely an angular shift results. Correspondingly, conventional beamforming is equivalent to a mechanical rotation of the antenna array (mechanical beam steering) [God97]. If the amplitudes of the received signals are also scaled before the combining step, then it is possible to modify also the shape of the overall antenna pattern.<sup>18</sup> In particular, an antenna array with  $N$  antenna elements provides  $(N-1)$  degrees of freedom, i.e., in principle  $(N-1)$  angles can be specified for which the overall antenna pattern is supposed to exhibit either a maximum or a minimum.

---

<sup>18</sup>Mathematically, the received signals are weighted by complex-valued antenna weights representing the phase shifts and the scaling of the individual signal amplitudes. In fact, these weighting operations (followed by the linear combining step) are very similar to those performed by diversity reception techniques in the baseband domain.



If the above narrowband assumption for the complex baseband signal is not met, the baseband signal can change during time intervals that are as small as the relative delays between the received RF signals. Thus, the individual antenna elements will observe different versions of the complex baseband signal. In this case, broadband beamforming techniques are required that combine narrowband beamforming (i.e., spatial filtering) with linear time-domain filtering, e.g., in the form of a two-dimensional linear finite-impulse-response (FIR) filter [God97].

### Array Gain

In a wireless communication scenario, transmitted signals often propagate via just a few distinct paths, for example via a line-of-sight path between transmitter and receiver and/or via paths that are associated with significant reflectors and diffractors in the environment (such as large buildings or mountains). If the directions of these dominant propagation paths are known at the receiver, beamforming techniques can be applied, in order to adjust the receiver beam pattern such that it has a high directivity towards the dominant angles of reception [God97]. By this means, significant SNR gains can be accomplished in comparison to an antenna array with an omni-directional beam pattern.<sup>19</sup> Such SNR gains due to beamforming techniques are often called antenna gains or array gains in the literature. Similarly, if the directions of the dominant propagation paths are known at the transmitter, the transmit power can be concentrated within the corresponding angular regions, and is not wasted for directions that do not contribute to the received signal. Beamforming techniques can also be useful, in order to reduce the delay spread of the physical channel caused by multipath signal propagation. To this end, the transmitter or receiver beam pattern is adjusted such that it exhibits minima (nulls) in the direction of dominant distant reflectors. Correspondingly, echoes with excessively large delays are eliminated from the received signal [God97]. The basic principle of beamforming is illustrated in Fig. 2.3. In the considered example, a beamformer is employed both at the transmitter and at the receiver.

In a practical system, the directions of dominant propagation paths must be estimated. This can, for example, be done by means of the well-known MUSIC algorithm [Sch86] or the ESPRIT algorithm [RK89]. Moreover, when transmitter or receiver are moving, the antenna patterns must be updated on a regular basis. Such adaptive antenna arrays are often called smart antennas or software antennas in the literature. Due to the required equipment and processing power, however, the use of smart antenna technologies is currently limited to fixed stations, such as base stations, or mobile stations that are fixed on vehicles. Yet, for future wireless communication systems it is anticipated that smart antennas will also be feasible for hand-held devices employing small phased arrays fabricated by microstrip technology [God97].

### Co-Channel Interference (CCI) Suppression and SDMA

Smart antennas are also beneficial in multiuser scenarios, in order to suppress CCI. Again, both transmitter- and receiver-sided beamforming techniques can be employed for miti-

---

<sup>19</sup>When multiple receive antennas are employed, an SNR gain is always obtained, because the overall average received power is increased. However, SNR gains due to beamforming come on top of that.

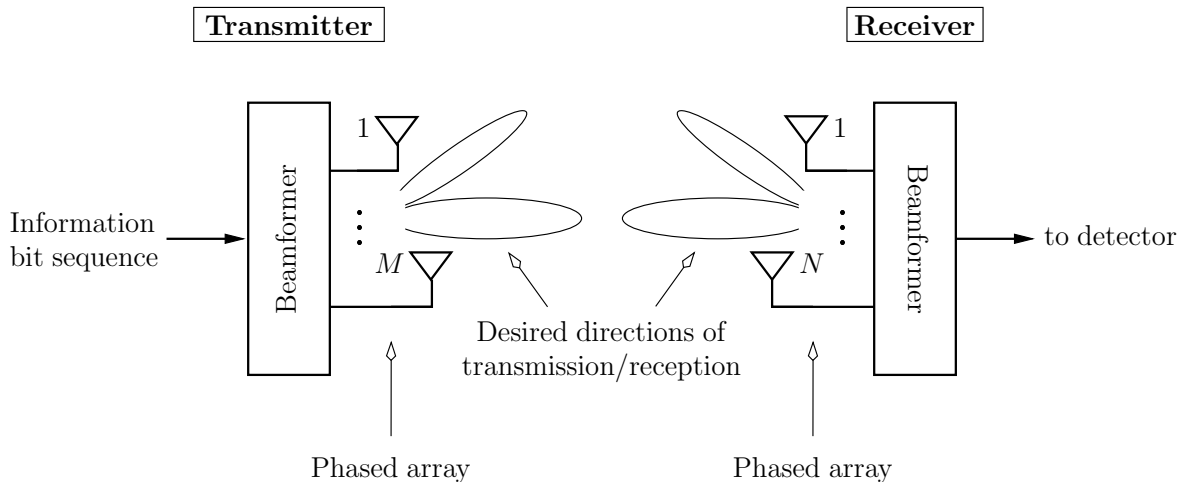


Figure 2.3: Basic principle of beamforming.

gating CCI. When transmitting, each user can adjust his beam pattern such that there are nulls in the directions of other co-channel users and a high directivity towards the desired direction(s) of transmission [Chr00]. By this means, the SINR for the other co-channel users is improved as well as the SNR at the desired receiver. Similarly, when receiving each user can adjust his beam pattern such that directions of co-channel interferers are nulled (or at least attenuated) and desired directions of reception are enhanced. By this means, each user can improve his own received SINR.<sup>20</sup> The use of smart antennas for CCI cancellation offers the opportunity to accommodate multiple co-channel users within the same frequency band. This concept is referred to as space-division multiple access (SDMA). For cellular networks, for example, it was shown that network capacity in terms of users per cell can be enhanced significantly by means of SDMA techniques [WSG94].

The concept of antenna arrays with adaptive beam patterns is not new. It has its origins in the field of radar and aerospace technology [Chr00], especially in applications such as target tracking and high-resolution remote sensing. Early publications on the use of antenna arrays for interference suppression date back to the 1960's [How65]. Similarly, publications on adaptive beamforming algorithms can be traced back to the 1970's [App76]. However, intensive research on smart antenna techniques for wireless communication systems started only in the 1990's, e.g. [SBEM90].

A detailed overview concerning the use of adaptive antenna arrays in wireless communication systems is provided in [God97]. Further tutorial-style articles that consider the topic of beamforming can be found in [Gab92, PP97, Win98, Koh98, SGGP99, Chr00, LFV01, ML02, SBM+04, AH04, SPSH04].

<sup>20</sup>In the case of exact nulling, the directions of all co-channel interferers must be known. Alternatively, it is also possible to optimize the SINR at the combiner output without explicit knowledge of the directions of all co-channel interferers [God97]. For example, the well-known Capon beamformer [Cap69] requires solely the direction of the desired source signal.

### Combinations with Spatial Multiplexing and Spatial Diversity Techniques

Smart antenna techniques employed for array gains or CCI suppression can readily be combined with spatial multiplexing or spatial diversity techniques. However, in order to achieve a good overall performance, the beamforming scheme should be adapted to the underlying spatial diversity/spatial multiplexing technique. MIMO transmission schemes that combine ideas of beamforming with spatial multiplexing or spatial diversity techniques were considered in [NBP01, WVF03, HLHS03, SS03, ZDZY03, CBRB04, KC04, NSL04, LL05a, GPPF05, LH05b, LH05c, RR06a] and [WSG94, JSO02, SP02, LI02, NTC02, LLC03, MWC03, CC03, ZG03a, PZS04, AQ04, BRW04, Lo04, BE04, JS04a, Ale04, vF04, HG04, LH05d, LJ05, CGZ05, LCL05a, PPPL06], respectively. A particularly simple solution is to build a hybrid system, where a switching between the different techniques is possible, see e.g., [FPKH05]. At any time, the best transmission strategy can thus be chosen, depending on the current properties of the wireless channel and the requested quality of service (QoS). An interesting performance comparison between beamforming, spatial multiplexing, and spatial diversity techniques (from a QoS point of view) was, for example, presented in [IN04].

#### 2.1.4 Other Classifications of Multiple-Antenna Techniques

As discussed above, transmission and reception techniques for multiple-antenna systems can roughly be divided into spatial multiplexing techniques, spatial diversity techniques, and smart antenna techniques (see Fig. 2.4 for an overview). In addition to this classification, there are other options for categorizing multiple-antenna techniques:

- *SIMO, MISO, and MIMO techniques*

Transmission techniques for multiple-antenna systems can be distinguished according to the number of transmit and receive antennas used. Techniques that utilize multiple receive antennas, but only a single transmit antenna (such as diversity reception schemes) are referred to as single-input multiple-output (SIMO) techniques in the literature. Similarly, techniques that utilize multiple transmit antennas, but only one receive antenna are called multiple-input single-output (MISO) techniques. Finally, techniques that require multiple antennas at both ends of the wireless link (e.g., spatial multiplexing techniques such as the BLAST scheme) are called multiple-input multiple-output (MIMO) techniques.

- *Open-loop, closed-loop, and non-coherent techniques*

Transmission techniques for multiple-antenna systems that require no channel knowledge at the transmitter are referred to as open-loop techniques, because no feedback of channel state information from the receiver to the transmitter is required [DGI+02, LH04b]. For example, space-time coding techniques and spatial multiplexing techniques such as the BLAST scheme are typical open-loop techniques. In contrast to this, transmission techniques that require full or partial channel knowledge at the transmitter (such as transmitter-sided beamforming techniques) are called closed-loop techniques. Transmission techniques that require channel knowledge neither at the transmitter nor at the receiver are called non-coherent

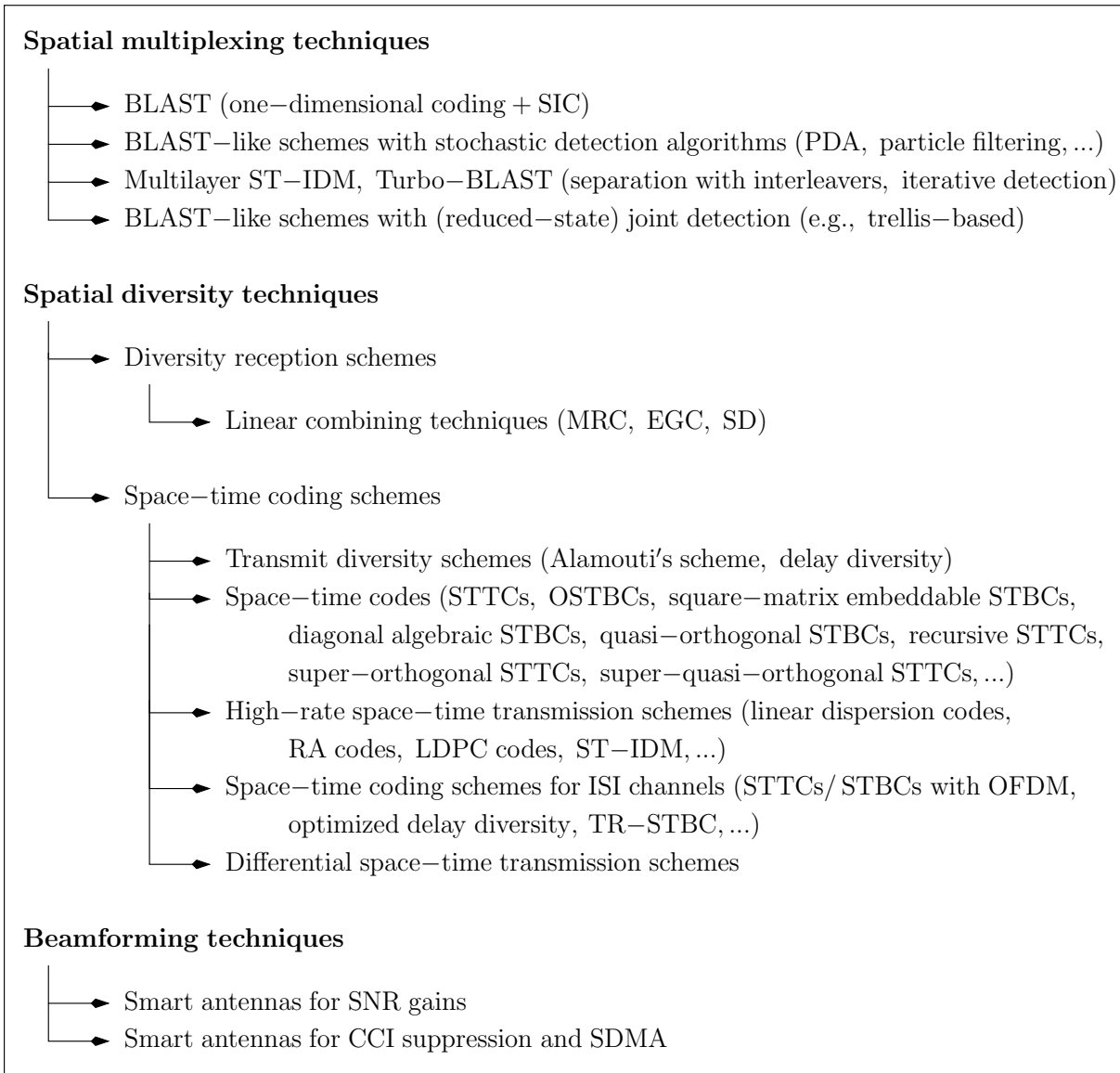


Figure 2.4: Overview of multiple-antenna techniques.

techniques [DASC04]. For example, the differential/non-coherent space-time transmission techniques discussed in Section 2.1.2 are an important class of non-coherent multiple-antenna techniques.

- *Narrowband and broadband techniques*

Transmission techniques that are designed for frequency-flat fading channels are called narrowband techniques. For example, OSTBCs or the original BLAST scheme are typical narrowband techniques. In contrast to this, transmission techniques that are suitable for frequency-selective fading channels (e.g., multiple-antenna techniques that are based on OFDM) are referred to as wideband or broadband techniques in the literature [AFS+02].

On a system level, MIMO systems can be categorized as follows:

- *Single-user and multiuser MIMO systems*

In a single-user MIMO system, a point-to-point communication with multiple antennas is performed between a single user and a remote network node (e.g., a base station, an access point, or another user). Correspondingly, in a multiuser MIMO system a point-to-multipoint communication (broadcast scenario) [SPSH04] or a multipoint-to-point communication (multiple-access scenario) [DASC04] is performed between multiple users and a remote network node.

- *Co-located and distributed MIMO systems*

In a co-located MIMO system, the antennas at transmitter and receiver are part of some sort of antenna array. In contrast to this, in a distributed MIMO system the antennas at the transmitter and/or the receiver side are spatially distributed on a large scale (cf. Section 1.2).

### 2.1.5 Focus of the Thesis

The focus of this thesis is on single-user systems (SIMO-, MISO-, or MIMO systems) with co-located or distributed antennas (see Chapter 3 for more details). Both narrow-band and broadband techniques are considered. Broadband techniques are of particular interest for distributed MIMO systems, because different relative propagation delays can cause ISI effects, as will be seen in Chapter 5. Throughout this thesis, focus will be on spatial diversity techniques operating in an open-loop fashion, although in Chapter 4 also the use of (statistical) channel knowledge at the transmitter side is investigated.

## 2.2 System and Channel Model

This section introduces the channel model for a general multiple-input multiple-output (MIMO) system, which constitutes the theoretical basis throughout this thesis. The topic of channel modeling for multiple-antenna systems has received much interest during the last couple of years, see [PP97, ECS+98, Koh98, GSS+03, PGNB04] for an overview. In fact, it is still an active field of research. On the one hand, accurate channel models are required, in order to predict the theoretical limits of real-world MIMO systems. On the other hand, they are indispensable for designing novel transmitter and receiver techniques and assessing their efficiency in realistic environments.

Channel models for MIMO systems can roughly be divided into physical and stochastic channel models. Physical channel models reflect certain physical characteristics of wireless communication scenarios. Often, they explicitly model signal propagation via distinct paths associated with significant reflectors and diffractors in the vicinity of transmitter and receiver. Typically, these models include several physical parameters such as antenna pattern characteristics, spatial scatterer distribution, and angles of departure and arrival. In contrast to this, stochastic channel models are rather abstract and try to reduce the number of required parameters to a minimum, while retaining a sufficiently accurate

description of the MIMO channel. Physical channel models for MIMO systems were, for example, proposed in [RC98, RJ99, WJ02, ZFW02], while stochastic channel models can be found in [PBKM00, KSP+02, XWL+04]. Moreover, numerous models have been suggested that try to build a bridge between physical and stochastic approaches, e.g., [PMF00, CFK+00, PMT01, BGP02, ITE02, Mue02a, Say02, GBGP02, XCHV04, BT04b]. In addition to this, there are some MIMO channel models which are based on extensive measurement campaigns, e.g., [WJSJ03, CLW+03, KCVW03]. However, the majority of channel models available in the literature is based on a statistical description, because an accurate deterministic description is often not feasible.

Within the scope of this thesis, we will make use of a stochastic channel model. To this end, we derive a statistical discrete-time channel model for a general MIMO system with  $M$  transmit and  $N$  receive antenna, which includes the effects of time-variance, intersymbol interference (ISI), and spatial fading correlations. Later, certain special cases being of particular interest will be derived from this model.

Throughout this thesis, the employed modulation scheme, the physical channel, and the receive filter are assumed to be linear. The first two steps of the channel modeling process are presented in detail in Appendix F. In the first step, a physical view on multipath signal propagation from a single transmit antenna to a single receive antenna is developed, see also [RC98, BGP02, Mue02a, XCHV04]. In the second step a statistical multipath signal propagation model is derived in a transparent fashion. A summary of the most important results required in the sequel is given in Section 2.2.1. Based on the statistical multipath signal propagation model, we then arrive at a discrete-time MIMO channel model (Section 2.2.2), where we basically follow [Hoe92, XWL+04]. As a novel contribution, a rigorous analysis of the statistical properties of the discrete-time MIMO channel model is presented, and a simple and statistically accurate method for simulating block-fading MIMO channels is stated (Section 2.2.3). Finally, alternative fading models that are of interest in this thesis are discussed in Section 2.2.4.

Since we consider digital communication systems, where all signal processing tasks of interest are carried out in the baseband domain, we will use the complex baseband representation throughout this thesis (i.e., we do not consider the up- and down-conversion of transmitted and received signals). The mathematical notation used in the sequel is introduced in Appendix B. Moreover, important mathematical definitions are included in Appendix C and D.

### 2.2.1 Statistical Multipath Signal Propagation Model

In the following, the most important results concerning the statistical multipath signal propagation model derived in Appendix F are summarized, and the underlying assumptions are highlighted.

We consider a point-to-point link between a transmitter equipped with  $M$  antenna elements and a receiver equipped with  $N$  antenna elements. It is assumed that transmitter and receiver are situated in a typical wireless communication scenario (see Fig. F.1 in Appendix F), where the transmitted signals are subject to multipath signal propagation, due to reflections, diffuse scattering, and diffraction [Jak74]. For the time being, we focus on a continuous-time signal propagation model. To this end, let  $s_\mu(t)$  denote the



continuous-time signal transmitted from the  $\mu$ th antenna element ( $1 \leq \mu \leq M$ ), where  $t$  denotes the absolute time.

In the sequel, let  $f_{\nu,\mu}(\tau_n, t)$  denote the overall complex gain factor associated with the  $\mu$ th transmit antenna element ( $1 \leq \mu \leq M$ ), the  $\nu$ th receive antenna element ( $1 \leq \nu \leq N$ ), the absolute time  $t$ , and the  $n$ th resolvable relative signal delay  $\tau_n$  ( $0 \leq n \leq N_\tau - 1$ ), where  $0 \leq \tau_0 < \dots < \tau_n < \dots < \tau_{N_\tau-1} =: \tau_{\max}$ . The gain factors  $f_{\nu,\mu}(\tau_n, t)$  exhibit a fading amplitude, due to constructive and non-constructive superposition of multiple signal components associated with the same relative delay  $\tau_n$ . Assuming a rich-scattering environment, the complex gain factors  $f_{\nu,\mu}(\tau_n, t)$  can be modeled as circularly symmetric complex Gaussian random variables [Hoe92], i.e.,

$$f_{\nu,\mu}(\tau_n, t) \sim \mathcal{CN}(\bar{f}_{\nu,\mu,n}, \sigma_{f_{\nu,\mu,n}}^2) \quad (2.1)$$

(cf. Definition C.9 in Appendix C), where  $\bar{f}_{\nu,\mu,n} := \mathbb{E}\{f_{\nu,\mu}(\tau_n, t)\}$  denotes the mean and  $\sigma_{f_{\nu,\mu,n}}^2 := \mathbb{E}\{|f_{\nu,\mu}(\tau_n, t) - \bar{f}_{\nu,\mu,n}|^2\}$  the variance of  $f_{\nu,\mu}(\tau_n, t)$ , i.e., the magnitudes of the gain factors  $f_{\nu,\mu}(\tau_n, t)$  are characterized by Rayleigh or Rice fading. Throughout this thesis, we assume that only the first gain factor  $f_{\nu,\mu}(\tau_0, t)$  may contain a line-of-sight (LoS) component ( $\tau_0=0$ ), cf. Remark F.2 in Appendix F. However, for the time being we assume  $\bar{f}_{\nu,\mu,0}=0$  for simplicity.

Throughout this thesis, we assume that the wireless channel is wide-sense stationary (WSS) with uncorrelated scattering (US) [Bel63], cf. Assumption F.3 in Appendix F. Uncorrelated scattering implies that two gain factors  $f_{\nu,\mu}(\tau_n, t)$  and  $f_{\nu',\mu'}(\tau_{n'}, t)$  associated with different discrete delays are uncorrelated, i.e., their covariance (for a fixed time  $t$ ) is given by

$$\sigma_{f_{\nu,\mu,n}, f_{\nu',\mu',n'}}^2 := \mathbb{E}\{f_{\nu,\mu}(\tau_n, t) f_{\nu',\mu'}^*(\tau_{n'}, t)\} = \sigma_{f_{\nu,\mu,n}}^2 \delta[n-n']. \quad (2.2)$$

Wide-sense stationarity implies that the statistical properties of the gain factors  $f_{\nu,\mu}(\tau_n, t)$ , such as the spatial covariances

$$\mathbb{E}\{f_{\nu,\mu}(\tau_n, t) f_{\nu',\mu'}^*(\tau_n, t)\} =: \begin{cases} \sigma_{f_{\nu,\mu,\nu',\mu',n}}^2 & \text{for } \mu' \neq \mu \text{ or } \nu' \neq \nu \\ \sigma_{f_{\nu,\mu,n}}^2 & \text{for } \mu' = \mu \text{ and } \nu' = \nu \end{cases}, \quad (2.3)$$

are time-invariant. Specifically, the auto-correlation function

$$R_{f_{\nu,\mu,n}}(t+\Delta t, t) := \mathbb{E}\{f_{\nu,\mu}(\tau_n, t) f_{\nu,\mu}^*(\tau_n, t+\Delta t)\} / \sigma_{f_{\nu,\mu,n}}^2 \quad (2.4)$$

depends only on the time difference  $\Delta t$ , but not on the absolute time  $t$ . Furthermore, we assume that spatial and temporal correlation properties may be modeled independently, cf. Assumption F.4. Correspondingly, we set the spatio-temporal correlations to

$$\frac{\mathbb{E}\{f_{\nu,\mu}(\tau_n, t) f_{\nu',\mu'}^*(\tau_n, t+\Delta t)\}}{\sqrt{\sigma_{f_{\nu,\mu,n}}^2 \sigma_{f_{\nu',\mu',n}}^2}} =: \rho_{f_{\nu,\mu,\nu',\mu',n}} \cdot R_{f_{\nu,\mu,n}}(t+\Delta t, t), \quad (2.5)$$

where the parameters

$$\rho_{f_{\nu,\mu,\nu',\mu',n}} := \frac{\sigma_{f_{\nu,\mu,\nu',\mu',n}}^2}{\sqrt{\sigma_{f_{\nu,\mu,n}}^2 \sigma_{f_{\nu',\mu',n}}^2}}, \quad (2.6)$$

denote the spatial fading correlations.

Finally, we will mainly employ the Kronecker correlation model throughout this thesis (cf. Assumption F.5), i.e., we assume that the spatial correlations  $\rho_{f_{\nu,\mu,\nu',\mu',n}}$  ( $\mu, \mu' = 1, \dots, M$ ,  $\nu, \nu' = 1, \dots, N$ ,  $n = 0, \dots, N_\tau - 1$ ) can be written as products

$$\rho_{f_{\nu,\mu,\nu',\mu',n}} = \rho_{f_{\nu,\mu,\nu,\mu',n}} \cdot \rho_{f_{\nu,\mu,\nu',\mu,n}} =: \rho_{f_{\mu,\mu',n}} \cdot \rho_{f_{\nu,\nu',n}} \quad (2.7)$$

of transmit and receive antenna correlations. The Kronecker correlation model was shown to be quite accurate, in order to model the spatial correlation properties of practical MIMO channels [XWL+04], at least for co-located systems with a moderate number of transmit and receive antennas [OHW+03]. Possible generalizations of the Kronecker model will be discussed in Section 3.3. As shown in Appendix F, the transmit and receive antenna correlations can be computed according to

$$\rho_{f_{\mu,\mu',n}} = \int_0^{2\pi} p_{\vartheta_d}(\vartheta_d) e^{j(\varphi_{\text{Tx},\mu}(\vartheta_d) - \varphi_{\text{Tx},\mu'}(\vartheta_d))} d\vartheta_d, \quad (2.8a)$$

$$\rho_{f_{\nu,\nu',n}} = \int_0^{2\pi} p_{\vartheta_a}(\vartheta_a) e^{j(\varphi_{\text{Rx},\nu}(\vartheta_a) - \varphi_{\text{Rx},\nu'}(\vartheta_a))} d\vartheta_a, \quad (2.8b)$$

where  $\vartheta_d$  denotes the angle of departure (AoD),  $\vartheta_a$  the angle of arrival (AoA),  $p_{\vartheta_d}(\vartheta_d)$  the angular probability density function (PDF) of the transmitter-sided power azimuth spectrum (PAS),  $p_{\vartheta_a}(\vartheta_a)$  the angular PDF of the receiver-sided PAS, and  $\varphi_{\text{Tx},\mu}(\vartheta_d)$  and  $\varphi_{\text{Rx},\nu}(\vartheta_a)$  the phase terms of the transmit and the receive antenna array, respectively. Numerical examples for the transmit and receive antenna correlations can be found in Example F.2 in Appendix F, for different antenna geometries and different power azimuth spectra.

We have now arrived at a statistical multipath signal propagation model for a general MIMO system with  $M$  transmit and  $N$  receive antennas, which includes the effects of spatial and temporal fading correlation. Altogether, the correlations of the complex gain factors  $f_{\nu,\mu}(\tau_n, t)$  are given by [XWL+04]

$$\frac{\mathbf{E}\{f_{\nu,\mu}(\tau_n, t) f_{\nu',\mu'}^*(\tau_{n'}, t + \Delta t)\}}{\sqrt{\sigma_{f_{\nu,\mu,n}}^2 \sigma_{f_{\nu',\mu',n'}}^2}} = \rho_{f_{\nu,\mu,\nu',\mu',n}} \cdot R_{f_{\nu,\mu,n}}(t + \Delta t, t) \cdot \delta[n - n'], \quad (2.9)$$

where  $\mu, \mu' = 1, \dots, M$ ,  $\nu, \nu' = 1, \dots, N$ , and  $n, n' = 0, \dots, N_\tau - 1$ . It should be noted that the above statistical multipath signal propagation model does not include antenna coupling effects (cf. Remark F.8 in Appendix F). Within the scope of this thesis, we will only focus on the aspect of antenna correlation, i.e., we will always assume that antenna spacings are large enough so that mutual coupling effects can be neglected.

So far, a continuous-time signal propagation model was considered. In a digital communication system, however, the transmitted signals  $s_\mu(t)$  carry discrete-time data symbols that are drawn from a finite alphabet  $\mathbb{A}$ . State-of-the-art receivers first filter and sample the received signals, and then recover the transmitted data symbols by means of discrete-time signal processing. Correspondingly, it is useful to define a discrete-time channel model [For72], which comprises the continuous-time physical channel model, (analog) filters at transmitter and receiver, and the sampling, including the sampling rate and



the sampling phase. Based on the above results, we derive in the following a statistical discrete-time channel model for a general MIMO system, which results in a convenient matrix-vector representation (see also [XWL+04]).

### 2.2.2 Statistical Discrete-Time Channel Model

From the above statistical multipath signal propagation model we move on to a statistical discrete-time MIMO channel model, which will constitute the theoretical basis for the remainder of the thesis. To this end, we consider the transmission model depicted in Fig. 2.5. For the time being, we focus on a single link from the  $\mu$ th transmit antenna to the  $\nu$ th receive antenna.

Throughout this thesis we assume a linear modulation scheme, i.e., the transmitted signals (in complex baseband representation) can be written as

$$s_\mu(t) = \sum_{k=-\infty}^{+\infty} x_\mu[k] g_{\text{Tx}}(t-kT), \quad (2.10)$$

( $\mu=1, \dots, M$ ), where  $x_\mu[k] \in \mathbb{C}$  denotes the  $k$ th data symbol transmitted via the  $\mu$ th antenna,  $k$  denotes the discrete time index,  $g_{\text{Tx}}(t)$  a (fixed) analog pulse shaping filter, which is assumed to be identical for all transmit antennas, and  $T$  denotes the symbol duration. The data symbols  $x_\mu[k]$  are assumed to be drawn from a (complex-valued)  $Q$ -ary signal constellation  $\mathbb{A}$ , for example a  $Q$ -ary phase-shift-keying (PSK) constellation. Moreover, we assume that the pulse shaping filter  $g_{\text{Tx}}(t)$  is strictly bandlimited with a one-sided bandwidth  $B$  that is small compared to the carrier frequency. Throughout this thesis, we consider coherent demodulation at the receiver. Correspondingly, the continuous-time received signal at the  $\nu$ th receive antenna before receive filtering (including multipath signal propagation and additive noise) results as<sup>21</sup>

$$r_\nu(t) = \sum_{\mu=1}^M \sum_{n=0}^{N_\tau-1} f_{\nu,\mu}(\tau_n, t) s_\mu(\tau-\tau_n) \Big|_{\tau=t} + w_\nu(t) \quad (2.11a)$$

$$= \sum_{\mu=1}^M \sum_{k=-\infty}^{+\infty} x_\mu[k] \sum_{n=0}^{N_\tau-1} f_{\nu,\mu}(\tau_n, t) g_{\text{Tx}}(\tau-\tau_n-kT) \Big|_{\tau=t} + w_\nu(t) \quad (2.11b)$$

( $1 \leq \nu \leq N$ ). As discussed in Appendix F, the resolvable delays  $0 \leq \tau_0 < \dots < \tau_{N_\tau-1} = \tau_{\max}$  are assumed to be identical for all transmit-receive antenna pairs. Moreover, the means  $\bar{f}_{\nu,\mu,n}$  of the complex gain factors  $f_{\nu,\mu}(\tau_n, t)$  are assumed to be zero for all delays  $\tau_n > 0$  (cf. Remark F.2 in Appendix F). Finally, the noise term  $w_\nu(t)$  is assumed to be an additive (temporally and spatially) white Gaussian noise (AWGN) process with

$$\mathbf{E}\{w_\nu(t) w_{\nu'}(t')\} = N_0 \cdot \delta(t-t') \cdot \delta[n-n'], \quad (2.12)$$

where  $N_0$  denotes the two-sided noise power density in the equivalent complex baseband.

<sup>21</sup>In the case of non-coherent reception, the complex gain factors  $f_{\nu,\mu}(\tau_n, t)$  will be associated with additional phase terms.

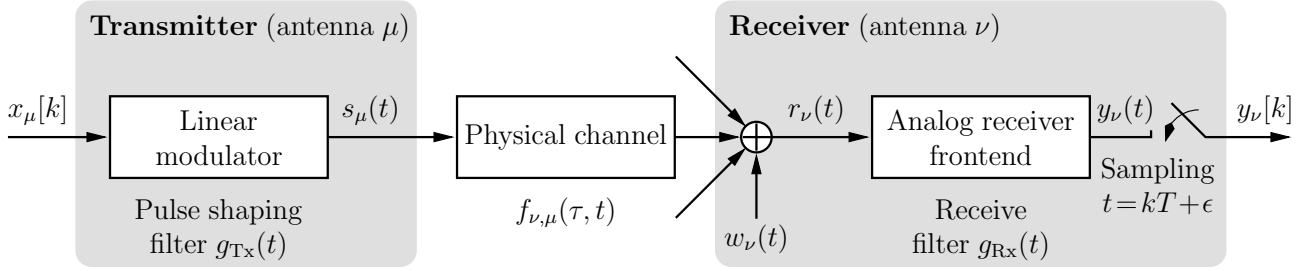


Figure 2.5: Transmission model under consideration.

At the receiver, the signals  $r_\nu(t)$  ( $\nu=1, \dots, N$ ) are filtered and sampled. In the case of a single transmit antenna ( $M=1$ ), the optimum linear receive filter (in the sense of maximizing the SNR at the filter output) is known to be a matched filter (MF) adapted to the time-varying impulse response composed by the pulse shaping filter  $g_{\text{Tx}}(t)$  and the physical channel<sup>22</sup> [For72]. However, in a practical system fixed receive filters are often more viable, due to a simpler implementation [Hoe92]. In the sequel, we therefore assume a fixed receive filter  $g_{\text{Rx}}(t)$  that is identical for all receive antennas. The (finite) one-sided bandwidth of the receive filter is denoted as  $B_{\text{Rx}} \geq B$ , and it is assumed that the filter  $g_{\text{Rx}}(t)$  does not exhibit any spectral zeros within the signal bandwidth  $B$ . This ensures that no spectral information is discarded through receive filtering. In the following, let

$$g(t) := \int_{-\infty}^{+\infty} g_{\text{Tx}}(t') g_{\text{Rx}}(t-t') dt' \quad (2.13)$$

denote the overall impulse response of transmit and receive filtering. Throughout this thesis, we assume that the physical channel is slowly time-varying, i.e., the complex gain factors  $f_{\nu,\mu}(\tau_n, t)$  can be regarded as constant during the time interval spanned by the impulse response  $g(t)$ . The filtered received signal of the  $\nu$ th receive antenna can then be written as

$$y_\nu(t) = \sum_{\mu=1}^M \sum_{k=-\infty}^{+\infty} x_\mu[k] \sum_{n=0}^{N_\tau-1} f_{\nu,\mu}(\tau_n, t) g(\tau - \tau_n - kT) \Big|_{\tau=t} + n_\nu(t), \quad (2.14)$$

where

$$n_\nu(t) := \int_{-\infty}^{+\infty} w_\nu(t') g_{\text{Rx}}(t-t') dt' \quad (2.15)$$

denotes the filtered noise process. The overall (time-varying) impulse response for the link from the  $\mu$ th transmit antenna to the  $\nu$ th receive antenna, containing the pulse shaping filter, the physical channel, and the receive filter, is in the following denoted as

$$h_{\nu,\mu}(\tau, t) := \sum_{n=0}^{N_\tau-1} f_{\nu,\mu}(\tau_n, t) g(\tau - \tau_n). \quad (2.16)$$

<sup>22</sup>Since the optimum receive filter colors the noise, it is often used in conjunction with a (discrete-time) whitening filter.

After receive filtering, the continuous-time signals  $y_\nu(t)$  are sampled. Within the scope of this thesis, we focus on symbol-rate sampling (sampling rate  $1/T$ ). Moreover, we assume that the same sampling phase  $\epsilon \in [0, T)$  is used for all receive antennas<sup>23</sup>. This yields the following discrete-time channel model for the  $\nu$ th receive antenna:

$$y_\nu[k] := y_\nu(t=kT+\epsilon) = \sum_{\mu=1}^M \sum_{l=0}^L h_{\nu,\mu,l}[k] x_\mu[k-l] + n_\nu[k], \quad (2.17)$$

where  $y_\nu[k]$  denotes the  $k$ th received sample of the  $\nu$ th receive antenna,  $L$  the effective memory length of the discrete-time channel model<sup>24</sup>, and  $n_\nu[k] := n_\nu(t=kT+\epsilon)$  the  $k$ th discrete-time noise sample at the  $\nu$ th receive antenna. The variance of the noise samples  $n_\nu[k]$  ( $\nu=1, \dots, N$ ) is in the sequel denoted as  $\sigma_n^2$ . The complex channel coefficients  $h_{\nu,\mu,l}[k]$  ( $l=0, \dots, L$ ) are defined as

$$h_{\nu,\mu,l}[k] := h_{\nu,\mu}(lT+\epsilon, kT+\epsilon) = \sum_{n=0}^{N_\tau-1} f_{\nu,\mu}(\tau_n, kT) g(lT+\epsilon-\tau_n), \quad (2.18)$$

where we have used that  $f_{\nu,\mu}(\tau_n, kT+\epsilon) = f_{\nu,\mu}(\tau_n, kT)$ , due to the assumption of a slowly time-varying physical channel. The channel coefficients  $h_{\nu,\mu,l}[k]$  ( $l=0, \dots, L$ ) can be interpreted as the coefficients of a time-varying discrete-time finite-impulse-response (FIR) filter. For convenience, they are collected in the vector

$$\mathbf{h}_{\nu,\mu}[k] := [h_{\nu,\mu,0}[k], \dots, h_{\nu,\mu,L}[k]]^T. \quad (2.19)$$

Since we have assumed identical transmit and receive filters for all antennas as well as identical discrete delays  $\tau_n$ , the effective memory length  $L$  is the same for all transmit-receive antenna pairs. The discrete-time channel model for the  $\nu$ th receive antenna is depicted in Fig. 2.6.

### Transmit and Receive Filter

Since the pulse shaping filter  $g_{\text{Tx}}(t)$  is required to be strictly bandlimited, the use of an ideal rectangular impulse response is not feasible, because the associated spectrum corresponds to a sinc function  $\sin(x)/x$ . Similarly, an ideal low-pass behavior of the (baseband) receive filter  $g_{\text{Rx}}(t)$  cannot be realized in practice, because this would require a  $\sin(x)/x$  pulse shaping filter in time domain. In this thesis, we assume that the pulse shaping filter  $g_{\text{Tx}}(t)$  is a square-root Nyquist filter, specifically, a root-raised cosine filter with roll-off factor  $r$  ( $0 \leq r \leq 1$ ) and one-sided bandwidth  $B$ . Note that root-raised cosine filters are widely used in practical systems [Pro01, Ch. 9.2]. Moreover, we assume that the receive filter  $g_{\text{Rx}}(t)$  is matched to  $g_{\text{Tx}}(t)$ , i.e.,  $g_{\text{Rx}}(t) := g_{\text{Tx}}^*(-t)$ .<sup>25</sup> This choice of  $g_{\text{Tx}}(t)$

<sup>23</sup>This assumption is not crucial, since different sampling phases may be represented by shifting the impulse responses of the physical channel accordingly.

<sup>24</sup>Strictly speaking, the memory length of the discrete-time channel model is, in general, infinite, because theoretically the overall impulse response  $g(t)$  is of infinite length (due to the limited bandwidth). However, practical impulse responses typically decay significantly for large absolute values of  $t$ . Correspondingly, one can find a certain window  $l \in [-L_1, +L_2]$  such that channel coefficients  $h_{\nu,\mu,l}[k]$  with  $l < -L_1$  or  $l > +L_2$  have a very small average power and can therefore be neglected [Hoe92]. For simplicity, we define the index  $l$  such that the window of interest is  $l \in [0, L]$ .

<sup>25</sup>Since  $g_{\text{Tx}}(t)$  is real-valued and symmetrical with respect to  $t=0$ , we actually have  $g_{\text{Rx}}(t) = g_{\text{Tx}}(t)$ .

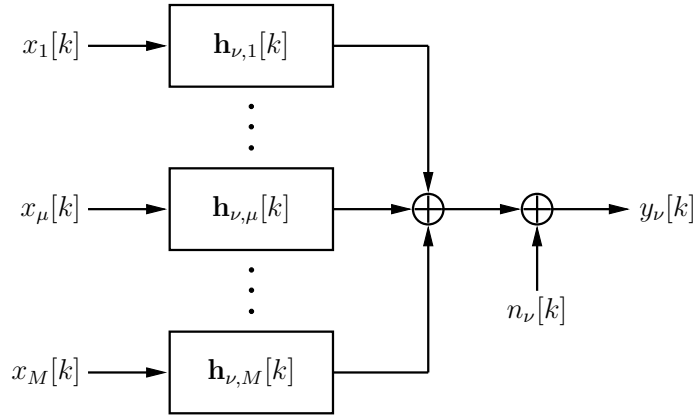


Figure 2.6: Discrete-time channel model for the  $\nu$ th receive antenna.

and  $g_{\text{Rx}}(t)$  has several important consequences:

- Due to the square-root Nyquist property of  $g_{\text{Rx}}(t)$ , the receive filter in conjunction with symbol-rate sampling does not color the sampled noise process, i.e., the sampled noise process at the receive filter output is still white.
- The overall impulse response of transmit and receive filtering,  $g(t)$ , is a cosine roll-off impulse with roll-off factor  $r$  and one-sided bandwidth  $B$  (cf. Definition C.1, Appendix C). Correspondingly, it fulfills the first Nyquist criterion [Pro01, Ch. 9.2], while the sampling rate has to be chosen as

$$\frac{1}{T} := \frac{2B}{1+r} \quad (2.20)$$

(symbol-rate sampling). We assume that the sampling is always performed with respect to the delay  $\tau_0$ , i.e., the sampling phase  $\epsilon$  is chosen such that

$$g(lT + \epsilon - \tau_0) = \delta[l - l_0], \quad (2.21)$$

where  $l_0$  is an appropriate integer number not necessarily equal to zero.

- Due to the Nyquist property of  $g(t)$ , the following holds: If the maximum delay  $\tau_{\text{max}}$  of the physical channel is very small in comparison with the symbol duration  $T$  (i.e.,  $N_\tau = 1$ ) and if the sampling phase  $\epsilon$  is chosen in accordance with (2.21), intersymbol-interference (ISI)-free transmission is possible. In this case, the effective channel memory length  $L$  is equal to zero (frequency-flat fading). However, if  $\tau_{\text{max}}$  is not significantly smaller than  $T$ , ISI effects between subsequent (in time domain) data symbols  $x_\mu[k]$  will in general be inevitable (frequency-selective fading,  $L > 0$ ).
- In the case of a slowly time-varying flat fading channel, the choice of the receive filter  $g_{\text{Rx}}(t)$  is optimal in the sense of maximizing the SNR at the filter output [Hoe92]. However, in the case of fast fading or significant delays  $\tau_n$ , this is typically not the case anymore.

- Given a frequency-flat fading channel with an arbitrary fading rate, the choice of the receive filter  $g_{\text{Rx}}(t)$  is still optimal in the sense that the received samples  $y_\nu[k]$  provide a set of sufficient statistics for maximum-likelihood (ML) detection of the transmitted data symbols  $x_\mu[k]$ , since no spectral information is discarded by the receive filter [MOP94].

### Matrix-Vector Model

In the subsequent chapters, we will often use the following matrix-vector representation of the above discrete-time MIMO channel model. The transmitted data symbols  $x_\mu[k]$ ,  $\mu=1, \dots, M$ , are collected in an  $(M \times 1)$ -transmitted vector

$$\mathbf{x}[k] := [x_1[k], \dots, x_\mu[k], \dots, x_M[k]]^T, \quad (2.22)$$

the noise samples  $n_\nu[k]$ ,  $\nu=1, \dots, N$ , are collected in an  $(N \times 1)$ -noise vector

$$\mathbf{n}[k] := [n_1[k], \dots, n_\nu[k], \dots, n_N[k]]^T, \quad (2.23)$$

and the received samples  $y_\nu[k]$ ,  $\nu=1, \dots, N$ , are collected in an  $(N \times 1)$ -received vector

$$\mathbf{y}[k] := [y_1[k], \dots, y_\nu[k], \dots, y_N[k]]^T. \quad (2.24)$$

Moreover, the channel coefficients  $h_{\nu,\mu,l}[k]$  associated with the same index  $0 \leq l \leq L$ , are collected in an  $(N \times M)$ -channel matrix

$$\mathbf{H}_l[k] := \begin{bmatrix} h_{1,1,l}[k] & \dots & h_{1,\mu,l}[k] & \dots & h_{1,M,l}[k] \\ \vdots & \ddots & \vdots & \ddots & \vdots \\ h_{\nu,1,l}[k] & \dots & h_{\nu,\mu,l}[k] & \dots & h_{\nu,M,l}[k] \\ \vdots & \ddots & \vdots & \ddots & \vdots \\ h_{N,1,l}[k] & \dots & h_{N,\mu,l}[k] & \dots & h_{N,M,l}[k] \end{bmatrix}. \quad (2.25)$$

The discrete-time MIMO channel model is thus given by<sup>26</sup>

$$\mathbf{y}[k] = \sum_{l=0}^L \mathbf{H}_l[k] \mathbf{x}[k-l] + \mathbf{n}[k]. \quad (2.26)$$

In the sequel, we consider some important special cases of (2.26).

(a) *Quasi-static fading/block fading*

We will often assume that the channel coefficients  $h_{\nu,\mu,l}[k]$  are (quasi-) static over a certain time interval, e.g., over the duration of a complete block of  $N_b$  subsequently transmitted data vectors  $\mathbf{x}[k]$ , where  $N_b$  denotes the block length. This assumption is reasonable when transmitter and receiver either have fixed positions or move with a moderate speed (provided that the block length is sufficiently small). Within a single data block, the time index  $k$  of the channel matrices  $\mathbf{H}_l[k]$  ( $l=0, \dots, L$ ) can therefore be dropped.

---

<sup>26</sup>In a MIMO system where strict channel reciprocity holds, the discrete-time MIMO channel model (2.26) can be used both for the forward and the reverse link (see Remark F.9 in Appendix F).

**Remark 2.1 (Block-fading assumption)**

We will often consider the average or the outage performance of (distributed and co-located) MIMO systems in terms of system capacity or error performance. To this end, we will assume that the MIMO channel changes randomly from one transmitted data block to the next. In other words, for different data blocks the channel matrices  $\mathbf{H}_l$  are modeled as statistically independent realizations of a matrix random variable  $\underline{\mathbf{H}}_l$ .

(b) *Flat fading*

In the case of frequency-flat fading ( $L=0$ ), the discrete-time MIMO channel model (2.26) reduces to

$$\mathbf{y}[k] = \mathbf{H}[k] \mathbf{x}[k] + \mathbf{n}[k], \quad (2.27)$$

where the index  $l=0$  of the channel matrix has been dropped for convenience. As discussed above, the assumption of flat fading is reasonable, when the maximum delay  $\tau_{\max}$  of the physical channel is small compared to the symbol duration  $T$ , due to the Nyquist property of  $g(t)$ . In addition to this, the flat-fading channel model (2.27) is also relevant for MIMO systems employing a multicarrier technique, such as OFDM or multicarrier (MC)-CDMA [HP97, HMCK03], for modeling data transmission within the quasi-flat sub-bands. Specifically, if  $N_c$  denotes the number of carriers, the overall multicarrier MIMO system can again be described by a larger matrix-vector model similar to (2.27), using a channel matrix of size  $(NN_c \times MN_c)$  comprising the correlation properties of the channel coefficients in the spatial and in the frequency domain.<sup>27</sup>

Finally, in the case of quasi-static flat fading, we will sometimes use the following convenient channel model for a block-wise transmission:

$$\mathbf{Y} = \mathbf{H} \mathbf{X} + \mathbf{N}, \quad (2.28)$$

where

$$\mathbf{Y} := [\mathbf{y}[0], \dots, \mathbf{y}[k], \dots, \mathbf{y}[N_b-1]], \quad (2.29a)$$

$$\mathbf{X} := [\mathbf{x}[0], \dots, \mathbf{x}[k], \dots, \mathbf{x}[N_b-1]], \quad (2.29b)$$

$$\mathbf{N} := [\mathbf{n}[0], \dots, \mathbf{n}[k], \dots, \mathbf{n}[N_b-1]]. \quad (2.29c)$$

For convenience, we have dropped the time index  $k$  and the index  $l=0$  for the channel matrix  $\mathbf{H}$ , cf. (2.26) and (2.27).

(c) *SIMO and MISO systems*

Given a SIMO system, the discrete-time MIMO channel model (2.26) reduces to

$$\mathbf{y}[k] = \sum_{l=0}^L \mathbf{h}_{\text{SIMO},l}[k] x[k-l] + \mathbf{n}[k], \quad (2.30)$$

<sup>27</sup>In the case of MIMO-OFDM, the resulting channel model can be decoupled for different carriers. Similarly, in the case of MIMO-MC-CDMA with frequency-domain spreading, the resulting channel model can be decoupled for different frequency ‘clusters’.

where the  $(N \times 1)$ -channel vector  $\mathbf{h}_{\text{SIMO},l}[k]$  is given by

$$\mathbf{h}_{\text{SIMO},l}[k] := [h_{1,1,l}[k], \dots, h_{\nu,1,l}[k], \dots, h_{N,1,l}[k]]^T. \quad (2.31)$$

The index  $\mu=1$  of the transmitted data symbol has been dropped for convenience. Similarly, given a MISO system, (2.26) reduces to

$$y[k] = \sum_{l=0}^L \mathbf{h}_{\text{MISO},l}[k] \mathbf{x}[k-l] + \mathbf{n}[k], \quad (2.32)$$

where the  $(1 \times M)$ -channel vector  $\mathbf{h}_{\text{MISO},l}[k]$  is given by

$$\mathbf{h}_{\text{MISO},l}[k] := [h_{1,1,l}[k], \dots, h_{1,\mu,l}[k], \dots, h_{1,M,l}[k]]. \quad (2.33)$$

The index  $\nu=1$  of the received sample has been dropped for convenience.

In the following, a rigorous analysis of the statistical properties of the discrete-time channel model (2.26) is presented.

### 2.2.3 Analysis of the Statistical Properties

According to (2.18), the channel coefficients  $h_{\nu,\mu,l}[k]$  result from a weighted sum of statistically independent (complex) Gaussian random variables and are thus also Gaussian distributed [Pro01, Ch. 2.1.4], i.e.,

$$h_{\nu,\mu,l}[k] \sim \mathcal{CN}(\bar{h}_{\nu,\mu,l}, \sigma_{h_{\nu,\mu,l}}^2). \quad (2.34)$$

Correspondingly, the (joint) statistical properties of the channel coefficients are fully captured by the means  $\bar{h}_{\nu,\mu,l}$ , the variances  $\sigma_{h_{\nu,\mu,l}}^2$ , and the complete set of covariances/ correlations between any two channel coefficients  $h_{\nu,\mu,l}[k]$  and  $h_{\nu',\mu',l'}[k']$ . In the case of a non-zero mean channel coefficient  $h_{\nu,\mu,l}[k]$ , the associated average power is in the sequel denoted as  $\Omega_{h_{\nu,\mu,l}} := \mathbb{E}\{|h_{\nu,\mu,l}[k]|^2\} = |\bar{h}_{\nu,\mu,l}|^2 + \sigma_{h_{\nu,\mu,l}}^2$ .

Since  $g(t)$  is a Nyquist impulse and sampling is performed with respect to the delay  $\tau_0$ , the mean values  $\bar{h}_{\nu,\mu,l}$  are given by

$$\bar{h}_{\nu,\mu,l} = \sum_{n=0}^{N_\tau-1} \mathbb{E}\{f_{\nu,\mu}(\tau_n, kT) g(lT + \epsilon - \tau_n)\} = \bar{f}_{\nu,\mu,0} \cdot \delta[l - l_0] \quad (2.35)$$

(since only the first gain factor  $f_{\nu,\mu}(\tau_0, t)$  may contain a LoS component). Correspondingly, the channel coefficient  $h_{\nu,\mu,l_0}[k]$  can be written as

$$h_{\nu,\mu,l_0}[k] = \bar{f}_{\nu,\mu,0} + \check{h}_{\nu,\mu,l_0}[k], \quad (2.36)$$

where  $\check{h}_{\nu,\mu,l_0}[k] \sim \mathcal{CN}(0, \sigma_{\check{h}_{\nu,\mu,l_0}}^2)$  represents the Rayleigh-fading component of  $h_{\nu,\mu,l_0}[k]$ . All other channel coefficients  $h_{\nu,\mu,l}[k]$  ( $l \neq l_0$ ) have zero means. The variances  $\sigma_{\check{h}_{\nu,\mu,l}}^2$  ( $l=0, \dots, L$ ) result as

$$\sigma_{\check{h}_{\nu,\mu,l}}^2 = \sum_{n=0}^{N_\tau-1} \sigma_{f_{\nu,\mu,n}}^2 g^2(lT + \epsilon - \tau_n), \quad (2.37)$$



where we have used that  $g(t)$  is real-valued and that  $f_{\nu,\mu}(\tau_n, t)$  and  $f_{\nu,\mu}(\tau_{n'}, t)$  are uncorrelated for  $n' \neq n$  (WSSUS model). The variances  $\sigma_{f_{\nu,\mu,n}}^2$  ( $n=0, \dots, N_\tau-1$ ) are specified in the corresponding power delay profile  $\mathbf{p}_{f_{\nu,\mu}}$  (cf. Definition F.1 in Appendix F). In the case of flat fading ( $N_\tau=1$ ), one obtains a single channel coefficient  $h_{\nu,\mu,l_0}[k] \sim \mathcal{CN}(\bar{f}_{\nu,\mu,0}, \sigma_{f_{\nu,\mu,0}}^2)$ . In this case, we will often set the index  $l_0$  to zero, in order to be in accordance with (2.26).

### Definition 2.1 (Channel power profile)

Similar to the power delay profile (cf. Definition F.1 in Appendix F), we define the *channel power profile* of the link between transmit antenna  $\mu$  ( $1 \leq \mu \leq M$ ) and receive antenna  $\nu$  ( $1 \leq \nu \leq N$ ) as

$$\mathbf{p}_{h_{\nu,\mu}} := [\sigma_{h_{\nu,\mu,0}}^2, \dots, |\bar{f}_{\nu,\mu,0}|^2 + \sigma_{h_{\nu,\mu,l_0}}^2, \dots, \sigma_{h_{\nu,\mu,L}}^2]^T. \quad (2.38)$$

In the case of pure Rayleigh fading, we have  $\bar{f}_{\nu,\mu,0} = 0$ . A numerical example concerning the channel power profile  $\mathbf{p}_{h_{\nu,\mu}}$  is provided in Example F.3 in Appendix F. •

### Triply-Selective MIMO System

In the sequel, we consider the case of pure Rayleigh fading for simplicity. Given Rician fading ( $\bar{f}_{\nu,\mu,0} \neq 0$ ), the following considerations apply only for the channel coefficients  $h_{\nu,\mu,l}[k]$ ,  $l \neq l_0$ , as well as for the Rayleigh component of  $h_{\nu,\mu,l_0}[k]$ . The LoS component of  $h_{\nu,\mu,l_0}[k]$  must be considered separately.

Based on Section 2.2.1, one obtains the following expression for the correlation between two channel coefficients  $h_{\nu,\mu,l}[k]$  and  $h_{\nu',\mu',l'}[k']$ :

$$\begin{aligned} \rho_{h_{\nu,\mu,\nu',\mu',l,l',k,k'}} &:= \frac{1}{\sqrt{\sigma_{h_{\nu,\mu,l}}^2 \sigma_{h_{\nu',\mu',l'}}^2}} \sum_{n=0}^{N_\tau-1} \sqrt{\sigma_{f_{\nu,\mu,n}}^2 \sigma_{f_{\nu',\mu',n}}^2} \cdot \rho_{f_{\nu,\mu,\nu',\mu',n}} \\ &\times R_{f_{\nu,\mu,n}}[k', k] \cdot g(lT + \epsilon - \tau_n) g(l'T + \epsilon - \tau_n), \end{aligned} \quad (2.39)$$

where

$$R_{f_{\nu,\mu,n}}[k', k] := R_{f_{\nu,\mu,n}}(t' = k'T + \epsilon, t = kT + \epsilon) = R_{f_{\nu,\mu,n}}(t' = k'T, t = kT). \quad (2.40)$$

In order to arrive at the expression (2.39), we have employed the WSSUS model and the assumption of independent spatial and temporal correlations. Due to the WSSUS assumption, the correlations  $\rho_{h_{\nu,\mu,\nu',\mu',l,l',k,k'}}$  depend only on the difference  $(k-k')$ , but not on the absolute time index  $k$ . For example, when using Clarke's model for the temporal correlations (cf. Remark F.7 in Appendix F), we obtain  $R_{f_{\nu,\mu,n}}[k', k] = J_0(2\pi f_{D,\max}(k-k')T)$ , where  $J_0(\cdot)$  denotes the Bessel function of the first kind and order zero (cf. Definition C.4 in Appendix C) and  $f_{D,\max}$  the maximum Doppler frequency.

In the most general case, the MIMO system exhibits selectivity in time (due to motion of transmitter or receiver), frequency (due to frequency-selective fading), and space (due to spatial diversity). In this case, the complete set of correlations  $\rho_{h_{\nu,\mu,\nu',\mu',l,l',k,k'}}$  must be taken into account, so as to obtain an accurate channel model. In this thesis, we will



mostly consider quasi-static or block-fading scenarios with  $f_{D,\max} = 0$ . Correspondingly, when considering a single data block, the expression (2.39) reduces to

$$\begin{aligned} \rho_{h_{\nu,\mu,\nu',\mu',l,l'}} &:= \frac{1}{\sqrt{\sigma_{h_{\nu,\mu,l}}^2 \sigma_{h_{\nu',\mu',l'}}^2}} \sum_{n=0}^{N_\tau-1} \sqrt{\sigma_{f_{\nu,\mu,n}}^2 \sigma_{f_{\nu',\mu',n}}^2} \cdot \rho_{f_{\nu,\mu,\nu',\mu',n}} \\ &\times g(lT + \epsilon - \tau_n) g(l'T + \epsilon - \tau_n). \end{aligned} \quad (2.41)$$

Setting  $l' := l$ , we obtain the spatial correlations between the channel coefficients  $h_{\nu,\mu,l}[k]$  and  $h_{\nu',\mu',l}[k]$  ( $\mu, \mu' = 1, \dots, M$ ,  $\nu, \nu' = 1, \dots, N$ ):

$$\rho_{h_{\nu,\mu,\nu',\mu',l}} := \frac{1}{\sqrt{\sigma_{h_{\nu,\mu,l}}^2 \sigma_{h_{\nu',\mu',l}}^2}} \sum_{n=0}^{N_\tau-1} \sqrt{\sigma_{f_{\nu,\mu,n}}^2 \sigma_{f_{\nu',\mu',n}}^2} \cdot \rho_{f_{\nu,\mu,\nu',\mu',n}} \cdot g^2(lT + \epsilon - \tau_n). \quad (2.42)$$

Furthermore, employing the Kronecker correlation model and considering the special cases  $\nu' = \nu$  and  $\mu' = \mu$ , we obtain

$$\rho_{h_{\mu,\mu',l}} := \frac{1}{\sqrt{\sigma_{h_{\nu,\mu,l}}^2 \sigma_{h_{\nu,\mu',l}}^2}} \sum_{n=0}^{N_\tau-1} \sqrt{\sigma_{f_{\nu,\mu,n}}^2 \sigma_{f_{\nu,\mu',n}}^2} \cdot \rho_{f_{\mu,\mu',n}} \cdot g^2(lT + \epsilon - \tau_n), \quad (2.43a)$$

$$\rho_{h_{\nu,\nu',l}} := \frac{1}{\sqrt{\sigma_{h_{\nu,\mu,l}}^2 \sigma_{h_{\nu,\mu',l}}^2}} \sum_{n=0}^{N_\tau-1} \sqrt{\sigma_{f_{\nu,\mu,n}}^2 \sigma_{f_{\nu,\mu',n}}^2} \cdot \rho_{f_{\nu,\nu',n}} \cdot g^2(lT + \epsilon - \tau_n), \quad (2.43b)$$

respectively. In particular, in the special case of flat fading ( $N_\tau = 1$ ), we obtain  $\rho_{h_{\mu,\mu',l}} = \rho_{f_{\mu,\mu',0}} \delta[l - l_0]$  and  $\rho_{h_{\nu,\nu',l}} = \rho_{f_{\nu,\nu',0}} \delta[l - l_0]$ . Finally, the intertap correlations between the channel coefficients  $h_{\nu,\mu,l}[k]$  and  $h_{\nu,\mu,l'}[k]$  ( $l, l' = 0, \dots, L$ ) are obtained from (2.41) by setting  $\mu' := \mu$  and  $\nu' := \nu$ :

$$\rho_{h_{\nu,\mu,l,l'}} := \frac{1}{\sqrt{\sigma_{h_{\nu,\mu,l}}^2 \sigma_{h_{\nu,\mu,l'}}^2}} \sum_{n=0}^{N_\tau-1} \sigma_{f_{\nu,\mu,n}}^2 \cdot g(lT + \epsilon - \tau_n) g(l'T + \epsilon - \tau_n). \quad (2.44)$$

A numerical example concerning the spatial correlations (2.43) is provided in Example F.3 in Appendix F.

### Correlation Structure

In [XWL+04] it is claimed that the correlations  $\rho_{h_{\nu,\mu,\nu',\mu',l,l',k,k'}}$  according to (2.39) can always be written as products of spatial correlations  $\rho_{h_{\nu,\mu,\nu',\mu',l}}$ , intertap correlations  $\rho_{h_{\nu,\mu,l,l'}}$  and temporal correlations

$$\rho_{h_{\nu,\mu,l,l',k,k'}} := \frac{1}{\sigma_{h_{\nu,\mu,l}}^2} \sum_{n=0}^{N_\tau-1} \sigma_{f_{\nu,\mu,n}}^2 \cdot R_{f_{\nu,\mu,n}}[k', k] \cdot g^2(lT + \epsilon - \tau_n). \quad (2.45)$$

However, it can easily be seen from (2.42), (2.44) and (2.45) that in general

$$\rho_{h_{\nu,\mu,\nu',\mu',l,l',k,k'}} \neq \rho_{h_{\nu,\mu,\nu',\mu',l}} \cdot \rho_{h_{\nu,\mu,l,l'}} \cdot \rho_{h_{\nu,\mu,l,k,k'}}. \quad (2.46)$$

Similarly, in the quasi-static scenario we find that in general

$$\rho_{h_{\nu,\mu,\nu',\mu',l,l'}} \neq \rho_{h_{\nu,\mu,\nu',\mu',l}} \cdot \rho_{h_{\nu,\mu,l,l'}}, \quad (2.47)$$

cf. (2.41), (2.42) and (2.44). Furthermore, it is claimed in [XWL+04] that the Kronecker correlation model (2.7) applies also for the channel coefficients  $h_{\nu,\mu,l}[k]$ . However, this is also not correct in general. Considering (2.42) and (2.43), it can be seen that in general

$$\rho_{h_{\nu,\mu,\nu',\mu',l}} \neq \rho_{h_{\mu,\mu',l}} \cdot \rho_{h_{\nu,\nu',l}}. \quad (2.48)$$

An exception is the case of frequency-flat fading ( $L=0$ ), where we can write

$$\rho_{h_{\nu,\mu,\nu',\mu',l}} = \rho_{h_{\mu,\mu',l}} \cdot \rho_{h_{\nu,\nu',l}} \cdot \delta[l-l_0] = \rho_{f_{\mu,\mu',0}} \cdot \rho_{f_{\nu,\nu',0}} \cdot \delta[l-l_0]. \quad (2.49)$$

Another exception is stated in the following Example 2.1.

**Example 2.1 (ISI channel with special spatial correlation property)**

Consider a MIMO channel model where the variances  $\sigma_{f_{\nu,\mu,n}}^2$  ( $n=0, \dots, N_\tau-1$ ) do not depend on the antenna indices  $\mu$  and  $\nu$ . Moreover, assume that the spatial correlations  $\rho_{f_{\mu,\mu',n}}$  and  $\rho_{f_{\nu,\nu',n}}$  are identical for all indices  $n=0, \dots, N_\tau-1$  ( $\rho_{f_{\mu,\mu',n}} =: \rho_{f_{\mu,\mu'}}$  and  $\rho_{f_{\nu,\nu',n}} =: \rho_{f_{\nu,\nu'}}$ ). In this case, (2.42) simplifies to

$$\rho_{h_{\nu,\mu,\nu',\mu',l}} := \frac{\sum_{n=0}^{N_\tau-1} \sigma_{f_{\nu,\mu,n}}^2 \cdot \rho_{f_{\mu,\mu'}} \rho_{f_{\nu,\nu'}} \cdot g^2(lT+\epsilon-\tau_n)}{\sum_{n=0}^{N_\tau-1} \sigma_{f_{\nu,\mu,n}}^2 \cdot g^2(lT+\epsilon-\tau_n)} = \rho_{f_{\mu,\mu'}} \rho_{f_{\nu,\nu'}} \quad (2.50)$$

for all  $\mu, \mu', \nu, \nu'$  and  $l=0, \dots, L$ . ◇

## Correlation and Covariance Matrices for Quasi-Static Scenarios

In the following, we define a covariance matrix  $\mathbf{Q}_{\mathbf{h}}$  for quasi-static scenarios, so as to represent the correlation properties of the channel coefficients  $h_{\nu,\mu,l}$  in a compact form. To this end, consider the overall channel coefficient vector

$$\mathbf{h}_{\text{ov}} := [\text{vec}(\mathbf{H}_0)^T, \dots, \text{vec}(\mathbf{H}_l)^T, \dots, \text{vec}(\mathbf{H}_L)^T]^T, \quad (2.51)$$

where

$$\text{vec}(\mathbf{H}_l) := [h_{1,1,l}, \dots, h_{N,1,l}, h_{1,2,l}, \dots, h_{N,2,l}, \dots, h_{1,M,l}, \dots, h_{N,M,l}]^T$$

denotes vectorization of the matrix  $\mathbf{H}_l$ , i.e., the column vectors of  $\mathbf{H}_l$  are stacked in a single column vector.

**Definition 2.2 (Overall correlation/covariance matrix)**

The overall covariance matrix,  $\mathbf{Q}_{\mathbf{h}}$ , of size  $MN(L+1) \times MN(L+1)$  is defined as

$$\mathbf{Q}_{\mathbf{h}} := \mathbf{E}\{\mathbf{h}_{\text{ov}} \mathbf{h}_{\text{ov}}^H\} = \begin{bmatrix} \mathbf{Q}_{\mathbf{h},0,0} & \cdots & \mathbf{Q}_{\mathbf{h},0,L} \\ \vdots & \ddots & \vdots \\ \mathbf{Q}_{\mathbf{h},L,0} & \cdots & \mathbf{Q}_{\mathbf{h},L,L} \end{bmatrix}, \quad (2.52)$$

where

$$\mathbf{Q}_{\mathbf{h},l,l'} := \begin{bmatrix} \sqrt{\sigma_{h_{1,1,l}}^2 \sigma_{h_{1,1,l'}}^2} \cdot \rho_{h_{1,1,1,1,l,l'}} & \cdots & \sqrt{\sigma_{h_{1,1,l}}^2 \sigma_{h_{N,M,l'}}^2} \cdot \rho_{h_{1,1,N,M,l,l'}} \\ \vdots & \ddots & \vdots \\ \sqrt{\sigma_{h_{N,M,l}}^2 \sigma_{h_{1,1,l'}}^2} \cdot \rho_{h_{N,M,1,1,l,l'}} & \cdots & \sqrt{\sigma_{h_{N,M,l}}^2 \sigma_{h_{N,M,l'}}^2} \cdot \rho_{h_{N,M,N,M,l,l'}} \end{bmatrix}. \quad (2.53)$$

Note that  $\mathbf{Q}_{\mathbf{h},l,l'}$  is in general not Hermitian for  $l' \neq l$ , whereas  $\mathbf{Q}_{\mathbf{h}}$  is always Hermitian ( $\mathbf{Q}_{\mathbf{h}} = \mathbf{Q}_{\mathbf{h}}^H$ ). Obviously,  $\mathbf{Q}_{\mathbf{h}}$  can be written as

$$\mathbf{Q}_{\mathbf{h}} := \mathbf{\Sigma}_{\mathbf{h}} \odot \mathbf{R}_{\mathbf{h}}, \quad (2.54)$$

where  $\odot$  denotes element-wise multiplication (Hadamard product, cf. Definition D.3 in Appendix D). Here

$$\mathbf{\Sigma}_{\mathbf{h}} = \begin{bmatrix} \mathbf{\Sigma}_{\mathbf{h},0,0} & \cdots & \mathbf{\Sigma}_{\mathbf{h},0,L} \\ \vdots & \ddots & \vdots \\ \mathbf{\Sigma}_{\mathbf{h},0,L}^T & \cdots & \mathbf{\Sigma}_{\mathbf{h},L,L} \end{bmatrix}, \quad \mathbf{\Sigma}_{\mathbf{h},l,l'} = \begin{bmatrix} \sqrt{\sigma_{h_{1,1,l}}^2 \sigma_{h_{1,1,l'}}^2} & \cdots & \sqrt{\sigma_{h_{1,1,l}}^2 \sigma_{h_{N,M,l'}}^2} \\ \vdots & \ddots & \vdots \\ \sqrt{\sigma_{h_{N,M,l}}^2 \sigma_{h_{1,1,l'}}^2} & \cdots & \sqrt{\sigma_{h_{N,M,l}}^2 \sigma_{h_{N,M,l'}}^2} \end{bmatrix} \quad (2.55)$$

denotes a weight matrix containing the variances of the channel coefficients  $h_{\nu,\mu,l}$ , and

$$\mathbf{R}_{\mathbf{h}} = \begin{bmatrix} \mathbf{R}_{\mathbf{h},0,0} & \cdots & \mathbf{R}_{\mathbf{h},0,L} \\ \vdots & \ddots & \vdots \\ \mathbf{R}_{\mathbf{h},0,L}^H & \cdots & \mathbf{R}_{\mathbf{h},L,L} \end{bmatrix}, \quad \mathbf{R}_{\mathbf{h},l,l'} = \begin{bmatrix} \rho_{h_{1,1,1,1,l,l'}} & \cdots & \rho_{h_{1,1,N,M,l,l'}} \\ \vdots & \ddots & \vdots \\ \rho_{h_{N,M,1,1,l,l'}} & \cdots & \rho_{h_{N,M,N,M,l,l'}} \end{bmatrix} \quad (2.56)$$

denotes the *overall correlation matrix*. Some important properties of covariance and correlation matrices are summarized in Appendix D, see Definition D.13. •

### Definition 2.3 (Antenna correlation matrices)

In the flat-fading case ( $L=0$ ), using the Kronecker correlation model we can write  $\rho_{h_{\nu,\mu,\nu'},\mu',l} = \rho_{h_{\mu,\mu',l}} \cdot \rho_{h_{\nu,\nu',l}} \cdot \delta[l-l_0]$ , cf. (2.49). For convenience, we set  $\rho_{h_{\mu,\mu',l_0}} =: \rho_{\text{Tx},\mu,\mu'}$  and  $\rho_{h_{\nu,\nu',l_0}} =: \rho_{\text{Rx},\nu,\nu'}$  in the sequel. The overall correlation matrix  $\mathbf{R}_{\mathbf{h}}$  can then be expressed as the Kronecker product

$$\mathbf{R}_{\mathbf{h}} = \mathbf{R}_{\mathbf{h},\text{Tx}} \otimes \mathbf{R}_{\mathbf{h},\text{Rx}} \quad (2.57)$$

(cf. Definition D.4 in Appendix D) of the *transmit* and *receive antenna correlation matrix*

$$\mathbf{R}_{\mathbf{h},\text{Tx}} := \begin{bmatrix} 1 & \cdots & \rho_{\text{Tx},1,M} \\ \vdots & \ddots & \vdots \\ \rho_{\text{Tx},1,M}^* & \cdots & 1 \end{bmatrix} \quad \text{and} \quad \mathbf{R}_{\mathbf{h},\text{Rx}} := \begin{bmatrix} 1 & \cdots & \rho_{\text{Rx},1,N} \\ \vdots & \ddots & \vdots \\ \rho_{\text{Rx},1,N}^* & \cdots & 1 \end{bmatrix}. \quad (2.58)$$

The corresponding overall covariance matrix  $\mathbf{Q}_{\mathbf{h}}$  thus results as

$$\mathbf{Q}_{\mathbf{h}} = \mathbf{\Sigma}_{\mathbf{h}} \odot (\mathbf{R}_{\mathbf{h},\text{Tx}} \otimes \mathbf{R}_{\mathbf{h},\text{Rx}}), \quad (2.59)$$

where

$$\Sigma_{\mathbf{h}} = \begin{bmatrix} \sigma_{h_{1,1,l_0}}^2 & \cdots & \sqrt{\sigma_{h_{1,1,l_0}}^2 \sigma_{h_{N,M,l_0}}^2} \\ \vdots & \ddots & \vdots \\ \sqrt{\sigma_{h_{1,1,l_0}}^2 \sigma_{h_{N,M,l_0}}^2} & \cdots & \sigma_{h_{N,M,l_0}}^2 \end{bmatrix}. \quad (2.60)$$

•

### Simple Method for Simulating Block-Fading Channels

To conclude this section, a simple and statistically accurate method is presented for simulating block-fading channels with selectivity in frequency and space. As earlier, we focus on the case of Rayleigh fading, i.e.,  $h_{\nu,\mu,l} \sim \mathcal{CN}(0, \sigma_{h_{\nu,\mu,l}}^2)$  for all indices  $\nu, \mu, l$ . Moreover, we employ the Kronecker correlation model (2.7). Finally, we assume that the power delay profiles  $\mathbf{p}_{f_{\nu,\mu}}$  ( $\mu=1, \dots, M$ ,  $\nu=1, \dots, N$ ) and the correlation values  $\rho_{f_{\mu,\mu'},n}$ ,  $\rho_{f_{\nu,\nu'},n}$  ( $n=0, \dots, N_{\tau}-1$ ) of the physical MIMO channel are given, as well as the overall impulse response  $g(t)$  of transmit and receive filtering. The proposed simulation method contains the following three steps:

- (i) Compute all entries of the overall covariance matrix  $\mathbf{Q}_{\mathbf{h}}$  according to (2.52)/(2.53), using (2.37) and (2.41). The calculation of  $\mathbf{Q}_{\mathbf{h}}$  has to be performed only once at the beginning of the simulation.
- (ii) For each new block of transmitted data symbols, generate an uncorrelated channel vector  $\mathbf{h}'_{\text{ov}}$  of size  $MN(L+1) \times 1$  with independent and identically distributed (i.i.d.) entries  $\sim \mathcal{CN}(0, 1)$ , i.e.,

$$\mathbf{Q}_{\mathbf{h}'} := \mathbb{E}\{\mathbf{h}'_{\text{ov}} \mathbf{h}'_{\text{ov}}{}^H\} = \mathbf{I}_{MN(L+1)}. \quad (2.61)$$

Note that the generated channel vectors  $\mathbf{h}'_{\text{ov}}$  must be statistically independent from one data block to the next.

- (iii) Compute the corresponding realization of the correlated channel vector according to

$$\mathbf{h}_{\text{ov}} := \mathbf{Q}_{\mathbf{h}}^{1/2} \mathbf{h}'_{\text{ov}} \quad (2.62)$$

(also for each block), where  $\mathbf{Q}_{\mathbf{h}}^{1/2} \mathbf{Q}_{\mathbf{h}}^{1/2H} = \mathbf{Q}_{\mathbf{h}}$ . By this means, the resulting channel vector  $\mathbf{h}_{\text{ov}}$  is characterized by the desired covariance matrix:

$$\mathbb{E}\{\mathbf{h}_{\text{ov}} \mathbf{h}_{\text{ov}}{}^H\} = \mathbf{Q}_{\mathbf{h}}^{1/2} \mathbb{E}\{\mathbf{h}'_{\text{ov}} \mathbf{h}'_{\text{ov}}{}^H\} \mathbf{Q}_{\mathbf{h}}^{1/2H} = \mathbf{Q}_{\mathbf{h}}. \quad (2.63)$$

The matrix  $\mathbf{Q}_{\mathbf{h}}^{1/2}$  has to be computed only once at the beginning of the simulation, e.g., based on the eigenvalue decomposition (EVD)  $\mathbf{Q}_{\mathbf{h}} = \mathbf{U} \mathbf{\Lambda} \mathbf{U}^H$  of  $\mathbf{Q}_{\mathbf{h}}$  (cf. Definition D.11 in Appendix D):

$$\mathbf{Q}_{\mathbf{h}}^{1/2} = \mathbf{U} \mathbf{\Lambda}^{1/2} \mathbf{U}^H. \quad (2.64)$$

Here  $\mathbf{U}$  is a unitary matrix (cf. Definition D.7) containing the eigenvectors of  $\mathbf{Q}_{\mathbf{h}}$ , and  $\mathbf{\Lambda}^{1/2}$  is a diagonal matrix containing the non-negative square-roots of the corresponding eigenvalues.<sup>28</sup> The EVD of  $\mathbf{Q}_{\mathbf{h}}$  can, for example, be obtained by means

<sup>28</sup>Since  $\mathbf{Q}_{\mathbf{h}}$  is a Hermitian matrix, all eigenvalues are real-valued and greater than or equal to zero.

of the Jacobian algorithm [Gv96, Ch. 8.4].

**Remark 2.2 (Special case of frequency-flat fading)**

In the special case of flat fading ( $L=0$ ), we can directly write the spatially correlated channel matrix  $\mathbf{H}$  according to

$$\mathbf{H} := \underline{\Xi}_{\mathbf{h}} \odot \left( \mathbf{R}_{\mathbf{h},\text{Rx}}^{1/2} \mathbf{H}' \mathbf{R}_{\mathbf{h},\text{Tx}}^{1/2} \right), \quad (2.65)$$

by using the Kronecker correlation model (2.49). Here,  $\mathbf{H}'$  denotes an uncorrelated  $(N \times M)$ -channel matrix with i.i.d. entries  $\sim \mathcal{CN}(0, 1)$  and the matrix  $\underline{\Xi}_{\mathbf{h}}$  is given by

$$\underline{\Xi}_{\mathbf{h}} := \begin{bmatrix} \sqrt{\sigma_{h_{1,1,l_0}}^2} & \cdots & \sqrt{\sigma_{h_{1,M,l_0}}^2} \\ \vdots & \ddots & \vdots \\ \sqrt{\sigma_{h_{N,1,l_0}}^2} & \cdots & \sqrt{\sigma_{h_{N,M,l_0}}^2} \end{bmatrix}. \quad (2.66)$$

In MIMO systems with co-located transmit and receive antennas, it is reasonable to assume that  $\sigma_{h_{\nu,\mu,l_0}}^2$  is the same for all indices  $\nu, \mu$  (cf. Remark F.3 in Appendix F). In this case, we set  $\sigma_{h_{\nu,\mu,l_0}}^2 := \sigma_h^2$  for all  $\nu, \mu$ , and (2.65) simplifies to

$$\mathbf{H} := \mathbf{R}_{\mathbf{h},\text{Rx}}^{1/2} \mathbf{H}' \mathbf{R}_{\mathbf{h},\text{Tx}}^{1/2}, \quad (2.67)$$

where  $\mathbf{H}'$  now has i.i.d. entries  $\sim \mathcal{CN}(0, \sigma_h^2)$ .

## 2.2.4 Other Types of Fading

So far, we have only considered Rayleigh- and Rice-fading channel models, which are widely used in the literature to model wireless communication systems in rich-scattering environments (with or without LoS components).

Another common fading model also considered within the scope of this thesis is the Nakagami- $m$  fading model [Nak60] (cf. Definition C.13), where  $m$  denotes the Nakagami-fading parameter. The Nakagami- $m$  model is useful to analyze non-LoS scenarios, where fading is either more severe or less severe than in the Rayleigh fading case. Possible values for  $m$  are  $0.5 \leq m < \infty$ , where  $m=1$  corresponds to Rayleigh fading,  $m < 1$  to more severe fading, and  $m > 1$  to milder fading conditions. Further details of the Nakagami- $m$  fading model will be discussed in Section 3.3.

All of the above fading models (Rayleigh-, Rice-, and Nakagami- $m$  fading) concern the modeling of microscopic fading effects due to a constructive and non-constructive superposition of scattered signal components. These fading models do not include shadowing effects caused by major obstacles between transmitter and receiver (macroscopic fading). For example, when a mobile user moves within an urban area, it can be expected that not only the instantaneous SNR is subject to fluctuations (due to microscopic fading), but also the average SNR (averaged over a medium time scale). A common model for capturing the impact of macroscopic fading, which is also adopted in this thesis, is the log-normal shadowing model [Suz77]. In this model, it is assumed that the average SNR itself is a random variable characterized by a log-normal PDF (cf. Definition C.14), i.e.,

the average SNR in dB is assumed to be Gaussian distributed. Within the scope of this thesis, macroscopic fading effects are of particular interest in the context of distributed MIMO systems (cf. Section 1.2). Further details of the log-normal shadowing model will be discussed in Section 3.4.

## 2.3 Details of Some Space-Time Coding Schemes

The primary goal of transmit diversity and space-time coding schemes is to mitigate the detrimental effects of fading on the error performance of wireless systems. This is accomplished on the basis of a diversity gain and a coding gain, by sending redundant signals over multiple transmit antennas. Indirectly, space-time codes can also be used to enhance bit rates, when employed in conjunction with an adaptive modulation/channel coding scheme [PSY+04].

The basic principle of space-time coding was already discussed in Section 2.1.2, along with a detailed overview concerning the literature on space-time trellis codes (STTCs) and space-time block codes (STBCs). In this chapter, some space-time coding schemes that are of particular interest in this thesis are highlighted and discussed in more detail. Alamouti's transmit diversity scheme [Ala98] and orthogonal STBCs (OSTBCs) [TJC99a, TJC99b] are considered in Section 2.3.1. As a new contribution, the orthogonality loss of OSTBCs due to a time-varying channel, intersymbol interference (ISI), and non-perfect channel knowledge at the receiver is discussed (see also [MHS03a]). Moreover, alternative receiver structures for Alamouti's transmit diversity scheme are considered (see also [MEH04b]).<sup>29</sup> For the case of frequency-selective fading, a maximum-likelihood sequence estimation (MLSE) algorithm for (O)STBCs is presented in Appendix J. In Section 2.3.2, quasi-orthogonal STBCs [Jaf01] are considered, and in Section 2.3.3 a simple space-time block coding technique suitable for MIMO channels with ISI is discussed [LP00]. Finally, delay diversity [Wit93, SW93] and STTCs [TSC98, TNSC99b] are addressed in Section 2.3.4.

### 2.3.1 Orthogonal Space-Time Block Codes

In 1998, Alamouti proposed a simple transmit diversity scheme for MIMO systems with two transmit antennas and an arbitrary number of receive antennas [Ala98]. The scheme was designed to achieve full spatial diversity in terms of the number of transmit and receive antennas. In particular, Alamouti's transmit diversity scheme performs an orthogonal transmission in space (i.e., across the transmit antennas) and time, which allows for maximum-likelihood (ML) symbol detection at the receiver by means of simple widely linear<sup>30</sup> linear processing. Motivated by the simple structure of Alamouti's transmit diversity scheme, orthogonal space-time block codes (OSTBCs) were introduced in [TJC99a, TJC99b]. OSTBCs constitute a generalization of Alamouti's scheme to more than two transmit antennas and are based on the mathematical theory of (generalized) orthogonal designs [Hur98, Rad22].

<sup>29</sup>Similar work was presented independently in [VLB04].

<sup>30</sup>The detection steps are not strictly linear, because in general they also include complex conjugation.

### System Model and Basic Principle of OSTBCs

Consider again the discrete-time MIMO channel model for frequency-flat fading introduced in Section 2.2.2:

$$\mathbf{y}[k] = \mathbf{H}[k] \mathbf{x}[k] + \mathbf{n}[k]. \quad (2.68)$$

Let  $M$  again denote the number of transmit antennas and  $N$  the number of receive antennas. The entries of the channel matrix  $\mathbf{H}[k]$  are assumed to be random variables, which may have arbitrary fading statistics and spatial correlation properties. As earlier, the means and the variances of the channel coefficients  $h_{\nu,\mu}$  ( $\mu=1, \dots, M$ ,  $\nu=1, \dots, N$ ) are denoted as  $\bar{h}_{\nu,\mu}$  and  $\sigma_{h_{\nu,\mu}}^2$ , respectively. Moreover, the average power of  $h_{\nu,\mu}$  is denoted as

$$\Omega_{h_{\nu,\mu}} := \mathbb{E}\{|h_{\nu,\mu}|^2\} = |\bar{h}_{\nu,\mu}|^2 + \sigma_{h_{\nu,\mu}}^2. \quad (2.69)$$

The entries  $x_\mu[k]$  ( $\mu=1, \dots, M$ ) of the transmitted vector  $\mathbf{x}[k]$  represent space-time encoded information symbols  $a[\kappa]$ , which are zero-mean and randomly drawn from a  $Q$ -ary signal constellation  $\mathbb{A}$ , e.g., a  $Q$ -PSK constellation. The index  $\kappa$  denotes the time index before the space-time encoder. The average power of the transmitted symbols  $x_\mu[k]$  is in the sequel denoted as  $\sigma_{x,\mu}^2$  and the average power of the information symbols  $a[\kappa]$  as  $\sigma_a^2$ . The entries  $n_\nu[k]$  ( $\nu=1, \dots, N$ ) of the noise vector  $\mathbf{n}[k]$  are assumed to be (temporally and spatially white) complex Gaussian random variables  $n_\nu[k] \sim \mathcal{CN}(0, \sigma_n^2)$ . Throughout this thesis it is assumed that  $\mathbf{H}[k]$ ,  $\mathbf{x}[k]$ , and  $\mathbf{n}[k]$  are statistically independent. Moreover, for the time being, we assume that the channel matrix  $\mathbf{H}[k]$  remains constant over  $p$  consecutive time indices  $k$ . For convenience, the time index  $k$  for the channel matrix is therefore dropped in the sequel. Finally, the instantaneous realizations of the channel matrix  $\mathbf{H}$  are assumed to be perfectly known at the receiver.

The basic principle of a general STBC is very similar to that of block codes used in channel coding. However, instead of one-dimensional code words, two-dimensional code matrices in space and time are used. In particular, the information symbols  $a[\kappa]$  are partitioned into groups of  $p_i$  symbols, which are subsequently mapped onto code matrices  $\mathbf{X}[k]$  of size  $(p \times M)$ , according to

$$\mathcal{S} : \mathbb{C}^{p_i} \rightarrow \mathbb{C}^{p \times M}, \quad \mathbf{a}[\kappa] := [a[\kappa], \dots, a[\kappa+p_i-1]]^T \mapsto \mathbf{X}[k], \quad (2.70)$$

where  $\mathbf{X}[k] := [\mathbf{x}[k], \dots, \mathbf{x}[k+p-1]]^T$ . The rows of the code matrix  $\mathbf{X}[k]$  are simultaneously transmitted via the  $M$  antennas using the same carrier frequency. More specifically, the entry  $[\mathbf{X}[k]]_{\xi,\mu}$  ( $1 \leq \xi \leq p$ ,  $1 \leq \mu \leq M$ ) of the code matrix is transmitted at time index  $k+\xi-1$  via the  $\mu$ th antenna.<sup>31</sup> Since altogether  $p$  time indices are required, in order to transmit  $p_i$  information symbols, the temporal rate of the STBC is given by

$$R_t := \frac{p_i}{p}. \quad (2.71)$$

In the case of an OSTBC orthogonal code matrices  $\mathbf{X}[k]$  are used, which allow for full spatial diversity<sup>32</sup> and a simple (widely) linear receiver structure. The maximum temporal

<sup>31</sup>The time indices  $k$  and  $\kappa$  cannot assume arbitrary values. Instead, we have  $k \in \{np \mid n \in \mathbb{Z}_{\geq 0}\}$  and  $\kappa \in \{np_i \mid n \in \mathbb{Z}_{\geq 0}\}$ . Note that there is a unique index  $k$  for every  $\kappa$ , and vice versa (via the integer  $n$ ).

<sup>32</sup>This means, that in a log-log plot the resulting frame or symbol error rate exhibits an asymptotic slope of  $-MN$  (i.e., for large SNR values).



rate of OSTBCs is  $R_t = 1$  ('full rate'), which corresponds to the rate of an uncoded single-antenna system.

### Orthogonal Designs

The difficulty in the design of OSTBCs is to find code matrices  $\mathbf{X}[k]$  that are always orthogonal, irrespective of the underlying information symbols  $a[\kappa]$ . To this end, the theory of (generalized) orthogonal designs [Hur98, Rad22], which dates back to the 1890s, was revisited in [TJC99a, TJC99b].

A generalized orthogonal design  $\mathfrak{D}$  is an orthogonal  $(p \times M)$ -matrix with entries  $[\mathfrak{D}]_{\xi, \mu}$  ( $\xi = 1, \dots, p$ ,  $\mu = 1, \dots, M$ ) that are linear combinations of  $p_i$  complex-valued variables  $a_1, \dots, a_{p_i}$  and their complex conjugates.<sup>33</sup> In particular, the product  $\mathfrak{D}^H \mathfrak{D}$  yields [SL02d]

$$\mathfrak{D}^H \mathfrak{D} = \zeta (|a_1|^2 + \dots + |a_{p_i}|^2) \mathbf{I}_M, \quad (2.72)$$

where  $\zeta$  is a positive constant that depends on the specific generalized orthogonal design  $\mathfrak{D}$  under consideration. Examples for generalized orthogonal designs are [TJC99a, TJC99b]

$$\mathfrak{D}_1 = \mathfrak{A} := \begin{bmatrix} a_1 & a_2 \\ -a_2^* & a_1^* \end{bmatrix} \quad (p=2, M=2, p_i=2, \zeta=1), \quad (2.73)$$

$$\mathfrak{D}_2 := \begin{bmatrix} a_1 & a_2 & \frac{a_3}{\sqrt{2}} & \frac{a_3}{\sqrt{2}} \\ -a_2^* & a_1^* & \frac{a_3}{\sqrt{2}} & -\frac{a_3}{\sqrt{2}} \\ \frac{a_3^*}{\sqrt{2}} & \frac{a_3^*}{\sqrt{2}} & \frac{-a_1 - a_1^* + a_2 - a_2^*}{2} & \frac{a_1 - a_1^* - a_2 - a_2^*}{2} \\ \frac{a_3^*}{\sqrt{2}} & -\frac{a_3^*}{\sqrt{2}} & \frac{a_1 - a_1^* + a_2 + a_2^*}{2} & \frac{-a_1 - a_1^* - a_2 + a_2^*}{2} \end{bmatrix} \quad (p=4, M=4, p_i=3, \zeta=1), \quad (2.74)$$

$$\mathfrak{D}_3 := \begin{bmatrix} a_1 & a_2 & a_3 & 0 \\ -a_2^* & a_1^* & 0 & a_3 \\ a_3^* & 0 & -a_1^* & a_2 \\ 0 & a_3^* & -a_2^* & -a_1 \end{bmatrix} \quad (p=4, M=4, p_i=3, \zeta=1), \quad (2.75)$$

and

$$\mathfrak{D}_4 := \begin{bmatrix} a_1 & a_2 & a_3 & a_4 \\ -a_2 & a_1 & -a_4 & a_3 \\ -a_3 & a_4 & a_1 & -a_2 \\ -a_4 & -a_3 & a_2 & a_1 \\ a_1^* & a_2^* & a_3^* & a_4^* \\ -a_2^* & a_1^* & -a_4^* & a_3^* \\ -a_3^* & a_4^* & a_1^* & -a_2^* \\ -a_4^* & -a_3^* & a_2^* & a_1^* \end{bmatrix} \quad (p=8, M=4, p_i=4, \zeta=2). \quad (2.76)$$

<sup>33</sup>In the original definition [Hur98, Rad22], an orthogonal design is a square matrix of size  $(M \times M)$  with entries taken from the set  $\{\pm a_1, \dots, \pm a_M\}$ , where  $a_1, \dots, a_M$  are real-valued variables. It was shown that orthogonal designs exist solely for  $M=2$ ,  $M=4$ , and  $M=8$ . The existence problem of orthogonal designs is known as the Hurwitz-Radon problem in the literature. Generalized orthogonal designs may be non-square with entries that depend on  $p_i \leq M$  complex-valued variables  $a_1, \dots, a_{p_i}$  and their complex conjugates.



The orthogonal design  $\mathfrak{D}_1$  with  $M=2$  is the well-known Alamouti matrix  $\mathfrak{A}$  [Ala98]. Generalized orthogonal designs with  $M=3$  can, for example, be obtained from  $\mathfrak{D}_2$ ,  $\mathfrak{D}_3$  or  $\mathfrak{D}_4$  by deleting the last column. Further examples of (generalized) orthogonal designs with different parameters  $(p, M, p_i)$  can be found in [TH00,GS01,SX03,Lia03a,Lia03b,LFX05].

Once a generalized orthogonal design  $\mathfrak{D}$  is found for a certain parameter set  $(p, M, p_i)$ , it can be used as an orthogonal code matrix  $\mathbf{X}[k]$ , by setting

$$[a_1, \dots, a_{p_i}]^T := [a[\kappa], \dots, a[\kappa+p_i-1]]^T. \quad (2.77)$$

Of special interest are those generalized orthogonal designs that offer a temporal rate  $R_t = p_i/p$  close to unity, so as to limit the rate loss compared to an uncoded single-antenna system. In the case of a real-valued signal constellation, e.g., an amplitude-shift keying (ASK)-constellation, full-rate OSTBCs exist for any number of transmit antennas [TJC99a]. However, given complex-valued information symbols  $a[\kappa]$ , the only full-rate OSTBC is Alamouti's transmit diversity scheme [Ala98] for two transmit antennas [LX03] (Alamouti matrix  $\mathfrak{A}$ ). In the case of three and four transmit antennas, the maximum possible rate is  $R_t = 3/4$  [TH00]. This rate is, for example, achieved by the generalized orthogonal designs  $\mathfrak{D}_2$  and  $\mathfrak{D}_3$ . In [TJC99a] it was shown that half-rate OSTBCs for complex-valued modulation schemes can be constructed for any number of transmit antennas. These half-rate designs consist of a full-rate orthogonal design constructed for real-valued signal constellations and the corresponding complex conjugate orthogonal design, see for example  $\mathfrak{D}_4$ . In fact, to find OSTBCs of high rates is, in general, not a trivial task. A systematic method to design high-rate OSTBCs for complex-valued modulation schemes and an arbitrary number of transmit antennas was presented in [SXL04].<sup>34</sup>

### Equivalent Single-Antenna System

The orthogonal property of the OSTBC code matrices  $\mathbf{X}[k]$  can be utilized, in order to transform the MIMO system with  $M$  transmit and  $N$  receive antennas into an equivalent single-antenna system. For this purpose, an appropriate (widely) linear combining scheme ('OSTBC decoder') is required at the receiver, see Fig. 2.7 a). For each receive antenna  $\nu$ , one first defines an equivalent MIMO system with  $2p_i$  inputs and  $p$  outputs, according to [BHS01]

$$\mathbf{y}_{\text{eq},\nu}[k] := \mathbf{H}_{\text{eq},\nu} \mathbf{a}_{\text{eq}}[\kappa] + \mathbf{n}_{\text{eq},\nu}[k], \quad (2.78)$$

where

$$\mathbf{y}_{\text{eq},\nu}[k] := [y_\nu[k], \dots, y_\nu[k+p-1]]^T, \quad (2.79a)$$

$$\mathbf{a}_{\text{eq}}[\kappa] := [a[\kappa], \dots, a[\kappa+p_i-1], a^*[\kappa], \dots, a^*[\kappa+p_i-1]]^T, \quad (2.79b)$$

$$\mathbf{n}_{\text{eq},\nu}[k] := [n_\nu[k], \dots, n_\nu[k+p-1]]^T. \quad (2.79c)$$

The equivalent channel matrix  $\mathbf{H}_{\text{eq},\nu}$  needs to be determined accordingly. Then, the following widely linear combining step is performed at the receiver [BHS01]:

$$\mathbf{z}[k] := \frac{1}{\|\mathbf{H}\|_{\text{F}}} \sum_{\nu=1}^N \mathbf{z}_{\text{eq},\nu}[k] := \frac{1}{\|\mathbf{H}\|_{\text{F}}} \sum_{\nu=1}^N \left( \mathbf{H}'_{1,\nu} \mathbf{y}_{\text{eq},\nu}[k] + \mathbf{H}'_{2,\nu} \mathbf{y}_{\text{eq},\nu}^*[k] \right), \quad (2.80)$$

<sup>34</sup>As an alternative to OSTBCs, orthogonal spreading sequences of length  $M$  can be used, in order to exploit full spatial diversity [ZG03a]. However, the temporal rate of such a system is only  $R_t = 1/M$ .

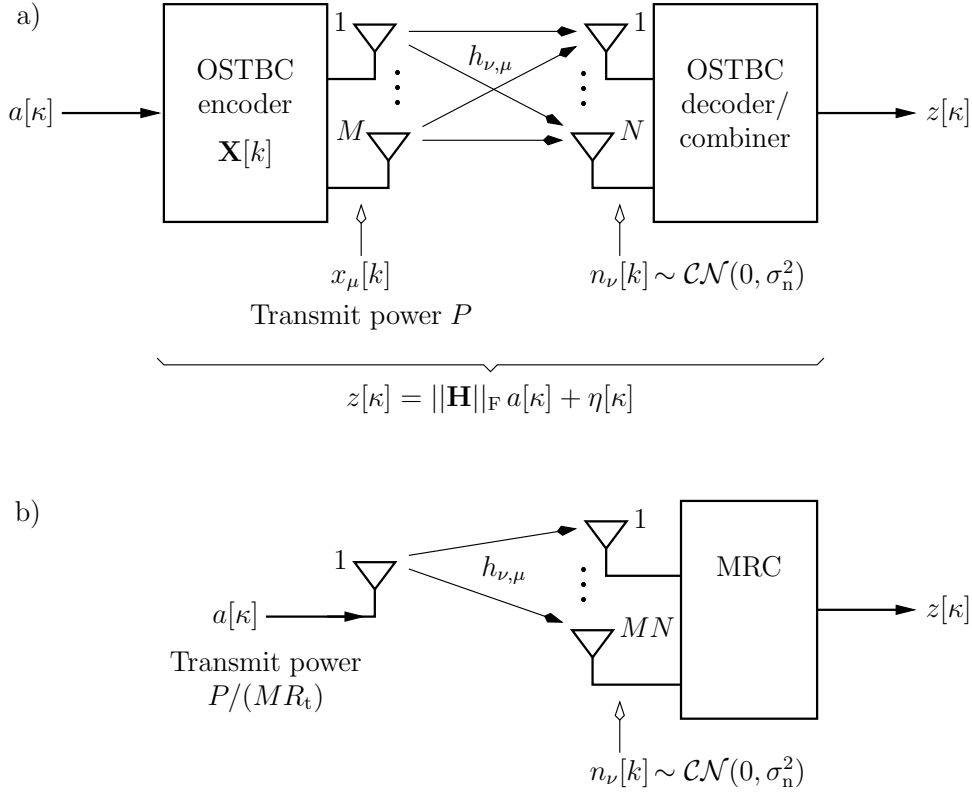


Figure 2.7: Transmission model for MIMO systems with OSTBC: a) OSTBC system with  $M$  transmit and  $N$  receive antennas and corresponding widely linear detector at the receiver b) Equivalent MRC system with a single transmit antenna and  $MN$  receive antennas.

where  $\mathbf{z}[\kappa] := [z[\kappa], \dots, z[\kappa + p_i - 1]]^T$ ,  $\|\mathbf{H}\|_F$  denotes the Frobenius norm of the original MIMO channel matrix in (2.68), and  $\mathbf{H}'_{1,\nu}$  and  $\mathbf{H}'_{2,\nu}$  denotes the upper and the lower  $(p_i \times p)$ -submatrix of  $\mathbf{H}_{\text{eq},\nu}^H$ , respectively. Due to the inherent orthogonality, the interference between the information symbols  $a[\kappa], \dots, a[\kappa + p_i - 1]$  is completely removed, such that (2.80) corresponds to an equivalent single-antenna system of form

$$z[\kappa] = \left( \sum_{\mu=1}^M \sum_{\nu=1}^N |h_{\nu,\mu}|^2 \right)^{1/2} a[\kappa] + \eta[\kappa] = \|\mathbf{H}\|_F a[\kappa] + \eta[\kappa], \quad (2.81)$$

cf. Fig. 2.7 a), where the noise samples  $\eta[\kappa]$  are temporally white complex Gaussian random variables  $\sim \mathcal{CN}(0, \sigma_n^2/\zeta)$  [SL02d]. Therefore, the detection rule for (symbol-by-symbol) maximum-likelihood (ML) detection of the information symbols  $a[\kappa]$  is given by

$$\hat{a}[\kappa] = \underset{\tilde{a}[\kappa]}{\operatorname{argmax}} p_{z[\kappa]|\tilde{a}[\kappa]}(z[\kappa]|\tilde{a}[\kappa]) = \underset{\tilde{a}[\kappa]}{\operatorname{argmin}} \mu_{\text{ML}}(z[\kappa], \tilde{a}[\kappa]), \quad (2.82)$$

where  $\hat{a}[\kappa]$  denotes a hard decision on the information symbol  $a[\kappa]$ ,  $\tilde{a}[\kappa]$  a hypothesis for  $a[\kappa]$ ,  $p_{z[\kappa]|\tilde{a}[\kappa]}(z[\kappa]|\tilde{a}[\kappa])$  the conditional PDF of  $z[\kappa]$  given the information symbol

hypothesis  $\tilde{a}[\kappa]$ , and  $\mu_{\text{ML}}(z[\kappa], \tilde{a}[\kappa])$  the associated ML detection metric

$$\mu_{\text{ML}}(z[\kappa], \tilde{a}[\kappa]) := \left| z[\kappa] - \|\mathbf{H}\|_{\text{F}} \tilde{a}[\kappa] \right|^2. \quad (2.83)$$

Note that due to the orthogonality of the code matrix  $\mathbf{X}[k]$ , the ML detection metrics  $\mu_{\text{ML}}(z[\kappa], \tilde{a}[\kappa])$  for the individual information symbols  $a[\kappa], \dots, a[\kappa + p_i - 1]$  are decoupled. Moreover, the effective channel coefficient  $\|\mathbf{H}\|_{\text{F}}$  in the equivalent single-antenna system reflects the achieved diversity advantage over a single-antenna system. If the channel coefficients  $h_{\nu, \mu}$  fade more or less independently, the probability is small that  $\|\mathbf{H}\|_{\text{F}}$  has a small magnitude.

### Equivalent Maximum-Ratio-Combining System

From (2.81) it can be seen that an OSTBC system with  $M$  transmit and  $N$  receive antennas (in conjunction with the corresponding widely linear detector at the receiver) is in essence equivalent to a maximum-ratio-combining (MRC) system with a single transmit antenna and  $MN$  receive antennas, as shown in Fig. 2.7 b) (see also Appendix I). Assuming identical fading statistics in both systems, the only difference concerns the overall received SNR [SL02d] (or equivalently, the overall average transmitted power).

In the following, let  $\bar{\gamma}_{\text{s}}$  denote the overall average received SNR per information symbol and  $\bar{\gamma}_{\text{b}}$  the overall average received SNR per information bit. Moreover, let  $\sigma_{x, \mu}^2$  denote the average energy of the code symbols  $x_{\mu}[k]$  in the OSTBC system transmitted via the  $\mu$ th antenna ( $1 \leq \mu \leq M$ ). We assume that the overall average transmit power per channel use is equal to  $P$ , i.e.,  $\sigma_{x, 1}^2 + \dots + \sigma_{x, M}^2 = P$ . Each code matrix  $\mathbf{X}[k]$  spans  $p$  consecutive time indices and is therefore associated with an overall average transmit power of  $P_{\text{ov}} = pP$ . On the other hand,  $P_{\text{ov}}$  can also be written as

$$P_{\text{ov}} = \mathbb{E} \{ \text{tr}(\mathbf{X}^{\text{H}}[k] \mathbf{X}[k]) \} = \zeta M \cdot \mathbb{E} \{ |a[\kappa]|^2 + \dots + |a[\kappa + p_i - 1]|^2 \} = \zeta M p_i \sigma_a^2. \quad (2.84)$$

Thus, the average energy per information symbol is given by

$$\sigma_a^2 = \frac{P}{M \zeta R_{\text{t}}}, \quad (2.85)$$

and the overall average received SNR per information symbol is equal to

$$\bar{\gamma}_{\text{s}} = \frac{P}{M R_{\text{t}} \sigma_{\text{n}}^2} \sum_{\mu=1}^M \sum_{\nu=1}^N \Omega_{h_{\nu, \mu}}. \quad (2.86)$$

Note that the parameter  $\zeta$  does not occur in the expression for  $\bar{\gamma}_{\text{s}}$ . Finally, the overall average received SNR per information bit results as  $\bar{\gamma}_{\text{b}} = \bar{\gamma}_{\text{s}} / \log_2(Q)$ .

For comparison, consider an MRC system with a single transmit antenna,  $MN$  receive antennas, an average transmit power  $P$ , and a noise variance  $\sigma_{\text{n}}^2$  per receive antenna. Assuming identical fading statistics as in the OSTBC system, the overall average received SNR per information symbol in the MRC system is given by

$$\bar{\gamma}_{\text{s}} = \frac{P}{\sigma_{\text{n}}^2} \sum_{\mu=1}^M \sum_{\nu=1}^N \Omega_{h_{\nu, \mu}}. \quad (2.87)$$

In comparison, the average received SNR in the OSTBC system is reduced by a factor  $1/(MR_t)$ . The factor  $1/M$  represents an SNR loss that is due to the smaller number of receive antennas compared to the MRC system. This SNR loss can (partly) be compensated by choosing a low temporal rate  $R_t$ , which comes, however, at the expense of a significant rate loss compared to an uncoded single-antenna system.

**Example 2.2 (Alamouti's transmit diversity scheme)**

In the following, the concept of the equivalent single-antenna system and the equivalent MRC system is illustrated for the example of Alamouti's transmit diversity scheme [Ala98] ( $M = 2$  transmit antennas,  $N$  receive antennas,  $R_t = 1$ ,  $\zeta = 1$ ). In Alamouti's scheme, pairs  $[a[\kappa], a[\kappa+1]]$  of  $Q$ -ary complex-valued information symbols are mapped onto the Alamouti matrix  $\mathfrak{A}$ , according to

$$\mathbf{X}[k] := \mathfrak{A} = \begin{array}{cc} \begin{bmatrix} a[\kappa] & a[\kappa+1] \\ -a^*[\kappa+1] & a^*[\kappa] \end{bmatrix} & \begin{array}{l} \longleftarrow \text{time index } k \\ \longleftarrow \text{time index } k+1 \end{array} \\ \begin{array}{c} \uparrow \qquad \uparrow \\ \text{antenna 1} \quad \text{antenna 2} \end{array} & \end{array} \quad (2.88)$$

cf. (2.73). At the receiver, the received samples  $y_\nu[k]$ ,  $y_\nu[k+1]$  of the  $\nu$ th antenna ( $1 \leq \nu \leq N$ ) are organized in a vector  $\mathbf{y}_{\text{eq},\nu}[k] := [y_\nu[k], y_\nu^*[k+1]]^T$ , which yields the equivalent matrix-vector system model<sup>35</sup>

$$\underbrace{\begin{bmatrix} y_\nu[k] \\ y_\nu^*[k+1] \end{bmatrix}}_{\mathbf{y}_{\text{eq},\nu}[k]} = \underbrace{\begin{bmatrix} h_{\nu,1} & h_{\nu,2} \\ h_{\nu,2}^* & -h_{\nu,1}^* \end{bmatrix}}_{=: \mathbf{H}_{\text{eq},\nu}} \underbrace{\begin{bmatrix} a[\kappa] \\ a[\kappa+1] \end{bmatrix}}_{=: \mathbf{a}[\kappa]} + \underbrace{\begin{bmatrix} n_\nu[k] \\ n_\nu^*[k+1] \end{bmatrix}}_{=: \mathbf{n}_{\text{eq},\nu}[k]}. \quad (2.89)$$

Due to the inherent orthogonality of the Alamouti matrix  $\mathfrak{A}$ , the equivalent channel matrix  $\mathbf{H}_{\text{eq},\nu}$  is also orthogonal, while

$$\mathbf{H}_{\text{eq},\nu}^H \mathbf{H}_{\text{eq},\nu} = (|h_{\nu,1}|^2 + |h_{\nu,2}|^2) \mathbf{I}_2. \quad (2.90)$$

Correspondingly, the (widely) linear detection step  $\mathbf{z}_{\text{eq},\nu}[\kappa] := \mathbf{H}_{\text{eq},\nu}^H \mathbf{y}_{\text{eq},\nu}[k]$  ('Alamouti decoding') yields

$$\mathbf{z}_{\text{eq},\nu}[\kappa] = \mathbf{H}_{\text{eq},\nu}^H \mathbf{y}_{\text{eq},\nu}[k] = (|h_{\nu,1}|^2 + |h_{\nu,2}|^2) \mathbf{a}[\kappa] + \boldsymbol{\eta}_\nu[\kappa], \quad (2.91)$$

where the noise vector  $\boldsymbol{\eta}_\nu[\kappa] := \mathbf{H}_{\text{eq},\nu}^H \mathbf{n}_{\text{eq},\nu}[k]$  is a complex Gaussian random vector with covariance matrix  $\mathbb{E}\{\boldsymbol{\eta}_\nu[\kappa] \boldsymbol{\eta}_\nu^H[\kappa]\} = (|h_{\nu,1}|^2 + |h_{\nu,2}|^2) \sigma_n^2 \mathbf{I}_2$ . In a final step, all vectors  $\mathbf{z}_{\text{eq},\nu}[\kappa]$  ( $\nu = 1, \dots, N$ ) are linearly combined according to

$$\mathbf{z}[\kappa] := \frac{1}{\|\mathbf{H}\|_F} \sum_{\nu=1}^N \mathbf{z}_{\text{eq},\nu}[\kappa] = \|\mathbf{H}\|_F \mathbf{a}[\kappa] + \boldsymbol{\eta}[\kappa], \quad (2.92)$$

where  $\mathbf{z}[\kappa] := [z[\kappa], z[\kappa+1]]^T$  and  $\boldsymbol{\eta}[\kappa] := [\eta[\kappa], \eta[\kappa+1]]^T$ . Note that symbol-by-symbol ML detection amounts to a simple hard decision on  $\mathbf{z}[\kappa]$ . In particular,

<sup>35</sup>Equation (2.89) constitutes a modified version of (2.78) that is valid for the special case of Alamouti's transmit diversity scheme. Alternatively, the equivalent system model can also be defined based on the vectors  $\mathbf{y}'_{\text{eq},\nu}[k] := [y_\nu[k], y_\nu[k+1]]^T$  and  $\mathbf{a}_{\text{eq}}[\kappa] := [a[\kappa], a[\kappa+1], a^*[\kappa], a^*[\kappa+1]]^T$ .

the noise vector  $\boldsymbol{\eta}[\kappa]$  is a complex Gaussian random vector with covariance matrix equal to  $\mathbf{E}\{\boldsymbol{\eta}[\kappa]\boldsymbol{\eta}^H[\kappa]\} = \sigma_n^2 \mathbf{I}_2$ . Thus, the overall average received SNR per information symbol is equal to

$$\bar{\gamma}_s = \frac{P}{2\sigma_n^2} \sum_{\mu=1}^M \sum_{\nu=1}^N \Omega_{h_{\nu,\mu}}, \quad (2.93)$$

cf. (2.86). As can be seen, the Alamouti-system with  $M=2$  transmit antennas and  $N$  receive antennas is equivalent to an MRC system with a single transmit antenna,  $2N$  receive antennas and an average energy per transmitted information symbol of  $\sigma_a^2 = P/2$ .  $\diamond$

### Orthogonality Loss

As discussed above, the key feature of OSTBCs is that the code matrix  $\mathbf{X}[k]$  is always orthogonal, irrespective of the transmitted information symbols  $a[\kappa]$ . This guarantees full spatial diversity and allows for simple, low-complexity symbol-by-symbol ML detection at the receiver. However, OSTBCs are based on somewhat idealized assumptions that might not be met in a practical MIMO system. For example, it was assumed above that the channel matrix  $\mathbf{H}$  remains constant over  $p$  consecutive time indices, i.e., over the duration of a complete code matrix  $\mathbf{X}[k]$ . Moreover, it was assumed that the instantaneous realizations of the channel matrix  $\mathbf{H}$  are perfectly known at the receiver. Finally, it was assumed that the system does not suffer from intersymbol interference (ISI) effects.

In the presence of ISI, a time-varying channel, or non-perfect channel knowledge at the receiver, the OSTBC system loses its orthogonality, i.e., the equivalent single-antenna system model (2.81) is not valid anymore. This causes interference between the information symbols  $a[\kappa]$ , which has two major effects. First, the interference will lead to a loss in error performance, which is adverse to the achieved spatial diversity gains. Second, the complexity of ML detection at the receiver increases, because symbol-by-symbol detection is no longer optimal. More specifically, if the channel is time-varying and/or not perfectly known at the receiver, interference can occur between all information symbols associated with the same code matrix  $\mathbf{X}[k]$ . Correspondingly, ML detection has to be performed on a matrix-by-matrix basis, i.e., jointly for groups of  $p_i$  information symbols [VLB04]. The number of required hypotheses per information symbol vector  $\mathbf{a}[\kappa] := [a[\kappa], \dots, a[\kappa+p_i-1]]^T$  is therefore equal to  $Q^{p_i}$ , while in the case of perfect orthogonality only  $Qp_i$  hypotheses are required (due to the decoupled ML detection metrics).

In the presence of ISI, interference will not only occur within a single code matrix  $\mathbf{X}[k]$ , but also between subsequent code matrices. In this case, the optimal receiver strategy is to perform maximum-likelihood sequence estimation (MLSE), e.g., by means of the Viterbi algorithm operating on an appropriately designed trellis structure.<sup>36</sup> The resulting trellis structure for a general STBC in the presence of ISI is discussed more detailed in Appendix J.

In the following, the orthogonality loss due to a time-varying channel and non-perfect channel knowledge at the receiver is illustrated for the example of Alamouti's transmit diversity scheme.

<sup>36</sup>In contrast to a single-antenna system, one trellis segment comprises the duration of a complete code matrix  $\mathbf{X}[k]$ , rather than a single time index  $k$  [Bau00, BHS01].

**Example 2.3 (Orthogonality loss for Alamouti's scheme)**

In the sequel, we drop the assumption that the channel matrix  $\mathbf{H}$  remains constant over the duration of a complete code matrix  $\mathbf{X}[k]$ , i.e., the channel coefficients for the time index  $k$  and  $k+1$  may now be different:

$$h_{\nu,\mu}[k+1] := h_{\nu,\mu}[k] + \Delta_{\nu,\mu}[k] \quad (2.94)$$

( $\mu=1, 2$ ,  $\nu=1, \dots, N$ ). The equivalent channel matrix for the  $\nu$ th receive antenna is thus given by

$$\mathbf{H}_{\text{eq},\nu}[k] = \begin{bmatrix} h_{\nu,1}[k] & h_{\nu,2}[k] \\ h_{\nu,2}^*[k+1] & -h_{\nu,1}^*[k+1] \end{bmatrix}, \quad (2.95)$$

cf. (2.89). Additionally, we drop the assumption that the receiver has perfect knowledge of the instantaneous channel realizations. To this end, let

$$\hat{h}_{\nu,\mu}[k] := h_{\nu,\mu}[k] + \varepsilon_{\nu,\mu}[k], \quad \hat{h}_{\nu,\mu}[k+1] := h_{\nu,\mu}[k+1] + \varepsilon_{\nu,\mu}[k+1] \quad (2.96)$$

denote noisy estimates of the channel coefficients associated with the  $\mu$ th transmit and the  $\nu$ th receive antenna. The Alamouti decoding step at the receiver will thus be performed using an erroneous channel matrix  $\hat{\mathbf{H}}_{\text{eq},\nu}[k]$ . Altogether, (2.91) becomes

$$\mathbf{z}'_{\text{eq},\nu}[\kappa] = \hat{\mathbf{H}}_{\text{eq},\nu}^{\text{H}}[\kappa] \mathbf{y}_{\text{eq},\nu}[\kappa] =: \mathbf{\Psi}_{\nu}[\kappa] \mathbf{a}[\kappa] + \boldsymbol{\eta}'_{\nu}[\kappa], \quad (2.97)$$

where

$$\begin{aligned} [\mathbf{\Psi}_{\nu}[k]]_{1,1} &= |h_{\nu,1}[k]|^2 + |h_{\nu,2}[k] + \Delta_{\nu,2}[k]|^2 \\ &\quad + \varepsilon_{\nu,1}^*[k] h_{\nu,1}[k] + \varepsilon_{\nu,2}^*[k+1] (h_{\nu,2}[k] + \Delta_{\nu,2}[k])^*, \end{aligned} \quad (2.98a)$$

$$\begin{aligned} [\mathbf{\Psi}_{\nu}[k]]_{1,2} &= (\varepsilon_{\nu,1}[k] - \Delta_{\nu,1}[k])^* h_{\nu,2}[k] \\ &\quad - (h_{\nu,1}[k] + \Delta_{\nu,1}[k])^* (\varepsilon_{\nu,2}[k+1] + \Delta_{\nu,2}[k]), \end{aligned} \quad (2.98b)$$

$$\begin{aligned} [\mathbf{\Psi}_{\nu}[k]]_{2,1} &= (\varepsilon_{\nu,2}[k] - \Delta_{\nu,2}[k])^* h_{\nu,1}[k] \\ &\quad - (h_{\nu,2}[k] + \Delta_{\nu,2}[k])^* (\varepsilon_{\nu,1}[k+1] + \Delta_{\nu,1}[k]), \end{aligned} \quad (2.98c)$$

$$\begin{aligned} [\mathbf{\Psi}_{\nu}[k]]_{2,2} &= |h_{\nu,1}[k] + \Delta_{\nu,1}[k]|^2 + |h_{\nu,2}[k]|^2 \\ &\quad + \varepsilon_{\nu,1}[k+1] (h_{\nu,1}[k] + \Delta_{\nu,1}[k])^* + \varepsilon_{\nu,2}^*[k] h_{\nu,2}[k]. \end{aligned} \quad (2.98d)$$

Obviously, the matrix  $\mathbf{\Psi}_{\nu}[k]$  is (in general) not diagonal anymore, which causes interference between the information symbols  $a[\kappa]$  and  $a[\kappa+1]$ . In addition to this, the information symbols are weighted with different factors, since  $[\mathbf{\Psi}_{\nu}[k]]_{1,1} \neq [\mathbf{\Psi}_{\nu}[k]]_{2,2}$ . Moreover, the covariance matrix of the noise vector  $\boldsymbol{\eta}'_{\nu}[\kappa]$  is given by

$$\mathbf{E}\{\boldsymbol{\eta}'_{\nu}[\kappa] \boldsymbol{\eta}'_{\nu}{}^{\text{H}}[\kappa]\} = \sigma_n^2 \mathbf{\Phi}_{\nu}[k], \quad (2.99)$$

where

$$[\mathbf{\Phi}_{\nu}[k]]_{1,1} = |h_{\nu,1}[k] + \varepsilon_{\nu,1}[k]|^2 + |h_{\nu,2}[k] + \Delta_{\nu,2}[k] + \varepsilon_{\nu,2}[k+1]|^2, \quad (2.100a)$$

$$\begin{aligned} [\mathbf{\Phi}_{\nu}[k]]_{1,2} &= (\varepsilon_{\nu,2}[k] - \varepsilon_{\nu,2}[k+1] - \Delta_{\nu,2}[k]) h_{\nu,1}^*[k] + (h_{\nu,2}[k] + \varepsilon_{\nu,2}[k]) \varepsilon_{\nu,1}^*[k] \\ &\quad - (\varepsilon_{\nu,1}[k+1] + \Delta_{\nu,1}[k])^* (h_{\nu,2}[k] + \Delta_{\nu,2}[k] + \varepsilon_{\nu,2}[k+1]) \\ &= [\mathbf{\Phi}_{\nu}[k]]_{2,1}^*, \end{aligned} \quad (2.100b)$$

$$[\mathbf{\Phi}_{\nu}[k]]_{2,2} = |h_{\nu,1}[k] + \Delta_{\nu,1}[k] + \varepsilon_{\nu,1}[k+1]|^2 + |h_{\nu,2}[k] + \varepsilon_{\nu,2}[k]|^2, \quad (2.100c)$$

i.e., the resulting noise term is not white anymore ( $\Phi_\nu[k] \neq \mathbf{I}_2$ ). Note that in the special case of a static channel ( $\Delta_{\nu,\mu}[k]=0$ ,  $\mu=1,2$ ), the non-diagonal elements of  $\Phi_\nu[k]$  vanish ( $\varepsilon_{\nu,\mu}[k]=\varepsilon_{\nu,\mu}[k+1]=:\varepsilon_{\nu,\mu}$ ). Moreover, the diagonal elements of  $\Phi_\nu[k]$  become equal in this case.

Altogether, we conclude that a hard symbol-by-symbol decision based on the vector  $\mathbf{z}'_{\text{eq}}[\kappa] := \sum_{\nu=1}^N \mathbf{z}'_{\text{eq},\nu}[\kappa]$  is no longer optimal in the sense of the ML criterion, cf. (2.97). Note that even in the case of perfect channel knowledge at the receiver (i.e., for  $\varepsilon_{\nu,1}[\cdot]=\varepsilon_{\nu,2}[\cdot]=0$ ) the matrix  $\Psi_\nu[k]$  is typically non-diagonal.  $\diamond$

### Alternative Receiver Structures for Alamouti's Transmit Diversity Scheme

In the case of a time-varying channel model and/or non-perfect channel knowledge at the receiver, the performance of Alamouti's transmit diversity scheme can sometimes be improved by means of a linear zero-forcing (ZF) or a linear minimum-mean-squared-error (MMSE) receiver, instead of performing the conventional Alamouti decoding step according to (2.97). Consider the following extended system model for Alamouti's transmit diversity scheme with multiple receive antennas [BHS01]:

$$\mathbf{y}_{\text{eq}}[k] = \mathbf{H}_{\text{eq}}[k] \mathbf{a}[k] + \mathbf{n}_{\text{eq}}[k], \quad (2.101)$$

where  $\mathbf{y}_{\text{eq}}[k] := [\mathbf{y}_{\text{eq},1}^T[k], \dots, \mathbf{y}_{\text{eq},N}^T[k]]^T$ ,  $\mathbf{n}_{\text{eq}}[k] := [\mathbf{n}_{\text{eq},1}^T[k], \dots, \mathbf{n}_{\text{eq},N}^T[k]]^T$ , and

$$\mathbf{H}_{\text{eq}}[k] := [\mathbf{H}_{\text{eq},1}^T[k], \dots, \mathbf{H}_{\text{eq},N}^T[k]]^T, \quad (2.102)$$

cf. (2.89). Note that for a static channel,  $\mathbf{H}_{\text{eq}}^H \mathbf{H}_{\text{eq}} = (|h_{1,1}|^2 + |h_{1,2}|^2 + \dots + |h_{N,1}|^2 + |h_{N,2}|^2) \mathbf{I}_2$  holds, i.e.,  $\mathbf{z}_{\text{eq}}[\kappa] := \mathbf{H}_{\text{eq}}^H[k] \mathbf{y}_{\text{eq}}[k] = \|\mathbf{H}\|_F^2 \mathbf{a}[\kappa] + \mathbf{H}_{\text{eq}}^H[k] \mathbf{n}_{\text{eq}}[k]$ , similar to (2.91). Given a time-varying channel and non-perfect channel knowledge at the receiver, the ZF receiver is given by

$$\mathbf{z}_{\text{ZF}}[\kappa] = \hat{\mathbf{H}}_{\text{eq}}^\dagger[k] \mathbf{y}_{\text{eq}}[k] = \left( \hat{\mathbf{H}}_{\text{eq}}^H[k] \hat{\mathbf{H}}_{\text{eq}}[k] \right)^{-1} \hat{\mathbf{H}}_{\text{eq}}^H[k] \mathbf{y}_{\text{eq}}[k], \quad (2.103)$$

where  $\hat{\mathbf{H}}_{\text{eq}}^\dagger[k]$  denotes the Moore-Penrose left-hand pseudoinverse of  $\hat{\mathbf{H}}_{\text{eq}}[k]$ . Similarly, the MMSE receiver is given by

$$\mathbf{z}_{\text{MMSE}}[\kappa] = \left( \hat{\mathbf{H}}_{\text{eq}}^H[k] \hat{\mathbf{H}}_{\text{eq}}[k] + \sigma_n^2 / \sigma_a^2 \cdot \mathbf{I}_2 \right)^{-1} \hat{\mathbf{H}}_{\text{eq}}^H[k] \mathbf{y}_{\text{eq}}[k]. \quad (2.104)$$

Note that in the case of a static channel and perfect channel knowledge at the receiver, the ZF receiver is (up to a scaling factor) equivalent to the conventional Alamouti decoding step, since

$$\mathbf{H}_{\text{eq}}^\dagger = (|h_{1,1}|^2 + |h_{1,2}|^2 + \dots + |h_{N,1}|^2 + |h_{N,2}|^2)^{-1} \mathbf{H}_{\text{eq}}^H. \quad (2.105)$$

Correspondingly, both the conventional Alamouti receiver and the ZF receiver are optimal in the sense of (symbol-by-symbol) ML detection in this case. Specifically, the use of the linear MMSE receiver will not give any benefit here. Interestingly, in the case of a time-varying channel and/or non-perfect channel knowledge at the receiver, we may rewrite (2.103) according to [Boe03]

$$\mathbf{z}_{\text{ZF}}[\kappa] = \left( \hat{\mathbf{H}}_{\text{eq}}^H[k] \hat{\mathbf{H}}_{\text{eq}}[k] \right)^{-1} \mathbf{z}'_{\text{eq}}[\kappa], \quad (2.106)$$



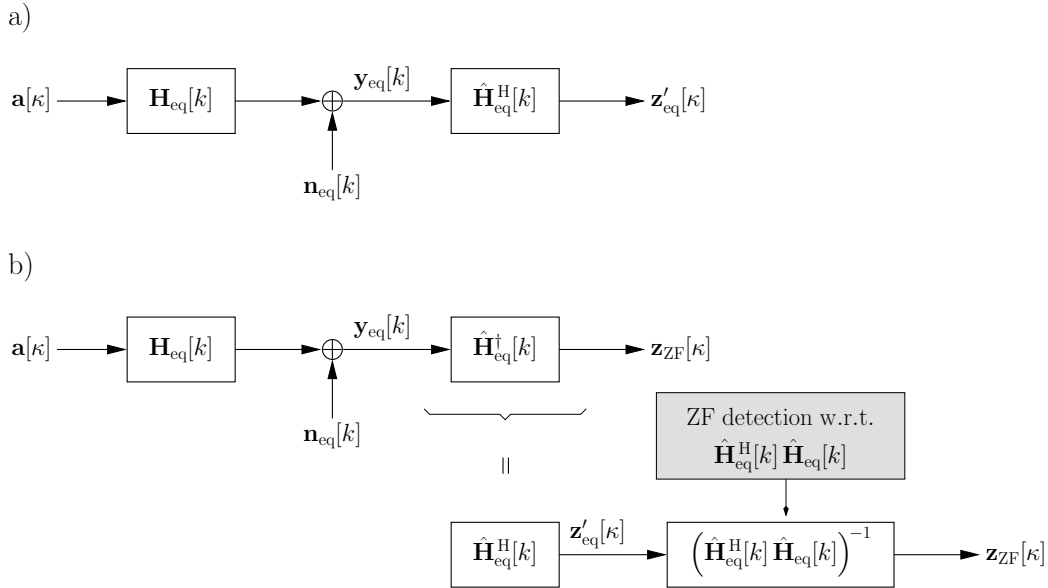


Figure 2.8: Interpretation of linear ZF detection as an add-on to conventional Alamouti decoding: a) Conventional Alamouti decoding b) Linear ZF detection.

where  $\mathbf{z}'_{\text{eq}}[\kappa] := \hat{\mathbf{H}}_{\text{eq}}^{\text{H}}[\kappa] \mathbf{y}_{\text{eq}}[\kappa]$  denotes the result obtained by conventional Alamouti decoding (cf. Example 2.3). Correspondingly, linear ZF detection may be interpreted as an add-on to conventional Alamouti decoding, as illustrated in Fig. 2.8. Similarly, (2.104) can be rewritten as

$$\mathbf{z}_{\text{MMSE}}[\kappa] = \left( \hat{\mathbf{H}}_{\text{eq}}^{\text{H}}[\kappa] \hat{\mathbf{H}}_{\text{eq}}[\kappa] + \sigma_{\text{n}}^2 / \sigma_{\text{a}}^2 \cdot \mathbf{I}_2 \right)^{-1} \mathbf{z}'_{\text{eq}}[\kappa], \quad (2.107)$$

i.e., linear MMSE detection corresponds to conventional Alamouti decoding followed by ZF detection with respect to the matrix  $(\hat{\mathbf{H}}_{\text{eq}}^{\text{H}}[\kappa] \hat{\mathbf{H}}_{\text{eq}}[\kappa] + \sigma_{\text{n}}^2 / \sigma_{\text{a}}^2 \mathbf{I}_2)$ .

The MMSE receiver is generally considered to be superior to the ZF receiver, because it provides an optimal trade-off (in the MMSE sense) between interference suppression and noise enhancement, whereas the ZF receiver exactly removes all interference. In particular, if  $\hat{\mathbf{H}}_{\text{eq}}^{\text{H}}[\kappa] \hat{\mathbf{H}}_{\text{eq}}[\kappa]$  is ill-conditioned, the ZF receiver typically causes significant coloring and enhancement of the noise. Interestingly, from [HZD05] it follows that the ZF receiver implicitly assumes that the transmitted vector  $\mathbf{a}[\kappa]$  is uniformly distributed on  $\mathbb{C}^{\text{pi}} = \mathbb{C}^2$ . In contrast to this, the MMSE receiver implicitly assumes that the joint PDF of  $\mathbf{a}[\kappa]$  is Gaussian on  $\mathbb{C}^2$ . Specifically, both types of receivers do not exploit the finite-alphabet property of  $\mathbf{a}[\kappa]$  that is typical for practical systems. Indeed, given a practical symbol alphabet  $\mathbb{A}$ , such as a phase-shift keying (PSK) or a quadrature amplitude modulation (QAM) constellation, the symbol-error-rate performance of the MMSE receiver is generally superior (or identical) to that of the ZF receiver. Obviously, this means that for practical symbol alphabets the implicit Gaussian assumption of the MMSE receiver is typically a ‘better’ fit to the actual distribution of  $\mathbf{a}[\kappa]$  than the uniform assumption made by the ZF receiver. However, it is possible to construct examples, for which the ZF receiver (slightly) outperforms the MMSE receiver [MH06a].

We will revisit the ZF and the MMSE receiver in Chapter 5, where we consider the impact of carrier frequency offsets and non-perfect channel tracking on the performance of distributed OSTBCs.

### 2.3.2 Quasi-Orthogonal Space-Time Block Codes

Although OSTBCs have many desirable properties, they have the drawback that for systems with more than two transmit antennas and a complex modulation scheme no full-rate designs exist. In [Jaf01] it was therefore suggested to sacrifice the strict constraint of perfect orthogonality, so as to enable a temporal rate of  $R_t = 1$  for more than two transmit antennas, while maintaining a spatial diversity gain and low-complexity ML detection at the receiver. An example of such a quasi-orthogonal STBC for  $M = 4$  transmit antennas is given by [Jaf01]

$$\mathbf{\Omega} := \begin{bmatrix} a_1 & a_2 & a_3 & a_4 \\ -a_2^* & a_1^* & -a_4^* & a_3^* \\ -a_3^* & -a_4^* & a_1^* & a_2^* \\ a_4 & -a_3 & -a_2 & a_1 \end{bmatrix} \quad (p=4, M=4, p_i=4, R_t=1), \quad (2.108)$$

which transmits  $p_i = 4$  information symbols using  $p = 4$  time indices. Further examples of quasi-orthogonal STBCs may be found in [SP03, PF03, BI03, SP04, SX04b, DG05, YGT05]. In contrast to OSTBCs, the product  $\mathbf{\Omega}^H \mathbf{\Omega}$  does not yield a scaled identity matrix anymore:

$$\mathbf{\Omega}^H \mathbf{\Omega} = (|a_1|^2 + |a_2|^2 + |a_3|^2 + |a_4|^2) \cdot \begin{bmatrix} 1 & 0 & 0 & \psi \\ 0 & 1 & -\psi & 0 \\ 0 & -\psi & 1 & 0 \\ \psi & 0 & 0 & 1 \end{bmatrix}, \quad (2.109)$$

where

$$\psi := 2 \cdot \frac{\operatorname{Re}\{a_1 a_4^*\} - \operatorname{Re}\{a_2 a_3^*\}}{|a_1|^2 + |a_2|^2 + |a_3|^2 + |a_4|^2}. \quad (2.110)$$

Due to this non-perfect orthogonality, the ML detection metrics for the individual information symbols are not decoupled anymore, as it is the case for OSTBCs. Still, it was shown in [Jaf01] that at least the ML detection metrics for the pairs  $(a_1, a_4)$  and  $(a_2, a_3)$  are decoupled, i.e., pairwise detection is optimal.<sup>37</sup> By this means, only  $2Q^2$  symbol hypotheses have to be considered for ML detection of  $a_1, a_2, a_3, a_4$ , rather than  $Q^4$  symbol hypotheses.

A drawback of quasi-orthogonal STBCs is that the intrinsic non-orthogonality leads to a reduced diversity order ( $< MN$ ). For example, in the case of a single receive antenna, the quasi-orthogonal STBC (2.108) achieves only a diversity order of two (just as Alamouti's

<sup>37</sup>Due to the inherent quasi-orthogonality, the interference between the pairs  $(a_1, a_4)$  and  $(a_2, a_3)$  can be removed completely by means of the linear combining steps (2.78)-(2.80) discussed earlier for the OSTBCs.

transmit diversity scheme), although four transmit antennas are employed. Due to this, an OSTBC designed for four transmit antennas will always be superior at high SNR values, despite the incurred rate loss [Jaf01]. Interestingly, in [SP03] it was shown that the performance of quasi-orthogonal STBCs can be improved using optimized rotations of the employed signal constellation (see also [SP04]). For example, in the case of the quasi-orthogonal STBC (2.108), the information symbols  $a_1$  and  $a_2$  are taken from a signal constellation  $\mathbb{A}$ , while  $a_3$  and  $a_4$  are taken from a rotated constellation  $\mathbb{A} \cdot e^{j\phi}$ , where  $\phi \in \mathbb{R}$  denotes a fixed rotation angle subject to optimization. However, it should be noted that substantial gains are only observed for error rates smaller than  $10^{-4}$  [SP03].

### 2.3.3 Time-Reversal Space-Time Block Code

In the case of intersymbol interference (ISI), the (quasi-) orthogonal property of OSTBCs and quasi-orthogonal STBCs gets lost, which typically causes significant performance degradations. One method to mitigate the impact of ISI is to employ an appropriate equalizer algorithm at the receiver. For example, the use of a trellis-based equalizer for arbitrary STBCs is discussed in Appendix J. As an alternative, an STBC with a time-reversal (TR) block structure was proposed in [LP00] (for the case of two transmit antennas), which is suitable for quasi-static MIMO channels with ISI. Due to the specific block structure, simple (widely) linear processing can be employed at the receiver, which allows for subsequent equalization by means of standard algorithms designed for single-antenna systems. In fact, the basic principle of the TR-STBC in [LP00] is very similar to that of Alamouti's transmit diversity scheme. However, in the case of the TR-STBC, pairs of information sequences are processed instead of pairs of information symbols. These are denoted as  $[\mathbf{a}_\kappa, \mathbf{a}_{\kappa+1}]$  in the sequel ( $\kappa \in \{0, 2, 4, \dots\}$ ), where

$$\mathbf{a}_\kappa := [a_\kappa[0], \dots, a_\kappa[k], \dots, a_\kappa[N_b - 1]]^T, \quad (2.111a)$$

$$\mathbf{a}_{\kappa+1} := [a_{\kappa+1}[0], \dots, a_{\kappa+1}[k], \dots, a_{\kappa+1}[N_b - 1]]^T. \quad (2.111b)$$

Similar to Alamouti's transmit diversity scheme, the TR-STBC is defined by a space-time code matrix

$$\begin{array}{cc} \left[ \begin{array}{cc} \mathbf{a}_\kappa & \mathbf{a}_{\kappa+1} \\ -\hat{\mathbf{a}}_{\kappa+1}^* & \hat{\mathbf{a}}_\kappa^* \end{array} \right] & \begin{array}{l} \leftarrow \text{block 1 } (N_b \text{ symbols}) \\ \leftarrow \text{block 2 } (N_b \text{ symbols}) \end{array} \\ \begin{array}{cc} \uparrow & \uparrow \\ \text{antenna 1} & \text{antenna 2} \end{array} & \end{array} \quad (2.112)$$

where

$$\hat{\mathbf{a}}_\kappa^* := [a_\kappa^*[N_b - 1], \dots, a_\kappa^*[k], \dots, a_\kappa^*[0]]^T. \quad (2.113)$$

Obviously, the complex conjugate operations in the Alamouti matrix  $\mathbf{A}$  have simply been replaced by complex conjugate and time-reversal operations. In fact, for the special case  $N_b = 1$ , the above matrix coincides with the Alamouti matrix  $\mathbf{A}$ . In the sequel, let

$$\mathbf{h}_{\nu,1} := [h_{\nu,1,0}, \dots, h_{\nu,1,l}, \dots, h_{\nu,1,L}]^T, \quad \mathbf{h}_{\nu,2} := [h_{\nu,2,0}, \dots, h_{\nu,2,l}, \dots, h_{\nu,2,L}]^T \quad (2.114)$$

denote the channel coefficient vectors associated with the first/second transmit antenna and the  $\nu$ th receive antenna, where  $L$  denotes the effective channel memory length of the MIMO channel. Moreover, let

$$\mathbf{y}_\nu^{(1)} := [y_\nu^{(1)}[0], \dots, y_\nu^{(1)}[k], \dots, y_\nu^{(1)}[N_b + L - 1]]^T, \quad (2.115a)$$

$$\mathbf{y}_\nu^{(2)} := [y_\nu^{(2)}[0], \dots, y_\nu^{(2)}[k], \dots, y_\nu^{(2)}[N_b + L - 1]]^T \quad (2.115b)$$

denote the received sequences at the  $\nu$ th receive antenna that are associated with the first and the second transmitted block of (2.112), including additive white Gaussian noise samples  $n_\nu^{(1)}[k]$  and  $n_\nu^{(2)}[k]$ , respectively. For simplicity it is assumed that the last  $L$  symbols of  $\mathbf{a}_\kappa$  and  $\mathbf{a}_{\kappa+1}$  are known and serve as tail symbols, so as to circumvent the problem of interblock interference.

The (widely) linear detection steps performed at the receiver are also very similar to that of Alamouti's scheme (cf. Example 2.2 in Section 2.3.1). First, the received sequence  $\mathbf{y}_\nu^{(2)}$  is time reversed and complex conjugated. Then, in order to recover the information sequence  $\mathbf{a}_\kappa$ , the received sequence  $\mathbf{y}_\nu^{(1)}$  is convolved with the complex conjugated and time-reversal version of  $\mathbf{h}_{\nu,1}$ , and the result is added to the convolution of  $\mathbf{h}_{\nu,2}$  with  $\hat{\mathbf{y}}_\nu^{(2)*}$ . This corresponds to the operation  $h_{\nu,1}^* y_\nu[k] + h_{\nu,2} y_\nu^*[k+1]$  performed in the case of Alamouti's transmit diversity scheme for computing the first entry of the vector  $\mathbf{z}_{\text{eq},\nu}[\kappa]$  (cf. Example 2.2). One thus obtains

$$z_{\text{eq},\nu}^{(1)}[k] := \sum_{l=0}^{2L} (h_{\text{eq},\nu,1,l} + h_{\text{eq},\nu,2,l}) a_\kappa[k-l] + \eta^{(1)}[k] \quad (2.116)$$

where

$$h_{\text{eq},\nu,\mu,l} := \sum_{l'=0}^L h_{\nu,\mu,l'} h_{\nu,\mu,L-l+l'}^* \quad (\mu=1,2) \quad (2.117)$$

and

$$\eta^{(1)}[k] := \sum_{l=0}^L \left( h_{\nu,1,L-l}^* \cdot n_\nu^{(1)}[k-l] + h_{\nu,2,l} \cdot n_\nu^{(2)*}[N_b - 1 - k + l] \right). \quad (2.118)$$

Similarly, in order to recover the information sequence  $\mathbf{a}_{\kappa+1}$ , the received sequence  $\mathbf{y}_\nu^{(1)}$  is convolved with  $\hat{\mathbf{h}}_{\nu,2}^*$ , and the convolution of  $\mathbf{h}_{\nu,1}$  with  $\hat{\mathbf{y}}_\nu^{(2)*}$  is subtracted. This yields

$$z_{\text{eq},\nu}^{(2)}[k] := \sum_{l=0}^{2L} (h_{\text{eq},\nu,1,l} + h_{\text{eq},\nu,2,l}) a_{\kappa+1}[k-l] + \eta^{(2)}[k], \quad (2.119)$$

where

$$\eta^{(2)}[k] := \sum_{l=0}^L \left( h_{\nu,2,L-l}^* \cdot n_\nu^{(1)}[k-l] - h_{\nu,1,l} \cdot n_\nu^{(2)*}[N_b - 1 - k + l] \right). \quad (2.120)$$

As can be seen, (2.116) and (2.119) constitute a discrete-time ISI channel model for an equivalent single-antenna system, which is valid for the first and the second information

sequence  $\mathbf{a}_\kappa$  and  $\mathbf{a}_{\kappa+1}$ , respectively. Note that the linear detection steps performed at the receiver correspond to a (channel-) matched filtering operation. Moreover, it should be noted that the additive noise terms  $\eta^{(1)}[k]$  and  $\eta^{(2)}[k]$  are no longer white [LP00].

In a final step, the contributions of all receive antennas can be added, according to  $z_{\text{eq}}^{(i)}[k] := \sum_{\nu=1}^N z_{\text{eq},\nu}^{(i)}[k]$  ( $i=1, 2$ ). Since the contributions of the information sequences  $\mathbf{a}_\kappa$  and  $\mathbf{a}_{\kappa+1}$  are completely decoupled, it is optimal to detect  $\mathbf{a}_\kappa$  and  $\mathbf{a}_{\kappa+1}$  separately on the basis of the sequences  $\mathbf{z}_{\text{eq}}^{(1)}$  and  $\mathbf{z}_{\text{eq}}^{(2)}$ , respectively ( $\mathbf{z}_{\text{eq}}^{(i)} := [z_{\text{eq}}^{(i)}[0], \dots, z_{\text{eq}}^{(i)}[N_b + 2L - 1]]^T$ ,  $i=1, 2$ ). In particular, a standard equalizer algorithm designed for single-antenna systems can be employed, e.g., a maximum-likelihood sequence estimator (MLSE) based on the Viterbi algorithm. However, due to the colored noise terms either a whitening prefilter or an Ungerboeck-type of path metric [Ung74] should be used.<sup>38</sup>

Finally, it should be noted that the above TR-STBC can also be extended to MIMO systems with more than two transmit antennas [JGS06], by generalizing other orthogonal designs along the same lines as discussed for Alamouti's transmit diversity scheme.

### 2.3.4 Delay Diversity and Space-Time Trellis Codes

In contrast to STBCs, which are strongly related to (algebraic) block codes used in channel coding, delay diversity and space-time trellis codes (STTCs) are rather related to convolutional codes and trellis-coded modulation (TCM) [Ung82, Ung87]. As in the case of (quasi-) orthogonal STBCs, multiple antennas at the receiver are optional. Both techniques are briefly recapitulated in the sequel.

#### Delay Diversity

Delay diversity is a particularly simple transmit diversity scheme, which was already proposed in 1993 as an enhancement for simulcast networks [Wit93, SW93].<sup>39</sup> Instead of using a complicated space-time mapping, the same information symbols  $a[k]$  are transmitted over all  $M$  antennas, while the information symbols at the  $\mu$ th transmit antenna are delayed by  $(\mu - 1)$  symbol durations ( $1 \leq \mu \leq M$ ). As can be seen in Fig. 2.9, the delay diversity scheme can be regarded as a simple convolutional encoder for systems with multiple transmit antennas. (In particular, if the block length is sufficiently large, the temporal rate of the scheme tends to one.) At the receiver, the information symbols  $a[k]$  can thus be recovered by means of maximum-likelihood sequence estimation (MLSE), e.g., using the Viterbi algorithm (probably, designed for multiple receive antennas). Since the effective memory length of the delay diversity 'encoder' is equal to  $(M - 1)$ , the corresponding trellis diagram will be characterized by  $Q^{M-1}$  trellis states, where  $Q$  again denotes the cardinality of the employed symbol alphabet. Therefore, the decoding complexity grows exponentially with the number of transmit antennas and the number of bits per information symbol, in contrast to the case of (quasi-) orthogonal STBCs.

<sup>38</sup>The application of the Ungerboeck metric is enabled due to the special form of the auto-correlation function of the filtered noise. The overall system is equivalent to an MRC system and is thus optimal.

<sup>39</sup>Simulcast networks are typically applied for broadcasting and paging application. Conventionally, multiple distributed transmitting nodes simultaneously transmit the same message using the same carrier frequency [Wit91].

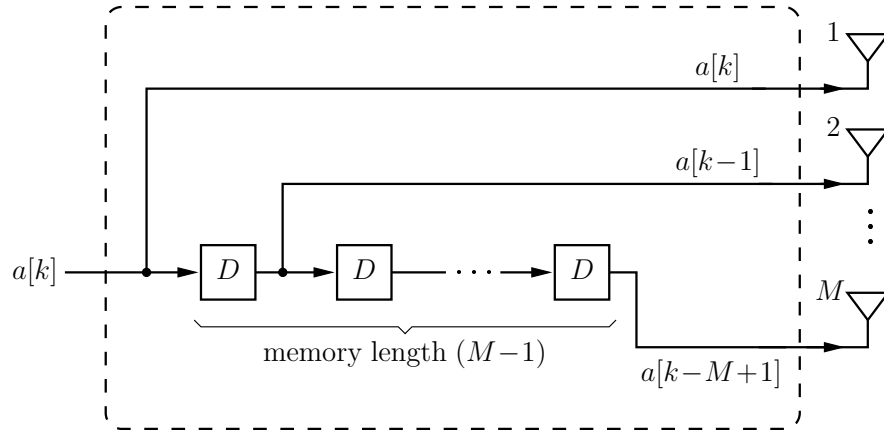


Figure 2.9: The delay diversity scheme interpreted as a simple convolutional encoder for systems with multiple transmit antennas ( $D$  denotes a delay by one symbol duration).

On the other hand, the delay elements employed by the delay diversity scheme can also be regarded as being part of the discrete-time channel model. In the case of a frequency-flat fading channel, the  $k$ th received sample at the  $\nu$ th receive antenna results as

$$y_\nu[k] = \sum_{\mu=1}^M h_{\nu,\mu}[k] a[k-\mu+1] + n_\nu[k], \quad (2.121)$$

where  $h_{\nu,\mu}[k]$  denotes the channel coefficient associated with the  $\mu$ th transmit antenna, and  $n_\nu[k]$  denotes an additive noise sample. Correspondingly, the above discrete-time channel model is equivalent to that of a single-antenna system in the presence of ISI, where

$$\mathbf{h}'[k] := [h'_0[k], \dots, h'_l[k], \dots, h'_{L'}[k]]^T := [h_{\nu,1}[k], \dots, h_{\nu,\mu}[k], \dots, h_{\nu,M}[k]]^T \quad (2.122)$$

denotes the channel vector of the equivalent single-antenna system (memory length  $L' = M - 1$ ). In other words, the delay diversity scheme introduces artificial ISI, i.e., the ‘convolutional decoder’ at the receiver can also be seen as an equalizer algorithm. Due to this, a spatial diversity gain is achieved, since the equalizer algorithm collects the contributions of all channel coefficients  $h_{\nu,1}[k], \dots, h_{\nu,M}[k]$ . To be specific, the delay diversity scheme in conjunction with MLSE at the receiver yields full spatial diversity with regard to the number of transmit and receive antennas [TSC98].

Due to the above properties, the delay diversity scheme is also well suited for MIMO channels with ISI. However, the equalizer at the receiver must be able to cope with the increased channel memory length. If the effective memory length of the given MIMO channel is equal to  $L$ , then the corresponding memory length in the equivalent single-antenna system will be equal to  $L' = L + M - 1$ , which leads to a trellis diagram with  $Q^{L+M-1}$  trellis states. Fig. 2.10 displays the resulting equivalent single-antenna system for the example of  $M = 2$  transmit antennas and a single receive antenna (see also [MH04a]).

Finally, it should be noted that the above choice of the delays is only optimal in the case of a frequency-flat fading channel. As will be discussed in Chapter 5, in the presence of

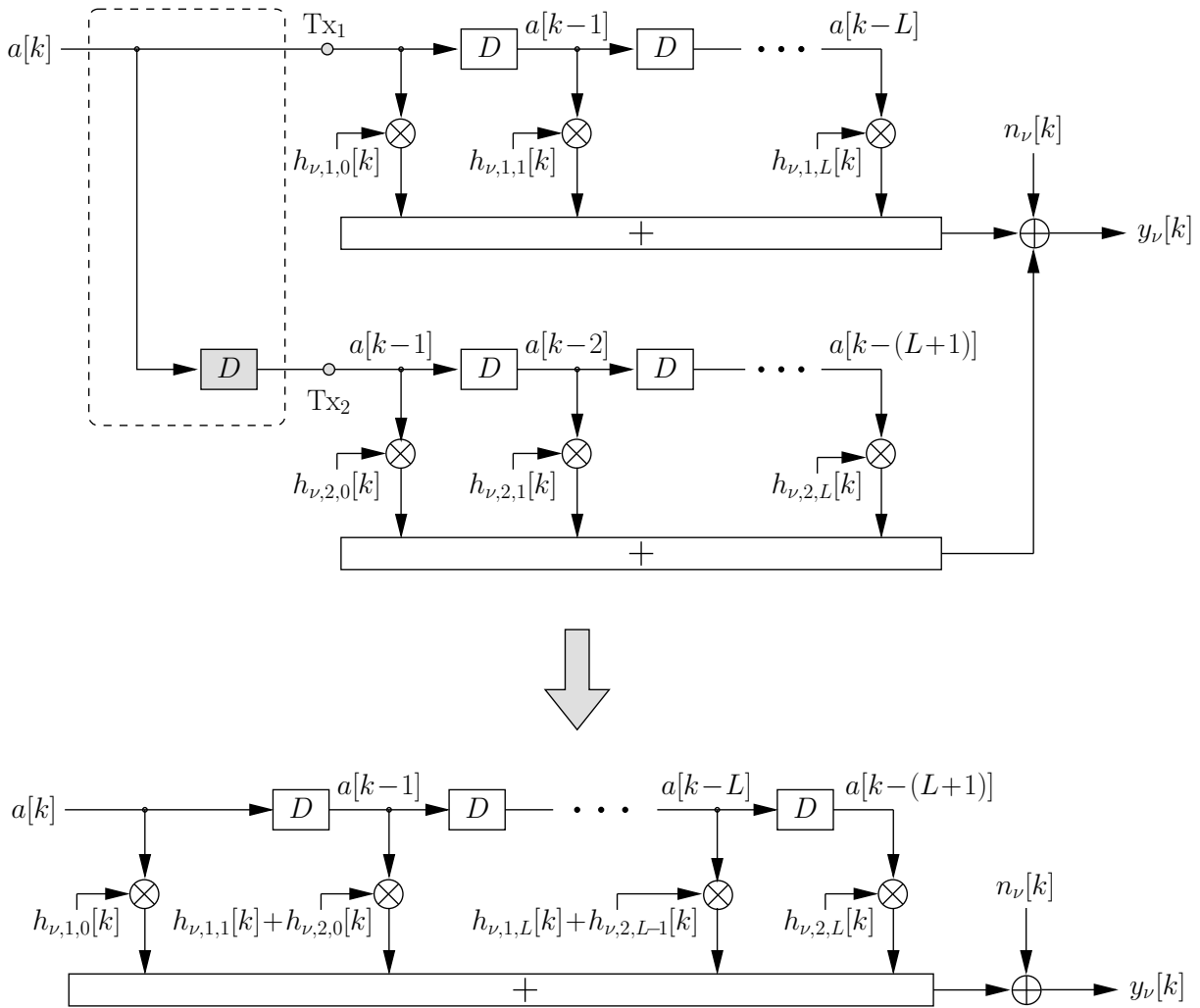


Figure 2.10: Delay diversity scheme in the presence of ISI ( $M=2$  transmit antennas).

frequency-selective fading the performance of delay diversity can be improved significantly by optimizing the delays for the individual transmitted signals (see also [MHS03a]). This gain comes, however, at the expense of a higher receiver complexity. Similar optimized versions of delay diversity for frequency-selective fading channels were also proposed in [GSP01, HSG05, YSG06], partly with regard to additional constraints (such as a fixed receiver complexity).

### Space-Time Trellis Codes

When the simple convolutional encoder depicted in Fig. 2.9 is replaced by a more sophisticated trellis encoder, it is possible to achieve an additional coding gain, while maintaining the full spatial diversity advantage offered by delay diversity [TSC98]. The resulting codes, referred to as space-time trellis codes (STTCs), thus combine modulation and an encoding process incorporating multiple transmit antennas. In this respect, delay di-



versity can be regarded as the simplest STTC, since it does not provide any additional coding gain (similar to a repetition code in channel coding). In principle, STTCs can be constructed for any desired  $Q$ -ary modulation scheme and any number of transmit antennas. In [TSC98] several examples were stated for 4-PSK, 8-PSK, and 16-QAM signal constellations. However, for any STTC the number of trellis states is at least equal to  $Q^{M-1}$  [TSC98], as for delay diversity. Given a fixed modulation scheme and number of antennas, increasing the number of trellis states typically leads to larger coding gains.

Under the assumption of uncorrelated transmit and receive antennas and quasi-static, frequency-flat Rayleigh fading, design criteria for optimal STTCs were derived in [TSC98]. Consider again the MIMO channel model (2.28) introduced in Section 2.2.2 for a block-wise transmission over a quasi-static, frequency-flat fading channel. Moreover, let  $\mathbf{X}$  denote the transmitted space-time code matrix of size  $(M \times N_b)$ , where  $N_b > M$  denotes the block length. The design criteria derived in [TSC98] are based on the pairwise error probability (PEP)

$$P(\mathbf{X} \rightarrow \mathbf{E}) := \mathbb{E} \left\{ \mathbb{Q} \left( \sqrt{\frac{P}{2M\sigma_n^2}} \|\mathbf{H}(\mathbf{X} - \mathbf{E})\|_{\text{F}} \right) \right\}, \quad (2.123)$$

i.e., on the probability that an MLSE detector decides in favor of an erroneous code matrix  $\mathbf{E} \neq \mathbf{X}$ , although the matrix  $\mathbf{X}$  was transmitted. Here  $\mathbb{Q}(x)$  denotes the Gaussian Q-function, cf. Definition C.2 in Appendix C. The expectation is taken with respect to the channel matrix  $\mathbf{H}$ . As earlier,  $P$  denotes the overall average transmit power per channel use. It can be shown that  $P(\mathbf{X} \rightarrow \mathbf{E})$  is bounded above as

$$P(\mathbf{X} \rightarrow \mathbf{E}) \leq \left( \prod_{i=1}^{r_{\text{Tx}}} \xi_{\text{Tx},i} \right)^{-N} \left( \frac{P}{4M\sigma_n^2} \right)^{-r_{\text{Tx}}N}, \quad (2.124)$$

where  $r_{\text{Tx}}$  denotes the rank of the matrix

$$\Psi_{\mathbf{X},\mathbf{E}} := (\mathbf{X} - \mathbf{E})(\mathbf{X} - \mathbf{E})^{\text{H}}, \quad (2.125)$$

and  $\xi_{\text{Tx},1}, \dots, \xi_{\text{Tx},r_{\text{Tx}}}$  denote the corresponding non-zero eigenvalues. Obviously, the upper bound (2.124) decays as  $(P/\sigma_n^2)^{-r_{\text{Tx}}N}$ , i.e., in a log-log plot one observes a slope of  $-r_{\text{Tx}}N$  with growing SNR. Correspondingly, the diversity order of the STTC is given by  $r_{\text{Tx}}N$ . In order to obtain the maximum diversity advantage, the matrix  $\Psi_{\mathbf{X},\mathbf{E}}$  should therefore always be of full rank, for any pair  $(\mathbf{X}, \mathbf{E})$  of code matrices ( $\mathbf{X} \neq \mathbf{E}$ ):

$$r_{\text{Tx}} = \text{rank}(\Psi_{\mathbf{X},\mathbf{E}}) \stackrel{!}{=} M. \quad (2.126)$$

By this means, the same diversity order as with delay diversity is achieved. Moreover, in order to minimize the upper bound (2.124), the expression

$$\left( \prod_{i=1}^M \xi_{\text{Tx},i} \right) = \det(\Psi_{\mathbf{X},\mathbf{E}}) \quad (2.127)$$

should be maximized. The expression  $\det(\Psi_{\mathbf{X},\mathbf{E}})$  thus represents an additional coding gain. Correspondingly, for a given modulation scheme, a given number of transmit antennas, and a given trellis complexity, one should search among all full-diversity STTCs, in order to find that STTC which offers the largest minimum determinant  $\det(\Psi_{\mathbf{X},\mathbf{E}})$ , i.e.,

$$\min_{\substack{(\mathbf{X},\mathbf{E}) \\ \mathbf{X} \neq \mathbf{E}}} \{\det(\Psi_{\mathbf{X},\mathbf{E}})\} \stackrel{!}{\rightarrow} \max. \quad (2.128)$$

The above performance criteria (2.126) and (2.128) are known as the *rank* and the *determinant criterion*, respectively.

In [TSC98], also modified design criteria were presented for the case of Rician fading, correlated transmit and receive antennas, and fast fading. Specifically, it was shown that in the case of correlated antennas, the rank criterion (2.126) is still valid, whereas a modified determinant criterion results. The case of correlated antennas will be discussed more detailed in Section 3.2.4. In a subsequent paper, the issues of frequency-selective fading, non-perfect channel estimation, and very large fading rates were treated [TNSC99b]. In particular, it was shown that the design criteria derived in [TSC98] are quite robust with regard to these effects. For example, the diversity order of the STTCs in [TSC98] is maintained. However, some degradations with regard to the coding gain were observed.<sup>40</sup> Further details concerning the literature on (optimized) STTCs as well as extensions to frequency-selective fading channels have already been discussed in Section 2.1.2.

## 2.4 Chapter Summary

Wireless systems with multiple transmit and receive antennas, so-called multiple-input multiple-output (MIMO) systems, offer huge advantages over systems employing a single antenna at either end of the link. In principle, multiple antennas can be utilized to increase the spectral efficiency and the error performance of a system. Moreover, beamforming gains can be achieved by steering the antenna patterns in certain desired directions.

In the first part of this chapter, a detailed overview of transmission and reception techniques for MIMO communication systems was provided. In particular, these techniques were categorized as spatial multiplexing techniques, spatial diversity techniques, and smart antenna techniques. Following this, further possible categorizations were discussed, and the focus of the thesis was highlighted. In the second part, the system and channel model for a general MIMO system was introduced, including spatial and temporal correlations as well as intersymbol interference effects due to frequency-selective fading. To this end, a statistical discrete-time MIMO channel model was derived in a transparent fashion, followed by a rigorous analysis of the statistical properties. In the final part of the chapter, certain space-time coding techniques that are of special interest in this thesis were discussed in more detail. As novel contributions, the orthogonality loss of orthogonal space-time block codes in the presence of various channel impairments was discussed, and improved receiver structures for Alamouti's transmit diversity scheme were proposed. The performance of the proposed receiver structures will be illustrated in Chapter 5.

<sup>40</sup>This is particularly true for the case of non-perfect channel estimation in conjunction with a large number of trellis states [TNSC99b].

## Chapter 3

# Distributed and Co-located MIMO Systems

**T**HE CAPACITY of MIMO systems, i.e., the highest data rate at which information can be transmitted with an arbitrarily small error probability [CT91, Ch. 8], was shown to grow (approximately) linearly with the minimum of the number of transmit and receive antennas [Fos96, FG98, Tel99]. Correspondingly, multiple antennas constitute a promising means to increase the spectral efficiency of a system. In addition to this, it was shown in [TSC98, Ala98, TJC99b] that multiple antennas can also be utilized, in order to provide a spatial diversity gain and thus to improve the error performance of a system.

In the literature on MIMO systems, typically quite restrictive assumptions are made concerning the antenna spacings at transmitter and receiver. On the one hand, it is typically assumed that the individual antenna elements are co-located, i.e., they belong to some sort of antenna array, cf. Fig. 1.2 (a) in Chapter 1. On the other hand, the antenna spacings are often assumed to be sufficiently large, so as to justify the assumption of statistically independent fading on the individual transmission links. In this thesis, these strict assumptions will be relaxed. On the one hand, sufficient antenna spacings in terms of low fading correlations cannot always be guaranteed in a practical system, cf. Fig. 1.2 (b).<sup>1</sup> On the other hand, the concept of MIMO systems can be transferred to cooperative wireless networks [NHH04], where multiple distributed transmitting or receiving nodes cooperate in terms of a joint transmission/reception strategy, cf. Fig. 1.2 (c). By this means, a virtual antenna array is established so that the cooperating nodes, possibly equipped with only a single antenna, can enjoy some of the benefits offered by (conventional) MIMO systems with co-located antennas.

In several publications, it was shown that spatial fading correlations caused by insufficient antenna spacings can lead to significant degradations in capacity and error performance. As will be seen, this is also the case when the individual transmit and/or receive antennas are distributed on a large scale. Although at the first glance, co-located

---

<sup>1</sup>Note that the notion of insufficient antenna spacings is relative, because it depends not only on the geometry of the employed antenna arrays, but also on the carrier frequency, the richness of scattering from the physical environment, and the angular power distribution of the transmitted and received signals (cf. Section F.3 in Appendix F).

and distributed MIMO systems might have little in common, we will show that these two types of systems can, in fact, be treated in a single unifying framework. In particular, for the case of flat Rayleigh fading, we will show that any MIMO system with co-located antennas obeying the Kronecker-correlation model (cf. Section 2.2.1), can be transformed into an equivalent (with regard to the capacity distribution) MIMO system with distributed antennas, and vice versa. With regard to space-time coding, we will show that (asymptotically) both MIMO systems lead to identical pairwise error probabilities (PEPs). Moreover, for the special case of orthogonal space-time block codes (OSTBCs), even identical symbol and bit error rates result. The equivalence proofs presented here are based on two unitary matrix transforms. The first transform associates a given co-located MIMO system with an equivalent distributed MIMO system. This transform is related to the well-known Karhunen-Loève transform (KLT) [SW02, Ch. 8.5], which is often used in the literature, in order to analyze correlated systems. As a novel contribution, we introduce a second transform which associates a given distributed MIMO system with an equivalent co-located MIMO system [MH05].

An important implication of the above equivalence is that optimal transmission and reception strategies originally developed for spatially correlated MIMO systems can be reused for distributed MIMO systems, and vice versa, without any loss of optimality. Optimal transmit power allocation strategies and diversity reception schemes for spatially correlated and distributed MIMO systems will be considered in Chapter 4.

The remainder of this chapter is organized as follows. To start with, examples of cooperative wireless networks are discussed in Section 3.1. The equivalence of distributed and co-located MIMO systems is addressed in Section 3.2. Specifically, a simple performance measure originally proposed for spatially correlated MIMO systems is considered [IN03], and the equivalent measure for distributed systems is derived. Generalizations of Section 3.2 to other fading models are considered in Section 3.3. In addition to this, more general spatial correlation models are discussed. Finally, the value of macroscopic diversity effects in distributed MIMO systems is studied in Section 3.4. The most important results of this chapter are summarized in Section 3.5.

### 3.1 Examples of Distributed MIMO Systems

The concept of cooperative wireless networks has recently gained considerable attention [NHH04]. On the one hand, cooperating network nodes build the basis of ad-hoc networks, which are envisioned for sensor networks [I05b], public safety communication networks [I06], or tactical networks for military applications [I04a, I05a]. For example, the benefits of cooperating nodes for wireless sensor networks were considered in [Li03b, CGB04, Li04, LCL05b]. On the other hand, cooperating nodes also promise benefits for hierarchical types of networks, e.g., cellular networks [PWS+04, HYFP04].

Throughout this thesis, we will regard cooperating transmitting or receiving nodes as a single entity, i.e., as a virtual antenna array. Algorithms and protocols that manage the interaction between the cooperating network nodes are beyond scope. In particular, in the case of distributed transmitting nodes, we assume that all nodes have the same (error-free) message to be transmitted at their disposal, just as in a co-located MIMO

system. Therefore, all performance results presented in this thesis constitute ultimate limits for practical systems. At the same time, these performance limits provide very general insights, since they do not depend on a specific protocol.

**Remark 3.1 (Distributed transmitting nodes)**

In a distributed scenario, the message to be transmitted must first be passed to all cooperating transmitting nodes. In the case of fixed stations (e.g., base stations), this can, for example, be realized via some fixed backbone network. In the case of mobile nodes, however, the exchange of messages must be performed using wireless resources [BS03a]. Strictly speaking, this causes a capacity penalty in comparison to a co-located system [Uts06a]. In addition to this, the messages passed to the individual transmitting nodes may be erroneous. This can lead to error propagation effects [SB05] and thus to further performance degradations, compared to a co-located system. As a counter measure, a cyclic redundancy check (CRC) code can be used. By this means, each transmitting node can first try to decode the received message correctly. In case of decoding errors, it can then decide not to take part in the cooperative transmission process, so as to prevent error propagation effects.

Consider first a MIMO system with distributed transmit antennas and co-located receive antennas, as depicted in Fig. 3.1. In general, all nodes within the network may be equipped with multiple antennas. To this end, let  $T_n$  denote the number of transmitting nodes, and  $M_i$  the number of antennas employed at the  $i$ th transmitting node ( $i = 1, \dots, T_n$ ). Moreover, let  $M$  denote the overall number of transmit antennas, i.e.,

$$\sum_{i=1}^{T_n} M_i =: M, \quad (3.1)$$

and let  $N$  denote the number of receive antennas used (as earlier).

The cooperating transmitting nodes may, for example, be part of a simulcast network employed for broadcasting or paging applications [Wit91, KSH97, WSW+06], serving a certain area around the receiving node. In this example, the receiving node would represent a single user (with fixed position) or a subscriber home equipped with a fixed antenna array. Another application example are future mobile radio systems, where joint transmission strategies based on distributed wireless access points are envisioned [ZZX+03, WSLW03]. Finally, the cooperating transmitting nodes may also be wireless (decode-and-forward) relays that forward messages of a certain source node to a certain destination node (in a cooperative fashion). In this example, the receiving node would represent the destination node. Relay-assisted cooperative wireless networks have already been addressed in a considerable number of papers, e.g. [ALK03, BS03a, KDA03, LW03, SEA03, Li03b, HA03, Doh03, JHHN04, ZHF04, DHDA04, CGB04, NBK04, AK04, SE04, PWS+04, BFY04, NHH04, MTH04, HYFP04, MMA04, Li04, LTW04, MHSD05, RCG05, SB05, LV05a, JH05b, LX05a, SE05, DH05, HSN06, AK06, BKRL06, YSL06a, UK06, WZA06, UCF06, WYG06, JH06, YS06, YSL06b, YB07]. These publications cover also relay-assisted networks, where received messages are only amplified and forwarded, rather than decoding and re-encoding them. Some of the above papers explicitly propose the use of distributed space-time codes among

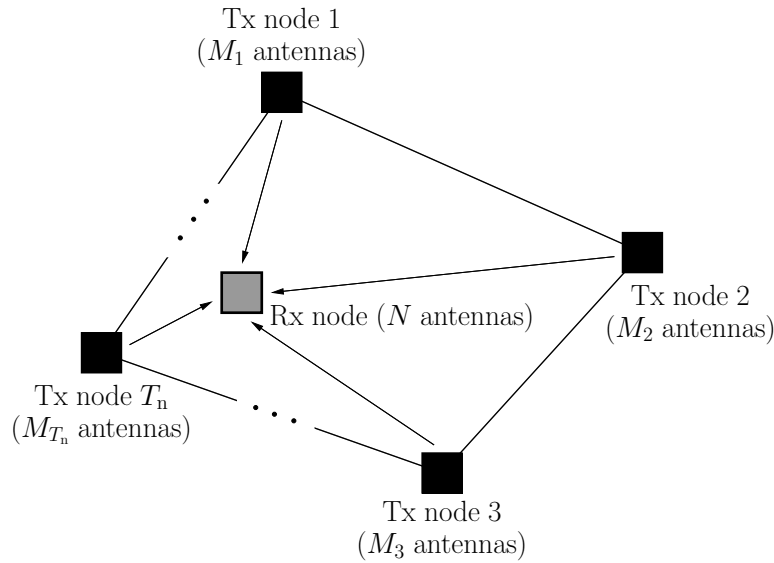


Figure 3.1: Cooperative wireless scenario with distributed transmit antennas and co-located receive antennas.

the cooperating relays. To this end, existing space-time coding techniques originally designed for co-located MIMO systems can be reused.

In the case of distributed receive antennas (and co-located transmit antennas), we assume  $R_n$  cooperating receiving nodes, each equipped with  $N_j$  antennas, where

$$\sum_{j=1}^{R_n} N_j =: N. \quad (3.2)$$

The receiving nodes are assumed to perform a joint reception strategy by passing (processed versions of) their received signals to a central entity (without errors). The cooperating receiving nodes may, for example, belong to a distributed wireless access network for mobile radio applications [ZZX+03, WSLW03]. Alternatively, they may be part of a reach-back network for wireless sensors serving a certain geographical area. The transmitting node would then represent a single wireless sensor broadcasting its measurements to the reach-back network.

The following section starts with specializing the statistical discrete-time channel model introduced in Section 2.2.2 to the case of distributed MIMO systems. Following this, the (asymptotic) equivalence of co-located and distributed MIMO systems is proven, in terms of the resulting capacity distribution, the pairwise error probability of a general space-time code, and the symbol error probability of an orthogonal space-time block code. The most important results are summarized in Theorems 3.1 to 3.3. For the time being, we restrict ourselves to the case of frequency-flat Rayleigh fading. Generalizations to other fading models are considered in Section 3.3.



## 3.2 Equivalence of Distributed and Co-located MIMO Systems

Consider a MIMO system with  $M$  transmit and  $N$  receive antennas, where the antennas at both ends are either co-located or distributed. All antennas are assumed to have quasi-fixed positions. For the time being, we assume perfect carrier frequency synchronization among all transmit and receive antennas. Moreover, we assume that the propagation delay differences between the individual transmission links are small compared to the symbol duration.<sup>2</sup> The impact of non-perfect timing and non-perfect carrier-frequency synchronization will be considered in Chapter 5.

In the sequel, we focus on the discrete-time channel model for quasi-static frequency-flat fading introduced in Section 2.2.2:

$$\mathbf{y}[k] = \mathbf{H}\mathbf{x}[k] + \mathbf{n}[k], \quad (3.3)$$

where  $\mathbf{y}[k] \in \mathbb{C}^N$  denotes the  $k$ th received vector,  $\mathbf{H} \in \mathbb{C}^{N \times M}$  the  $(N \times M)$ -channel matrix,  $\mathbf{x}[k] \in \mathbb{C}^M$  the  $k$ th transmitted vector, and  $\mathbf{n}[k] \in \mathbb{C}^N$  the  $k$ th additive noise vector. The time index  $k$  of the channel matrix has been dropped for convenience. We assume that  $\mathbf{H}$ ,  $\mathbf{x}[k]$  and  $\mathbf{n}[k]$  are statistically independent. The channel matrix  $\mathbf{H}$  is assumed to be constant over an entire block of  $N_b$  transmitted vectors  $\mathbf{x}[k]$ , and changes randomly from one block to the next. Correspondingly, we will sometimes use the system model (2.28) for block-wise transmission (cf. Section 2.2.2). For the time being we assume Rayleigh fading, i.e., the entries  $h_{\nu,\mu}$  of  $\mathbf{H}$  ( $\mu = 1, \dots, M$ ,  $\nu = 1, \dots, N$ ) are zero-mean circularly symmetric complex Gaussian random variables with variance  $\sigma_{h_{\nu,\mu}}^2/2$  per real dimension, i.e.,  $h_{\nu,\mu} \sim \mathcal{CN}(0, \sigma_{h_{\nu,\mu}}^2)$ . The instantaneous realizations of the channel matrix  $\mathbf{H}$  are assumed to be perfectly known at the receiver. The entries  $x_\mu[k]$  of the transmitted vector  $\mathbf{x}[k]$  are treated as zero-mean random variables with variance  $\sigma_{x,\mu}^2$ . Possibly, they are correlated due to some underlying space-time code. We assume an overall average transmit power constraint of  $P$ , i.e.,

$$\sum_{\mu=1}^M \sigma_{x,\mu}^2 \stackrel{!}{\leq} P. \quad (3.4)$$

For the time being, we consider the case of equal power allocation among the transmit antennas, i.e.,  $\sigma_{x,\mu}^2 = P/M$  for all  $\mu = 1, \dots, M$ . Alternative transmit power allocation strategies will be considered in Chapter 4. Finally, the entries of  $\mathbf{n}[k]$  are assumed to be zero-mean, spatially and temporally white complex Gaussian random variables with variance  $\sigma_n^2/2$  per real dimension, i.e.,  $n_\nu[k] \sim \mathcal{CN}(0, \sigma_n^2)$  and

$$\mathbb{E} \{ \mathbf{n}[k] \mathbf{n}^H[k'] \} = \sigma_n^2 \cdot \delta[k-k'] \cdot \mathbf{I}_N. \quad (3.5)$$

Next, we specialize the above model to the case of co-located and distributed antennas.

<sup>2</sup>This is a reasonable assumption, as long as the distributed transmit or receive antennas are not spaced too far apart from each other, or if, in the case of distributed transmit antennas, sufficiently accurate timing advance techniques are employed at the transmitter side. In the case of distributed receive antennas, propagation delay differences can be compensated by adjusting the sampling phase accordingly.



### 3.2.1 System Model for Co-located MIMO Systems

In the case of co-located antennas, the individual transmission links from the transmit to the receive antennas may be correlated, due to insufficient antenna spacings. Let

$$\sigma_{h_{\nu,\mu},\nu',\mu'}^2 := \mathbb{E}\{h_{\nu,\mu} h_{\nu',\mu'}^*\} = \sigma_{h_{\nu',\mu'},\nu,\mu}^{2*} \quad (3.6)$$

denote the covariance between two channel coefficients  $h_{\nu,\mu}$  and  $h_{\nu',\mu'}$ , and let

$$\rho_{h_{\nu,\mu},\nu',\mu'} := \sigma_{h_{\nu,\mu},\nu',\mu'}^2 / \sqrt{\sigma_{h_{\nu,\mu}}^2 \sigma_{h_{\nu',\mu'}}^2} \quad (3.7)$$

denote the corresponding spatial correlation. For the time being, we consider the Kronecker correlation model (cf. Section 2.2.1), i.e.,

$$\rho_{h_{\nu,\mu},\nu',\mu'} := \rho_{\text{Tx},\mu,\mu'} \cdot \rho_{\text{Rx},\nu,\nu'} \quad (3.8)$$

for all indices  $\mu, \mu', \nu, \nu'$ . The channel matrix  $\mathbf{H}$  can thus be written as

$$\mathbf{H} := \mathbf{\Xi}_{\mathbf{h}} \odot \left( \mathbf{R}_{\mathbf{h},\text{Rx}}^{1/2} \mathbf{H}' \mathbf{R}_{\mathbf{h},\text{Tx}}^{1/2} \right) \quad (3.9)$$

(cf. Remark 2.2), where the matrix  $\mathbf{\Xi}_{\mathbf{h}}$  is given by

$$\mathbf{\Xi}_{\mathbf{h}} := \begin{bmatrix} \sqrt{\sigma_{h_{1,1}}^2} & \cdots & \sqrt{\sigma_{h_{1,M}}^2} \\ \vdots & \ddots & \vdots \\ \sqrt{\sigma_{h_{N,1}}^2} & \cdots & \sqrt{\sigma_{h_{N,M}}^2} \end{bmatrix}, \quad (3.10)$$

and

$$\mathbf{R}_{\mathbf{h},\text{Tx}} := \begin{bmatrix} 1 & \cdots & \rho_{\text{Tx},1,M} \\ \vdots & \ddots & \vdots \\ \rho_{\text{Tx},1,M}^* & \cdots & 1 \end{bmatrix} \quad \text{and} \quad \mathbf{R}_{\mathbf{h},\text{Rx}} := \begin{bmatrix} 1 & \cdots & \rho_{\text{Rx},1,N} \\ \vdots & \ddots & \vdots \\ \rho_{\text{Rx},1,N}^* & \cdots & 1 \end{bmatrix} \quad (3.11)$$

denote the transmitter and receiver correlation matrix ( $\text{tr}(\mathbf{R}_{\mathbf{h},\text{Tx}}) = M$ ,  $\text{tr}(\mathbf{R}_{\mathbf{h},\text{Rx}}) = N$ ). Finally,  $\mathbf{H}'$  denotes an uncorrelated ( $N \times M$ )-channel matrix with entries  $h'_{\nu,\mu} \sim \mathcal{CN}(0, 1)$ .

If congenerous, co-located antenna elements are used at the transmitter and the receiver side, it is reasonable to assume that the variance of the channel coefficients  $h_{\nu,\mu}$  is the same for all transmission links, since all links experience, on average, similar propagation conditions. In particular, the individual link lengths are the same. Correspondingly, we define  $\sigma_{h_{\nu,\mu}}^2 := \sigma_h^2$  for all indices  $\mu, \nu$  and write  $\mathbf{H}$  according to

$$\mathbf{H} := \mathbf{R}_{\mathbf{h},\text{Rx}}^{1/2} \mathbf{H}' \mathbf{R}_{\mathbf{h},\text{Tx}}^{1/2} \quad (3.12)$$

( $h'_{\nu,\mu} \sim \mathcal{CN}(0, \sigma_h^2)$  and uncorrelated). The transmitter and receiver correlation matrix can then be written as

$$\mathbf{R}_{\mathbf{h},\text{Tx}} = \mathbb{E}\{\mathbf{H}^{\text{H}}\mathbf{H}\} / (N\sigma_h^2) \quad \text{and} \quad \mathbf{R}_{\mathbf{h},\text{Rx}} = \mathbb{E}\{\mathbf{H}\mathbf{H}^{\text{H}}\} / (M\sigma_h^2). \quad (3.13)$$

In the sequel, we denote the eigenvalue decompositions (EVDs) of  $\mathbf{R}_{\mathbf{h},\text{Tx}}$  and  $\mathbf{R}_{\mathbf{h},\text{Rx}}$  as

$$\mathbf{R}_{\mathbf{h},\text{Tx}} = \mathbf{U}_{\text{Tx}} \mathbf{\Lambda}_{\mathbf{h},\text{Tx}} \mathbf{U}_{\text{Tx}}^{\text{H}} \quad \text{and} \quad \mathbf{R}_{\mathbf{h},\text{Rx}} = \mathbf{U}_{\text{Rx}} \mathbf{\Lambda}_{\mathbf{h},\text{Rx}} \mathbf{U}_{\text{Rx}}^{\text{H}}, \quad (3.14)$$

where  $\mathbf{\Lambda}_{\mathbf{h},\text{Tx}} := \text{diag}([\lambda_{\text{Tx},1}, \dots, \lambda_{\text{Tx},M}])$  and  $\mathbf{\Lambda}_{\mathbf{h},\text{Rx}} := \text{diag}([\lambda_{\text{Rx},1}, \dots, \lambda_{\text{Rx},N}])$  contain the eigenvalues of  $\mathbf{R}_{\mathbf{h},\text{Tx}}$  and  $\mathbf{R}_{\mathbf{h},\text{Rx}}$ , and  $\mathbf{U}_{\text{Tx}}$  and  $\mathbf{U}_{\text{Rx}}$  are unitary matrices ( $\mathbf{U}_{\text{Tx}}^{\text{H}} \mathbf{U}_{\text{Tx}} = \mathbf{I}_M$ ,  $\mathbf{U}_{\text{Rx}}^{\text{H}} \mathbf{U}_{\text{Rx}} = \mathbf{I}_N$ ), cf. Section D.4 in Appendix D.

### 3.2.2 System Model for Distributed MIMO Systems

Next, we consider a MIMO system with distributed antennas. To start with, we focus on the case of distributed transmit antennas and co-located receive antennas, as depicted in Fig. 3.1. The general expression (3.9) for the channel matrix  $\mathbf{H}$  applies also for MIMO systems with distributed (transmit) antennas. For simplicity we assume in the sequel that all transmit antennas are uncorrelated. (For antennas belonging to different transmitting nodes, this condition is surely fulfilled.)

Similar to Section 3.2.1, it is again reasonable to assume that all channel coefficients associated with the same transmitting node  $i$  ( $i = 1, \dots, T_n$ ) have the same variance  $\sigma_{h,i}^2$ . Correspondingly, assuming an appropriate order of the columns of  $\mathbf{H}$ , we obtain

$$\mathbb{E}\{\mathbf{H}^H\mathbf{H}\}/N = \text{diag}([\sigma_{h,1}^2, \dots, \sigma_{h,i}^2, \dots, \sigma_{h,T_n}^2]) =: \mathbf{\Sigma}_{\mathbf{h},\text{Tx}}, \quad (3.15)$$

where each variance  $\sigma_{h,i}^2$  occurs  $M_i$  times. Following the Kronecker-correlation model, we can thus write

$$\mathbf{H} = \mathbf{R}_{\mathbf{h},\text{Rx}}^{1/2} \mathbf{H}' \mathbf{\Sigma}_{\mathbf{h},\text{Tx}}^{1/2} \quad (3.16)$$

( $h'_{\nu,\mu} \sim \mathcal{CN}(0, 1)$  and uncorrelated), cf. (3.12). Typically, the variances  $\sigma_{h,i}^2$  (and thus the average link SNRs) vary significantly between the individual transmitting nodes, (mainly) due to different link lengths. Since in a rich-scattering environment the average received power decays at least with the square of the link length [Ste94, Ch. 1.2], comparatively small link length differences already lead to considerable differences in the average link SNRs. Additionally, the variances  $\sigma_{h,i}^2$  may include shadowing effects.<sup>3</sup>

Similarly, in a MIMO system with co-located transmit antennas and distributed receive antennas, we have

$$\mathbb{E}\{\mathbf{H}\mathbf{H}^H\}/M = \text{diag}([\sigma_{h,1}^2, \dots, \sigma_{h,j}^2, \dots, \sigma_{h,R_n}^2]) =: \mathbf{\Sigma}_{\mathbf{h},\text{Rx}} \quad (3.17)$$

and

$$\mathbf{H} = \mathbf{\Sigma}_{\mathbf{h},\text{Rx}}^{1/2} \mathbf{H}' \mathbf{R}_{\mathbf{h},\text{Tx}}^{1/2} \quad (3.18)$$

( $h'_{\nu,\mu} \sim \mathcal{CN}(0, 1)$  and uncorrelated), where  $\sigma_{h,j}^2$  ( $1 \leq j \leq R_n$ ) denotes the channel variance associated with the  $j$ th receiving node.

In order to treat co-located and distributed MIMO systems in a single, unifying framework, we normalize the overall average power of the channel coefficients as follows:<sup>4</sup>

$$\text{tr}(\mathbb{E}\{\text{vec}(\mathbf{H})\text{vec}(\mathbf{H})^H\}) \stackrel{!}{=} MN. \quad (3.19)$$

For MIMO systems with co-located antennas, cf. (3.12) and (3.13), this means we set  $\sigma_h^2 := 1$ . In this case, we get

$$\mathbb{E}\{\text{vec}(\mathbf{H})\text{vec}(\mathbf{H})^H\} = \mathbf{R}_{\mathbf{h},\text{Tx}} \otimes \mathbf{R}_{\mathbf{h},\text{Rx}}. \quad (3.20)$$

For MIMO systems with distributed transmit/receive antennas, it means we set

$$\text{tr}(\mathbf{\Sigma}_{\mathbf{h},\text{Tx}}) \stackrel{!}{=} M \quad \text{or} \quad \text{tr}(\mathbf{\Sigma}_{\mathbf{h},\text{Rx}}) \stackrel{!}{=} N. \quad (3.21)$$

<sup>3</sup>As long as the transmitting nodes have quasi-fixed positions and a single receiving node is considered (also with a fixed position), no macroscopic diversity is available. Shadowing effects are fully captured by the channel variances  $\sigma_{h,i}^2$ . The benefits of macroscopic diversity become only apparent, when some mobility is assumed and different positions of the receiving node are considered. The value of macroscopic diversity in distributed MIMO systems is addressed in Section 3.4.

<sup>4</sup>In order to provide a fair comparison between distributed and co-located MIMO systems, the overall average received power must be fixed.

### 3.2.3 Capacity Distribution of MIMO Systems

In the sequel, we will show that for any MIMO system with co-located antennas obeying the Kronecker-correlation model (3.12), an equivalent MIMO system with distributed antennas can be found, and vice versa, in the sense that both systems are characterized by identical capacity distributions.

For the time being, we assume that channel state information is solely available at the receiver, but not at the transmitter. (The case of instantaneous and statistical channel knowledge at the transmitter side is considered in Chapter 4.) In this case, given a fixed realization of the random channel matrix  $\underline{\mathbf{H}}$ , the capacity of the MIMO system (3.3) is given by [FG98]

$$C(\mathbf{H}) = \log_2 \det \left( \mathbf{I}_N + \frac{P}{M\sigma_n^2} \mathbf{H}\mathbf{H}^H \right) \text{ bit/channel use} \quad (3.22)$$

(cf. Appendix G). The capacity  $C(\mathbf{H})$  is in the following called instantaneous capacity. Obviously,  $C(\mathbf{H}) =: r$  itself is a random variable, and its probability density function (PDF) is denoted as  $p_r(r)$  in the sequel.

#### MIMO Systems with Co-located Antennas

To start with, consider a MIMO system with co-located transmit and receive antennas and an overall spatial covariance matrix according to (3.20). Let

$$\mathbf{R}_A := \begin{cases} \mathbf{R}_{\mathbf{h},\text{Tx}} & \text{if } M < N \\ \mathbf{R}_{\mathbf{h},\text{Rx}} & \text{else} \end{cases} \quad \text{and} \quad \mathbf{R}_B := \begin{cases} \mathbf{R}_{\mathbf{h},\text{Rx}} & \text{if } M < N \\ \mathbf{R}_{\mathbf{h},\text{Tx}} & \text{else} \end{cases}, \quad (3.23)$$

i.e., the correlation matrix  $\mathbf{R}_A$  is always related to the side with less antennas. Moreover, let

$$\tilde{M} := \min(M, N), \quad \tilde{N} := \max(M, N). \quad (3.24)$$

Finally, let  $\lambda_{A,1}, \dots, \lambda_{A,\tilde{M}}$  denote the eigenvalues of  $\mathbf{R}_A$  and  $\lambda_{B,1}, \dots, \lambda_{B,\tilde{N}}$  the eigenvalues of  $\mathbf{R}_B$ . Without loss of generality, we assume in the sequel that both  $\mathbf{R}_A$  and  $\mathbf{R}_B$  have full rank.<sup>5</sup> Moreover, for simplicity, we assume that both matrices  $\mathbf{R}_A$  and  $\mathbf{R}_B$  have distinct eigenvalues, while the following order is employed in the sequel:

$$0 < \lambda_{A,1} < \dots < \lambda_{A,\tilde{M}} \quad \text{and} \quad 0 < \lambda_{B,1} < \dots < \lambda_{B,\tilde{N}}. \quad (3.25)$$

Under these premises, a closed-form expression for the characteristic function (cf. Definition C.17, Appendix C) of the instantaneous capacity  $r = C(\mathbf{H})$  was evaluated in [PSL04]. The result is of form

$$\mathbb{C}\{r\}(\mathbf{j}\omega) := \mathbb{E}\{e^{\mathbf{j}\omega r}\} = \frac{K_{\text{SNR}} \varphi(\mathbf{j}\omega)}{\psi(\mathbf{R}_A, \mathbf{R}_B)} \det \left( \begin{bmatrix} \mathbf{V}(\mathbf{R}_B) \\ \mathbf{M}(\mathbf{R}_A, \mathbf{R}_B, \mathbf{j}\omega) \end{bmatrix} \right), \quad (3.26)$$

where  $\omega \in \mathbb{R}$  and

$$K_{\text{SNR}} = \left( \frac{P}{M\sigma_n^2} \right)^{-\tilde{M}(\tilde{M}-1)/2}, \quad (3.27)$$

<sup>5</sup>Any MIMO system with rank-deficient transmitter/receiver correlation matrix can be transformed into an equivalent MIMO system with full-rank correlation matrices [Kie05].

$$\varphi(j\omega) = \prod_{i=1}^{\tilde{M}-1} (i + j\omega \log_2 e)^{-i}, \quad (3.28)$$

and

$$\psi(\mathbf{R}_A, \mathbf{R}_B) = \prod_{1 \leq j < i \leq \tilde{M}} (\lambda_{A,i} - \lambda_{A,j}) \prod_{1 \leq j < i \leq \tilde{N}} (\lambda_{B,i} - \lambda_{B,j}). \quad (3.29)$$

Moreover,  $\mathbf{V}(\mathbf{R}_B)$  is a Vandermonde matrix of dimension  $(\tilde{N} - \tilde{M}) \times \tilde{N}$  with entries

$$[\mathbf{V}(\mathbf{R}_B)]_{i,j} = \lambda_{B,j}^{i-1}, \quad i = 1, \dots, (\tilde{N} - \tilde{M}), \quad j = 1, \dots, \tilde{N}, \quad (3.30)$$

and  $\mathbf{M}(\mathbf{R}_A, \mathbf{R}_B, j\omega)$  is an  $(\tilde{M} \times \tilde{N})$ -matrix with entries

$$[\mathbf{M}(\mathbf{R}_A, \mathbf{R}_B, j\omega)]_{i,j} = \lambda_{B,j}^{\tilde{N}-\tilde{M}-1} \int_0^\infty e^{-x/\lambda_{B,j}} \left(1 + \frac{P}{M\sigma_n^2} \lambda_{A,i} x\right)^{\tilde{M}-1+j\omega \log_2 e} dx \quad (3.31)$$

( $i=1, \dots, \tilde{M}$ ,  $j=1, \dots, \tilde{N}$ ).<sup>6</sup> An alternative closed-form expression for  $\mathbf{C}\{r\}(j\omega)$  that is based on a specific hypergeometric function of matrix arguments was derived in [Kie05]. In particular, specialized expressions were derived in [Kie05] for the case of one-sided spatial correlation (i.e.,  $\mathbf{R}_{\mathbf{h},\text{Tx}} = \mathbf{I}_M$  or  $\mathbf{R}_{\mathbf{h},\text{Rx}} = \mathbf{I}_N$ ) and for the case of uncorrelated antennas. (For the uncorrelated case, a closed-form expression for  $\mathbf{C}\{r\}(j\omega)$  was also stated in [PSL04].)

Obviously, the characteristic function  $\mathbf{C}\{r\}(j\omega)$  depends solely on the eigenvalues of  $\mathbf{R}_{\mathbf{h},\text{Tx}}$  and  $\mathbf{R}_{\mathbf{h},\text{Rx}}$ , but not on specific entries of  $\mathbf{R}_{\mathbf{h},\text{Tx}}$  or  $\mathbf{R}_{\mathbf{h},\text{Rx}}$ . Correspondingly, any MIMO system having an overall spatial covariance matrix

$$\mathbf{E}\{\text{vec}(\mathbf{H})\text{vec}(\mathbf{H})^H\} = (\mathbf{U}_M \mathbf{R}_{\mathbf{h},\text{Tx}} \mathbf{U}_M^H) \otimes (\mathbf{U}_N \mathbf{R}_{\mathbf{h},\text{Rx}} \mathbf{U}_N^H) =: \mathbf{R}'_{\text{Tx}} \otimes \mathbf{R}'_{\text{Rx}}, \quad (3.32)$$

where  $\mathbf{U}_M$  is an arbitrary unitary  $(M \times M)$ -matrix<sup>7</sup> and  $\mathbf{U}_N$  an arbitrary unitary  $(N \times N)$ -matrix, will exhibit exactly the same characteristic function (3.26) of the instantaneous capacity (since the eigenvalues of  $\mathbf{R}'_{\text{Tx}}$  and  $\mathbf{R}_{\text{Tx}}$  and of  $\mathbf{R}'_{\text{Rx}}$  and  $\mathbf{R}_{\text{Rx}}$  are identical). Specifically, we may choose  $\mathbf{U}_M := \mathbf{U}_{\text{Tx}}^H$  and/or  $\mathbf{U}_N := \mathbf{U}_{\text{Rx}}^H$ , in order to find an equivalent MIMO system with distributed transmit and/or distributed receive antennas, cf. (3.14):

$$\mathbf{U}_{\text{Tx}}^H \mathbf{R}_{\mathbf{h},\text{Tx}} \mathbf{U}_{\text{Tx}} = \mathbf{\Lambda}_{\mathbf{h},\text{Tx}} =: \mathbf{\Sigma}_{\mathbf{h},\text{Tx}} \quad (3.33a)$$

$$\mathbf{U}_{\text{Rx}}^H \mathbf{R}_{\mathbf{h},\text{Rx}} \mathbf{U}_{\text{Rx}} = \mathbf{\Lambda}_{\mathbf{h},\text{Rx}} =: \mathbf{\Sigma}_{\mathbf{h},\text{Rx}}. \quad (3.33b)$$

**Remark 3.2 (Capacity distribution, ergodic capacity, outage capacity)**

The characteristic function  $\mathbf{C}\{r\}(j\omega)$  contains the complete information about the statistical properties of  $r = C(\mathbf{H})$ . Specifically, the PDF of  $r$  can be calculated as<sup>8</sup>

$$p_r(r) = \frac{1}{2\pi} \int_{-\infty}^{+\infty} \mathbf{C}\{r\}(j\omega) e^{-j\omega r} d\omega. \quad (3.34)$$

<sup>6</sup>If the eigenvalues of  $\mathbf{R}_A$  or  $\mathbf{R}_B$  are not distinct, the characteristic function of  $r = C(\mathbf{H})$  can be obtained as a limiting case of (3.26) [PSL04].

<sup>7</sup>Unitary matrices can, for example, be constructed using Givens rotations, Householder reflections, the matrix exponential function, or the Cayley transform (cf. Remark D.1, Appendix D).

<sup>8</sup>The characteristic function of a random variable can be interpreted as the Fourier transform of the corresponding PDF, evaluated at  $-j\omega$  (cf. Definition C.17). Therefore, the PDF can be obtained from the characteristic function via the corresponding inverse transform.

Based on the characteristic function  $C\{r\}(j\omega)$  and the capacity distribution  $p_r(r)$ , further statistical characteristics of  $r=C(\mathbf{H})$  can be obtained, such as the cumulative distribution function (CDF),

$$\Pr\{r \leq C_0\} := \int_0^{C_0} p_r(r) \, dr. \quad (3.35)$$

Another important quantity is the  $p\%$ -outage capacity  $C_{\text{out}}^{p\%}$ , i.e., the capacity value  $C_0$  for which the CDF (3.35) yields a value of  $p\%$  [FG98]. Moreover, based on the characteristic function, the mean and the variance of the capacity distribution can be calculated in closed form, according to

$$\bar{C} := E\{r\} = \frac{1}{j} \cdot \frac{\partial}{\partial \omega} C\{r\}(j\omega) \Big|_{\omega=0} \quad (3.36)$$

and

$$\sigma_C^2 := E\{(r-\bar{C})^2\} = -2 \cdot \frac{\partial}{\partial \omega^2} C\{r\}(j\omega) \Big|_{\omega=0} - \bar{C}^2 \quad (3.37)$$

(cf. Definition C.17). The mean capacity  $\bar{C}$  is also called ergodic capacity in the literature. The variance  $\sigma_C^2$  (in conjunction with the mean capacity  $\bar{C}$ ) is, for example, useful for Gaussian approximations of the capacity distribution  $p_r(r)$ . As will be seen below, this often yields a good approximation, provided that the number of transmit and receive antennas is not too small. Closed-form expressions for the ergodic capacity  $\bar{C}$  in the case of spatially correlated Rayleigh fading can be found in [PSL04, Kie05]. For the uncorrelated case, a closed-form expression for the ergodic capacity (based on Laguerre polynomials) was first presented in [Tel95]. Closed-form expressions for the variance  $\sigma_C^2$  can be found in [PSL04].

## MIMO Systems with Distributed Antennas

The above results have shown that for any co-located MIMO system following the Kronecker correlation model an equivalent (with regard to the resulting capacity PDF) distributed MIMO system can be found (based on (3.33)). Vice versa, given a MIMO system with distributed transmit and/or distributed receive antennas, the diagonal elements of the matrix  $\Sigma_{\mathbf{h},\text{Tx}} / \Sigma_{\mathbf{h},\text{Rx}}$  may be interpreted as the eigenvalues of a corresponding correlation matrix  $\mathbf{R}_{\mathbf{h},\text{Tx}} / \mathbf{R}_{\mathbf{h},\text{Rx}}$ .

Employing the normalization according to (3.21), a unitary matrix  $\tilde{\mathbf{U}}_M$  or  $\tilde{\mathbf{U}}_N$  can be found for any number of transmit and receive antennas such that the transform

$$\tilde{\mathbf{U}}_M \Sigma_{\mathbf{h},\text{Tx}} \tilde{\mathbf{U}}_M^H =: \mathbf{R}_{\mathbf{h},\text{Tx}} \quad (3.38a)$$

$$\tilde{\mathbf{U}}_N \Sigma_{\mathbf{h},\text{Rx}} \tilde{\mathbf{U}}_N^H =: \mathbf{R}_{\mathbf{h},\text{Rx}} \quad (3.38b)$$

yields a correlation matrix  $\mathbf{R}_{\mathbf{h},\text{Tx}} / \mathbf{R}_{\mathbf{h},\text{Rx}}$  with diagonal entries equal to one and non-diagonal entries with magnitudes  $\leq 1$ . As shown in Appendix 1 at the end of this chapter, suitable unitary matrices are, for example, the  $(n \times n)$ -Fourier matrix  $\mathfrak{F}_n$  (cf. Definition D.8, Appendix D), which exists for any number  $n$ , or the normalized  $(n \times n)$ -

Hadamard matrix  $\mathfrak{H}_n$  (cf. Definition D.6), which is known to exist for all numbers  $n=2^\nu$ , where  $\nu$  is an arbitrary positive integer number.<sup>9</sup>

**Remark 3.3 (Spatial correlations in the equivalent co-located system)**

Note that for  $\Sigma_{\mathbf{h},\text{Tx}} \neq \mathbf{I}_M$  or  $\Sigma_{\mathbf{h},\text{Rx}} \neq \mathbf{I}_N$ , at least some non-diagonal entries of  $\mathbf{R}_{\mathbf{h},\text{Tx}}/\mathbf{R}_{\mathbf{h},\text{Rx}}$  will have a magnitude greater than zero. Correspondingly, a MIMO system with distributed antennas and unequal average link SNRs is transformed into an equivalent co-located MIMO system with correlated antennas. Specifically, if all but one elements of  $\Sigma_{\mathbf{h},\text{Tx}}/\Sigma_{\mathbf{h},\text{Rx}}$  are equal to zero (because the corresponding links are completely obstructed), one obtains an equivalent co-located MIMO system with fully correlated transmit or receive antennas, i.e., all elements of  $\mathbf{R}_{\mathbf{h},\text{Tx}}/\mathbf{R}_{\mathbf{h},\text{Rx}}$  have a magnitude equal to one. However, if all average link SNRs are the same, the distributed MIMO system is equivalent to a co-located MIMO system with uncorrelated transmit and receive antennas.

**Remark 3.4**

In Appendix H, the unitary matrix transforms (3.33) and (3.38) considered above are illustrated by means of two simple examples. Moreover, examples for virtual antenna arrays (VAAs) in cellular mobile radio systems are considered, and specific results are derived concerning the associated spatial correlation properties in the equivalent co-located MIMO system.

The above findings are summarized in the following theorem:

**Theorem 3.1 (Equivalence of distributed and co-located MIMO systems I)**

*For any MIMO system with co-located transmit and receive antennas, which is subject to frequency-flat Rayleigh fading obeying the Kronecker correlation model, an equivalent MIMO system with distributed transmit and/or distributed receive antennas can be found, and vice versa, such that both systems are characterized by identical capacity distributions.*

*Proof.* The capacity distribution according to (3.26) and (3.34) is invariant under a unitary transform of the transmitter or receiver correlation/covariance matrix. Thus, using the unitary matrix transform (3.33), any co-located MIMO system can be transformed into an equivalent distributed MIMO system. Similarly, using the unitary matrix transform (3.38), any distributed MIMO system can be transformed into an equivalent co-located MIMO system.  $\square$

**Numerical Capacity Results**

In order to illustrate the above findings, some numerical capacity results are presented in Fig. 3.2, for different MIMO systems with four transmit and three receive antennas. Displayed are the capacity distributions  $p_{\underline{r}}(r)$  resulting for

- (i) a co-located MIMO system with uncorrelated links ('conventional MIMO system'),
- (ii) a co-located MIMO system with correlated transmit and receive antennas, and

<sup>9</sup>It should be noted that a unitary matrix transform of form (3.38) was also employed in [Say02], in order to establish a so-called 'virtual' channel representation of physical MIMO channel models.

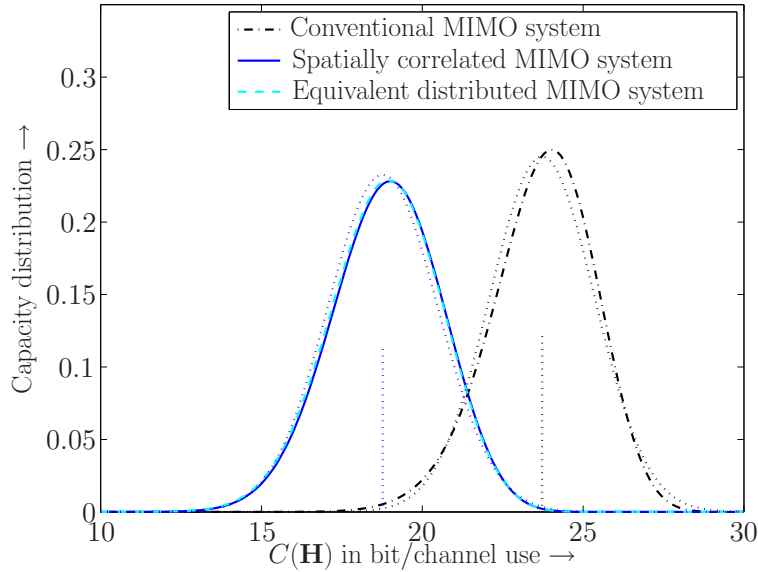


Figure 3.2: Capacity distributions  $p_r(r)$  for different MIMO systems with four transmit and three receive antennas, at an SNR of  $10 \log_{10}(P/\sigma_n^2) = 26$  dB.

(iii) the corresponding equivalent distributed MIMO system,

at an SNR of  $10 \log_{10}(P/\sigma_n^2) = 26$  dB. The associated ergodic capacities are marked by dotted vertical lines. Moreover, corresponding Gaussian approximations of  $p_r(r)$  have been included in Fig. 3.2 (also marked by dotted lines). As an example, a single-parameter  $(n \times n)$ -correlation matrix

$$\mathbf{R}_{n,\rho} := \begin{bmatrix} 1 & \rho & \rho^4 & \dots & \rho^{(n-1)^2} \\ \rho & 1 & \rho & \dots & \rho^{(n-2)^2} \\ \rho^4 & \rho & & & \vdots \\ \vdots & \vdots & & \ddots & \vdots \\ \rho^{(n-1)^2} & \rho^{(n-2)^2} & \dots & \dots & 1 \end{bmatrix} \quad (3.39)$$

( $\rho \in \mathbb{R}$ ) was used for the matrices  $\mathbf{R}_{\mathbf{h},\text{Tx}}$  and  $\mathbf{R}_{\mathbf{h},\text{Rx}}$  in the spatially correlated MIMO system.<sup>10</sup> For the transmitter, the parameters  $n=M=4$  and  $\rho_{\text{Tx}}=0.8$  were chosen, and for the receiver the parameters  $n=N=3$  and  $\rho_{\text{Rx}}=0.7$ . The corresponding matrices  $\mathbf{\Sigma}_{\mathbf{h},\text{Tx}}$  and  $\mathbf{\Sigma}_{\mathbf{h},\text{Rx}}$  in the equivalent distributed MIMO system are given by

$$\mathbf{\Sigma}_{\mathbf{h},\text{Tx}} = \text{diag}([0.0198 \ 0.2125 \ 1.0459 \ 2.7217]), \quad (3.40a)$$

$$\mathbf{\Sigma}_{\mathbf{h},\text{Rx}} = \text{diag}([0.1228 \ 0.7599 \ 2.1173]). \quad (3.40b)$$

The capacity distributions for the co-located MIMO system with uncorrelated links and the co-located MIMO system with correlated antennas were obtained based on the analytical results presented in [PSL04] (cf. (3.26) and (3.34) for the correlated case). The capacity

<sup>10</sup>The single-parameter correlation matrix (3.39) was proposed in [vH02a] for uniform linear antenna arrays (ULAAAs) with  $n$  antenna elements.



distribution for the equivalent distributed system was obtained by means of Monte-Carlo simulations over  $10^7$  independent channel realizations. As expected, the capacity distributions for the spatially correlated MIMO system and the equivalent distributed MIMO system are identical.<sup>11</sup> As can be seen, the ergodic capacity is significantly reduced compared to the co-located MIMO system with uncorrelated links, from 23.7 bit/channel use to 18.9 bit/channel use. (Moreover, the width of the capacity distribution is slightly increased, which is of interest for the outage capacity.) Note that this is an important result. It implies that distributed MIMO systems with unequal link lengths have an inferior performance compared to co-located MIMO systems with uncorrelated antennas (at least as long as no macroscopic diversity gains are available in the distributed MIMO system). Finally, we note that the Gaussian approximation of the capacity distributions fits well, for both the uncorrelated MIMO system and the correlated/distributed MIMO system.

If only a single antenna is employed either at the transmitter or the receiver, the loss in ergodic capacity turns out to be significantly smaller. For example, in a MIMO system with  $M=4$  transmit antennas and a single receive antenna, the ergodic capacity is reduced from 8.5 bit/channel use in the uncorrelated MIMO system to 8.2 bit/channel use in the case of a spatially correlated MIMO system with  $\mathbf{R}_{\mathbf{h},\text{Tx}} = \mathbf{R}_{M,\rho}$  and  $\rho=0.9$  (at an SNR of  $10 \log_{10}(P/\sigma_n^2) = 26$  dB).

### Further Capacity Results for Co-located and Distributed MIMO Systems

Due to the equivalence of co-located and distributed MIMO systems, many capacity results reported for co-located MIMO systems can be reused, in order to gain insights for distributed MIMO systems. A comprehensive survey of existing capacity results for MIMO systems with uncorrelated and correlated antennas can be found in [GJJV03]. In particular, different scenarios concerning the amount of channel knowledge available at the transmitter are considered (see also Appendix G). With regard to the receiver, focus is on the case of perfect and statistical channel knowledge. (Capacity results for the case where channel knowledge is neither available at the transmitter nor the receiver can be found in [ZT02].) Another excellent survey on the topic can be found in [BT04a].

Capacity results for co-located MIMO systems that can directly be transferred to distributed MIMO systems were, for example, presented in [SFGK00,GSS+03,SL03,CWZ03,JB04a,KSB04,OAA04,MO04,PSL04,Kie05,KA06]. For instance, in [SFGK00] simulation results were presented for the PDFs of the eigenvalues of the matrix  $\mathbf{H}\mathbf{H}^H$  (for the case of Rayleigh fading and the Kronecker correlation model). They show that in the presence of spatial correlations, the probability is comparatively large that the number of significant eigenvalues of  $\mathbf{H}\mathbf{H}^H$  is small.<sup>12</sup> Moreover, simulation results for the CDF of  $r=C(\mathbf{H})$  were included (for the case where no channel knowledge is available at the transmitter), and it was shown that spatial correlations can result in a significantly reduced ergodic capacity.

<sup>11</sup>As an example, both correlation matrices  $\mathbf{R}_{\mathbf{h},\text{Tx}}$  and  $\mathbf{R}_{\mathbf{h},\text{Rx}}$  were replaced by  $\Sigma_{\mathbf{h},\text{Tx}}$  and  $\Sigma_{\mathbf{h},\text{Rx}}$ , respectively, which corresponds to a MIMO system with distributed transmit and distributed receive antennas. Of course, the capacity distribution will not change if only one of the correlation matrices  $\mathbf{R}_{\mathbf{h},\text{Tx}}$  and  $\mathbf{R}_{\mathbf{h},\text{Rx}}$  is replaced by the corresponding matrix  $\Sigma_{\mathbf{h},\text{Tx}}/\Sigma_{\mathbf{h},\text{Rx}}$ .

<sup>12</sup>Analytical expressions for the (joint) distribution of the eigenvalues of  $\mathbf{H}\mathbf{H}^H$  in the case of spatial correlations can be found in [CWZ03,MO04,TV04b]. We will return to this topic in Chapter 4.

Analytical results that are based on majorization theory were presented in [JB04a], again for Rayleigh fading and the Kronecker correlation model. An  $(1 \times M)$ -vector  $\mathbf{a}$  is said to majorize another  $(1 \times M)$ -vector  $\mathbf{b}$  if  $\sum_{i=1}^m a_i \geq \sum_{i=1}^m b_i$  for all  $m=1, \dots, M$ . Let  $\boldsymbol{\lambda}_{\mathbf{h},\text{Tx}}$  and  $\boldsymbol{\lambda}_{\mathbf{h},\text{Rx}}$  denote the vector containing the ordered eigenvalues of the transmitter and receiver correlation matrix, respectively, where  $\lambda_{\text{Tx},1} \geq \dots \geq \lambda_{\text{Tx},M}$  and  $\lambda_{\text{Rx},1} \geq \dots \geq \lambda_{\text{Rx},N}$ . Assuming an equal power allocation strategy at the transmitter, a fixed receiver correlation matrix  $\mathbf{R}_{\mathbf{h},\text{Rx}}$  and two different transmitter correlation matrices  $\mathbf{R}_{\mathbf{h},\text{Tx}}$  and  $\mathbf{R}'_{\mathbf{h},\text{Tx}}$  with corresponding eigenvalue vectors  $\boldsymbol{\lambda}_{\mathbf{h},\text{Tx}}$  and  $\boldsymbol{\lambda}'_{\mathbf{h},\text{Tx}}$ , the following was shown in [JB04a]. If  $\boldsymbol{\lambda}'_{\mathbf{h},\text{Tx}}$  majorizes  $\boldsymbol{\lambda}_{\mathbf{h},\text{Tx}}$ , the ergodic capacity associated with the correlation matrix  $\mathbf{R}'_{\mathbf{h},\text{Tx}}$  is always smaller than the one associated with the correlation matrix  $\mathbf{R}_{\mathbf{h},\text{Tx}}$ . The same principle holds also if  $\boldsymbol{\lambda}_{\mathbf{h},\text{Tx}}$  is fixed and different vectors  $\boldsymbol{\lambda}_{\mathbf{h},\text{Rx}}$  are compared. Correspondingly, the maximum ergodic capacity results for  $\boldsymbol{\lambda}_{\mathbf{h},\text{Tx}} = [1, \dots, 1]$  and  $\boldsymbol{\lambda}_{\mathbf{h},\text{Rx}} = [1, \dots, 1]$ , i.e., for uncorrelated transmit and receive antennas, and the minimum ergodic capacity results for  $\boldsymbol{\lambda}_{\mathbf{h},\text{Tx}} = [M, 0, \dots, 0]$  and  $\boldsymbol{\lambda}_{\mathbf{h},\text{Rx}} = [N, 0, \dots, 0]$ , i.e., for fully correlated antennas.

More specialized capacity results for doubly- and triply-selective co-located MIMO systems were, for example, presented in [GCSS03, IUN03, XZ04, PJ05]. The topic of capacity scaling for a growing number of transmit and receive antennas was, for example, addressed in [CTKV02, RS03, MFP03]. Specifically, in [RS03] it was shown that in the case of spatial correlations, the ergodic capacity  $\bar{C}$  still scales (approximately) linearly with  $\tilde{M} = \min(M, N)$ . However, the slope of  $\bar{C}$  as a function of  $\tilde{M}$  is smaller than in the uncorrelated case. In [MFP03] the case where the number of transmit and receive antennas grows to infinity was considered, while the ratio  $M/N$  is kept constant. By this means, asymptotic expressions were derived for the capacity  $r = C(\mathbf{H})$  which indicate that spatial correlations are more harmful when arising at the side with less antennas. As shown in [MFP03], these asymptotic capacity results are also relevant for MIMO systems with a moderate number of antennas. Finally, some papers report specific capacity results for MIMO systems with correlated antennas, which include certain assumptions regarding the geometry of the antenna arrays and/or the volume available for deploying them, e.g. [PAK03, WGJ03, HF03a, Chi03].

To conclude this section, further results concerning the ergodic capacity of distributed and co-located MIMO systems are presented in the sequel. In particular, the impact of the overall received SNR and the available number of antennas is illustrated.

### Ergodic Capacity of Distributed and Co-located MIMO Systems

Consider again a co-located MIMO system with  $M$  transmit and  $N$  receive antennas. As earlier, we assume frequency-flat Rayleigh fading which follows the Kronecker correlation model. Moreover, we assume that no channel state information is available at the transmitter, whereas the receiver has perfect instantaneous channel knowledge. The case of instantaneous and statistical channel knowledge at the transmitter will be considered in Chapter 4. A tight upper bound on the ergodic capacity  $\bar{C} = \mathbf{E}\{r\}$  can be found as follows [BT04a, Ch. 4.3]. Since the log-function is convex- $\cap$  on  $\mathbb{R}_{>0}$  (cf. Section E.2 in Appendix E), we can apply Jensen's inequality to the expression for  $\bar{C}$ , which yields

$$\bar{C} \leq \log_2 \mathbf{E} \left\{ \det \left( \mathbf{I}_N + \frac{P}{M\sigma_n^2} \mathbf{H}\mathbf{H}^H \right) \right\} \text{ bit/channel use.} \quad (3.41)$$

**Remark 3.5**

Jensen's inequality says that for any function  $f$ , which is convex- $\cap$  on a certain set  $\mathbb{S}$ , the following holds:  $\mathbf{E}\{f(x)\} \leq f(\mathbf{E}\{x\})$  for all  $x \in \mathbb{S}$ . Interestingly, an alternative (less tight) upper bound on  $\bar{C}$  can be obtained by applying Jensen's inequality to the  $\log_2 \det$ -function [BT04a, Ch. 4.2]. Since  $\log_2 \det(\mathbf{A})$  is convex- $\cap$  on the set of all non-negative definite Hermitian matrices  $\mathbf{A}$ , the ergodic capacity  $\bar{C}$  is bounded above by the minimum of

$$\log_2 \det \left( \mathbf{I}_N + \frac{P}{\sigma_n^2} \mathbf{R}_{\mathbf{h}, \text{Rx}} \right) \quad \text{and} \quad \log_2 \det \left( \mathbf{I}_M + \frac{PN}{M\sigma_n^2} \mathbf{R}_{\mathbf{h}, \text{Tx}} \right), \quad (3.42)$$

where  $\sigma_h^2 = 1$  has been assumed.

In [SL03], the right-hand side of (3.41) was further evaluated, based on the principal minor determinants of  $\mathbf{R}_{\mathbf{h}, \text{Tx}}$  and  $\mathbf{R}_{\mathbf{h}, \text{Rx}}$ . The result is given by

$$\bar{C} \leq \log_2 \left( 1 + \sum_{\mu=1}^{\tilde{M}} \left( \frac{P}{M\sigma_n^2} \right)^\mu \mu! \sum_{\mathbf{i} \in \mathbb{I}_\mu} \det(\mathbf{R}_{\mathbf{h}, \text{Tx}})_{\mathbf{i}} \sum_{\mathbf{j} \in \mathbb{J}_\mu} \det(\mathbf{R}_{\mathbf{h}, \text{Rx}})_{\mathbf{j}} \right), \quad (3.43)$$

where  $\mathbf{i}$  and  $\mathbf{j}$  denote index vectors taken from the sets

$$\mathbb{I}_\mu := \{\mathbf{i} := [i_1, \dots, i_\mu] \mid 1 \leq i_1 < i_2 < \dots < i_\mu \leq M\} \quad (3.44a)$$

$$\mathbb{J}_\mu := \{\mathbf{j} := [j_1, \dots, j_\mu] \mid 1 \leq j_1 < j_2 < \dots < j_\mu \leq N\}. \quad (3.44b)$$

Moreover,  $\det(\mathbf{A})_{\mathbf{i}}$  denotes the minor determinant of  $\mathbf{A}$ , which is associated with the quadratic submatrix of  $\mathbf{A}$  specified by the index vector  $\mathbf{i}$ . The right-hand side of (3.43) can be further simplified by replacing  $\mathbf{R}_{\mathbf{h}, \text{Tx}}$  and  $\mathbf{R}_{\mathbf{h}, \text{Rx}}$  by the corresponding eigenvalue matrices  $\mathbf{\Lambda}_{\mathbf{h}, \text{Tx}}$  and  $\mathbf{\Lambda}_{\mathbf{h}, \text{Rx}}$ . By this means, the minor determinants  $\det(\mathbf{R}_{\mathbf{h}, \text{Tx}})_{\mathbf{i}}$  and  $\det(\mathbf{R}_{\mathbf{h}, \text{Rx}})_{\mathbf{j}}$  are replaced by simple products of eigenvalues:

$$\bar{C} \leq \log_2 \left( 1 + \sum_{\mu=1}^{\tilde{M}} \left( \frac{P}{M\sigma_n^2} \right)^\mu \mu! \sum_{\mathbf{i} \in \mathbb{I}_\mu} \lambda_{\text{Tx}, i_1} \cdots \lambda_{\text{Tx}, i_\mu} \sum_{\mathbf{j} \in \mathbb{J}_\mu} \lambda_{\text{Rx}, j_1} \cdots \lambda_{\text{Rx}, j_\mu} \right). \quad (3.45)$$

(The order of the eigenvalues is arbitrary.) In particular, the above expression can directly be utilized for distributed MIMO systems, by setting  $\mathbf{\Lambda}_{\mathbf{h}, \text{Tx}} := \mathbf{\Sigma}_{\mathbf{h}, \text{Tx}}$  and  $\mathbf{\Lambda}_{\mathbf{h}, \text{Rx}} := \mathbf{\Sigma}_{\mathbf{h}, \text{Rx}}$ . In the case of uncorrelated transmit and receive antennas, the upper bound (3.45) simplifies to

$$\bar{C} \leq \log_2 \left( 1 + \sum_{\mu=1}^{\tilde{M}} \left( \frac{P}{M\sigma_n^2} \right)^\mu \mu! \binom{M}{M-\mu} \binom{N}{N-\mu} \right). \quad (3.46)$$

As an example, some numerical results concerning the ergodic capacity of a MIMO system with four distributed transmit antennas and three co-located receive antennas are presented in the following. At the transmitter side, two different transmitter covariance matrices are considered. The first represents the case of equal average links SNRs ( $\mathbf{\Sigma}_{\mathbf{h}, \text{Tx}} = \mathbf{I}_M$ ), whereas the second represents the case of a significant SNR imbalance:

$$\mathbf{\Sigma}_{\mathbf{h}, \text{Tx}} := \text{diag}([2.5 \ 1.0 \ 0.3 \ 0.2]). \quad (3.47)$$

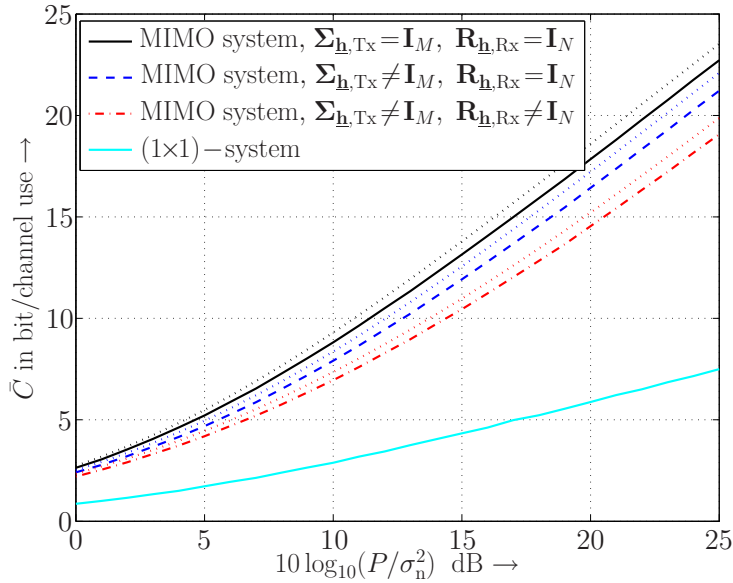


Figure 3.3: Ergodic capacity  $\bar{C}$  of a MIMO system with four distributed transmit and three co-located receive antennas, resulting for equal/unequal average link SNRs and uncorrelated/correlated receive antennas. (Simulative results were obtained by means of Monte-Carlo simulations; dotted lines: Corresponding analytical upper bounds.) For comparison, the ergodic capacity of a single-antenna system has also been included (‘(1x1)-system’).

Equivalently, we could also consider a MIMO system with co-located transmit and receive antennas and a transmitter correlation matrix with eigenvalue matrix  $\Lambda_{\mathbf{h},\text{Tx}} = \Sigma_{\mathbf{h},\text{Tx}}$ . At the receiver we also consider two different receiver correlation matrices, namely  $\mathbf{R}_{\mathbf{h},\text{Rx}} = \mathbf{I}_N$  (uncorrelated receive antennas) and a single-parameter correlation matrix  $\mathbf{R}_{\mathbf{h},\text{Rx}} = \mathbf{R}_{N,\rho_{\text{Rx}}}$  with  $\rho_{\text{Rx}} = 0.7$ , cf. (3.39).

In Fig. 3.3, the ergodic capacities  $\bar{C}$  resulting for the different cases are plotted as a function of the average SNR  $P/\sigma_n^2$  in dB. The exact ergodic capacities (solid, dashed and dashed-dotted line) were obtained by means of Monte-Carlo simulations over 10.000 independent channel realizations, whereas the dotted lines represent the corresponding upper bounds on  $\bar{C}$ , which were obtained on the basis of (3.45) and (3.46). As can be seen, the upper bounds are reasonably tight throughout the complete SNR range. Moreover, for medium to large SNR values the ergodic capacity is reduced significantly if the average link SNRs are unbalanced due to distributed transmit antennas, especially if the receive antennas are correlated. However, in all cases huge gains are achieved compared to a single-antenna system (‘(1x1)-system’), especially in the case of high SNR values.

In Fig. 3.4, the impact of the number of receive antennas is illustrated, for a fixed SNR of  $10 \log_{10}(P/\sigma_n^2) = 20$  dB. As can be seen, for  $N < 4$  the ergodic capacity grows (approximately) linearly with  $\min(M, N) = N$  in all cases, whereas for larger  $N$  the rate of growth diminishes. Interestingly, for small numbers  $N$  the performance of the system with  $\Sigma_{\mathbf{h},\text{Tx}} \neq \mathbf{I}_M$  and  $\mathbf{R}_{\mathbf{h},\text{Rx}} = \mathbf{I}_N$  is superior to that of the system with  $\Sigma_{\mathbf{h},\text{Tx}} = \mathbf{I}_M$  and  $\mathbf{R}_{\mathbf{h},\text{Rx}} \neq \mathbf{I}_N$ , whereas for large numbers  $N$  the situation is reversed. This result is

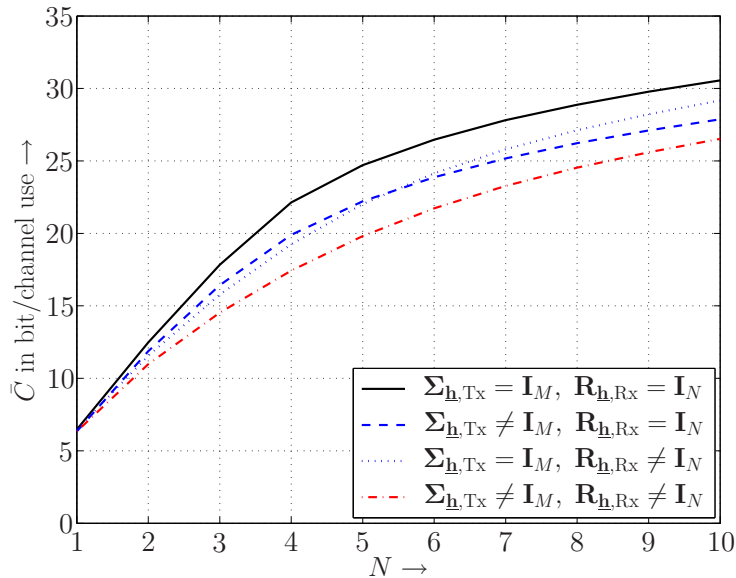


Figure 3.4: Ergodic capacity  $\bar{C}$  of a MIMO system with four distributed transmit and  $N$  co-located receive antennas as a function of  $N$ , at an SNR of  $10 \log_{10}(P/\sigma_n^2) = 20$  dB: Equal/unequal average link SNRs and uncorrelated/correlated receive antennas (simulative results obtained by means of Monte-Carlo simulations).

supported by the finding of [MFP03] that spatial correlations (or unbalanced link SNRs) are more harmful when occurring at the side with less antennas. Moreover, it can be seen that the performance gap between the system with  $\Sigma_{\mathbf{h},\text{Tx}} = \mathbf{I}_M$  and  $\mathbf{R}_{\mathbf{h},\text{Rx}} = \mathbf{I}_N$  and the system with  $\Sigma_{\mathbf{h},\text{Tx}} \neq \mathbf{I}_M$  and  $\mathbf{R}_{\mathbf{h},\text{Rx}} \neq \mathbf{I}_N$  is virtually the same for all numbers  $N \geq 4$ . Finally, in the case of a single receive antenna (which is of particular interest for practical applications requiring a simple receiver), the reduction of the ergodic capacity due to unbalanced link SNRs is negligible.

### 3.2.4 Pairwise Error Probability of Space-Time Codes

The results in Section 3.2.3 were very general and are relevant for coded MIMO systems with co-located or distributed antennas. In the following, we focus on an important class of coded MIMO systems, namely on space-time coded MIMO systems. Specifically, we will show that space-time coded MIMO systems with spatially correlated antennas and space-time coded MIMO systems with distributed antennas lead (asymptotically) to identical pairwise error probabilities (PEPs).

To this end, consider again channel model (2.28) introduced in Section 2.2.2 for a block-wise transmission over quasi-static, frequency-flat fading MIMO channels. As earlier, the block length is denoted as  $N_b$  in the sequel. We assume that a space-time encoder with memory length  $\nu$  (e.g., a space-time trellis encoder) is used at the transmitter, possibly in a distributed fashion. The space-time encoder maps a sequence of  $(N_b - \nu)$  information symbols  $a[\kappa]$  (followed by  $\nu$  known tailing symbols) onto an  $(M \times N_b)$  space-time transmission matrix  $\mathbf{X}$ , where  $N_b > M$ . The matrix  $\mathbf{X}$  is called the code matrix in

the following. Assuming that the channel matrix  $\mathbf{H}$  is perfectly known at the receiver, the metric for maximum-likelihood sequence estimation (MLSE) is given by [UG04]

$$\mu(\mathbf{Y}, \tilde{\mathbf{X}}) := \|\mathbf{Y} - \mathbf{H}\tilde{\mathbf{X}}\|_{\text{F}}^2, \quad (3.48)$$

where  $\tilde{\mathbf{X}}$  denotes a hypothesis for the code matrix  $\mathbf{X}$ . Moreover,  $\|\cdot\|_{\text{F}}$  denotes the Frobenius norm, cf. Definition D.2 in Appendix D. The PEP  $P(\mathbf{X} \rightarrow \mathbf{E})$ , i.e., the probability that the MLSE decoder decides in favor of an erroneous code matrix  $\mathbf{E} \neq \mathbf{X}$ , although the matrix  $\mathbf{X}$  was transmitted, is given by [WSFY04]

$$\begin{aligned} P(\mathbf{X} \rightarrow \mathbf{E}) &= \Pr\{\mu(\mathbf{Y}, \mathbf{E}) \leq \mu(\mathbf{Y}, \mathbf{X})\} \\ &= \mathbb{E} \left\{ Q \left( \sqrt{\frac{P}{2M\sigma_n^2}} \|\mathbf{H}(\mathbf{X} - \mathbf{E})\|_{\text{F}} \right) \right\}, \end{aligned} \quad (3.49)$$

cf. (2.123), where  $Q(x)$  denotes the Gaussian Q-function, cf. Definition C.2 in Appendix C. The expectation is taken with respect to the channel matrix  $\mathbf{H}$ . The PEP is often used in the literature, in order to derive design criteria for space-time codes (cf. Section 2.3.4). With regard to performance analysis the PEP can, for example, be used to approximate the bit error rate provided by space-time codes [UG04].

### MIMO Systems with Co-located Antennas

Consider again a MIMO system with co-located transmit and receive antennas, and an overall spatial covariance matrix  $\mathbb{E}\{\text{vec}(\mathbf{H})\text{vec}(\mathbf{H})^{\text{H}}\} = \mathbf{R}_{\mathbf{h},\text{Tx}} \otimes \mathbf{R}_{\mathbf{h},\text{Rx}}$ . As earlier, we denote

$$\Psi_{\mathbf{X},\mathbf{E}} := (\mathbf{X} - \mathbf{E})(\mathbf{X} - \mathbf{E})^{\text{H}} \quad (3.50)$$

(cf. Section 2.3.4). In the sequel, we assume that the employed space-time code achieves full spatial diversity. This implies that the matrix  $\Psi_{\mathbf{X},\mathbf{E}}$  has always full rank, i.e.,

$$\text{rank}(\Psi_{\mathbf{X},\mathbf{E}}) = M \quad (3.51)$$

for any pair of code matrices ( $\mathbf{X} \neq \mathbf{E}$ ). In [WSFY04], it was shown that the PEP (3.49) can be expressed in the form of a single finite-range integral, according to

$$P(\mathbf{X} \rightarrow \mathbf{E}) = \frac{1}{\pi} \int_0^{\pi/2} \prod_{i=1}^M \prod_{j=1}^N \left[ 1 + \frac{P}{4M\sigma_n^2} \frac{\xi_{\text{Tx},i} \lambda_{\text{Rx},j}}{\sin^2 \theta} \right]^{-1} d\theta, \quad (3.52)$$

where  $\xi_{\text{Tx},1}, \dots, \xi_{\text{Tx},M}$  denote the eigenvalues of the matrix  $\Psi_{\mathbf{X},\mathbf{E}} \mathbf{R}_{\mathbf{h},\text{Tx}}$  and  $\lambda_{\text{Rx},1}, \dots, \lambda_{\text{Rx},N}$  the eigenvalues of  $\mathbf{R}_{\mathbf{h},\text{Rx}}$  (as earlier). Specifically, it was shown in [WSFY04] that the presence of receive antenna correlations ( $\mathbf{R}_{\mathbf{h},\text{Rx}} \neq \mathbf{I}_N$ ) always degrades the PEP (for any SNR value, particularly for high SNRs). In contrast to this, the impact of transmit antenna correlations depends on the employed space-time code. In the low SNR regime, the presence of transmit antenna correlations ( $\mathbf{R}_{\mathbf{h},\text{Tx}} \neq \mathbf{I}_M$ ) can improve the PEP, whereas for large SNR values the PEP is always degraded.



### MIMO Systems with Distributed Antennas

Based on the same arguments as in Section 3.2.3, we can always find a MIMO system with distributed receive antennas, which leads to exactly the same PEP as the above co-located system. Any MIMO system with overall spatial covariance matrix

$$\mathbb{E}\{\text{vec}(\mathbf{H})\text{vec}(\mathbf{H})^H\} = \mathbf{R}_{\mathbf{h},\text{Tx}} \otimes (\mathbf{U}_N \mathbf{R}_{\mathbf{h},\text{Rx}} \mathbf{U}_N^H) =: \mathbf{R}_{\mathbf{h},\text{Tx}} \otimes \mathbf{R}'_{\mathbf{h},\text{Rx}} \quad (3.53)$$

will lead to the same PEP (3.52), where  $\mathbf{U}_N$  is an arbitrary unitary ( $N \times N$ )-matrix. In particular, we may again choose  $\mathbf{U}_N := \mathbf{U}_{\mathbf{h},\text{Rx}}^H$  to obtain  $\mathbf{R}'_{\mathbf{h},\text{Rx}} = \mathbf{\Lambda}_{\mathbf{h},\text{Rx}} =: \mathbf{\Sigma}_{\mathbf{h},\text{Rx}}$ . Similarly, given a MIMO system with distributed receive antennas, we can always find an equivalent co-located MIMO system by evaluating (3.38b).

In contrast to this, a MIMO system with distributed transmit antennas and overall spatial covariance matrix

$$\mathbb{E}\{\text{vec}(\mathbf{H})\text{vec}(\mathbf{H})^H\} = \mathbf{\Sigma}_{\mathbf{h},\text{Tx}} \otimes \mathbf{R}_{\mathbf{h},\text{Rx}} \quad (3.54)$$

( $\mathbf{\Sigma}_{\mathbf{h},\text{Tx}} := \mathbf{U}_{\mathbf{h},\text{Tx}}^H \mathbf{R}_{\mathbf{h},\text{Tx}} \mathbf{U}_{\mathbf{h},\text{Tx}}$ ) will not lead to the same PEP expression (3.52), because the eigenvalues of  $\mathbf{\Psi}_{\mathbf{X},\mathbf{E}} \mathbf{R}_{\mathbf{h},\text{Tx}}$  and  $\mathbf{\Psi}_{\mathbf{X},\mathbf{E}} \mathbf{\Sigma}_{\mathbf{h},\text{Tx}}$  are, in general, different. Note that we obtain a PEP expression for space-time coded MIMO systems with distributed transmit antennas, by replacing  $\xi_{\text{Tx},1}, \dots, \xi_{\text{Tx},M}$  in (3.52) by the eigenvalues of the matrix  $\mathbf{\Psi}_{\mathbf{X},\mathbf{E}} \mathbf{\Sigma}_{\mathbf{h},\text{Tx}}$ . This PEP expression might, for example, be utilized as a design criterion for distributed space-time trellis codes.

Asymptotically (i.e., for large SNR values) the PEP expressions for co-located and distributed MIMO systems again become the same. In [BP00a] it was shown that for large SNR values the PEP (3.52) is well approximated by

$$P(\mathbf{X} \rightarrow \mathbf{E}) \leq \left( \frac{P}{4M\sigma_n^2} \right)^{-MN} \det(\mathbf{\Psi}_{\mathbf{X},\mathbf{E}} \mathbf{R}_{\mathbf{h},\text{Tx}})^{-N} \det(\mathbf{R}_{\mathbf{h},\text{Rx}})^{-M}, \quad (3.55)$$

where it was assumed that  $\mathbf{R}_{\mathbf{h},\text{Tx}}$  and  $\mathbf{R}_{\mathbf{h},\text{Rx}}$  have full rank. Since  $\mathbf{\Psi}_{\mathbf{X},\mathbf{E}}$  was also assumed to always have full rank, we obtain

$$\det(\mathbf{\Psi}_{\mathbf{X},\mathbf{E}} \mathbf{R}_{\mathbf{h},\text{Tx}}) = \det(\mathbf{\Psi}_{\mathbf{X},\mathbf{E}}) \det(\mathbf{R}_{\mathbf{h},\text{Tx}}) = \det(\mathbf{\Psi}_{\mathbf{X},\mathbf{E}}) \det(\mathbf{\Sigma}_{\mathbf{h},\text{Tx}}), \quad (3.56)$$

i.e., the expression (3.55) does not change when the matrix  $\mathbf{R}_{\mathbf{h},\text{Tx}}$  is replaced by  $\mathbf{\Sigma}_{\mathbf{h},\text{Tx}}$ . Given a MIMO system with distributed transmit/receive antennas, we can find an asymptotically equivalent co-located MIMO system by evaluating (3.38).<sup>13</sup>

The above findings are summarized in the following theorem:

#### Theorem 3.2 (Equivalence of distributed and co-located MIMO systems II)

*For any MIMO system with co-located transmit and receive antennas, which is subject to frequency-flat Rayleigh fading obeying the Kronecker correlation model and which*

<sup>13</sup>Note that if  $\mathbf{R}_{\mathbf{h},\text{Tx}}$  and  $\mathbf{R}_{\mathbf{h},\text{Rx}}$  (or  $\mathbf{\Sigma}_{\mathbf{h},\text{Tx}}$  and  $\mathbf{\Sigma}_{\mathbf{h},\text{Rx}}$ ) have full rank, the achieved diversity order is equal to  $MN$ . In the case of a MIMO system with distributed transmit antennas, it may happen that a random subset of the transmit antennas is completely obstructed due to severe shadowing, which renders the transmitter covariance matrix  $\mathbf{\Sigma}_{\mathbf{h},\text{Tx}}$  rank-deficient. In this case, the achieved diversity order is equal to  $\text{rank}(\mathbf{\Sigma}_{\mathbf{h},\text{Tx}}) \cdot N$ , since  $\mathbf{\Psi}_{\mathbf{X},\mathbf{E}}$  was assumed to always have full rank.



employs a space-time coding scheme designed to achieve full spatial diversity, an equivalent MIMO system with distributed transmit and/or distributed receive antennas can be found, and vice versa, such that asymptotically (i.e., for large signal-to-noise ratios) both systems are characterized by identical pair-wise error probabilities.

*Proof.* The pair-wise error probability according to (3.52) is invariant under a unitary transform of the receiver correlation/covariance matrix and asymptotically invariant under a unitary transform of the transmitter correlation/covariance matrix. Thus, using the unitary matrix transform (3.33), any co-located MIMO system can be transformed into an (asymptotically) equivalent distributed MIMO system. Similarly, using the unitary matrix transform (3.38), any distributed MIMO system can be transformed into an (asymptotically) equivalent co-located MIMO system.  $\square$

### 3.2.5 Error Rates of Orthogonal Space-Time Block Codes

In the sequel, we further specialize the above results and focus on co-located and distributed MIMO systems that employ an orthogonal space-time block code (OSTBC) at the transmitter. As will be seen, in this case identical symbol and bit error rates result for co-located and distributed systems (for any SNR value). As a new contribution, closed-form expressions [MHKX06a] as well as high-SNR approximations for the average symbol error probability of co-located and distributed OSTBC systems are derived.<sup>14</sup> Moreover, a simple tight upper bound on the ergodic maximum mutual information of OSTBC systems is presented.

#### MIMO Systems with Co-located Antennas

Consider again a MIMO system with co-located transmit and receive antennas, and an overall spatial covariance matrix  $\mathbf{E}\{\text{vec}(\mathbf{H})\text{vec}(\mathbf{H})^H\} =: \mathbf{R}_{\mathbf{h}}$ .<sup>15</sup> In Section 2.3.1, it was shown that any MIMO system with  $M$  transmit and  $N$  receive antennas employing an OSTBC in conjunction with the corresponding (widely) linear decoding step at the receiver can be transformed into an equivalent maximum ratio combining (MRC) system with one transmit antenna and  $MN$  receive antennas. Using the normalization introduced in Section 3.2.2 ( $\mathbf{E}\{|h_{\nu,\mu}|^2\} = \sigma_h^2 = 1$  for all  $\mu = 1, \dots, M$ ,  $\nu = 1, \dots, N$ ), the overall average received SNR per information symbol in the OSTBC system is given by

$$\bar{\gamma}_s = \frac{PN}{R_t \sigma_n^2} \quad (3.57)$$

(cf. Section 2.3.1), where  $P$  denotes the overall average transmit power and  $R_t$  the temporal rate of the OSTBC under consideration. For performance analysis, we therefore consider an equivalent  $(1 \times MN)$ -system

$$\mathbf{y}[k] = \mathbf{h} a[k] + \mathbf{n}[k] \quad (3.58)$$

<sup>14</sup>Similar results can also be found in [JS04b].

<sup>15</sup>The analytical performance results presented in this section are valid for a general covariance matrix  $\mathbf{R}_{\mathbf{h}}$ , which does not have to obey the Kronecker correlation model considered in Section 3.2.3 and 3.2.4.

with MRC at the receiver, where

$$\mathbf{h} := [h_1, \dots, h_{MN}]^T, \quad \mathbf{E}\{\mathbf{h}\mathbf{h}^H\} := \mathbf{R}_{\mathbf{h}} \quad (3.59)$$

( $h_\nu \sim \mathcal{CN}(0, 1)$ ,  $\nu = 1, \dots, MN$ ),

$$\mathbf{n}[k] := [n_1[k], \dots, n_{MN}[k]]^T, \quad \mathbf{E}\{\mathbf{n}[k]\mathbf{n}^H[k]\} := \sigma_n^2 \cdot \mathbf{I}_{MN} \quad (3.60)$$

( $n_\nu[k] \sim \mathcal{CN}(0, \sigma_n^2)$ ,  $\nu = 1, \dots, MN$ ), and

$$\mathbf{E}\{|a[k]|^2\} := \frac{P}{MR_t}. \quad (3.61)$$

The instantaneous and the average received SNR of the  $\nu$ th receive antenna in the equivalent MRC system is thus given by

$$\gamma_{s,\nu} := \frac{P |h_\nu|^2}{MR_t \sigma_n^2} \quad \text{and} \quad \bar{\gamma}_{s,\nu} := \frac{P}{MR_t \sigma_n^2} = \frac{\bar{\gamma}_s}{MN}, \quad (3.62)$$

respectively, cf. (3.57). In the following, let

$$z[k] := \|\mathbf{h}\|_2 a[k] + \eta[k] \quad (3.63)$$

denote the  $k$ th output sample of the maximum ratio combiner, where  $\eta[k] \sim \mathcal{CN}(0, \sigma_n^2)$ . The metric for maximum-likelihood (ML) detection of the information symbols  $a[k]$  is thus given by

$$\mu_{\text{ML}}(z[k], \tilde{a}[k]) := |z[k] - \|\mathbf{h}\|_2 \tilde{a}[k]|^2 \quad (3.64)$$

(cf. Section 2.3.1), where  $\tilde{a}[k]$  denotes a hypothesis for  $a[k]$ .

### Uncorrelated Antennas

In order to determine the average symbol or bit error probability provided by the system, the PDF  $p_{\gamma_s}(\gamma_s)$  of the overall instantaneous received SNR  $\gamma_s$  after maximum ratio combining is of interest (see Appendix I), where  $\gamma_s := \sum_{\nu=1}^{MN} \gamma_{s,\nu}$ . In the case of uncorrelated antennas ( $\mathbf{R}_{\mathbf{h}} = \mathbf{I}_{MN}$ ), the moment-generating function (MGF) of  $\gamma_s$ ,

$$\mathbf{M}\{\gamma_s\}(s) := \mathbf{E}\{e^{s\gamma_s}\} = \int_0^{+\infty} e^{s\gamma_s} p_{\gamma_s}(\gamma_s) d\gamma_s, \quad (3.65)$$

is given by the product of the individual MGFs of the instantaneous received SNRs  $\gamma_{s,\nu}$  ( $\nu = 1, \dots, MN$ ), i.e.,

$$\mathbf{M}\{\gamma_s\}(s) = \prod_{\nu=1}^{MN} \mathbf{M}\{\gamma_{s,\nu}\}(s) \quad (3.66)$$

(see Appendix I). Since in many cases closed-form expressions are known for the MGFs  $\mathbf{M}\{\gamma_{s,\nu}\}(s)$ , cf. Definition C.17 in Appendix C, it is in principle possible to find analytical

expressions for the PDF  $p_{\gamma_s}(\gamma_s)$ , basically via an inverse Laplace transform of  $\mathbf{M}\{\gamma_s\}(s)$ . For example, in the case of Rayleigh fading, the MGFs  $\mathbf{M}\{\gamma_{s,\nu}\}(s)$  are given by

$$\mathbf{M}\{\gamma_{s,\nu}\}(s) = \frac{1}{1 - s\bar{\gamma}_{s,\nu}} \quad (\nu = 1, \dots, MN). \quad (3.67)$$

For example, given unequal average SNRs  $\bar{\gamma}_{s,\nu}$ , one obtains the following closed-form expression for the PDF  $p_{\gamma_s}(\gamma_s)$  [Pro01, Ch. 14.5]:

$$p_{\gamma_s}(\gamma_s) = \sum_{\nu=1}^{MN} \frac{1}{\bar{\gamma}_{s,\nu}} \left( \prod_{\substack{\nu'=1 \\ \nu' \neq \nu}}^{MN} \frac{\bar{\gamma}_{s,\nu}}{\bar{\gamma}_{s,\nu} - \bar{\gamma}_{s,\nu'}} \right) e^{-\gamma_s/\bar{\gamma}_{s,\nu}} \quad (\gamma_s \geq 0). \quad (3.68)$$

Moreover, using Craig's alternative representation of the Gaussian Q-function [Cra91], one can directly find closed-form expressions for the resulting average symbol or bit error probability, which are in the form of finite-range integrals over known functions (see Appendix I). For example, in the case of Rayleigh fading and a  $Q$ -ary phase-shift keying (PSK) signal constellation, the average symbol error probability can be calculated as

$$\bar{P}_s = \frac{1}{\pi} \int_0^{\frac{(Q-1)\pi}{Q}} \mathbf{M}\{\gamma_s\}(s = \varsigma_{\text{PSK}}(\phi)) \, d\phi = \frac{1}{\pi} \int_0^{\frac{(Q-1)\pi}{Q}} \prod_{\nu=1}^{MN} \frac{1}{1 - \varsigma_{\text{PSK}}(\phi) \bar{\gamma}_{s,\nu}} \, d\phi, \quad (3.69)$$

where  $\varsigma_{\text{PSK}}(\phi) := -\sin^2(\pi/Q)/\sin^2(\phi)$ . Further examples can be found in Appendix I.

### Correlated Antennas

In the case of correlated antennas ( $\mathbf{R}_{\mathbf{h}} \neq \mathbf{I}_{MN}$ ), closed-form expressions for  $p_{\gamma_s}(\gamma_s)$  or  $\mathbf{M}\{\gamma_s\}(s)$  are in general hard to obtain. Correspondingly, a direct extension of the above performance analysis to the case of correlated antennas is difficult. However, in [DB02] it was shown that in the case of Rayleigh fading a unitary transform

$$\mathbf{y}'[k] := \mathbf{U} \mathbf{y}[k] \quad (3.70)$$

of the received vector  $\mathbf{y}[k]$  in (3.58), where  $\mathbf{U}$  is an arbitrary unitary matrix, does not change the statistical properties of the MRC system. In particular, the above unitary transform yields a  $(1 \times MN)$ -system

$$\mathbf{y}'[k] = \mathbf{U} \mathbf{h} a[k] + \mathbf{U} \mathbf{n}[k] =: \mathbf{h}' a[k] + \mathbf{n}'[k] \quad (3.71)$$

with

$$\mathbf{E}\{\mathbf{h}'\mathbf{h}'^H\} = \mathbf{U} \mathbf{R}_{\mathbf{h}} \mathbf{U}^H \quad \text{and} \quad \mathbf{E}\{\mathbf{n}'[k]\mathbf{n}'^H[k]\} = \sigma_n^2 \cdot \mathbf{I}_{MN}. \quad (3.72)$$

(The complex Gaussian distribution of the channel coefficients and the noise samples is preserved.) The transformed MRC system is thus given by

$$z'[k] := \|\mathbf{h}'\|_2 a[k] + \eta'[k] = \|\mathbf{h}\|_2 a[k] + \eta'[k], \quad (3.73)$$

where we have exploited that the Euclidean norm is invariant under a unitary transform. The transformed noise samples  $\eta'[k]$  have the same statistical properties as in the original MRC system, i.e.,  $\eta'[k] \sim \mathcal{CN}(0, \sigma_n^2)$ . Correspondingly, the transformed MRC system (3.73) and the original MRC system (3.63) are equivalent.

As will be seen, this observation simplifies the task of performance analysis for spatially correlated MRC systems significantly. Let

$$\mathbf{R}_{\mathbf{h}} = \mathbf{U}_{\mathbf{h}} \mathbf{\Lambda}_{\mathbf{h}} \mathbf{U}_{\mathbf{h}}^H \quad (3.74)$$

denote the eigenvalue decomposition (EVD) of  $\mathbf{R}_{\mathbf{h}}$ , where  $\mathbf{\Lambda}_{\mathbf{h}} := \text{diag}[\lambda_1, \dots, \lambda_{MN}]$ . Choosing  $\mathbf{U} := \mathbf{U}_{\mathbf{h}}^H$ , the spatially correlated MRC system (3.63) can be transformed into an equivalent MRC system with uncorrelated antennas and an overall spatial covariance matrix

$$\mathbf{R}_{\mathbf{h}'} = \mathbb{E}\{\mathbf{h}'\mathbf{h}'^H\} = \mathbf{\Lambda}_{\mathbf{h}}. \quad (3.75)$$

The performance analysis can then be done on the basis of the transformed MRC system, along the same lines as in the case of uncorrelated antennas (and unequal average SNRs).<sup>16</sup> Specifically, the average received SNRs in the transformed MRC system are given by

$$\bar{\gamma}'_{s,\nu} := \frac{P\lambda_{\nu}}{MR_t\sigma_n^2}. \quad (3.76)$$

Moreover, since  $\text{tr}(\mathbf{\Lambda}_{\mathbf{h}}) = \text{tr}(\mathbf{R}_{\mathbf{h}}) = MN$ , the overall average received SNR per information symbol is still given by (3.57).

It should be noted that the above analysis can also be generalized to the case of Rician fading [Ric48], i.e., to the case where line-of-sight (LoS) signal components are present [DB02]. However, in general the Rice factors in the equivalent, transformed system (3.71) will be different from those in the original system (3.58).

### MIMO Systems with Distributed Antennas

As shown above, the average symbol error probability of a correlated  $(1 \times MN)$ -MRC system (and thus of the equivalent  $(M \times N)$ -OSTBC system) can be calculated by evaluating a finite-range integral<sup>17</sup>, where the average received SNRs  $\bar{\gamma}_{s,\nu}$  in the original MRC system have to be replaced by the average received SNRs  $\bar{\gamma}'_{s,\nu}$  obtained for the decorrelated MRC system, cf. (3.62) and (3.76).

As earlier, note that the complete performance analysis depends solely on the eigenvalues of the overall spatial covariance matrix  $\mathbf{R}_{\mathbf{h}}$  (via the transformed average received

<sup>16</sup>The transformed, decorrelated MRC system is often called ‘virtual’ system in the literature. The corresponding unitary transform, which transforms the spatially correlated MRC system into the equivalent decorrelated MRC system, is called Karhunen-Loève transform (KLT) [SW02, Ch. 8.5] and is often used in the literature, in order to analyze correlated systems.

<sup>17</sup>Note that, although (3.69) was for the example of Rayleigh fading and a PSK signal constellation, similar finite-range integral expressions result also for other types of fading and for other signal constellations (see Appendix I). Moreover, the performance analysis can be generalized, in order to calculate the resulting bit error probability.

SNRs  $\bar{\gamma}'_{s,\nu}$ ), but not on specific entries of  $\mathbf{R}_{\mathbf{h}}$ . Correspondingly, if we again focus on an  $(M \times N)$ -OSTBC system characterized by the Kronecker correlation model

$$\mathbf{R}_{\mathbf{h}} = \mathbf{R}_{\mathbf{h},\text{Tx}} \otimes \mathbf{R}_{\mathbf{h},\text{Rx}}, \quad (3.77)$$

where

$$\mathbf{R}_{\mathbf{h},\text{Tx}} = \mathbf{U}_{\text{Tx}} \mathbf{\Lambda}_{\mathbf{h},\text{Tx}} \mathbf{U}_{\text{Tx}}^H \quad \text{and} \quad \mathbf{R}_{\mathbf{h},\text{Rx}} = \mathbf{U}_{\text{Rx}} \mathbf{\Lambda}_{\mathbf{h},\text{Rx}} \mathbf{U}_{\text{Rx}}^H, \quad (3.78)$$

it is clear that the symbol and bit error performance will stay exactly the same, if we replace the transmitter correlation matrix  $\mathbf{R}_{\mathbf{h},\text{Tx}}$  by  $\mathbf{\Sigma}_{\mathbf{h},\text{Tx}} := \mathbf{U}_{\text{Tx}}^H \mathbf{R}_{\mathbf{h},\text{Tx}} \mathbf{U}_{\text{Tx}}$  and/or the receiver correlation matrix  $\mathbf{R}_{\mathbf{h},\text{Rx}}$  by  $\mathbf{\Sigma}_{\mathbf{h},\text{Rx}} := \mathbf{U}_{\text{Rx}}^H \mathbf{R}_{\mathbf{h},\text{Rx}} \mathbf{U}_{\text{Rx}}$ . By this means, we have again found an equivalent  $(M \times N)$ -OSTBC system with distributed transmit or distributed receive antennas. Similarly, given an  $(M \times N)$ -OSTBC system with distributed transmit or distributed receive antennas, we can find an equivalent co-located OSTBC system by evaluating (3.38a) or (3.38b).

The above findings are summarized in the following theorem:

**Theorem 3.3 (Equivalence of distributed and co-located MIMO systems III)**

*For any MIMO system with co-located transmit and receive antennas, which is subject to frequency-flat Rayleigh fading obeying the Kronecker correlation model and which employs an orthogonal space-time block code (OSTBC) with corresponding (widely) linear detection at the receiver, an equivalent MIMO system with distributed transmit and/or distributed receive antennas can be found, and vice versa, such that both systems are characterized by identical average symbol and bit error probabilities.*

*Proof.* In the case of Rayleigh fading, the average symbol and bit error probability of an OSTBC system is invariant under a unitary transform of the transmitter or receiver correlation/covariance matrix. Thus, using the unitary matrix transform (3.33), any co-located OSTBC system can be transformed into an equivalent distributed OSTBC system. Similarly, using the unitary matrix transform (3.38), any distributed OSTBC system can be transformed into an equivalent co-located OSTBC system.  $\square$

### Diversity Advantage of OSTBCs

In the following, the impact of spatial correlations or, equivalently, of unbalanced average link SNRs, on the diversity advantage of OSTBCs is illustrated and compared with a single-antenna system.

As already discussed in Section 2.3.1, the diversity advantage of an OSTBC is reflected by the effective channel coefficient  $\|\mathbf{h}\|_2$  in the equivalent MRC system, cf. (3.63). If the channel coefficients  $h_1, \dots, h_{MN}$  fade more or less independently, the probability for a small magnitude of  $\|\mathbf{h}\|_2$  is comparatively small. This fact is illustrated in Fig 3.5, for the example of an OSTBC system with two co-located transmit antennas, a single receive antenna, and a transmitter correlation matrix<sup>18</sup>

$$\mathbf{R}_{\mathbf{h},\text{Tx}} = \begin{bmatrix} 1 & \rho \\ \rho^* & 1 \end{bmatrix}, \quad (0 \leq |\rho| \leq 1). \quad (3.79)$$

<sup>18</sup>As earlier, we consider the case of Rayleigh fading, where  $h_1, h_2 \sim \mathcal{CN}(0, 1)$ .

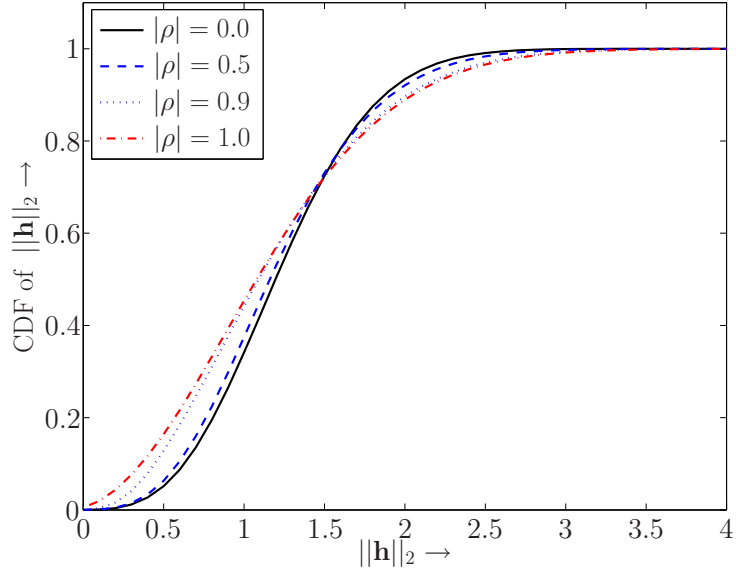


Figure 3.5: CDF of the effective channel coefficient  $\|\mathbf{h}\|_2$  in an OSTBC system with two co-located transmit antennas and a single receive antenna, for different values of the correlation parameter  $|\rho|$  (simulative results obtained by means of Monte-Carlo simulations).

Equivalently, we could consider a  $(2 \times 1)$ -OSTBC system with distributed transmit antennas and transmitter covariance matrix  $\Sigma_{\mathbf{h}, \text{Tx}} = \Lambda_{\mathbf{h}, \text{Tx}}$ , while  $\Lambda_{\mathbf{h}, \text{Tx}} := \text{diag}([1 - |\rho|, 1 + |\rho|])$ , cf. Example H.1 in Appendix H. Fig. 3.5 displays the CDF  $\Pr\{\|\underline{\mathbf{h}}\|_2 \leq \|\mathbf{h}\|_2\}$  of the effective channel coefficient  $\|\mathbf{h}\|_2$ , for different values of  $|\rho|$ . As expected, for large values of  $|\rho|$  the probability of small magnitudes of  $\|\mathbf{h}\|_2$  grows significantly. However, note that for correlation values  $|\rho| \leq 0.5$  the resulting CDF deviates only slightly from the uncorrelated case. Correspondingly, a large fraction of the diversity advantage offered by the OSTBC is retained for  $|\rho| \leq 0.5$  (see also [MH04a], where similar considerations were made). Finally, when  $|\rho|$  approaches one, the same CDF results as in a single-antenna system characterized by a channel coefficient  $h \sim \mathcal{CN}(0, 2)$ , since for a fair comparison the channel variance in the single-antenna system has to be doubled. In this case, the diversity advantage of the OSTBC is completely lost.

In the following, we will have a closer look at the symbol and bit error rates achieved by OSTBC systems with distributed and co-located antennas. To start with, we focus on the special case of binary antipodal transmission ( $Q=2$ ), and consider certain analytical results that provide further insights to the performance of OSTBCs in the presence of antenna correlations and/or unbalanced average link SNRs. Afterwards, some numerical performance results will be presented (also analytical), that cover also higher-order modulation schemes ( $Q>2$ ). As earlier, we focus on the case of Rayleigh fading and the Kronecker correlation model. More general fading scenarios will be considered in Section 3.3.

### Analytical Symbol Error Rate for the Case of Binary Transmission

As discussed above, the error performance of OSTBCs can be assessed on the basis of an equivalent MRC system. In the case of Rayleigh fading and binary antipodal transmission, the average symbol error probability (or, equivalently, the average bit error probability) can be calculated in closed-form, using analytical expressions derived for MRC systems, cf. Appendix I.

Consider an OSTBC system with  $M$  transmit antennas and  $N$  receive antennas (either co-located or distributed). As earlier, let  $\bar{\gamma}_s = PN/(R_t\sigma_n^2)$  denote the overall average received SNR per information symbol, where we again use the normalization introduced in Section 3.2.2. The average symbol error probability can thus be calculated utilizing the expression (I.21) in Appendix I:

$$\bar{P}_s = \frac{1}{2} \sum_{\nu=1}^{MN} \left( \prod_{\substack{\nu'=1 \\ \nu' \neq \nu}}^{MN} \frac{\bar{\gamma}_{s,\nu}}{\bar{\gamma}_{s,\nu} - \bar{\gamma}_{s,\nu'}} \right) \left( 1 - \sqrt{\frac{\bar{\gamma}_{s,\nu}}{1 + \bar{\gamma}_{s,\nu}}} \right), \quad (3.80)$$

where

$$\bar{\gamma}_{s,\nu} := \frac{P\lambda_\nu}{MR_t\sigma_n^2} \quad (\bar{\gamma}_{s,1} + \dots + \bar{\gamma}_{s,MN} = \bar{\gamma}_s) \quad (3.81)$$

and  $\lambda_1, \dots, \lambda_{MN}$  denote the eigenvalues of the overall spatial covariance matrix  $\mathbf{R}_{\mathbf{h}}$ . When we again focus on a co-located OSTBC system obeying the Kronecker correlation model ( $\mathbf{R}_{\mathbf{h}} = \mathbf{R}_{\mathbf{h},\text{Tx}} \otimes \mathbf{R}_{\mathbf{h},\text{Rx}}$ ), the set of eigenvalues  $\{\lambda_\nu | \nu=1, \dots, MN\}$  of  $\mathbf{R}_{\mathbf{h}}$  is given by all pairwise products

$$\{\lambda_{\text{Tx},\mu} \cdot \lambda_{\text{Rx},\nu} | \mu=1, \dots, M, \nu=1, \dots, N\} \quad (3.82)$$

of the eigenvalues of  $\mathbf{R}_{\mathbf{h},\text{Tx}}$  and  $\mathbf{R}_{\mathbf{h},\text{Rx}}$  [LT85, Ch. 12.2]. Therefore, we can rewrite (3.80) according to

$$\bar{P}_s = \frac{1}{2} \sum_{\mu=1}^M \sum_{\nu=1}^N \left( \prod_{\substack{\mu'=1 \\ (\mu',\nu') \neq (\mu,\nu)}}^M \prod_{\nu'=1}^N \frac{1}{1 - \frac{\lambda_{\text{Tx},\mu'} \lambda_{\text{Rx},\nu'}}{\lambda_{\text{Tx},\mu} \lambda_{\text{Rx},\nu}}} \right) \left( 1 - \sqrt{\frac{\lambda_{\text{Tx},\mu} \lambda_{\text{Rx},\nu}}{\lambda_{\text{Tx},\mu} \lambda_{\text{Rx},\nu} + \xi}} \right), \quad (3.83)$$

where  $\xi := MR_t\sigma_n^2/P$ . Again, the above expression can directly be utilized for OSTBC systems with distributed antennas, by setting  $\mathbf{\Lambda}_{\mathbf{h},\text{Tx}} := \mathbf{\Sigma}_{\mathbf{h},\text{Tx}}$  and/or  $\mathbf{\Lambda}_{\mathbf{h},\text{Rx}} := \mathbf{\Sigma}_{\mathbf{h},\text{Rx}}$ .

A high-SNR approximation ( $\bar{\gamma}_s \rightarrow \infty$ ) of (3.83) yields

$$\bar{P}_s \approx \left( \frac{MN}{4\bar{\gamma}_s} \right)^{MN} \binom{2MN-1}{MN} \prod_{\mu=1}^M \prod_{\nu=1}^N \frac{1}{\lambda_{\text{Tx},\mu} \lambda_{\text{Rx},\nu}} \quad (3.84)$$

(cf. [Pro01, Ch. 14.5]), where it was assumed for simplicity that  $\mathbf{R}_{\mathbf{h},\text{Tx}}$  and  $\mathbf{R}_{\mathbf{h},\text{Rx}}$  have full rank, i.e., all eigenvalues are greater than zero. Two important observations can be



made in (3.84). First, asymptotically  $\bar{P}_s$  is always proportional to  $\bar{\gamma}_s^{-MN}$ , i.e., the achieved diversity order of the system (in a log-log plot),

$$d := - \lim_{\bar{\gamma}_s \rightarrow \infty} \frac{\log \bar{P}_s}{\log \bar{\gamma}_s} = MN \quad (3.85)$$

[ZT03], is not reduced as long as  $\mathbf{R}_{\mathbf{h},\text{Tx}}$  and  $\mathbf{R}_{\mathbf{h},\text{Rx}}$  have full rank.<sup>19</sup> Second, the product term in (3.84), which is solely determined by the eigenvalues of  $\mathbf{R}_{\mathbf{h},\text{Tx}}$  and  $\mathbf{R}_{\mathbf{h},\text{Rx}}$ , causes an asymptotic up-shift of the symbol-error-rate curve (again in a log-log plot). As stated by the following lemma, the product term is always greater than or equal to one, with equality if and only if  $\mathbf{R}_{\mathbf{h},\text{Tx}} = \mathbf{I}_M$  and  $\mathbf{R}_{\mathbf{h},\text{Rx}} = \mathbf{I}_N$  holds. Correspondingly, in a co-located OSTBC system any type of antenna correlation at the transmitter or receiver (or any type of SNR imbalance in a distributed OSTBC system) will cause an asymptotic loss with regard to the average symbol error probability (see also [MH05]).

**Lemma 3.1**

Let  $\lambda_1, \dots, \lambda_n$  denote the eigenvalues of an  $(n \times n)$ -correlation matrix  $\mathbf{R}$  with rank  $n$ , i.e.,  $\lambda_1, \dots, \lambda_n$  are real-valued and positive, and  $\lambda_1 + \dots + \lambda_n = n$ . Then, the product term

$$\prod_{j=1}^n \frac{1}{\lambda_j} \quad (3.86)$$

is always greater than or equal to one, with equality if and only if  $\mathbf{R} = \mathbf{I}_n$ .

*Proof.* The product term (3.86) is equal to  $\det(\mathbf{R})^{-1}$ , while  $\det(\mathbf{R})$  is known to be always between zero and one, and equal to one if and only if  $\mathbf{R} = \mathbf{I}_n$  [Gra83, Ch. 8.7].  $\square$

A direct (and very simple) proof of Lemma 3.1, which is based on convex optimization (cf. Appendix E), is provided in Appendix 2 at the end of this chapter.

**Remark 3.6 (Approximations for higher-order modulation schemes)**

High-SNR approximations for the average symbol error probability that are similar to (3.84) can also be found for higher-order modulation schemes, by utilizing the finite-range integral expressions stated in Appendix I. For example, for a  $Q$ -ary PSK signal constellation, one obtains

$$\bar{P}_s \approx \left( \frac{MN}{\sin^2(\pi/Q) \bar{\gamma}_s} \right)^{MN} \frac{g(M, N, Q)}{\pi} \prod_{\mu=1}^M \prod_{\nu=1}^N \frac{1}{\lambda_{\text{Tx},\mu} \lambda_{\text{Rx},\nu}}, \quad (3.87)$$

cf. (3.69), where 
$$g(M, N, Q) := \int_0^{\frac{(Q-1)\pi}{Q}} (\sin \phi)^{2MN} d\phi. \quad (3.88)$$

Correspondingly, the above observations for binary transmission apply also for higher-order modulation schemes. In particular, Lemma 3.1 is still relevant.

<sup>19</sup>In general, the diversity order is given by  $d = \text{rank}(\mathbf{R}_{\mathbf{h},\text{Tx}}) \text{rank}(\mathbf{R}_{\mathbf{h},\text{Rx}})$ .

### Numerical Performance Results

In order to illustrate the impact of spatial correlations or unbalanced average link SNRs on the performance of co-located and distributed OSTBC systems, some numerical performance results are presented in the following. As an example, we focus on an OSTBC system with four distributed transmit antennas and a single receive antenna. The temporal rate of the employed OSTBC is assumed to be  $R_t = 3/4$ , which is the maximum possible rate for four transmit antennas [TH00]. For simplicity, channel coding is not taken into account. However, an outer channel code can be added, so as to further improve performance (see, for example, [LH02] for a comprehensive overview).

To start with, we consider the case of binary antipodal transmission ( $Q=2$ ). Fig. 3.6 displays the average symbol error rate, which results for different transmitter covariance matrices  $\Sigma_{\mathbf{h},\text{Tx}}$  (all with full rank) representing different degrees of SNR imbalance:

$$\Sigma_{\mathbf{h},\text{Tx},1} := \text{diag}([1.0 \ 1.0 \ 1.0 \ 1.0]) = \mathbf{I}_M \quad (3.89a)$$

$$\Sigma_{\mathbf{h},\text{Tx},2} := \text{diag}([0.5 \ 0.7 \ 0.8 \ 2.0]) \quad (3.89b)$$

$$\Sigma_{\mathbf{h},\text{Tx},3} := \text{diag}([0.2 \ 0.3 \ 0.5 \ 3.0]) \quad (3.89c)$$

$$\Sigma_{\mathbf{h},\text{Tx},4} := \text{diag}([0.1 \ 0.2 \ 0.2 \ 3.5]). \quad (3.89d)$$

Again, we could equivalently consider an OSTBC system with four co-located transmit antennas and a correlation matrix  $\mathbf{R}_{\mathbf{h},\text{Tx}}$  with eigenvalue matrix  $\Lambda_{\mathbf{h},\text{Tx}} = \Sigma_{\mathbf{h},\text{Tx}}$ . The resulting symbol-error-rate curves are plotted as a function of  $P/\sigma_n^2$  in dB, while the overall average received SNR per information symbol in the OSTBC system is given by  $\bar{\gamma}_s = P/(R_t\sigma_n^2) = 1.333 \cdot P/\sigma_n^2$ . The curves were obtained on the basis of (3.83) and (I.19) in Appendix I, and were validated by means of Monte-Carlo simulations. For comparison, the corresponding curve for a single-antenna system has also been included (average received SNR  $P/\sigma_n^2$ ). As predicted by the high-SNR approximation (3.84), the best performance is achieved by the OSTBC system with  $\Sigma_{\mathbf{h},\text{Tx}} = \mathbf{I}_M$  (also for low and medium SNR values). Interestingly, although the SNR imbalance for  $\Sigma_{\mathbf{h},\text{Tx}} = \Sigma_{\mathbf{h},\text{Tx},2}$  is already quite significant, the resulting symbol-error-rate curve is still close to the optimal curve. However, when the SNR imbalance becomes more significant, the resulting performance loss can be quite large (e.g., for  $\Sigma_{\mathbf{h},\text{Tx}} = \Sigma_{\mathbf{h},\text{Tx},4}$  a loss of about 4 dB is observed at a symbol error rate of  $10^{-4}$ ). Yet, a significant performance improvement over the single-antenna system is achieved, especially for large SNR values. In particular, the symbol-error-rate curve of the OSTBC system is always characterized by an asymptotic slope of  $-4$ , as predicted by (3.84), whereas the asymptotic slope for the single-antenna system is  $-1$ .

Fig. 3.7 displays corresponding performance results for 8-PSK modulation (for the same transmitter covariance matrices  $\Sigma_{\mathbf{h},\text{Tx}}$ ), which were obtained on the basis of (3.69). As can be seen, the main observations are the same as for binary antipodal transmission.

### Capacity Results for OSTBC Systems

To conclude this section on OSTBCs, some numerical results are presented in the following that concern the maximum mutual information achieved by co-located and distributed OSTBC systems.

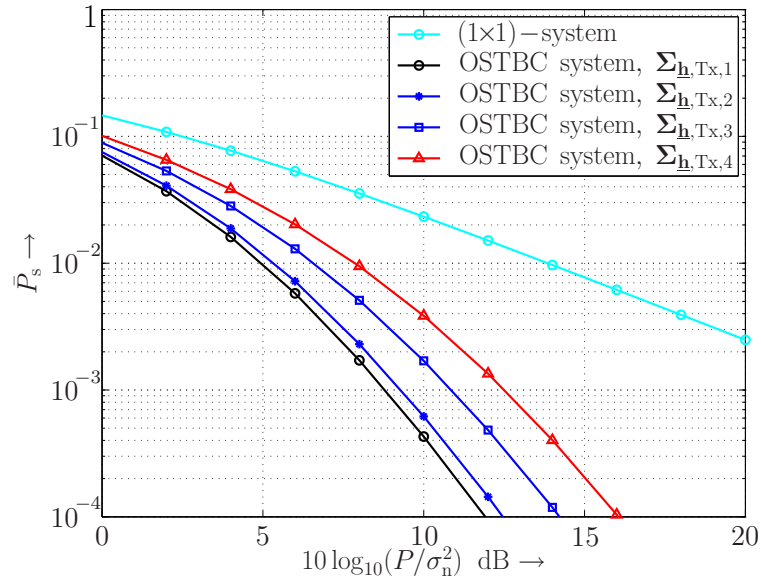


Figure 3.6: Average symbol error rate of an OSTBC system with four distributed transmit antennas and a single receive antenna: Analytical results for binary antipodal transmission ( $Q=2$ ) and different transmitter covariance matrices  $\Sigma_{\mathbf{h}, \text{Tx}}$ .

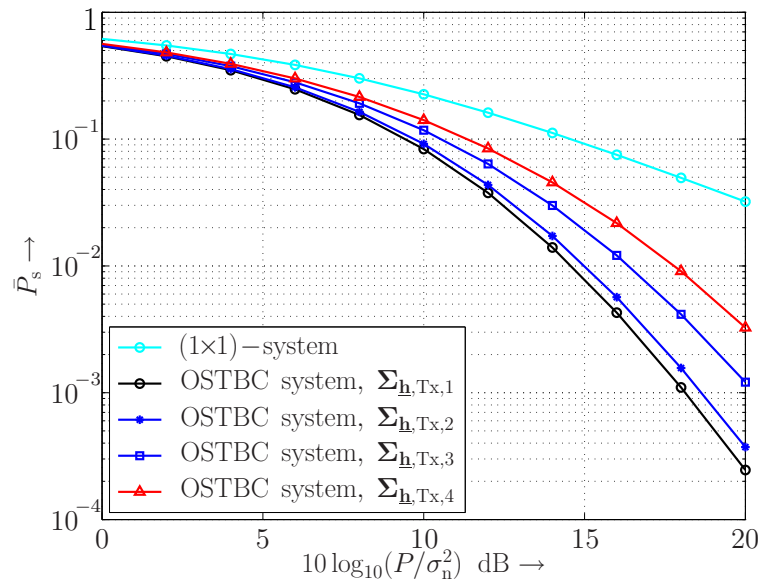


Figure 3.7: Average symbol error rate of an OSTBC system with four distributed transmit antennas and a single receive antenna: Analytical results for an 8-PSK signal constellation ( $Q=8$ ) and different transmitter covariance matrices  $\Sigma_{\mathbf{h}, \text{Tx}}$ .

Similar to the average symbol error rate, the (instantaneous) maximum mutual information of an OSTBC system,  $C_{\text{OSTBC}}(\mathbf{h})$ , can again be assessed on the basis of the equivalent MRC system (3.63). The result is [SP00, Doh03]

$$C_{\text{OSTBC}}(\mathbf{h}) = R_t \cdot \log_2 \left( 1 + \frac{P}{MR_t \sigma_n^2} \|\mathbf{h}\|_2^2 \right) \text{ bit/channel use.} \quad (3.90)$$

In other words, the maximum mutual information achieved by an OSTBC system is in essence equal to the capacity of a scaled AWGN channel. Note that in the case of a single receive antenna ( $N=1$ ) and a temporal rate of  $R_t \rightarrow 1$ , the above expression tends to the MIMO capacity expression (3.22), i.e., in this case the OSTBC system is capacity achieving. Otherwise, the maximum mutual information of an OSTBC system is inferior to that of a general MIMO system [SP00].

As earlier, we note that the Euclidean norm is invariant under a unitary matrix transform. Correspondingly, any co-located OSTBC system obeying the Kronecker correlation model can be transformed into an equivalent distributed OSTBC system and vice versa (via the equivalent MRC systems, cf. (3.70)-(3.76)), such that both systems are characterized by exactly the same capacity distribution. Concerning the ergodic maximum mutual information  $\bar{C}_{\text{OSTBC}}$ , we can find an upper bound by applying Jensen's inequality:

$$\bar{C}_{\text{OSTBC}} \leq R_t \cdot \log_2 \left( 1 + \frac{PN}{R_t \sigma_n^2} \right). \quad (3.91)$$

Note that the upper bound does not depend on the transmitter or receiver correlation/covariance matrix anymore and is thus a generic upper bound.

As an example, we revisit the MIMO system with four distributed transmit antennas and three co-located receive antennas, which was earlier considered in Section 3.2.3 (cf. Fig. 3.3). Again we assume that an OSTBC with a temporal rate of  $R_t = 3/4$  is employed at the transmitter side. In Fig. 3.8, the ergodic maximum mutual informations  $\bar{C}_{\text{OSTBC}}$  resulting for different transmitter and receiver correlation/covariance matrices are plotted as a function of the average SNR  $P/\sigma_n^2$  in dB (simulative results obtained by means of Monte-Carlo simulations). The dotted curve represents the corresponding upper bound (3.91). Interestingly, the maximum mutual information of the OSTBC system is virtually not influenced by the transmitter or receiver covariance matrix. Moreover, the generic upper bound (3.91) is very tight throughout the whole SNR range. Compared to a general MIMO system, the achieved ergodic maximum mutual information is significantly reduced, especially for high SNR values (cf. Fig. 3.3). Moreover, the gain compared to a single-antenna system tends to be comparatively small. For very large SNR values (greater than 27.3 dB in this example), the single-antenna system even outperforms the OSTBC system (not shown in Fig. 3.8).

### 3.2.6 A Simple Performance Measure

The previous sections have shown that co-located and distributed MIMO systems are (asymptotically) equivalent with regard to many important performance measures, such as the capacity distribution (and thus the ergodic and outage capacity) as well as the

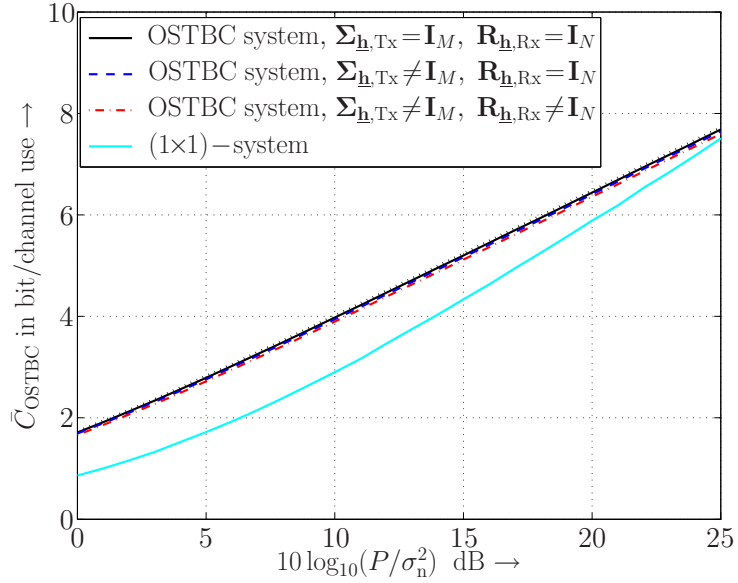


Figure 3.8: Ergodic maximum mutual information  $\bar{C}_{\text{OSTBC}}$  of an OSTBC system with four distributed transmit and three co-located receive antennas, resulting for equal/unequal average link SNRs and uncorrelated/correlated receive antennas. (Simulative results were obtained by means of Monte-Carlo simulations; dotted line: Analytical upper bound.) For comparison, the ergodic capacity of a single-antenna system has also been included.

(pairwise or symbol) error probability of space-time codes. Specifically, it was shown that antenna correlations (or, equivalently, an imbalance in the average link SNRs) can cause significant performance degradations, both with regard to capacity and error performance. However, the antenna correlation matrices  $\mathbf{R}_{\mathbf{h},\text{Tx}}$  and  $\mathbf{R}_{\mathbf{h},\text{Rx}}$  (or the covariance matrices  $\Sigma_{\mathbf{h},\text{Tx}}$  and  $\Sigma_{\mathbf{h},\text{Rx}}$ ) do not directly reflect the associated performance loss in terms of capacity or error rate. It is therefore not immediately obvious, how two MIMO systems with different transmitter or receiver correlation matrices behave in comparison with each other.

To this end, a simple performance measure  $\Delta(\mathbf{R}_{\mathbf{h}})$  between zero and one is considered in the following, which allows for a classification of different MIMO systems. The performance measure was earlier proposed in [IN03], in order to categorize spatially correlated MIMO systems with regard to their ergodic capacity. As will be seen in the sequel, it can also be used, in order to categorize space-time coded MIMO-systems (with co-located or distributed antennas) with regard to the associated error performance (see also [MH05]).

Consider again a MIMO system with co-located transmit and receive antennas and an overall spatial covariance matrix  $\mathbf{R}_{\mathbf{h}} = \mathbf{R}_{\mathbf{h},\text{Tx}} \otimes \mathbf{R}_{\mathbf{h},\text{Rx}}$ . The corresponding performance measure  $\Delta(\mathbf{R}_{\mathbf{h}})$  is defined as [IN03]

$$\Delta(\mathbf{R}_{\mathbf{h}}) = \frac{1}{\sqrt{MN(MN-1)}} \sqrt{\sum_{i=1}^{MN} \sum_{\substack{j=1 \\ j \neq i}}^{MN} |[\mathbf{R}_{\mathbf{h}}]_{i,j}|^2}. \quad (3.92)$$

Note that  $\Delta(\mathbf{R}_{\mathbf{h}})$  is always between zero and one, while zero corresponds to the uncorrelated case ( $\Delta(\mathbf{I}_{MN}) = 0$ ) and one to the fully correlated case with  $|\mathbf{R}_{\mathbf{h}}]_{i,j}| = 1$  for all indices  $i, j = 1, \dots, MN$ .

In the following, we reformulate (3.92) such that it can directly be used for MIMO systems with distributed transmit or receive antennas. To this end, we rewrite (3.92) according to

$$\Delta(\mathbf{R}_{\mathbf{h}}) = \frac{\|\mathbf{R}_{\mathbf{h}} - \mathbf{I}_{MN}\|_{\text{F}}}{\sqrt{MN(MN - 1)}}. \quad (3.93)$$

As earlier, let

$$\mathbf{R}_{\mathbf{h}} := \mathbf{U}_{\mathbf{h}} \mathbf{\Lambda}_{\mathbf{h}} \mathbf{U}_{\mathbf{h}}^{\text{H}}, \quad (3.94)$$

denote the eigenvalue decomposition of  $\mathbf{R}_{\mathbf{h}}$ , where  $\mathbf{U}_{\mathbf{h}} \mathbf{U}_{\mathbf{h}}^{\text{H}} = \mathbf{I}_{MN}$ . Since  $\mathbf{R}_{\mathbf{h}}$  is the Kronecker product of  $\mathbf{R}_{\mathbf{h},\text{Tx}}$  and  $\mathbf{R}_{\mathbf{h},\text{Rx}}$ , the eigenvalues of  $\mathbf{R}_{\mathbf{h}}$  are again given by all pairwise products  $\lambda_{\text{Tx},\mu} \lambda_{\text{Rx},\nu}$  of the eigenvalues of  $\mathbf{R}_{\mathbf{h},\text{Tx}}$  and  $\mathbf{R}_{\mathbf{h},\text{Rx}}$ . Utilizing the fact that the Frobenius norm is invariant under a unitary matrix transform, we have

$$\|\mathbf{R}_{\mathbf{h}} - \mathbf{I}_{MN}\|_{\text{F}} = \|\mathbf{\Lambda}_{\mathbf{h}} - \mathbf{I}_{MN}\|_{\text{F}}, \quad (3.95)$$

i.e., (3.93) can be reformulated as

$$\Delta(\mathbf{R}_{\mathbf{h}}) = \frac{1}{\sqrt{MN(MN - 1)}} \sqrt{\sum_{\mu=1}^M \sum_{\nu=1}^N (\lambda_{\text{Tx},\mu} \lambda_{\text{Rx},\nu} - 1)^2}. \quad (3.96)$$

We have thus found a new expression for  $\Delta(\mathbf{R}_{\mathbf{h}})$  as a function of the eigenvalues of  $\mathbf{R}_{\mathbf{h},\text{Tx}}$  and  $\mathbf{R}_{\mathbf{h},\text{Rx}}$ , which can directly be used for MIMO systems with distributed transmit or receive antennas (again by setting  $\mathbf{\Lambda}_{\mathbf{h},\text{Tx}} := \mathbf{\Sigma}_{\mathbf{h},\text{Tx}}$  and/or  $\mathbf{\Lambda}_{\mathbf{h},\text{Rx}} := \mathbf{\Sigma}_{\mathbf{h},\text{Rx}}$ ).

In [IN03] it was shown that the above performance measure is well suited, in order to categorize co-located and distributed MIMO systems according to their ergodic capacity. In the following, it is demonstrated that the performance measure is also well suited for categorizing OSTBC systems according to the resulting error performance (provided that all associated matrices  $\mathbf{R}_{\mathbf{h}}$  have the same rank). As earlier, we consider an OSTBC system with four distributed transmit antennas, a single receive antenna, and different transmitter covariance matrices (all with full rank):

$$\mathbf{\Sigma}_{\mathbf{h},\text{Tx},1} := \text{diag}([0.222 \ 0.222 \ 0.444 \ 3.111]), \quad (3.97a)$$

$$\mathbf{\Sigma}_{\mathbf{h},\text{Tx},2} := \text{diag}([0.154 \ 0.154 \ 0.615 \ 3.077]), \quad (3.97b)$$

$$\mathbf{\Sigma}_{\mathbf{h},\text{Tx},3} := \text{diag}([0.154 \ 0.308 \ 0.462 \ 3.077]). \quad (3.97c)$$

All of the above transmitter covariance matrices lead to a performance measure of about  $\Delta(\mathbf{R}_{\mathbf{h}}) = \Delta(\mathbf{\Sigma}_{\mathbf{h},\text{Tx}}) \approx 0.7$ . In the following, we restrict ourselves to the case of binary antipodal transmission ( $Q = 2$ ). As earlier, we assume that an OSTBC with a temporal rate of  $R_t = 3/4$  is employed at the transmitter side. Fig. 3.9 displays the average symbol error rates as a function of  $P/\sigma_n^2$  in dB, which result for the different transmitter covariance matrices under consideration. As can be seen, the resulting symbol error rates

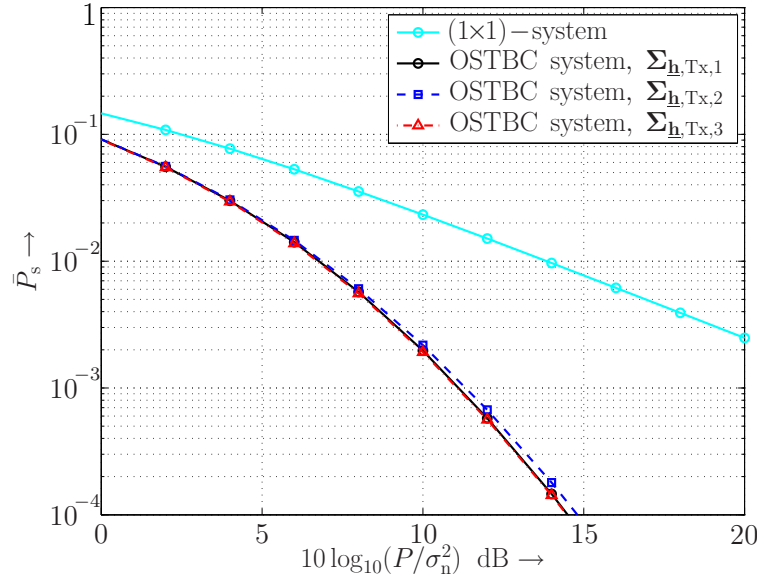


Figure 3.9: Average symbol error rate of an OSTBC system with four distributed transmit antennas and a single receive antenna: Analytical results for binary antipodal transmission ( $Q=2$ ) and different transmitter covariance matrices  $\Sigma_{\mathbf{h},Tx}$  with  $\Delta(\Sigma_{\mathbf{h},Tx}) \approx 0.7$ .

are very similar throughout the whole SNR range under consideration, i.e., the performance measure  $\Delta(\mathbf{R}_{\mathbf{h}})$  predicts the system behavior quite accurately. Additionally, the product term in (3.84) can be taken as a performance measure, so as to predict the error performance resulting for large SNR values.

### 3.3 Generalization to other Channel Models

So far, we have focussed on the special case of Rayleigh fading in conjunction with the Kronecker correlation model. Under these assumptions, it was shown that MIMO systems with distributed antennas are (asymptotically) equivalent to MIMO systems with co-located antennas, with respect to many important performance measures. In particular, any co-located MIMO system with correlated antennas can be transformed into an (asymptotically) equivalent distributed MIMO system with unequal average link SNRs, and vice versa. In this section, more general fading models are considered. As will be seen, the most important results presented in the previous section also apply when the assumption of Rayleigh fading is dropped.

#### 3.3.1 Generalized Fading Models

The Rayleigh fading model is widely used in the literature, in order to model wireless communication systems in rich-scattering environments, where no line-of-sight link between transmitter and receiver is available. In the following, we consider the more gen-



eral Nakagami- $m$  fading model [Nak60], which is another popular fading model for rich-scattering scenarios without line of sight. (The presence of line-of-sight signal components will be considered in Section 3.4.) For the time being, we employ the Kronecker correlation model (3.12) for simplicity. More general spatial correlation models will be discussed in Section 3.3.2.

The Nakagami- $m$  distribution (cf. Definition C.13 in Appendix C) is used to model wireless scenarios where fading is either more severe than in the case of Rayleigh fading ( $m < 1$ ) or milder ( $m > 1$ ), cf. Section 2.2.4. In fact, it was shown that the Nakagami- $m$  distribution (with suitably chosen fading parameter  $m$ ) often yields a better fit to practical measurements than the Rayleigh distribution [SA00, Ch. 2.2]. Possible values for  $m$  are  $0.5 \leq m < \infty$ , where  $m = 0.5$  corresponds to the most severe type of fading and  $m \rightarrow \infty$  to a non-fading AWGN link (similar to the Rician fading model with Rice factor  $K \rightarrow \infty$ ). For  $m = 1$ , the Nakagami- $m$  distribution coincides with the Rayleigh distribution. Moreover, for large values of  $m$  (say,  $m \geq 10$ ), the Nakagami- $m$  distribution well approximates a Rician distribution with Rice factor  $K = \sqrt{m^2 - m} / (m - \sqrt{m^2 - m})$ , cf. Definition C.13. The results presented in the sequel are thus also relevant for Rician fading.

Consider first a MIMO system with co-located transmit and receive antennas. According to the Kronecker correlation model, we assume that the channel matrix  $\mathbf{H}$  can be written as

$$\mathbf{H} := \mathbf{R}_{\mathbf{h},\text{Rx}}^{1/2} \mathbf{H}' \mathbf{R}_{\mathbf{h},\text{Tx}}^{1/2} \quad (3.98)$$

As earlier, the entries  $h'_{\nu,\mu}$  of the matrix  $\mathbf{H}'$  ( $\mu = 1, \dots, M$ ,  $\nu = 1, \dots, N$ ) are assumed to be independent and identically distributed (i.i.d.) random variables. The amplitudes  $|h'_{\nu,\mu}|$  are assumed to follow the Nakagami- $m$  distribution (C.22), and the phases are uniformly distributed in  $[0, 2\pi)$ . For simplicity, we assume that the fading parameter  $m$  is the same for all channel coefficients  $h'_{\nu,\mu}$ . Note that in contrast to the Rician fading model, the channel coefficients in the Nakagami- $m$  fading model have always zero means. Following the normalization introduced in Section 3.2.2, we set  $\mathbf{E}\{|h'_{\nu,\mu}|^2\} = 1$  for all indices  $\mu$  and  $\nu$ . In the case of distributed antennas, the matrices  $\mathbf{R}_{\mathbf{h},\text{Tx}}$  and  $\mathbf{R}_{\mathbf{h},\text{Rx}}$  are again replaced by diagonal matrices  $\mathbf{\Sigma}_{\mathbf{h},\text{Tx}}$  and  $\mathbf{\Sigma}_{\mathbf{h},\text{Rx}}$ , respectively, where  $\text{tr}(\mathbf{\Sigma}_{\mathbf{h},\text{Tx}}) := M$  and  $\text{tr}(\mathbf{\Sigma}_{\mathbf{h},\text{Rx}}) := N$ .

In the following, we consider the capacity distribution of a coded MIMO system with co-located or distributed antennas under Nakagami- $m$  fading. Afterwards, we will focus on the average symbol error rate of OSTBC systems.

### Capacity Distribution of Co-located and Distributed MIMO Systems

As discussed earlier in Section 3.2.3, in the case of Rayleigh fading the capacity distribution of a co-located MIMO system with correlated antennas can be calculated analytically, via the corresponding characteristic function, cf. (3.26). To the best of the author's knowledge, similar analytical expressions are not known for Nakagami- $m$  fading (neither for co-located nor for distributed MIMO systems). We therefore resort to simulative results in the sequel. As an example, Fig. 3.10 and 3.11 display the capacity distributions  $p_r(r)$  ( $r := C(\mathbf{H})$ ) resulting for different MIMO systems with four transmit and three receive antennas under Nakagami- $m$  fading (for an SNR of  $10 \log_{10}(P/\sigma_n^2) = 26$  dB). The associated ergodic capacities are marked by dashed vertical lines. In Fig 3.10, a fading

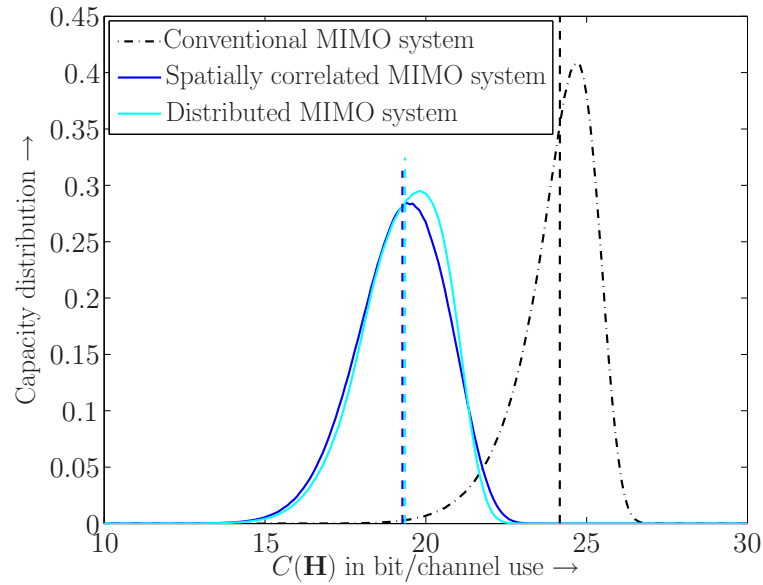


Figure 3.10: Capacity distributions  $p_r(r)$  for different MIMO systems with four transmit and three receive antennas, at an SNR of  $10 \log_{10}(P/\sigma_n^2) = 26$  dB: Nakagami- $m$  fading with fading parameter  $m=10$  for all transmission links (approximated by Rician fading with a Rice factor of  $K = 18.487$ , cf. Fig. C.4 in Appendix C); simulative results obtained by means of Monte-Carlo simulations over  $10^6$  independent channel realizations.

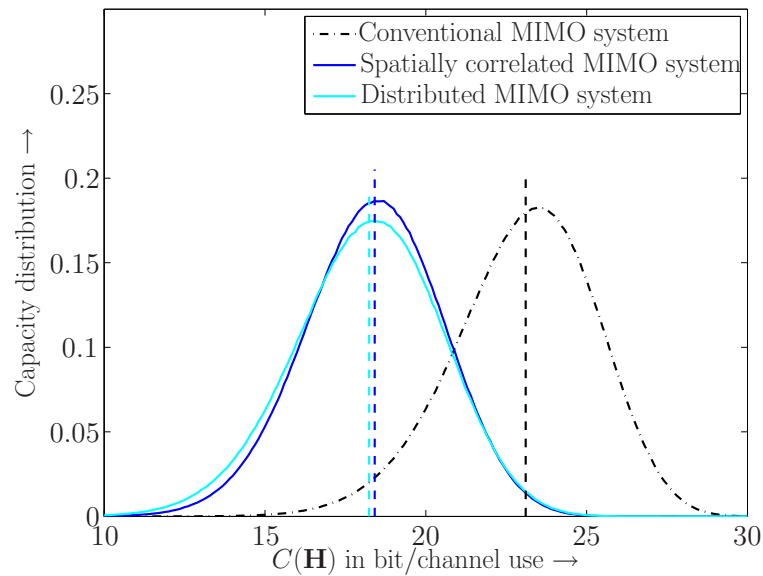


Figure 3.11: Corresponding capacity distributions  $p_r(r)$  for Nakagami- $m$  fading with fading parameter  $m=0.5$  for all transmission links.

parameter of  $m=10$  was chosen for all transmission links and in Fig 3.11 a fading parameter of  $m=0.5$ . Similar to Section 3.2.3, three different MIMO systems are considered: A co-located MIMO system with statistically independent links (‘conventional MIMO system’), a co-located MIMO system with correlated transmit and receive antennas, and a distributed MIMO system with unequal average link SNRs. As earlier, the co-located MIMO system is characterized by a transmitter correlation matrix  $\mathbf{R}_{\mathbf{h},\text{Tx}} = \mathbf{R}_{M,\rho_{\text{Tx}}}$  with  $\rho_{\text{Tx}}=0.8$ , cf. (3.39), and a receiver correlation matrix  $\mathbf{R}_{\mathbf{h},\text{Rx}} = \mathbf{R}_{N,\rho_{\text{Rx}}}$  with  $\rho_{\text{Rx}}=0.7$ . The distributed MIMO system is again characterized by the covariance matrices (3.40).

In the case of Rayleigh fading, the co-located MIMO system and the distributed MIMO system lead to exactly the same capacity distribution, cf. Fig. 3.2. As can be seen in Fig. 3.10 and 3.11, in the presence of Nakagami- $m$  fading this strict equivalence does not hold anymore (or at least the unitary matrix transforms (3.33) and (3.38) established for Rayleigh fading do not yield equivalent systems). Still, it can be seen that the co-located MIMO system with correlated antennas and the distributed MIMO system exhibit a very similar behavior. In both cases ( $m=10$  and  $m=0.5$ ), the ergodic capacity of the distributed and the spatially correlated MIMO system is significantly reduced compared to the co-located MIMO system with statistically independent links. For example, in the case  $m=0.5$  the ergodic capacity is reduced from 23.1 bit/channel use in the ‘conventional’ MIMO system to 18.4 bit/channel use in the spatially correlated MIMO system, and to 18.2 bit/channel use in the distributed MIMO system. Moreover, the capacity distributions resulting for the distributed and the spatially correlated MIMO system have a similar width. Interestingly, the impact of the Nakagami fading parameter on the ergodic capacity is quite small in the considered example. In the case of mild fading ( $m=10$ ), the ergodic capacities are only slightly larger than for Rayleigh fading (cf. Fig. 3.2), and in the case of severe fading ( $m=0.5$ ) they are only slightly decreased. However, for  $m=10$  the capacity distributions are significantly narrower than for Rayleigh fading, which is relevant for the associated outage capacity. Similarly, a Nakagami fading parameter of  $m=0.5$  leads to significantly wider capacity distributions.

### Symbol Error Rates of Co-located and Distributed OSTBC Systems

As earlier, we focus on a co-located or distributed OSTBC system with  $M$  transmit and  $N$  receive antennas. In order to assess the resulting average symbol error probability in the presence of Nakagami- $m$  fading, we again utilize the equivalent MRC system

$$z[k] = \|\mathbf{h}\|_2 a[k] + \eta[k], \quad \mathbf{h} = [h_1, \dots, h_{MN}]^T, \quad \eta[k] \sim \mathcal{CN}(0, \sigma_n^2), \quad (3.99)$$

cf. Section 2.3.1 and Section 3.2.5. The instantaneous received SNR (per information symbol) of the  $\nu$ th receive antenna ( $\nu=1, \dots, MN$ ) in the equivalent MRC system is again given by

$$\gamma_{s,\nu} := \frac{P |h_\nu|^2}{MR_t \sigma_n^2}. \quad (3.100)$$

An analytical expression for the PDF of  $\gamma_{s,\nu}$  in the case of Nakagami- $m$  fading is given by (C.25) in Appendix C. Some example PDFs are displayed in Fig. C.4, for different values of the Nakagami fading parameter  $m$  ( $\bar{\gamma}_{s,\nu}=1$  in all cases). Note that for  $m > 1$ ,

the PDF of  $\gamma_{s,\nu}$  is less concentrated at small values than in the case of Rayleigh fading. In other words, the probability for small instantaneous SNR values is markedly reduced (as expected). However, given a small Nakagami fading parameter ( $m \rightarrow 0.5$ ), the probability for small values of  $\gamma_{s,\nu}$  is significantly larger than for Rayleigh fading.

Consider first an OSTBC system with co-located transmit and co-located receive antennas. As earlier, we assume that the channel vector  $\mathbf{h}$  is characterized by a covariance matrix  $\mathbf{E}\{\mathbf{h}\mathbf{h}^H\} =: \mathbf{R}_{\mathbf{h}}$ . For the case of Rayleigh fading, it was shown in Section 3.2.5 that the average symbol error probability of a spatially correlated OSTBC system can be assessed by transforming the equivalent (correlated) MRC system (3.99) into a statistically equivalent uncorrelated MRC system

$$z'[k] = \|\mathbf{h}'\|_2 a[k] + \eta'[k], \quad \mathbf{h}' = \mathbf{U}_{\mathbf{h}}^H \mathbf{h}, \quad \eta'[k] \sim \mathcal{CN}(0, \sigma_n^2), \quad (3.101)$$

where the unitary matrix  $\mathbf{U}_{\mathbf{h}}$  is taken from the eigenvalue decomposition of  $\mathbf{R}_{\mathbf{h}}$  (cf. Section 3.2.5). In fact, the above MRC system is always statistically equivalent to the MRC system (3.99), irrespective of the underlying fading model. This becomes evident when considering the instantaneous SNR after maximum ratio combining, which is exactly the same in both systems (for any realization of the channel vector  $\mathbf{h}$ ):

$$\gamma_s = \sum_{\nu=1}^{MN} \gamma_{s,\nu} = \frac{P \|\mathbf{h}\|_2^2}{MR_t \sigma_n^2} = \frac{P \|\mathbf{h}'\|_2^2}{MR_t \sigma_n^2}, \quad (3.102)$$

see also [DB02].<sup>20</sup> As earlier, the average received SNRs  $\bar{\gamma}'_{s,\nu}$  in the equivalent uncorrelated MRC system are given by (3.76), i.e., the complete performance analysis again depends only on the eigenvalues of the overall spatial covariance matrix  $\mathbf{R}_{\mathbf{h}} = \mathbf{R}_{\mathbf{h},\text{Tx}} \otimes \mathbf{R}_{\mathbf{h},\text{Rx}}$ , just as in the case of Rayleigh fading. Correspondingly, the symbol error performance will not change if we replace  $\mathbf{R}_{\mathbf{h},\text{Tx}}$  and/or  $\mathbf{R}_{\mathbf{h},\text{Rx}}$  by the corresponding eigenvalue matrices  $\mathbf{\Lambda}_{\mathbf{h},\text{Tx}}$  and  $\mathbf{\Lambda}_{\mathbf{h},\text{Rx}}$ . In other words, the unitary matrix transform (3.33) still yields an equivalent distributed OSTBC system, even if the assumption of Rayleigh fading is dropped. Similarly, by means of the unitary matrix transform (3.38) any given distributed OSTBC system can again be transformed into an equivalent OSTBC system with co-located antennas. Due to the above equivalence, the average symbol error probability of a spatially correlated OSTBC system can again be obtained analytically, based on the moment-generating functions (MGFs) of the instantaneous SNRs  $\gamma_{s,\nu}$  (cf. Table C.1 in Appendix C). For example, in the case of Nakagami- $m$  fading and a  $Q$ -ary PSK signal constellation, the average symbol error probability can be calculated as

$$\bar{P}_s = \frac{1}{\pi} \int_0^{\frac{(Q-1)\pi}{Q}} \mathbf{M}\{\gamma_s\}(s = \varsigma_{\text{PSK}}(\phi)) d\phi = \frac{1}{\pi} \int_0^{\frac{(Q-1)\pi}{Q}} \prod_{\nu=1}^{MN} \left( \frac{m}{m - \varsigma_{\text{PSK}}(\phi) \bar{\gamma}'_{s,\nu}} \right)^m d\phi, \quad (3.103)$$

similar to the case of Rayleigh fading, cf. (3.69). For fading parameters  $m < \infty$ , the corresponding high-SNR approximation ( $\bar{\gamma}_s \rightarrow \infty$ ) reads

$$\bar{P}_s \approx \frac{1}{\pi} \left( \frac{MNm}{\sin^2(\pi/Q) \bar{\gamma}_s} \right)^{MNm} \left( \prod_{\mu=1}^M \prod_{\nu=1}^N \frac{1}{\lambda_{\text{Tx},\mu} \lambda_{\text{Rx},\nu}} \right)^m \int_0^{\frac{(Q-1)\pi}{Q}} (\sin \phi)^{2MNm} d\phi. \quad (3.104)$$

<sup>20</sup>The statistics of the noise terms  $\eta[k]$  and  $\eta'[k]$  are independent of the underlying fading model, cf. Section 2.3.1 and Appendix I.

Interestingly, in the above expression the same product term occurs as in the case of Rayleigh fading. Correspondingly, Lemma 3.1 is also relevant for Nakagami- $m$  fading. Moreover, note that compared to Rayleigh fading the diversity order of the OSTBC system is altered from  $MN$  to  $MNm$ .<sup>21</sup>

In the following, numerical performance results are presented, again for the examples  $m=10$  and  $m=0.5$ . Similar to Section 3.2.5, an OSTBC system with four distributed transmit antennas and a single receive antenna is considered. (Alternatively, one could also consider the equivalent co-located OSTBC system.) As earlier, different transmitter covariance matrices are taken into account, which represent different degrees of SNR imbalance, cf. (3.89). The temporal rate of the employed OSTBC is assumed to be  $R_t=3/4$ . For simplicity, we focus on the case of binary antipodal transmission ( $Q=2$ ). Fig. 3.12 displays the average symbol error rates resulting for  $m=10$  and  $m=0.5$  and the different transmitter covariance matrices  $\Sigma_{\mathbf{h},\text{Tx}}$ . The curves were obtained on the basis of (3.103) and were validated by means of Monte-Carlo simulations. As can be seen, similar to the case of Rayleigh fading the best performance is again achieved by the OSTBC system with  $\Sigma_{\mathbf{h},\text{Tx}} = \Sigma_{\mathbf{h},\text{Tx},1} = \mathbf{I}_M$  (both for  $m=10$  and  $m=0.5$ ), as expected. With growing SNR imbalance, the resulting performance loss becomes more and more significant. However, when fading is light ( $m=10$ ) the OSTBC system is generally much less sensitive to unbalanced average link SNRs than in the case of severe fading ( $m=0.5$ ). In any case, significant performance improvements over the corresponding single-antenna system are achieved, particularly for  $m=0.5$ .

Finally, it is demonstrated that the performance measure introduced in Section 3.2.6 is also useful for the case of Nakagami- $m$  fading. To this end, we again consider the different transmitter covariance matrices in (3.97), which are all associated with a performance measure of about  $\Delta(\Sigma_{\mathbf{h},\text{Tx}}) \approx 0.7$ . Fig. 3.13 displays the corresponding average symbol error rates that result for the example  $m=0.5$  and  $Q=2$ . As can be seen, the symbol error rates are very similar throughout the whole SNR range under consideration, just as in the case of Rayleigh fading. Similar results were also obtained for the example  $m=10$ .

### MIMO Systems with Intersymbol Interference

The above discussion has shown that many important results presented in Section 3.2 are still valid when a more general fading model is considered. In particular, it was seen that distributed MIMO systems with unequal average link SNRs generally have an inferior performance compared to co-located MIMO systems with uncorrelated antennas, at least when no macroscopic diversity gains are available in the distributed MIMO system. (The benefits of macroscopic diversity effects will be considered in Section 3.4.)

For simplicity, all performance results presented so far were restricted to MIMO systems without intersymbol interference (ISI). From a practical point of view, this restriction is reasonable since many (current and future) wireless communication systems are based on OFDM with a guard interval of sufficient length so that the impact of ISI can be neglected. Due to this fact, most papers on MIMO systems disregard ISI effects completely,

<sup>21</sup>For simplicity, we have assumed that the fading parameter  $m$  is the same for all transmission links. However, it is straightforward to generalize the above results to the case of unequal fading parameters, which might be of interest for OSTBC systems with distributed antennas.

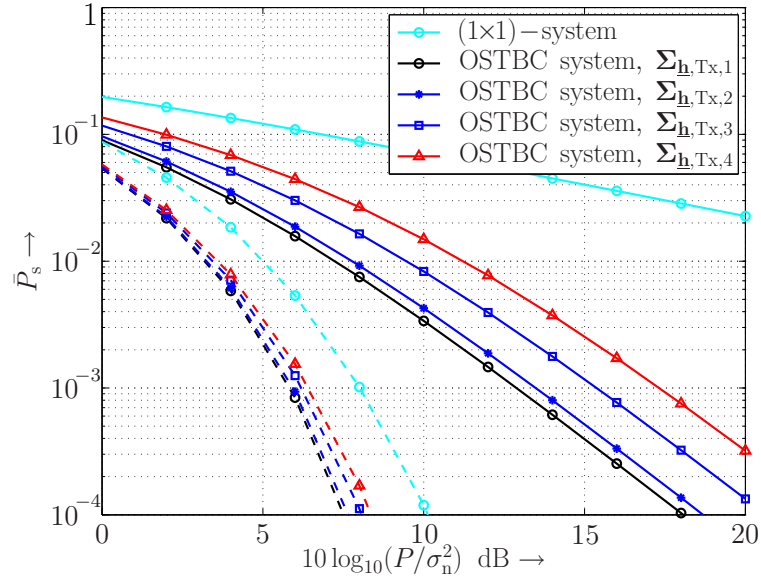


Figure 3.12: Average symbol error rate of an OSTBC system with four distributed transmit antennas and a single receive antenna under Nakagami- $m$  fading: Analytical results for binary antipodal transmission ( $Q=2$ ) and different transmitter covariance matrices  $\Sigma_{\mathbf{h},\text{Tx}}$  according to (3.89). Solid lines: Nakagami fading parameter  $m=0.5$ ; dashed lines:  $m=10$ .

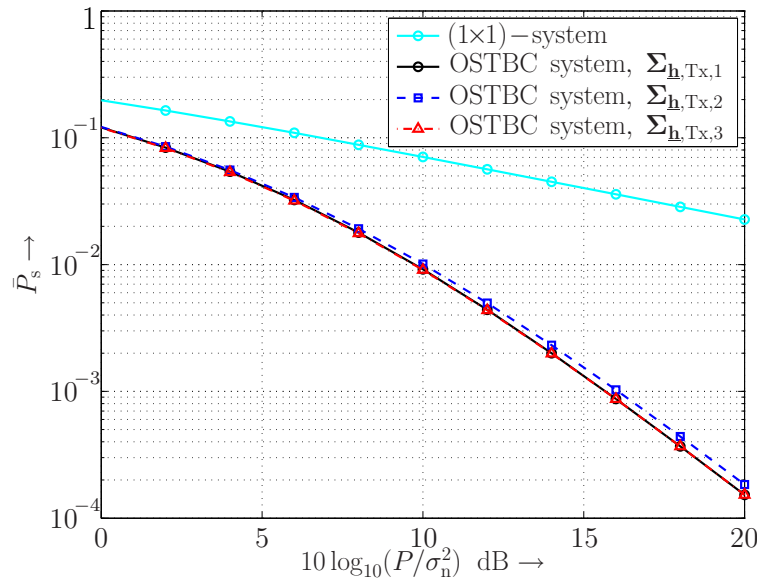


Figure 3.13: Average symbol error rate of an OSTBC system with four distributed transmit antennas and a single receive antenna under Nakagami- $m$  fading ( $m=0.5$ ): Analytical results for binary antipodal transmission ( $Q=2$ ) and different transmitter covariance matrices  $\Sigma_{\mathbf{h},\text{Tx}}$  according to (3.97) with  $\Delta(\Sigma_{\mathbf{h},\text{Tx}}) \approx 0.7$ .



cf. Section 2.1. We therefore note that all results presented above are also relevant for MIMO-OFDM systems, as long as a single (frequency-flat) sub-carrier is considered and no coding across multiple sub-carriers is employed. Yet, in Chapter 5 we will also consider the more general case where the impact of ISI cannot be (completely) neglected. As will be seen, the above conclusion that distributed MIMO systems are typically inferior to co-located MIMO systems with uncorrelated antennas is still valid in this case.

### 3.3.2 Generalized Spatial Correlation Models

The equivalence proofs for co-located and distributed MIMO systems presented above were based on the assumption that the channel matrix  $\mathbf{H}$  follows the Kronecker correlation model, where the transmitter and receiver correlations are clearly separable. For the sake of completeness, more general spatial correlation models are discussed in this section. Moreover, specific scenarios are highlighted for which the Kronecker model typically provides an accurate description.

#### MIMO Systems with Co-located Antennas

For practical MIMO systems with a moderate number of co-located transmit and receive antennas, the Kronecker correlation model

$$\mathbf{H} := \mathbf{R}_{\mathbf{h},\text{Rx}}^{1/2} \mathbf{H}' \mathbf{R}_{\mathbf{h},\text{Tx}}^{1/2}, \quad \mathbf{R}_{\mathbf{h}} = \text{E}\{\text{vec}(\mathbf{H})\text{vec}(\mathbf{H})^H\}/\sigma_h^2 := \mathbf{R}_{\mathbf{h},\text{Tx}} \otimes \mathbf{R}_{\mathbf{h},\text{Rx}} \quad (3.105)$$

(cf. Section 3.2.1 and 3.2.2) was shown to be quite accurate [OHW+03,XWL+04]. As will be seen below, the Kronecker model is also suitable for an important class of distributed MIMO systems. Finally, note that the Kronecker correlation model is always accurate for the trivial, but practically important case of a MISO or a SIMO system, where multiple antennas are only employed at one end of the wireless link.

A generalized spatial correlation model, which is known as the W-model, was proposed in [WHOB06]. Compared to the Kronecker model, the W-model contains (in essence) an additional coupling matrix  $\mathbf{\Omega}_{\mathbf{h}}$  which captures certain dependencies between the transmitter and receiver correlations.

In the most general case, the MIMO channel matrix is characterized by an overall spatial covariance matrix  $\mathbf{R}_{\mathbf{h}}$  with an arbitrary structure (apart from the usual conditions met by any covariance matrix, cf. Definition D.13). In this case, the channel matrix  $\mathbf{H}$  can be expressed as

$$\mathbf{H} := \text{vec}^{-1}\left(\mathbf{R}_{\mathbf{h}}^{1/2} \text{vec}(\mathbf{H}')\right), \quad (3.106)$$

where  $\text{vec}^{-1}(\cdot)$  denotes the inverse operation to  $\text{vec}(\cdot)$ , i.e., the  $MN$  elements of a row vector are aligned column-wise in a matrix of size  $(N \times M)$ . In both spatial correlation models, the transmitter and receiver correlations are not clearly separable anymore. A direct generalization of the equivalence proofs presented in Section 3.2 is therefore not possible.



### MIMO Systems with Distributed Antennas

In the case of distributed MIMO systems, additional constraints apply for the overall spatial covariance matrix  $\mathbf{R}_{\mathbf{h}}$ . For example, in the case of  $M$  distributed transmit antennas and  $N$  co-located receive antennas, the matrix  $\mathbf{R}_{\mathbf{h}}$  has the following structure:

$$\mathbf{R}_{\mathbf{h}} = \begin{bmatrix} \mathbf{R}_{\mathbf{h},1,1} & \cdots & \mathbf{0}_N \\ \vdots & \ddots & \vdots \\ \mathbf{0}_N & \cdots & \mathbf{R}_{\mathbf{h},M,M} \end{bmatrix}, \quad (3.107)$$

where  $\mathbf{R}_{\mathbf{h},\mu,\mu} := \mathbb{E}\{\mathbf{h}_\mu \mathbf{h}_\mu^H\}$  ( $\mu = 1, \dots, M$ ) and  $\mathbf{h}_\mu := [h_{1,\mu}, \dots, h_{N,\mu}]^T$  denotes the  $\mu$ th column vector of  $\mathbf{H}$ . (As earlier, we have assumed that the distributed transmit antennas are uncorrelated.) In general, the structure of the matrices  $\mathbf{R}_{\mathbf{h},\mu,\mu}$  will vary for different indices  $\mu$ , because the corresponding received signals arrive from different directions and may thus exhibit different angular spreads and power azimuth spectra. In many scenarios, however, it is reasonable to assume that the matrices  $\mathbf{R}_{\mathbf{h},\mu,\mu}$  are at least approximately the same, apart from a power weighting factor  $\sigma_{h,i}^2$  ( $i = 1, \dots, M$ ) which depends on the transmit antenna under consideration, cf. (3.15).<sup>22</sup> In this case, the overall spatial covariance matrix  $\mathbf{R}_{\mathbf{h}}$  can again be written as a Kronecker product

$$\mathbf{R}_{\mathbf{h}} \approx \Sigma_{\mathbf{h},\text{Tx}} \otimes \mathbf{R}_{\mathbf{h},\text{Rx}}. \quad (3.108)$$

Specifically, in the case of uncorrelated receive antennas, the covariance matrix  $\mathbf{R}_{\mathbf{h}}$  can always be written as

$$\mathbf{R}_{\mathbf{h}} = \Sigma_{\mathbf{h},\text{Tx}} \otimes \mathbf{I}_N \quad (3.109)$$

(without any approximation). Similarly, in the case of co-located, uncorrelated transmit antennas and distributed receive antennas, the covariance matrix  $\mathbf{R}_{\mathbf{h}}$  can always be written as

$$\mathbf{R}_{\mathbf{h}} = \mathbf{I}_M \otimes \Sigma_{\mathbf{h},\text{Rx}}. \quad (3.110)$$

Altogether, it can be concluded that the Kronecker correlation model is suitable for a fairly large class of practical (co-located or distributed) MIMO systems. Correspondingly, the theoretical results presented in Section 3.2 and 3.3.1 are of great practical relevance.

## 3.4 Benefits of Macroscopic Diversity

In order to conclude this chapter, the benefits of macroscopic spatial diversity in distributed MIMO systems are discussed (see also [MH06c]). We start with a brief summary and discussion of the most important results presented so far.

<sup>22</sup>A typical example is the downlink of a simulcast system consisting of multiple cooperating base stations, where the mobile station is surrounded by a uniform ring of local scatterers. In this case, the mobile station will always observe a received signal with a uniform power azimuth spectrum, irrespective of the transmit antenna under consideration. Correspondingly, the receiver correlations will not depend on the transmit antenna index  $\mu$ , cf. Section F.3 in Appendix F.

### 3.4.1 Discussion of Previous Results

In the previous sections, we have focussed on distributed MIMO systems where the position of all transmitting and receiving nodes is (quasi-) fixed. Under the assumption of Rayleigh fading obeying the Kronecker correlation model, we have shown in Section 3.2 that distributed MIMO systems are (asymptotically) equivalent to co-located MIMO systems (with respect to many important performance measures). More specifically, distributed MIMO systems that are characterized by unbalanced average link SNRs (due to unequal link lengths and/or shadowing effects) are equivalent to spatially correlated MIMO systems. As we have seen in Section 3.2 and 3.3, unbalanced average link SNRs can cause significant performance degradations compared to co-located MIMO systems with uncorrelated antennas (given the same overall average received power). Still, significant gains over single-antenna systems are achieved, even in the case of a strong SNR imbalance. Correspondingly, distributed MIMO systems constitute an attractive option for wireless systems, where nodes equipped with multiple antennas are either not feasible or not desired. By establishing a virtual antenna array, single-antenna nodes can still enjoy a good part of the benefits offered by co-located, spatially uncorrelated MIMO systems.

Another potential benefit of distributed MIMO systems, which was not considered in the previous sections, is that of macroscopic spatial diversity. As long as the position of the transmitting and receiving nodes is fixed, no macroscopic spatial diversity gains are available. Correspondingly, we have so far focussed on microscopic (small-scale) spatial diversity gains that are due to fading effects caused by multipath signal propagation. However, as soon as some larger-scale mobility is presumed and different (random) positions of the transmitting and/or receiving nodes are taken into account, additional macroscopic diversity gains might be available (depending on the physical environment under consideration). In this case, the above equivalence between distributed and co-located MIMO systems cannot be established anymore, simply because co-located MIMO systems do not offer any macroscopic spatial diversity gains. Therefore, when macroscopic diversity gains come into play, the performance of distributed MIMO systems can also be superior to that of (uncorrelated) MIMO systems with co-located antennas.

In the remainder of this section, the benefits of macroscopic diversity in distributed MIMO systems are illustrated by means of analytical and simulative performance results.

### 3.4.2 System Model with Macroscopic Diversity

As an example, we consider the downlink of a simulcast network consisting of  $M$  cooperating base stations  $BS_1$  to  $BS_M$  and a single mobile receiver MS (see Fig. 3.14). Conventionally, simulcasting means that the base stations simultaneously transmit the same signal on the same carrier frequency. Mobile users within the intersection of the coverage areas are thus provided with a comparatively small probability of shadowing and a high probability of at least one line-of-sight link (macroscopic spatial diversity). However, conventional simulcasting does not yield any microscopic spatial diversity gains [Wit91]. Correspondingly, in order to accomplish microscopic spatial diversity, the base stations are in the sequel assumed to employ a distributed space-time block coding scheme.

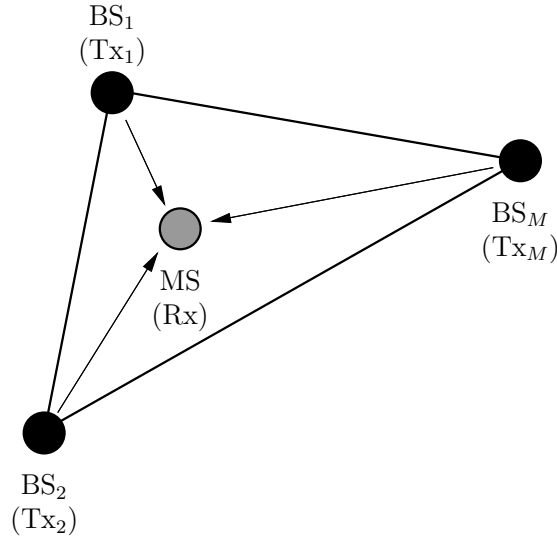


Figure 3.14: Simulcast network consisting of  $M$  cooperating base stations

### Further Assumptions

For simplicity, we assume in the following that the base stations and the mobile receiver are each equipped with a single antenna. A generalization to the case of multiple antennas is, however, straightforward. The mobile station is assumed to (randomly) move around a certain nominal position within the intersection of the coverage areas of all base stations. In particular, we assume that the velocity of the mobile receiver is sufficiently slow such that the quasi-static channel model (3.3) considered in Section 3.2 is still valid. As earlier, we consider a frequency-flat block-fading channel model for simplicity.<sup>23</sup> Moreover, we assume that the area, in which the mobile station is moving, is sufficiently small so that the path losses occurring on the individual transmission links (without shadowing effects) remain constant. Correspondingly, the average received SNRs (averaged over a medium to large time scale) can be considered time-invariant. On a shorter time scale, however, fluctuations of the average received SNRs may occur due to shadowing effects. Finally, we assume that the average transmit power is equally distributed among the different transmit antennas and that the differences between the individual propagation delays are small compared to the symbol duration. The case of large relative propagation delays is discussed in Chapter 5.

As an example, we assume that an OSTBC with a temporal rate of  $R_t \leq 1$  is employed at the transmitter (in conjunction with the corresponding widely linear decoding step at the receiver). For performance analysis, we again consider the equivalent MRC system

$$z[k] = \|\mathbf{h}\|_2 a[k] + \eta[k], \quad \mathbf{h} := [h_1, \dots, h_M]^T, \quad (3.111)$$

where  $\mathbf{E}\{|a[k]|^2\} = P/(M\zeta R_t)$  and  $\mathbf{E}\{|\eta[k]|^2\} = \sigma_n^2/\zeta$ , cf. Section 2.3.1 and 3.2.5. The overall average received SNR per information symbol is given by  $\bar{\gamma}_s = P/(R_t \sigma_n^2)$ .

<sup>23</sup>Again, the results presented in the following are also relevant for frequency-selective channel models. For example, they can directly be applied to space-time block coded MIMO-OFDM systems.

### Fading Models

In order to model the effects of microscopic fading, we consider random fading amplitudes  $|h_\mu|$  ( $\mu=1, \dots, M$ ) that are either Nakagami- $m$  distributed or Rician distributed. Both fading models are valid for rich-scattering environments and include Rayleigh fading as a special case. In the case of Rician fading, the channel coefficients  $h_\mu$  ( $\mu=1, \dots, M$ ) can be written as  $h_\mu := \bar{h}_\mu + \check{h}_\mu$ , where  $\bar{h}_\mu \in \mathbb{C}$  represents a non-fading line-of-sight (LoS) component and  $\check{h}_\mu \sim \mathcal{CN}(0, \sigma_{\check{h}_\mu}^2)$  the scattered components. As earlier, the average power of channel coefficient  $h_\mu$  is denoted as  $\Omega_{h_\mu} := \mathbf{E}\{|h_\mu|^2\} = |\bar{h}_\mu|^2 + \sigma_{\check{h}_\mu}^2$ . The Rice factor  $K_\mu \in [0, \infty)$  is defined as the ratio between LoS signal power and average power of the scattered components, i.e.,  $K_\mu = |\bar{h}_\mu|^2 / \sigma_{\check{h}_\mu}^2$ . Specifically, the cases  $K_\mu = 0$  and  $K_\mu \rightarrow \infty$  correspond to pure Rayleigh fading and to a non-fading AWGN link, respectively.

In the case of pure Rayleigh fading, the PDF of the instantaneous received SNR (per information symbol) of the  $\mu$ th transmission link,  $\gamma_{s,\mu} := P |h_\mu|^2 / (MR_t \sigma_n^2)$ , is given by

$$p_{\underline{\gamma}_{s,\mu}}(\gamma_{s,\mu}) = \frac{1}{\bar{\gamma}_{s,\mu}} \exp\left(-\frac{\gamma_{s,\mu}}{\bar{\gamma}_{s,\mu}}\right) \quad (\gamma_{s,\mu} \geq 0) \quad (3.112)$$

(cf. Definition C.11 in Appendix C). The corresponding PDF for Rice fading is given by (C.21a), and the PDF for Nakagami- $m$  fading with  $m \neq 1$  is given by (C.25), cf. Definition C.12 and C.13, respectively. Fig. C.3 and C.4 in Appendix C display some example PDFs  $p_{\underline{\gamma}_{s,\mu}}(\gamma_{s,\mu})$  for Rice fading and for Nakagami- $m$  fading.

In order to account for macroscopic fading caused by shadowing effects, the average SNRs  $\bar{\gamma}_{s,\mu}$  themselves are regarded as random variables characterized by a log-normal distribution. This means that the average SNRs in dB

$$\bar{\gamma}_{s,\text{dB},\mu} := 10 \log_{10} \bar{\gamma}_{s,\mu} \text{ dB} \quad (3.113)$$

are assumed to be Gaussian distributed. In the sequel, let  $\bar{\bar{\gamma}}_{s,\text{dB},\mu}$  and  $\sigma_{\text{dB},\mu}^2$  denote the mean and the variance of  $\bar{\gamma}_{s,\text{dB},\mu}$  in dB, respectively, i.e.,  $\bar{\gamma}_{s,\text{dB},\mu} \sim \mathcal{N}(\bar{\bar{\gamma}}_{s,\text{dB},\mu}, \sigma_{\text{dB},\mu}^2)$ . The corresponding PDF of  $\bar{\gamma}_{s,\mu}$  is given by

$$p_{\bar{\gamma}_{s,\mu}}(\bar{\gamma}_{s,\mu}) = \frac{10}{\sqrt{2\pi\sigma_{\text{dB},\mu}^2} \ln 10} \frac{1}{\bar{\gamma}_{s,\mu}} \exp\left(-\frac{(10 \log_{10} \bar{\gamma}_{s,\mu} - \bar{\bar{\gamma}}_{s,\text{dB},\mu})^2}{2\sigma_{\text{dB},\mu}^2}\right) \quad (3.114)$$

(cf. Definition C.14). To combine, for example, Rayleigh fading with log-normal shadowing, the PDF (3.112) is conditioned on  $\bar{\gamma}_{s,\mu}$  and then averaged over the log-normal PDF of  $\bar{\gamma}_{s,\mu}$ , cf. (C.27) in Definition C.14 [AG99]. By this means, one obtains the PDF of the instantaneous SNR  $\gamma_{s,\mu}$  of the composite fading/log-normal shadowing process.

In Fig. C.5 in Appendix C, some example PDFs of the instantaneous SNR  $\gamma_{s,\mu}$  are shown for composite Nakagami- $m$  fading/log-normal shadowing, for different values of the fading parameter  $m$  and the variance  $\sigma_{\text{dB},\mu}^2 =: \sigma_{x_{\text{dB}}}^2$ , while  $\bar{\bar{\gamma}}_{s,\text{dB},\mu} = 1$  in all cases. (The dark curves are for composite Rayleigh fading/log-normal shadowing.) The PDFs for  $\sigma_{x_{\text{dB}}} = 1$  dB represent very light shadowing, i.e.,  $p_{\underline{\gamma}_{s,\mu}}(\gamma_{s,\mu})$  is virtually the same as for pure Rayleigh or pure Nakagami- $m$  fading (cf. Fig. C.4). As can be seen in Fig. C.5, when shadowing is more severe (e.g.  $\sigma_{x_{\text{dB}}} = 10$  dB), the probability of small instantaneous SNR values increases significantly (also for comparatively large values of  $m$  such as  $m=5$ ).

### 3.4.3 Influence of Line-of-Sight Signal Components

For the time being, we restrict the discussion to Rayleigh and Rice fading (without any shadowing effects). To start with, consider again the simulcast network depicted in Fig. 3.14, and suppose that all  $M$  transmission links are characterized by pure Rayleigh fading (i.e., the Rice-factor  $K_\mu$  is zero for all indices  $\mu=1, \dots, M$ ).

In the following, it will be shown that the average symbol error probability,  $\bar{P}_s$ , is already significantly improved, if only a single link  $\mu'$  contains a pronounced LoS component. To this end, we examine the corresponding moment-generating function (MGF) of the instantaneous SNR  $\gamma_{s,\mu'}$ ,

$$\mathbf{M}\{\gamma_{s,\mu'}\}(s) = \int_0^{+\infty} e^{s\gamma_{s,\mu'}} p_{\gamma_{s,\mu'}}(\gamma_{s,\mu'}) d\gamma_{s,\mu'}. \quad (3.115)$$

Closed-form expressions for  $\mathbf{M}\{\gamma_{s,\mu'}\}(s)$  for the case of Rayleigh and Rice fading can be found in Table C.1 in Appendix C.

For simplicity, we focus on a  $Q$ -ary PSK signal constellation in the sequel. However, in principle the following discussion is also valid for  $Q$ -ary ASK or  $Q$ -ary QAM signal constellations. The average symbol error probability for  $Q$ -ary PSK is calculated as

$$\bar{P}_s = \frac{1}{\pi} \int_0^{\frac{(Q-1)\pi}{Q}} f(\phi) d\phi = \frac{1}{\pi} \int_0^{\frac{(Q-1)\pi}{Q}} \prod_{\mu=1}^M f_\mu(\phi) d\phi, \quad (3.116)$$

where

$$f_\mu(\phi) := \mathbf{M}\{\gamma_{s,\mu}\}(s = \varsigma_{\text{PSK}}(\phi)), \quad \varsigma_{\text{PSK}}(\phi) := -\sin^2(\pi/Q) / \sin^2(\phi) \quad (3.117)$$

(cf. Section 3.2.5 and Appendix I). In order to obtain the function  $f_{\mu'}(\phi)$  for the index  $\mu'$ , the PDF  $p_{\gamma_{s,\mu'}}(\gamma_{s,\mu'})$  is (for each value of  $\phi$ ) multiplied with the exponential term

$$g(\gamma_{s,\mu'}, \phi) := e^{\varsigma_{\text{PSK}}(\phi)\gamma_{s,\mu'}} \quad (3.118)$$

and integrated over  $\gamma_{s,\mu'}$ , cf. (3.115). For  $K_{\mu'} > 0$ , the PDF of  $\gamma_{s,\mu'}$  is less concentrated at small values than it is for  $K_{\mu'} = 0$ . This can, for example, be seen in Fig. C.3 in Appendix C. Since for any value of  $\phi$  the exponential term  $g(\gamma_{s,\mu'}, \phi)$  decreases with growing  $\gamma_{s,\mu'}$ , the area under the function  $g(\gamma_{s,\mu'}, \phi) \cdot p_{\gamma_{s,\mu'}}(\gamma_{s,\mu'})$  thus tends to be smaller when  $K_{\mu'}$  is greater than zero. Correspondingly, the functions  $f_{\mu'}(\phi)$  and  $f(\phi)$  tend to be smaller, i.e., the average symbol error probability  $\bar{P}_s$  according to (3.116) is reduced.

This fact is illustrated in Fig. 3.15, where the function  $f(\phi)$  is displayed for the example of  $M = 4$  transmit antennas, an overall average received SNR of  $10 \log_{10} \bar{\gamma}_s = 10$  dB, and different PSK constellations with cardinalities  $Q = 2, 4, 8$ . For simplicity, it has been assumed that the average SNR  $\bar{\gamma}_{s,\mu}$  is the same for all transmission links (i.e.,  $\bar{\gamma}_{s,\mu} = \bar{\gamma}_s/M$ ,  $\mu = 1, \dots, M$ ). Two different cases are depicted in Fig. 3.15:

- (i) Rice factors  $K_\mu = 0$  for all indices  $\mu = 1, \dots, M$  (pure Rayleigh fading) and
- (ii) Rice factors  $K_{\mu'} = 10$  and  $K_\mu = 0$  for all indices  $\mu \neq \mu'$ .

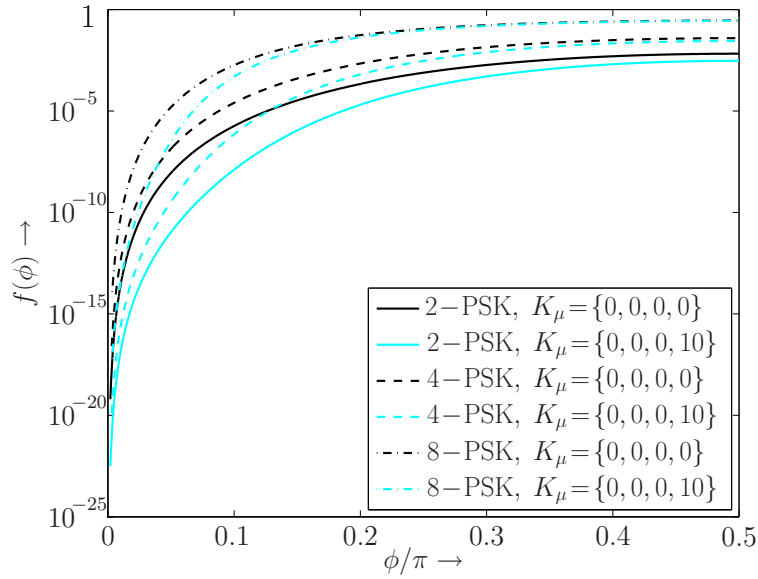


Figure 3.15: Function  $f(\phi)$  for the example  $M=4$  and an SNR of  $10 \log_{10} \bar{\gamma}_s = 10$  dB with (i) Rice-factors  $K_\mu=0$  for all  $\mu$  and (ii) Rice-factors  $K_{\mu'}=10$  and  $K_\mu=0$  for  $\mu \neq \mu'$ . Different PSK signal constellations are considered ( $Q=2, 4, 8$ ).

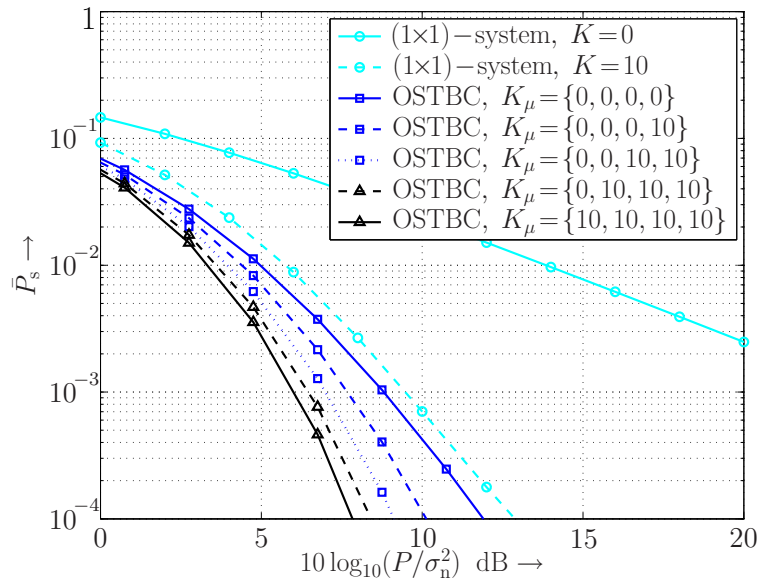


Figure 3.16: Average symbol error probability of an OSTBC system with four distributed transmit antennas and a single receive antenna: Analytical results for binary antipodal transmission ( $Q=2$ ). One or more links contain a LoS component with a Rice factor of  $K_\mu=10$ , while the remaining links are characterized by Rayleigh fading ( $K_\mu=0$ ).



As can be seen, for all considered PSK constellations the area under the function  $f(\phi)$  (and thus the average symbol error probability) is significantly reduced, when a single LoS component with  $K_{\mu'} = 10$  is present.

Fig. 3.16 displays corresponding symbol-error-probability results for the case of binary antipodal transmission ( $Q = 2$ ). It also includes results for the case that more than one link exhibits a Rice-factor of  $K_{\mu} = 10$ . As earlier, the average symbol error probabilities are plotted as a function of  $P/\sigma_n^2$  in dB. The overall average received SNR in the OSTBC system is given by  $\bar{\gamma}_s = P/(R_t\sigma_n^2)$ , where a temporal rate of  $R_t = 3/4$  was assumed. The curves were obtained analytically on the basis of (3.116) and (3.117) and were validated by means of Monte-Carlo simulations. In a system with co-located transmit antennas, one can assume that either all links simultaneously contain a LoS component (leftmost dark curve) or none of them (pure Rayleigh fading, rightmost dark curve). The line-of-sight probability is therefore (more or less) the same as in a single-antenna system, i.e., the use of multiple co-located antennas does not yield any advantage in this respect. In a system with distributed transmit antennas, however, there is a comparatively high probability that at least one link contains a LoS component. As can be seen in Fig. 3.16, already a single link with a Rice factor of  $K_{\mu} = 10$  (dashed curve, marked with squares) yields a gain of about 1.8 dB compared to the case of pure Rayleigh fading (at a symbol error rate of  $10^{-4}$ ). Compared to this, the additional gains accomplished with further LoS links are relatively small. In particular, it should be noted that the performance gains achieved in the OSTBC system are much smaller than in the single-antenna system, even if all four links contain a LoS component with  $K_{\mu} = 10$ .

In the following, the performance of the distributed and the co-located OSTBC system is compared, using simple assumptions about the corresponding LoS probabilities.<sup>24</sup> Moreover, it is assumed for simplicity that the antennas in the co-located OSTBC system are uncorrelated. Let  $P_{\text{LoS}}$  denote the LoS probability in the single-antenna system, i.e., with probability  $P_{\text{LoS}}$  the Rice factor is equal to  $K = 10$  (otherwise  $K = 0$ ). According to the above arguments, we assume that the LoS probability in the co-located OSTBC system is also given by  $P_{\text{LoS}}$ , i.e., with probability  $P_{\text{LoS}}$  all four links are characterized by a Rice factor of  $K_{\mu} = 10$ , and otherwise  $K_{\mu} = 0$  for all links. In the distributed OSTBC system, however, the LoS probability is assumed to be  $P_{\text{LoS}}$  for each link, while the individual links are statistically independent. As earlier, all links containing a LoS component are assumed to have a Rice factor of  $K_{\mu} = 10$ . Fig. 3.17 displays the average symbol error probability resulting for the single-antenna system, the co-located OSTBC system, and the distributed OSTBC system. The curves are plotted as a function of the LoS probability  $P_{\text{LoS}}$ , where the average SNR  $P/\sigma_n^2$  was set to 7 dB. As can be seen, the distributed OSTBC system is generally superior to the co-located OSTBC system. For example, in order to achieve an average symbol error probability of  $10^{-3}$ , the co-located OSTBC system requires a LoS probability of  $P_{\text{LoS}} \geq 0.73$ , whereas for the distributed OSTBC system a LoS probability of  $P_{\text{LoS}} \geq 0.46$  is already sufficient. As expected, the

<sup>24</sup>For a more rigorous performance comparison, an accurate model of the morphology of the physical environment would be required. Based on such a model, LoS probabilities could then be determined using ray-tracing simulations (similar to [DTN+03]) in conjunction with a mobility model for the mobile receiver, e.g. [MLTS97].



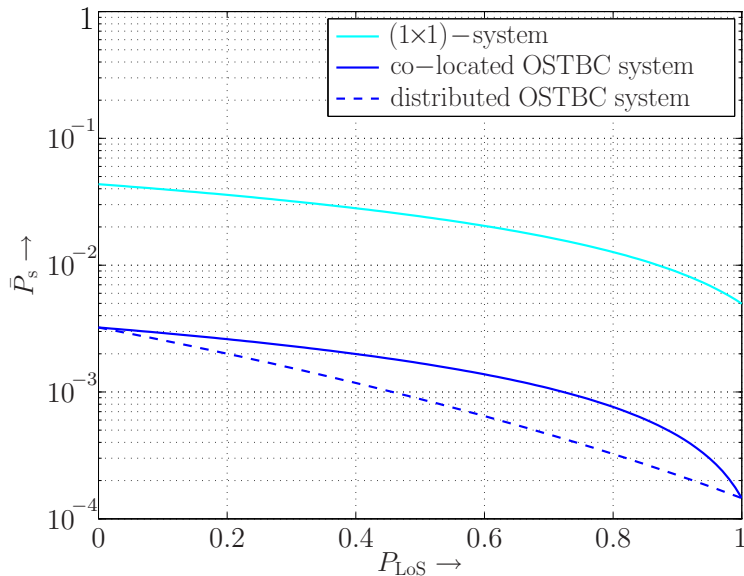


Figure 3.17: Average symbol error probability resulting for the single-antenna system, the co-located OSTBC system, and the distributed OSTBC system, as a function of the LoS probability  $P_{LoS}$  (for an SNR of  $10 \log_{10} P/\sigma_n^2 = 7$  dB).

performance of both systems coincides if  $P_{LoS}$  is either close to zero (pure Rayleigh fading) or close to one (pure Rice fading).

### 3.4.4 Influence of Shadowing

In the sequel, we examine the influence of shadowing effects on the error performance of distributed and co-located (and spatially uncorrelated) OSTBC systems. To this end, we consider different scenarios with composite Rayleigh fading/log-normal shadowing, i.e., the average SNRs  $\bar{\gamma}_{s,dB,\mu}$  in dB are now assumed to be Gaussian distributed, and no LoS components are available.<sup>25</sup> Unfortunately, a closed-form expression for the corresponding functions  $f_\mu(\phi)$  is not known in this case [AS02]. An analytical evaluation of the average symbol error probability is therefore difficult. Correspondingly, we resort to numerical performance results obtained by Monte-Carlo simulations.

Consider again the simulcast network depicted in Fig. 3.14. With regard to shadowing, the use of multiple co-located transmit antennas is again not advantageous. Large-scale objects between transmitter and receiver will most likely obstruct either all links simultaneously or none of them. Therefore, the probability of shadowing is not significantly reduced compared to a single-antenna system. In other words, with co-located transmit antennas the average SNRs  $\bar{\gamma}_{s,dB,\mu}$  will be strongly correlated. However, in a system with distributed transmit antennas (with sufficient spacing), the average SNRs  $\bar{\gamma}_{s,dB,\mu}$  can be assumed statistically independent [EKA02], which yields huge macroscopic diversity

<sup>25</sup>The results presented in the following apply, in principle, also for Nakagami- $m$  fading with a fading parameter  $m \neq 1$ .

gains. This is illustrated in Fig. 3.18, where symbol-error-rate (SER) curves are presented for the example of  $M=4$  transmit antennas, an OSTBC with a temporal rate of  $R_t=3/4$ , binary antipodal transmission ( $Q=2$ ), and identical average SNRs  $\bar{\gamma}_{s,\mu}$  for all transmission links ( $\mu=1, \dots, M$ ). Moreover, for simplicity identical variances  $\sigma_{\text{dB},\mu}^2 =: \sigma_{\text{dB}}^2$  were considered for all transmission links. In the case of the co-located OSTBC system, it was assumed that the average SNRs  $\bar{\gamma}_{s,\text{dB},\mu}$  are fully correlated, i.e.

$$\mathbb{E}\{(\bar{\gamma}_{s,\text{dB},\mu} - \bar{\gamma}_{s,\text{dB},\mu})(\bar{\gamma}_{s,\text{dB},\mu'} - \bar{\gamma}_{s,\text{dB},\mu'})\} / \sigma_{\text{dB}}^2 = 1 \quad (3.119)$$

for all indices  $\mu$  and  $\mu'$ . As can be seen in Fig. 3.18, in the case of very light shadowing ( $\sigma_{\text{dB}}=1$  dB), the average SER performance with distributed transmit antennas is virtually the same as with co-located transmit antennas (as expected). In both cases, significant (microscopic) diversity gains are obtained compared to the single-antenna system.<sup>26</sup>

Considering a more practical scenario ( $\sigma_{\text{dB}}=10$  dB), one first observes that the performance of the single-antenna system degrades significantly. Interestingly, the use of  $M=4$  co-located transmit antennas yields only moderate performance improvements, i.e., a large fraction of the microscopic diversity gain obtained for  $\sigma_{\text{dB}}=1$  dB is lost. In contrast to this, in the case of distributed transmit antennas one again obtains huge diversity gains compared to the single-antenna system. These gains are not only due to macroscopic diversity, but also to microscopic diversity accomplished by the distributed OSTBC. This becomes evident, when comparing the SER performance to that of (conventional) simulcasting, where identical signals are transmitted from each antenna.<sup>27</sup> As can be seen, simulcasting performs about 1.5 dB worse than the distributed OSTBC (at a BER of  $10^{-3}$ ). Altogether, it can be concluded that in the presence of significant shadowing, systems with distributed transmit antennas are superior to systems with co-located transmit antennas, and distributed space-time codes are superior to (co-phased) simulcasting.

Another interesting observation is that for low SNR values the SER performance of a distributed OSTBC system with significant shadowing ( $\sigma_{\text{dB}}=10$  dB) is even better than for very light shadowing ( $\sigma_{\text{dB}}=1$  dB), which is a rather unexpected result. There is a cross-over point of the respective SER curves at 3.5 dB. (In the case of the single-antenna system, there is also a cross-over point at approximately -2.5 dB.) An intuitive explanation for this is as follows. In the low SNR regime channel conditions are already bad, and a further reduction of the SNR due to shadowing does not have much impact on the average SER performance. However, a large variance  $\sigma_{\text{dB}}^2$  of the average SNR  $\bar{\gamma}_{s,\text{dB},\mu}$  leads to some very good channel realizations, which is obviously beneficial for the average SER performance. This cross-over behavior can also be observed when considering the corresponding functions  $f_\mu(\phi)$ , cf. (3.115)-(3.117). In the case of moderate to high SNR values (e.g.  $\bar{\gamma}_{s,\mu}=1$ ), the PDFs  $p_{\gamma_{s,\mu}}(\gamma_{s,\mu})$  are less concentrated at small values of  $\gamma_{s,\mu}$ , when the variance  $\sigma_{\text{dB}}^2$  is small (cf. Fig. C.5 in Appendix C). Correspondingly, the function  $f(\phi)$ , and thus the average symbol error probability, is smaller than for large variances  $\sigma_{\text{dB}}^2$ . In

<sup>26</sup>Since the shadowing effect is negligible, the composite fading is virtually independent for the individual links, both for co-located and for distributed transmit antennas.

<sup>27</sup>To be specific, an improved version of simulcasting is already considered here, where the phases of the individual transmitted signals are adjusted such that constructive superposition is obtained at the receiver.

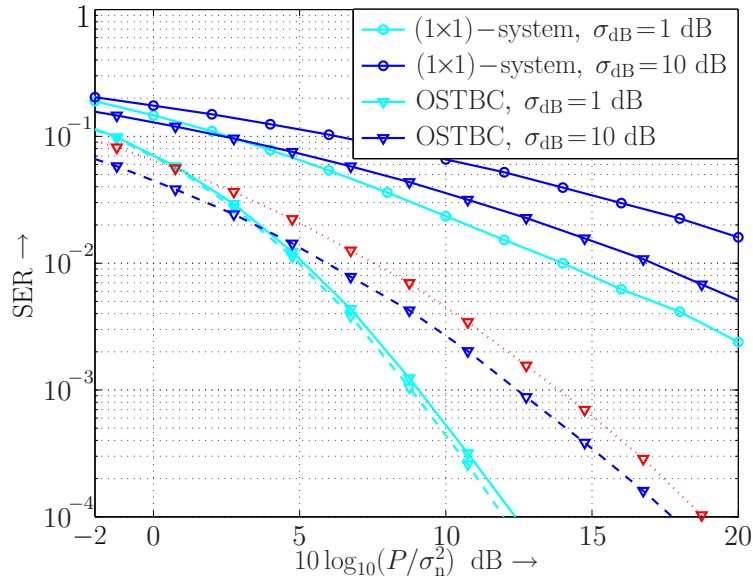


Figure 3.18: Comparison of the average SER performance of a co-located (solid lines) and a distributed OSTBC system (dashed lines) with  $M = 4$  transmit antennas and a single receive antenna: Simulative results for binary antipodal transmission ( $Q = 2$ ) and composite Rayleigh fading/log-normal shadowing (equal average link SNRs  $\bar{\gamma}_{s,\text{dB},\mu}$ , equal variances  $\sigma_{\text{dB},\mu}^2$  for  $\mu = 1, \dots, M$ ). The dotted curve is for simulcasting with co-phased received signals ( $\sigma_{\text{dB}} = 10$  dB).

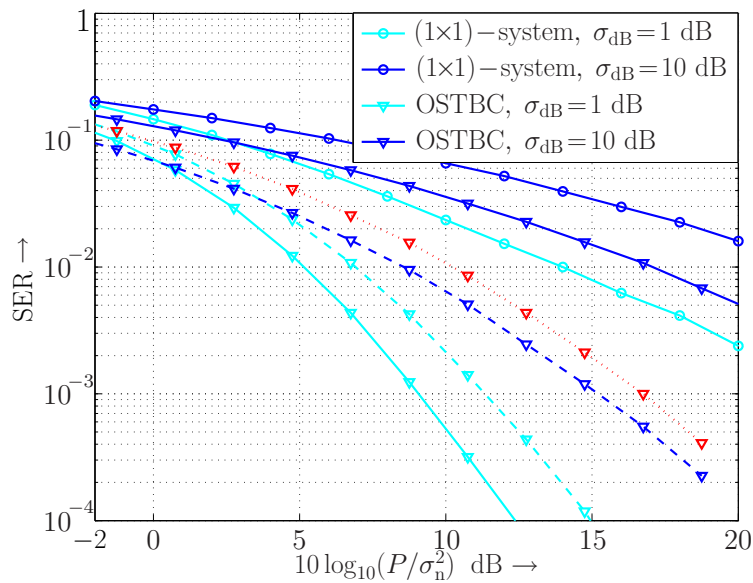


Figure 3.19: Corresponding results for unequal average link SNRs  $\bar{\gamma}_{s,\text{dB},\mu}$  in the distributed OSTBC system, where  $\Sigma_{\mathbf{h},\text{Tx}} = \text{diag}([0.154 \ 0.154 \ 0.615 \ 3.077])$  was assumed.

the case of low SNR values, however, the PDF  $p_{\gamma_{s,\mu}}(\gamma_{s,\mu})$  is already concentrated at very small values  $\gamma_{s,\mu}$ . Given a large variance  $\sigma_{\text{dB}}^2$ , the PDF  $p_{\gamma_{s,\mu}}(\gamma_{s,\mu})$  exhibits a tail that tends to higher values of  $\gamma_{s,\mu}$  (not depicted in Fig. C.5). Due to this, the function  $f(\phi)$  and thus the average symbol error probability becomes smaller with growing variance  $\sigma_{\text{dB}}^2$ .

For simplicity, we have so far assumed that the average SNRs  $\bar{\gamma}_{s,\mu}$  are the same for all transmission links, i.e., the transmitter covariance matrix is equal to  $\Sigma_{\mathbf{h},\text{Tx}} = \mathbf{I}_4$ . As will be seen, the main conclusions drawn from Fig. 3.18 apply also for the case of unequal average SNRs  $\bar{\gamma}_{s,\mu}$ . As an example, we consider the transmitter covariance matrix

$$\Sigma_{\mathbf{h},\text{Tx}} := \text{diag}([0.154 \ 0.154 \ 0.615 \ 3.077]) \quad (3.120)$$

in the case of the distributed system. The corresponding SER results are displayed in Fig. 3.19. As can be seen, the SER performance of the distributed system is significantly degraded due to the unequal average link SNRs (cf. Fig. 3.18). In the case of light shadowing ( $\sigma_{\text{dB}} = 1$  dB), where the achieved diversity gains are mainly due to microscopic spatial diversity, the OSTBC system with co-located transmit antennas thus clearly outperforms the distributed OSTBC system. However, in the case of significant shadowing ( $\sigma_{\text{dB}} = 10$  dB) the situation is reversed. Due to huge macroscopic diversity gains, the distributed OSTBC system still yields a much better SER performance than the co-located OSTBC system. Moreover, the advantage of the distributed OSTBC over conventional (co-phased) simulcasting is maintained. Altogether, it can be concluded that in the presence of very light shadowing, one should employ co-located antennas, if possible. In the case of significant shadowing effects, however, distributed antennas are preferable.

## 3.5 Chapter Summary

The concept of cooperating wireless networks (e.g., in the form of simulcast networks or relay-assisted wireless networks, cf. Section 3.1) has recently gained considerable attention. In such networks multiple network nodes, possibly equipped with only a single antenna, cooperate in terms of a joint transmission or reception strategy. In effect, the cooperating nodes establish a MIMO system with distributed antennas. By this means, the nodes can share their antennas and enjoy some of the benefits offered by ‘conventional’ MIMO systems with co-located antennas.

In this chapter, it was shown that MIMO systems with distributed antennas and MIMO systems with co-located antennas can be treated in a single, unifying framework, although at the first glance both types of systems might have little in common. In particular, under certain assumptions MIMO systems with distributed antennas and MIMO systems with co-located antennas were shown to be (asymptotically) equivalent with regard to many important performance measures. The results presented in Section 3.2.3 apply for (arbitrary) coded MIMO systems. For the case of frequency-flat Rayleigh fading, it was shown that for any co-located MIMO system obeying the Kronecker correlation model an equivalent distributed MIMO system can be found and vice versa, in the sense that both systems are characterized by identical capacity distributions. In particular, antenna correlations in the co-located MIMO system correspond to unequal average link signal-to-noise

ratios (SNRs) in the distributed MIMO system. The results presented in Section 3.2.4 apply for space-time coded MIMO systems employing an arbitrary space-time code designed to achieve full spatial diversity. These results have shown that co-located and distributed space-time coded MIMO systems lead (asymptotically) to identical pairwise error probabilities. Finally, the results presented in Section 3.2.5 apply for MIMO systems employing an orthogonal space-time block code (OSTBC) at the transmitter side (in conjunction with the corresponding widely linear combining at the receiver). As a new contribution, closed-form expressions as well as high-SNR approximations were derived for the average symbol error probability of co-located and distributed OSTBC systems. In particular, it was shown that co-located and distributed systems lead to identical average symbol error rates, irrespective of the average received SNR. Moreover, a simple performance measure was considered (Section 3.2.6), which allows for a classification of different MIMO systems with regard to their ergodic capacity and the average symbol error rate achieved by OSTBCs.

As long as no macroscopic diversity gains are available, it can be concluded that distributed MIMO systems typically have an inferior performance compared to co-located MIMO systems with uncorrelated antennas (due to unequal average link SNRs). In fact, this conclusion is still valid when the assumption of frequency-flat Rayleigh fading is dropped and more general fading models are considered (cf. Section 3.3). Still, one typically observes substantial performance gains over single-antenna systems, even if the average link SNRs are highly unbalanced (or, in the case of a co-located MIMO system, if antennas are highly correlated).

In the final part of this chapter, the benefits of macroscopic spatial diversity effects in distributed MIMO systems were considered (Section 3.4). For example, in a distributed MIMO system the probability that at least one transmission link offers a line-of-sight (LoS) component is typically larger than in a co-located MIMO system, which can lead to substantial performance improvements (cf. Section 3.4.3). With regard to shadowing, it was shown that huge macroscopic and microscopic diversity gains can be obtained in a distributed MIMO system, cf. Section 3.4.4. In particular, it was shown that distributed space-time codes are superior to conventional simulcasting, even in the case of severe shadowing. In contrast to this, in a system with co-located antennas, the performance improvements compared to a single-antenna system tend to be rather small, when shadowing is taken into account. To conclude, as soon as significant macroscopic diversity gains are available, distributed MIMO systems are typically superior to co-located MIMO systems, even in the case of unbalanced average link SNRs.



## Appendix 1

The following theorem provides the basis for the unitary matrix transform (3.38), which is used to transform a given distributed MIMO system into an equivalent co-located MIMO system.

### Theorem 3.4 (Existence of unitary matrix transform)

For any positive (semi-)definite diagonal  $(n \times n)$ -matrix  $\mathbf{\Sigma}$  with  $\text{tr}(\mathbf{\Sigma}) = n$ , where  $n$  is an arbitrary number  $\geq 2$ , a unitary  $(n \times n)$ -matrix  $\tilde{\mathbf{U}}_n$  can be found such that the transform

$$\tilde{\mathbf{U}}_n \mathbf{\Sigma} \tilde{\mathbf{U}}_n^H = \mathbf{R} \quad (3.121)$$

yields a correlation matrix  $\mathbf{R}$  with diagonal entries equal to one and non-diagonal entries having magnitudes  $\leq 1$ .

*Proof.* By definition, the resulting matrix  $\mathbf{R}$  is a Hermitian matrix. Choosing  $\tilde{\mathbf{U}}_n$  such that  $|\tilde{u}_{ij}| = 1/\sqrt{n}$  for all  $i, j = 1, \dots, n$ , one obtains for the diagonal entries of  $\mathbf{R}$ :

$$[\mathbf{R}]_{i,i} = \sum_{j=1}^n |u_{ij}|^2 [\mathbf{\Sigma}]_{j,j} = \frac{\text{tr}(\mathbf{\Sigma})}{n} = 1. \quad (3.122)$$

Moreover, since  $\tilde{\mathbf{U}}_n$  is a unitary matrix,  $|r_{ij}| \leq 1$  holds for all  $i, j$ . Unitary matrices  $\tilde{\mathbf{U}}_n$  with the desired property are, for example, the  $(n \times n)$ -Fourier matrix  $\tilde{\mathbf{F}}_n$  with entries  $\tilde{u}_{ij} = e^{-j2\pi(i-1)(j-1)/n}/\sqrt{n}$  ( $i, j = 1, \dots, n$ ), which exists for any number  $n$ , or the normalized  $(n \times n)$ -Hadamard matrix  $\tilde{\mathbf{H}}_n$ , which is known to exist for all  $n = 2^\nu$ , where  $\nu$  is an arbitrary positive integer number (cf. Definition D.6 in Appendix D).  $\square$

## Appendix 2

In the following, an alternative proof is given for Lemma 3.1, which is based on convex optimization (cf. Appendix E).

*Proof.* It has to be shown that the product term in (3.86) is equal to one, if and only if all eigenvalues  $\lambda_1, \dots, \lambda_n$  are equal to one, and otherwise greater than one ( $> 1$ ). Correspondingly, we can formulate the following optimization problem:

$$\begin{aligned} \text{minimize} \quad & f(\boldsymbol{\lambda}) := \prod_{j=1}^n \frac{1}{\lambda_j}, \quad \boldsymbol{\lambda} := [\lambda_1, \dots, \lambda_n]^T \\ \text{subject to} \quad & \sum_{j=1}^n \lambda_j = n \quad \text{and} \quad \lambda_j > 0 \quad \text{for all } j = 1, \dots, n. \end{aligned} \quad (3.123)$$

We can reformulate the above optimization problem according to

$$\begin{aligned} & \text{minimize} \quad \tilde{f}(\boldsymbol{\lambda}) := - \sum_{j=1}^n \log(\lambda_j), \quad \boldsymbol{\lambda} := [\lambda_1, \dots, \lambda_n]^T & (3.124) \\ & \text{subject to} \quad \sum_{j=1}^n \lambda_j = n \quad \text{and} \quad \lambda_j > 0 \quad \text{for all } j = 1, \dots, n, \end{aligned}$$

since the  $\log(\cdot)$ -function is a monotonic increasing function. The above optimization problem is convex, since  $-\log(\cdot)$  is a convex- $\cup$  function. In fact, (3.124) is just a special case of the well-known water-filling problem [Boe05], cf. Example E.1 in Appendix E and [BV04, Ch. 5.5]. Correspondingly, we simply obtain

$$\lambda_j^\bullet = \max(0, \Theta) \quad \text{subject to} \quad \sum_{j=1}^n \Theta = n. \quad (3.125)$$

Thus, we get  $\lambda_j^\bullet = \Theta = 1$  for all  $j = 1, \dots, n$ . Moreover, since the solution is unique we will always have  $\tilde{f}(\boldsymbol{\lambda}) > \tilde{f}(\boldsymbol{\lambda}^\bullet) = 0$  or, equivalently,  $f(\boldsymbol{\lambda}) > f(\boldsymbol{\lambda}^\bullet) = 1$  for any  $\boldsymbol{\lambda} \neq \boldsymbol{\lambda}^\bullet$ .  $\square$



# Chapter 4

## Optimal Transmitter and Receiver Strategies

**T**HE PREVIOUS chapter has shown that MIMO systems with co-located or distributed antennas offer substantial performance advantages over single-antenna systems, despite possible antenna correlations or unbalanced average link SNRs.

So far, we have focussed on scenarios where no channel knowledge is available at the transmitter. Correspondingly, we have assumed that the available transmit power is, on average, equally distributed among the transmit antennas.<sup>1</sup> In practice, this assumption is often reasonable, since channel knowledge at the transmitter can be costly or even infeasible. On the other hand, an optimization of the transmitter strategy might not always be desired. Consider, for example, a simulcast network established by multiple cooperating base stations (cf. Fig 3.14 in Section 3.4). Simulcast networks are typically employed for broadcasting applications, where many mobile users are simultaneously served with the same message. In this case, an optimization of the transmitter strategy with respect to a specific user is typically not reasonable.

In this chapter, we consider a general scenario where channel knowledge at the transmitter is both available and utilized in terms of an optimal transmitter strategy. In fact, several publications have shown that the performance of MIMO systems can be improved significantly by using some form of channel knowledge at the transmitter, see e.g. [GJJV03]. The use of (possibly imperfect) full and partial instantaneous channel knowledge at the transmitter was, for example, considered in [Tel99, SSP01, JSO02, KC02, MWC03, WVF03, PL03, ZDZY03, CBRB04, HSA04, NAP04, Ale04, LJ05, GPPF05, LT05, PPPL06] and [JBM+02, OD02, Blu03, LH03b, MSEA03, LHS03, SH03a, RR04, LH04a, MWC04, BRW04, NSL04, Lo04, XG04, BE04, JS04a, SKL04, LH05a, LH05b, LH05c, LH05d, MGJ05, YW05a, KGK05, HL05, RSB05, CH05, RR06a, RR06b, LH06, MGJ06, YKY06, DLWZ06, LSG06, ZLW06], respectively. As an alternative, the use of statistical channel knowledge was studied in [Cav99, NBP01, FWLH02, SP02, ZG02, GJJV03, HLHS03, ZG03a, SS03, AQ04, KT04, JB04b, HG04, MA04, JB04c, Kie04, CGZ05, LY05, LL05a, XLRP05, AG05, HG05, MH06b, MHKX06b, YSG06]. While instantaneous chan-

---

<sup>1</sup>Equal power allocation is the optimal strategy if the transmitter does not have any channel knowledge available [BT04a, App. B.2].

nel knowledge at the transmitter might be difficult to acquire in a practical system, statistical channel knowledge can be gained quite easily [ZG03a], for example off-line through field measurements, ray-tracing simulations or based on physical channel models, or on-line based on long-term averaging of the channel coefficients. Optimal statistical transmit power allocation schemes for spatially correlated MIMO systems were, for example, derived in [SP02, ZG03a, JB04b] with regard to different optimization criteria: Minimum symbol error probability [ZG03a], minimum pairwise error probability of space-time codes [SP02], and maximum ergodic capacity [JB04b]. Due to the (asymptotic) equivalence of co-located and distributed MIMO systems, these power allocation strategies can also be used in MIMO systems with distributed antennas, without any loss of optimality.

In Section 4.1, optimal transmitter strategies for distributed and co-located MIMO systems are discussed in more detail, with focus on schemes that are based on statistical channel knowledge at the transmitter. As novel contributions, a rigorous performance analysis is presented, and the impact of estimation errors concerning the transmitter correlation matrix is analyzed (see also [MHKX06b]). Moreover, a simple transmit power allocation strategy for space-time coded MIMO systems is proposed, which provides a near-optimum performance over a wide SNR range. In Section 4.2, the use of statistical channel knowledge at the receiver is investigated, so as to provide an optimal trade-off between performance and receiver complexity. It is shown that there is a strong duality between the receiver structure under consideration and the statistical transmit power allocation schemes discussed in Section 4.1 (see also [MHKX06a]). Specifically, the impact of estimation errors concerning the receiver correlation matrix can be analyzed along the same lines as for the transmitter side. The most important results of this chapter are summarized in Section 4.3.

## 4.1 Optimal Transmit Power Allocation Schemes

Within the scope of this thesis, we will focus on transmit power allocation schemes that are based on statistical channel knowledge at the transmitter. To start with, we consider the benefits of a statistical transmit power allocation scheme with regard to the ergodic capacity of a coded MIMO system with co-located or distributed antennas. We will also briefly discuss the use of instantaneous channel knowledge at the transmitter. Afterwards, we combine the statistical transmit power allocation scheme with an outer space-time code and analyze the resulting performance gains in comparison to equal power allocation among the individual transmit antennas.

### 4.1.1 System Model with Statistical Transmit Power Allocation

For the time being, we again focus on the case of frequency-flat Rayleigh fading for simplicity. Later on, we will also consider Nakagami- $m$  fading with  $m \neq 1$ . To start with, consider a MIMO system with  $M$  co-located transmit antennas and  $N$  co-located receive antennas. As earlier, we focus on the discrete-time channel model

$$\mathbf{y}[k] = \mathbf{H}\mathbf{x}[k] + \mathbf{n}[k] \quad (4.1)$$

introduced in Section 2.2.2 for quasi-static frequency-flat fading. In essence, the same statistical properties are assumed as in Section 3.2. In particular, we again assume that the channel matrix  $\mathbf{H}$  follows the Kronecker correlation model

$$\mathbf{H} := \mathbf{R}_{\mathbf{h},\text{Rx}}^{1/2} \mathbf{H}' \mathbf{R}_{\mathbf{h},\text{Tx}}^{1/2}, \quad h'_{\nu,\mu} \sim \mathcal{CN}(0, \sigma_h^2), \quad (4.2)$$

while the entries of  $\mathbf{H}'$  are independent and identically distributed (i.i.d.) random variables. As earlier, let  $\mathbf{R}_{\mathbf{h},\text{Tx}} := \mathbf{U}_{\text{Tx}} \mathbf{\Lambda}_{\mathbf{h},\text{Tx}} \mathbf{U}_{\text{Tx}}^H$  and  $\mathbf{R}_{\mathbf{h},\text{Rx}} := \mathbf{U}_{\text{Rx}} \mathbf{\Lambda}_{\mathbf{h},\text{Rx}} \mathbf{U}_{\text{Rx}}^H$  denote the eigenvalue decompositions of  $\mathbf{R}_{\mathbf{h},\text{Tx}}$  and  $\mathbf{R}_{\mathbf{h},\text{Rx}}$ , respectively. The instantaneous realizations of the channel matrix  $\mathbf{H}$  are assumed to be perfectly known at the receiver, while at the transmitter only statistical channel knowledge is available. More precisely, the transmitter is assumed to have perfect knowledge of the complete set of second-order channel statistics, in terms of the transmitter correlation matrix  $\mathbf{R}_{\mathbf{h},\text{Tx}}$ , the receiver correlation matrix  $\mathbf{R}_{\mathbf{h},\text{Rx}}$ , the channel variance  $\sigma_h^2$ , and the noise variance  $\sigma_n^2$ . Finally, the entries  $x_\mu[k]$  of the transmitted vector  $\mathbf{x}[k]$  are again treated as zero-mean (possibly correlated) random variables with variance  $\sigma_{x,\mu}^2$ . As earlier, we assume an overall average transmit power constraint of  $P$ , i.e.,

$$\sum_{\mu=1}^M \sigma_{x,\mu}^2 \stackrel{!}{\leq} P. \quad (4.3)$$

Thus, a fair comparison between different transmit power allocation strategies is possible. In the following, we consider a simple statistical transmit power allocation scheme for spatially correlated MIMO systems, which is based on the Karhunen-Loève transform (KLT) [SW02, Ch. 8.5].<sup>2</sup> The transmit power allocation scheme does not require any knowledge of instantaneous realizations of the channel matrix  $\mathbf{H}$  and is thus of great practical interest.

The system model under consideration is depicted in Fig. 4.1. The  $(M \times 1)$ -vector  $\mathbf{x}_s[k]$  contains the information symbols to be transmitted, which are possibly encoded by some outer space-time coding scheme. (The statistical transmit power allocation scheme considered here can be used in conjunction with any outer space-time code.) For simplicity, the entries  $x_{s,\mu}[k]$  of the vector  $\mathbf{x}_s[k]$  are assumed to have zero means and equal variances, i.e.,  $\mathbf{E}\{|x_{s,\mu}[k]|^2\} := P/M$  for all  $\mu=1, \dots, M$ . Even if an outer space-time coding scheme is employed, the entries of  $\mathbf{x}_s[k]$  can typically be regarded as statistically independent random variables (only across the individual transmit antennas, not in time direction), i.e.,

$$\mathbf{Q}_{\mathbf{x}_s} := \mathbf{E}\{\mathbf{x}_s[k] \mathbf{x}_s^H[k]\} = P/M \cdot \mathbf{I}_M. \quad (4.4)$$

The statistical transmit power allocation scheme consists of an inner decorrelation stage based on the KLT and an outer power weighting stage with weighting matrix<sup>3</sup>

$$\mathbf{W} := \text{diag}([w_1, \dots, w_M]), \quad \text{tr}(\mathbf{W}) = M. \quad (4.5)$$

The overall transmission model can be written as (cf. Fig. 4.1):

$$\mathbf{y}[k] = \mathbf{H} \mathbf{x}[k] + \mathbf{n}[k] = \mathbf{H} \mathbf{U}_{\text{Tx}} \mathbf{W}^{1/2} \mathbf{x}_s[k] + \mathbf{n}[k] \quad (4.6a)$$

$$=: \mathbf{H}_v \mathbf{x}_v[k] + \mathbf{n}[k] =: \mathbf{H}_s \mathbf{x}_s[k] + \mathbf{n}[k], \quad (4.6b)$$

<sup>2</sup>The basic transmitter structure was earlier considered in [SP02, HLHS03, ZG03a, JB04b].

<sup>3</sup>The optimality of the considered transmitter structure was proven in [ZG03a].

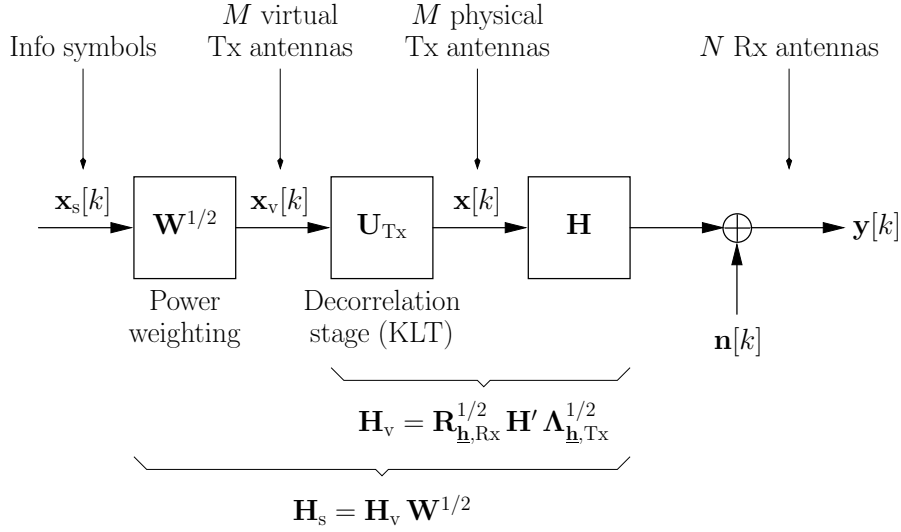


Figure 4.1: System model with statistical transmit power allocation scheme based on the Karhunen-Loève transform.

with  $\mathbf{H}_v := \mathbf{H} \mathbf{U}_{\text{Tx}}$ ,  $\mathbf{x}_v[k] := \mathbf{W}^{1/2} \mathbf{x}_s[k]$ , and  $\mathbf{H}_s := \mathbf{H}_v \mathbf{W}^{1/2}$ . The decorrelation stage transforms the given channel matrix  $\mathbf{H}$  according to (4.2) into a semi-correlated channel matrix  $\mathbf{H}_v = \mathbf{R}_{\mathbf{h},\text{Rx}}^{1/2} \mathbf{H}' \boldsymbol{\Lambda}_{\mathbf{h},\text{Tx}}^{1/2}$ , using the unitary matrix  $\mathbf{U}_{\text{Tx}}$  from the eigenvalue decomposition of  $\mathbf{R}_{\mathbf{h},\text{Tx}}$  as a precoding matrix. Correspondingly, we have

$$\mathbf{E} \{ \mathbf{H}_v^H \mathbf{H}_v \} = \mathbf{U}_{\text{Tx}}^H \mathbf{E} \{ \mathbf{H}^H \mathbf{H} \} \mathbf{U}_{\text{Tx}} = N \sigma_h^2 \boldsymbol{\Lambda}_{\mathbf{h},\text{Tx}}, \quad (4.7)$$

where we have used that  $\mathbf{E} \{ \mathbf{H}^H \mathbf{H} \} = N \sigma_h^2 \mathbf{R}_{\mathbf{h},\text{Tx}}$  (cf. Section 3.2.2 in Chapter 3). The channel matrix  $\mathbf{H}_v$  is often called virtual channel matrix in the literature, and the  $M$  inputs to the precoding matrix  $\mathbf{U}_{\text{Tx}}$  (vector  $\mathbf{x}_v[k]$ ) represent virtual transmit antennas. Finally, note that due to the trace constraint on  $\mathbf{W}$ , the transmitted vector  $\mathbf{x}[k]$  will always meet the same overall power constraint as the vector  $\mathbf{x}_s[k]$ , i.e.,

$$\text{tr}(\mathbf{E} \{ \mathbf{x}[k] \mathbf{x}^H[k] \}) =: \text{tr}(\mathbf{Q}_{\mathbf{x}}) = P/M \cdot \text{tr}(\mathbf{U}_{\text{Tx}} \mathbf{W} \mathbf{U}_{\text{Tx}}^H) = P = \text{tr}(\mathbf{Q}_{\mathbf{x}_s}), \quad (4.8)$$

cf. (4.4). Thus, a fair comparison between different transmit power allocation strategies is possible. Based on the statistical channel knowledge at the transmitter, the weighting matrix  $\mathbf{W}$  can now be optimized with respect to a given optimization criterion. For example, one option is to maximize the (overall) average received SNR.

### Maximizing the Average Received SNR

By choosing an appropriate weighting matrix  $\mathbf{W}$ , the average received SNR can be improved, compared with the case of equal power allocation ( $\mathbf{W} = \mathbf{I}_M$ ). This can be seen

when considering the covariance matrix of the received vector  $\mathbf{y}[k]$ :

$$\mathbf{Q}_{\underline{\mathbf{y}}} = \mathbb{E} \{ \mathbf{y}[k] \mathbf{y}^H[k] \} = \mathbb{E} \{ \mathbf{H}_v \mathbf{W}^{1/2} \mathbb{E} \{ \mathbf{x}_s[k] \mathbf{x}_s^H[k] \} \mathbf{W}^{1/2} \mathbf{H}_v^H \} + \sigma_n^2 \mathbf{I}_N \quad (4.9a)$$

$$= \frac{P}{M} \cdot \mathbb{E} \{ \mathbf{H} \mathbf{U}_{\text{Tx}} \mathbf{W} \mathbf{U}_{\text{Tx}}^H \mathbf{H}^H \} + \sigma_n^2 \mathbf{I}_N \quad (4.9b)$$

$$= \frac{P}{M} \cdot \mathbf{R}_{\underline{\mathbf{h}}, \text{Rx}}^{1/2} \mathbb{E} \left\{ \mathbf{H}' \mathbf{U}_{\text{Tx}} \mathbf{W} \mathbf{\Lambda}_{\underline{\mathbf{h}}, \text{Tx}} \mathbf{U}_{\text{Tx}}^H \mathbf{H}'^H \right\} \mathbf{R}_{\underline{\mathbf{h}}, \text{Rx}}^{1/2} + \sigma_n^2 \mathbf{I}_N \quad (4.9c)$$

$$= \frac{P \sigma_h^2}{M} \underbrace{\sum_{\mu=1}^M w_\mu \lambda_{\text{Tx}, \mu}}_{=: f_{\text{snr}}(\mathbf{W}, \mathbf{\Lambda}_{\underline{\mathbf{h}}, \text{Tx}})} \mathbf{R}_{\underline{\mathbf{h}}, \text{Rx}} + \sigma_n^2 \mathbf{I}_N \quad (4.9d)$$

[Boe03]. In the case of equal power allocation, one obtains

$$f_{\text{snr}}(\mathbf{I}_M, \mathbf{\Lambda}_{\underline{\mathbf{h}}, \text{Tx}}) = P \sigma_h^2. \quad (4.10)$$

However, using an appropriate transmit power allocation strategy, it is possible to achieve an SNR gain ( $f_{\text{snr}}(\mathbf{W}, \mathbf{\Lambda}_{\underline{\mathbf{h}}, \text{Tx}}) > P \sigma_h^2$ ). In particular, from Lemma 4.1 below it follows that the average received SNR is maximized when the complete transmit power  $P$  is concentrated on the strongest eigenvalue  $\lambda_{\text{Tx}, \text{max}}$  of the transmitter correlation matrix  $\mathbf{R}_{\underline{\mathbf{h}}, \text{Tx}}$ . This power allocation strategy is in the sequel denoted as (one-dimensional) eigenbeamforming (EBF).<sup>4</sup>

#### Lemma 4.1

Let  $\lambda_1 < \dots < \lambda_n$  denote the eigenvalues of a  $(n \times n)$ -correlation matrix  $\mathbf{R}$ , i.e.,  $\lambda_1, \dots, \lambda_n$  are real-valued and non-negative, and  $\lambda_1 + \dots + \lambda_n = n$ . Moreover, let  $w_1, \dots, w_n$  denote a set of arbitrary real-valued non-negative numbers with sum constraint  $w_1 + \dots + w_n = n$ . Then, the term

$$\sum_{j=1}^n w_j \lambda_j \quad (4.11)$$

is maximized for  $w_n := n$  and  $w_j := 0$  for all  $j \neq n$ .

*Proof.* Follows from many results reported in the literature, e.g. [SP02, ZG03a].  $\square$

A simple alternative proof, which is based on convex optimization (cf. Appendix E), is provided in Appendix 1 at the end of this chapter.

Note that the optimal choice of the weighting matrix  $\mathbf{W}$  depends only on the transmitter correlation matrix  $\mathbf{R}_{\underline{\mathbf{h}}, \text{Tx}}$  (or, more precisely, on the eigenvalues  $\lambda_{\text{Tx}, \mu}$ ), but not on the receiver correlation matrix  $\mathbf{R}_{\underline{\mathbf{h}}, \text{Rx}}$ . In particular, the EBF solution can be reused for MIMO systems with distributed (transmit and/or receive) antennas without any loss of optimality. In particular, in the case of distributed transmit antennas (with a transmitter covariance matrix  $\mathbf{\Sigma}_{\underline{\mathbf{h}}, \text{Tx}} := \mathbf{\Lambda}_{\underline{\mathbf{h}}, \text{Tx}}$ ), the decorrelation stage  $\mathbf{U}_{\text{Tx}}$  can be dropped (i.e.,  $\mathbf{U}_{\text{Tx}} := \mathbf{I}_M$ ).

<sup>4</sup>Note that the maximum (temporal) rate that can be accomplished with EBF corresponds to that of a single-antenna system (similar to a full-rate STBC system with equal power allocation).

Maximizing the average received SNR is just one (particularly simple) criterion for an optimal choice of the weighting matrix  $\mathbf{W}$ . In the following, we consider the benefits of a (statistical) transmit power allocation scheme with regard to the ergodic capacity of distributed and co-located MIMO systems.

### 4.1.2 Benefits with Regard to Ergodic Capacity

Consider again a MIMO system with co-located antennas which follows the Kronecker correlation model (4.2), where we set  $\sigma_h^2 := 1$ . We again assume that the transmitter has perfect knowledge of the complete set of second-order channel statistics, while the receiver has perfect instantaneous channel knowledge. In order to maximize the ergodic capacity, it was shown in [JB04b] that the optimal strategy is to transmit in the directions of the eigenvectors of the transmitter correlation matrix  $\mathbf{R}_{\mathbf{h},\text{Tx}}$ . In other words, the transmitter structure depicted in Fig. 4.1 is capacity achieving, provided that an optimal power weighting matrix  $\mathbf{W} = \text{diag}([w_1, \dots, w_M])$  is chosen. Given a fixed covariance matrix

$$\mathbf{Q}_{\mathbf{x}} = \mathbb{E}\{\mathbf{x}[k]\mathbf{x}^H[k]\} = P/M \cdot \mathbf{U}_{\text{Tx}} \mathbf{W} \mathbf{U}_{\text{Tx}}^H \quad (4.12)$$

of the transmitted vector  $\mathbf{x}[k]$ , the instantaneous MIMO capacity is given by

$$C(\mathbf{H}, \mathbf{Q}_{\mathbf{x}}) = \log_2 \det \left( \mathbf{I}_N + \frac{1}{\sigma_n^2} \mathbf{H} \mathbf{Q}_{\mathbf{x}} \mathbf{H}^H \right) \text{ bit/channel use} \quad (4.13)$$

(cf. (G.9) in Appendix G). Unfortunately, a closed-form solution for the optimal weighting matrix  $\mathbf{W}^\bullet$ , which maximizes the ergodic capacity  $\bar{C}(\mathbf{Q}_{\mathbf{x}}) := \mathbb{E}\{C(\mathbf{H}, \mathbf{Q}_{\mathbf{x}})\}$ , is not known. The optimal power weighting results from solving the optimization problem [JB04b]

$$\begin{aligned} & \text{maximize} \quad f(\mathbf{w}) := \mathbb{E} \left\{ \log_2 \det \left( \mathbf{I}_N + \sum_{\mu=1}^M \frac{w_\mu \lambda_{\text{Tx},\mu} \mathbf{z}_\mu \mathbf{z}_\mu^H}{\sigma_n^2} \right) \right\}, \quad \mathbf{w} := [w_1, \dots, w_M]^T \\ & \text{subject to} \quad \sum_{\mu=1}^M w_\mu = M \quad \text{and} \quad w_\mu \geq 0 \quad \text{for all} \quad \mu = 1, \dots, M, \end{aligned} \quad (4.14)$$

where the vectors  $\mathbf{z}_\mu \in \mathbb{C}^N$  are i.i.d. complex Gaussian random vectors with zero mean and covariance matrix  $\mathbf{\Lambda}_{\mathbf{h},\text{Rx}}$ , i.e.,  $z_{\mu,\nu} \sim \mathcal{CN}(0, \lambda_{\text{Rx},\nu})$  for all  $\mu = 1, \dots, M$ . Note that the optimal power weighting depends both on the eigenvalues of  $\mathbf{R}_{\mathbf{h},\text{Tx}}$  and on the eigenvalues of  $\mathbf{R}_{\mathbf{h},\text{Rx}}$ . As earlier, the resulting transmit power weighting will also be optimal for a distributed MIMO system with transmitter covariance matrix  $\mathbf{\Sigma}_{\mathbf{h},\text{Tx}} := \mathbf{\Lambda}_{\mathbf{h},\text{Tx}}$  and/or receiver covariance matrix  $\mathbf{\Sigma}_{\mathbf{h},\text{Rx}} := \mathbf{\Lambda}_{\mathbf{h},\text{Rx}}$ . (In the case of distributed transmit antennas the decorrelation stage  $\mathbf{U}_{\text{Tx}}$  can again be dropped.)

The above expression for  $f(\mathbf{w})$  is, in general, difficult to evaluate. In the following, we will therefore consider a tight upper bound on  $\bar{C}(\mathbf{Q}_{\mathbf{x}})$ , which is again based on Jensen's inequality, cf. (3.41) in Section 3.2.3. As will be seen, this greatly simplifies the optimization of  $\mathbf{W}$ . One obtains

$$\bar{C}(\mathbf{Q}_{\mathbf{x}}) \leq \log_2 \mathbb{E} \left\{ \det \left( \mathbf{I}_N + \frac{1}{\sigma_n^2} \mathbf{H} \mathbf{Q}_{\mathbf{x}} \mathbf{H}^H \right) \right\}. \quad (4.15)$$

The term  $\mathbf{H}\mathbf{Q}_{\mathbf{x}}\mathbf{H}^H$  can be further evaluated as

$$\mathbf{H}\mathbf{Q}_{\mathbf{x}}\mathbf{H}^H = \mathbf{R}_{\mathbf{h},\text{Rx}}^{1/2} \mathbf{H}' \mathbf{U}_{\text{Tx}} \mathbf{W} \mathbf{\Lambda}_{\mathbf{h},\text{Tx}} \mathbf{U}_{\text{Tx}}^H \mathbf{H}^H \mathbf{R}_{\mathbf{h},\text{Rx}}^{1/2}, \quad (4.16)$$

where  $\mathbf{U}_{\text{Tx}} \mathbf{W} \mathbf{\Lambda}_{\mathbf{h},\text{Tx}} \mathbf{U}_{\text{Tx}}^H =: \mathbf{R}'_{\mathbf{h},\text{Tx}}$  can be interpreted as an effective transmitter correlation matrix with eigenvalues  $w_1 \lambda_{\text{Tx},1}, \dots, w_M \lambda_{\text{Tx},M}$ . For the special case of equal power allocation we have  $\mathbf{R}'_{\mathbf{h},\text{Tx}} = \mathbf{R}_{\mathbf{h},\text{Tx}}$ . Correspondingly, for a given arbitrary power weighting matrix  $\mathbf{W}$  we can reuse the result (3.45) from Section 3.2.3 by replacing the eigenvalues  $\lambda_{\text{Tx},1}, \dots, \lambda_{\text{Tx},M}$  by  $w_1 \lambda_{\text{Tx},1}, \dots, w_M \lambda_{\text{Tx},M}$ , respectively. We thus obtain

$$\begin{aligned} \bar{C}(\mathbf{Q}_{\mathbf{x}}) \leq & \log_2 \left( 1 + \sum_{\mu=1}^{\tilde{M}} \left( \frac{P}{M\sigma_n^2} \right)^\mu \mu! \times \right. \\ & \left. \times \sum_{\mathbf{i} \in \mathbb{I}_\mu} w_{i_1} \lambda_{\text{Tx},i_1} \cdots w_{i_\mu} \lambda_{\text{Tx},i_\mu} \sum_{\mathbf{j} \in \mathbb{J}_\mu} \lambda_{\text{Rx},j_1} \cdots \lambda_{\text{Rx},j_\mu} \right), \end{aligned} \quad (4.17)$$

where  $\tilde{M} := \min(M, N)$  and  $\mathbf{i}$  and  $\mathbf{j}$  again denote index vectors taken from the sets (3.44), cf. Section 3.2.3. For a fixed SNR value  $P/(M\sigma_n^2)$ , the right-hand side of (4.17) can now be maximized numerically, in order to find the optimal power weighting matrix  $\mathbf{W}^\bullet$ .

## Numerical Results

As an example, we consider a co-located MIMO system with four transmit antennas and three receive antennas, where the correlation matrices  $\mathbf{R}_{\mathbf{h},\text{Tx}}$  and  $\mathbf{R}_{\mathbf{h},\text{Rx}}$  are given by  $\mathbf{R}_{\mathbf{h},\text{Tx}} = \mathbf{R}_{M,\rho_{\text{Tx}}}$  with  $\rho_{\text{Tx}} = 0.8$  and  $\mathbf{R}_{\mathbf{h},\text{Rx}} = \mathbf{R}_{N,\rho_{\text{Rx}}}$  with  $\rho_{\text{Rx}} = 0.7$ , cf. (3.39) in Section 3.2.3. In Fig. 4.2, the ergodic capacities  $\bar{C}(\mathbf{Q}_{\mathbf{x}})$  resulting for different power allocations are plotted as a function of the average SNR  $P/(M\sigma_n^2)$  in dB. The exact ergodic capacities (solid, dashed and dashed-dotted line) were obtained by means of Monte-Carlo simulations over  $10^5$  independent channel realizations, whereas the dotted lines represent the corresponding upper bounds on  $\bar{C}(\mathbf{Q}_{\mathbf{x}})$ , which were obtained on the basis of (4.17). As can be seen, the upper bounds are reasonably tight throughout the complete SNR range. Compared to the uncorrelated system (solid line, dark color), the ergodic capacity of the correlated system with equal power allocation (dashed-dotted line) is significantly reduced, especially for large SNR values (cf. Section 3.2.3). For the light-colored curve and the dashed curve, the transmit power weights  $w_1, \dots, w_M$  were optimized numerically, based on (4.17). The light-colored curve represents the case, where both  $\mathbf{R}_{\mathbf{h},\text{Tx}}$  and  $\mathbf{R}_{\mathbf{h},\text{Rx}}$  is known at the transmitter. For the dashed curve, however, it was assumed that the transmitter knows only  $\mathbf{R}_{\mathbf{h},\text{Tx}}$  (i.e., the transmitter presumes  $\mathbf{R}_{\mathbf{h},\text{Rx}} = \mathbf{I}_N$ ). As can be seen, in both cases the ergodic capacity of the correlated system is improved significantly compared to equal power allocation, especially in the low SNR regime. For SNR values smaller than  $-2$  dB, the achieved capacity is even larger than in the uncorrelated case. Interestingly, although the upper bound (4.17) depends both on the eigenvalues of  $\mathbf{R}_{\mathbf{h},\text{Tx}}$  and  $\mathbf{R}_{\mathbf{h},\text{Rx}}$ , the difference between the light-colored curve and the dashed curve is negligible in the considered example, i.e., the knowledge of  $\mathbf{R}_{\mathbf{h},\text{Rx}}$  at the transmitter is of little or no benefit. Finally, it should be noted that for  $P/(M\sigma_n^2) \rightarrow 0$  the optimal power weighting tends to the



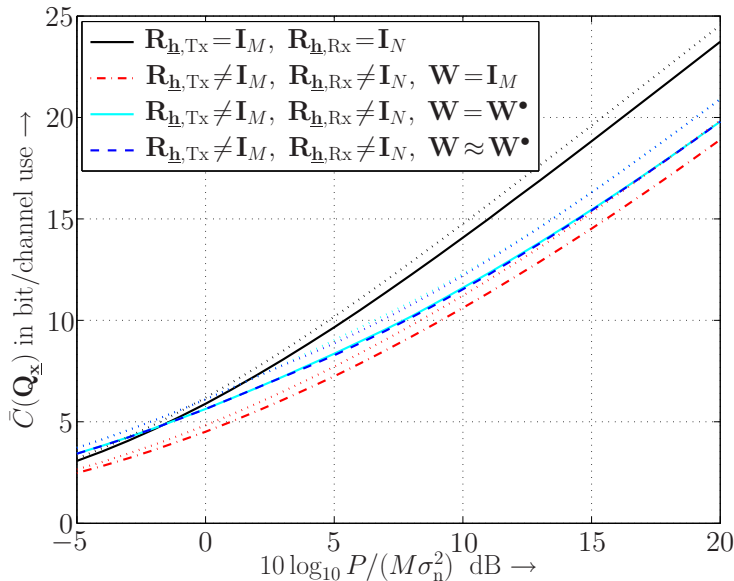


Figure 4.2: Ergodic capacity  $\bar{C}(\mathbf{Q}_x)$  of a co-located MIMO system with four transmit and three receive antennas, resulting for different transmit power allocation strategies. (Simulative results were obtained by means of Monte-Carlo simulations; dotted lines: Corresponding analytical upper bounds.)

(one-dimensional) EBF solution, where the complete transmit power is focussed on the largest eigenvalue of  $\mathbf{R}_{\mathbf{h},\text{Tx}}$  (see also [JB04b]). However, for  $P/(M\sigma_n^2) \rightarrow \infty$  one obtains (in the considered example) an equal power allocation solution over the  $\tilde{M} = \min\{M, N\} = 3$  largest eigenvalues of  $\mathbf{R}_{\mathbf{h},\text{Tx}}$ .

### Instantaneous Channel Knowledge at the Transmitter

In the following, we briefly consider the case of perfect instantaneous channel knowledge at the transmitter. In particular, we will again see that optimal transmit power allocation schemes originally designed for co-located MIMO systems can be reused for distributed MIMO systems (and vice versa), without any loss of optimality.

Consider again a MIMO system with co-located antennas which follows the Kronecker correlation model (4.2), where  $\sigma_h^2 = 1$ . In the case of perfect instantaneous channel knowledge at the transmitter and the receiver, the instantaneous MIMO capacity is given by

$$C(\mathbf{H}) = \sum_{\mu=1}^{\tilde{M}} \left[ \log_2 \left( \frac{\chi_\mu}{\sigma_n^2} \Theta \right) \right]_+ =: r \quad \text{bit/channel use}, \quad (4.18)$$

where  $[\chi_1, \dots, \chi_{\tilde{M}}] =: \boldsymbol{\chi}$  denote the  $\tilde{M} = \min(M, N)$  eigenvalues of the matrix  $\mathbf{H}\mathbf{H}^H$  (for  $N \leq M$ ) or the matrix  $\mathbf{H}^H\mathbf{H}$  (for  $N > M$ ), cf. Appendix G. Moreover,  $\Theta$  denotes the waterlevel which results from the well-known waterfilling solution (cf. Appendix E). The waterlevel  $\Theta$  depends on the available transmit power  $P$ , the noise variance  $\sigma_n^2$  and the eigenvalues  $\chi_1, \dots, \chi_{\tilde{M}}$  (cf. (G.15) in Appendix G), i.e.,  $\Theta = \Theta(\boldsymbol{\chi})$ . Thus, the capacity

distribution  $p_r(r)$  is solely determined by the joint PDF  $p_{\underline{\boldsymbol{\chi}}}(\boldsymbol{\chi})$  of the (unordered) eigenvalues  $\chi_1, \dots, \chi_{\tilde{M}}$ . Recently, a closed-form expression for  $p_{\underline{\boldsymbol{\chi}}}(\boldsymbol{\chi})$  was derived in [RV05] (for the case  $N \geq M$ ).<sup>5</sup> The result is of form

$$p_{\underline{\boldsymbol{\chi}}}(\boldsymbol{\chi}) = \frac{v(\mathbf{R}_{\mathbf{h},\text{Tx}}, \mathbf{R}_{\mathbf{h},\text{Rx}}, \boldsymbol{\chi})}{K_{M,N} \cdot \varsigma(\mathbf{R}_{\mathbf{h},\text{Tx}}, \mathbf{R}_{\mathbf{h},\text{Rx}})} \cdot \prod_{\mu=1}^M \chi_{\mu}^{N-M} \prod_{\substack{\mu'=1 \\ \mu' > \mu}}^M (\chi_{\mu} - \chi_{\mu'})^2, \quad (4.19)$$

where

$$v(\mathbf{R}_{\mathbf{h},\text{Tx}}, \mathbf{R}_{\mathbf{h},\text{Rx}}, \boldsymbol{\chi}) := \sum_{k=0}^{\infty} \sum_{\boldsymbol{\kappa} \in \mathbb{K}_k} \frac{C_{\boldsymbol{\kappa}}(-\mathbf{R}_{\mathbf{h},\text{Tx}}^{-1}) C_{\boldsymbol{\kappa}}(\mathbf{R}_{\mathbf{h},\text{Rx}}^{-1}) C_{\boldsymbol{\kappa}}(\text{diag}(\boldsymbol{\chi}))}{k! C_{\boldsymbol{\kappa}}(\mathbf{I}_M) C_{\boldsymbol{\kappa}}(\mathbf{I}_N)}, \quad (4.20)$$

$$K_{M,N} := M! \prod_{\mu=1}^M \Gamma(N - \mu + 1) \Gamma(M - \mu + 1) \quad (4.21)$$

( $\Gamma(x)$  denotes the Gamma function, cf. Definition C.3 in Appendix C), and

$$\varsigma(\mathbf{R}_{\mathbf{h},\text{Tx}}, \mathbf{R}_{\mathbf{h},\text{Rx}}) := (\lambda_{\text{Tx},1} \cdots \lambda_{\text{Tx},M})^N (\lambda_{\text{Rx},1} \cdots \lambda_{\text{Rx},N})^M. \quad (4.22)$$

The vector  $\boldsymbol{\kappa}$  in (4.20) denotes an index vector taken from the set

$$\mathbb{K}_k := \{\boldsymbol{\kappa} := [k_1, \dots, k_M] \mid k_1 \geq k_2 \geq \cdots \geq k_M \geq 0, k_1 + k_2 + \cdots + k_M = k\}. \quad (4.23)$$

Moreover,  $C_{\boldsymbol{\kappa}}(\mathbf{X})$  denotes a so-called complex zonal polynomial of a complex Hermitian matrix  $\mathbf{X}$  (see [RVA03, RV05] for further details). In fact, if  $\mathbf{X} := \mathbf{U}_{\mathbf{X}} \boldsymbol{\Lambda}_{\mathbf{X}} \mathbf{U}_{\mathbf{X}}^{\text{H}}$  denotes the eigenvalue decomposition of  $\mathbf{X}$ , we have  $C_{\boldsymbol{\kappa}}(\mathbf{X}) = C_{\boldsymbol{\kappa}}(\boldsymbol{\Lambda}_{\mathbf{X}})$  [RVA03]. Correspondingly we can rewrite (4.20) according to

$$C_{\boldsymbol{\kappa}}(-\mathbf{R}_{\mathbf{h},\text{Tx}}^{-1}) = C_{\boldsymbol{\kappa}}(-\boldsymbol{\Lambda}_{\mathbf{h},\text{Tx}}^{-1}), \quad C_{\boldsymbol{\kappa}}(\mathbf{R}_{\mathbf{h},\text{Rx}}^{-1}) = C_{\boldsymbol{\kappa}}(\boldsymbol{\Lambda}_{\mathbf{h},\text{Rx}}^{-1}). \quad (4.24)$$

As earlier, we note that the joint PDF of the eigenvalues of  $\mathbf{H}^{\text{H}}\mathbf{H}$  depends solely on the eigenvalues of  $\mathbf{R}_{\mathbf{h},\text{Tx}}$  and  $\mathbf{R}_{\mathbf{h},\text{Rx}}$ , but not on specific entries of  $\mathbf{R}_{\mathbf{h},\text{Tx}}$  and  $\mathbf{R}_{\mathbf{h},\text{Rx}}$ . Correspondingly, a distributed MIMO system with transmitter covariance matrix  $\boldsymbol{\Sigma}_{\mathbf{h},\text{Tx}} := \boldsymbol{\Lambda}_{\mathbf{h},\text{Tx}}$  and/or receiver covariance matrix  $\boldsymbol{\Sigma}_{\mathbf{h},\text{Rx}} := \boldsymbol{\Lambda}_{\mathbf{h},\text{Rx}}$  will be characterized by exactly the same capacity distribution  $p_r(r)$  as the co-located MIMO system considered above.

### 4.1.3 Combination with Outer Space-Time Code

In the following, we focus on space-time coded MIMO systems and study the benefits of the above statistical transmit power allocation scheme with regard to the resulting error performance. As an example, we combine the transmitter structure in Fig. 4.1 with an outer orthogonal space-time block code (OSTBC) and evaluate the average symbol error probability (see also [ZG03a]). Consider again the transmission model

$$\mathbf{y}[k] = \mathbf{H}_s \mathbf{x}_s[k] + \mathbf{n}[k] \quad (4.25)$$

<sup>5</sup>Specialized expressions for the cases  $\mathbf{R}_{\mathbf{h},\text{Tx}} = \mathbf{I}_M$  and  $\mathbf{R}_{\mathbf{h},\text{Rx}} = \mathbf{I}_N$  can be found in [CWZ03, TV04b] and [RVA03], respectively.

introduced in Section 4.1.1. The vector  $\mathbf{x}_s[k]$  is now assumed to be part of a  $(p \times M)$ -OSTBC code matrix  $\mathbf{X}_s[k] := [\mathbf{x}_s[k], \dots, \mathbf{x}_s[k+p-1]]^T$ , cf. Section 2.3.1 in Chapter 2. As discussed above, the channel matrix  $\mathbf{H}_s$  can be written as

$$\mathbf{H}_s = \mathbf{R}_{\mathbf{h},\text{Rx}}^{1/2} \mathbf{H}' \mathbf{\Lambda}_{\mathbf{h},\text{Tx}}^{1/2} \mathbf{W}^{1/2} \quad (4.26)$$

( $\sigma_h^2 := 1$ ). The channel matrix  $\mathbf{H}_s$  therefore constitutes a semi-correlated channel matrix with effective transmitter covariance matrix  $\mathbf{\Lambda}_{\mathbf{h},\text{Tx}} \mathbf{W}$ . Correspondingly, we can reuse the analytical SER results from Section 3.2.5 by replacing the eigenvalues  $\lambda_{\text{Tx},1}, \dots, \lambda_{\text{Tx},M}$  by  $w_1 \lambda_{\text{Tx},1}, \dots, w_M \lambda_{\text{Tx},M}$ , respectively (similar to Section 4.1.2).

In the case of binary antipodal transmission ( $Q=2$ ), for example, the average symbol error probability thus results as

$$\bar{P}_s = \frac{1}{2} \sum_{\mu=1}^M \sum_{\nu=1}^N \left( \prod_{\substack{\mu'=1 \\ (\mu',\nu') \neq (\mu,\nu)}}^M \prod_{\nu'=1}^N \frac{1}{1 - \frac{w_{\mu'} \lambda_{\text{Tx},\mu'} \lambda_{\text{Rx},\nu'}}{w_{\mu} \lambda_{\text{Tx},\mu} \lambda_{\text{Rx},\nu}}} \right) \left( 1 - \sqrt{\frac{w_{\mu} \lambda_{\text{Tx},\mu} \lambda_{\text{Rx},\nu}}{w_{\mu} \lambda_{\text{Tx},\mu} \lambda_{\text{Rx},\nu} + \xi}} \right) \quad (4.27)$$

( $w_{\mu} > 0$  assumed for all  $\mu = 1, \dots, M$ ), cf. (3.83), where  $\xi := MR_t \sigma_n^2 / P$ .<sup>6</sup> The corresponding high-SNR approximation of (4.27) is given by

$$\bar{P}_s \approx \left( \frac{MN}{4 \bar{\gamma}_s} \right)^{MN} \binom{2MN-1}{MN} \underbrace{\prod_{\mu=1}^M \prod_{\nu=1}^N \frac{1}{w_{\mu} \lambda_{\text{Tx},\mu} \lambda_{\text{Rx},\nu}}}_{=: f_{\text{div}}(\mathbf{W}, \mathbf{\Lambda}_{\mathbf{h},\text{Tx}}, \mathbf{\Lambda}_{\mathbf{h},\text{Rx}})}, \quad (4.28)$$

cf. (3.84), where  $\bar{\gamma}_s = PN / (R_t \sigma_n^2)$ . As earlier, the product term  $f_{\text{div}}(\mathbf{W}, \mathbf{\Lambda}_{\mathbf{h},\text{Tx}}, \mathbf{\Lambda}_{\mathbf{h},\text{Rx}})$  is also relevant for higher-order modulation schemes (cf. Remark 3.6 in Chapter 3). For example, for a  $Q$ -ary phase-shift-keying (PSK) signal constellation, one obtains

$$\bar{P}_s \approx \left( \frac{MN}{\sin^2(\pi/Q) \bar{\gamma}_s} \right)^{MN} \frac{f_{\text{div}}(\mathbf{W}, \mathbf{\Lambda}_{\mathbf{h},\text{Tx}}, \mathbf{\Lambda}_{\mathbf{h},\text{Rx}})}{\pi} \int_0^{\frac{(Q-1)\pi}{Q}} (\sin \phi)^{2MN} d\phi, \quad (4.29)$$

cf. (3.87) and (3.88). Similar expressions also result for  $Q$ -ary ASK- and  $Q$ -ary QAM-signal constellations.

### Optimal Transmit Power Allocation

For high SNR values, in order to maximize the diversity advantage, the product term  $f_{\text{div}}(\mathbf{W}, \mathbf{\Lambda}_{\mathbf{h},\text{Tx}}, \mathbf{\Lambda}_{\mathbf{h},\text{Rx}})$  has to be minimized. In fact, from Lemma 4.2 below it follows that the optimal power allocation strategy in this case is to use equal power allocation, i.e.,  $\mathbf{W}^{\bullet} = \mathbf{I}_M$ . In other words, the asymptotic up-shift of the symbol-error-rate curve (with respect to the case of uncorrelated transmit and receive antennas), which is caused

<sup>6</sup>Again, the above expression can directly be used for OSTBC systems with distributed antennas and a transmitter covariance matrix  $\mathbf{\Sigma}_{\mathbf{h},\text{Tx}} := \mathbf{\Lambda}_{\mathbf{h},\text{Tx}}$  and/or a receiver covariance matrix  $\mathbf{\Sigma}_{\mathbf{h},\text{Rx}} := \mathbf{\Lambda}_{\mathbf{h},\text{Rx}}$ .

by the product term  $f_{\text{div}}(\mathbf{I}_M, \mathbf{\Lambda}_{\mathbf{h}, \text{Tx}}, \mathbf{\Lambda}_{\mathbf{h}, \text{Rx}})$  (cf. Section 3.2.5), cannot be reduced by any statistical transmit power allocation strategy.<sup>7</sup> On the other hand, any statistical transmit power allocation scheme which yields an SNR gain with respect to equal power allocation (cf. Section 4.1.1) will at the same time lower the diversity advantage at high SNR values.

**Lemma 4.2**

Let  $\lambda_1, \dots, \lambda_n$  denote the eigenvalues of an  $(n \times n)$ -correlation matrix  $\mathbf{R}$  with rank  $n$ , i.e.,  $\lambda_1, \dots, \lambda_n$  are real-valued and positive, and  $\lambda_1 + \dots + \lambda_n = n$ . Moreover, let  $w_1, \dots, w_n$  denote a set of arbitrary real-valued positive numbers with sum constraint  $w_1 + \dots + w_n = n$ . Then, the product term

$$\prod_{j=1}^n \frac{1}{w_j \lambda_j} \quad (4.30)$$

is minimized for  $w_1 = \dots = w_n := 1$ .

*Proof.* Follows from many results reported in the literature, e.g. [ZG03a].  $\square$

A simple alternative proof, which is based on convex optimization (cf. Appendix E), is provided in Appendix 2 at the end of this chapter.

For arbitrary SNR values and a single receive antenna ( $N=1$ ), the optimal statistical transmit power allocation strategy in terms of a minimum symbol error probability was derived in [ZG03a].<sup>8</sup> As shown in [ZG03a], the optimization of the weighting matrix  $\mathbf{W}$  amounts to solving the following convex optimization problem:

$$\begin{aligned} \text{minimize} \quad & f(\mathbf{w}) := - \sum_{\mu=1}^M \log \left( 1 + w_{\mu} \lambda_{\text{Tx}, \mu} \frac{g \bar{\gamma}_s}{M} \right), \quad \mathbf{w} := [w_1, \dots, w_M]^T \\ \text{subject to} \quad & \sum_{\mu=1}^M w_{\mu} = M \quad \text{and} \quad w_{\mu} \geq 0 \quad \text{for all } \mu = 1, \dots, M. \end{aligned} \quad (4.31)$$

Depending on the signal constellation under consideration, the parameter  $g$  is equal to  $g_{\text{PSK}}$ ,  $g_{\text{ASK}}$ , or  $g_{\text{QAM}}$ , cf. (I.23), (I.25), and (I.27) in Appendix I. The result is a waterfilling solution (cf. Appendix E) with respect to the inverse eigenvalues  $1/\lambda_{\text{Tx}, \mu}$  of the transmitter correlation matrix  $\mathbf{R}_{\mathbf{h}, \text{Tx}}$ . It is straightforward to show that the result in [ZG03a] can be also be utilized for OSTBC systems with multiple uncorrelated receive antennas

<sup>7</sup>Note that this is a consequence of the transmit power constraint (4.3) or, equivalently, of the trace constraint  $\text{tr}(\mathbf{W}) := M$ . Without this constraint one could, for example, compensate for the transmit antenna correlations by choosing  $w_{\mu} := 1/\lambda_{\text{Tx}, \mu}$ . However, as discussed above a fair comparison between different transmit power allocation strategies is only possible when the overall transmit power is kept constant. As will be seen, under these premises an inversion of the eigenvalues  $\lambda_{\text{Tx}, \mu}$  typically leads to a poor performance.

<sup>8</sup>To be specific, the unifying upper bound (I.28) on  $\bar{P}_s$ , which applies for any  $Q$ -ary PSK-, ASK-, or QAM-signal constellation (cf. Appendix I), was minimized in [ZG03a]. Moreover, focus was on a slightly different transmitter structure, where Alamouti's transmit diversity scheme [Ala98] for two transmit antennas was combined with an  $(M \times M)$  unitary precoder matrix ( $M \geq 2$ ).

( $\mathbf{R}_{\mathbf{h},\text{Rx}} := \mathbf{I}_N$ ). One obtains:

$$w_\mu^\bullet = M \left[ \frac{1}{M'} - \frac{1}{g} \frac{N}{\bar{\gamma}_s} \left( \frac{1}{\lambda_{\text{Tx},\mu}} - \frac{1}{M'} \sum_{\mu' \in \mathbb{W}_{>0}} \frac{1}{\lambda_{\text{Tx},\mu'}} \right) \right]_+, \quad (4.32)$$

where  $M'$  denotes the number of virtual transmit antennas actually used, i.e., the number of power weights  $w_\mu^\bullet > 0$ . Moreover,  $\mathbb{W}_{>0}$  denotes the corresponding index set comprising all indices  $\mu$  with  $w_\mu^\bullet > 0$  (i.e.,  $|\mathbb{W}_{>0}| = M'$ ).

**Remark 4.1 (Determination of the index set  $\mathbb{W}_{>0}$ )**

The number  $M'$  and the index set  $\mathbb{W}_{>0}$  can be determined as follows [ZG03a]: One first sets  $M' := M$  and checks whether the resulting optimal power weight  $w_\mu^\bullet$  associated with the smallest eigenvalue  $\lambda_{\text{Tx},\mu}$  of  $\mathbf{R}_{\mathbf{h},\text{Tx}}$  is greater than zero. If this is the case, the index set  $\mathbb{W}_{>0}$  is equal to  $\mathbb{W}_{>0} = \{1, \dots, M\}$ . Otherwise, one continues with  $M' := (M-1)$  and excludes the index  $\mu$  associated with the smallest eigenvalue  $\lambda_{\text{Tx},\mu}$  from the index set  $\mathbb{W}_{>0}$ . Based on the updated index set, one now checks whether the resulting optimal power weight associated with the second smallest eigenvalue of  $\mathbf{R}_{\mathbf{h},\text{Tx}}$  is greater than zero, and so on.

Note that the optimal waterfilling solution depends on the overall SNR  $\bar{\gamma}_s = PN/(R_t \sigma_n^2)$ . For high SNR values, the waterfilling solution (4.32) tends to the EBF solution ( $M' = M$ ), and for low SNR values one obtains the one-dimensional eigen-beamforming solution ( $M' = 1$ ). Moreover, for the special case  $\mathbf{R}_{\mathbf{h},\text{Tx}} = \mathbf{I}_M$  the waterfilling solution also tends to the equal-power-allocation solution, just as in the case of high SNR values.

As earlier, we note that the optimal waterfilling solution (4.32) can be reused for OSTBC systems with distributed transmit antennas, without any loss of optimality. In this case, the decorrelation stage  $\mathbf{U}_{\text{Tx}}$  in Fig. 4.1 can again be dropped. Moreover, note that for  $\Sigma_{\mathbf{h},\text{Tx}} \neq \mathbf{I}_M$  and low SNR values, some of the cooperating transmitting nodes will not at all take part in the cooperative transmission process.

Further transmitter strategies for space-time coded MIMO systems requiring statistical channel knowledge at the transmitter can, for example, be found in [SP02, AQ04, HG04]. In particular, [SP02, AQ04] treat the case of uncorrelated receive antennas, whereas [HG04] covers also scenarios with correlated transmit and correlated receive antennas.

## Numerical Results

As an example, we consider an OSTBC system with  $M=4$  co-located transmit antennas and a single receive antenna ( $\sigma_h^2=1$ ), and focus on the case of binary antipodal transmission ( $Q=2$ ) for simplicity. As earlier, we assume a transmitter correlation matrix  $\mathbf{R}_{\mathbf{h},\text{Tx}} = \mathbf{R}_{M,\rho_{\text{Tx}}}$  with correlation parameter  $\rho_{\text{Tx}}=0.8$ , cf. (3.39). Again, we could equivalently consider an OSTBC system with four distributed transmit antennas and a transmitter covariance matrix  $\Sigma_{\mathbf{h},\text{Tx}} := \Lambda_{\mathbf{h},\text{Tx}}$ . Fig. 4.3 displays the average SER performance of the OSTBC system resulting for the different statistical transmit power allocation strategies discussed above. As earlier, the average symbol error probabilities are plotted as a function of  $P/\sigma_n^2$  in dB. The overall average received SNR in the OSTBC system is

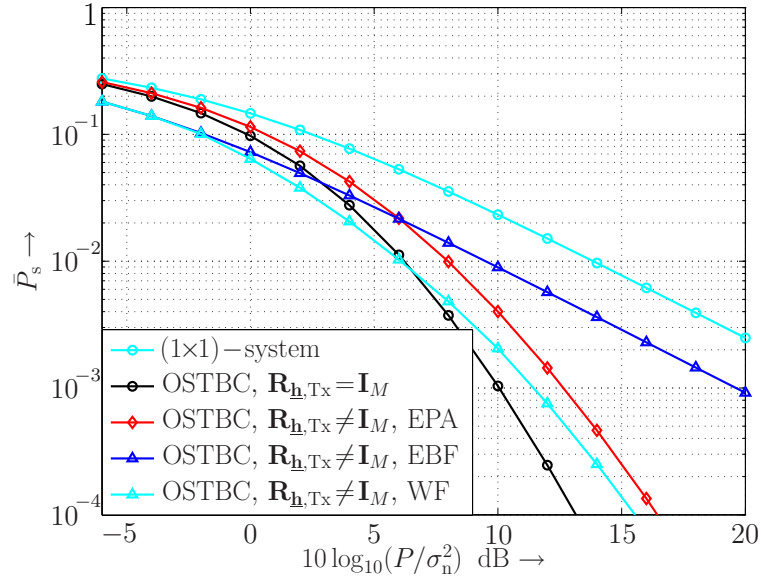


Figure 4.3: Average SER performance of a (4×1)-OSTBC system with different statistical transmit power allocation strategies: Equal power allocation (EPA), one-dimensional eigen-beamforming (EBF), and optimal waterfilling (WF). Analytical results for binary antipodal transmission ( $Q=2$ ), frequency-flat Rayleigh fading, and a transmitter correlation matrix  $\mathbf{R}_{\mathbf{h},\text{Tx}} = \mathbf{R}_{M,\rho_{\text{Tx}}}$  with  $\rho_{\text{Tx}}=0.8$ .

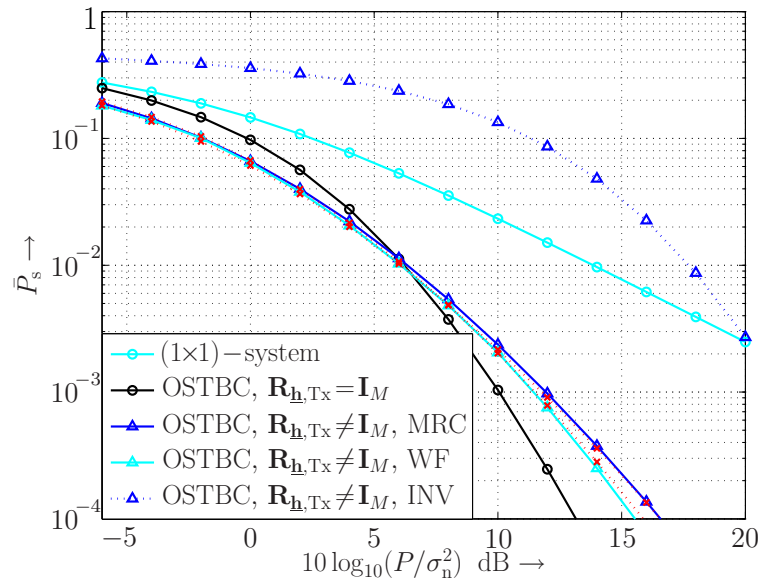


Figure 4.4: Corresponding performance results for transmitter-sided maximum-ratio-combining (MRC) and eigenvalue inversion (INV). The dotted curves marked with ‘×’ illustrate the impact of estimation errors concerning the transmitter correlation matrix, which will be discussed in Section 4.1.4.

given by  $\bar{\gamma}_s = P/(R_t\sigma_n^2)$ , while a temporal rate of  $R_t = 1$  was assumed for simplicity. The curves were obtained analytically on the basis of (4.27) and were validated by means of Monte-Carlo simulations. As a reference, the SER curves of a single-antenna system and of a (4×1)-OSTBC system with uncorrelated antennas have been included.

As can be seen, throughout the complete SNR range under consideration, the optimal waterfilling (WF) strategy according to (4.32) yields significant performance gains with respect to equal power allocation (EPA). As expected, for low SNR values the waterfilling strategy coincides with the one-dimensional eigen-beamforming (EBF) solution.<sup>9</sup> Altogether, depending on the SNR value the waterfilling strategy provides a gain of up to 2 dB over one-dimensional eigen-beamforming/equal power allocation (taking the superior of both strategies). In the low SNR regime the performance of the spatially correlated OSTBC system with optimal waterfilling is even superior to that of the uncorrelated OSTBC system, similar to the capacity results presented in Section 4.1.2.

As an alternative to the optimal waterfilling solution (4.32), we propose to use a simple transmitter-sided maximum-ratio-combining (MRC) scheme, where the eigenvalues  $\lambda_{T_x,\mu}$  themselves are used as weighting factors ( $\mathbf{W} := \mathbf{\Lambda}_{\mathbf{h},T_x}$ ). Thus, strong eigenvalues  $\lambda_{T_x,\mu}$  are strongly weighted and weak eigenvalues are weakly weighted, similar to the waterfilling solution, cf. Fig. E.1 in Appendix E ( $\alpha_\mu := 1/\lambda_{T_x,\mu}$ ). As can be seen in Fig. 4.4, the transmitter-sided MRC strategy provides a good performance over the complete SNR range under consideration and is quite close to the optimal waterfilling solution. Especially for low SNR values the difference is barely visible. Interestingly, even for SNR values up to 15 dB the transmitter-sided MRC scheme still outperforms the equal-power-allocation strategy (cf. Fig. 4.3). However, for larger SNR values, equal power allocation becomes superior. For the sake of completeness, Fig. 4.4 also displays the SER curve which results for a transmitter-sided eigenvalue inversion (INV) strategy. In the case of an OSTBC system with distributed transmit antennas, this power allocation strategy corresponds to levelling the unequal average link SNRs. The transmit power weights  $w_\mu$  were chosen as  $w_\mu := c/\lambda_{T_x,\mu}$ , where the normalization factor  $c := M/(\sum_{\mu'=1}^M 1/\lambda_{T_x,\mu'})$  guarantees that the trace constraint  $\text{tr}(\mathbf{W}) = M$  is met. As can be seen, the eigenvalue inversion strategy leads to a very poor performance, because the resulting normalization factor  $c$  is quite small in the considered example. Note that in this case the asymptotic slope of the SER curve corresponds to that of the uncorrelated OSTBC system, as expected.

### Optimal Transmit Power Allocation for Distributed OSTBC Systems

The above considerations were restricted to the case where all transmission links are subject to frequency-flat Rayleigh fading. However, given an OSTBC system with distributed transmit antennas, the individual transmission links may be subject to different fading characteristics.

In this section, we consider the general case where the individual transmission links are characterized by Nakagami- $m$  fading (cf. Section 3.3.1 in Chapter 3) with different fading

<sup>9</sup>Note that the SER curve of the EBF scheme has the same asymptotic slope as the curve of the single-antenna system. This is because the EBF scheme reduces the diversity order from  $M = 4$  to one. However, compared to the single-antenna system an SNR gain of  $10 \log_{10}(2.72)$  dB  $\approx 4.4$  dB is achieved, since the maximum eigenvalue of the transmitter correlation matrix  $\mathbf{R}_{\mathbf{h},T_x}$  is given by  $\lambda_{T_x,\max} = 2.72$ .



parameters  $m_\mu$ , where Rayleigh fading is included as a special case ( $m_\mu = 1$ ).<sup>10</sup> Consider again the distributed MIMO system depicted in Fig. 3.1, which consists of  $T_n$  cooperating transmitting nodes, equipped with altogether  $M$  antennas, and a single receiving node equipped with  $N$  antennas. We again assume that an OSTBC with a temporal rate of  $R_t$  is employed at the transmitter side. As earlier, let

$$\Sigma_{\mathbf{h}, \text{Tx}} = \mathbf{E}\{\mathbf{H}^H \mathbf{H}\} / N = \text{diag}([\sigma_{h,1}^2, \dots, \sigma_{h,\mu}^2, \dots, \sigma_{h,M}^2]) \quad (4.33)$$

denote the transmitter covariance matrix ( $\text{tr}(\Sigma_{\mathbf{h}, \text{Tx}}) := M$ ), which represents the unequal average link SNRs due to the distributed transmit antennas (cf. Section 3.2.2). The  $\mu$ th transmit antenna ( $1 \leq \mu \leq M$ ) is assumed to be associated with a Nakagami fading parameter  $m_\mu$  ( $0.5 \leq m_\mu < \infty$ ). The receive antennas are again assumed to be uncorrelated ( $\mathbf{R}_{\mathbf{h}, \text{Rx}} = \mathbf{I}_N$ ). Correspondingly, the channel matrix  $\mathbf{H}$  can be written as

$$\mathbf{H} := \mathbf{H}' \Sigma_{\mathbf{h}, \text{Tx}}^{1/2}, \quad (4.34)$$

where the entries of the  $\mu$ th column of  $\mathbf{H}'$  are i.i.d. complex random variables with Nakagami- $m_\mu$  distributed amplitudes and phases uniformly distributed in  $[0, 2\pi)$ .

In the following, we again consider the statistical transmit power allocation scheme depicted in Fig. 4.1 (without the decorrelation stage  $\mathbf{U}_{\text{Tx}}$ ). As earlier, we assume that the complete set of second-order channel statistics, in terms of the transmitter covariance matrix  $\Sigma_{\mathbf{h}, \text{Tx}}$  and the noise variance  $\sigma_n^2$  is perfectly known at the transmitter. Additionally, we assume that the fading parameters  $m_1, \dots, m_M$  are known at the transmitter side.<sup>11</sup> Given an arbitrary power weighting matrix  $\mathbf{W} = \text{diag}([w_1, \dots, w_M])$ , the average symbol error probability, e.g., for the case of a  $Q$ -ary PSK signal constellation, is thus given by

$$\bar{P}_s = \frac{1}{\pi} \int_0^{\frac{(Q-1)\pi}{Q}} \prod_{\mu=1}^M \left( \frac{MN m_\mu \sin^2(\phi)}{MN m_\mu \sin^2(\phi) + w_\mu \sigma_{h,\mu}^2 g_{\text{PSK}} \bar{\gamma}_s} \right)^{Nm_\mu} d\phi, \quad (4.35)$$

cf. Section 3.3.1 and Appendix I, where  $g_{\text{PSK}} = \sin^2(\pi/Q)$  and  $\bar{\gamma}_s = PN/(R_t \sigma_n^2)$ . Similar expressions result also for  $Q$ -ary ASK and  $Q$ -ary QAM signal constellations. For fading parameters  $m_\mu < \infty$  ( $\mu = 1, \dots, M$ ), the corresponding high-SNR approximation ( $\bar{\gamma}_s \rightarrow \infty$ ) results as

$$\begin{aligned} \bar{P}_s &\approx \frac{1}{\pi} \prod_{\mu=1}^M \left( \frac{MN}{g_{\text{PSK}} \bar{\gamma}_s} \right)^{Nm_\mu} \underbrace{\prod_{\mu=1}^M \left( \frac{m_\mu}{w_\mu \sigma_{h,\mu}^2} \right)^{Nm_\mu}}_{=: f'_{\text{div}}(\mathbf{W}, \Sigma_{\mathbf{h}, \text{Tx}})} \int_0^{\frac{(Q-1)\pi}{Q}} \prod_{\mu=1}^M (\sin \phi)^{2Nm_\mu} d\phi. \end{aligned} \quad (4.36)$$

Note that the diversity order of the system is given by  $N(m_1 + \dots + m_M)$ . Moreover, for pure Rayleigh fading ( $m_1 = \dots = m_M = 1$ ) the above expression reduces to (4.29) with

<sup>10</sup>Interestingly, most papers on optimal transmit power allocation strategies focus on Rayleigh fading, while the literature on corresponding strategies for Nakagami- $m$  fading scenarios is surprisingly sparse, e.g., [LG01, HA02, KA03].

<sup>11</sup>Different techniques for estimating the Nakagami-fading parameter were discussed, e.g., in [KA03].

$\mathbf{\Lambda}_{\mathbf{h},\text{Tx}} := \mathbf{\Sigma}_{\mathbf{h},\text{Tx}}$  and  $\mathbf{\Lambda}_{\mathbf{h},\text{Rx}} := \mathbf{I}_N$ . Finally, the unifying upper bound (I.28) on  $\bar{P}_s$  (cf. Appendix I), which applies for any  $Q$ -ary PSK-, ASK-, or QAM-signal constellation [ZG03a], results as

$$\bar{P}_s \leq \frac{Q-1}{Q} \prod_{\mu=1}^M \left( \frac{MNm_\mu}{MNm_\mu + w_\mu \sigma_{h,\mu}^2 g \bar{\gamma}_s} \right)^{m_\mu N}. \quad (4.37)$$

As earlier, the parameter  $g$  is equal to  $g_{\text{PSK}}$ ,  $g_{\text{ASK}}$ , or  $g_{\text{QAM}}$ , cf. (I.23), (I.25), and (I.27) in Appendix I, depending on the signal constellation under consideration.

In the sequel, we again assume that the power weighting matrix  $\mathbf{W}$  is subject to the trace constraint  $\text{tr}(\mathbf{W}) := M$ , so as to fix the overall average transmit power. Similar to the case of pure Rayleigh fading, minimizing the right-hand side of (4.37) amounts to solving the following convex optimization problem, cf. (4.31):

$$\begin{aligned} & \text{minimize} \quad f(\mathbf{w}) := - \sum_{\mu=1}^M m_\mu \log \left( 1 + w_\mu \frac{\sigma_{h,\mu}^2 g \bar{\gamma}_s}{m_\mu MN} \right), \quad \mathbf{w} := [w_1, \dots, w_M]^T \\ & \text{subject to} \quad \sum_{\mu=1}^M w_\mu = M \quad \text{and} \quad w_\mu \geq 0 \quad \text{for all} \quad \mu = 1, \dots, M. \end{aligned} \quad (4.38)$$

The above optimization problem can be solved along the same lines as the corresponding problem (4.31) for pure Rayleigh fading [ZG03a]. One obtains:

$$w_\mu^\bullet = Mm_\mu \left[ \frac{1}{\Phi(M')} - \frac{1}{g \bar{\gamma}_s} \left( \frac{1}{\sigma_{h,\mu}^2} - \frac{1}{\Phi(M')} \sum_{\mu' \in \mathbb{W}_{>0}} \frac{m_{\mu'}}{\sigma_{h,\mu'}^2} \right) \right]_+, \quad (4.39)$$

where

$$\Phi(M') := \sum_{\mu' \in \mathbb{W}_{>0}} m_{\mu'}. \quad (4.40)$$

For the sake of convenience, the details of the derivation of (4.39) have been included in Appendix 3 at the end of this chapter.<sup>12</sup> As earlier,  $M'$  denotes the number of power weights  $w_\mu^\bullet > 0$  and  $\mathbb{W}_{>0}$  the corresponding index set comprising all indices  $\mu$  with  $w_\mu^\bullet > 0$ . In the special case of i.i.d. Nakagami- $m$  fading ( $m_1 = \dots = m_M =: m$ ), the above expression reduces to

$$w_\mu^\bullet = Mm \left[ \frac{1}{M'm} - \frac{1}{g \bar{\gamma}_s} \left( \frac{1}{\sigma_{h,\mu}^2} - \frac{1}{M'} \sum_{\mu' \in \mathbb{W}_{>0}} \frac{1}{\sigma_{h,\mu'}^2} \right) \right]_+. \quad (4.41)$$

In particular, for i.i.d. Rayleigh fading (4.39) reduces to the waterfilling solution (4.32), where  $\sigma_{h,\mu}^2 := \lambda_{\text{Tx},\mu}$ . Finally, note that the waterfilling solution (4.39) is also relevant for scenarios with mixed Rayleigh and Rice fading (cf. Section 3.4.3 in Chapter 3). As

<sup>12</sup>An alternative derivation of (4.39) was presented in [KA03]. However, the system model considered in [KA03] is different from the one considered here. At the transmitter, perfect orthogonal spreading was assumed (instead of an OSTBC), and focus was on a single receive antenna. Note that the temporal rate of this system is equal to  $R_t = 1/M$ . As discussed in [KA03], the number  $M'$  and the index set  $\mathbb{W}_{>0}$  can be determined in a similar way as discussed earlier for the case of pure Rayleigh fading (cf. Remark 4.1).

discussed in Section 3.3.1, for large values of the fading parameter  $m$  (say,  $m \geq 10$ ), the Nakagami- $m$  distribution well approximates a Rician distribution with Rice factor  $K = \sqrt{m^2 - m} / (m - \sqrt{m^2 - m})$ . Moreover, for  $m \rightarrow 0.5$  the Nakagami- $m$  distribution can also be utilized, in order to approximate composite Rayleigh fading/log-normal shadowing distributions (cf. Fig. C.4 and Fig. C.5 in Appendix C).

In order to maximize the diversity advantage for high SNR values ( $\bar{\gamma}_s \rightarrow \infty$ ), the product term  $f'_{\text{div}}(\mathbf{W}, \boldsymbol{\Sigma}_{\mathbf{h}, \text{Tx}})$  in (4.36) has to be minimized. (As earlier, the product term  $f'_{\text{div}}(\mathbf{W}, \boldsymbol{\Sigma}_{\mathbf{h}, \text{Tx}})$  is also relevant for  $Q$ -ary ASK- and  $Q$ -ary QAM-signal constellations.) In contrast to pure Rayleigh fading, in the case of non-i.i.d. Nakagami- $m$  fading equal power allocation is no longer the optimal power allocation strategy for high SNR values. Instead, the diversity advantage is maximized by choosing

$$w_{\mu}^{\bullet} = \frac{M m_{\mu}}{\Phi(M)}, \quad \Phi(M) := \sum_{\mu'=1}^M m_{\mu'} \quad (M' = M), \quad (4.42)$$

cf. (4.39) and (4.40). Correspondingly, transmission links with a large fading parameter  $m_{\mu}$  are stronger weighted than links with a small fading parameter, i.e., the transmit power is focussed on those links characterized by particularly mild fading conditions. Interestingly, for the special case  $\boldsymbol{\Sigma}_{\mathbf{h}, \text{Tx}} = \mathbf{I}_M$  and arbitrary SNR values  $\bar{\gamma}_s$ , (4.39) becomes

$$w_{\mu}^{\bullet} = M m_{\mu} \left[ \frac{1}{\Phi(M')} \right]_{+} = \frac{M m_{\mu}}{\Phi(M)}, \quad (4.43)$$

i.e., the same solution results as for high SNR values (given an arbitrary transmitter covariance matrix  $\boldsymbol{\Sigma}_{\mathbf{h}, \text{Tx}}$ ).

## Numerical Results

As an example, we consider an OSTBC system with  $M = 4$  distributed transmit antennas, a single receive antenna, and a transmitter covariance matrix

$$\boldsymbol{\Sigma}_{\mathbf{h}, \text{Tx}} = \text{diag}([2.0 \ 0.8 \ 0.7 \ 0.5]). \quad (4.44)$$

For simplicity, we again focus on the case of binary antipodal transmission ( $Q = 2$ ). Fig. 4.5 displays the average SER performance of the OSTBC system that results for Nakagami-fading parameters  $m_1 = 5$ ,  $m_2 = 2$ ,  $m_3 = 1$ ,  $m_4 = 0.5$  and different statistical transmit power allocation strategies. The average symbol error probabilities are again plotted as a function of  $P/\sigma_n^2$  in dB. For simplicity, a temporal rate of  $R_t = 1$  was assumed for the OSTBC. The curves were obtained analytically on the basis of (4.35) and were validated by means of Monte-Carlo simulations. As a reference, the SER curve of a single-antenna system for the case of Rayleigh fading ( $m = 1$ ) has been included. As can be seen, the optimal waterfilling (WF) strategy according to (4.39) yields significant performance gains over equal power allocation (EPA), throughout the complete SNR range under consideration. As in the case of pure Rayleigh fading, for low SNR values the waterfilling strategy coincides with the one-dimensional eigen-beamforming (EBF) solution. However, in the

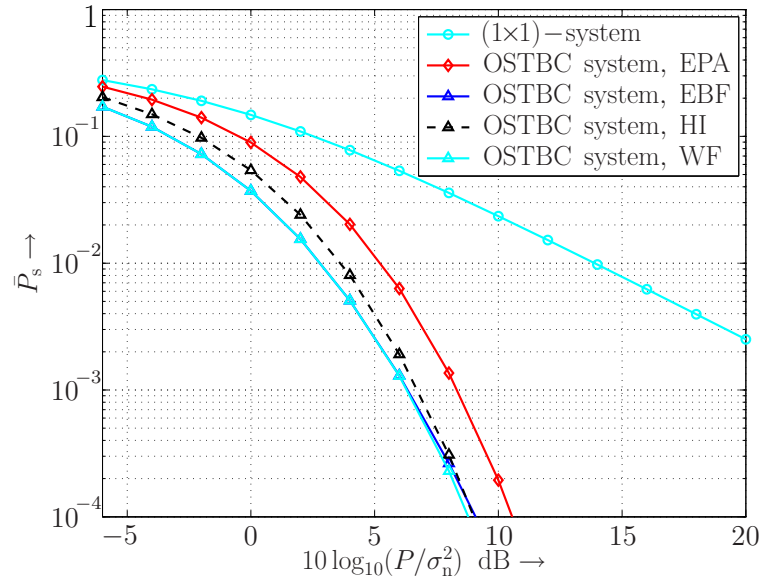


Figure 4.5: Average SER performance of a distributed  $(4 \times 1)$ -OSTBC system with different statistical transmit power allocation strategies: Equal power allocation (EPA), one-dimensional eigen-beamforming (EBF), high-SNR solution (HI), and optimal waterfilling (WF). Analytical results for binary antipodal transmission ( $Q=2$ ), frequency-flat non-i.i.d. Nakagami- $m$  fading ( $m_1=5$ ,  $m_2=2$ ,  $m_3=1$ ,  $m_4=0.5$ ), and a transmitter covariance matrix  $\Sigma_{\mathbf{h},\text{Tx}} = \text{diag}([2.0 \ 0.8 \ 0.7 \ 0.5])$ .

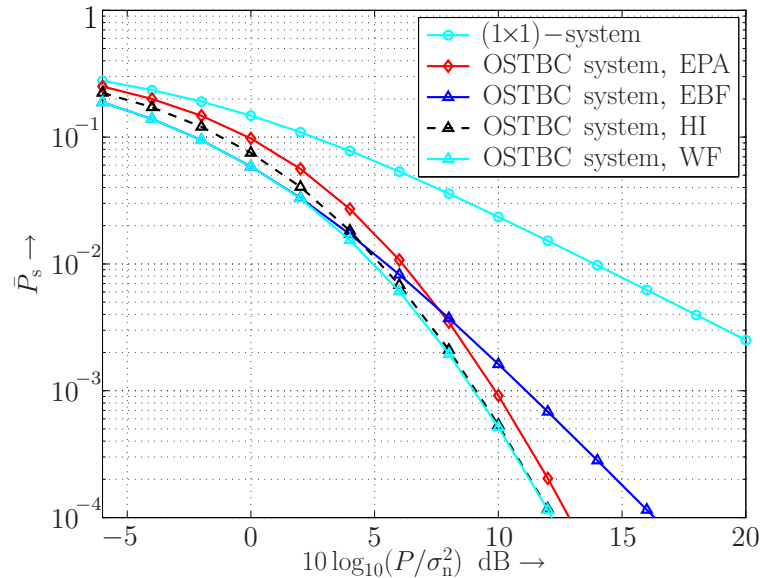


Figure 4.6: Corresponding performance results for  $m_1=2$ ,  $m_2=1$ ,  $m_3=0.75$  and  $m_4=0.5$  (same transmitter covariance matrix  $\Sigma_{\mathbf{h},\text{Tx}}$ ).

considered example the difference between the optimal waterfilling solution and the eigen-beamforming solution is only visible at an SNR of 8 dB. As expected, for large values of  $P/\sigma_n^2$  the waterfilling strategy approaches the high-SNR (HI) solution (4.42).

As a second example, Fig. 4.6 displays corresponding performance results for Nakagami-fading parameters  $m_1=2$ ,  $m_2=1$ ,  $m_3=0.75$  and  $m_4=0.5$  (same transmitter covariance matrix  $\mathbf{\Sigma}_{\mathbf{h},\text{Tx}}$ ). As can be seen, the gains with respect to equal power allocation are smaller in this example. Moreover, for SNR values greater than 5 dB the eigen-beamforming solution is clearly outperformed by the optimal waterfilling solution. On the other hand, for SNR values greater than 6 dB the waterfilling solution is closely approximated by the high-SNR solution (4.42). Only in the area around 5 dB, the waterfilling solution outperforms both the eigen-beamforming and the high-SNR solution. However, compared to the case of pure Rayleigh fading the difference is rather small (cf. Fig. 4.3). Altogether, in many cases the optimal waterfilling solution (4.39) turned out to be closely approximated either by the eigen-beamforming solution or by the high-SNR solution (depending on the SNR value under consideration). This allows for a simple calculation of the power weights  $w_\mu$  while achieving near-optimal performance.

#### 4.1.4 Impact of Estimation Errors

Consider again an OSTBC system with co-located antennas that is subject to frequency-flat Rayleigh fading. So far, we have assumed that the correlation matrix  $\mathbf{R}_{\mathbf{h},\text{Tx}}$  is perfectly known at the transmitter. In the case of estimation errors, however, the statistical transmit power allocation scheme will be based on an erroneous transmitter correlation matrix  $\hat{\mathbf{R}}_{\mathbf{h},\text{Tx}}$ . In general, both the eigenvectors and the eigenvalues of  $\hat{\mathbf{R}}_{\mathbf{h},\text{Tx}}$  will be different from those of the actual correlation matrix  $\mathbf{R}_{\mathbf{h},\text{Tx}}$ , i.e.,

$$\hat{\mathbf{R}}_{\mathbf{h},\text{Tx}} = \hat{\mathbf{U}}_{\text{Tx}} \hat{\mathbf{\Lambda}}_{\mathbf{h},\text{Tx}} \hat{\mathbf{U}}_{\text{Tx}}^H, \quad (4.45)$$

where  $\hat{\mathbf{U}}_{\text{Tx}} \neq \mathbf{U}_{\text{Tx}}$  and  $\hat{\mathbf{\Lambda}}_{\mathbf{h},\text{Tx}} \neq \mathbf{\Lambda}_{\mathbf{h},\text{Tx}}$ . (We assume that  $\hat{\mathbf{R}}_{\mathbf{h},\text{Tx}}$  is still a Hermitian matrix.) This has the following two effects. First, the transmitter will use a mismatched decorrelation stage  $\hat{\mathbf{U}}_{\text{Tx}}$ . If  $\hat{\mathbf{U}}_{\text{Tx}} \neq \mathbf{U}_{\text{Tx}}$ , the product  $\hat{\mathbf{U}}_{\text{Tx}}^H \mathbf{U}_{\text{Tx}}$  does no longer yield the identity matrix  $\mathbf{I}_M$ , i.e., equation (4.7) does not hold anymore and generalizes to

$$\mathbb{E} \{ \mathbf{H}_v^H \mathbf{H}_v \} = N \sigma_h^2 \hat{\mathbf{U}}_{\text{Tx}}^H \mathbf{U}_{\text{Tx}} \mathbf{\Lambda}_{\mathbf{h},\text{Tx}} \mathbf{U}_{\text{Tx}}^H \hat{\mathbf{U}}_{\text{Tx}}. \quad (4.46)$$

Second, the power weighting stage will be based on an erroneous eigenvalue matrix  $\hat{\mathbf{\Lambda}}_{\mathbf{h},\text{Tx}}$ .<sup>13</sup> This means that a mismatched weighting matrix  $\hat{\mathbf{W}}$  will be used, which might lower the obtained performance gains.<sup>14</sup> Altogether, (4.9) generalizes to

$$\mathbf{Q}_y = \frac{P \sigma_h^2}{M} \cdot \text{tr} \left( \hat{\mathbf{U}}_{\text{Tx}}^H \mathbf{U}_{\text{Tx}} \hat{\mathbf{W}} \mathbf{\Lambda}_{\mathbf{h},\text{Tx}} \mathbf{U}_{\text{Tx}}^H \hat{\mathbf{U}}_{\text{Tx}} \right) \mathbf{R}_{\mathbf{h},\text{Rx}} + \sigma_n^2 \mathbf{I}_N, \quad (4.47)$$

<sup>13</sup>Bounds for the absolute difference between the eigenvalues  $\hat{\lambda}_{\text{Tx},\mu}$  and  $\lambda_{\text{Tx},\mu}$  [Uts06b], given some perturbation  $\hat{\mathbf{R}}_{\mathbf{h},\text{Tx}} := \mathbf{R}_{\mathbf{h},\text{Tx}} + \mathbf{E}$ , where  $\mathbf{E}$  denotes an error matrix, can be found in [HJ85, EI99]. For example, it can be shown that the maximum absolute difference  $|\hat{\lambda}_{\text{Tx},\mu} - \lambda_{\text{Tx},\mu}|$  (over all indices  $\mu$ ) is bounded above by  $\sup_{\mathbf{x} \neq \mathbf{0}} \|\mathbf{E}\mathbf{x}\|_2 / \|\mathbf{x}\|_2$ .

<sup>14</sup>If the optimal waterfilling solution (4.32) is employed, the mismatched weighting matrix  $\hat{\mathbf{W}}$  will clearly be suboptimal. Specifically, an erroneous eigenvalue matrix  $\hat{\mathbf{\Lambda}}_{\mathbf{h},\text{Tx}}$  might lead to a suboptimal choice of the dimension  $M'$ , i.e., to a suboptimal number of virtual antennas.

i.e., there will be an overall mismatch in the power weighting, which is captured by the diagonal elements of the  $(M \times M)$ -matrix

$$\mathbf{\Xi}_{\text{Tx}} := \hat{\mathbf{U}}_{\text{Tx}}^{\text{H}} \mathbf{U}_{\text{Tx}} \hat{\mathbf{W}} \mathbf{\Lambda}_{\mathbf{h}, \text{Tx}} \mathbf{U}_{\text{Tx}}^{\text{H}} \hat{\mathbf{U}}_{\text{Tx}}. \quad (4.48)$$

(If  $\mathbf{R}_{\mathbf{h}, \text{Tx}}$  is perfectly known at the transmitter, one obtains  $\mathbf{\Xi}_{\text{Tx}} = \mathbf{W} \mathbf{\Lambda}_{\mathbf{h}, \text{Tx}}$ .) Correspondingly, we can reuse the analytical SER results from Section 4.1.3 by replacing the terms  $w_1 \lambda_{\text{Tx},1}, \dots, w_M \lambda_{\text{Tx},M}$  by  $[\mathbf{\Xi}_{\text{Tx}}]_{1,1}, \dots, [\mathbf{\Xi}_{\text{Tx}}]_{M,M}$ , respectively. For example, in the case of binary antipodal transmission ( $Q=2$ ), one obtains

$$\bar{P}_s = \frac{1}{2} \sum_{\mu=1}^M \sum_{\nu=1}^N \left( \prod_{\substack{\mu'=1 \\ (\mu', \nu') \neq (\mu, \nu)}}^M \prod_{\nu'=1}^N \frac{1}{1 - \frac{[\mathbf{\Xi}_{\text{Tx}}]_{\mu', \mu'} \lambda_{\text{Rx}, \nu'}}{[\mathbf{\Xi}_{\text{Tx}}]_{\mu, \mu} \lambda_{\text{Rx}, \nu}}} \right) \left( 1 - \sqrt{\frac{[\mathbf{\Xi}_{\text{Tx}}]_{\mu, \mu} \lambda_{\text{Rx}, \nu}}{[\mathbf{\Xi}_{\text{Tx}}]_{\mu, \mu} \lambda_{\text{Rx}, \nu} + \xi}} \right) \quad (4.49)$$

( $[\mathbf{\Xi}_{\text{Tx}}]_{\mu, \mu} > 0$  assumed for all  $\mu = 1, \dots, M$ ), cf. (4.27), where  $\xi := MR_t \sigma_n^2 / P$ .

In the case of distributed transmit antennas, where an erroneous transmitter covariance matrix  $\hat{\Sigma}_{\mathbf{h}, \text{Tx}} \neq \Sigma_{\mathbf{h}, \text{Tx}}$  is available at the transmitter side, (4.48) simplifies to  $\mathbf{\Xi}_{\text{Tx}} = \hat{\mathbf{W}} \Sigma_{\mathbf{h}, \text{Tx}}$ , since no decorrelation stage  $\mathbf{U}_{\text{Tx}}$  is required in this case.

## Numerical Examples

In the following, the impact of estimation errors concerning the transmitter correlation matrix is illustrated by means of simple examples. To this end, we again assume that the transmitter correlation matrix  $\mathbf{R}_{\mathbf{h}, \text{Tx}}$  is of form (3.39), and that a direct estimate  $\hat{\rho}_{\text{Tx}} := |\hat{\rho}_{\text{Tx}}| e^{j\hat{\phi}_{\text{Tx}}}$  of the correlation parameter  $\rho_{\text{Tx}} := |\rho_{\text{Tx}}| e^{j\phi_{\text{Tx}}}$  is available at the transmitter. Correspondingly, the statistical transmit power allocation scheme will be based on an erroneous transmitter correlation matrix  $\hat{\mathbf{R}}_{\mathbf{h}, \text{Tx}} = \mathbf{R}_{M, \hat{\rho}_{\text{Tx}}}$ .

### Example 4.1 (Power weighting mismatch for two transmit antennas)

In the case of  $M=2$  transmit antennas, the diagonal entries of the matrix  $\mathbf{\Xi}_{\text{Tx}}$  can be calculated in closed form. Utilizing the eigenvalue decomposition of  $\mathbf{R}_{\mathbf{h}, \text{Tx}} = \mathbf{R}_{2, \rho_{\text{Tx}}}$  (cf. Example H.1 in Appendix H), one obtains

$$[\mathbf{\Xi}_{\text{Tx}}]_{1,1} = \frac{1}{2} \left( \hat{w}_1 \lambda_{\text{Tx},1} (1 + \cos \Delta \phi_{\text{Tx}}) + \hat{w}_2 \lambda_{\text{Tx},2} (1 - \cos \Delta \phi_{\text{Tx}}) \right), \quad (4.50a)$$

$$[\mathbf{\Xi}_{\text{Tx}}]_{2,2} = \frac{1}{2} \left( \hat{w}_1 \lambda_{\text{Tx},1} (1 - \cos \Delta \phi_{\text{Tx}}) + \hat{w}_2 \lambda_{\text{Tx},2} (1 + \cos \Delta \phi_{\text{Tx}}) \right), \quad (4.50b)$$

where  $\Delta \phi_{\text{Tx}} := \phi_{\text{Tx}} - \hat{\phi}_{\text{Tx}}$ ,  $\lambda_{\text{Tx},1} := 1 - |\rho_{\text{Tx}}|$ , and  $\lambda_{\text{Tx},2} := 1 + |\rho_{\text{Tx}}|$ . Obviously, for perfect knowledge of  $\mathbf{R}_{\mathbf{h}, \text{Tx}}$  at the transmitter we have  $\hat{w}_{1,2} = w_{1,2}$  and  $\Delta \phi = 0$ , i.e.,  $[\mathbf{\Xi}_{\text{Tx}}]_{\mu, \mu} = w_{\mu} \lambda_{\text{Tx}, \mu}$  ( $\mu = 1, 2$ ), as expected.  $\diamond$

### Example 4.2 (Impact on the transmitter-sided MRC scheme)

Next, we consider the case of  $M=4$  transmit antennas. As an example, numerical results for the co-located  $(4 \times 1)$ -OSTBC system considered in Section 4.1.3 have

been included in Fig. 4.4 ( $\rho_{\text{Tx}}=0.8$ ) for the case of the transmitter-sided MRC scheme (dotted curves marked with ‘×’). Specifically, for  $|\hat{\rho}_{\text{Tx}}|$  values of  $0.9\rho_{\text{Tx}}$  (lower curve) and  $1.1\rho_{\text{Tx}}$  (upper curve) were assumed, and for  $\Delta\phi_{\text{Tx}}$  a value of 0.1 rad. As can be seen, the SER performance of the transmitter-sided MRC scheme is quite robust with regard to these estimation errors. Note that the estimation errors considered here are already quite large. Usually, such an estimation accuracy can easily be achieved, for example, by averaging the channel coefficients over a reasonable number of channel realizations. Interestingly, since the transmitter-sided MRC scheme is not optimal, estimation errors can even improve the performance slightly (cf. Fig. 4.4).  $\diamond$

## 4.2 Use of Statistical Channel Knowledge at the Receiver

In this section, we consider the use of statistical channel knowledge at the receiver, so as to provide an optimal trade-off between system performance and receiver complexity. The receiver structure under consideration can, for example, be combined with the statistical transmit power allocation scheme discussed in Section 4.1. In fact, it will be seen that the structures of the transmitter and the considered receiver scheme are somewhat dual to each other. In particular, the impact of estimation errors concerning the receiver correlation matrix can be analyzed along the same lines as for the transmitter scheme (cf. Section 4.1.4). Although focus is on MIMO systems with co-located receive antennas, the receiver structure can also be employed in MIMO systems with distributed receive antennas, again without any loss of optimality. Moreover, all considerations made in the following apply also for MIMO systems with distributed transmit antennas.

### 4.2.1 System Model with Reduced-Dimension Receiver

In the following, we consider a MIMO system with  $M$  co-located transmit antennas and  $N$  co-located receive antennas. As earlier, we focus on the case of quasi-static frequency-flat Rayleigh fading. Correspondingly, the discrete-time channel model is given by

$$\mathbf{y}[k] = \mathbf{H}\mathbf{x}[k] + \mathbf{n}[k] \quad (4.51)$$

(cf. Section 2.2.2), where in essence the same statistical properties are assumed as in Section 3.2 and Section 4.1.1. In particular, we again assume that the channel matrix  $\mathbf{H}$  follows the Kronecker correlation model (4.2).

The receiver structure under consideration is depicted in Fig. 4.7. Similar to the statistical transmit power allocation scheme discussed above, the considered receiver structure consists of an inner decorrelation stage based on the Karhunen-Loève transform (KLT) [SW02, Ch. 8.5] and an outer selection stage. The general structure of this reduced-dimension receiver was earlier considered in [JF02] (see also [Jel01]). Here, we combine it with subsequent space-time decoding.<sup>15</sup> The benefit of such a receiver structure is that

<sup>15</sup>The considered receiver structure can also be used in the case of frequency-selective fading, by combining it with an appropriate space-time equalizer (see [MHKX06a] for further details).



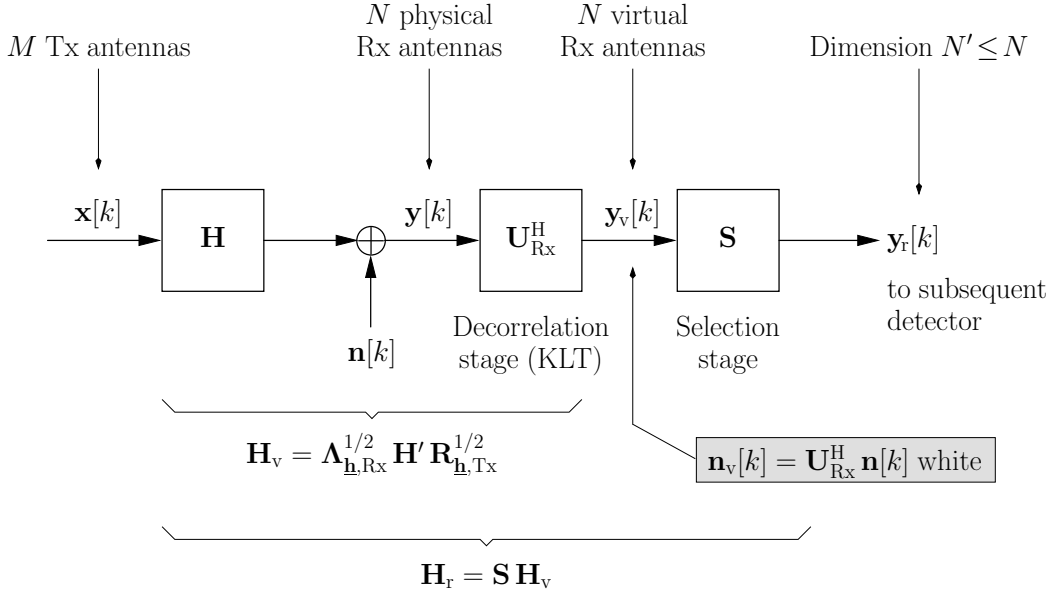


Figure 4.7: System model with reduced-dimension receiver.

it provides a flexible trade-off between complexity and performance. Using all spatial dimensions offered by the individual receive antennas is of course optimal, but it leads to a comparatively high complexity for subsequent receiver stages (especially in the case of frequency-selective fading). However, if the receive antennas are correlated, an appropriate subset of spatial dimensions is usually sufficient, in order to achieve a performance close to the optimum (since the eigenvalues of the receiver correlation matrix  $\mathbf{R}_{\mathbf{h},\text{Rx}}$  are not equally strong). In other words, the complexity of subsequent receiver stages can be reduced significantly at the expense of only a small performance loss. This complexity reduction is carried out by the selection stage, by choosing an appropriate subset of the eigenvalues (and the associated eigenvectors) of the receiver correlation matrix  $\mathbf{R}_{\mathbf{h},\text{Rx}}$  for further processing.

As earlier, the  $(M \times 1)$ -vector  $\mathbf{x}[k]$ , cf. Fig. 4.7, contains the information symbols to be transmitted, which are possibly encoded by some outer space-time coding scheme.<sup>16</sup> Moreover, the vector  $\mathbf{x}[k]$  may be subject to some statistical transmit power weighting strategy (cf. Fig. 4.1). Correspondingly, the covariance matrix of the transmitted vector is assumed as  $\mathbf{Q}_{\mathbf{x}} = \mathbf{E}\{\mathbf{x}[k]\mathbf{x}^H[k]\} := P/M \cdot \mathbf{U}_{\text{Tx}} \mathbf{W} \mathbf{U}_{\text{Tx}}^H$  in the sequel. Similar to Section 4.1.1, the decorrelation stage at the receiver transforms the given channel matrix  $\mathbf{H}$  according to (4.2) into a semi-correlated channel matrix  $\mathbf{H}_v = \boldsymbol{\Lambda}_{\mathbf{h},\text{Rx}}^{1/2} \mathbf{H}' \mathbf{R}_{\mathbf{h},\text{Tx}}^{1/2}$ , using the unitary matrix  $\mathbf{U}_{\text{Rx}}^H$  from the eigenvalue decomposition of  $\mathbf{R}_{\mathbf{h},\text{Rx}}$  as a linear filter:

$$\mathbf{E}\{\mathbf{H}_v \mathbf{H}_v^H\} = \mathbf{U}_{\text{Rx}}^H \mathbf{E}\{\mathbf{H} \mathbf{H}^H\} \mathbf{U}_{\text{Rx}} = M \sigma_h^2 \boldsymbol{\Lambda}_{\mathbf{h},\text{Rx}}, \quad (4.52)$$

where  $\mathbf{H}_v := \mathbf{U}_{\text{Rx}}^H \mathbf{H}$ . The overall transmission model (without selection stage) can thus be written as

$$\mathbf{y}_v[k] := \mathbf{H}_v \mathbf{x}[k] + \mathbf{n}_v[k], \quad (4.53)$$

<sup>16</sup>The reduced-dimension receiver can be used in conjunction with any outer space-time code.

where  $\mathbf{n}_v[k] := \mathbf{U}_{\text{Rx}}^H \mathbf{n}[k]$ . Note that the resulting noise vector  $\mathbf{n}_v[k]$  is still spatially white (with unaltered variance):

$$\mathbb{E} \{ \mathbf{n}_v[k] \mathbf{n}_v^H[k] \} = \mathbf{U}_{\text{Rx}}^H \mathbb{E} \{ \mathbf{n}[k] \mathbf{n}^H[k] \} \mathbf{U}_{\text{Rx}} = \sigma_n^2 \cdot \mathbf{I}_N. \quad (4.54)$$

Similar to Section 4.1.1, the  $N$  outputs of the decorrelation stage  $\mathbf{U}_{\text{Rx}}^H$  (vector  $\mathbf{y}_v[k]$ ) represent virtual receive antennas.

### Selection Stage

In order to provide an optimal trade-off between complexity and performance, the selection stage selects those  $N'$  components of the vector  $\mathbf{y}_v[k]$  for further processing that correspond to the strongest eigenvalues  $\lambda_{\text{Rx},\nu}$  (and the associated eigenvectors) of the receiver correlation matrix  $\mathbf{R}_{\text{h,Rx}}$ .<sup>17</sup> The overall transmission model including the selection stage is thus given by

$$\mathbf{y}_r[k] = \mathbf{S} \mathbf{y}_v[k] = \mathbf{S} \mathbf{H}_v \mathbf{x}[k] + \mathbf{S} \mathbf{n}_v[k] =: \mathbf{H}_r \mathbf{x}[k] + \mathbf{n}_r[k], \quad (4.55)$$

where  $\mathbf{S}$  denotes an appropriate  $(N' \times N)$ -puncturing matrix. For example, if the first  $N'$  virtual receive antennas are retained for further processing, the matrix  $\mathbf{S}$  is of form

$$\mathbf{S} = [\mathbf{I}_{N'} \mathbf{0}_{N-N'}]. \quad (4.56)$$

(In general, a column-permuted version of the above puncturing matrix will be used.) On the one hand, the dimension  $N'$  should be chosen as small as possible, in order to keep the complexity of subsequent receiver stages small. On the other hand, if the number of discarded eigenvalues  $\lambda_{\text{Rx},\nu}$  is too large, an unacceptable performance loss might occur.

As an example, we again assume that an orthogonal space-time block code (OSTBC) with a temporal rate of  $R_t \leq 1$  is employed at the transmitter. In order to find the optimal dimension  $N'$ , closed-form expressions for the resulting SER performance can be utilized. To this end, the SER expressions according to Section 4.1.3 have to be generalized to the case of  $N' < N$  virtual receive antennas. For example, for binary antipodal transmission ( $Q=2$ ) and perfect knowledge of the transmitter and receiver correlation matrix, one obtains:

$$\bar{P}_s = \frac{1}{2} \sum_{\mu=1}^M \sum_{\nu \in \mathbb{S}_{\text{ret}}} \left( \prod_{\substack{\mu'=1 \\ (\mu',\nu') \neq (\mu,\nu)}}^M \prod_{\nu' \in \mathbb{S}_{\text{ret}}} \frac{1}{1 - \frac{w_{\mu'} \lambda_{\text{Tx},\mu'} \lambda_{\text{Rx},\nu'}}{w_{\mu} \lambda_{\text{Tx},\mu} \lambda_{\text{Rx},\nu}}} \right) \left( 1 - \sqrt{\frac{w_{\mu} \lambda_{\text{Tx},\mu} \lambda_{\text{Rx},\nu}}{w_{\mu} \lambda_{\text{Tx},\mu} \lambda_{\text{Rx},\nu} + \xi}} \right) \quad (4.57)$$

( $w_{\mu} > 0$  assumed for all  $\mu = 1, \dots, M$ ), where the index set  $\mathbb{S}_{\text{ret}} \subseteq \{1, \dots, N\}$  represents all eigenvalues  $\lambda_{\text{Rx},\nu}$  retained for further processing ( $|\mathbb{S}_{\text{ret}}| = N'$ ). Moreover, as earlier we have  $\xi = MR_t \sigma_n^2 / P$ , cf. (4.27). Clearly, for  $N' < N$  the diversity order of the system is reduced

<sup>17</sup>Given a MIMO system with distributed receive antennas, the decorrelation stage  $\mathbf{U}_{\text{Rx}}^H$  in Fig. 4.7 can again be dropped. In this case, the selection stage operates directly on the physical receive antennas.

from  $MN$  to  $MN'$ , which can be seen when considering the corresponding high-SNR approximation ( $\bar{\gamma}_s \rightarrow \infty$ ):

$$\bar{P}_s \approx \left( \frac{MN}{4\bar{\gamma}_s} \right)^{MN'} \binom{2MN' - 1}{MN'} \prod_{\mu=1}^M \prod_{\nu \in \mathbb{S}_{\text{ret}}} \frac{1}{w_\mu \lambda_{\text{Tx},\mu} \lambda_{\text{Rx},\nu}}. \quad (4.58)$$

As earlier, similar high-SNR approximations also result for higher-order PSK-, ASK-, or QAM-modulation schemes. For a given (finite) SNR value  $\bar{\gamma}_s$  and a predefined desired target SER  $\bar{P}_{s,t}$ , the analytical expression (4.57) can now be utilized, in order to find the minimum dimension  $N'$  that still guarantees an average SER of  $\bar{P}_s \leq \bar{P}_{s,t}$ . Note that for a certain dimension  $N'$  all possible index sets  $\mathbb{S}_{\text{ret}}$  with  $|\mathbb{S}_{\text{ret}}| = N'$  have to be tested.<sup>18</sup> Note that it is straightforward to extend (4.57) to more general fading scenarios (such as non-i.i.d. Nakagami- $m$  fading scenarios), which might be of interest for OSTBC systems with distributed receive antennas.

**Remark 4.2 (Value of receiver structure for distributed MIMO systems)**

It should be noted that the above reduced-dimension receiver structure (without decorrelation stage) is of special interest for MIMO systems with distributed receive antennas. In such a system, multiple cooperating receiving nodes perform a joint reception strategy and pass (processed versions of) their received signals to a central entity (cf. Section 3.1). Based on long-term statistical channel knowledge (in terms of the average link SNRs/the individual Nakagami-fading parameters), an appropriate subset  $\mathbb{S}_{\text{ret}}$  of the available receiving nodes can be selected. By this means, the overall data traffic between the cooperating receiving nodes and the central entity can be minimized, while guaranteeing a SER of  $\bar{P}_s \leq \bar{P}_{s,t}$ .

## 4.2.2 Impact of Estimation Errors

The impact of estimation errors concerning the receiver correlation matrix  $\mathbf{R}_{\mathbf{h},\text{Rx}}$  can be analyzed along the same lines as for the statistical transmit power allocation scheme (cf. Section 4.1.4). As earlier, let  $\hat{\mathbf{R}}_{\mathbf{h},\text{Rx}}$  denote an estimate of  $\mathbf{R}_{\mathbf{h},\text{Rx}}$ , and let

$$\hat{\mathbf{R}}_{\mathbf{h},\text{Rx}} = \hat{\mathbf{U}}_{\text{Rx}} \hat{\mathbf{\Lambda}}_{\mathbf{h},\text{Rx}} \hat{\mathbf{U}}_{\text{Rx}}^H \quad (4.59)$$

denote the corresponding eigenvalue decomposition, where  $\hat{\mathbf{U}}_{\text{Rx}} \neq \mathbf{U}_{\text{Rx}}$  and  $\hat{\mathbf{\Lambda}}_{\mathbf{h},\text{Rx}} \neq \mathbf{\Lambda}_{\mathbf{h},\text{Rx}}$ . (We again assume that  $\hat{\mathbf{R}}_{\mathbf{h},\text{Rx}}$  is still a Hermitian matrix.) Due to the mismatched decorrelation stage  $\hat{\mathbf{U}}_{\text{Rx}}^H$ , (4.52) generalizes to

$$\mathbb{E} \{ \mathbf{H}_v \mathbf{H}_v^H \} = M \sigma_h^2 \hat{\mathbf{U}}_{\text{Rx}}^H \mathbf{U}_{\text{Rx}} \mathbf{\Lambda}_{\mathbf{h},\text{Rx}} \mathbf{U}_{\text{Rx}}^H \hat{\mathbf{U}}_{\text{Rx}}. \quad (4.60)$$

This causes a certain shift between the received powers of the individual virtual receive antennas (desired signal), which is captured by the diagonal elements of the  $(N \times N)$ -matrix

$$\mathbf{\Xi}_{\text{Rx}} := \hat{\mathbf{U}}_{\text{Rx}}^H \mathbf{U}_{\text{Rx}} \mathbf{\Lambda}_{\mathbf{h},\text{Rx}} \mathbf{U}_{\text{Rx}}^H \hat{\mathbf{U}}_{\text{Rx}}. \quad (4.61)$$

<sup>18</sup>Since the statistical channel properties can be regarded as slowly time-varying, an infrequent update of the choice of the dimension  $N'$  is sufficient. Correspondingly, the additional receiver complexity required for the selection stage can be neglected.

For the example of binary antipodal transmission, (4.57) thus becomes

$$\bar{P}_s = \frac{1}{2} \sum_{\mu=1}^M \sum_{\nu \in \mathbb{S}_{\text{ret}}} \left( \prod_{\substack{\mu'=1 \\ (\mu', \nu') \neq (\mu, \nu)}}^M \prod_{\nu' \in \mathbb{S}_{\text{ret}}} \frac{1}{1 - \frac{w_{\mu'} \lambda_{\text{Tx}, \mu'} [\mathbf{\Xi}_{\text{Rx}}]_{\nu', \nu'}}{w_{\mu} \lambda_{\text{Tx}, \mu} [\mathbf{\Xi}_{\text{Rx}}]_{\nu, \nu}}} \right) \left( 1 - \sqrt{\frac{w_{\mu} \lambda_{\text{Tx}, \mu} [\mathbf{\Xi}_{\text{Rx}}]_{\nu, \nu}}{w_{\mu} \lambda_{\text{Tx}, \mu} [\mathbf{\Xi}_{\text{Rx}}]_{\nu, \nu} + \xi}} \right), \quad (4.62)$$

where we have assumed for simplicity that the transmitter correlation matrix  $\mathbf{R}_{\mathbf{h}, \text{Tx}}$  is perfectly known at the transmitter. (Otherwise, the terms  $w_{\mu} \lambda_{\text{Tx}, \mu}$  again have to be replaced by  $[\mathbf{\Xi}_{\text{Tx}}]_{\mu, \mu}$ , respectively, cf. Section 4.1.4.) Note that (4.62) describes the actual SER resulting for a given index set  $\mathbb{S}_{\text{ret}}$ . In contrast to this, the estimated SER at the receiver, which builds the basis for the selection stage  $\mathbf{S}$ , is given by

$$\hat{P}_s = \frac{1}{2} \sum_{\mu=1}^M \sum_{\nu \in \mathbb{S}_{\text{ret}}} \left( \prod_{\substack{\mu'=1 \\ (\mu', \nu') \neq (\mu, \nu)}}^M \prod_{\nu' \in \mathbb{S}_{\text{ret}}} \frac{1}{1 - \frac{w_{\mu'} \lambda_{\text{Tx}, \mu'} \hat{\lambda}_{\text{Rx}, \nu'}}{w_{\mu} \lambda_{\text{Tx}, \mu} \hat{\lambda}_{\text{Rx}, \nu}}} \right) \left( 1 - \sqrt{\frac{w_{\mu} \lambda_{\text{Tx}, \mu} \hat{\lambda}_{\text{Rx}, \nu}}{w_{\mu} \lambda_{\text{Tx}, \mu} \hat{\lambda}_{\text{Rx}, \nu} + \xi}} \right). \quad (4.63)$$

Correspondingly, if the quality of the estimate of  $\mathbf{R}_{\mathbf{h}, \text{Rx}}$  is poor, erroneous decisions might occur concerning the choice of the index set  $\mathbb{S}_{\text{ret}}$ , in the sense that the actual SER  $\bar{P}_s$  exceeds the predefined target SER  $\bar{P}_{s,t}$ , although the condition  $\hat{P}_s \leq \bar{P}_{s,t}$  is met. On the other hand, it might also happen that the number  $N'$  of virtual receive antennas chosen is larger than required for guaranteeing  $\bar{P}_s \leq \bar{P}_{s,t}$ , which leads to an unnecessarily high receiver complexity. Further details can be found in [MHKX06a], where a numerical example for the case of frequency-selective fading is given.

### 4.3 Chapter Summary

Based on the fact that the performance of MIMO systems can be enhanced using some form of channel knowledge at the transmitter side, in the first part of this chapter appropriate transmit power allocation strategies were developed for MIMO systems with distributed or correlated transmit antennas, and their benefits with regard to ergodic capacity and error performance were evaluated. Specifically, it was shown that transmit power allocation schemes originally developed for MIMO systems with correlated transmit antennas can be reused for MIMO systems with distributed transmit antennas, and vice versa, without any loss of optimality. The main focus was on a simple transmit power allocation scheme for OSTBC systems with correlated transmit antennas, which requires solely statistical channel knowledge at the transmitter side. First, closed-form expressions for the resulting symbol error rate were stated, which were then utilized in order to find the optimal transmit power allocation strategy. In particular, it was shown that significant performance gains compared to equal power allocation are achieved. Moreover, a simple transmitter-sided maximum-ratio-combining strategy was proposed, which provides a near-optimum performance over a wide SNR range. Next, the optimal statistical transmit power allocation strategy for distributed MIMO systems in the presence

of non-i.i.d. Nakagami- $m$  fading was derived. In particular, it was shown that for large SNR values equal power allocation is no longer optimal – as opposed to the case of pure Rayleigh fading. Instead, the transmit power has to be focussed on those transmission links that are characterized by particularly mild fading conditions. Finally, for the case of correlated transmit antennas the impact of estimation errors concerning the transmitter correlation matrix was analyzed, and it was demonstrated that the considered transmitter scheme provides quite a robust performance.

In the second part of the chapter, the use of statistical channel knowledge at the receiver side was investigated, so as to provide an optimal trade-off between performance and receiver complexity. In particular, the value of the considered reduced-dimension receiver for MIMO systems with distributed receive antennas was highlighted. It was shown, that there is a strong duality between the reduced-dimension receiver structure and the above statistical transmit power allocation scheme. This duality was then exploited in order to find closed-form expressions for the resulting average symbol error rate. Moreover, it was shown that the impact of estimation errors concerning the receiver correlation matrix can be analyzed along the same lines as for the statistical transmit power allocation scheme.

◇ ◇ ◇

## Appendix 1

In the following, an alternative proof is given for Lemma 4.1, which is based on convex optimization (cf. Appendix E).

*Proof.* We have to solve the following convex optimization problem:

$$\begin{aligned} & \text{minimize} && f(\mathbf{w}) := - \sum_{j=1}^n w_j \lambda_j, && \mathbf{w} := [w_1, \dots, w_n]^T && (4.64) \\ & \text{subject to} && \sum_{j=1}^n w_j = n && \text{and} && w_j \geq 0 \text{ for all } j = 1, \dots, n. \end{aligned}$$

After deriving the corresponding Lagrangian function  $L(\mathbf{w}, \boldsymbol{\mu}, \nu)$ , where  $\nu \in \mathbb{R}$  and  $\boldsymbol{\mu} = [\mu_1, \dots, \mu_n]^T \in \mathbb{R}^n$  denote Lagrangian multipliers for the equality constraint and the  $n$  inequality constraints, respectively, and inspecting the Karush-Kuhn-Tucker (KKT) conditions for an optimal choice of  $\mathbf{w}$ ,  $\boldsymbol{\mu}$  and  $\nu$ , one obtains the following condition for  $\nu^\bullet$ :

$$\nu^\bullet \stackrel{!}{=} \begin{cases} = \lambda_j & \text{for } \mu_j^\bullet = 0, \quad w_j^\bullet > 0 \\ > \lambda_j & \text{for } \mu_j^\bullet > 0, \quad w_j^\bullet = 0 \end{cases}, \quad (4.65)$$

i.e.,  $\nu^\bullet < \lambda_j$  is not allowed for any  $j$ . Correspondingly, we choose  $\nu^\bullet \geq \lambda_n$ , i.e.,  $w_j^\bullet = 0$  for all  $j \neq n$ . Finally, in order to meet the equality constraint on  $\mathbf{w}$ , we choose  $\nu^\bullet = \lambda_n$  and  $w_n^\bullet = n$ .  $\square$

## Appendix 2

In the following, an alternative proof is given for Lemma 4.2, which is based on convex optimization (cf. Appendix E).

*Proof.* We have to solve the following optimization problem:

$$\begin{aligned} & \text{minimize} && f(\mathbf{w}) := - \sum_{j=1}^n \log(w_j \lambda_j), && \mathbf{w} := [w_1, \dots, w_n]^T && (4.66) \\ & \text{subject to} && \sum_{j=1}^n w_j = n && \text{and} && w_j > 0 \text{ for all } j = 1, \dots, n. \end{aligned}$$

After deriving the corresponding Lagrangian function  $L(\mathbf{w}, \boldsymbol{\mu}, \nu)$ , where  $\nu \in \mathbb{R}$  and  $\boldsymbol{\mu} = [\mu_1, \dots, \mu_n]^T \in \mathbb{R}^n$  denote Lagrangian multipliers for the equality constraint and the  $n$  inequality constraints, respectively, and inspecting the KKT conditions for an optimal choice of  $\mathbf{w}$ ,  $\boldsymbol{\mu}$  and  $\nu$ , one obtains the following condition for  $\nu^\bullet$ :

$$\nu^\bullet \stackrel{!}{=} 1/w_j^\bullet \text{ for all } j = 1, \dots, n, \quad (4.67)$$

which can only be fulfilled for  $w_1^\bullet = \dots = w_n^\bullet$ . In order to meet the equality constraint on  $\mathbf{w}$ , we choose  $w_j^\bullet = 1$  for all  $j = 1, \dots, n$ .  $\square$

## Appendix 3

For the sake of completeness, the details of the derivation of the optimal waterfilling solution (4.39) for the case of non-i.i.d. Nakagami- $m$  fading are presented in the following.

We have to solve the convex optimization problem (4.38). Ignoring the inequality constraints  $w_\mu \geq 0$  for a moment, the Lagrangian function  $L(\mathbf{w}, \nu)$  is given by

$$L(\mathbf{w}, \nu) = - \sum_{\mu=1}^M m_\mu \log \left( 1 + w_\mu \frac{\sigma_{h,\mu}^2 g \bar{\gamma}_s}{m_\mu MN} \right) + \nu \left( \sum_{\mu=1}^M w_\mu - M \right), \quad (4.68)$$

where  $\nu \in \mathbb{R}$  denotes the Lagrangian multiplier for the equality constraint. Inspecting the KKT conditions for an optimal choice of  $\mathbf{w}$  and  $\nu$  yields the following condition:

$$\frac{\partial}{\partial w_\mu} L(\mathbf{w}^\bullet, \nu^\bullet) = - \frac{m_\mu \sigma_{h,\mu}^2 g \bar{\gamma}_s}{MN m_\mu + w_\mu^\bullet \sigma_{h,\mu}^2 g \bar{\gamma}_s} + \nu^\bullet = 0 \quad (\mu = 1, \dots, M). \quad (4.69)$$

Thus, we obtain

$$w_\mu^\bullet = \left[ \frac{m_\mu}{\nu^\bullet} - \frac{MN m_\mu}{\sigma_{h,\mu}^2 g \bar{\gamma}_s} \right]_+ \quad (\mu = 1, \dots, M), \quad (4.70)$$

where we have incorporated the inequality constraint  $w_\mu^\bullet \geq 0$ . Revisiting the equality constraint, we find

$$\sum_{\mu' \in \mathbb{W}_{>0}} \left( \frac{m_{\mu'}}{\nu^\bullet} - \frac{MN m_{\mu'}}{\sigma_{h,\mu'}^2 g \bar{\gamma}_s} \right) = M, \quad (4.71)$$

where  $\mathbb{W}_{>0}$  denotes the index set comprising all  $|\mathbb{W}_{>0}| =: M'$  indices  $\mu'$  with  $w_{\mu'}^{\bullet} > 0$ . Thus, we obtain

$$\frac{1}{\nu^{\bullet}} = \frac{M}{\Phi(M')} \left( 1 + \frac{1}{g} \frac{N}{\bar{\gamma}_s} \sum_{\mu' \in \mathbb{W}_{>0}} \frac{m_{\mu'}}{\sigma_{h,\mu'}^2} \right) \quad (4.72)$$

where

$$\Phi(M') := \sum_{\mu' \in \mathbb{W}_{>0}} m_{\mu'}. \quad (4.73)$$

Plugging (4.72) into (4.70) yields the desired result.



## Chapter 5

# Distributed MIMO Systems with Non-perfect Synchronization

**I**N THIS FINAL chapter, we will focus on MIMO systems with distributed transmit antennas and co-located receive antennas. So far, it was always assumed that the cooperating transmitting nodes are perfectly synchronized in time and frequency. However, due to the distributed nature of the system, this might not be the case in practice. First, the individual transmitting nodes will employ independent local oscillators for converting the transmitted signals into bandpass domain. This can cause carrier-frequency offsets (CFOs) between the different transmission links resulting in time-varying channel impulse responses. Second, if the individual transmitting nodes are spaced very far apart, large differences can occur between the corresponding link lengths. If no timing-advance techniques are applied at the transmitter side, the differences between the individual propagation delays might not be negligible anymore (in comparison to the symbol duration). This will lead to intersymbol interference (ISI) effects at the receiver, which can significantly compromise the achievable spatial diversity gains.

The impact of CFOs on the performance of different space-time coding techniques is investigated in Section 5.1. As a novel contribution, improved detection schemes for Alamouti's transmit diversity scheme [Ala98] are considered and a blind CFO estimation technique for phase-shift-keying (PSK) signal constellations is proposed (see also [MEH04b]). In Section 5.2, distributed MIMO systems with imperfect timing synchronization are addressed (see also [MH04b]) and suitable space-time coding techniques are identified, which maintain a diversity advantage over a single-antenna system. As a novel contribution, an optimization of the delay diversity scheme [Wit93, SW93] based on the Rake Receiver Bound (RRB) is presented (see also [MHS03a]). Moreover, the distance properties of Alamouti's transmit diversity scheme in the presence of imperfect timing synchronization are considered. The most important results of this chapter are summarized in Section 5.3. It should be noted that the literature on unsynchronized distributed MIMO systems is yet surprisingly sparse. The problem of imperfect timing synchronization was, for example, addressed in [Wit91, KSH97, Li03b, MH04b, Li04, MHSD05, LX05a]. The problem of imperfect carrier-frequency synchronization was, for example, addressed in [MEH04b, Li04].

## 5.1 Imperfect Carrier-Frequency Synchronization

Consider again the wireless network depicted in Fig. 3.1 consisting of  $T_n$  cooperating transmitting nodes and a single receiving node. As earlier, we assume that the  $i$ th transmitting node is equipped with  $M_i$  antennas, where  $M_1 + \dots + M_{T_n} =: M$ . Moreover, we assume that the receiving node is equipped with  $N$  antennas. The cooperating transmitting nodes are again assumed to simultaneously transmit the same message on the same carrier-frequency, while employing a distributed space-time coding scheme, so as to accomplish a spatial diversity advantage.

### 5.1.1 System Model with Carrier-Frequency Offsets

For simplicity, we again focus on the case of quasi-static frequency-flat Rayleigh fading. However, it is straightforward to extend the following considerations to time-varying fading, frequency-selective fading and/or other fading models, such as Nakagami- $m$  fading or Rician fading. We again focus on the discrete-time channel model

$$\mathbf{y}[k] = \mathbf{H}\mathbf{x}[k] + \mathbf{n}[k] \quad (5.1)$$

introduced earlier in Section 2.2.2.

In the following, let  $f_c$  denote the nominal carrier frequency. In practice, the local oscillators employed by the individual network nodes will not be ideal. This is particularly true for wireless networks, where network nodes are supposed to be simple and cost-effective, as in wireless sensor networks. Correspondingly, the actual carrier frequencies employed for up- and down-conversion of the transmitted and received signals will deviate from the nominal carrier frequency  $f_c$ . In the sequel, it is assumed that the  $i$ th transmitting node employs the frequency

$$f_{\text{Tx},i} := f_c + \Delta f_{\text{Tx},i} \quad (5.2)$$

for up-conversion. In the case of a multi-antenna node, we assume that the same local oscillator is used for all  $M_i$  transmit antennas. Similarly, the receiving node is assumed to use the frequency

$$f_{\text{Rx}} := f_c + \Delta f_{\text{Rx}} \quad (5.3)$$

for down-conversion (again for all  $N$  receive antennas). Correspondingly, the effective CFO associated with the transmission links between the  $i$ th transmitting node and the receiving node is given by

$$\Delta f_i := f_{\text{Tx},i} - f_{\text{Rx}} = \Delta f_{\text{Tx},i} - \Delta f_{\text{Rx}}. \quad (5.4)$$

Throughout this section, we will always refer to normalized CFOs

$$\varpi_i := \Delta f_i \cdot T, \quad (5.5)$$

where  $T$  denotes the symbol duration. The channel coefficients  $h_{\nu,\mu}$  ( $\mu=1, \dots, M$ ,  $\nu=1, \dots, N$ ) are thus equipped with a time-varying phase term, according to

$$h_{\nu,\mu}[k] := h_{\nu,\mu}[0] e^{j2\pi\varpi_i k}, \quad (5.6)$$

where it was assumed that  $h_{\nu,\mu}[k]$  is associated with the  $i$ th transmitting node. In other words, the quasi-static channel model (5.1) is changed into a time-varying channel model

$$\mathbf{y}[k] = \mathbf{H}[k]\mathbf{x}[k] + \mathbf{n}[k]. \quad (5.7)$$

In fact, since most space-time coding schemes proposed in the literature are designed for quasi-static MIMO channels (cf. Section 2.1.2), CFOs can cause significant performance degradations.<sup>1</sup> Moreover, in a MIMO system with distributed transmit antennas, the individual CFOs  $\varpi_i$  will in general be different. For example, if all transmitting nodes are equipped with a single antenna, i.e.,  $M_1 = \dots = M_{T_n} := 1$  ( $T_n := M$ ), we can write (5.7) according to

$$\mathbf{y}[k] = \mathbf{H}[0] \mathbf{D}_{\varpi}[k] \mathbf{x}[k] + \mathbf{n}[k], \quad (5.8)$$

where  $\mathbf{D}_{\varpi}[k] := \text{diag}([e^{j2\pi\varpi_1 k}, \dots, e^{j2\pi\varpi_M k}])$ . However, a joint correction of the CFOs at the receiver (based on explicit estimates  $\hat{\varpi}_i$ ) is only possible when all CFOs  $\varpi_i$  are identical.<sup>2</sup> In the following section, the impact of CFOs on the performance of different space-time coding schemes is investigated.

**Remark 5.1 (Wireless systems with a resilient transmitter structure)**

The above system model is also relevant for wireless systems with a so-called resilient transmitter structure. In wireless communication networks it is often crucial to keep the probability of link failure as small as possible. One option to accomplish this goal is to employ a resilient transmitter structure, where the transmitter is equipped with multiple independent, parallel transmitter chains (see [MKH03, MEH04a] for further details). In particular, the individual transmitter chains are equipped with independent local oscillators and dedicated transmit antennas. Resilient transmitter structures are, for example, used in microwave radio links to interconnect base stations or other fixed nodes within cellular mobile radio networks [N00]. Other application examples include satellite links to fixed earth stations as well as fixed broadband wireless access networks connecting residential sites to a high-data-rate backbone network ('last mile').

Conventionally, in such systems only a single transmitter chain is active at a time, while the others are kept in a 'hot-stand-by' mode and serve as back-up units. Alternatively, all transmitter chains can be used simultaneously, e.g., in conjunction with a suitable space-time coding scheme. For the special case of two independent transmitter chains, for example, a resilient system design based on Alamouti's transmit diversity scheme [Ala98] was proposed in [MKH03]. Since Alamouti's scheme provides a temporal rate of one, the data rate of the conventional hot-stand-by system is retained. Additionally, a spatial diversity gain is achieved. Moreover, the alternative system design is still resilient, because Alamouti's scheme is backward compatible, i.e., one transmitter chain may fail without causing a rate loss. However, a drawback of the alternative system design is that due to the independent transmitter chains the individual transmitted signals might be subject to different CFOs, just as in the case of a MIMO system with distributed transmit antennas.

<sup>1</sup>Note that no temporal diversity gains can be expected from the time-varying phase terms.

<sup>2</sup>In a simulcast system with dominant line-of-sight signal components and a fixed receiver position, CFOs can also have beneficial effects. In such a static scenario, the receiver might permanently be located within an interference minimum of the carrier signal. In the presence of CFOs, however, the interference pattern is periodically shifted, thus preventing the receiver from durable failure [SSX99].

### 5.1.2 Performance Loss of Orthogonal Space-Time Block Codes

For simplicity, we assume that the cooperating transmitting nodes are each equipped with a single transmit antenna, i.e.,  $M_i := 1$  for all  $i = 1, \dots, T_n$  ( $T_n := M$ ). As discussed in Section 2.3.1, the key feature of orthogonal space-time block codes (OSTBCs) [TJC99b, TJC99a] is that the code matrix  $\mathbf{X}[k]$  is always orthogonal, irrespective of the information symbols  $a[\kappa]$ . In the case of a frequency-flat block-fading channel, this orthogonality leads to an equivalent single-antenna system model

$$z[\kappa] = \left( \sum_{\mu=1}^M \sum_{\nu=1}^N |h_{\nu,\mu}|^2 \right)^{1/2} a[\kappa] + \eta[\kappa] = \|\mathbf{H}\|_F a[\kappa] + \eta[\kappa], \quad (5.9)$$

which allows for low-complexity optimal detection in terms of a simple symbol-by-symbol maximum-likelihood (ML) detection rule (cf. Section 2.3.1). However, given a time-varying channel model, e.g., due to CFOs, the OSTBC system will lose its orthogonality. In this case, the single-antenna system model (5.9) is not valid anymore. As a consequence, interference occurs between the information symbols  $a[\kappa]$  which leads to a loss in error performance. Moreover, the complexity of ML detection increases, because symbol-by-symbol detection is no longer optimal (cf. Section 2.3.1).

The design of (near-)optimal receiver structures for OSTBCs and Alamouti's transmit diversity scheme in the presence of CFOs or time-varying fading was, for example, addressed in [LMG02, AB03, MEH04b, VLB04, KBJP04]. Further papers on the topic, including analytical performance results for various settings, can be found in [SKKY04, HC04, Ohn04, LCL05c, AKB05, JZP05]. Finally, the topic of joint channel and CFO estimation for both general and space-time coded MIMO systems was addressed in [BS03b, VVL03, MMPL03, MEH04b, MPM04, SGG05].

For the time being, we focus on Alamouti's transmit diversity scheme for  $M = 2$  transmit antennas [Ala98]. To start with, we consider a simple example, which shows how explicit estimates of the CFOs  $\varpi_1$  and  $\varpi_2$  can be obtained without the need for any training symbols.

**Example 5.1 (Explicit blind CFO estimation for Alamouti's scheme)**

Given a single-antenna system which employs a  $Q$ -ary phase-shift keying (PSK) signal constellation, a common blind CFO estimation method [See03] is to raise the received samples to the power of  $Q$  and perform a subsequent (fast) Fourier transform [GHW92, Ch. 6.3.1]. The same principle can be utilized for Alamouti's transmit diversity scheme. One obtains:

$$y^Q[k] = (h_{1,1}[k] a[\kappa])^Q + (h_{1,2}[k] a[\kappa+1])^Q + \text{noise and error terms}, \quad (5.10a)$$

$$y^Q[k+1] = (h_{1,2}[k] a^*[\kappa])^Q + (h_{1,1}[k] a^*[\kappa+1])^Q + \text{noise and error terms}, \quad (5.10b)$$

cf. (2.89), where  $N = 1$  receive antenna was assumed for simplicity. Moreover, it was utilized that  $Q$  is typically an even integer. Using that

$$a[\kappa] = e^{jq2\pi/Q} \quad (q \in \{0, \dots, Q-1\}) \quad (5.11)$$

and disregarding the noise and error terms, we have

$$y^Q[k] = (h_{1,1}[0])^Q e^{j2\pi Q\varpi_1 k} + (h_{1,2}[0])^Q e^{j2\pi Q\varpi_2 k}, \quad (5.12a)$$

$$y^Q[k+1] = (h_{1,1}[0])^Q e^{j2\pi Q\varpi_1(k+1)} + (h_{1,2}[0])^Q e^{j2\pi Q\varpi_2(k+1)}. \quad (5.12b)$$

Correspondingly, a Fourier transform of the sequence  $[y^Q[0], \dots, y^Q[k], \dots, y^Q[N_b-1]]$ , where  $N_b$  denotes the block length, will yield spectral lines at  $Q\varpi_1$  and  $Q\varpi_2$  plus spectral noise and error terms. If the received SNR is sufficiently large, the CFOs  $\varpi_1$  and  $\varpi_2$  can thus be obtained by means of a simple maximum search. Note, however, that the resolution of the Fourier transform must be chosen sufficiently large. By this means, explicit CFO estimates are obtained without requiring any training symbols. Further details as well as a numerical example for  $Q = 4$  can be found in [MEH04b].  $\diamond$

Within the scope of this section, we focus on linear receivers with subsequent symbol-by-symbol detection. The option of ML detection is not considered further, due to its increased complexity. To start with, we consider the orthogonality loss occurring when conventional Alamouti detection is performed at the receiver. Later on, we will also investigate the use of a linear zero-forcing (ZF) receiver and a linear minimum-mean-squared-error (MMSE) receiver (cf. Section 2.3.1).

In the sequel, we assume that the receiver employs some channel estimation/tracking algorithm (such as [SGG05]), which provides estimates

$$\hat{h}_{\nu,\mu}[k] := h_{\nu,\mu}[k] + \varepsilon_{\nu,\mu}[k] \quad (\mu = 1, 2, \nu = 1, \dots, N) \quad (5.13)$$

of the channel coefficients  $h_{\nu,\mu}[k]$ , according to (5.6).<sup>3</sup> In particular, we assume that the channel estimation errors  $\varepsilon_{\nu,\mu}[k]$  can be modeled as a spatially and temporally white zero-mean complex Gaussian random variables with variance  $\sigma^2$ , i.e.,

$$\varepsilon_{\nu,\mu}[k] \sim \mathcal{CN}(0, \sigma^2), \quad \mathbf{E}\{\varepsilon_{\nu,\mu}[k] \varepsilon_{\nu',\mu'}^*[k']\} = \sigma^2 \cdot \delta[\mu - \mu'] \delta[\nu - \nu'] \delta[k - k']. \quad (5.14)$$

The impact of channel estimation errors on the orthogonality of Alamouti's transmit diversity scheme (in conjunction with the conventional widely linear detection steps at the receiver) was already addressed in Section 2.3.1, cf. Example 2.3. Additionally, the effect of a time-varying channel model was included. Correspondingly, the results in Example 2.3 can be reused here, by setting

$$h_{\nu,\mu}[k] := h_{\nu,\mu}[0] e^{j2\pi\varpi_\mu k} \quad \text{and} \quad \Delta_{\nu,\mu}[k] := h_{\nu,\mu}[k] (e^{j2\pi\varpi_\mu} - 1) \quad (5.15)$$

( $\mu = 1, 2$ ). Obviously, for small CFOs  $\varpi_1, \varpi_2 \rightarrow 0$ , we have  $\Delta_{\nu,1}[k] \approx \Delta_{\nu,2}[k] \approx 0$  for all  $\nu = 1, \dots, N$  and all time indices  $k$  (as expected). Interestingly, in the case  $\varpi_1 \neq \varpi_2$  the orthogonality of Alamouti's transmit diversity scheme is lost even in the case of perfect channel tracking, i.e., if  $\varepsilon_{\nu,\mu}[k] = 0$  for all  $\mu = 1, 2, \nu = 1, \dots, N$  and all time indices  $k$  ( $\sigma^2 = 0$ ). In this case, the entries of the matrix  $\Psi_\nu[k]$  in (2.97) are given by

$$[\Psi_\nu[k]]_{1,1} = |h_{\nu,1}[0]|^2 + |h_{\nu,2}[0]|^2 = [\Psi_\nu[k]]_{2,2}, \quad (5.16a)$$

$$[\Psi_\nu[k]]_{1,2} = h_{\nu,1}^*[k] h_{\nu,2}[k] (1 - e^{j2\pi(\varpi_2 - \varpi_1)}) = [\Psi_\nu[k]]_{2,1}^*. \quad (5.16b)$$

<sup>3</sup>In contrast to Example 5.1, the CFOs are thus estimated implicitly by tracking the time-varying channel coefficients.

The entries of the covariance matrix  $\Phi_\nu[k]$  of the noise vector  $\boldsymbol{\eta}'_\nu[k]$  in (2.97) are identical to that of the matrix  $\Psi_\nu[k]$ . Obviously, the second product term in (5.16b) is time-invariant and can be close to zero. In particular, for  $\varpi_1 = \varpi_2$  one obtains  $\Psi_\nu[k] = (|h_{\nu,1}[0]|^2 + |h_{\nu,2}[0]|^2) \mathbf{I}_2$ , i.e., the CFOs do not have any impact on the performance. Moreover, if the absolute difference between  $\varpi_1$  and  $\varpi_2$  is small, the magnitude of the non-diagonal elements of  $\Psi_\nu[k]$  can be approximated as

$$|[\Psi_\nu[k]]_{1,2}| = |[\Psi_\nu[k]]_{2,1}| \approx |h_{\nu,1}[0] h_{\nu,2}[0]| |2\pi(\varpi_2 - \varpi_1)|. \quad (5.17)$$

In the following, numerical results are presented, which illustrate the impact of CFOs and channel estimation errors on the resulting symbol error rate (SER) performance.

### Numerical Performance Results

Fig. 5.1 displays numerical results for the SER performance of Alamouti's transmit diversity scheme in the presence of CFOs and non-perfect channel tracking, for the example of two distributed transmit antennas, a single receive antenna, and binary antipodal transmission. For simplicity, the variances of the channel coefficients  $h_{1,\mu}[k]$ ,  $\mu = 1, 2$ , were assumed to be equal. As an example, CFOs  $\varpi_1 = 0.04$  and  $\varpi_2 = -0.04$  were considered.<sup>4</sup> Moreover, a variance  $\sigma^2 = 0.01$  of the channel estimation error  $\varepsilon_{\nu,\mu}[k]$  was taken into account. For simplicity, it was assumed that  $\sigma^2$  does not depend on the average SNR  $P/\sigma_n^2$ . At the receiver, conventional Alamouti decoding with subsequent symbol-by-symbol detection was performed. As a reference, analytical curves for a single-antenna system and for an 'ideal' (2×1)-Alamouti system without CFOs and perfect channel tracking ( $\sigma^2 = 0$ ) have been included. As can be seen, given perfect channel tracking the impact of the CFOs is quite small in this case. The performance loss at a SER of  $10^{-3}$  is only about 0.5 dB. However, in the case of non-perfect channel tracking (and the same CFOs), one observes a significant performance loss, which is mainly due to channel estimation errors. Still, a substantial performance advantage compared to the single-antenna system is achieved. In Fig. 5.2, corresponding performance results for the case of an 8-ary PSK signal constellation and  $N = 2$  receive antennas are displayed. As can be seen, the impact of the CFOs is significantly more severe than for binary antipodal transmission, since the 8-PSK scheme is more sensitive to constellation rotations. However, note that the considered example ( $\varpi_1 = 0.04$ ,  $\varpi_2 = -0.04$ ) is an extreme case, since both CFOs have the same magnitude but opposite signs, cf. (5.16).

This can also be seen in Fig. 5.3, where different pairs of CFOs were considered for the same setting and a fixed average SNR of  $10 \log_{10}(P/\sigma_n^2) = 15$  dB. For the first CFO the value  $\varpi_1 = 0.04$  was chosen (as earlier), while the value for the second CFO was varied between  $\varpi_2 = -0.04, \dots, +0.04$ . In addition to conventional Alamouti decoding, the use of a linear zero-forcing (ZF) and a linear minimum-mean-squared-error (MMSE) receiver was considered (with subsequent symbol-by-symbol detection). The case of perfect channel tracking (i.e., the receiver has perfect knowledge of the channel coefficients for all time indices  $k$ ) is represented by solid curves and the case of non-perfect channel tracking ( $\sigma^2 = 0.01$ ) by dashed curves. As can be seen, compared to Fig. 5.2, the SER performance

<sup>4</sup>A magnitude of  $|\varpi_\mu| \leq 0.04$  appears to be relevant for most practical wireless communication systems.



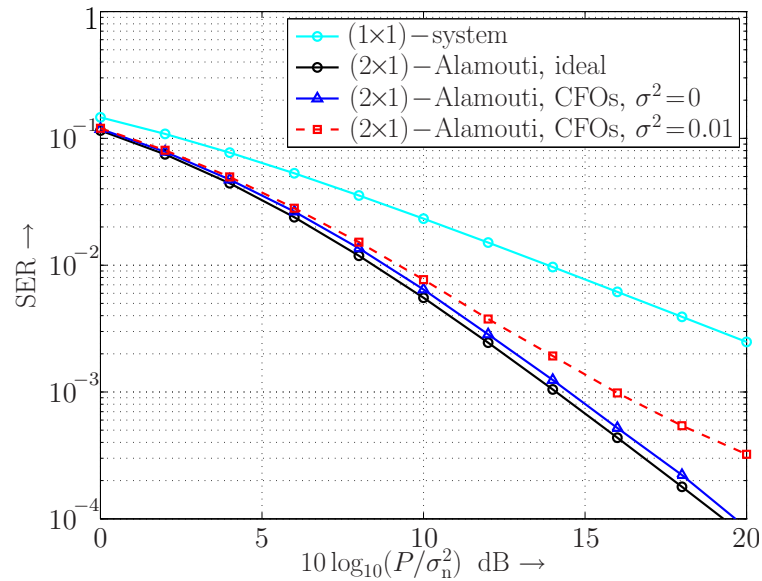


Figure 5.1: Average SER performance of Alamouti's transmit diversity scheme with  $M=2$  distributed transmit antennas and a single receive antenna (binary antipodal transmission,  $Q=2$ ): Impact of CFOs  $\varpi_1 = 0.04$ ,  $\varpi_2 = -0.04$  and non-perfect channel tracking ( $\sigma^2 = 0.01$ ). The SER curves were obtained by means of Monte-Carlo simulations over a sufficiently large number of channel realizations.

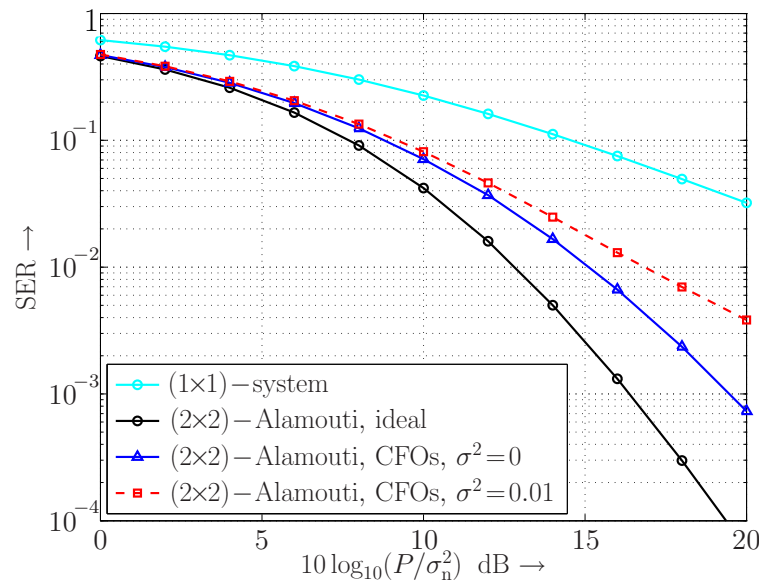


Figure 5.2: Corresponding performance results for the case of an 8-ary phase-shift-keying (PSK) signal constellation and  $N=2$  receive antennas.



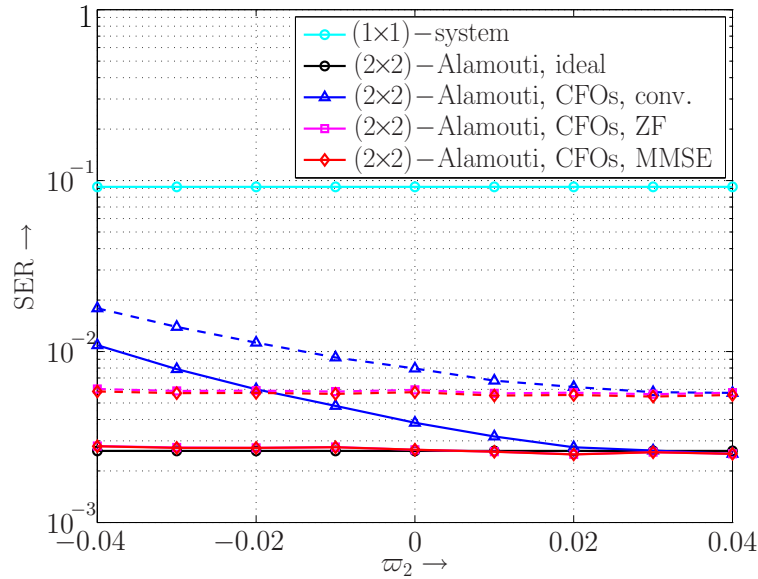


Figure 5.3: Performance results for the case of an 8-ary PSK signal constellation and  $N=2$  receive antennas with varying CFOs ( $\varpi_1=0.04$ ,  $\varpi_2=-0.04$ , ...,  $+0.04$ ) and different linear detection schemes at the receiver ( $10 \log_{10}(P/\sigma_n^2) = 15$  dB). Solid lines: Perfect channel tracking ( $\sigma^2=0$ ). Dashed lines: Non-perfect channel tracking ( $\sigma^2=0.01$ ). The SER curves were obtained by means of Monte-Carlo simulations.

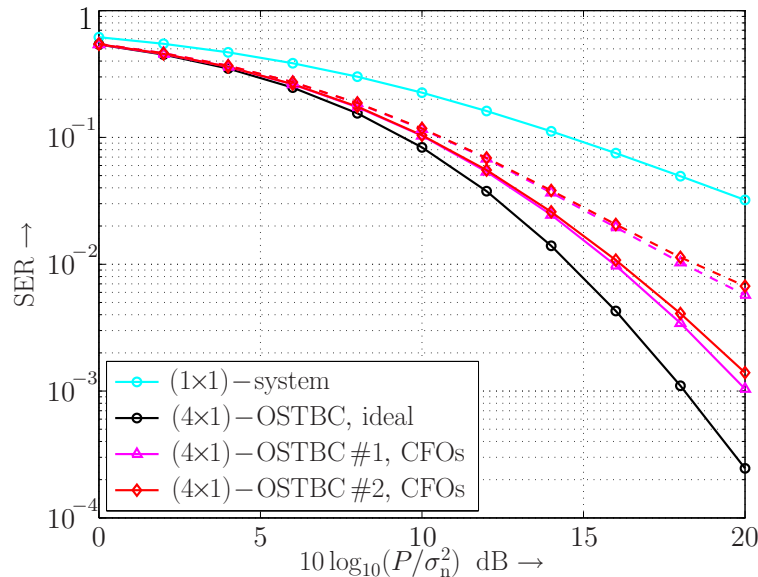


Figure 5.4: Average SER performance of two different OSTBCs with  $M=4$  transmit antennas, a single receive antenna, and a temporal rate of  $R_t = 3/4$  (8-ary PSK signal constellation): Impact of CFOs  $\varpi_1=0.02$ ,  $\varpi_2=-0.02$ ,  $\varpi_3=0.01$ ,  $\varpi_4=-0.01$ . Solid lines: Perfect channel tracking ( $\sigma^2=0$ ). Dashed lines: Non-perfect channel tracking ( $\sigma^2=0.01$ ).

of conventional Alamouti decoding improves significantly as soon as the absolute difference between  $\varpi_1$  and  $\varpi_2$  is reduced. Specifically, for  $\varpi_1 = \varpi_2 = 0.04$  and perfect channel tracking, the same performance is achieved as in the ideal case of no CFOs and perfect channel knowledge at the receiver. Interestingly, the performance of the linear ZF receiver and the linear MMSE receiver is very robust for the considered values of  $\varpi_1$  and  $\varpi_2$ . In particular, in the case of perfect channel tracking, the corresponding SER performance is very close to the ideal case.<sup>5</sup> Therefore, when the difference  $|\varpi_1 - \varpi_2|$  is large, significant performance improvements over conventional Alamouti detection are achieved, both for perfect and for non-perfect channel tracking. At the same time we note that in a system with co-located transmit and receive antennas the use of a linear ZF/MMSE receiver will be of little benefit, since  $\varpi_1$  and  $\varpi_2$  will typically be the same.

So far, we have focussed on Alamouti's transmit diversity scheme, which is the simplest case of an OSTBC. In Fig. 5.4, the performance of two more general OSTBCs for  $M = 4$  transmit antennas is displayed, for a single receive antenna and an 8-PSK signal constellation. The first OSTBC ('#1') is based on the generalized orthogonal design  $\mathfrak{D}_2$ , while the second OSTBC ('#2') is based on  $\mathfrak{D}_3$ , cf. (2.74) and (2.75) in Section 2.3.1. Both OSTBCs are characterized by a temporal rate of  $R_t = 3/4$ . In both cases, the impact of CFOs  $\varpi_1 = 0.02$ ,  $\varpi_2 = -0.02$ ,  $\varpi_3 = 0.01$ , and  $\varpi_4 = -0.01$  on the resulting average SER performance was studied. The solid curves again represent the case of perfect channel tracking and the dashed curves the case of non-perfect channel tracking, where  $\sigma^2 = 0.01$  (same CFOs). At the receiver, conventional linear OSTBC decoding was performed, i.e., no linear ZF or MMSE receiver was used. As can be seen, the basic behavior of the SER curves is quite similar to the case of Alamouti's scheme (cf. Fig. 5.2). In particular, the performance of both OSTBCs is very similar. As soon as all CFOs  $\varpi_1, \dots, \varpi_4$  are equal, the same performance as in the ideal case of no CFOs is achieved, similar to Alamouti's transmit diversity scheme.

### 5.1.3 Performance Loss of Other Space-Time Coding Schemes

To conclude this section, the impact of CFOs  $\varpi_1, \dots, \varpi_M$  on the performance of alternative space-time coding schemes is investigated in the sequel. As an example, the quasi-orthogonal STBC [Jaf01] introduced in Section 2.3.2 is considered as well as the simple delay diversity scheme [Wit93, SW93] discussed in Section 2.3.4.

#### Quasi-Orthogonal Space-Time Block Code

Fig. 5.5 displays the performance of the quasi-orthogonal STBC ('QOSTBC') introduced in Section 2.3.2 (temporal rate  $R_t = 1$ ,  $M = 4$  transmit antennas), for a single receive antenna and an 8-PSK signal constellation. In all cases, the (widely) linear combining steps (2.78)-(2.80) were performed at the receiver (with subsequent symbol-by-symbol detection), as discussed in Section 2.3.1 for the case of OSTBCs. Moreover, an optimal rotation angle  $\phi$  for the second signal constellation (info symbols  $a_3$  and  $a_4$ , cf. Section 2.3.2) was used in all cases. However, it should be noted that the performance gains achieved by the constellation rotation are rather small, as long as symbol error rates greater than  $10^{-3}$  are

<sup>5</sup>Due to the relatively large average SNR, the performance of both receivers is nearly identical.

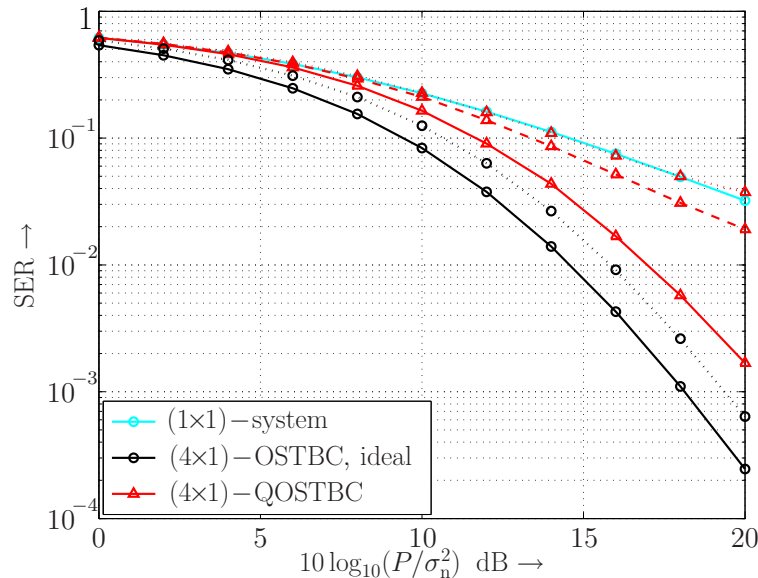


Figure 5.5: Average SER performance of the quasi-orthogonal STBC (2.108) with  $M=4$  transmit antennas and a single receive antenna (8-ary PSK signal constellation): Impact of CFOs  $\varpi_1=0.02$ ,  $\varpi_2=-0.02$ ,  $\varpi_3=0.01$ ,  $\varpi_4=-0.01$  (perfect and non-perfect channel tracking with  $\sigma^2=0.01$  considered).

considered. (This finding coincides with the results reported in [SP03].) Consider first the ideal case of no CFOs and perfect channel knowledge at the receiver (solid line, marked with triangles). As can be seen, a significant performance loss compared to an OSTBC with  $R_t=3/4$  has to be accepted (solid line, marked with circles), due to the intrinsic non-orthogonality. However, for a fair comparison one would have to take an OSTBC with a temporal rate of one as a reference, as marked by the dotted line. In the presence of CFOs  $\varpi_1=0.02$ ,  $\varpi_2=-0.02$ ,  $\varpi_3=0.01$  and  $\varpi_4=-0.01$  and perfect channel tracking<sup>6</sup> (dashed line), a significant additional performance loss is observed. In fact, compared to the OSTBCs considered in Fig. 5.4, the quasi-orthogonal STBC appears to be more sensitive to the CFOs. Finally, in the case of non-perfect channel tracking (same CFOs,  $\sigma^2=0.01$ , dotted line marked with triangles), the performance advantage over the single-antenna system (with perfect channel knowledge at the receiver) is completely lost. Altogether it can be concluded that, concerning robustness against CFOs and non-perfect channel tracking, the quasi-orthogonal STBC (2.108) does not yield a very attractive alternative to the OSTBCs considered in Fig. 5.4.

### Delay Diversity

So far, we have focussed on space-time coding techniques that are (quasi-) orthogonal, a property that is lost in the presence of CFOs and/or non-perfect channel tracking. An interesting question is, how the performance of alternative space-time coding tech-

<sup>6</sup>In other words, for each time index  $k$  the correct channel coefficients were employed for the combining steps (2.78)-(2.80) at the receiver.

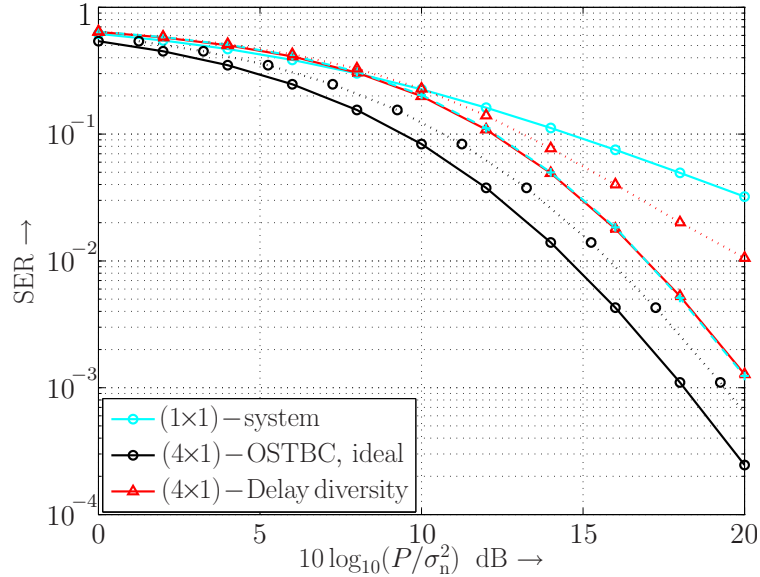


Figure 5.6: Average SER performance of delay diversity with  $M=4$  transmit antennas and a single receive antenna (8-ary PSK signal constellation): Impact of CFOs  $\varpi_1=0.02$ ,  $\varpi_2=-0.02$ ,  $\varpi_3=0.01$ ,  $\varpi_4=-0.01$  for perfect and non-perfect channel tracking ( $\sigma^2=0.01$ ).

niques behaves that are not based on an intrinsic orthogonality. As an example, Fig. 5.6 displays the performance of the delay diversity scheme discussed in Section 2.3.4 (temporal rate  $R_t \approx 1$ , due to termination symbols;  $M=4$  transmit antennas), for a single receive antenna and an 8-PSK signal constellation. In all cases, a maximum-likelihood-sequence-estimation (MLSE) equalizer based on the Viterbi algorithm was employed at the receiver. As earlier, the impact of CFOs  $\varpi_1=0.02$ ,  $\varpi_2=-0.02$ ,  $\varpi_3=0.01$ ,  $\varpi_4=-0.01$  and non-perfect channel tracking with an error variance of  $\sigma^2=0.01$  has been considered. Note that the delay diversity scheme constitutes a particularly simple alternative to a quasi-orthogonal STBC, since it causes (virtually) no temporal rate loss and can be applied for any number of transmit antennas. As can be seen, in the ideal case of no CFOs and perfect channel tracking (solid line, marked with triangles), one again observes a performance loss compared to an OSTBC with  $R_t=3/4$  (similar to the case of the quasi-orthogonal STBC), which is in this case due to the artificial ISI introduced by the delay diversity scheme, cf. Section 2.3.4. (Again, an OSTBC with a temporal rate of one, marked by the dotted line, would be more suitable as a reference.) As long as the channel coefficients are perfectly tracked and appropriately taken into account in the branch metrics of the Viterbi equalizer, the CFOs do not have any impact on the performance of the delay diversity scheme (dashed line, light color, marked with ‘x’). In fact, this is a major advantage over the quasi-orthogonal STBC considered in Fig. 5.5. At high SNR values (e.g., 20 dB), the resulting performance is even comparable to that of the OSTBCs considered in Fig. 5.4, although a higher temporal rate is achieved. In the case of non-perfect channel tracking, however, a substantial performance loss occurs, which again renders the delay diversity scheme inferior to the OSTBCs in Fig. 5.4. The loss at a SER of  $10^{-2}$  is approximately equal to 2 dB. Still, a significant diversity advantage

over the quasi-orthogonal STBC is accomplished. Altogether it can be concluded that the delay diversity scheme constitutes an attractive alternative to an OSTBC, as long as channel tracking is sufficiently accurate.

## 5.2 Imperfect Timing Synchronization

Consider again the distributed MIMO system depicted in Fig. 3.1. So far, we have always assumed that the difference between the propagation delays associated with the individual transmission links is small in comparison with the symbol duration  $T$ . This is a reasonable assumption, as long as the cooperating transmitting nodes are not spaced too far apart from each other, or if a sufficiently accurate timing advance technique is employed at the transmitter side. In this section, we investigate the general case where the propagation delay differences cannot be neglected. Possible applications include simulcast networks established by multiple cooperating satellites (cf. Fig. 5.7), where mobile users or subscriber homes have intervisibility with more than one satellite, or simulcast networks established by multiple base stations with no or only very coarse timing advance at the transmitter.

### 5.2.1 System Model with Propagation Delay Differences

In the sequel, we assume a block-fading channel model with either frequency-flat or frequency-selective fading. Throughout this section, we restrict ourselves to the case of Rayleigh fading for simplicity. However, generalizations to other types of fading are straightforward. As earlier, we focus on MIMO systems with distributed transmit antennas and co-located, uncorrelated receive antennas. In particular, an equal power allocation scheme with an overall average transmission power  $P$  is assumed. In order to accomplish a spatial diversity gain, the cooperating transmitting nodes are again assumed to employ a distributed space-time coding scheme. For simplicity we assume that the normalized CFOs  $\varpi_i$  between the individual transmission links are negligible. Moreover, we assume that each transmitting node is equipped with a single antenna.

In the sequel, let  $\delta_\mu$  denote the relative<sup>7</sup> propagation delay associated with the  $\mu$ th transmit antenna. Since the receive antennas are co-located, it can be assumed that the delay  $\delta_\mu$  does not depend on the receive antenna  $\nu$  under consideration. Without loss of generality, we assume  $\delta_1 = 0$  and  $\delta_\mu > 0$  for all indices  $\mu \neq 1$ . The system model under consideration is given by

$$\mathbf{y}[k] = \sum_{l=0}^L \mathbf{H}_l \mathbf{x}[k-l] + \mathbf{n}[k] \quad (5.18)$$

(cf. Section 2.2.2). The channel coefficients  $h_{\nu,\mu,l}$  ( $l = 0, \dots, L$ ) associated with the  $\mu$ th transmit antenna and the  $\nu$ th receive antenna result as

$$h_{\nu,\mu,l} = \sum_{n=0}^{N_\tau-1} f_{\nu,\mu}(\tau_n) g(lT + \epsilon - \tau_n - \delta_\mu). \quad (5.19)$$

<sup>7</sup>As discussed in Section F.1 in Appendix F, the absolute time required for signal propagation from the transmitting nodes to the receiving node is not considered further.

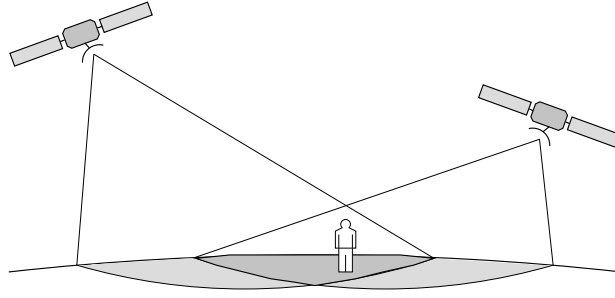


Figure 5.7: Simulcast network established by two cooperating satellites.

As earlier,  $N_\tau$  denotes the number of resolvable delays  $\tau_n$  (assumed identical for all transmission links),  $f_{\nu,\mu}(\tau_n) \sim \mathcal{CN}(0, \sigma_{f_{\nu,\mu,n}}^2)$  denotes the complex gain factor associated with transmit antenna  $\mu$ , receive antenna  $\nu$  and discrete delay  $\tau_n$ ,  $g(t)$  denotes the overall impulse response of transmit and receive filtering,  $T$  denotes the symbol duration, and  $\epsilon \in [0, T)$  denotes the sampling phase assumed to be identical for each receive antenna, cf. Section 2.2.2.<sup>8</sup> For simplicity, we assume  $\tau_0 = 0$  in the sequel. Moreover, we assume that  $g(t)$  constitutes a Nyquist filter with cosine roll-off and a roll-off factor  $0 \leq r \leq 1$ . Finally, note that the statistical properties of the channel coefficients  $h_{\nu,\mu,l}$  can in general be different for different indices  $\mu$ , since the individual transmit antennas might be associated with different power delay profiles

$$\mathbf{p}_{f_{\nu,\mu}} = [\sigma_{f_{\nu,\mu,0}}^2, \sigma_{f_{\nu,\mu,1}}^2, \dots, \sigma_{f_{\nu,\mu,N_\tau-1}}^2]^T, \quad (5.20)$$

cf. Definition F.1 in Appendix F. Moreover, for different indices  $\mu$  the channel coefficients  $h_{\nu,\mu,l}$  will be subject to different channel variances, representing unbalanced average SNRs caused by different link lengths. In the sequel, the variances of the channel coefficients are normalized such that  $\sum_{l=0}^L \mathbf{E}\{\|\mathbf{H}_l\|_F^2\} = MN$ .

**Example 5.2 (Numerical examples)**

As an example, consider a symbol duration of  $T = 1 \mu\text{s}$ . In this case, a relative propagation delay of  $\delta_\mu = T$  corresponds to a link length difference between the first and the  $\mu$ th transmit antenna of 300 meters ( $\delta_1 := 0$ ). The corresponding difference in the average received SNR depends on the absolute distance  $D_1$  between the first transmit antenna and the receiver. For example, assuming a path-loss exponent  $p = 2$ , an absolute distance of  $D_1 = 100$  m leads to an SNR difference of 24 dB, whereas a distance of  $D_1 = 200$  m leads to an SNR difference of about 8 dB.  $\diamond$

**Remark 5.2 (Simulcast system established by cooperating satellites)**

In the case of a simulcast system established by cooperating satellites, as depicted in Fig. 5.7, we assume that at least a coarse timing advance scheme is employed at the transmitter side so that the relative propagation delays  $\delta_\mu$  are in the order of a few multiples of the symbol duration  $T$ . Moreover, we assume that at least a

<sup>8</sup>Due to the block-fading assumption, the absolute time  $t$  has been dropped for the complex gain factors  $f_{\nu,\mu}(\tau, t)$ .



coarse power control scheme is employed so that the average received SNRs of all transmission links are significantly greater than zero. For simplicity these coarse synchronization measures are not considered further, but are modeled as part of the physical channel. Having cooperating satellites in mind, the relative delays  $\delta_\mu$  and the channel variances can therefore be interpreted as effective quantities, which include the effects of coarse timing synchronization and power control.

Throughout this section, we assume that the power delay profiles are characterized by an exponential decay (cf. Definition F.1 in Appendix F). We will mainly consider the case that the sampling phase is chosen as  $\epsilon=0$ , i.e., the receiver is perfectly synchronized with respect to the first transmit antenna. In particular, in the case of frequency-flat fading ( $N_\tau=1$ ) we thus obtain

$$h_{\nu,1,l} = f_{\nu,1}(\tau_0) g(lT + \epsilon - \tau_0 - \delta_1) = f_{\nu,1}(\tau_0) g(lT) = f_{\nu,1}(\tau_0) \delta[l - l_0], \quad (5.21)$$

where  $l_0$  is an appropriate integer number, cf. Section 2.2.2. This assumption appears to be reasonable as long as the average SNR associated with the first transmit antenna is significantly larger than the SNRs associated with the remaining transmit antennas. (Since we have assumed  $\delta_1=0$ , the first link will be characterized by the largest average received SNR.) However, if the average received SNRs of all (or at least of some) transmission links are approximately the same and multiple dominant signals with different relative propagation delays superimpose, a practical receiver will not be able to synchronize with respect to a specific transmit antenna [MHSD05]. For the sake of completeness we will therefore also consider the case that the sampling phase  $\epsilon$  has an arbitrary value between  $0 \leq \epsilon < T$ , according to a uniform distribution.

Given a sampling phase of  $\epsilon=0$ , it is important to note that all transmission links with  $\mu \neq 1$  will (in general) suffer from ISI effects, even in the case of frequency-flat fading. This is due to the fact that the signals received from the  $\mu$ th transmit antenna are sampled with timing offset  $\delta_\mu$ , while typically  $g(lT + \delta_\mu) \neq \delta[l - l_0]$ , cf. Fig. C.1 in Appendix C. (Obviously, in the case of an arbitrary sampling phase  $\epsilon$ , ISI effects will occur on all transmission links.) Note that in the case of frequency-flat fading, the ISI effects can solely cause a performance degradation, but no performance improvement. Diversity gains due to ISI effects can only be gained in the case of frequency-selective fading.<sup>9</sup> As discussed in Section 2.1.2, most space-time coding schemes proposed in the literature were designed for MIMO channels without ISI. In the presence of ISI effects, one option is to employ a multicarrier transmission scheme with quasi-flat sub-bands (e.g. MC-CDMA or OFDM). Another option is to use a space-time coding scheme originally designed for frequency-flat fading and mitigate the impact of ISI at the receiver using an appropriate equalizer algorithm. Finally, one can refine or generalize existing space-time coding schemes such that they are suited for MIMO channels with ISI. A detailed discussion on existing solutions has already been presented in Section 2.1.2.

<sup>9</sup>In [MHS03a] the notion of ‘static’ and ‘dynamic’ ISI was introduced. The static part of the ISI is due to the overall impulse response  $g(t)$  of transmit and receive filtering and can solely cause performance degradations. In contrast to this, the dynamic part of the ISI is due to the delay spread of the physical channel and can lead to an additional multipath diversity gain.



In the following, we will focus on the case of  $M=2$  transmit antennas for simplicity. In particular, we will investigate the use of Alamouti's transmit diversity scheme [Ala98] in conjunction with an appropriate trellis-based equalizer algorithm at the receiver (cf. Appendix J). As an alternative, we will consider the time-reversal STBC [LP00] discussed in Section 2.3.3 as well as the delay diversity scheme [Wit93, SW93], which is inherently suited for MIMO channels with ISI (cf. Section 2.3.4). For the delay diversity scheme, we will also briefly discuss transmitter-sided optimization measures as well as possible receiver structures for the case of very large relative signal delays. It should be noted that the use of the time-reversal STBC in distributed MIMO systems with imperfect timing synchronization was also investigated in [Li03b, Li04, MHSD05]. The performance of Alamouti's transmit diversity scheme in conjunction with OFDM was considered in [MHSD05]. Finally, a construction of distributed STTCs without the requirement of perfect timing synchronization was presented in [LX05a].

### 5.2.2 Performance of Alamouti's Transmit Diversity Scheme

In this section, numerical performance results for Alamouti's transmit diversity scheme ( $M=2$ ) in the presence of propagation delay differences are presented. For simplicity, we focus on binary antipodal transmission ( $Q=2$ ) and a single receive antenna ( $N=1$ ). In order to mitigate the impact of ISI effects, we consider the use of a suitable trellis-based equalizer algorithm, which performs maximum-likelihood sequence estimation (MLSE) on the basis of the Viterbi algorithm [For72]. The structure of the corresponding trellis diagram as well as the calculation of the branch metrics is in detail discussed in Appendix J. The memory length that is taken into account by the equalizer algorithm is denoted as  $L_{\text{eq}}$  in the following, where  $L_{\text{eq}} \leq L$ . As explained in Appendix J, the number of required trellis states is equal to  $Q^{L_{\text{eq}}}$ , if  $L_{\text{eq}}$  is an even number, and otherwise equal to  $Q^{L_{\text{eq}}+1}$ .

According to the above system model, we assume relative propagation delays of  $\delta_1=0$  and  $\delta_2 \geq 0$  in the sequel. As an example, we consider the case that the average received signal power of the second link is 10 dB below that of the first link, i.e.,

$$\frac{\sum_{l=0}^L \sigma_{h_{1,1,l}}^2}{\sum_{l=0}^L \sigma_{h_{1,2,l}}^2} =: \frac{\sigma_{h_{1,1}}^2}{\sigma_{h_{1,2}}^2} = 10. \quad (5.22)$$

Moreover, we assume for simplicity that the power delay profiles  $\mathbf{p}_{f_{1,\mu}}$  ( $\mu = 1, 2$ ) are identical and characterized by an exponential decay according to (F.10) in Appendix F, where  $c_\tau := T$ .

#### Frequency-Flat Fading

To start with, we focus on the case of frequency-flat Rayleigh fading ( $N_\tau=1$ ) and assume that the receiver is perfectly synchronized with respect to the first transmit antenna (i.e.,  $\epsilon=0$ ). Fig. 5.8 displays the resulting SER performance as a function of  $P/\sigma_n^2$  in dB, for a roll-off factor of  $r=0$ , an equalizer length of  $L_{\text{eq}}=4$ , and different relative delays  $\delta_2$  between zero and  $2T$ . As a reference, the SER performance resulting for  $\delta_2=0$  has been included (marked with circles), where the dotted curve is for equal average received SNRs

on the two links and the solid curve for unequal average SNRs according to (5.22).<sup>10</sup> As earlier, we note that unequal average received SNRs cause a significant performance degradation. Moreover, as can be seen, a relative delay  $\delta_2 > 0$  can cause a substantial (additional) performance loss. In particular, when  $\delta_2$  is equal to the symbol duration  $T$ , a large fraction of the diversity gain compared to the single-antenna system (with perfect time synchronization) is lost. Interestingly, larger delays such as  $\delta_2 = 1.5T$  or  $\delta_2 = 2T$  again lead to an improved SER performance. In fact, for  $\delta_2 = 2T$  the resulting performance is quite close to the optimum.

This interesting behavior can be observed more clearly in Fig. 5.9, where the average SER performance is displayed for a fixed SNR of 20 dB and different relative delays  $\delta_2$  between zero and  $5T$  (for roll-off factors  $r=0$  and  $r=1$  and equalizer lengths  $L_{\text{eq}}=4$  and  $L_{\text{eq}}=6$ ). Clearly, there is a pronounced peak at  $\delta_2 = T$ . This effect can be explained based on the distance properties of Alamouti's transmit diversity scheme in the presence of ISI (see the appendix at the end of this chapter). Moreover, it can be seen that an equalizer with memory length  $L_{\text{eq}}=4$  can only tolerate relative propagation delays of  $\delta_2 \leq 3T$ . If the delay  $\delta_2$  becomes larger, the equalizer suspends a significant fraction  $\psi_{\text{susp}}$  of the overall channel variance  $\sum_{l=0}^L \mathbf{E}\{|h_{1,2,l}|^2\}$  of the second transmission link, as illustrated in Fig. 5.10. The numerical values for  $\psi_{\text{susp}}$  were calculated analytically based on (5.19) and (C.1) in Appendix C. As can be seen, between  $\delta_2 = 3T$  and  $\delta_2 = 4T$  the fraction  $\psi_{\text{susp}}$  increases from zero to (nearly) one, which significantly degrades the corresponding SER performance due to residual ISI (cf. Fig. 5.9). However, at the expense of an increased equalizer complexity ( $L_{\text{eq}}=6$ ) it is again possible to achieve a near-optimum SER performance, at least for the considered values of the propagation delay  $\delta_2$ . Finally, we note that the undesired behavior at  $\delta_2 = T$  can be circumvented by delaying the signal associated with the longer transmission link by two or more symbol durations. Note that the exact value of  $\delta_2$  does not need to be known, in order to apply this coarse timing adjustment. However, in order to achieve a near-optimum performance, the equalizer length  $L_{\text{eq}}$  has to be chosen sufficiently large.

In order to conclude the discussion on frequency-flat fading, Fig. 5.11 displays the corresponding SER performance resulting for the case that the receiver is not synchronized with respect to a certain transmit antenna, while  $\epsilon \sim \mathcal{U}([0, T])$  was assumed. As can be seen, the resulting SER performance looks quite similar to that in the case  $\epsilon=0$  (and  $L_{\text{eq}}=4$ ). However, note that now an equalizer length of  $L_{\text{eq}}=6$  has been employed, so as to mitigate precursor ISI effects resulting for the first transmission link (cf. Fig. C.1 in Appendix C). In other words, the maximum relative propagation delay  $\delta_2$  that can be tolerated by an equalizer of length  $L_{\text{eq}}=6$  is smaller than in the case  $\epsilon=0$ .

### Frequency-Selective Fading

Finally, we consider the case of frequency-selective Rayleigh fading, where we focus again on the case  $\epsilon=0$ . Fig. 5.12 displays the SER performance as a function of  $P/\sigma_n^2$  in dB, which results for a physical channel model with  $N_\tau=10$  equally spaced resolvable delays  $\tau_n$  between zero and  $T$  (i.e.,  $\tau_0=0$  and  $\tau_{\text{max}}=T$ ) and a power delay profile characterized

<sup>10</sup>As earlier, the overall average received SNR was fixed, irrespective of the relative propagation delay  $\delta_2$ .

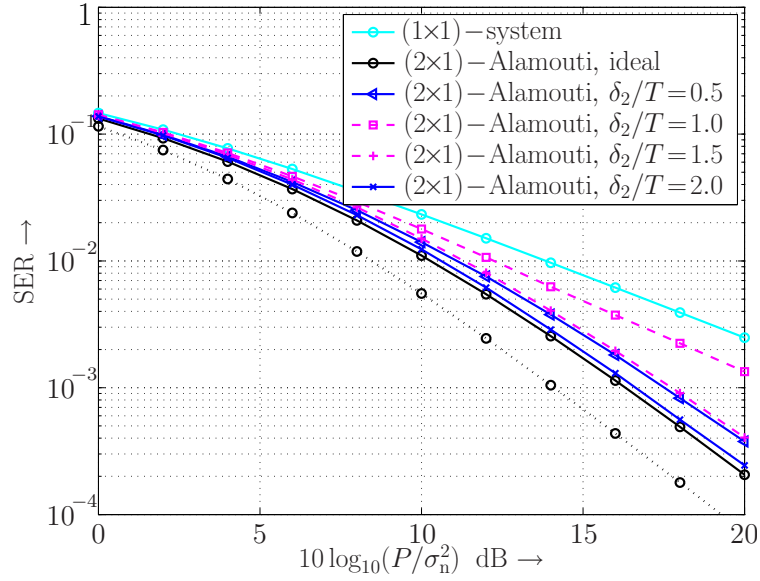


Figure 5.8: Average SER performance of Alamouti's transmit diversity scheme for different relative delays  $\delta_2$  between zero and  $2T$  ( $N=1$  receive antenna, frequency-flat Rayleigh fading, unequal average received SNRs according to (5.22), binary antipodal transmission, sampling phase  $\epsilon=0$ , roll-off factor  $r=0$ , equalizer length  $L_{\text{eq}}=4$ ).

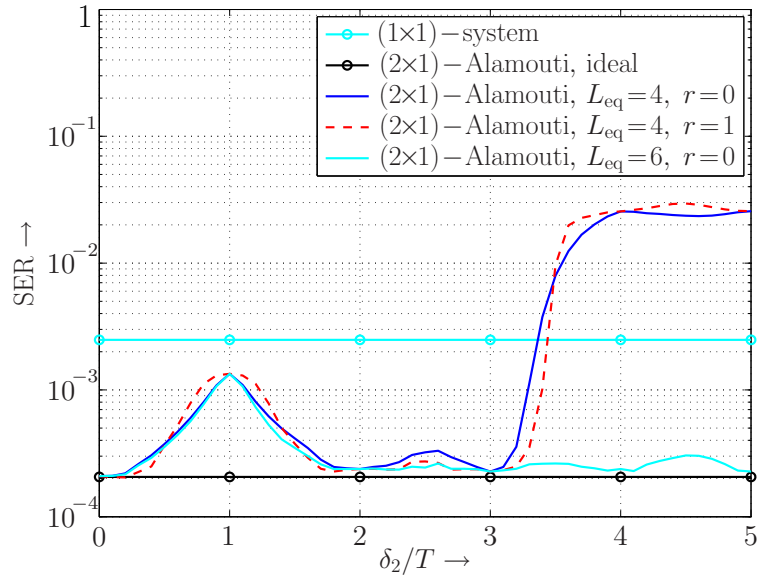


Figure 5.9: Average SER performance of Alamouti's transmit diversity scheme for a fixed SNR of 20 dB and different relative delays  $\delta_2$  between zero and  $5T$  ( $N=1$  receive antenna, frequency-flat Rayleigh fading, unequal average received SNRs according to (5.22), binary antipodal transmission, sampling phase  $\epsilon=0$ , roll-off factors  $r=0$  and  $r=1$ , equalizer lengths  $L_{\text{eq}}=4$  and  $L_{\text{eq}}=6$ ).

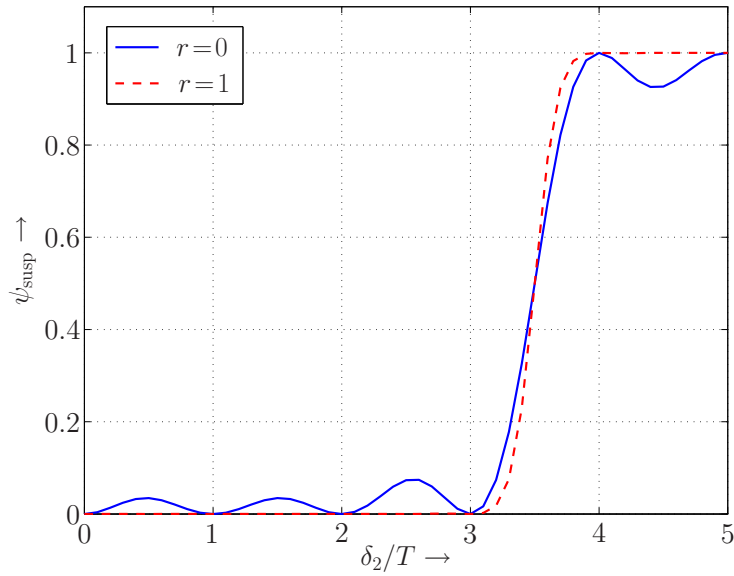


Figure 5.10: Fraction  $\psi_{\text{susp}}$  of the overall channel variance  $\sum_{l=0}^L \mathbf{E}\{|h_{1,2,l}|^2\}$  of the second transmission link suspended by an equalizer with memory length  $L_{\text{eq}}=4$ .

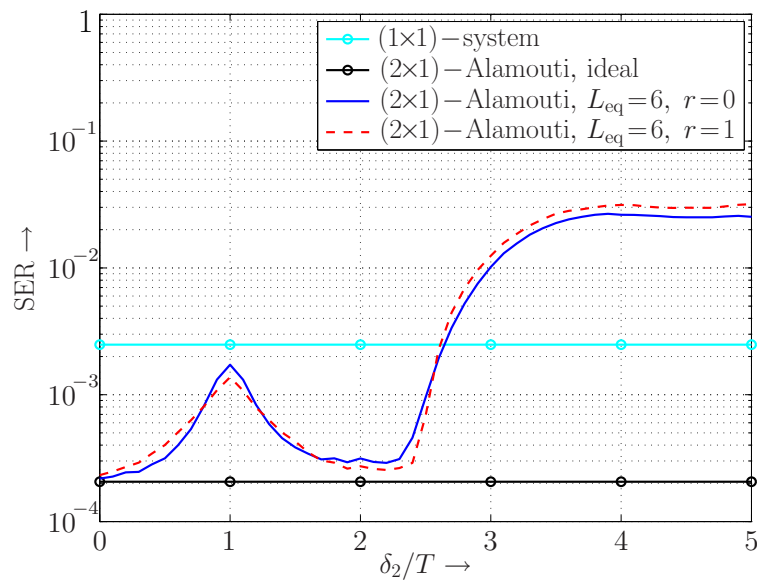


Figure 5.11: Average SER performance of Alamouti's transmit diversity scheme for a fixed SNR of 20 dB and different relative delays  $\delta_2$  between zero and  $5T$  ( $N=1$  receive antenna, frequency-flat Rayleigh fading, unequal average received SNRs according to (5.22), binary antipodal transmission, sampling phase  $\epsilon \sim \mathcal{U}([0, T])$ , roll-off factors  $r=0$  and  $r=1$ , equalizer length  $L_{\text{eq}}=6$ ).

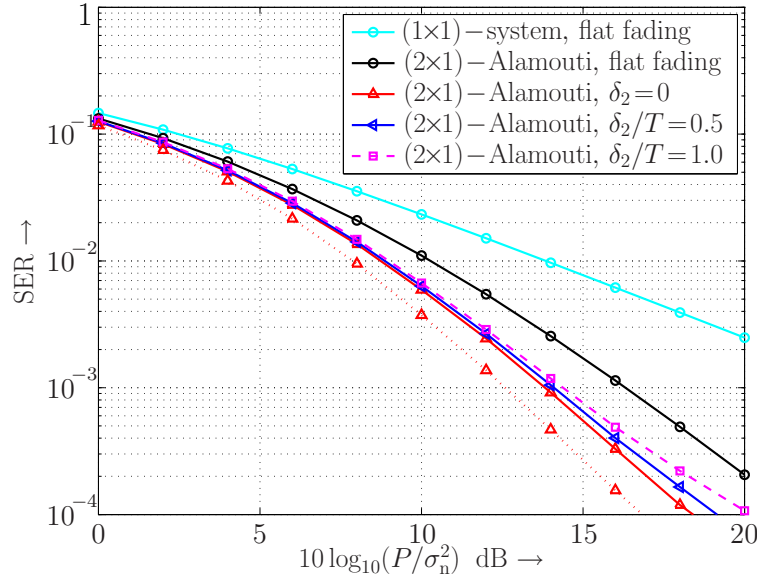


Figure 5.12: Average SER performance of Alamouti's transmit diversity scheme for different relative delays  $\delta_2$  ( $N = 1$  receive antenna, frequency-selective Rayleigh fading, unequal average received SNRs according to (5.22), binary antipodal transmission, sampling phase  $\epsilon = 0$ , roll-off factor  $r = 0$ , equalizer length  $L_{\text{eq}} = 4$ ).

by an exponential decay ( $c_\tau = T$ ). As earlier, a roll-off factor of  $r = 0$  has been considered and an equalizer length of  $L_{\text{eq}} = 4$ . Moreover, relative propagation delays  $\delta_2 = 0$ ,  $\delta_2 = 0.5T$  and  $\delta_2 = T$  have been taken into account. As can be seen, compared to the curve resulting for frequency-flat fading ( $\delta_2 = 0$ , marked with circles) a significant performance gain is achieved due to an increased amount of multipath diversity. Similar to the flat-fading case, the unequal average received SNRs according to (5.22) cause a significant performance loss compared to the case of equal average link SNRs (dotted curve). Interestingly, for relative propagation delays  $\delta_2$  greater than zero, comparatively small performance degradations are observed (when compared to the flat-fading case), provided that the memory length of the equalizer algorithm is chosen sufficiently large.<sup>11</sup>

Still, in the presence of frequency-selective fading, Alamouti's scheme is not able to extract the full diversity order<sup>12</sup> that is offered by the physical channel (see also [Che05, Ch. 9.5.1]), not even in the case  $\delta_2 = 0$ . In order to illustrate this fact, an analytical lower bound on the resulting SER performance is derived in the following.

<sup>11</sup>As can be seen, given a fixed equalizer length  $L_{\text{eq}}$  the performance loss increases with growing delay  $\delta_2$ . Moreover, the performance loss is particularly pronounced for large SNR values, which is due to the residual ISI. Similar SER peaks as in the case of frequency-flat fading (for  $\delta_2 = T$ , cf. Fig. 5.9 and Fig. 5.11) are not observed in the frequency-selective case.

<sup>12</sup>In general, the overall diversity order offered by a spatially uncorrelated frequency-selective MIMO system with  $M$  transmit antennas,  $N$  receive antennas, and a channel memory length of  $L$  is given by  $MN(L+1)$ , see e.g. [SR05].

### 5.2.3 Rake Receiver Bound for Frequency-Selective Fading

Given a quasi-static frequency-selective fading channel and perfect channel knowledge at the receiver, a lower bound on the error performance of an MLSE equalizer is the so-called Rake Receiver Bound (RRB) or Matched Filter Bound [HB98, Pro01]. In order to derive this lower bound for a single-antenna system, it is assumed that the transmitter sends single information symbols  $a[k]$  that are followed by a pause intervals of  $\geq L$  consecutive time indices, where  $L$  denotes the channel memory length. By this means, the receiver can collect all contributions from a transmitted information symbol (without any interference) and combine the corresponding received samples according to the maximum-ratio-combining (MRC) principle.<sup>13</sup> Therefore, the RRB corresponds to the average symbol error rate accomplished by an MRC system with a single input and  $(L+1)$  outputs, where the  $l$ th branch ( $l=0, \dots, L$ ) is associated with the  $l$ th channel coefficient,  $h_{1,1,l}$ , in the original single-antenna system. The corresponding system model thus reads

$$z[k] := \sum_{l=0}^L \left( |h_{1,1,l}|^2 a[k] + h_{1,1,l}^* n_l[k] \right), \quad (5.23)$$

where  $n_l[k]$  are zero-mean, temporally and spatially white complex Gaussian noise samples having the same variance  $\sigma_n^2$  as the noise samples in the original single-antenna system. Since such a (theoretical) system does not suffer from any ISI effects, the resulting symbol error rate will always constitute a lower bound on the performance of a practical MLSE equalizer.<sup>14</sup>

It is important to note that the channel coefficients  $h_{1,1,l}$  in the original single-antenna system comprise both a ‘static’ and a ‘dynamic’ ISI component [MHS03a]. As mentioned above, the static part is due to the overall impulse response  $g(t)$  of transmit and receive filtering and can only cause a performance loss. Specifically, the impulse response  $g(t)$  leads to certain intertap correlations between the channel coefficients  $h_{1,1,l}$ , cf. (2.44) in Chapter 2. In contrast to this, the dynamic part of the ISI is due to the delay spread of the physical channel and might yield an additional multipath diversity gain. For the purpose of analysis, one can try to eliminate the influence of the impulse response  $g(t)$  (and thus of the static ISI component) by means of linear filtering of the channel coefficients  $h_{1,1,l}$  [MHS03a]. Otherwise, the RRB will overestimate the available multipath diversity gain and will therefore be too optimistic. Here, we focus on the option to decorrelate the channel coefficient vector  $\mathbf{h} := [h_{1,1,0}, \dots, h_{1,1,L}]^T$  based on the eigenvalue decomposition of the covariance matrix  $\mathbf{Q}_{\mathbf{h},\text{ISI}} := \mathbf{E}\{\mathbf{h}\mathbf{h}^H\}$ . As discussed earlier in Section 3.2.5, if  $\mathbf{Q}_{\mathbf{h},\text{ISI}} := \mathbf{U}\mathbf{\Lambda}\mathbf{U}^H$  denotes the eigenvalue decomposition of  $\mathbf{Q}_{\mathbf{h},\text{ISI}}$ , we obtain the corresponding uncorrelated channel vector with covariance matrix  $\mathbf{\Lambda} := \text{diag}([\lambda_0, \dots, \lambda_L])$  by computing  $\mathbf{h}' := \mathbf{U}^H \mathbf{h}$ . Based on the equivalent uncorrelated MRC system [DB02]

$$z'[k] := \sum_{l=0}^L \left( |h'_{1,1,l}|^2 a[k] + h'_{1,1,l} n_l[k] \right) \quad (5.24)$$

<sup>13</sup>This resembles a Rake receiver in a DS-CDMA system with perfect orthogonality, hence the name Rake Receiver Bound.

<sup>14</sup>The error performance of a practical MLSE equalizer typically suffers from a certain SNR loss due to ISI effects [Pro01, Ch. 10.1].

it is now possible to find closed-form expressions for the RRB for arbitrary  $Q$ -ary PSK, ASK, and QAM signal constellations, cf. Appendix I. The average SNR associated with the  $l$ th branch in the equivalent uncorrelated MRC system is given by  $\bar{\gamma}_l := \sigma_a^2 \lambda_l / \sigma_n^2$ , where  $\sigma_a^2 := \mathbb{E}\{|a[k]|^2\}$ . Assuming that  $\mathbf{Q}_{\mathbf{h}, \text{ISI}}$  has full rank, the diversity order offered by the system is thus given by  $(L+1)$ , cf. Section 3.2.5.<sup>15</sup>

In the following, we generalize the above concept to the case of Alamouti's transmit diversity scheme<sup>16</sup> with distributed transmit antennas and co-located, uncorrelated receive antennas. To this end, an idealized MRC receiver is considered which is able to combine all contributions from a transmitted information symbol  $a[k]$  without any spatial or intertap interference. Assuming that  $N$  antennas are employed at the receiver, the RRB thus corresponds to the average symbol error rate accomplished by an MRC system with a single input and  $MN(L+1)$  outputs, where  $M=2$  in this case. The corresponding system model is thus given by

$$z[k] := \sum_{\mu=1}^2 \sum_{\nu=1}^N \sum_{l=0}^L \left( |h_{\nu, \mu, l}|^2 a[k] + h_{\nu, \mu, l}^* n_{\nu, \mu, l}[k] \right). \quad (5.25)$$

Based on the overall covariance matrix  $\mathbf{Q}_{\mathbf{h}} := \mathbb{E}\{\mathbf{h}_{\text{ov}} \mathbf{h}_{\text{ov}}^H\}$  of the channel coefficient vector

$$\mathbf{h}_{\text{ov}} := [\text{vec}(\mathbf{H}_0)^T, \dots, \text{vec}(\mathbf{H}_l)^T, \dots, \text{vec}(\mathbf{H}_L)^T]^T \quad (5.26)$$

(cf. Section 2.2.3), and the corresponding eigenvalue decomposition  $\mathbf{Q}_{\mathbf{h}} := \mathbf{U} \mathbf{\Lambda} \mathbf{U}^H$ , we can again find an equivalent uncorrelated MRC system by transforming the channel vector  $\mathbf{h}_{\text{ov}}$  as  $\mathbf{h}'_{\text{ov}} := \mathbf{U}^H \mathbf{h}_{\text{ov}}$ . In particular, assuming that  $\mathbf{Q}_{\mathbf{h}}$  has full rank the diversity order offered by the (idealized) system is given by  $2N(L+1)$ .

### Numerical Example

As an example, we revisit the numerical performance results presented for Alamouti's transmit diversity scheme in the presence of frequency-selective Rayleigh fading ( $N=1$ ), cf. Fig. 5.12. For simplicity, we focus on the case  $\delta_2=0$ . As can be seen in Fig. 5.13, the gap between the RRB (solid curve, marked with 'x') and the average SER accomplished by Alamouti's transmit diversity scheme is quite significant, especially for large SNR values. In particular, the RRB exhibits a steeper asymptotic slope. Therefore, we conclude that Alamouti's transmit diversity scheme is not able to capture the full diversity order of  $2(L+1)$  that is offered by the physical channel. Finally, we note that the RRB should always be determined based on the decorrelated MRC system, so as to take the intertap correlations due to the impulse response  $g(t)$  into account (static ISI component). Otherwise, the available multipath diversity gain might be overestimated significantly, as illustrated by the dashed curve.

<sup>15</sup>Although the RRB is only a lower bound, it is known to accurately predict the performance behavior of an MLSE equalizer in the presence of frequency-selective fading, see e.g. [BS92].

<sup>16</sup>It should be noted that the resulting RRB will also apply for the time-reversal STBC [LP00] discussed in Section 2.3.3. Moreover, a generalization to OSTBC systems or time-reversal STBC systems with more than two transmit antennas is straightforward.



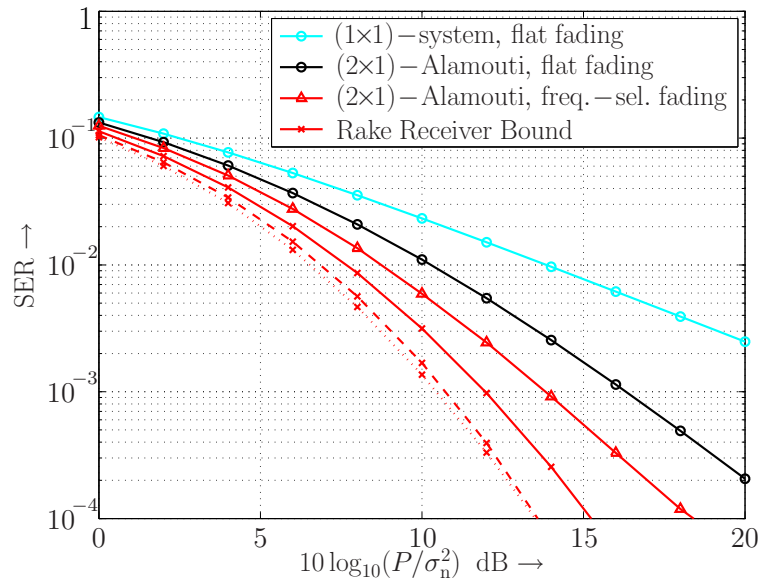


Figure 5.13: Average SER performance of Alamouti's transmit diversity scheme for frequency-selective Rayleigh fading and corresponding Rake Receiver Bound ( $N=1$  receive antenna, unequal average received SNRs according to (5.22), binary antipodal transmission,  $\delta_2=0$ ).

**Remark 5.3 (Distributed and co-located MIMO systems)**

For the flat-fading case, the conclusion was made in Chapter 3 that distributed MIMO systems are typically inferior to co-located MIMO systems with uncorrelated antennas (at least when no macroscopic diversity gains are available in the distributed MIMO system). The RRB illustrates that this conclusion holds also for frequency-selective fading channels. As an example, the RRB resulting for the case of equal average SNRs (but identical intertap correlations) has been included in Fig. 5.13 (dotted curve, marked with 'x'), which represents a co-located MIMO system with uncorrelated antennas. As can be seen, the bound is significantly below the RRB for the distributed MIMO system (solid curve, marked with 'x').

## 5.2.4 Use of the Time-Reversal Space-Time Block Code

In the case of relative propagation delays  $\delta_2 > 0$  and/or frequency-selective Rayleigh fading, the time-reversal (TR-) STBC scheme [LP00] discussed in Section 2.3.3 might sometimes be more suitable than Alamouti's transmit diversity scheme in conjunction with a corresponding MLSE equalizer at the receiver. In the following, the advantages and disadvantages of the TR-STBC are briefly discussed.

To start with, consider again the case of frequency-flat Rayleigh fading discussed in Section 5.2.2. As earlier, we focus on the case of  $N=1$  receive antenna, binary antipodal transmission, a Nyquist filter  $g(t)$  with cosine roll-off ( $r=0$ ), a fixed sampling phase of  $\epsilon=0$ , and relative propagation delays  $\delta_1=0$  and  $\delta_2 > 0$ . For Alamouti's transmit diversity scheme it was shown in Section 5.2.2 that relative propagation delays  $\delta_2 > 0$  can cause a significant performance loss. In particular, a propagation delay of  $\delta_2 = T$  degrades the SER

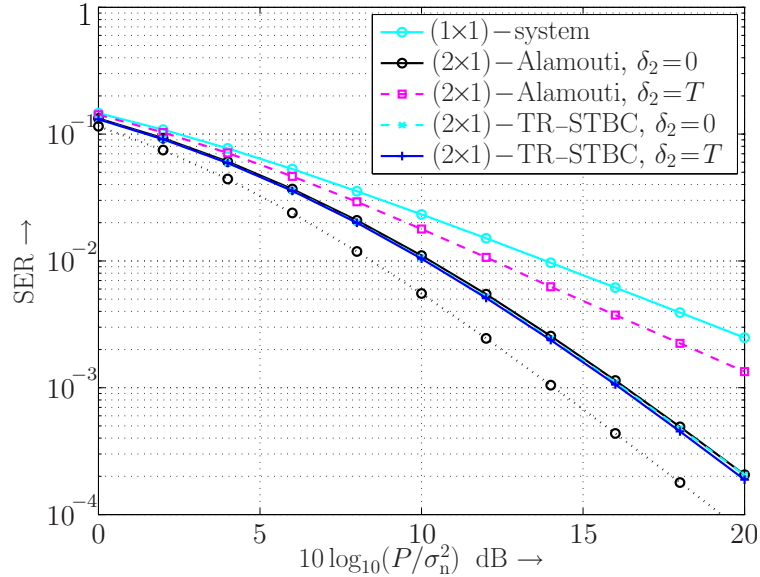


Figure 5.14: Average SER performance of the TR-STBC for relative delays  $\delta_2=0$  and  $\delta_2=T$  ( $N=1$  receive antenna, frequency-flat Rayleigh fading, unequal average received SNRs according to (5.22), binary antipodal transmission, sampling phase  $\epsilon=0$ ). As a reference, the SER performance resulting for  $\delta_2=0$  and equal average received SNRs has been included (dotted curve, cf. Fig. 5.8).

performance of Alamouti's transmit diversity scheme by almost a decade (cf. Fig. 5.8). This undesired behavior does not occur when the TR-STBC is employed.<sup>17</sup> As can be seen in Fig. 5.14, the SER performance of the TR-STBC remains unchanged when the propagation delay  $\delta_2$  increases from  $\delta_2=0$  to  $\delta_2=T$ . In both cases, the same performance is accomplished as with Alamouti's transmit diversity scheme in the ideal case  $\delta_2=0$ .

The TR-STBC is also advantageous in the case of quasi-static frequency-selective fading (with or without a relative propagation delay  $\delta_2>0$ ), because it is able to capture the full diversity order offered by the physical channel [ZG03b]. When compared to Alamouti's transmit diversity scheme in conjunction with MLSE equalization, the TR-STBC will therefore achieve a smaller performance gap with respect to the RRB (cf. Fig. 5.13), especially at high SNR values. However, in the presence of carrier-frequency offsets (cf. Section 5.1) or a time-varying channel model, the TR-STBC can suffer from significant performance degradations, since it relies on the assumption that the channel coefficients are quasi-static. In this case, Alamouti's transmit diversity scheme in conjunction with MLSE equalization might be more favorable, because the employed MLSE equalizer can easily be combined with a suitable channel tracking algorithm, so as to adapt to a time-varying channel behavior [GOS+04].

<sup>17</sup>As in the case of Alamouti's transmit diversity scheme, we assume that the channel coefficients comprise both a square-root Nyquist pulse shaping filter  $g_{Tx}(t)$  and a square-root Nyquist receive filter  $g_{Rx}(t)$ . Correspondingly, in the case of flat fading and propagation delays  $\delta_1=0$  and  $\delta_2=T$ , the effective memory length of the MIMO channel is equal to  $L=1$ .

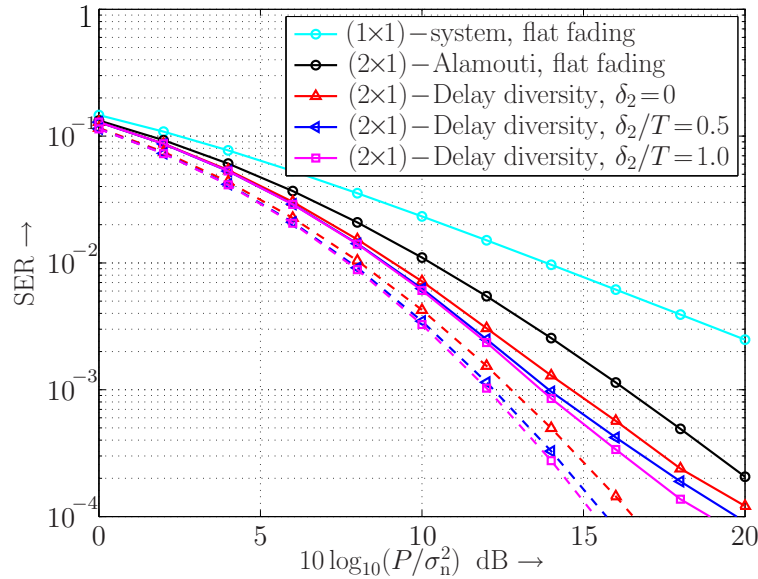


Figure 5.15: Average SER performance of the standard delay diversity scheme ( $\Delta_{DD}=T$ ) for different relative delays  $\delta_2$  ( $N=1$  receive antenna, frequency-selective Rayleigh fading, unequal average received SNRs according to (5.22), binary antipodal transmission, sampling phase  $\epsilon=0$ , roll-off factor  $r=0$ , equalizer length  $L_{eq}=5$ ). The dashed curves represent the corresponding Rake Receiver Bounds.

### 5.2.5 Performance and Optimization of Delay Diversity

As an alternative to the TR-STBC, the delay diversity scheme [Wit93, SW93] discussed in Section 2.3.4 constitutes another transmit diversity scheme suitable for frequency-selective fading scenarios (with or without relative propagation delays  $\delta_\mu \neq 0$ ).

As an example, we focus again on the case of two distributed transmit antennas ( $\delta_1=0$  and  $\delta_2 \geq 0$ ), a single receive antenna, and frequency-selective Rayleigh fading. As earlier, we assume that the average received signal power of the second link is 10 dB below that of the first link. For the time being, we focus on the standard delay diversity scheme employing a delay of zero at the first transmit antenna and a delay of  $T$  ( $=: \Delta_{DD}$ ) at the second transmit antennas. As earlier, we consider a physical channel model with  $N_\tau=10$  equally spaced resolvable delays  $\tau_n$  between zero and  $T$  and a power delay profile characterized by an exponential decay ( $c_\tau=T$ ). Moreover, we consider a roll-off factor of  $r=0$ , a fixed sampling phase  $\epsilon=0$ , and an equalizer length of  $L_{eq}=5$ .

Fig. 5.15 displays the average SER performance as a function of  $P/\sigma_n^2$  in dB, which results for relative propagation delays  $\delta_2=0$ ,  $\delta_2=0.5T$  and  $\delta_2=T$ . As can be seen, a similar performance is obtained as with Alamouti's transmit diversity scheme (cf. Fig 5.12), at the expense of a slightly increased equalizer complexity. Still, at high SNR values the impact of residual ISI is visible. Interestingly, in contrast to Alamouti's scheme the SER performance improves when the relative propagation delay  $\delta_2$  increases from zero to  $T$ . Obviously, with growing delay  $\delta_2$  a larger diversity gain is captured. This finding is

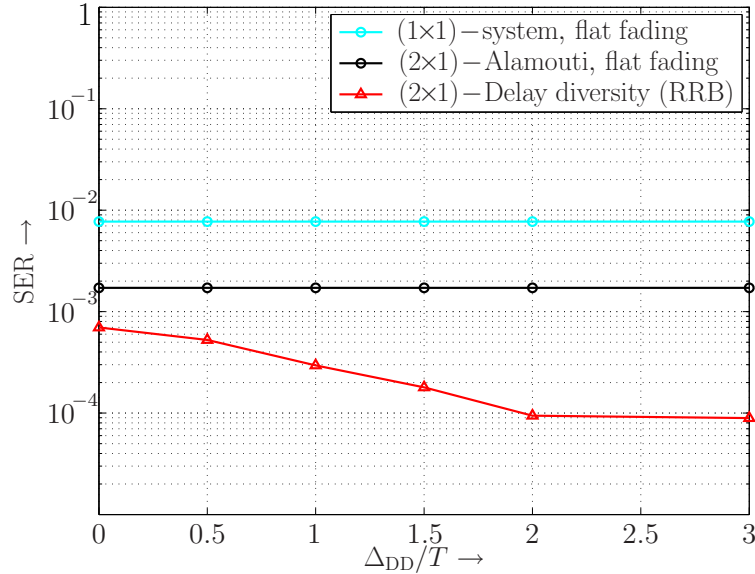


Figure 5.16: Rake Receiver Bound resulting for  $\delta_2=0$  and different delays  $\Delta_{DD}$  between zero and  $3T$  ( $N=1$  receive antenna, frequency-selective Rayleigh fading, unequal average received SNRs according to (5.22), binary antipodal transmission, sampling phase  $\epsilon=0$ , roll-off factor  $r=0$ ).

supported by the corresponding Rake Receiver Bounds (RRBs)<sup>18</sup> for  $\delta_2=0$ ,  $\delta_2=0.5T$  and  $\delta_2=T$ , which have also been included in Fig. 5.15 (dashed lines).

On the other hand, if the propagation delay  $\delta_2$  and the power delay profile of the physical channel are known, the performance of the delay diversity scheme can be optimized by adjusting the delay  $\Delta_{DD}$  employed at the second transmit antenna accordingly. This optimization can, for example, be performed based on the RRB (see also [MHS03a]). As an example, consider the case  $\delta_2=0$ . Fig. 5.16 displays the RRB resulting for different delays  $\Delta_{DD}$  between zero and  $3T$  for a fixed SNR of 15 dB. The same power delay profile as in Fig. 5.15 was assumed. Again, the average received signal power of the second link was 10 dB below that of the first link. Still, it can be seen that the performance of the delay diversity scheme can be improved significantly, by choosing a delay  $\Delta_{DD} \geq 2T$ , provided that the equalizer length  $L_{eq}$  is chosen sufficiently large.<sup>19</sup> For the choice  $\Delta_{DD}=0$ , however, the worst performance results.

Similar optimized versions of the delay diversity scheme for frequency-selective fading channels were also presented in [GSP01, HSG05, YSG06].

<sup>18</sup>The RRB for the delay diversity scheme (with given relative propagation delay  $\delta_2$ ) was derived based on the resulting equivalent single-antenna system, cf. Fig. 2.10 in Section 2.3.4, as described in Section 5.2.3. Note, that the channel coefficient vector in the equivalent single-antenna system actually depends on the propagation delay  $\delta_2$ .

<sup>19</sup>It is also possible to take the impact of a fixed equalizer length  $L_{eq}$  into account, by modeling the occurring residual ISI as an additional Gaussian noise term. As a consequence, the resulting RRB increases significantly, when the delay  $\Delta_{DD}$  becomes too large. As shown in [MHS03a], the modified RRB clearly indicates the maximum delay  $\Delta_{DD}$  that can be tolerated by the equalizer.

**Remark 5.4 (Statistical transmit power allocation for delay diversity)**

The RRB can also be utilized, in order to optimize the transmit power allocation among the individual transmit antennas. This is of particular interest for systems with distributed transmit antennas, where the individual transmission links are associated with different power delay profiles offering different amounts of diversity. To this end, the propagation delays  $\delta_\mu$ , the relative signal attenuations, and the power delay profiles associated with the individual transmission links must be known. The transmit power weights  $w_\mu$  to be optimized can be incorporated in the channel coefficient vector of the equivalent single-antenna system (in the form of effective relative signal attenuations). By this means, the resulting RRB can then be optimized as a function of the transmit power weights  $w_\mu$ . However, it appears that the RRB needs to be re-computed for each new choice of the transmit power weights  $w_\mu$ , which renders the optimization rather complex.

**Large Relative Propagation Delays**

In the case of large relative propagation delays  $\delta_\mu$ , the equivalent single-antenna system will be characterized by a large effective channel memory length  $L'$ . At the same time, the corresponding channel coefficient vector is likely to contain a large number of zero coefficients. Due to the large channel memory length  $L'$ , equalization/detection with a reasonable receiver complexity is a demanding task. An attractive option to limit the receiver complexity is to reuse equalizer algorithms designed for so-called sparse ISI channels.<sup>20</sup> Such algorithms explicitly utilize the sparse channel structure, in order to achieve a complexity reduction (see also [MBLH06]). The topics of linear and decision-feedback equalization (DFE) for sparse ISI channels were, e.g., addressed in [LM04], where the sparse structure of the channel was utilized for the design of the corresponding finite-impulse-response (FIR) filter(s). DFE for sparse ISI channels was also considered in [FGF99, HBA00, CR00, RB03].

Trellis-based equalization for sparse ISI channels was addressed in [BM96, MKH98, McG98, LM02, MBLH06]. In [BM96] it was observed that given a sparse channel there is only a comparatively small number of possible branch metrics within each trellis segment. By avoiding to compute the same branch metric several times, the computational complexity is reduced significantly without any loss of optimality. However, the complexity in terms of trellis states remains the same. As an alternative, another equalizer concept called multitrellis Viterbi algorithm was proposed in [BM96] which is based on multiple parallel irregular trellis diagrams (i.e., time-variant trellis diagrams). The multitrellis Viterbi algorithm was claimed to be optimal while having a significantly reduced computational complexity and number of trellis states. However, based on a factor-graph framework [Loe04] for complexity reduction without loss of optimality, it was demonstrated in [MBLH06] that the multitrellis Viterbi algorithm is in fact clearly suboptimal. A particularly simple solution to reduce the complexity of the conventional Viterbi algorithm [For72] without loss of optimality can be found in [MKH98, McG98]. The parallel-trellis Viterbi algorithm is based on multiple parallel regular trellis diagrams. However,

<sup>20</sup>Sparse ISI channels are encountered in a wide range of communication systems, such as aeronautical or satellite communication systems or high-data-rate mobile radio systems (especially in hilly terrain, where the delay spread of the physical channel is large).

it can only be applied for sparse channels with a so-called zero-pad structure, where the non-zero channel coefficients are placed on a regular grid (see also [MBLH06]). In order to tackle more general sparse ISI channels with a structure close to a zero-pad channel, it was proposed in [MKH98,McG98] to exchange tentative decisions between the parallel trellises, so as to cancel residual ISI.<sup>21</sup> Generalizations of the (suboptimal) parallel-trellis Viterbi algorithm, which are based on the Bahl-Cocke-Jelinek-Raviv (BCJR) algorithm [BCJR74], were presented in [LM02] along with some interesting enhancements.

In [MBLH06], the effort was made to compare the performance of the above algorithms with that of standard (suboptimal) reduced-complexity receivers which are not specifically designed for sparse channels. In particular, it was demonstrated that the use of a linear prefilter for an overall minimum-phase channel impulse response [Bad01,GOMH02,BH04] renders the application of efficient reduced-state trellis-based equalizer algorithms such as [EQ88,DH89] feasible, without significant loss of optimality.<sup>22</sup> Such a receiver structure is notably simple, because the employed equalizer algorithm is a standard algorithm. (The sparse channel structure is typically lost after prefiltering.) Only the linear filter has to be adjusted to the current channel impulse response, which is particularly favorable with regard to fading channels. Moreover, the filter coefficients can be computed using standard techniques available in the literature.

Alternatives to trellis-based equalization are the tree-based list-sequential (LISS) algorithm [Hag03,Kuh05,Kuh06] and the Joint Gaussian approach in [PLWL06]. A factor-graph approach for sparse ISI channels, based on the sum-product algorithm [Loe04], was presented in [CG05]. Turbo equalization [DJB+95] for sparse channels was addressed in [PG04]. Finally, a non-trellis based equalizer algorithm for fast-fading sparse ISI channels, based on the symbol-by-symbol maximum a-posteriori (MAP) criterion, was presented in [CM99].

### 5.3 Chapter Summary

In the previous chapters it was shown that many of the benefits provided by MIMO systems with co-located antennas can also be gained in distributed MIMO systems with cooperating transmitting or receiving nodes. In this chapter, the issue of non-perfect carrier-frequency and timing synchronization between cooperating transmitting nodes was addressed. While carrier-frequency offsets (CFOs) cause a time-varying channel impulse response, timing synchronization errors leads to intersymbol interference (ISI) effects.

First, the impact of CFOs on the performance of OSTBCs was considered. In the case of binary antipodal transmission and perfect channel tracking, the performance of OSTBCs turned out to be quite robust. However, if a higher-order modulation scheme is employed, a significant performance loss can occur, which is due to an orthogonality loss caused by the CFOs. For the example of Alamouti's transmit diversity scheme, it was demonstrated that the performance can be improved significantly by using linear zero-forcing (ZF) or linear minimum-mean-squared-error (MMSE) detection at the

<sup>21</sup>It should be noted that this modified version of the parallel-trellis Viterbi algorithm is suboptimal.

<sup>22</sup>As an alternative, the use of a linear channel shortening filter [Kam94] was investigated in [MBLH06], in conjunction with a conventional Viterbi algorithm operating on a shortened channel memory length.



receiver rather than conventional Alamouti decoding. In addition to OSTBCs, the quasi-orthogonal STBC introduced in Section 2.3.2 and the delay diversity scheme discussed in Section 2.3.4 were considered. In comparison with an OSTBC, the quasi-orthogonal STBC appeared to be more sensitive to the impact of CFOs. In the case of perfect channel tracking, the delay diversity scheme turned out to be superior to an OSTBC, but was inferior when the channel coefficients were not perfectly tracked.

In the second part of the chapter, the impact of non-perfect timing synchronization was investigated. First, the performance of Alamouti's transmit diversity scheme in conjunction with maximum-likelihood sequence estimation (MLSE) at the receiver was considered. It was demonstrated that in the case of frequency-flat fading, significant performance degradations can occur due to poor distance properties of Alamouti's scheme in the presence of ISI. In contrast to this, in the case of frequency-selective fading the performance appeared to be quite robust. Yet, Alamouti's scheme was shown to be unable to extract the full diversity order that is offered by the frequency-selective fading channel. In the case of a quasi-static fading scenario, the time-reversal STBC discussed in Section 2.3.3 therefore seems to be more attractive. Finally, the use of the delay diversity scheme was considered, which constitutes an attractive alternative to the time-reversal STBC. In particular, if the relative propagation delays and the power delay profile(s) of the physical channel are known, the performance of the delay diversity scheme can be improved significantly by optimizing the delay(s) employed at the transmitter side. Moreover, it was argued that in the case of large relative propagation delays, equalization techniques originally designed for so-called sparse ISI channels can be reused.



## Appendix

The poor performance of Alamouti's transmit diversity scheme resulting for frequency-flat fading in conjunction with a relative propagation delay of  $\delta_2 = T$  (cf. Fig. 5.9) can be explained based on the distance properties of Alamouti's transmit diversity scheme in the presence of ISI.

To this end, a so-called difference trellis diagram [Hub92, Ch. 5.1.2] is defined, as explained in Section J.3 in Appendix J. The difference trellis diagram contains all possible error sequences  $\boldsymbol{\epsilon} = \mathbf{a} - \mathbf{a}'$ , where  $\mathbf{a} := [\dots, a[\kappa-1], a[\kappa], a[\kappa+1], \dots]$  denotes the sequence of information symbols actually transmitted and  $\mathbf{a}'$  a (possible erroneous) sequence that is detected by an MLSE equalizer.<sup>23</sup> The corresponding distance spectrum comprises all squared Euclidean distances  $d_{\text{E}}^2(\boldsymbol{\epsilon}) = d_{\text{E}}^2(\mathbf{a}, \mathbf{a}')$  associated with the individual error sequences  $\boldsymbol{\epsilon}$  (after the STBC encoder and the ISI channel, cf. Fig. J.4 in Appendix J) along with their relative frequencies. The distance spectrum is useful, in order to bound above the so-called error event probability  $\Pr\{\mathcal{E}_{\text{error}, k_0}\}$ , i.e., the probability that at a certain time index  $k_0$  the MLSE equalizer diverts from the correct trellis path representing the transmitted information sequence  $\mathbf{a}$ . In particular, if there are relatively few squared

<sup>23</sup>The error sequence  $\boldsymbol{\epsilon} = \mathbf{0}$  thus represents the case of error-free transmission.



Euclidean distances  $d_E^2(\boldsymbol{\epsilon})$  with a value close to zero, the upper bound on  $\Pr\{\mathcal{E}_{\text{error},k_0}\}$  will be comparatively small, implying a good resulting error performance.

For the case of co-located transmit antennas ( $\delta_2=0$ ) and a single receive antenna, the distance properties of Alamouti's transmit diversity scheme in the presence of ISI are discussed in more detail in Appendix J, with focus on the special case  $L=1$  (cf. Example J.2). In particular, it is shown that the distance spectrum can be evaluated based on a state transition matrix  $\mathbf{T}(D, E, J)$ , cf. (J.34). The entries of  $\mathbf{T}(D, E, J)$  are polynomials with symbolic bases  $D, E, J$ , while the exponents of  $D$  represent the squared Euclidean distances  $d_{E,k}^2$  acquired in a single trellis segment, depending on the error sequence  $\boldsymbol{\epsilon}$  under consideration:

$$d_E^2(\boldsymbol{\epsilon}) := \sum_k d_{E,k}^2. \quad (5.27)$$

In the case  $L=1$ , the squared Euclidean distances  $d_{E,k}^2$  take on the values summarized in Table J.1 in Appendix J.

In order to explain the pronounced peak in the SER curve resulting for distributed transmit antennas, frequency-flat fading, and a relative propagation delay of  $\delta_2=T$ , we compare the distance spectra resulting for  $\delta_2=0$  and  $\delta_2=T$ . Since  $g(t)$  was assumed to constitute a Nyquist filter (cf. Section 5.2.1), the results obtained in Example J.2 can be utilized by setting the channel coefficient vectors  $\mathbf{h}$  and  $\mathbf{g}$  to  $\mathbf{h} := [h_0, 0]^T$ ,  $\mathbf{g} := [g_0, 0]^T$  ( $\delta_2=0$ ) or  $\mathbf{h} := [h_0, 0]^T$ ,  $\mathbf{g} := [0, g_1]^T$  ( $\delta_2=T$ ), respectively. In the case  $\delta_2=0$ , the squared Euclidean distances  $d_{E,k}^2$  of all branches within the difference trellis diagram, which lead to a target state other than the zero state, either take on the value  $4(|h_0+g_0|^2+|h_0-g_0|^2)$  or the value  $4(|h_0|^2+|g_0|^2)$ , cf. Table J.1. Correspondingly, unless both channel coefficients  $h_0$  and  $g_0$  have a small magnitude, the acquired squared Euclidean distances  $d_{E,k}^2$  will always have a value significantly larger than zero. This again reflects the achieved diversity gain in comparison with a single-antenna system. In contrast to this, in the case  $\delta_2=T$  one can construct examples for which some of the squared Euclidean distances  $d_{E,k}^2$  are zero or close to zero, which leads to a (quasi-) catastrophic error performance.

As an example, we consider the case where all channel coefficients have a value of  $h_0=g_0=g_1=1$ . The corresponding distance spectra resulting for  $\delta_2=0$  and  $\delta_2=T$  are depicted in Fig. 5.17, where an error path length of  $S=10$  trellis segments was taken into account.<sup>24</sup> As can be seen, for  $\delta_2=0$  there are relatively few squared Euclidean distances  $d_E^2(\boldsymbol{\epsilon})$  with a small value (say,  $d_E^2(\boldsymbol{\epsilon}) < 40$ ), which will lead to a comparatively good error performance. In contrast to this, for  $\delta_2=T$  the fraction of small squared Euclidean distances  $d_E^2(\boldsymbol{\epsilon})$  is comparatively large. In particular, there are error sequences  $\boldsymbol{\epsilon} \neq \mathbf{0}$  that are associated with a squared Euclidean distance equal to zero, which will lead to a catastrophic performance.

<sup>24</sup>The distance spectra have been evaluated based on the polynomial  $P_S(D, E, J)$ , as explained in Section J.3 in Appendix J.

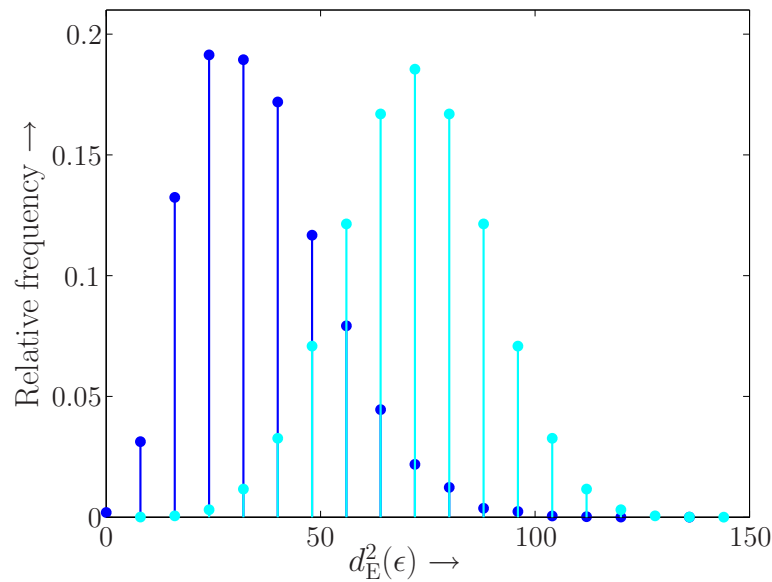


Figure 5.17: Distance spectrum for Alamouti's transmit diversity scheme resulting for channel coefficient vectors  $\mathbf{h} := [1, 0]^T$ ,  $\mathbf{g} := [1, 0]^T$  (light color) and channel coefficient vectors  $\mathbf{h} := [1, 0]^T$ ,  $\mathbf{g} := [0, 1]^T$  (dark color), given an error path length of  $S=10$  trellis segments.

# Chapter 6

## Summary and Conclusions

**D**UE TO THE disruptive characteristics of wireless channels, it is a demanding task to build wireless communication systems that offer high bit rates and small error rates at the same time. A bandwidth-efficient and thus cost-effective option to accomplish this goal is the use of multiple transmit and receive antennas. In fact, multiple-antenna systems, called multiple-input multiple-output (MIMO) systems, are currently regarded as a key technology for future wireless multimedia applications.

The great potential of MIMO systems has only become apparent during the last decade. Since then, researchers from academia and industry have generated an enormous number of yearly publications. On the one hand, it was shown that the capacity of MIMO systems grows (approximately) linearly with the minimum of the number of transmit and receive antennas. Correspondingly, multiple antennas provide a promising means to accomplish enhanced bit rates in comparison with a single-antenna system. On the other hand, multiple antennas can also be utilized, in order to provide a spatial diversity gain and thus to improve the error performance of a system. A detailed overview of the exciting research field of MIMO systems has been presented in Section 2.1.

### Contributions of the Thesis

In the literature on MIMO systems, typically quite restrictive assumptions are made concerning the antenna spacings at transmitter and receiver. On the one hand, it is typically assumed that the individual antenna elements are co-located, i.e., they belong to some sort of antenna array. On the other hand, the antenna spacings are often assumed to be sufficiently large, so as to justify the assumption of uncorrelated antenna elements. The objective of this thesis was to relax these strict assumptions, based on the following motivations. First, sufficient antenna spacings cannot always be guaranteed in practical MIMO systems, which leads to spatially correlated transmission links. Second, in order to shift the limits of wireless communications, the concept of cooperative wireless networks has recently gained considerable interest. In such networks, multiple nodes that are spatially distributed on a large scale cooperate in terms of a joint transmission or reception strategy. By this means, virtual antenna arrays are established, so that the cooperating nodes (possibly equipped with only a single antenna) are able to enjoy some of the benefits offered by conventional MIMO systems with co-located antennas.

For co-located MIMO systems, it is well known that spatially correlated links can cause significant performance degradations, both with regard to capacity and error rates. Based on the statistical discrete-time channel model, which was derived and thoroughly analyzed in Section 2.2, it was shown in Chapter 3 that MIMO systems with distributed antennas and MIMO systems with co-located antennas can be treated in a single, unifying framework. As a result, the above performance degradations will also occur, when antennas are spatially distributed on a large scale, which is due to unequal average signal-to-noise ratios on the individual transmission links. More specifically, it was proven that any co-located MIMO system, which obeys the so-called Kronecker correlation model, can be transformed into an (asymptotically) equivalent distributed MIMO system, and vice versa (Section 3.2). This equivalence was proven for the resulting capacity distribution, the pairwise error probability of a general full-diversity space-time code, and the average symbol error rate of an orthogonal space-time block code.<sup>1</sup>

Potential advantages of distributed MIMO systems in comparison with co-located MIMO systems were investigated in Section 3.4. First, in a distributed MIMO system the line-of-sight probability is typically larger than in a co-located MIMO system. Based on numerical performance results, it was shown that this often leads to substantial performance improvements. Second, in distributed MIMO systems additional macroscopic diversity gains due to shadowing effects may be available. It was shown that distributed space-time codes are able to capture both macroscopic and microscopic spatial diversity gains, and are thus superior to conventional simulcasting techniques. Altogether, it was concluded that as soon as significant macroscopic diversity gains are available, distributed MIMO systems are typically superior to co-located MIMO systems, even in the case of unbalanced signal-to-noise ratios.

Several publications have shown that the performance of MIMO systems can be improved significantly when exploiting some form of channel knowledge at the transmitter side. Motivated by this fact, optimal transmit power allocation strategies for distributed and co-located MIMO systems were developed in Chapter 4 (Section 4.1), utilizing the equivalence results from Chapter 3. In particular, fading scenarios were taken into account that occur especially in distributed MIMO systems. Focus was on power allocation schemes that require solely statistical channel knowledge at the transmitter side, which can easily be acquired in practical systems. By means of analytical results, it was shown that significant performance gains in comparison with equal power allocation can be achieved. Moreover, the impact of estimation errors concerning the transmitter correlation matrix was studied, and it was shown that the considered power allocation schemes offer quite a robust performance.

In the second part of Chapter 4, the use of statistical channel knowledge at the receiver was investigated, for providing an optimal trade-off between performance and receiver complexity (Section 4.2). It was shown that there is a strong duality between the considered reduced-dimension receiver and the statistical transmit power allocation schemes investigated in Section 4.1. Specifically, the impact of estimation errors concerning the receiver correlation matrix can be analyzed along the same lines as for the transmitter side.

---

<sup>1</sup>Yet, typically substantial performance gains over a single-antenna system were observed, even in the case of highly correlated antennas or highly unbalanced signal-to-noise ratios.

Finally, in Chapter 5 two problems were studied that are of particular interest for MIMO systems with distributed transmit antennas. First, the individual transmitting nodes will employ independent local oscillators for converting the transmitted signals into bandpass domain. This can cause carrier-frequency offsets between the different transmission links resulting in time-varying channel impulse responses. Second, if the individual transmitting nodes are spaced very far apart, large differences can occur between the corresponding link lengths. If no timing-advance technique is employed at the transmitter side, the different propagation delays can cause intersymbol interference effects compromising the achieved diversity gains. Since the above effects do typically not occur in co-located MIMO systems, they are usually not addressed in the standard literature on space-time coding techniques. On the other hand, they are also neglected in most publications on cooperative wireless networks, where focus is usually rather on algorithms and protocols managing the interaction between the individual network nodes. In Section 5.1, the impact of carrier-frequency offsets on the performance of different space-time coding techniques was investigated, and possible counter measures were discussed. For example, for Alamouti's transmit diversity scheme, improved (linear) receiver structures were proposed that offer a near-optimum performance. In Section 5.2, the influence of non-negligible relative propagation delays was studied. Specifically, suitable space-time coding and equalization techniques were identified, so as to maintain a diversity advantage over a single-antenna system.

A more detailed account of specific contributions made by this thesis can be found in the conclusions offered at the end of each chapter.

### **Directions for Future Work**

Throughout this thesis, focus was on transmitter and receiver techniques that concern mainly the physical layer of distributed and co-located MIMO systems. With regard to distributed MIMO systems, the influence of several effects, such as macroscopic diversity effects and non-negligible relative propagation delays, was investigated, and it was demonstrated that these effects have a significant impact on the resulting system performance. These results can be seen as a first step towards a more realistic performance evaluation for cooperative wireless systems. Yet, significantly more work is required, so as to accurately predict the benefits of virtual antenna arrays for practical systems. In particular, further work on efficient protocols, suitable distributed space-time coding techniques, and robust receiver structures is required, taking the above effects into account. Concerning the transmitter and receiver techniques considered in Chapter 4, suitable algorithms for estimating the spatial correlation matrices have to be developed, and their performance needs to be assessed. For example, [DIU06] could serve as a starting point here. Similarly, in the case of significant carrier-frequency offsets, efficient channel tracking algorithms are needed, so as to limit the performance loss of distributed space-time coding techniques. Finally, while in this thesis focus was on spatial diversity techniques, it will also be interesting to study the use of spatial multiplexing techniques in distributed MIMO systems.





# Appendix A

## Acronyms and Abbreviations

### Frequently Used Abbreviations

|         |   |
|---------|---|
| 3G      | Third generation  |
| 4G      | Fourth generation   |
| AoA     | Angle of arrival  |
| AoD     | Angle of departure  |
| ASK     | Amplitude-shift keying  |
| AWGN    | Additive white Gaussian noise                                       |
| BCJR    | Bahl-Cocke-Jelinek-Raviv  |
| BER     | Bit error rate  |
| BLAST   | Bell-Labs Layered Space-Time Architecture                           |
| BS      | Base station  |
| CAA     | Circular antenna array  |
| CCI     | Co-channel interference   |
| CDF     | Cumulative distribution function                                    |
| CDMA    | Code-division multiple access                                       |
| CF      | Characteristic function   |
| CFO     | Carrier-frequency offset  |
| CRC     | Cyclic redundancy check   |
| D-BLAST | Diagonal BLAST  |
| DDFSE   | Delayed-decision feedback sequence estimator                        |
| DFE     | Decision-feedback equalizer   |
| DMMT    | Discrete matrix multitone   |
| DMT     | Discrete multitone  |
| DPSK    | Differential phase-shift keying                                     |
| DS-CDMA | Direct-sequence CDMA  |
| EBF     | Eigen-beamforming   |
| EGC     | Equal gain combining  |
| EPA     | Equal power allocation  |
| ESPRIT  | Estimation of signal parameters via rotational invariance technique |
| EVD     | Eigenvalue decomposition  |



|         |   |
|---------|---|
| EXIT    | Extrinsic information transfer                |
| FDE     | Frequency-domain equalization                 |
| FFT     | Fast Fourier transform                        |
| FIR     | Finite impulse response                       |
| HI      | Power allocation solution for high SNR values |
| IDMA    | Interleave-division multiple access           |
| IFFT    | Inverse fast Fourier transform                |
| i.i.d.  | independent and identically distributed       |
| INV     | Eigenvalue inversion                          |
| ISI     | Intersymbol interference                      |
| JLSCE   | Joint least squares channel estimation        |
| KKT     | Karush-Kuhn-Tucker                            |
| KLT     | Karhunen-Loève transform                      |
| LDPC    | Low-density parity-check                      |
| LE      | Linear equalizer                              |
| LISS    | List sequential                               |
| LoS     | Line of sight                                 |
| MAP     | Maximum a-posteriori                          |
| MC-CDMA | Multicarrier CDMA                             |
| MF      | Matched filter                                |
| MGF     | Moment-generating function                    |
| MIMO    | Multiple-input multiple-output                |
| MISO    | Multiple-input single-output                  |
| ML      | Maximum likelihood                            |
| MLSE    | Maximum-likelihood sequence estimation        |
| MMSE    | Minimum mean squared error                    |
| MRC     | Maximum ratio combining                       |
| MS      | Mobile station                                |
| MUSIC   | Multiple signal classification                |
| OFDM    | Orthogonal frequency-division multiplexing    |
| OSTBC   | Orthogonal STBC                               |
| PAS     | Power azimuth spectrum                        |
| PCC     | Parallel concatenated code                    |
| PDA     | Probabilistic data association                |
| PDF     | Probability density function                  |
| PDP     | Power delay profile                           |
| PEP     | Pairwise error probability                    |
| PRUS    | Perfect roots-of-unity sequence               |
| PSK     | Phase-shift keying                            |
| QAM     | Quadrature amplitude modulation               |
| QoS     | Quality of service                            |
| RA      | Repeat-accumulate                             |
| RF      | Radio frequency                               |
| RRB     | Rake Receiver Bound                           |

---

|         |   |
|---------|---|
| Rx      | Receiver                                  |
| SD      | Selection diversity                       |
| SDMA    | Space-division multiple access            |
| SER     | Symbol error rate                         |
| SF      | Space-frequency                           |
| SIC     | Successive interference cancellation      |
| SINR    | Signal-to-interference-plus-noise ratio   |
| SiSo    | Soft-input soft-output                    |
| SIMO    | Single-input multiple-output              |
| SNR     | Signal-to-noise ratio                     |
| s.t.    | subject to                                |
| ST      | Space-time                                |
| STC     | Space-time code                           |
| STBC    | Space-time block code                     |
| STF     | Space-time-frequency                      |
| ST-IDM  | Space-time IDMA scheme                    |
| STTC    | Space-time trellis code                   |
| SVD     | Singular-value decomposition              |
| TCM     | Trellis-coded modulation                  |
| TDD     | Time-division duplex                      |
| TDMA    | Time-division multiple access             |
| TR      | Time-reversal                             |
| Tx      | Transmitter                               |
| ULAA    | Uniform linear antenna array              |
| UMTS    | Universal Mobile Telecommunication System |
| US      | Uncorrelated scattering                   |
| VAA     | Virtual antenna array                     |
| V-BLAST | Vertical BLAST                            |
| WF      | Waterfilling                              |
| WSS     | Wide-sense stationarity                   |
| ZF      | Zero forcing                              |

## Units and Pseudo-Units

|     |  |
|-----|--|
| bit | Pseudo-unit for entropy/information (based on $\text{ld}(\cdot)$ -logarithm) |
| dB  | decibel  |
| Hz  | Hertz  |
| m   | meter  |
| nat | Pseudo-unit for entropy/information (based on $\text{ln}(\cdot)$ -logarithm) |
| rad | Radiant  |
| s   | second   |



# Appendix B

## Notation

### Use of Fonts

Throughout this thesis, vectors are written in lower-case bold face and matrices in upper-case bold face. Scalar random variables, random vectors, and random matrices are marked by an underscore. General sets are written in blackboard type, e.g.  $\mathbb{S}$ . Specific operators, such as statistical expectation, are denoted by Sans Serif fonts with argument in curly brackets, e.g.  $\mathbf{E}\{x\}$ . Specific matrices are denoted by bold-face Gothic fonts. For example, the  $(n \times n)$ -Fourier matrix is denoted by  $\mathfrak{F}_n$ .

|                                |  |
|--------------------------------|--|
| $x, \xi$                       | Scalar or realization of a scalar random variable $\underline{x}, \underline{\xi}$                       |
| $\mathbf{x}, \boldsymbol{\xi}$ | Vector or realization of a vector random variable $\underline{\mathbf{x}}, \underline{\boldsymbol{\xi}}$ |
| $\mathbf{X}, \boldsymbol{\Xi}$ | Matrix or realization of a matrix random variable $\underline{\mathbf{X}}, \underline{\boldsymbol{\Xi}}$ |
| $\mathfrak{X}$                 | Specific matrix  |
| $\mathbb{X}$                   | General set  |
| $\mathbf{X}\{.\}$              | Specific operator  |

### Conventions

Continuous-time functions such as signals are written using parentheses for the argument, e.g.  $s(t)$ . Quantities such as data symbols, which depend on a discrete time index, are written using square brackets for the argument, e.g.  $d[k]$ .

The probability of an event  $\mathcal{E}$  is denoted by  $\Pr\{\mathcal{E}\}$ . Statistical expectation of a scalar, vector, or matrix random variable is denoted by  $\mathbf{E}\{.\}$ . (For notational convenience, we write  $\mathbf{E}\{x\}$  instead  $\mathbf{E}\{\underline{x}\}$ .) The probability density function (PDF) of a continuous scalar random variable  $\underline{x}$  is denoted by  $p_{\underline{x}}(x)$  and the corresponding cumulative distribution function (CDF) by  $\Pr\{\underline{x} \leq x\}$ . The joint PDF of a vector random variable  $\underline{\mathbf{x}}$  is denoted by  $p_{\underline{\mathbf{x}}}(\mathbf{x})$ . The characteristic function (CF) and the moment-generating function (MGF) of a scalar random variable  $\underline{x}$  is denoted as  $\mathbf{C}\{x\}$  and  $\mathbf{M}\{x\}$ , respectively.

If not stated otherwise, vectors are regarded as column vectors. The  $i$ th element of a vector  $\mathbf{v}$  is denoted by  $v_i$ . The  $(i, j)$ -element of a matrix  $\mathbf{M}$  is denoted by  $m_{ij}$  or by  $[\mathbf{M}]_{i,j}$ . The  $i$ th column vector of a matrix  $\mathbf{M}$  is represented by  $\mathbf{m}_i$ . For a given  $(m \times n)$  matrix  $\mathbf{M}$ ,  $\text{vec}(\mathbf{M})$  denotes vectorization, where the column vectors of  $\mathbf{M}$  are successively

stacked in a single column vector of size  $(mn \times 1)$ . Moreover,  $\text{diag}(\mathbf{v})$  denotes a diagonal matrix with diagonal entries given by the vector  $\mathbf{v}$ . The determinant, trace, and rank of a matrix  $\mathbf{M}$  is denoted by  $\det(\mathbf{M})$ ,  $\text{tr}(\mathbf{M})$  and  $\text{rank}(\mathbf{M})$ , respectively.

Complex conjugation of a complex number is denoted by  $(\cdot)^*$ . Moreover,  $(\cdot)^T$  marks the transposed of a vector or a matrix and  $(\cdot)^H$  the Hermitian transposed. The inverse of a scalar or a square matrix is marked by  $(\cdot)^{-1}$ . The Moore-Penrose left-hand pseudoinverse of a non-square/rank-deficient matrix is denoted by  $(\cdot)^\dagger$ . Average values, hypotheses, and hard decisions/estimates are marked by  $(\bar{\cdot})$ ,  $(\tilde{\cdot})$  and  $(\hat{\cdot})$ , respectively.

A list of all specific symbols, notations, and variables used throughout this thesis is given below.

## List of Specific Symbols and Notations

### Constants

|       |                                       |
|-------|---------------------------------------|
| $e$   | Euler's number ( $e \approx 2.7183$ ) |
| $j$   | Imaginary unit ( $j = \sqrt{-1}$ )    |
| $\pi$ | Pi ( $\pi \approx 3.1416$ )           |

### Specific Sets

|                               |   |
|-------------------------------|---|
| $\mathbb{A}$                  | Symbol alphabet                             |
| $\mathbb{C}$                  | Set of all complex numbers                  |
| $\mathbb{I}$                  | Index set                                   |
| $\mathbb{R}, \mathbb{R}_{>0}$ | Set of all real numbers (greater than zero) |
| $\mathbb{S}_n$                | Stiefel manifold (see Definition D.7)       |
| $\mathbb{Z}$                  | Set of all integers                         |

### Known Functions

|   |  |
|---|--|
| $\cos(x)$   | Cosine function  |
| $\delta(x), \delta[x]$                              | Dirac-impulse at $x=0$   |
| $\text{erfc}(x)$                                    | Complementary error function (see Definition C.2)                          |
| $\exp(x)$   | Exponential function   |
| $\Gamma(x)$   | Gamma function (see Definition C.3)  |
| $\inf(\cdot)$                                       | Infimum  |
| $I_n(x)$  | Modified Bessel function of the first kind, order $n$ (see Definition C.5) |
| $J_n(x)$  | Bessel function of the first kind, order $n$ (see Definition C.4)          |
| $\text{ld}(x)$                                      | Logarithm to the base 2  |
| $\log_a(x)$   | Logarithm to the base $a$  |
| $L(\mathbf{x}, \boldsymbol{\mu}, \boldsymbol{\nu})$ | Lagrangian function  |
| $\max(\cdot)$                                       | Maximum  |
| $\min(\cdot)$                                       | Minimum  |
| $\sin(x)$   | Sine function  |
| $\sup(\cdot)$                                       | Supremum   |
| $Q(x)$  | Q-function (see Definition C.2)  |

### Functions of Matrices

|                                 |   |
|---------------------------------|---|
| $\text{cp}_{\mathbf{X}}(x)$     | Characteristic polynomial of a square matrix $\mathbf{X}$ (see Definition D.10)             |
| $C_{\kappa}(\mathbf{X})$        | Complex zonal polynomial of a complex Hermitian matrix $\mathbf{X}$                         |
| $\det(\mathbf{X})$              | Determinant of a square matrix $\mathbf{X}$   |
| $\det(\mathbf{X})_{\mathbf{i}}$ | Minor determinant of a square matrix $\mathbf{X}$ associated with index vector $\mathbf{i}$ |
| $\text{rank}(\mathbf{X})$       | Rank of a matrix $\mathbf{X}$ (see Definition D.10)   |
| $\text{tr}(\mathbf{X})$         | Trace of a matrix $\mathbf{X}$ (sum over all diagonal elements $x_{ii}$ )                   |

### Functions and Operators Concerning Random Variables

|  |   |
|--|---|
| $\mathbb{C}\{x\}(j\omega)$               | Characteristic function (CF) of a scalar random variable $\underline{x}$ , evaluated at $j\omega$ , $\omega \in \mathbb{R}$ (see Definition C.17) |
| $\mathbb{E}\{.\}$                        | Statistical expectation of a scalar, vector, or matrix random variable  |
| $\mathbb{M}\{x\}(s)$                     | Moment-generating function (MGF) of a scalar random variable $\underline{x}$ , evaluated at $s \in \mathbb{C}$ (see Definition C.17)              |
| $p_{\underline{x}}(x)$                   | Probability density function (PDF) of a scalar random variable $\underline{x}$  |
| $p_{\underline{\mathbf{x}}}(\mathbf{x})$ | Joint PDF of a vector random variable $\underline{\mathbf{x}}$  |
| $\Pr\{\underline{x} \leq x\}$            | Cumulative distribution function (CDF) of a scalar random variable $\underline{x}$  |

### Specific Operators and Transforms

|                               |  |
|-------------------------------|--|
| $\nabla$                      | Gradient   |
| $\frac{\partial}{\partial x}$ | Derivative with respect to $x$   |
| $\text{argmax}\{.\}$          | argmax operator  |
| $\text{argmin}\{.\}$          | argmin operator  |
| $\mathbb{F}\{f(x)\}(j\omega)$ | Fourier transform of a scalar function $f(x)$ , evaluated at $j\omega$ , $\omega \in \mathbb{R}$ |
| $\text{Im}\{.\}$              | Imaginary part of a complex number   |
| $\lim_{a \rightarrow b}$      | Limes for $a \rightarrow b$  |
| $\mathbb{L}\{f(x)\}(s)$       | Laplace transform of a scalar function $f(x)$ , evaluated at $s \in \mathbb{C}$                  |
| $\Pr\{\mathcal{E}\}$          | Probability of an event $\mathcal{E}$  |
| $\text{Re}\{.\}$              | Real part of a complex number  |

### Specific Matrices

|                  |   |
|------------------|---|
| $\mathbf{0}$     | Matrix or vector with entries 0                             |
| $\mathfrak{A}$   | Alamouti matrix   |
| $\mathfrak{F}_n$ | Fourier matrix of size $(n \times n)$ , see Definition D.8  |
| $\mathfrak{H}_n$ | Hadamard matrix of size $(n \times n)$ , see Definition D.6 |
| $\mathbf{I}_n$   | Identity matrix of size $(n \times n)$                      |
| $\mathfrak{D}$   | (Generalized) orthogonal design                             |
| $\mathfrak{Q}$   | Quasi-orthogonal design                                     |

### Specific Distributions

|                                     |   |
|-------------------------------------|---|
| $\mathcal{CN}(\bar{x}, \sigma_x^2)$ | Circularly symmetric complex Gaussian distribution with mean $\bar{x}$ and variance $\sigma_x^2$ (see Definition C.9) |
|-------------------------------------|---|

|   |   |
|---|---|
| $\mathcal{CN}(\bar{\mathbf{x}}, \mathbf{Q}_{\mathbf{x}})$ | Multivariate complex Gaussian distribution with mean $\bar{\mathbf{x}}$ and covariance matrix $\mathbf{Q}_{\mathbf{x}}$ (see Definition C.10) |
| $\mathcal{L}(\bar{x}, \sigma_x^2)$                        | Laplacian distribution with mean $\bar{x}$ and variance $\sigma_x^2$ (see Definition C.8)   |
| $\mathcal{N}(\bar{x}, \sigma_x^2)$                        | Gaussian distribution with mean $\bar{x}$ and variance $\sigma_x^2$ (see Definition C.7)  |
| $\mathcal{U}([a, b])$                                     | Uniform distribution on the interval $[a, b]$ (see Definition C.6)  |

### Operations on Scalars, Vectors, and Matrices

|                               |   |
|-------------------------------|---|
| *                             | Convolution   |
| $\odot$                       | Hadamard product of two matrices (see Definition D.3)                                       |
| $\otimes$                     | Kronecker product of two matrices (see Definition D.4)                                      |
| $\binom{n}{k}$                | Binomial coefficient $\left(= \frac{n!}{(n-k)!k!}\right)$                                   |
| $[x]_+$                       | Maximum of $x$ and 0  |
| $x^*$                         | Complex conjugation of a complex number $x$   |
| $x^{-1}$                      | Inverse of a scalar $x$   |
| $x_i$                         | $i$ th element of a vector $\mathbf{x}$   |
| $x_{i,j}, [\mathbf{X}]_{i,j}$ | $(i, j)$ -element of a matrix $\mathbf{X}$  |
| $\mathbf{x}_i$                | $i$ th column vector of a matrix $\mathbf{X}$   |
| $\mathbf{X}^\dagger$          | Moore-Penrose left-hand pseudoinverse of a non-square or rank-deficient matrix $\mathbf{X}$ |
| $\mathbf{X}^{-1}$             | Inverse of a square matrix $\mathbf{X}$   |
| $(\cdot)^H$                   | Hermitian transposed of a vector or matrix, $(\cdot)^H = ((\cdot)^T)^* = ((\cdot)^*)^T$     |
| $(\cdot)^T$                   | Transposed of a vector or matrix  |
| $\text{diag}(\mathbf{x})$     | Diagonal matrix with diagonal elements given by the vector $\mathbf{x}$                     |
| $\text{vec}(\mathbf{X})$      | Vectorization of a matrix (stacking of the column vectors)                                  |

### Norms and Distance Measures

|                                    |  |
|------------------------------------|--|
| $\ \mathbf{x}\ _2, \ \mathbf{x}\ $ | Euclidean norm of a vector $\mathbf{x}$ (see Definition D.1) |
| $\ \mathbf{X}\ _F$                 | Frobenius norm of a matrix $\mathbf{X}$ (see Definition D.2) |
| $\mu_{\text{ML}}(\cdot, \cdot)$    | Metric for maximum-likelihood detection                      |

### Mathematical Symbols

|           |   |
|-----------|---|
| $[, ]$    | Limits of a closed interval                   |
| $(, )$    | Limits of an open interval                    |
| $ \cdot $ | Magnitude of a number or cardinality of a set |
| !         | Factorial                                     |
| $\in$     | Element of                                    |
| $\infty$  | Infinity                                      |

### Mathematical Accents

|                 |                       |
|-----------------|-----------------------|
| $\bar{(\cdot)}$ | Average value or mean |
| $\hat{(\cdot)}$ | Hard decision         |



|                           |  |
|---------------------------|--|
| $\tilde{(\cdot)}$         | Hypothesis   |
| $\overleftarrow{(\cdot)}$ | Time reversed version of a sequence                        |
| $\cdot^{\bullet}$         | Solution of an optimization problem                        |
| $\check{(\cdot)}$         | Rayleigh component of a Rician distributed random variable |

## List of Variables

### General Variables

|                    |  |
|--------------------|--|
| $f$                | Frequency  |
| $\Lambda$          | Diagonal matrix containing eigenvalues                 |
| $\mu_{x,i}$        | $i$ th moment of $x$ (see Definition C.15)             |
| $\mu_{x,i}^{(c)}$  | $i$ th centralized moment of $x$ (see Definition C.16) |
| $\boldsymbol{\mu}$ | Lagrangian multipliers for inequality constraints      |
| $\boldsymbol{\nu}$ | Lagrangian multipliers for equality constraints        |
| $\mathbf{O}$       | Orthogonal matrix (see Definition D.5)                 |
| $\mathbf{Q}$       | Covariance matrix (see Definition D.13)                |
| $R$                | Radius   |
| $\mathbf{R}$       | Correlation matrix (see Definition D.13)               |
| $\rho_{x,y}$       | Correlation between $x$ and $y$ (see Definition C.18)  |
| $\sigma_x^2$       | Variance of $x$  |
| $\sigma_{x,y}^2$   | Covariance of $x$ and $y$ (see Definition C.18)        |
| $t$                | Absolute time  |
| $\tau$             | Relative propagation delay                             |
| $\mathbf{U}$       | Unitary matrix (see Definition D.7)                    |

### Variables Used for System Modeling

|                            |  |
|----------------------------|--|
| $a[k]$                     | Information symbols ( $Q$ -ary symbol alphabet)  |
| $B$                        | One-sided signal bandwidth   |
| $B_{\text{Rx}}$            | One-sided bandwidth of the analog receive filter   |
| $d$                        | Antenna spacing  |
| $D$                        | Distance between transmitter and receiver  |
| $\delta_{\mu}$             | Relative propagation delay associated with the $\mu$ th transmission link  |
| $\epsilon$                 | Sampling phase   |
| $f_c$                      | Carrier frequency  |
| $\Delta f$                 | Carrier frequency offset (CFO)   |
| $g(t)$                     | Overall impulse response of transmit and receive filtering   |
| $g_{\text{Rx}}(t)$         | Analog receive filter  |
| $g_{\text{Tx}}(t)$         | Analog pulse shaping filter  |
| $h_{\nu,\mu,l}[k]$         | Channel coefficients for the link from the $\mu$ th transmit antenna to the $\nu$ th receive antenna ( $l = 0, \dots, L$ ) |
| $\check{h}_{\nu,\mu,l}[k]$ | Rayleigh component of channel coefficient $h_{\nu,\mu,l}[k]$   |

|   |  |
|---|--|
| $h_{\nu,\mu}(\tau, t)$                    | Overall time-varying impulse response for the link from the $\mu$ th transmit antenna to the $\nu$ th receive antenna      |
| $\mathbf{h}_{\nu,\mu}[k]$                 | Channel coefficient vector   |
| $\mathbf{h}_{\text{SIMO}}[k]$             | Channel vector for a SIMO system   |
| $\mathbf{h}_{\text{MISO}}[k]$             | Channel vector for a MISO system   |
| $\mathbf{H}[k]$                           | Channel matrix for frequency-flat fading   |
| $\mathbf{H}_l[k]$                         | Channel matrix for frequency-selective fading ( $l = 0, \dots, L$ )  |
| $\mathbf{H}'[k]$                          | Spatially uncorrelated channel matrix  |
| $k$                                       | Discrete time index  |
| $L$                                       | Effective channel memory length  |
| $\lambda_c$                               | Carrier wavelength   |
| $\lambda_{\text{Rx},\nu}$                 | Eigenvalues of $\mathbf{R}_{\mathbf{h},\text{Rx}}$ ( $\nu = 1, \dots, N$ )   |
| $\lambda_{\text{Tx},\mu}$                 | Eigenvalues of $\mathbf{R}_{\mathbf{h},\text{Tx}}$ ( $\mu = 1, \dots, M$ )   |
| $\mathbf{\Lambda}_{\mathbf{h},\text{Rx}}$ | Eigenvalue matrix of $\mathbf{R}_{\mathbf{h},\text{Rx}}$   |
| $\mathbf{\Lambda}_{\mathbf{h},\text{Tx}}$ | Eigenvalue matrix of $\mathbf{R}_{\mathbf{h},\text{Tx}}$   |
| $M$                                       | Number of transmit antennas  |
| $M'$                                      | Number of virtual transmit antennas used by a transmit power weighting scheme  |
| $\mu$                                     | Transmit antenna index ( $\mu = 1, \dots, M$ )   |
| $n_\nu[k]$                                | $k$ th noise sample at the $\nu$ th receive antenna  |
| $n_\nu(t)$                                | Filtered noise at receive antenna $\nu$ (continuous time)  |
| $N$                                       | Number of receive antennas   |
| $N'$                                      | Number of virtual receive antennas used by a reduced-dimension receiver  |
| $N_0$                                     | Two-sided noise power density in the equivalent complex baseband   |
| $N_b$                                     | Block length   |
| $N_c$                                     | Number of carriers in a MIMO-OFDM system   |
| $N_i$                                     | Number of STBC code matrices per info block  |
| $\mathbf{n}[k]$                           | $k$ th noise vector  |
| $\mathbf{N}$                              | Matrix of $N_b$ subsequent noise vectors $\mathbf{n}[k]$   |
| $\nu$                                     | Receive antenna index ( $\nu = 1, \dots, N$ )  |
| $p$                                       | Path-loss exponent   |
| $p_t$                                     | Training block length  |
| $P$                                       | Overall average transmit power (per channel use)   |
| $P_{\text{LoS}}$                          | Line-of-sight probability  |
| $\mathbf{p}_{h_{\nu,\mu}}$                | Channel power profile for the link from the $\mu$ th transmit antenna to the $\nu$ th receive antenna (see Definition 2.1) |
| $\varpi$                                  | Normalized carrier frequency offset (CFO)  |
| $Q$                                       | Cardinality of the finite symbol alphabet  |
| $\mathbf{Q}_{\mathbf{h}}$                 | Overall covariance matrix of the channel coefficients (see Definition 2.2)   |
| $\mathbf{Q}_{\mathbf{x}}$                 | Covariance matrix of the transmitted vector $\mathbf{x}[k]$  |
| $r$                                       | Roll-off factor  |
| $r_\nu(t)$                                | Overall received signal at receive antenna $\nu$ (continuous time)   |

|  |  |
|--|--|
| $\mathbf{R}_{\mathbf{h}}$                | Overall correlation matrix of the channel coefficients<br>(see Definition 2.2)                 |
| $\mathbf{R}_{\mathbf{h},\text{Rx}}$      | Receive antenna correlation matrix (see Definition 2.3)  |
| $\mathbf{R}_{\mathbf{h},\text{Tx}}$      | Transmit antenna correlation matrix (see Definition 2.3)                                       |
| $\mathbf{R}_{n,\rho}$                    | Single-parameter antenna correlation matrix, see (3.39)  |
| $\rho_{h_{\nu,\mu,\nu'},\mu',l,l',k,k'}$ | Correlation between two channel coefficients $h_{\nu,\mu,l}[k]$ and $h_{\nu',\mu',l'}[k']$     |
| $\rho_{h_{\nu,\mu,\nu'},\mu',l,l'}$      | Correlation between $h_{\nu,\mu,l}[k]$ and $h_{\nu',\mu',l'}[k']$ in the quasi-static case     |
| $\rho_{h_{\nu,\mu,\nu'},\mu',l}$         | Spatial correlation between $h_{\nu,\mu,l}[k]$ and $h_{\nu',\mu',l}[k]$                        |
| $\rho_{h_{\mu,\mu'},l}$                  | Spatial correlation between $h_{\nu,\mu,l}[k]$ and $h_{\nu,\mu',l}[k]$                         |
| $\rho_{h_{\nu,\nu'},l}$                  | Spatial correlation between $h_{\nu,\mu,l}[k]$ and $h_{\nu',\mu,l}[k]$                         |
| $\rho_{h_{\nu,\mu,l,l'}}$                | Intertap correlation between $h_{\nu,\mu,l}[k]$ and $h_{\nu,\mu,l'}[k]$                        |
| $\rho_{h_{\nu,\mu,l,k,k'}}$              | Temporal correlation between $h_{\nu,\mu,l}[k]$ and $h_{\nu,\mu,l}[k']$                        |
| $\rho_{\text{Rx},\nu,\nu'}$              | Receive antenna correlation ( $= \rho_{h_{\nu,\nu'},l}$ )                                      |
| $\rho_{\text{Tx},\mu,\mu'}$              | Transmit antenna correlation ( $= \rho_{h_{\mu,\mu'},l}$ )                                     |
| $s_{\mu}(t)$                             | Signal transmitted via transmit antenna $\mu$ (continuous-time)                                |
| $\mathbf{S}$                             | Puncturing matrix representing a selection stage at the receiver                               |
| $\sigma_a^2$                             | Variance of information symbols  |
| $\sigma_{\text{dB}}^2$                   | Variance of average SNR in dB (log-normal shadowing)   |
| $\sigma_h^2$                             | Channel variance ( $= \sigma_{h_{\nu,\mu,l}}^2$ )  |
| $\sigma_{h_{\nu,\mu,l}}^2$               | Variance of channel coefficient $h_{\nu,\mu,l}[k]$   |
| $\sigma_{h_{\nu,\mu,\nu'},\mu'}$         | Covariance of channel coefficients $h_{\nu,\mu}[k]$ and $h_{\nu',\mu'}[k]$                     |
| $\sigma_n^2$                             | Noise variance (after receive filtering)   |
| $\sigma_{x,\mu}^2$                       | Variance of the $\mu$ th transmitted data symbol $x_{\mu}[k]$ ( $1 \leq \mu \leq M$ )          |
| $\Sigma_{\mathbf{h}}$                    | Weight matrix for the overall covariance matrix $\mathbf{Q}_{\mathbf{h}}$ (see Definition 2.2) |
| $\Sigma_{\mathbf{h},\text{Rx}}$          | Receiver covariance matrix (distributed receive antennas)                                      |
| $\Sigma_{\mathbf{h},\text{Tx}}$          | Transmitter covariance matrix (distributed transmit antennas)                                  |
| $T$                                      | Symbol duration  |
| $\mathbf{U}_{\text{Rx}}$                 | Eigenvector matrix of $\mathbf{R}_{\mathbf{h},\text{Rx}}$                                      |
| $\mathbf{U}_{\text{Tx}}$                 | Eigenvector matrix of $\mathbf{R}_{\mathbf{h},\text{Tx}}$                                      |
| $w_{\mu}$                                | Transmit power weight of the $\mu$ th transmit antenna   |
| $w_{\nu}(t)$                             | Additive white Gaussian noise at receive antenna $\nu$ (continuous time)                       |
| $\mathbf{W}$                             | Transmit power weighting matrix  |
| $x_{\mu}[k]$                             | $k$ th data symbol transmitted via the $\mu$ th transmit antenna                               |
| $\mathbf{x}[k]$                          | $k$ th transmitted vector  |
| $\mathbf{x}_t[k]$                        | Training vector  |
| $\mathbf{X}$                             | Matrix of $N_b$ subsequently transmitted vectors $\mathbf{x}[k]$                               |
| $\Xi_{\mathbf{h}}$                       | Weight matrix for the Kronecker correlation model  |
| $y_{\nu}[k]$                             | $k$ th received sample of the $\nu$ th receive antenna   |
| $y_{\nu}(t)$                             | Filtered received signal at receive antenna $\nu$ (continuous time)                            |
| $\mathbf{y}[k]$                          | $k$ th received vector   |
| $\mathbf{Y}$                             | Matrix of $N_b$ subsequently received vectors $\mathbf{y}[k]$                                  |
| $\Omega_{h_{\nu,\mu,l}}$                 | Average power of channel coefficient $h_{\nu,\mu,l}[k]$  |

### Variables Used for Channel Modeling

|                                      |  |
|--------------------------------------|--|
| $a_i$                                | Complex gain factor of the $i$ th propagation path   |
| $a_{s,i}$                            | Complex gain factor of the $s$ th scattered component of propagation path $i$  |
| $c_\tau$                             | Constant for an exponentially decaying power delay profile (PDP)   |
| $f_{D,\max}$                         | Maximum Doppler frequency  |
| $f_{\nu,\mu}(\tau_n, t)$             | Overall complex gain factor between transmit antenna $\mu$ and receive antenna $\nu$ associated with time delay $\tau_n$       |
| $K$                                  | Rice factor  |
| $\mathbf{k}_{a,i}$                   | Directional vector (direction of arrival, $i$ th propagation path)   |
| $\mathbf{k}_{d,i}$                   | Directional vector (direction of departure, $i$ th propagation path)   |
| $m$                                  | Nakagami-fading parameter  |
| $N_P$                                | Overall number of propagation paths  |
| $N_{P,n}$                            | Number of propagation paths associated with delay $\tau_n$   |
| $N_{S,i}$                            | Number of scattered components associated with the $i$ th propagation path   |
| $N_\tau$                             | Number of resolvable delays  |
| $P_{a_i}$                            | Average power of the $i$ th propagation path   |
| $p_{\vartheta_a}(\vartheta_a)$       | Angular PDF of transmitter-sided power azimuth spectrum (PAS)  |
| $p_{\vartheta_d}(\vartheta_d)$       | Angular PDF of receiver-sided power azimuth spectrum (PAS)   |
| $P_n(\vartheta_a)$                   | Receiver-sided power azimuth spectrum (see Definition F.2)   |
| $P_n(\vartheta_d)$                   | Transmitter-sided power azimuth spectrum (see Definition F.2)  |
| $\mathbf{p}_{f_{\nu,\mu}}$           | Power delay profile of the link between transmit antenna $\mu$ and receive antenna $\nu$ (see Definition F.1)                  |
| $r_{\nu,i}(t)$                       | Signal received at receive antenna $\nu$ via propagation path $i$  |
| $R_{f_{\nu,\mu,n}}(t', t)$           | Auto-correlation function of complex gain factor $f_{\nu,\mu}(\tau_n, t)$  |
| $R_{f_{\nu,\mu,n}}[k', k]$           | Discrete-time version of $R_{f_{\nu,\mu,n}}(t', t)$  |
| $\mathbf{r}_{Tx,\mu}$                | Position vector of the $\mu$ th transmit antenna element   |
| $\mathbf{r}_{Rx,\nu}$                | Position vector of the $\nu$ th receive antenna element  |
| $\rho_{f_{\nu,\mu},\nu',\mu',n}$     | Spatial correlation between gain factors $f_{\nu,\mu}(\tau_n, t)$ and $f_{\nu',\mu'}(\tau_n, t)$                               |
| $\rho_{f_{\mu,\mu'},n}$              | Spatial correlation between gain factors $f_{\nu,\mu}(\tau_n, t)$ and $f_{\nu,\mu'}(\tau_n, t)$ (transmit antenna correlation) |
| $\rho_{f_{\nu,\nu'},n}$              | Spatial correlation between gain factors $f_{\nu,\mu}(\tau_n, t)$ and $f_{\nu',\mu}(\tau_n, t)$ (receive antenna correlation)  |
| $\sigma_{f_{\nu,\mu,n}}^2$           | Variance of complex gain factor $f_{\nu,\mu}(\tau_n, t)$   |
| $\sigma_{f_{\nu,\mu,n,n'}}^2(t', t)$ | Covariance of complex gain factors $f_{\nu,\mu}(\tau_n, t)$ and $f_{\nu,\mu}(\tau_{n'}, t')$                                   |
| $\sigma_{f_{\nu,\mu,n,n'}}^2$        | Covariance of complex gain factors $f_{\nu,\mu}(\tau_n, t)$ and $f_{\nu,\mu}(\tau_{n'}, t)$                                    |
| $\sigma_{f_{\nu,\mu,\mu',\nu',n}}^2$ | Covariance of complex gain factors $f_{\nu,\mu}(\tau_n, t)$ and $f_{\nu',\mu'}(\tau_n, t)$                                     |
| $\tau_{c,i}$                         | Relative delay of the $i$ th propagation path  |
| $\tau_{\max}$                        | Maximum delay  |
| $\tau_n$                             | Resolvable, discrete delays ( $n = 0, \dots, N_\tau - 1$ )   |
| $\vartheta_{a,i}$                    | Angle of arrival of the $i$ th propagation path  |
| $\vartheta_{d,i}$                    | Angle of departure of the $i$ th propagation path  |

|  |   |
|--|---|
| $\varphi_{\text{Rx},\nu}(\vartheta_{a,i})$ | Phase offset of receive antenna $\nu$ with respect to receive antenna 1   |
| $\varphi_{\text{Tx},\mu}(\vartheta_{d,i})$ | Phase offset of transmit antenna $\mu$ with respect to transmit antenna 1 |

### Variables Used in the Context of Space-Time Coding

|                                 |  |
|---------------------------------|--|
| $\bar{\gamma}_b$                | Overall average received SNR per information bit                     |
| $\bar{\gamma}_s$                | Overall average received SNR per information symbol                  |
| $D$                             | Delay by one symbol duration   |
| $\Delta_{\text{DD}}$            | Delay employed by the delay diversity scheme (two transmit antennas) |
| $\eta[k]$                       | Noise sample after OSTBC decoding or maximum ratio combining         |
| $\boldsymbol{\eta}[k]$          | Noise vector after OSTBC decoding or maximum ratio combining         |
| $\mathbf{H}_{\text{eq},\nu}$    | Channel matrix in equivalent MIMO-system (OSTBC)                     |
| $\kappa$                        | Time index before the space-time encoder (information symbols)       |
| $L'$                            | Effective channel memory length resulting for delay diversity        |
| $\mathbf{n}_{\text{eq},\nu}[k]$ | Noise vector in equivalent MIMO-system (OSTBC)                       |
| $p$                             | Number of time indices associated with a single STBC code-matrix     |
| $p_i$                           | Number of information symbols mapped onto STBC code-matrix           |
| $P_{\text{ov}}$                 | Overall average transmit power per code matrix                       |
| $R_t$                           | Temporal rate of an STBC   |
| $\mathcal{S}$                   | Space-time mapping (STBC)  |
| $\mathbf{X}[k]$                 | Code matrix of an STBC   |
| $\mathbf{y}_{\text{eq},\nu}[k]$ | Received vector in equivalent MIMO-system (OSTBC)                    |
| $\boldsymbol{\Psi}_\nu[k]$      | Matrix reflecting the orthogonality loss of Alamouti's scheme        |
| $z[k]$                          | Received sample after OSTBC decoding or maximum ratio combining      |
| $\mathbf{z}[k]$                 | Received vector after OSTBC decoding or maximum ratio combining      |
| $\mathbf{z}_{\text{MMSE}}[k]$   | Received vector after linear MMSE receiver                           |
| $\mathbf{z}_{\text{ZF}}[k]$     | Received vector after linear ZF receiver                             |

### Variables Used in the Context of Cooperative Networks

|       |   |
|-------|---|
| $M_i$ | Number of transmit antennas at the $i$ th cooperating transmitting node |
| $N_j$ | Number of receive antennas at the $j$ th cooperating receiving node     |
| $R_n$ | Number of cooperating receiving nodes                                   |
| $T_n$ | Number of cooperating transmitting nodes                                |

### Variables Used in the Context of Channel Capacity

|                                |   |
|--------------------------------|---|
| $\bar{C}$                      | Ergodic capacity  |
| $C(\mathbf{H})$                | Instantaneous capacity of a MIMO channel (channel matrix $\mathbf{H}$ )             |
| $C_{\text{OSTBC}}(\mathbf{h})$ | Instantaneous capacity of an OSTBC system (equivalent channel vector $\mathbf{h}$ ) |
| $h(\cdot)$                     | Differential entropy (see Definition C.20)  |
| $H(\cdot)$                     | Entropy (see Definition C.19)   |
| $I(\cdot; \cdot)$              | Mutual information  |
| $\tilde{M}$                    | Minimum of $M$ and $N$  |
| $\tilde{N}$                    | Maximum of $M$ and $N$  |

$\Theta$  Waterlevel

### Variables Used for Error Performance Analysis

|   |   |
|---|---|
| $\mathbf{a}$                            | Sequence of information symbols   |
| $d$                                     | Diversity order   |
| $d_E^2(\boldsymbol{\epsilon})$          | Squared Euclidean distance associated with error sequence $\boldsymbol{\epsilon}$   |
| $d_H(\boldsymbol{\epsilon})$            | Hamming distance associated with error sequence $\boldsymbol{\epsilon}$   |
| $\Delta(\mathbf{R}_h)$                  | Performance measure for co-located/distributed MIMO systems   |
| $\epsilon[k]$                           | Error symbol used for evaluating the performance of MLSE  |
| $\varepsilon_{\nu,\mu}[k]$              | Channel estimation error (channel coefficient $h_{\nu,\mu}[k]$ )  |
| $\boldsymbol{\epsilon}$                 | Error sequence used for evaluating the performance of MLSE  |
| $g$                                     | Specific parameter depending on the employed signal constellation (equal to $g_{\text{PSK}}$ , $g_{\text{ASK}}$ , or $g_{\text{QAM}}$ , cf. (I.23), (I.25), (I.27) in Appendix I) |
| $\mathbf{h}'$                           | Decorrelated channel vector (maximum-ratio-combining system)  |
| $\mathbf{n}'[k]$                        | Noise vector after decorrelation (maximum-ratio-combining system)   |
| $\Lambda_k(D, E, J)$                    | Symbolic branch label used for evaluating the performance of MLSE   |
| $P(\mathbf{a} \rightarrow \mathbf{a}')$ | Pairwise error probability of MLSE  |
| $P(\mathbf{X} \rightarrow \mathbf{E})$  | Pairwise error probability for a general STC  |
| $\bar{P}_b$                             | Average bit error probability   |
| $\bar{P}_s$                             | Average symbol error probability  |
| $P_S(D, E, J)$                          | Symbolic polynomial used for evaluating the performance of MLSE   |
| $\Pr\{\mathcal{E}_{\text{error},k_0}\}$ | Error event probability   |
| $S$                                     | Error path length in terms of trellis segments  |
| $\mathbf{T}(D, E, J)$                   | State transition matrix used for evaluating the performance of MLSE   |
| $\Xi_{\text{Rx}}$                       | Matrix reflecting the impact of estimation errors concerning the receiver correlation matrix $\mathbf{R}_{h,\text{Rx}}$ (reduced-dimension receiver)                              |
| $\Xi_{\text{Tx}}$                       | Matrix reflecting the impact of estimation errors concerning the transmitter correlation matrix $\mathbf{R}_{h,\text{Tx}}$ (statistical transmit power allocation)                |
| $\mathbf{y}'[k]$                        | Decorrelated received vector (maximum-ratio-combining system)   |
| $\Psi_{\mathbf{X},\mathbf{E}}$          | Difference matrix for code matrices $\mathbf{X}$ and $\mathbf{E}$   |

### Variables Used in the Context of Trellis-Based Equalization

|                      |   |
|----------------------|---|
| $\Gamma_b[k]$        | Metric increment for the trellis-based equalizer (branch $b$ )  |
| $L_{\text{eq}}$      | Memory length of the trellis-based equalizer  |
| $\psi_{\text{susp}}$ | Fraction of the overall channel variance discarded by a trellis-based equalizer with finite memory length $L_{\text{eq}}$ |

# Appendix C

## Mathematical Definitions

Please, refer to Appendix B for conventions and notations employed in the following.

### C.1 Special Functions

#### Definition C.1 (Cosine roll-off impulse)

A *cosine roll-off impulse*  $g(t)$  has the following impulse response [Pro01, Ch. 9.2]:

$$g(t) := \frac{\sin(\pi t/T)}{\pi t/T} \frac{\cos(\pi r t/T)}{1 - (2r t/T)^2}, \quad (\text{C.1})$$

where  $T$  denotes the symbol duration and  $r \in [0, 1]$  the *roll-off factor*. The cosine roll-off impulse is depicted in Fig. C.1 for different roll-off factors  $r$ . The corresponding transfer function  $G(f)$  is given by

$$G(f) = \begin{cases} T & \text{for } |f| \leq \frac{1-r}{2T} \\ \frac{T}{2} \left[ 1 + \cos \left( \frac{\pi T}{r} \left( |f| - \frac{1-r}{2T} \right) \right) \right] & \text{for } \frac{1-r}{2T} \leq |f| \leq \frac{1+r}{2T} \\ 0 & \text{for } \frac{1+r}{2T} \leq |f| \end{cases} . \quad (\text{C.2})$$

In the case  $r=0$ , an ideal low-pass filter results. •

#### Definition C.2 (Gaussian Q-function)

The *Gaussian Q-function* is traditionally defined as [AG99, SA00]

$$Q(x) := \frac{1}{\sqrt{2\pi}} \int_x^\infty e^{-t^2/2} dt. \quad (\text{C.3})$$

An alternative representation for  $x \geq 0$ , which is of particular interest in this thesis, was proposed in [Cra91]:

$$Q(x) = \frac{1}{\pi} \int_0^{\pi/2} \exp \left( -\frac{x^2}{2 \sin^2 \phi} \right) d\phi \quad (x \geq 0). \quad (\text{C.4})$$



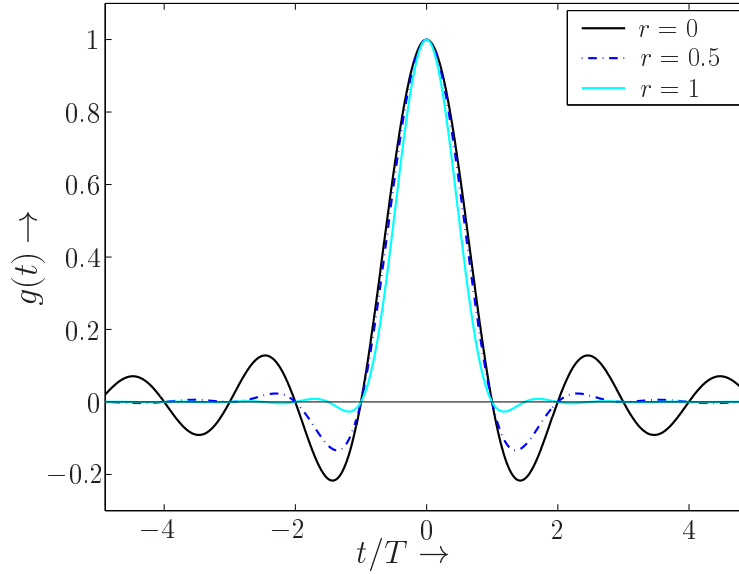


Figure C.1: Cosine roll-off impulse for different roll-off factors  $r$ .

The Gaussian Q-function is closely related to the *complementary error function*:

$$Q(x) = \frac{1}{2} \operatorname{erfc} \left( \frac{x}{\sqrt{2}} \right). \quad (\text{C.5})$$

Special functional characteristics of the Gaussian Q-function are

$$Q(-\infty) = 1, \quad Q(0) = 0.5, \quad \text{and} \quad Q(+\infty) = 0. \quad (\text{C.6})$$

Moreover, we have  $Q(-x) = 1 - Q(x)$  for all  $x \in \mathbb{R}$ . •

### Definition C.3 (Gamma function)

The *Gamma function* is defined as [BS91, p. 103]

$$\Gamma(x) := \int_0^{\infty} \xi^{x-1} e^{-\xi} d\xi \quad (x \in \mathbb{R}_{>0}). \quad (\text{C.7})$$

Special functional characteristics are

$$\Gamma(0.5) = \sqrt{\pi} \quad \text{and} \quad \Gamma(1) = 1. \quad (\text{C.8})$$

Moreover, if  $x$  is a natural number  $\Gamma(x+1) = x!$  holds. •

### Definition C.4 (Bessel function of the first kind)

The *Bessel function of the first kind and order  $n$*  is defined as follows [BS91, p. 441]:

$$J_n(x) := \sum_{\nu=0}^{\infty} \frac{(-1)^{\nu}}{\nu! \Gamma(n+\nu+1)} \left( \frac{x}{2} \right)^{n+2\nu} \quad (x \in \mathbb{R}), \quad (\text{C.9})$$

where  $\Gamma(\cdot)$  denotes the Gamma function (cf. Definition C.3). There are many alternative representations of  $J_n(\cdot)$ . The following integral representation is of special interest in this thesis:

$$J_n(x) := \frac{1}{2\pi j^n} \int_0^{2\pi} e^{jn\xi} e^{jx \cos(\xi)} d\xi. \quad (\text{C.10})$$

A special functional characteristic of  $J_0(\cdot)$  is  $J_0(0) = 1$ . •

**Definition C.5 (Modified Bessel function of the first kind)**

The *modified Bessel function of the first kind and order  $n$*  is defined as [BS91, p. 441]

$$I_n(x) := \frac{J_n(jx)}{j^n} \quad (x \in \mathbb{R}), \quad (\text{C.11})$$

where  $J_n(\cdot)$  is the Bessel function of the first kind and order  $n$  (see Definition C.4). •

## C.2 Important Statistical Distributions

**Definition C.6 (Uniform distribution)**

A random variable  $\underline{x}$  with probability density function (PDF)

$$p_{\underline{x}}(x) = \begin{cases} 1/|b-a| & \text{for } x \in [a, b] \\ 0 & \text{else} \end{cases} \quad (\text{C.12})$$

is called *uniformly distributed* on the interval  $[a, b]$  ( $x \sim \mathcal{U}([a, b])$ ). •

**Definition C.7 (Gaussian distribution)**

The PDF of a real-valued, *Gaussian* (or *normal*) *distributed* random variable  $\underline{x}$  with mean  $\bar{x} := \mathbb{E}\{x\}$  and variance  $\sigma_x^2 := \mathbb{E}\{(x - \bar{x})^2\}$  ( $x \sim \mathcal{N}(\bar{x}, \sigma_x^2)$ ) is given by [BS91, p. 664]

$$p_{\underline{x}}(x) := \frac{1}{\sqrt{2\pi\sigma_x^2}} \exp\left(-\frac{(x - \bar{x})^2}{2\sigma_x^2}\right). \quad (\text{C.13})$$

The Gaussian distribution is fully characterized by the first moment  $\mu_{x,1} = \bar{x}$  and the second central moment  $\mu_{x,2}^{(c)} = \sigma_x^2$ , cf. Definitions C.15 and C.16. •

**Definition C.8 (Laplacian distribution)**

A real-valued random variable  $\underline{x}$  with mean  $\bar{x} := \mathbb{E}\{x\}$ , variance  $\sigma_x^2 := \mathbb{E}\{(x - \bar{x})^2\}$ , and PDF

$$p_{\underline{x}}(x) := \frac{1}{\sqrt{2\sigma_x^2}} \exp\left(-\frac{|x - \bar{x}|}{\sqrt{\sigma_x^2/2}}\right) \quad (\text{C.14})$$

is called *Laplacian distributed* ( $x \sim \mathcal{L}(\bar{x}, \sigma_x^2)$ ) [PMF00]. The Laplace distribution is, for example, used to model the power azimuth spectrum (PAS) observed at a base station in a typical urban scenario. The Laplace distribution is illustrated in Fig. C.2, for the case  $\bar{x} = 0$  and  $\sigma_x^2 = 1$ . For comparison, the Gaussian distribution has also been included. •

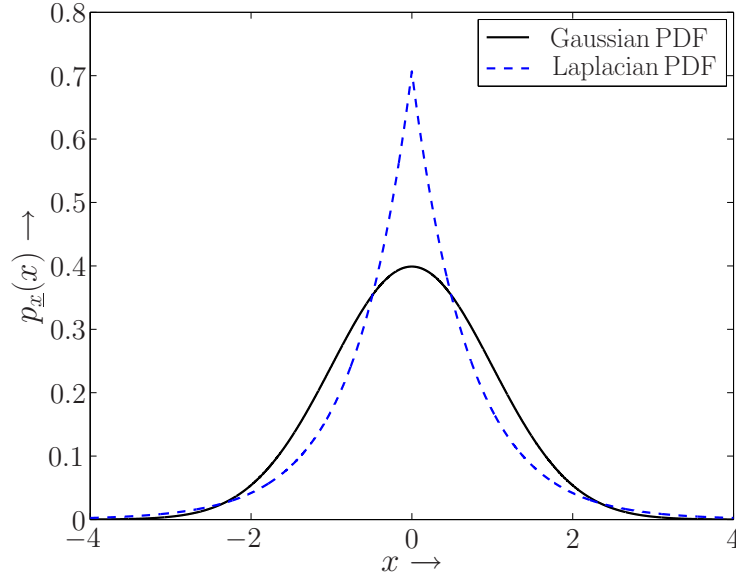


Figure C.2: Gaussian and Laplacian PDF ( $\bar{x}=0$  and  $\sigma_x^2=1$  in both cases).

**Definition C.9 (Circularly symmetric complex Gaussian distribution)**

The PDF of a complex-valued, *circularly symmetric Gaussian distributed* random variable  $\underline{x} = \underline{x}_i + j\underline{x}_q$  with mean  $\bar{x} := \mathbb{E}\{x\} = \bar{x}_i + j\bar{x}_q$  and variance  $\sigma_x^2 := \mathbb{E}\{|x - \bar{x}|^2\}$  ( $x \sim \mathcal{CN}(\bar{x}, \sigma_x^2)$ ) is given by [Kam96, p. 707]

$$p_{\underline{x}}(x) := \frac{1}{\pi\sigma_x^2} \exp\left(-\frac{|x - \bar{x}|^2}{\sigma_x^2}\right). \quad (\text{C.15})$$

For the quadrature components of  $\underline{x}$  the following holds:

$$x_i \sim \mathcal{N}(\bar{x}_i, \sigma_x^2/2), \quad x_q \sim \mathcal{N}(\bar{x}_q, \sigma_x^2/2), \quad \text{and} \quad \mathbb{E}\{x_i x_q^*\} = 0. \quad (\text{C.16})$$

and  $\mathbb{E}\{(x_i - \bar{x}_i)(x_q - \bar{x}_q)^*\} = 0$ . •

**Remark C.1 (Application examples)**

The zero-mean complex Gaussian distribution is commonly used to model complex additive white Gaussian noise (AWGN) or the random channel coefficients  $h[k]$  of a rich-scattering fading channel without line-of-sight (LoS) component (Rayleigh fading). A rich-scattering fading channel with LoS component is usually modeled by a complex Gaussian distribution with mean  $\bar{x} \neq 0$  (Rician fading).

**Definition C.10 (Multivariate complex Gaussian distribution)**

The joint PDF of a random vector  $\underline{\mathbf{x}} \in \mathbb{C}^m$  with entries  $x_\mu \sim \mathcal{CN}(\bar{x}_\mu, \sigma_{x_\mu}^2)$ ,  $\mu = 1, \dots, m$ , and covariance matrix  $\mathbf{Q}_{\underline{\mathbf{x}}}$  (cf. Definition D.13) is given by<sup>1</sup> [BT04a, p. 113]

$$p_{\underline{\mathbf{x}}}(\mathbf{x}) = \frac{1}{\pi^m \det(\mathbf{Q}_{\underline{\mathbf{x}}})} \exp\left(-(\mathbf{x} - \bar{\mathbf{x}})^H \mathbf{Q}_{\underline{\mathbf{x}}}^{-1} (\mathbf{x} - \bar{\mathbf{x}})\right), \quad (\text{C.17})$$

where  $\bar{\mathbf{x}} := [\bar{x}_1, \dots, \bar{x}_m]^T$ . As a short-hand notation, we write  $\mathbf{x} \sim \mathcal{CN}(\bar{\mathbf{x}}, \mathbf{Q}_{\underline{\mathbf{x}}})$ . •

<sup>1</sup>It is assumed that the covariance matrix  $\mathbf{Q}_{\underline{\mathbf{x}}}$  has full rank so that the inverse  $\mathbf{Q}_{\underline{\mathbf{x}}}^{-1}$  exists.

**Definition C.11 (Rayleigh distribution)**

The magnitude  $\underline{\alpha} = |\underline{x}|$  of a zero-mean complex Gaussian random variable  $\underline{x}$  with variance  $\sigma_x^2$ , ( $x \sim \mathcal{CN}(0, \sigma_x^2)$ ), is *Rayleigh distributed* with PDF [SA00, p. 18]

$$p_{\underline{\alpha}}(\alpha) = \frac{2\alpha}{\Omega_{\alpha}} \exp\left(-\frac{\alpha^2}{\Omega_{\alpha}}\right) \quad (\alpha \geq 0), \quad (\text{C.18})$$

where  $\Omega_{\alpha} := \mathbf{E}\{\alpha^2\} = \sigma_x^2$ . The Rayleigh distribution describes the random channel amplitude  $\alpha[k] := |h[k]|$  of a rich-scattering flat-fading channel without LoS component, while the phase of  $h[k]$  is uniformly distributed in  $[0, 2\pi)$ . The PDF of the corresponding instantaneous SNR  $\gamma := c\alpha^2$  ( $c$  constant) is given by

$$p_{\underline{\gamma}}(\gamma) = \frac{1}{\bar{\gamma}} \exp\left(-\frac{\gamma}{\bar{\gamma}}\right) \quad (\gamma \geq 0), \quad (\text{C.19})$$

where  $\bar{\gamma} := \mathbf{E}\{\gamma\} = c\Omega_{\alpha}$  denotes the average SNR. The PDF  $p_{\underline{\gamma}}(\gamma)$  is displayed in Fig. C.3 for the example  $\bar{\gamma} = 1$  (see case  $K = 0$ ). •

**Definition C.12 (Rician distribution)**

The magnitude  $\underline{\alpha} = |\underline{x}|$  of a complex Gaussian random variable  $\underline{x}$  with mean  $\bar{x}$  and variance  $\sigma_x^2$  ( $x \sim \mathcal{CN}(\bar{x}, \sigma_x^2)$ ) is *Rician distributed* [Ric48] with PDF [SA00, p. 21]

$$p_{\underline{\alpha}}(\alpha) = \frac{2\alpha(1+K)}{\Omega_{\alpha}} \exp\left(-K - \frac{\alpha^2(1+K)}{\Omega_{\alpha}}\right) \text{I}_0\left(2\alpha\sqrt{\frac{K(1+K)}{\Omega_{\alpha}}}\right) \quad (\text{C.20a})$$

$$= \frac{2\alpha}{\sigma_x^2} \exp\left(-\frac{\alpha^2 + |\bar{x}|^2}{\sigma_x^2}\right) \text{I}_0\left(\frac{2\alpha|\bar{x}|}{\sigma_x^2}\right) \quad (\alpha \geq 0), \quad (\text{C.20b})$$

where  $\Omega_{\alpha} := \mathbf{E}\{\alpha^2\} = |\bar{x}|^2 + \sigma_x^2$ . Moreover,  $K := |\bar{x}|^2/\sigma_x^2$  denotes the Rice factor and  $\text{I}_0(x)$  the modified Bessel function of the first kind and order zero (cf. Definition C.5). The Rician distribution describes the random channel amplitude  $\alpha[k] := |h[k]|$  of a rich-scattering flat-fading channel with LoS component. The Rice factor  $K$  is given by the ratio between LoS signal power and average power of the scattered components ( $K \in [0, \infty)$ ). The special case  $K = 0$  corresponds to a Rayleigh-fading channel model (cf. Definition C.11), and the case  $K \rightarrow \infty$  to a non-fading AWGN channel model. The PDF of the corresponding instantaneous SNR  $\gamma := c\alpha^2$  ( $c$  constant) is generally given by

$$p_{\underline{\gamma}}(\gamma) = \frac{1+K}{\bar{\gamma}} \exp\left(-K - \frac{\gamma(1+K)}{\bar{\gamma}}\right) \text{I}_0\left(2\sqrt{\frac{\gamma K(1+K)}{\bar{\gamma}}}\right) \quad (\text{C.21a})$$

$$= \frac{1}{c\sigma_x^2} \exp\left(-\frac{\gamma + c|\bar{x}|^2}{c\sigma_x^2}\right) \text{I}_0\left(\frac{2|\bar{x}|}{\sigma_x^2} \sqrt{\frac{\gamma}{c}}\right) \quad (\gamma \geq 0), \quad (\text{C.21b})$$

where  $\bar{\gamma} := \mathbf{E}\{\gamma\} = c\Omega_{\alpha}$  denotes the average SNR. As an example, the PDF  $p_{\underline{\gamma}}(\gamma)$  is displayed in Fig. C.3, for the example  $\bar{\gamma} = 1$  and different Rice factors  $K$ . •

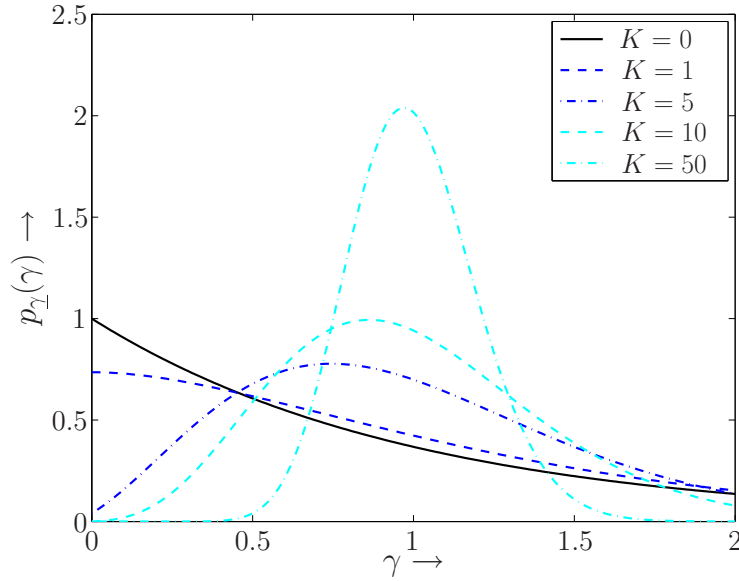


Figure C.3: PDF  $p_\gamma(\gamma)$  of the instantaneous SNR  $\gamma$  in the case of Rayleigh fading ( $K=0$ ) and Rice fading (different Rice factors  $K$ ) for the example  $\bar{\gamma}=1$ .

**Definition C.13 (Nakagami- $m$  distribution)**

The *Nakagami- $m$  distribution* is given by [SA00, p. 22]

$$p_\alpha(\alpha) = \frac{2m^m \alpha^{2m-1}}{\Omega_\alpha^m \Gamma(m)} \exp\left(-\frac{m\alpha^2}{\Omega_\alpha}\right) \quad (\alpha \in \mathbb{R}_{\geq 0}), \quad (\text{C.22})$$

where  $\Omega_\alpha := \mathbf{E}\{\alpha^2\}$ . Moreover,  $m \in [0.5, \infty)$  denotes the Nakagami-fading parameter, and  $\Gamma(x)$  the Gamma function (cf. Definition C.3). The Nakagami- $m$  distribution can be seen as a generalization of the Rayleigh distribution (C.18) and describes the random channel amplitude  $\alpha[k] := |h[k]|$  of a rich-scattering flat-fading channel without LoS component. The phase of  $h[k]$  is uniformly distributed in  $[0, 2\pi)$ . For the special case  $m=1$ , the Nakagami- $m$  distribution and the Rayleigh distribution are identical. Values  $m \neq 1$  either model more severe fading ( $m < 1$ ) or milder fading conditions ( $m > 1$ ) than in the Rayleigh case. The most severe fading results for  $m=0.5$ , where the PDF (C.22) becomes a one-sided Gaussian distribution. The other extreme,  $m \rightarrow \infty$ , corresponds to a non-fading AWGN channel model (similar to the Rician fading model with  $K \rightarrow \infty$ , cf. Definition C.12). Moreover, for  $m \gg 1$  the Nakagami- $m$  distribution is well approximated by a Rician distribution with Rice factor [SA00, p. 23]

$$K := \frac{\sqrt{m^2 - m}}{m - \sqrt{m^2 - m}}, \quad (\text{C.23})$$

cf. (C.20a). Vice versa, for  $K \gg 0$  the Rician distribution is well approximated by a Nakagami- $m$  distribution with

$$m := \frac{(1+K)^2}{1+2K}. \quad (\text{C.24})$$

For an arbitrary fading parameter  $m$ , the PDF of the corresponding instantaneous SNR  $\gamma := c\alpha^2$  ( $c$  constant) is given by

$$p_{\underline{\gamma}}(\gamma) = \frac{m^m \gamma^{m-1}}{\bar{\gamma}^m \Gamma(m)} \exp\left(-\frac{m\gamma}{\bar{\gamma}}\right) \quad (\gamma \geq 0), \quad (\text{C.25})$$

where  $\bar{\gamma} := \mathbb{E}\{\gamma\} = c\Omega_\alpha$  denotes the average SNR. The PDF  $p_{\underline{\gamma}}(\gamma)$  is displayed in Fig. C.4, for the example  $\bar{\gamma} = 1$  and different values of the fading parameter  $m$ . As an example, the PDF for  $m = 10$  has been approximated using a Rician distribution with a Rice factor according to (C.23). As can be seen, the approximation fits quite well. •

#### Definition C.14 (Log-normal distribution)

A random variable  $\underline{x}$  is called *log-normal distributed* if  $\underline{x}_{\text{dB}} := 10 \log_{10} \underline{x}$  dB is Gaussian distributed (cf. Definition C.7). Let  $\bar{x}_{\text{dB}}$  and  $\sigma_{x_{\text{dB}}}^2$  denote the mean and the variance of  $\underline{x}_{\text{dB}}$ , i.e.,  $x_{\text{dB}} \sim \mathcal{N}(\bar{x}_{\text{dB}}, \sigma_{x_{\text{dB}}}^2)$ . Then, the PDF of  $\underline{x}$  can be expressed as [SA00, p. 24]

$$p_{\underline{x}}(x) = \frac{10}{\sqrt{2\pi\sigma_{x_{\text{dB}}}^2} \ln 10} \frac{1}{x} \exp\left(-\frac{(10 \log_{10} x - \bar{x}_{\text{dB}})^2}{2\sigma_{x_{\text{dB}}}^2}\right). \quad (\text{C.26})$$

The log-normal distribution is often used to model macroscopic fading due to shadowing effects [Stu96, Ch. 2.4], where the average SNR  $\bar{\gamma}_{\text{dB}} := 10 \log_{10} \bar{\gamma}$  in dB (averaged over a medium time scale) is assumed to be Gaussian distributed (i.e.,  $\underline{x} := \bar{\gamma}$  in the above PDF, while  $\bar{\gamma}$  denotes the average SNR on a linear scale). In order to combine log-normal shadowing with Rayleigh-, Rice-, or Nakagami- $m$  fading (cf. Definitions C.11 to C.13), the PDF of the instantaneous SNR,  $p_{\underline{\gamma}}(\gamma)$ , is conditioned on the average SNR  $\bar{\gamma}$  ( $\rightarrow p_{\underline{\gamma}|\bar{\gamma}}(\gamma|\bar{\gamma})$ ) and is then averaged over the log-normal PDF  $p_{\bar{\gamma}}(\bar{\gamma})$  [HS93]. This yields the (new) PDF of the instantaneous SNR within the composite fading model:

$$p_{\underline{\gamma}}(\gamma) = \int_0^\infty p_{\underline{\gamma}|\bar{\gamma}}(\gamma|\bar{\gamma}) p_{\bar{\gamma}}(\bar{\gamma}) d\bar{\gamma}. \quad (\text{C.27})$$

As an example, the PDF  $p_{\underline{\gamma}}(\gamma)$  is displayed in Fig. C.5, for composite Nakagami- $m$  fading/log-normal shadowing with different values of the fading parameter  $m$  and the variance  $\sigma_{x_{\text{dB}}}^2$  ( $\mathbb{E}\{\bar{\gamma}\} = 1$ ). •

## C.3 Moments of a Statistical Distribution

#### Definition C.15 (Moments of a one-dimensional distribution)

The  $i$ th *moment* of a random variable  $\underline{x}$  with PDF  $p_{\underline{x}}(x)$  is defined as [BS91, p. 667]

$$\mu_{x,i} := \mathbb{E}\{x^i\} = \int_{-\infty}^{+\infty} x^i p_{\underline{x}}(x) dx. \quad (\text{C.28})$$

The mean of  $\underline{x}$  is given by the first moment, i.e.,  $\bar{x} := \mu_{x,1}$ . •

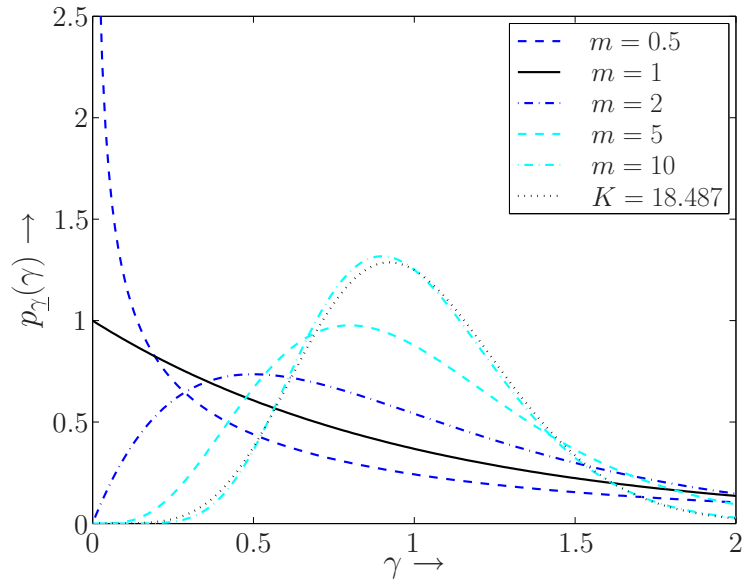


Figure C.4: PDF  $p_{\bar{\gamma}}(\gamma)$  of the instantaneous SNR  $\gamma$  in the case of Nakagami- $m$  fading, for the example  $\bar{\gamma}=1$  and different values of the fading parameter  $m$  (the case  $m=1$  corresponds to Rayleigh fading). For comparison, the PDF resulting for Rician fading with  $K=18.487$  has also been included.

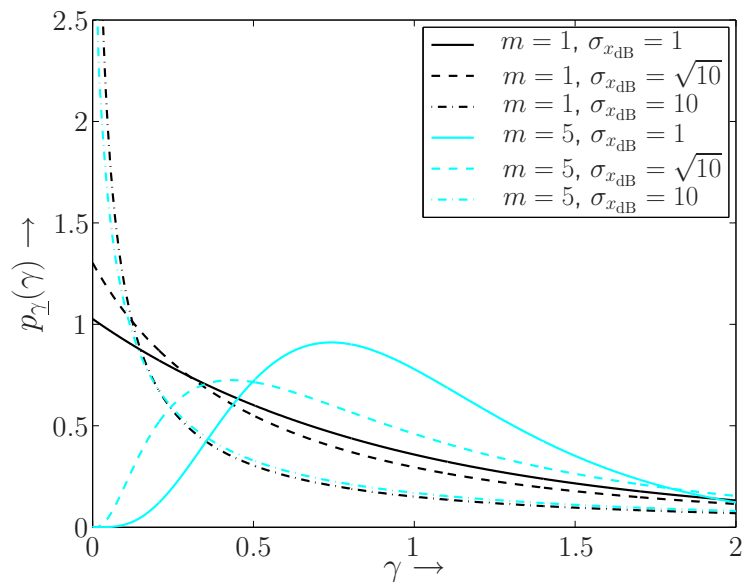


Figure C.5: PDF  $p_{\bar{\gamma}}(\gamma)$  of the instantaneous SNR  $\gamma$  in the case of composite Nakagami- $m$  fading/log-normal shadowing, for the example  $\mathbb{E}\{\bar{\gamma}\}=1$  and different values of the fading parameter  $m$  and the variance  $\sigma_{x_{\text{dB}}}^2$ .



**Definition C.16 (Central moments of a one-dimensional distribution)**

The  $i$ th *central moment* of a random variable  $\underline{x}$  with PDF  $p_{\underline{x}}(x)$  is defined as [BS91, p. 667]

$$\mu_{x,i}^{(c)} := \mathbf{E}\{(x - \bar{x})^i\} = \int_{-\infty}^{+\infty} (x - \bar{x})^i p_{\underline{x}}(x) dx. \quad (\text{C.29})$$

The variance of  $\underline{x}$  is given by the second central moment, i.e.,  $\sigma_x^2 := \mu_{x,2}^{(c)}$ . •

**Definition C.17 (Moment-generating function, characteristic function)**

The *moment-generating function (MGF)* of a random variable  $\underline{x}$  with PDF  $p_{\underline{x}}(x)$  is defined as [SA00, p. 4]

$$\mathbf{M}\{x\}(s) := \mathbf{E}\{e^{sx}\} = \int_{-\infty}^{+\infty} e^{sx} p_{\underline{x}}(x) dx \quad (\text{C.30})$$

(provided that the integral exists). The MGF corresponds to the Laplace transform of the PDF of  $\underline{x}$ , evaluated at  $-s$ , i.e.

$$\mathbf{M}\{x\}(s) = \mathbf{L}\{p_{\underline{x}}(x)\}(-s). \quad (\text{C.31})$$

The name of the MGF comes from the fact that a series expansion of  $\mathbf{M}\{x\}(s)$  yields all (non-central) moments of  $\underline{x}$ :

$$\mathbf{M}\{x\}(s) = \mathbf{E}\left\{\sum_{i=0}^{\infty} \frac{(sx)^i}{i!}\right\} = \sum_{i=0}^{\infty} \frac{s^i}{i!} \cdot \mu_{x,i}, \quad (\text{C.32})$$

cf. Definition C.15. For many statistical distributions, closed-form expressions are known for the corresponding MGF. Table C.1 states some examples that are of further interest in this thesis [AG99, SA00]. In this case, the moments  $\mu_{x,i}$  may be calculated analytically, according to

$$\mu_{x,i} = i! \cdot \left. \frac{\partial}{\partial s^i} \mathbf{M}\{x\}(s) \right|_{s=0}. \quad (\text{C.33})$$

Some authors prefer to use the so-called *characteristic function (CF)*, which is defined in a very similar fashion as the MGF [Pro01, Ch. 2.1.3]:

$$\mathbf{C}\{x\}(j\omega) := \mathbf{E}\{e^{j\omega x}\} = \int_{-\infty}^{+\infty} e^{j\omega x} p_{\underline{x}}(x) dx \quad (\text{C.34})$$

(provided that the integral exists). The CF corresponds to the Fourier transform of the PDF of  $\underline{x}$ , evaluated at  $-j\omega$ , i.e.

$$\mathbf{C}\{x\}(j\omega) = \mathbf{F}\{p_{\underline{x}}(x)\}(-j\omega). \quad (\text{C.35})$$

Specifically, we have  $\mathbf{C}\{x\}(j\omega) = \mathbf{M}\{x\}(s = j\omega)$ , provided that the imaginary axis lies within the convergence area of the MGF. Similar to (C.33), the  $i$ th moment of  $\underline{x}$  can be calculated as

$$\mu_{x,i} = \frac{i!}{j^i} \cdot \left. \frac{\partial}{\partial \omega^i} \mathbf{C}\{x\}(j\omega) \right|_{\omega=0}. \quad (\text{C.36})$$

•

| PDF   | Eq.     | Corresponding MGF  |
|---|---------|--|
| Gaussian distribution $p_{\underline{x}}(x)$            | (C.13)  | $M\{x\}(s) = \exp(s\bar{x}) \exp\left(\frac{s^2\sigma_x^2}{2}\right)$                                      |
| $p_{\underline{\gamma}}(\gamma)$ , Rayleigh fading      | (C.19)  | $M\{\gamma\}(s) = \frac{1}{1-s\bar{\gamma}}$   |
| $p_{\underline{\gamma}}(\gamma)$ , Rice fading          | (C.21a) | $M\{\gamma\}(s) = \frac{1+K}{1+K-s\bar{\gamma}} \exp\left(\frac{Ks\bar{\gamma}}{1+K-s\bar{\gamma}}\right)$ |
| $p_{\underline{\gamma}}(\gamma)$ , Nakagami- $m$ fading | (C.25)  | $M\{\gamma\}(s) = \left(\frac{m}{m-s\bar{\gamma}}\right)^m$  |

Table C.1: Some important PDFs with closed-form MGFs.

**Definition C.18 (Covariance and correlation)**

Let  $\underline{x}$  and  $\underline{y}$  be two random variables with joint PDF  $p_{\underline{x},\underline{y}}(x, y)$ . The *covariance* of  $x$  and  $y$  is defined as

$$\sigma_{x,y}^2 := \mathbf{E}\{(x-\bar{x})(y-\bar{y})^*\} = \int_{-\infty}^{+\infty} \int_{-\infty}^{+\infty} (x-\bar{x})(y-\bar{y})^* p_{\underline{x},\underline{y}}(x, y) dx dy. \quad (\text{C.37})$$

The *correlation* between  $x$  and  $y$  is defined as

$$\rho_{x,y} := \frac{\sigma_{x,y}^2}{\sqrt{\sigma_x^2\sigma_y^2}}, \quad (\text{C.38})$$

where  $\sigma_x^2 := \mathbf{E}\{|x-\bar{x}|^2\}$  and  $\sigma_y^2 := \mathbf{E}\{|y-\bar{y}|^2\}$ . If  $\underline{x}$  and  $\underline{y}$  are complex random variables, the covariance  $\sigma_{x,y}^2$  and the correlation  $\rho_{x,y}$  are in general complex-valued. The magnitude of  $\rho_{x,y}$  is always between zero and one, while  $|\rho_{x,y}|=0$  represents the uncorrelated case and  $|\rho_{x,y}|=1$  the case of full correlation. •

## C.4 Entropy and Mutual Information

**Definition C.19 (Entropy of a Random Variable)**

Let  $\underline{x}$  denote a scalar random variable with realizations  $x$  that are drawn from a finite alphabet  $\mathbb{X} := \{\xi_1, \dots, \xi_Q\}$  of cardinality  $Q$ . Moreover, let  $p_q$  denote the probability that a realization of  $\underline{x}$  is equal to  $\xi_q$  ( $1 \leq q \leq Q$ ). The *entropy* of  $\underline{x}$  is then defined as [CT91, p. 5]

$$H(x) := - \sum_{q=1}^Q p_q \log_a(p_q) = -\mathbf{E}\{\log_a(p_q)\}. \quad (\text{C.39})$$

The entropy is a measure for the average uncertainty or the average information of  $\underline{x}$ . Correspondingly, entropy is sometimes referred to as self-information of a random variable. Throughout this thesis, the logarithm  $\log_2(\cdot) = \text{ld}(\cdot)$  is used, and the entropy is associated with the pseudo-unit ‘bits’. (Some authors use the natural logarithm instead, in conjunction with the pseudo-unit ‘nats’ [Gal68, p. 16].) A generalization of (C.39) to vector random variables is straightforward. •

**Definition C.20 (Differential entropy)**

The *differential entropy* constitutes the generalization of entropy to continuous random variables. Let  $\underline{x}$  denote a scalar random variable with realizations  $x$  that are drawn from a continuous set  $\mathbb{X}$ . Moreover, let  $p_{\underline{x}}(x)$  denote the PDF of  $\underline{x}$ . The *differential entropy* of  $\underline{x}$  is then defined as [CT91, p. 224]

$$h(x) := - \int_{\mathbb{X}} p_{\underline{x}}(x) \log_a p_{\underline{x}}(x) dx = -\mathbf{E}\{\log_a p_{\underline{x}}(x)\}. \quad (\text{C.40})$$

Throughout this thesis, the logarithm  $\log_2(\cdot) = \text{ld}(\cdot)$  is used, and the entropy is associated with the pseudo-unit ‘bits’. A generalization of (C.40) to vector random variables is straightforward. •

**Definition C.21 (Mutual information)**

The *mutual information*  $I(x; y)$  between two scalar random variables  $\underline{x}$  and  $\underline{y}$  is defined as [CT91, p. 19, 231]

$$I(x; y) := H(y) - H(y|x) \quad \text{or} \quad I(x; y) := h(y) - h(y|x), \quad (\text{C.41})$$

depending on whether the realizations of  $\underline{x}$  and  $\underline{y}$  are taken from a finite alphabet or from a continuous set (cf. Definition C.19 and C.20). The mutual information  $I(x; y)$  can be interpreted as the average information gain about  $\underline{x}$  that can be obtained by observing  $\underline{y}$  (or vice versa, since  $I(x; y) = I(y; x)$  holds). Specifically, we have

$$I(x; x) = H(x) \quad \text{or} \quad I(x; x) = h(x). \quad (\text{C.42})$$

A generalization of (C.41) and (C.42) to vector random variables is straightforward. •

## C.5 Important Theorems

**Theorem C.1 (Weak law of large numbers/Bernoulli’s theorem)**

Let  $\{\underline{x}_1, \dots, \underline{x}_N\}$  be a set of  $N$  independent and identically distributed (i.i.d.) random variables with an arbitrary PDF  $p_{\underline{x}}(x)$ , finite mean  $\bar{x}$ , and finite variance  $\sigma_x^2$ . Furthermore, let  $\underline{y}$  be the so-called sample mean of  $\{\underline{x}_1, \dots, \underline{x}_N\}$ , defined as [Pro01, Ch. 2.1.6]

$$\underline{y} := \frac{1}{N} \sum_{n=1}^N \underline{x}_n. \quad (\text{C.43})$$

Then,  $\underline{y}$  can be interpreted as an estimate for  $\bar{x}$ . Specifically, it can be shown that  $\bar{y} = \mathbb{E}\{\underline{y}\} = \bar{x}$ . The variance of  $\underline{y}$  can be shown to be

$$\mathbb{E}\{(y - \bar{y})^2\} = \frac{\sigma_x^2}{N}. \quad (\text{C.44})$$

Correspondingly, for  $N \rightarrow \infty$  the variance of  $\underline{y}$  approaches zero, i.e. the sample mean (C.43) converges to the true mean  $\bar{x}$ .

**Theorem C.2 (Central limit theorem)**

Let  $\{\underline{x}_1, \dots, \underline{x}_N\}$  be a set of  $N$  independent and identically distributed (i.i.d.) random variables with an arbitrary PDF  $p_{\underline{x}}(x)$ , a finite mean  $\bar{x}$ , and a finite variance  $\sigma_x^2$ . Then, the random variable

$$\underline{y} := \lim_{N \rightarrow \infty} \frac{1}{\sqrt{N}} \sum_{n=1}^N \frac{(\underline{x}_n - \bar{x})}{\sqrt{\sigma_x^2}} \quad (\text{C.45})$$

is Gaussian distributed with zero mean and unit variance [Pro01, Ch. 2.1.6].

**Theorem C.3 (Relaxed central limit theorem)**

Let  $\{\underline{x}_1, \dots, \underline{x}_N\}$  be a set of  $N$  independent, not necessarily identically distributed random variables with finite means  $\bar{x}_n$  and finite variances  $\sigma_{x,n}^2$  ( $n = 1, \dots, N$ ). Then, the random variable

$$\underline{y} := \lim_{N \rightarrow \infty} \frac{\sum_{n=1}^N (\underline{x}_n - \bar{x}_n)}{\sqrt{\sum_{n=1}^N \sigma_{x,n}^2}} \quad (\text{C.46})$$

is almost surely Gaussian distributed with zero mean and unit variance [PKB99, p. 203].

# Appendix D

## Matrix Calculus

Please, refer to Appendix B for conventions and notations employed in the following.

### D.1 Vector and Matrix Norms

#### Definition D.1 (Euclidean norm)

The *Euclidean norm* of an  $(m \times 1)$ -vector  $\mathbf{x}$  is defined as [Gv96, p. 52]:

$$\|\mathbf{x}\|_2 := \sqrt{\sum_{\mu=1}^m |x_{\mu}|^2} = \sqrt{\text{tr}(\mathbf{x}\mathbf{x}^H)}. \quad (\text{D.1})$$

We often use  $\|\mathbf{x}\|$  as a short-hand notation. •

#### Definition D.2 (Frobenius norm)

The *Frobenius norm* of an  $(m \times n)$ -matrix  $\mathbf{X}$  is defined as [Gra83, Ch. 5.6]:

$$\|\mathbf{X}\|_F := \sqrt{\sum_{\mu=1}^m \sum_{\nu=1}^n |x_{\mu\nu}|^2} = \sqrt{\sum_{\nu=1}^n \|\mathbf{x}_{\nu}\|^2} = \sqrt{\text{tr}(\mathbf{X}\mathbf{X}^H)}, \quad (\text{D.2})$$

where  $\mathbf{x}_{\nu}$  denotes the  $\nu$ th column vector of  $\mathbf{X}$ . •

### D.2 Special Matrix Products

#### Definition D.3 (Hadamard product)

The *Hadamard product* of two  $(m \times n)$ -matrices  $\mathbf{X}$  and  $\mathbf{Y}$  is defined as:

$$\mathbf{X} \odot \mathbf{Y} := \begin{bmatrix} x_{11} y_{11} & \cdots & x_{1n} y_{1n} \\ \vdots & \ddots & \vdots \\ x_{m1} y_{m1} & \cdots & x_{mn} y_{mn} \end{bmatrix} \quad (\text{D.3})$$

(element-wise multiplication). •

**Definition D.4 (Kronecker product)**

The *Kronecker product* of an  $(m \times n)$ -matrix  $\mathbf{X}$  and an  $(m' \times n')$ -matrix  $\mathbf{Y}$  is defined as:

$$\mathbf{X} \otimes \mathbf{Y} := \begin{bmatrix} x_{11} \mathbf{Y} & \dots & x_{1n} \mathbf{Y} \\ \vdots & \ddots & \vdots \\ x_{m1} \mathbf{Y} & \dots & x_{mn} \mathbf{Y} \end{bmatrix}, \quad (\text{D.4})$$

where the resulting matrix is of size  $m m' \times n n'$ . •

### D.3 Orthogonal Matrices

**Definition D.5 (Orthogonal matrix)**

A real-valued  $(n \times n)$ -matrix  $\mathbf{O}$ , for which

$$\mathbf{O}\mathbf{O}^T = \mathbf{I}_n \quad (\text{D.5})$$

holds (i.e.,  $\mathbf{O}^T = \mathbf{O}^{-1}$ ), is called an *orthogonal matrix* [Gv96, Ch. 2.5.1]. Orthogonal matrices have some important properties. For example, for any orthogonal matrix  $\mathbf{O}$   $\det(\mathbf{O}) = \pm 1$  holds, i.e., orthogonal matrices are always non-singular. Also, the matrix product of two arbitrary orthogonal matrices  $\mathbf{O}_1$  and  $\mathbf{O}_2$  always yields an orthogonal matrix:  $\mathbf{O}_1\mathbf{O}_2(\mathbf{O}_1\mathbf{O}_2)^T = \mathbf{O}_1\mathbf{O}_2\mathbf{O}_2^T\mathbf{O}_1^T = \mathbf{I}_n$ . •

**Definition D.6 (Hadamard matrix)**

A specific orthogonal matrix that is of particular interest in this thesis is the normalized *Hadamard matrix*  $\mathfrak{H}_n$  of size  $n \times n$ , which contains solely entries  $\pm 1/\sqrt{n}$  [Gra83, Ch. 8.14]. Unfortunately, normalized Hadamard matrices do not exist for arbitrary  $n$ . Moreover, although it is conjectured that normalized Hadamard matrices exist for  $n=2$  and any  $n$  that is a multiple of 4, a strict proof is yet to be found. A normalized Hadamard matrix of size  $2 \times 2$  is, for example, given by

$$\mathfrak{H}_2 = \frac{1}{\sqrt{2}} \begin{bmatrix} +1 & +1 \\ +1 & -1 \end{bmatrix}. \quad (\text{D.6})$$

If  $\mathfrak{H}_n$  is a normalized Hadamard matrix of size  $n \times n$  this is also the case for any column- or row-permuted version of  $\mathfrak{H}_n$ . Normalized Hadamard matrices of size  $2n \times 2n$  can, for example, be constructed by building the Kronecker product

$$\mathfrak{H}_{2n} = \mathfrak{H}_2 \otimes \mathfrak{H}_n = \frac{1}{\sqrt{2}} \begin{bmatrix} \mathfrak{H}_n & \mathfrak{H}_n \\ \mathfrak{H}_n & -\mathfrak{H}_n \end{bmatrix}, \quad (\text{D.7})$$

with  $\mathfrak{H}_n$  being a normalized Hadamard matrix of size  $n \times n$ . •

## D.4 Unitary Matrix Transforms

### Definition D.7 (Unitary matrix, Stiefel manifold)

A complex-valued  $(n \times n)$ -matrix  $\mathbf{U}$ , for which

$$\mathbf{U}\mathbf{U}^{\text{H}} = \mathbf{I}_n \quad (\text{D.8})$$

holds (i.e.,  $\mathbf{U}^{\text{H}} = \mathbf{U}^{-1}$ ), is called a *unitary matrix* [Gv96, Ch. 2.5.6]. Unitary matrices play an important role throughout this thesis. Similar to real-valued orthogonal matrices, unitary matrices have some important properties. For example, for any unitary matrix  $\mathbf{U}$   $|\det(\mathbf{U})| = 1$  holds, i.e., unitary matrices are always non-singular. Moreover, the matrix product of two arbitrary unitary matrices  $\mathbf{U}_1$  and  $\mathbf{U}_2$  always yields a unitary matrix. The set of all unitary  $(n \times n)$ -matrices is referred to as *Stiefel manifold* [HH02a] and is denoted as

$$\mathbb{S}_n := \{\mathbf{U} \mid \mathbf{U} \in \mathbb{C}^{n \times n}, \mathbf{U} \text{ unitary}\} \quad (\text{D.9})$$

in the sequel.<sup>1</sup> •

### Remark D.1 (Parameterizations of the Stiefel manifold)

Any unitary matrix  $\mathbf{U} \in \mathbb{S}_n$  is associated with  $n^2$  real-valued free parameters, whereas an arbitrary complex-valued  $(n \times n)$ -matrix is associated with  $2n^2$  real-valued parameters [HH02a]. This reduced number of free parameters is due to the fact that the column vectors  $\mathbf{u}_\nu$  ( $\nu = 1, \dots, n$ ) of a unitary matrix are required to have unit norms  $\|\mathbf{u}_\nu\|$  ( $n$  constraints) and are required to be mutually orthogonal, i.e.,  $\mathbf{u}_\nu^{\text{H}}\mathbf{u}_{\nu'} = 0$  for all  $\nu, \nu' = 1, \dots, n$  ( $n^2 - n$  constraints). Given a set of  $n^2$  real-valued parameters, there are several techniques to generate a unitary  $(n \times n)$ -matrix [HH02a]:

- *Givens rotations*: Let  $\mathbf{D}$  be a unitary diagonal  $(n \times n)$ -matrix, i.e., the diagonal entries of  $\mathbf{D}$  are given by  $d_\nu := e^{j\varphi_\nu}$  ( $\nu = 1, \dots, n$ ). Furthermore, let  $\mathbf{O}_1$  and  $\mathbf{O}_2$  denote two arbitrary real-valued (non-diagonal) orthogonal  $(n \times n)$ -matrices. Then, the matrix product

$$\mathbf{U} := \mathbf{O}_1 \mathbf{D} \mathbf{O}_2 \quad (\text{D.10})$$

yields a unitary (non-diagonal) matrix, i.e.,  $\mathbf{U} \in \mathbb{S}_n$ . Any orthogonal  $(n \times n)$ -matrix  $\mathbf{O}$  can in turn be written as the product of  $(n-1)n/2$  Givens matrices:

$$\mathbf{O} := \mathbf{G}_1 \mathbf{G}_2 \cdots \mathbf{G}_{(n-1)n/2}. \quad (\text{D.11})$$

Each Givens matrix  $\mathbf{G}_i$ ,  $1 \leq i \leq (n-1)n/2$ , represents a planar rotation on one of the  $(n-1)n/2$  two-dimensional hyperplanes, and is determined by a single real-valued parameter  $\phi$ , which represents the angle of rotation. Therefore, according to (D.10) altogether  $n + 2(n-1)n/2 = n^2$  real-valued parameters are required, in order to generate a unitary matrix  $\mathbf{U}$  by means of Givens rotations (as expected).

---

<sup>1</sup>In a more general definition, unitary matrices may also be non-square. Correspondingly, the Stiefel manifold is typically defined as the set of all unitary  $(m \times n)$ -matrices, where  $m = n$  or  $m \neq n$ .



- *Householder reflections:* This construction is similar to the above construction based on Givens rotations. Again, let  $\mathbf{D}$  be a unitary diagonal  $(n \times n)$ -matrix. Then the matrix product

$$\mathbf{U} := \mathbf{D}\mathbf{H}_1\mathbf{H}_2 \cdots \mathbf{H}_n \quad (\text{D.12})$$

yields a unitary (non-diagonal) matrix  $\mathbf{U}$ , where the  $(n \times n)$ -Householder matrices  $\mathbf{H}_\nu$  ( $\nu=1, \dots, n$ ) are defined as

$$\mathbf{H}_\nu := \mathbf{I}_n - 2 \cdot \frac{\boldsymbol{\xi}^{(\nu)} \boldsymbol{\xi}^{(\nu)\text{H}}}{\|\boldsymbol{\xi}^{(\nu)}\|^2}, \quad \boldsymbol{\xi}^{(\nu)} := [0, \dots, 0, 1, \xi_{\nu+1}^{(\nu)}, \dots, \xi_n^{(\nu)}]^\text{T}. \quad (\text{D.13})$$

Here,  $\xi_{\nu+1}^{(\nu)}, \dots, \xi_n^{(\nu)}$  ( $1 \leq \nu \leq n$ ) are  $(n-1)n$  real-valued parameters.

- *Matrix exponential function:* Given an arbitrary Hermitian matrix  $\mathbf{A} \in \mathbb{C}^{n \times n}$  (i.e.,  $\mathbf{A} = \mathbf{A}^\text{H}$ ), the mapping

$$\mathbf{U} := e^{\mathbf{j}\mathbf{A}} = \sum_{i=0}^{\infty} \frac{(\mathbf{j}\mathbf{A})^i}{i!} \quad (\text{D.14})$$

always yields a unitary matrix  $\mathbf{U}$ . The mapping (D.14) can be interpreted as a matrix generalization of the scalar mapping  $u := e^{\mathbf{j}a}$  ( $a \in \mathbb{R}$ ), which maps the real axis onto the unit circle within the complex plane. It should be noted that the mapping (D.14) is not a one-to-one mapping (similar to the scalar case, where  $a \in \mathbb{R}$  and  $a \pm N2\pi$  yield the same complex number  $u$  for any  $N \in \mathbb{Z}$ ).

- *Cayley transform:* This construction is similar to the one based on the matrix exponential function. Given an arbitrary Hermitian matrix  $\mathbf{A} \in \mathbb{C}^{n \times n}$ , the so-called Cayley transform of  $\mathbf{j}\mathbf{A}$ ,

$$\mathbf{U} := (\mathbf{I}_n + \mathbf{j}\mathbf{A})^{-1}(\mathbf{I}_n - \mathbf{j}\mathbf{A}), \quad (\text{D.15})$$

always yields a unitary matrix  $\mathbf{U}$ . Similar to the mapping (D.14), the mapping (D.15) can be interpreted as a matrix generalization of the scalar mapping  $u := (1 - \mathbf{j}a)/(1 + \mathbf{j}a)$  ( $a \in \mathbb{R}$ ), which maps the real axis onto the unit circle within the complex plane.

### Definition D.8 (Fourier matrix)

A specific unitary matrix, that is of particular interest in this thesis, is the  $(n \times n)$ -*Fourier matrix*  $\mathfrak{F}_n$  with entries  $[\mathfrak{F}_n]_{\mu,\nu} = e^{-\mathbf{j}2\pi(\mu-1)(\nu-1)/n} / \sqrt{n}$ , which exists for any number  $n$  [Gra83, Ch. 8.12]:

$$\mathfrak{F}_n := \frac{1}{\sqrt{n}} \begin{bmatrix} 1 & 1 & 1 & \cdots & 1 \\ 1 & \omega & \omega^2 & \cdots & \omega^{n-1} \\ 1 & \omega^2 & \omega^4 & \cdots & \omega^{(n-1) \cdot 2} \\ \vdots & \vdots & \vdots & \ddots & \vdots \\ 1 & \omega^{n-1} & \omega^{2 \cdot (n-1)} & \cdots & \omega^{(n-1) \cdot (n-1)} \end{bmatrix}, \quad \omega := e^{-\mathbf{j}2\pi/n}. \quad (\text{D.16})$$

•

**Definition D.9 (Unitary matrix transformation)**

A *unitary matrix transformation* is a linear mapping  $\mathbf{A} \mapsto \mathbf{U}\mathbf{A}\mathbf{U}^H$ , where  $\mathbf{A}$  is an arbitrary complex-valued  $(n \times n)$ -matrix and  $\mathbf{U} \in \mathbb{S}_n$  an arbitrary unitary matrix [Gv96, Ch. 2.5.6]. Unitary matrix transformations are often useful, because they preserve a number of fundamental matrix properties. For example,

$$|\det(\mathbf{U}\mathbf{A}\mathbf{U}^H)| = |\det(\mathbf{U})|^2 |\det(\mathbf{A})| = |\det(\mathbf{A})|. \quad (\text{D.17})$$

Moreover, we have  $\text{tr}(\mathbf{U}\mathbf{A}\mathbf{U}^H) = \text{tr}(\mathbf{A})$  [Gra83, Ch. 9.1] and

$$\|\mathbf{U}\mathbf{A}\mathbf{U}^H\|_F = \sqrt{\text{tr}(\mathbf{U}\mathbf{A}\mathbf{U}^H\mathbf{U}\mathbf{A}^H\mathbf{U}^H)} = \|\mathbf{A}\|_F. \quad (\text{D.18})$$

(cf. Definition D.2). •

## D.5 Eigenvalue and Singular-Value Decomposition

**Definition D.10 (Eigenvalues and eigenvectors)**

The *eigenvalues*  $\lambda_1, \dots, \lambda_n$  of a square matrix  $\mathbf{A} \in \mathbb{C}^{n \times n}$  are the  $n$  roots of the characteristic polynomial [Gv96, Ch. 7.1]

$$\text{cp}_{\mathbf{A}}(x) := \det(x\mathbf{I}_n - \mathbf{A}). \quad (\text{D.19})$$

The non-zero vectors  $\mathbf{x}_\nu \in \mathbb{C}^n$  ( $\nu = 1, \dots, n$ ) that satisfy

$$\mathbf{A}\mathbf{x}_\nu = \lambda_\nu \mathbf{x}_\nu \quad (\text{D.20})$$

are called the *eigenvectors* of  $\mathbf{A}$ . The *rank* of  $\mathbf{A}$ , denoted as  $\text{rank}(\mathbf{A})$ , is defined as the number of non-zero eigenvalues  $\lambda_\nu$ . •

**Definition D.11 (Eigenvalue decomposition)**

Any square matrix  $\mathbf{A} \in \mathbb{C}^{n \times n}$  with unequal eigenvalues  $\lambda_1 \neq \dots \neq \lambda_n$  can be written as the product of a non-singular square matrix  $\mathbf{X} \in \mathbb{C}^{n \times n}$ , a diagonal matrix  $\mathbf{\Lambda}$ , and the inverse of  $\mathbf{X}$ , according to

$$\mathbf{A} = \mathbf{X}\mathbf{\Lambda}\mathbf{X}^{-1}. \quad (\text{D.21})$$

This follows directly from rewriting (D.20) according to  $\mathbf{A}\mathbf{X} = \mathbf{X}\mathbf{\Lambda}$ , where  $\mathbf{X} := [\mathbf{x}_1, \dots, \mathbf{x}_n]$  contains the eigenvectors of  $\mathbf{A}$  and  $\mathbf{\Lambda} := \text{diag}([\lambda_1, \dots, \lambda_n])$  the corresponding eigenvalues. Correspondingly, (D.21) is called *eigenvalue decomposition (EVD)* of  $\mathbf{A}$ . The EVD can, for example, be obtained by means of the Jacobian algorithm [Gv96, Ch. 8.4]. •

**Remark D.2 (EVD of Hermitian matrices)**

If  $\mathbf{A}$  is Hermitian ( $\mathbf{A} = \mathbf{A}^H$ ), its eigenvectors constitute a unitary basis, i.e.,

$$\mathbf{U} := [\mathbf{x}_1, \dots, \mathbf{x}_n] \quad (\text{D.22})$$

is a unitary matrix [HJ85, Ch. 2.5]. Correspondingly,  $\mathbf{A}$  can be written as

$$\mathbf{A} = \mathbf{U}\mathbf{\Lambda}\mathbf{U}^H. \quad (\text{D.23})$$

Specifically, all eigenvalues are real-valued in this case [HJ85, Ch. 2.5]. If, additionally,  $\mathbf{A}$  can be written as a product  $\mathbf{A} = \mathbf{B}\mathbf{B}^H$ , where  $\mathbf{B}$  is an arbitrary complex-valued matrix, all eigenvalues of  $\mathbf{A}$  are greater than or equal to zero (since the eigenvalues of  $\mathbf{A}$  are the squares of the non-zero singular values of  $\mathbf{B}$ , cf. Definition D.12).

**Definition D.12 (Singular-value decomposition)**

The *singular-value decomposition (SVD)* can be seen as a generalization of the EVD to non-square matrices. Any matrix  $\mathbf{B} \in \mathbb{C}^{m \times n}$  can be written as a product [Gv96, Ch. 2.5]

$$\mathbf{B} = \mathbf{U}\mathbf{\Lambda}\mathbf{V}^H, \quad (\text{D.24})$$

where  $\mathbf{U}$  is a unitary  $(m \times m)$ -matrix containing the eigenvectors of  $\mathbf{B}\mathbf{B}^H$ , and  $\mathbf{V}$  is a unitary  $(n \times n)$ -matrix containing the eigenvectors of  $\mathbf{B}^H\mathbf{B}$ . The matrix  $\mathbf{\Lambda}$  is an  $(m \times n)$ -diagonal matrix containing the non-negative square-roots of the  $\tilde{m} := \min(m, n)$  eigenvalues  $\chi_1, \dots, \chi_{\tilde{m}}$  of  $\mathbf{B}\mathbf{B}^H$  ( $m \leq n$ ) or  $\mathbf{B}^H\mathbf{B}$  ( $m > n$ ):

$$\mathbf{\Lambda} := \left[ \begin{array}{ccc|c} \lambda_1 & & 0 & \\ & \ddots & & \\ 0 & & \lambda_m & \\ \hline & & & \mathbf{0}_{m,n-m} \end{array} \right] (m \leq n), \quad \mathbf{\Lambda} := \left[ \begin{array}{ccc|c} \lambda_1 & & & 0 \\ & \ddots & & \\ & & & \lambda_n \\ \hline 0 & & & \\ & & & \mathbf{0}_{m-n,n} \end{array} \right] (m > n), \quad (\text{D.25})$$

where the parameters  $\lambda_{\tilde{\mu}} := \sqrt{\chi_{\tilde{\mu}}}$  ( $\tilde{\mu} = 1, \dots, \tilde{m}$ ) are called *singular values* of  $\mathbf{B}$ . Obviously, the eigenvalues  $\chi_{\tilde{\mu}}$  are always real-valued, since  $\mathbf{B}\mathbf{B}^H$  and  $\mathbf{B}^H\mathbf{B}$  are Hermitian matrices. In the case of a Hermitian matrix  $\mathbf{B} \in \mathbb{C}^{n \times n}$ , we have  $\mathbf{B}\mathbf{B}^H = \mathbf{B}^H\mathbf{B}$ , i.e., the SVD (D.24) reduces to the EVD (D.23). •

## D.6 Covariance and Correlation Matrices

**Definition D.13 (Covariance and correlation matrix)**

The *covariance matrix* of a complex-valued vector random variable

$$\underline{\mathbf{x}} := [\underline{x}_1, \dots, \underline{x}_m]^T \quad (\text{D.26})$$

is defined as

$$\mathbf{Q}_{\underline{\mathbf{x}}} := \mathbf{E}\{(\mathbf{x} - \bar{\mathbf{x}})(\mathbf{x} - \bar{\mathbf{x}})^H\} = \mathbf{\Sigma}_{\underline{\mathbf{x}}} \odot \mathbf{R}_{\underline{\mathbf{x}}}, \quad (\text{D.27})$$

where  $\bar{\mathbf{x}} := \mathbf{E}\{\mathbf{x}\}$  denotes the mean of  $\mathbf{x}$ ,

$$\mathbf{\Sigma}_{\underline{\mathbf{x}}} := \begin{bmatrix} \sigma_{x_1}^2 & \cdots & \sqrt{\sigma_{x_1}^2 \sigma_{x_m}^2} \\ \vdots & \ddots & \vdots \\ \sqrt{\sigma_{x_1}^2 \sigma_{x_m}^2} & \cdots & \sigma_{x_m}^2 \end{bmatrix} \quad (\text{D.28})$$

is a weight matrix determined by the variances  $\sigma_{x_i}^2 = \mathbf{E}\{|x_i - \bar{x}_i|^2\}$  ( $i = 1, \dots, m$ ) of the elements of  $\mathbf{x}$ , and  $\mathbf{R}_{\underline{\mathbf{x}}}$  denotes the corresponding *correlation matrix*. Covariance and correlation matrices are always Hermitian, i.e.,  $\mathbf{Q}_{\underline{\mathbf{x}}} = \mathbf{Q}_{\underline{\mathbf{x}}}^H$  and  $\mathbf{R}_{\underline{\mathbf{x}}} = \mathbf{R}_{\underline{\mathbf{x}}}^H$ . The entries of  $\mathbf{Q}_{\underline{\mathbf{x}}}$  and

$\mathbf{R}_{\underline{x}}$  are in general complex-valued. Moreover, the entries of  $\mathbf{R}_{\underline{x}}$  always have magnitudes that are smaller than or equal to one. Specifically, we have  $[\mathbf{R}_{\underline{x}}]_{i,i} = 1$  for all  $i = 1, \dots, m$ . Moreover, the determinant of  $\mathbf{R}_{\underline{x}}$  is always between zero and one [Gra83, Ch. 8.7], i.e.,

$$0 \leq \det(\mathbf{R}_{\underline{x}}) \leq 1, \quad (\text{D.29})$$

where  $\det(\mathbf{R}_{\underline{x}}) = 1$  if and only if  $\mathbf{R}_{\underline{x}} = \mathbf{I}_m$ . Due to the left-hand side of (D.27), the covariance matrix  $\mathbf{Q}_{\underline{x}}$  can be written as a product  $\mathbf{B}\mathbf{B}^H$ , where  $\mathbf{B}$  denotes an appropriate  $(m \times m)$ -matrix [HE95, Ch. 1.5]. Correspondingly, the eigenvalues of  $\mathbf{Q}_{\underline{x}}$  and  $\mathbf{R}_{\underline{x}}$  are always greater than or equal to zero, i.e.,  $\mathbf{Q}_{\underline{x}}$  and  $\mathbf{R}_{\underline{x}}$  are always non-negative definite.<sup>2</sup> •

**Remark D.3 (Estimation of covariance and correlation matrices)**

Covariance and correlation matrices can be measured/estimated by averaging over a sufficiently large number of independent realizations  $\mathbf{x}_n$  of the random vector  $\underline{x}$  under consideration, e.g., for zero-mean random variables

$$\hat{\mathbf{Q}}_{\underline{x}, N_s} := \frac{1}{N_s} \sum_{n=1}^{N_s} \mathbf{x}_n \mathbf{x}_n^H. \quad (\text{D.30})$$

For  $N_s \rightarrow \infty$ , we have

$$\lim_{N_s \rightarrow \infty} \hat{\mathbf{Q}}_{\underline{x}, N_s} = \mathbf{Q}_{\underline{x}}, \quad (\text{D.31})$$

i.e., the sample mean of  $\mathbf{x}_n \mathbf{x}_n^H$  tends to the expected value (cf. Theorem C.1). In general, the properties of estimated covariance/correlation matrices may deviate from the properties stated in Definition D.13. For example, the determinant of an estimated correlation matrix  $\hat{\mathbf{R}}_{\underline{x}}$  might be greater than one. In particular, if the individual entries of the covariance/correlation matrix are estimated separately, one might obtain a negative definite estimate  $\hat{\mathbf{Q}}_{\underline{x}} / \hat{\mathbf{R}}_{\underline{x}}$ .

Within the scope of this thesis, channel covariance/correlation matrices are of special interest. These can, for example, be estimated at the receiver by employing appropriate training sequences. Estimation techniques that guarantee positive (semi-) definite estimates of the channel covariance/correlation matrix were, for example, considered in [DIU06].

---

<sup>2</sup>Note that the non-negative definite property of  $\mathbf{R}_{\underline{x}}$  is also reflected in the left inequality of (D.29). The right inequality follows from the so-called Hadamard inequality, which states that for any non-negative definite  $(m \times m)$ -matrix  $\mathbf{A}$ ,  $\det(\mathbf{A}) \leq a_{11} \cdot a_{22} \cdot \dots \cdot a_{mm}$  holds, with equality if and only if  $\mathbf{A}$  is diagonal [BT04a, App. B.2].



# Appendix E

## Convex Optimization

SOME OF THE theorems presented in this thesis are proven using techniques from convex optimization. To this end, a brief introduction to convex optimization is provided in the following. Further details can be found in the excellent book by Boyd and Vandenberghe [BV04] or in the tutorial paper [LY06] by Luo and Yu.

### E.1 Optimization Problems and Strong Duality

Consider the following (general) optimization problem:

$$\begin{aligned} & \text{minimize} && f(\mathbf{x}) && \text{(E.1)} \\ & \text{subject to} && g_i(\mathbf{x}) \leq 0 && (i = 1, \dots, l), \\ & && h_j(\mathbf{x}) = 0 && (j = 1, \dots, m), \end{aligned}$$

where  $\mathbf{x} \in \mathbb{R}^n$  denotes the optimization variable of the problem,  $f : \mathbb{R}^n \rightarrow \mathbb{R}$  the objective function, and  $g_i : \mathbb{R}^n \rightarrow \mathbb{R}$  ( $i = 1, \dots, l$ ) and  $h_j : \mathbb{R}^n \rightarrow \mathbb{R}$  ( $j = 1, \dots, m$ ) denote some constraint functions.

For any optimization problem of the above form, a dual problem can be found which is based on the so-called Lagrangian function  $L(\mathbf{x}, \boldsymbol{\mu}, \boldsymbol{\nu})$ . The Lagrangian function is obtained by augmenting the objective function  $f$  by a weighted sum of the constraint functions  $g_i$  and  $h_j$ , according to

$$L(\mathbf{x}, \boldsymbol{\mu}, \boldsymbol{\nu}) := f(\mathbf{x}) + \sum_{i=1}^l \mu_i g_i(\mathbf{x}) + \sum_{j=1}^m \nu_j h_j(\mathbf{x}) \quad \text{(E.2)}$$

( $L : \mathbb{R}^n \times \mathbb{R}^l \times \mathbb{R}^m \rightarrow \mathbb{R}$ ), where the parameters  $\mu_i$  and  $\nu_j$  are called Lagrangian multipliers for the (in)equality constraints, and  $\boldsymbol{\mu} := [\mu_1, \dots, \mu_l]^T$  and  $\boldsymbol{\nu} := [\nu_1, \dots, \nu_m]^T$  are called the dual variables. The dual optimization problem corresponding to (E.1) is then given by

$$\begin{aligned} & \text{maximize} && f_a(\boldsymbol{\mu}, \boldsymbol{\nu}) := \min_{\mathbf{x} \in \mathbb{R}^n} L(\mathbf{x}, \boldsymbol{\mu}, \boldsymbol{\nu}) && \text{(E.3)} \\ & \text{subject to} && \mu_i \geq 0 && (i = 1, \dots, l), \end{aligned}$$

where the function  $f_d : \mathbb{R}^l \times \mathbb{R}^m \rightarrow \mathbb{R}$  is called the Lagrangian dual function. The significance of the dual optimization problem is explained as follows. Let  $\mathbf{x}^\bullet \in \mathbb{R}^n$  denote a solution of the primal optimization problem (E.1), i.e.,  $\mathbf{x}^\bullet$  minimizes the objective function  $f$  under the given constraints. Moreover, let  $f(\mathbf{x}^\bullet) =: p^\bullet$  denote the corresponding minimum value of  $f$ . Then it can be shown [BV04, Ch. 5.1] that the Lagrangian dual function always provides a lower bound on  $p^\bullet$ , as long as all Lagrangian multipliers  $\mu_i$  are greater than or equal to zero, i.e.,

$$f_d(\boldsymbol{\mu}, \boldsymbol{\nu}) \leq p^\bullet \quad (\text{E.4})$$

for all  $\boldsymbol{\mu} \in \mathbb{R}_{\geq 0}^l$  and  $\boldsymbol{\nu} \in \mathbb{R}^m$ . Correspondingly, the dual optimization problem can be interpreted as finding the best lower bound on  $p^\bullet$ , given the constraint that all Lagrangian multipliers  $\mu_i$  are greater than or equal to zero. Now, let  $(\boldsymbol{\mu}^\bullet, \boldsymbol{\nu}^\bullet) \in \mathbb{R}_{\geq 0}^l \times \mathbb{R}^m$  denote a solution of the dual optimization problem (E.3), i.e.,  $(\boldsymbol{\mu}^\bullet, \boldsymbol{\nu}^\bullet)$  maximizes the Lagrangian dual function  $f_d$  under the given constraints. Moreover, let  $f_d(\boldsymbol{\mu}^\bullet, \boldsymbol{\nu}^\bullet) =: d^\bullet$  denote the corresponding maximum value of  $f_d$ . If now  $d^\bullet = p^\bullet$  holds, i.e., the so-called (optimal) duality gap ( $p^\bullet - d^\bullet$ ) is zero, the two optimization problems (E.1) and (E.3) are said to be strongly dual (otherwise weakly dual).

### Karush-Kuhn-Tucker Conditions

In the following, we assume that the objective function  $f$  and the constraint functions  $g_i$  and  $h_j$  of the primal optimization problem (E.1) are differentiable on  $\mathbb{R}^n$ . Moreover, we assume that strong duality is given. Under these prerequisites, it can be shown [BV04, Ch. 5.5] that any pair of primal and dual optimal points,  $\mathbf{x}^\bullet, (\boldsymbol{\mu}^\bullet, \boldsymbol{\nu}^\bullet)$ , must satisfy the so-called Karush-Kuhn-Tucker (KKT) conditions, which are given by

$$g_i(\mathbf{x}^\bullet) \leq 0 \quad \text{for all } i = 1, \dots, l \quad (\text{1st primal problem constraint}) \quad (\text{E.5a})$$

$$h_j(\mathbf{x}^\bullet) = 0 \quad \text{for all } j = 1, \dots, m \quad (\text{2nd primal problem constraint}) \quad (\text{E.5b})$$

$$\mu_i^\bullet \geq 0 \quad \text{for all } i = 1, \dots, l \quad (\text{dual problem constraint}) \quad (\text{E.5c})$$

$$\mu_i^\bullet g_i(\mathbf{x}^\bullet) = 0 \quad \text{for all } i = 1, \dots, l \quad (\text{complementary slackness}) \quad (\text{E.5d})$$

$$\nabla L(\mathbf{x}^\bullet, \boldsymbol{\mu}^\bullet, \boldsymbol{\nu}^\bullet) = 0 \quad (\text{gradient condition}) \quad (\text{E.5e})$$

$(\nabla f(\mathbf{x})) := [\partial f(\mathbf{x})/\partial x_1, \dots, \partial f(\mathbf{x})/\partial x_n]^T$  denotes the gradient of a function  $f : \mathbb{R}^n \rightarrow \mathbb{R}$ .

## E.2 Convex Optimization Problems

A function  $f : \mathbb{R}^n \rightarrow \mathbb{R}$  is called convex, if for all  $\mathbf{x}, \mathbf{y} \in \mathbb{R}^n$  and all parameters  $\vartheta \in [0, 1]$  the following holds:<sup>1</sup>

$$f(\vartheta \mathbf{x} + (1-\vartheta)\mathbf{y}) \leq \vartheta f(\mathbf{x}) + (1-\vartheta)f(\mathbf{y}). \quad (\text{E.6})$$

<sup>1</sup>For fixed points  $\mathbf{x}, \mathbf{y} \in \mathbb{R}^n$ , the set  $\mathbb{S} := \{\vartheta \mathbf{x} + (1-\vartheta)\mathbf{y} \mid \vartheta \in [0, 1]\}$  marks a straight line in  $\mathbb{R}^n$ , which starts in  $\mathbf{y}$  ( $\vartheta=0$ ) and ends in  $\mathbf{x}$  ( $\vartheta=1$ ). Similarly, the set  $\mathbb{S}' := \{\vartheta f(\mathbf{x}) + (1-\vartheta)f(\mathbf{y}) \mid \vartheta \in [0, 1]\}$  marks a straight line in  $\mathbb{R}^{n+1}$ , which starts in  $(\mathbf{y}, f(\mathbf{y}))$  and ends in  $(\mathbf{x}, f(\mathbf{x}))$ . If  $f$  is convex, the line  $\mathbb{S}'$ , which is called the chord between  $\mathbf{x}$  and  $\mathbf{y}$ , lies always above the graph of  $f$  (for any choice of  $\mathbf{x}, \mathbf{y} \in \mathbb{R}^n$ ).



Moreover,  $f$  is called concave if  $-f$  is convex. In order to avoid confusions, convex functions are often called convex- $\cup$ , whereas concave functions are called convex- $\cap$ . An important special case are linear and affine functions (i.e., linear functions plus a constant), because they satisfy the above condition with equality and are thus convex- $\cup$  and convex- $\cap$  at the same time.

A (primal) optimization problem of form (E.1) is called a convex optimization problem, if the objective function  $f$  as well as all constraint functions  $g_i$  and  $h_j$  are convex- $\cup$ .<sup>2</sup> (If all functions are linear, the optimization problem is called a linear program.) Convex optimization problems are an important class of optimization problems, because they have two amicable properties [BV04, pp. 226, 244]. First, if the primal optimization problem is convex, usually (but not always) strong duality is given. Second, the KKT conditions (E.5) are not only necessary conditions for a pair of primal and dual optimal points  $\mathbf{x}^\bullet, (\boldsymbol{\mu}^\bullet, \boldsymbol{\nu}^\bullet)$ , but also sufficient conditions. Correspondingly, assuming strong duality the KKT conditions can be utilized, in order to find a pair  $\mathbf{x}^\bullet, (\boldsymbol{\mu}^\bullet, \boldsymbol{\nu}^\bullet)$  of primal and dual optimal points. However, if the primal problem is not convex, the KKT conditions can only be utilized in order to check, whether a given pair of points,  $\mathbf{x}, (\boldsymbol{\mu}, \boldsymbol{\nu})$ , is primal and dual optimal.

An example for a convex optimization problem, which is of special interest within this thesis, is the well-known water-filling problem:

**Example E.1 (Water-filling problem)**

The water-filling problem is given by

$$\begin{aligned} \text{minimize} \quad & f(\mathbf{x}) := -\sum_{j=1}^n \log(\alpha_j + x_j) && (\mathbf{x} \in \mathbb{R}^n) && \text{(E.7)} \\ \text{subject to} \quad & \sum_{j=1}^n x_j = 1 \quad \text{and} \quad x_j \geq 0 \quad \text{for all } j = 1, \dots, n. \end{aligned}$$

It occurs, for example, in the derivation of the capacity of multiple parallel additive white Gaussian noise (AWGN) channels with unequal average signal-to-noise ratios [Gal68, Ch. 7.5]. The solution of (E.7) is very well documented in [BV04, Ch. 5.5] and is therefore not repeated here. (Moreover, a similar derivation can be found in Appendix 3 at the end of Chapter 4.) One obtains:

$$x_j^\bullet = [\Theta - \alpha_j]_+ \quad \text{subject to} \quad \sum_{j=1}^n [\Theta - \alpha_j]_+ = 1, \quad \text{(E.8)}$$

where

$$[\xi]_+ := \max\{0, \xi\}. \quad \text{(E.9)}$$

Equation (E.8) has to be solved numerically, in order to obtain the so-called water-level  $\Theta$ . The water-filling solution is illustrated in Fig. E.1.  $\diamond$

---

<sup>2</sup>Interestingly, the dual optimization problem (E.3) is always convex, irrespective of the primal optimization problem [BV04, Ch. 5.2].

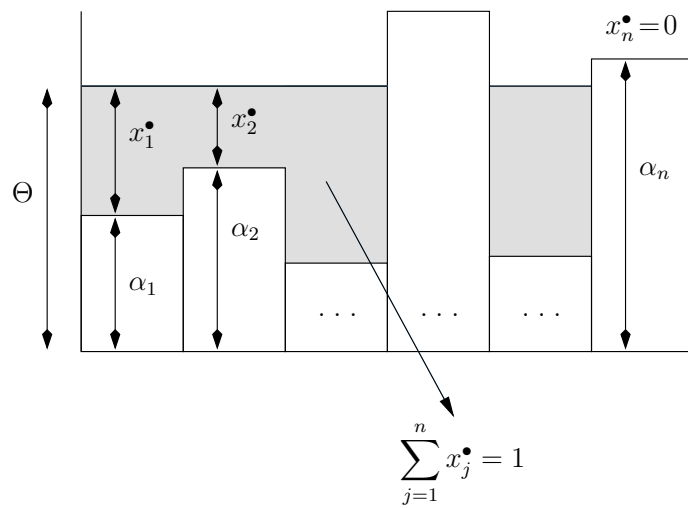


Figure E.1: Illustration of the water-filling solution.

# Appendix F

## Channel Modeling

**I**N THE FOLLOWING, we derive a statistical model for multipath signal propagation in a typical wireless communication setting. We start with a physical view on multipath signal propagation from a single transmit antenna to a single receive antenna, see [RC98, BGP02, Mue02a, XCHV04]. Based on this, the statistical multipath signal propagation model is derived in a transparent fashion. Throughout this thesis, it is assumed that the physical channel is linear. The most important results obtained in the following are summarized in Section 2.2.1. The statistical multipath signal propagation model is later utilized in Section 2.2.2, in order to derive the discrete-time MIMO channel model, which builds the theoretical basis throughout this thesis.

### F.1 Physical Perspective on Multipath Propagation

Consider a point-to-point link between a transmitter and a receiver situated in a typical wireless communication scenario<sup>1</sup>, as depicted in Fig. F.1. Transmitter and receiver are equipped with  $M$  and  $N$  co-located antenna elements, respectively. For the time being, we focus on signal propagation from a single transmit antenna  $\mu$  ( $1 \leq \mu \leq M$ ) to a single receive antenna  $\nu$  ( $1 \leq \nu \leq N$ ). Let  $s_\mu(t) \in \mathbb{C}$  denote the corresponding transmitted signal, where  $t$  denotes the absolute time. The transmitted signal  $s_\mu(t)$  arrives at the receiver via multiple paths, due to reflections, diffuse scattering, and diffraction [Jak74]. Possibly, there is also a direct line-of-sight (LoS) path from the transmitter to the receiver. In the following, we assume that there are altogether  $N_P$  propagation paths that yield a significant contribution to the received signal. For the moment we consider a static scenario, i.e, the positions of transmitter and receiver are fixed, and there are no changes in the physical environment.

Let us focus on the  $i$ th propagation path ( $1 \leq i \leq N_P$ ) between transmit antenna  $\mu$  and receive antenna  $\nu$ , which might be associated with one or more significant reflectors or scatterers<sup>2</sup> (e.g., buildings or hills). Moreover, let us assume that the transmitted

---

<sup>1</sup>For simplicity, we restrict ourselves to a two-dimensional model here. It is straightforward to generalize the model to three-dimensional signal propagation.

<sup>2</sup>We assume that the individual propagation paths  $i = 1, \dots, N_P$  are associated with different scatterers.

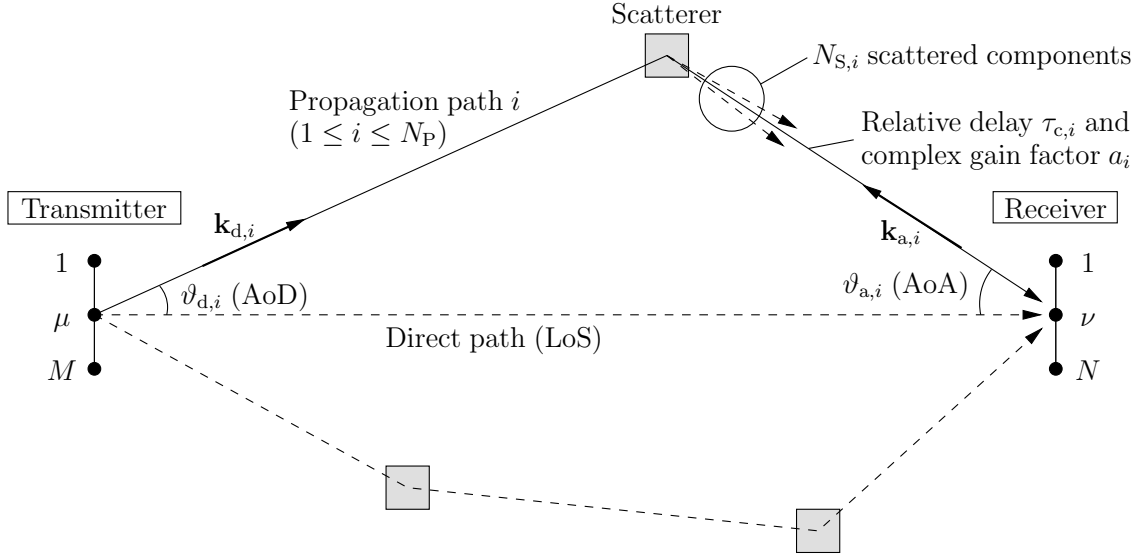


Figure F.1: Typical wireless communication scenario with multipath signal propagation.

signal is an ideal Dirac-impulse at  $t = 0$ , i.e.,  $s_\mu(t) := \delta(t)$ . Let  $\vartheta_{d,i} \in [0, 2\pi)$  denote the angle of departure (AoD),  $\vartheta_{a,i} \in [0, 2\pi)$  the angle of arrival (AoA), and  $\tau_{c,i} \in \mathbb{R}$  the relative delay associated with the  $i$ th propagation path (cf. Fig. F.1). Without loss of generality, the direct path from the transmitter to the receiver is taken as a reference, i.e., the AoD and AoA associated with the LoS path is set to  $\vartheta_d = 0$  and  $\vartheta_a = 0$ . Moreover, we set the relative delay of the LoS path to zero, i.e., the absolute time required for signal propagation from the transmitter to the receiver is not considered further. The received signal component (without noise) associated with the  $i$ th propagation path can generally be written as [RC98, Mue02a, XCHV04]

$$r_{\nu,i}(t) = \sum_{s=1}^{N_{S,i}} a_{s,i} e^{j(\varphi_{\text{Tx},\mu}(\vartheta_{d,i}) + \varphi_{\text{Rx},\nu}(\vartheta_{a,i}))} \delta(t - \tau_{c,i}) \quad (\text{F.1a})$$

$$=: a_i e^{j(\varphi_{\text{Tx},\mu}(\vartheta_{d,i}) + \varphi_{\text{Rx},\nu}(\vartheta_{a,i}))} \delta(t - \tau_{c,i}), \quad (\text{F.1b})$$

where  $N_{S,i}$  denotes the number of scattered components associated with the  $i$ th propagation path (diffuse scattering) and  $a_{s,i} \in \mathbb{C}$  the complex gain factor of the  $s$ th scattered component, including path loss, attenuation due to reflection(s), as well as the array gains in the direction of  $\vartheta_{d,i}$  and  $\vartheta_{a,i}$ . Moreover,  $a_i := \sum_s a_{s,i}$  represents the overall complex gain factor associated with the  $i$ th propagation path,  $\varphi_{\text{Tx},\mu}(\vartheta_{d,i})$  denotes an additional phase offset of transmit antenna  $\mu$  with respect to the first transmit antenna (we take  $\varphi_{\text{Tx},1}(\vartheta_{d,i}) := 0$  as a reference), and  $\varphi_{\text{Rx},\nu}(\vartheta_{a,i})$  the corresponding phase offset of receive antenna  $\nu$  with respect to the first receive antenna ( $\varphi_{\text{Rx},1}(\vartheta_{a,i}) := 0$ ). Assuming planar wave fronts (far-field assumption), the phase terms of a general transmit or receive antenna array are calculated as [XCHV04]

$$\varphi_{\text{Tx},\mu}(\vartheta_{d,i}) = (\mathbf{r}_{\text{Tx},\mu} - \mathbf{r}_{\text{Tx},1})^T \cdot \mathbf{k}_{d,i}, \quad \varphi_{\text{Rx},\nu}(\vartheta_{a,i}) = (\mathbf{r}_{\text{Rx},\nu} - \mathbf{r}_{\text{Rx},1})^T \cdot \mathbf{k}_{a,i}, \quad (\text{F.2})$$

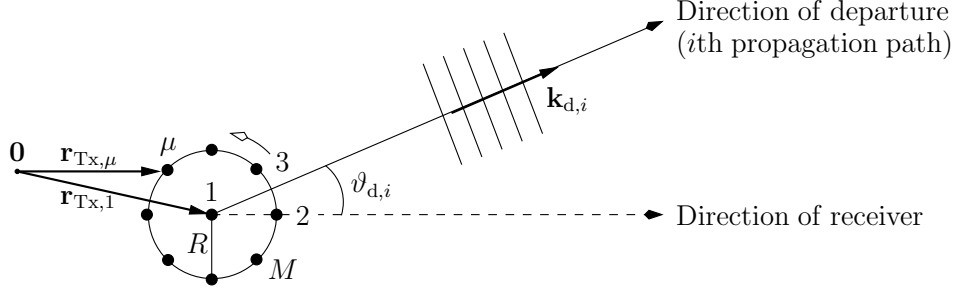


Figure F.2: Circular antenna array.

where  $\mathbf{r}_{\text{Tx},\mu}$  ( $\mathbf{r}_{\text{Rx},\nu}$ ) denotes the position vector of the  $\mu$ th transmit antenna (the  $\nu$ th receive antenna) and  $\mathbf{k}_{\text{d},i}$  ( $\mathbf{k}_{\text{a},i}$ ) the directional vector representing the direction of departure (of arrival) associated with the  $i$ th propagation path. The Euclidean norms of the directional vectors are given by  $\|\mathbf{k}_{\text{d},i}\| = 2\pi/\lambda_c = \|\mathbf{k}_{\text{a},i}\|$ , where  $\lambda_c$  denotes the carrier wavelength.<sup>3</sup>

**Example F.1 (Array phase terms)**

The array phase terms of a uniform linear antenna array (ULAA) with antenna spacing  $d$  and broad-side orientation (cf. Fig. F.1) are given by

$$\varphi_{\text{Tx},\mu}(\vartheta_{\text{d},i}) = -\frac{2\pi d(\mu-1)}{\lambda_c} \sin(\vartheta_{\text{d},i}), \quad \varphi_{\text{Rx},\nu}(\vartheta_{\text{a},i}) = -\frac{2\pi d(\nu-1)}{\lambda_c} \sin(\vartheta_{\text{a},i}). \quad (\text{F.3})$$

In the case of a circular antenna array (CAA) with radius  $R$  and orientation as shown in Fig. F.2, the array phase terms are given by

$$\varphi_{\text{Tx},\mu}(\vartheta_{\text{d},i}) = -\frac{2\pi R}{\lambda_c} \cos\left(\vartheta_{\text{d},i} - \frac{2\pi(\mu-2)}{M-1}\right), \quad (\text{F.4a})$$

$$\varphi_{\text{Rx},\nu}(\vartheta_{\text{a},i}) = -\frac{2\pi R}{\lambda_c} \cos\left(\vartheta_{\text{a},i} - \frac{2\pi(\nu-2)}{N-1}\right), \quad (\text{F.4b})$$

where  $\mu=2, \dots, M$  and  $\nu=2, \dots, N$  ( $\varphi_{\text{Tx},1}(\vartheta_{\text{d},i}) = \varphi_{\text{Rx},1}(\vartheta_{\text{a},i}) = 0$ ).  $\diamond$

**Assumption F.1 (Resolvable delays)**

In practice, the delays  $\tau_{c,i}$  can only be resolved up to a certain limit (due to a limited system bandwidth), i.e., two delays that are closely together cannot be distinguished at the receiver. Due to this, the assumption of discrete delays is often employed in the literature (see for example [Mue02a, XWL+04]), which leads to a quantized multipath signal propagation model. Such a model is easier to handle than a model with continuous delays, especially with regard to computer simulations. If the number of discrete delays is chosen sufficiently large, the quantized multipath signal propagation model will still be accurate. For simplicity, we define a common set of  $N_\tau$  discrete (not necessarily uniformly spaced) delays  $0 \leq \tau_0 < \dots < \tau_{N_\tau-1}$  for all transmit-receive antenna pairs. The average received power associated with a certain delay  $\tau_n$  may, however, differ from one transmit-receive antenna pair to another. Specifically, it may be zero for certain transmit-receive antenna pairs. The maximum relative delay  $\tau_{N_\tau-1}$  is in the sequel denoted as  $\tau_{\text{max}}$ .

<sup>3</sup>Note that in a multicarrier system the array phase terms  $\varphi_{\text{Tx},\mu}(\vartheta_{\text{d},i})$  and  $\varphi_{\text{Rx},\nu}(\vartheta_{\text{a},i})$  differ from one carrier to another.

**Remark F.1 (Geometrical interpretation)**

A geometrical interpretation of the quantized multipath signal propagation model can be found in [Mue02a]. Assuming that all propagation paths are due to a single reflector (single-bounce model), all reflectors associated with a certain delay  $\tau_n$  are located on an ellipse around transmitter and receiver, while the positions of transmitter and receiver mark the foci of the ellipse.

With the quantized model at hand, the overall received signal can readily be written as

$$r_\nu(t) = \sum_{n=0}^{N_\tau-1} \sum_{i=1}^{N_{P,n}} a_{\nu,\mu,n,i} e^{j(\varphi_{T_x,\mu}(\vartheta_{d,i}) + \varphi_{R_x,\nu}(\vartheta_{a,i}))} \delta(t - \tau_n), \quad (\text{F.5})$$

where  $N_{P,n}$  denotes the number of propagation paths associated with delay  $\tau_n$ , while  $N_{P,0} + \dots + N_{P,N_\tau-1} = N_P$ .

In the following, we drop the assumption of a static scenario. In this case, the complex gain factors  $a_{\nu,\mu,n,i}$  as well as the angles of departure and arrival are time-varying, while the AoDs  $\vartheta_{d,i}$  and the AoAs  $\vartheta_{a,i}$  typically vary slowly. Correspondingly, the received signal is now given by

$$r_\nu(t) = \sum_{n=0}^{N_\tau-1} \sum_{i=1}^{N_{P,n}} a_{\nu,\mu,n,i}(t) e^{j(\varphi_{T_x,\mu}(\vartheta_{d,i}(t)) + \varphi_{R_x,\nu}(\vartheta_{a,i}(t)))} \delta(t - \tau_n) \quad (\text{F.6a})$$

$$=: \sum_{n=0}^{N_\tau-1} f_{\nu,\mu}(\tau_n, t) \delta(t - \tau_n), \quad (\text{F.6b})$$

where  $f_{\nu,\mu}(\tau_n, t)$  represents the overall complex gain factor associated with delay  $\tau_n$ . The gain factors  $f_{\nu,\mu}(\tau_n, t)$  exhibit a fading amplitude, due to constructive and non-constructive superposition of the  $N_{P,n}$  signal components associated with delay  $\tau_n$ .

## F.2 Statistical Multipath Propagation Model

Since the complex gain factors  $a_{\nu,\mu,n,i}(t)$  in (F.6a) result from a quasi-random, incoherent superposition of several complex terms, cf. (F.1), an accurate deterministic description is typically difficult. In addition to this, as soon as the number of propagation paths,  $N_P$ , is large, a deterministic model becomes quite involved. It is therefore advisable to model the complex gain factors  $a_{\nu,\mu,n,i}(t)$  as random variables [BGP02].

In the sequel, three common assumptions are discussed that are adopted within the scope of this thesis: (i) The assumption of a rich-scattering environment [Hoe92], (ii) the assumption of wide-sense stationarity (WSS) and uncorrelated scattering (US) [Bel63], and (iii) the assumption of independent spatial and temporal correlations [XWL+04].

### Three Common Assumptions

Although a statistical view significantly simplifies the multipath signal propagation model, it is still a challenging task to find an accurate statistical description for arbitrary scattering [Mue02a]. This is because the probability density functions (PDFs) of the gain

factors  $a_{\nu,\mu,n,i}(t)$  depend on many parameters, e.g., the distance between transmitter and receiver, the scatterer topology, the morphology of the environment, the weather conditions, the antenna array beam patterns, and the employed carrier frequency. In order to further simplify the description, the assumption of a rich-scattering environment is often made in the literature [Hoe92,XWL+04]. We will adopt this assumption in the following, in order to arrive at a tractable statistical multipath signal propagation model, which includes time-variance and spatial correlation.

**Assumption F.2 (Rich-scattering environment)**

We assume that for all discrete delays  $\tau_n$  ( $n=0, \dots, N_\tau-1$ ) the number  $N_{P,n}$  of corresponding propagation paths tends to infinity. According to the relaxed central limit theorem (cf. Theorem C.3 in Appendix C), the gain factors  $f_{\nu,\mu}(\tau_n, t)$  can thus be modeled as (circularly symmetric) complex Gaussian random variables<sup>4</sup> [Hoe92], i.e.,

$$f_{\nu,\mu}(\tau_n, t) \sim \mathcal{CN}(\bar{f}_{\nu,\mu,n}, \sigma_{f_{\nu,\mu,n}}^2), \quad (\text{F.7})$$

where  $\bar{f}_{\nu,\mu,n} := \mathbf{E}\{f_{\nu,\mu}(\tau_n, t)\}$  denotes the mean and  $\sigma_{f_{\nu,\mu,n}}^2 := \mathbf{E}\{|f_{\nu,\mu}(\tau_n, t) - \bar{f}_{\nu,\mu,n}|^2\}$  the variance of  $f_{\nu,\mu}(\tau_n, t)$  (cf. Definition C.9). Due to the Gaussian assumption (F.7), the statistical properties of the complex gain factors  $f_{\nu,\mu}(\tau_n, t)$ ,  $n=0, \dots, N_\tau-1$ , are fully captured by the means  $\bar{f}_{\nu,\mu,n}$ , the variances  $\sigma_{f_{\nu,\mu,n}}^2$ , and the covariances

$$\sigma_{f_{\nu,\mu,n},n'}^2(t', t) := \mathbf{E}\{(f_{\nu,\mu}(\tau_n, t) - \bar{f}_{\nu,\mu,n})(f_{\nu,\mu}(\tau_{n'}, t') - \bar{f}_{\nu,\mu,n'})^*\} \quad (\text{F.8})$$

(cf. Definition C.18).

**Remark F.2 (Rayleigh and Rice fading)**

The first gain factor  $f_{\nu,\mu}(\tau_0, t) \sim \mathcal{CN}(\bar{f}_{\nu,\mu,0}, \sigma_{f_{\nu,\mu,0}}^2)$  may contain a LoS component. In this case, we have  $\tau_0=0$  and  $\bar{f}_{\nu,\mu,0} \neq 0$ , and the fading amplitude  $|f_{\nu,\mu}(\tau_0, t)|$  is Rician distributed [Ric48] (cf. Definition C.12) with Rice factor  $K_{\nu,\mu} := |\bar{f}_{\nu,\mu,0}|^2 / \sigma_{f_{\nu,\mu,0}}^2$ . The Rice factor  $K_{\nu,\mu}$  represents the ratio between LoS signal power and the average power of the scattered components. All other gain factors  $f_{\nu,\mu}(\tau_n, t)$  with  $\tau_n > 0$  are zero mean, and the fading amplitudes  $|f_{\nu,\mu}(\tau_n, t)|$  are Rayleigh distributed (cf. Definition C.11).

The average powers of the individual gain factors  $f_{\nu,\mu}(\tau_n, t)$ ,  $n=0, \dots, N_\tau-1$ , are collected in the so-called power delay profile:

**Definition F.1 (Power delay profile)**

The *power delay profile (PDP)* of the link between transmit antenna  $\mu$  ( $1 \leq \mu \leq M$ ) and receive antenna  $\nu$  ( $1 \leq \nu \leq N$ ) is defined as

$$\mathbf{P}f_{\nu,\mu} := [ |\bar{f}_{\nu,\mu,0}|^2 + \sigma_{f_{\nu,\mu,0}}^2, \sigma_{f_{\nu,\mu,1}}^2, \dots, \sigma_{f_{\nu,\mu,N_\tau-1}}^2 ]^T. \quad (\text{F.9})$$

Signal components with a large relative delay are typically subject to stronger attenuation than those with a smaller delay (due to larger propagation path lengths). Correspondingly,

<sup>4</sup>In practice, a finite number of propagation paths, e.g.  $N_{P,n} > 20$ , is sufficient, in order to generate gain factors  $f_{\nu,\mu}(\tau_n, t)$  that are virtually Gaussian distributed.



it is reasonable to assume that the PDP decays with growing delay  $\tau_n$ . A common assumption often found in the literature is an exponential decay of the PDP [PBKM00, ITE02], i.e.,

$$\sigma_{f_{\nu,\mu,n}}^2 \propto \exp\left(-\frac{\tau_n}{c_\tau}\right), \quad (\text{F.10})$$

where  $c_\tau$  is an appropriate constant. •

**Remark F.3 (Co-located and distributed MIMO systems)**

In the case of a co-located MIMO system, cf. Fig. 1.2 a) in Section 1.2, it is reasonable to assume that the PDP is the same for all transmission links. On average, all links from a certain transmit antenna to a certain receive antenna experience the same physical environment. In a distributed system, however, different PDPs may result for the individual links. In particular, the overall average power of the gain factors  $f_{\nu,\mu}(\tau_n, t)$  (i.e., the sum over the elements of  $\mathbf{p}_{f_{\nu,\mu}}$ ) will in general be different from one link to another, due to different distances between the transmit and the receive antennas.

In the following, we specify the covariances  $\sigma_{f_{\nu,\mu,n,n'}}^2(t', t)$  of the complex gain factors  $f_{\nu,\mu}(\tau_n, t)$ , cf. (F.8), where we focus on zero-mean gain factors for simplicity<sup>5</sup>. In this context, we adopt an assumption which is widely used in the literature, namely the assumption of wide-sense stationarity (WSS) and uncorrelated scattering (US). The WSSUS model for wireless communication channels [Bel63] was shown to be a good model for many wireless channels of practical interest.

**Assumption F.3 (WSSUS model)**

We assume a wireless communication channel that is wide-sense stationary with uncorrelated scattering. Uncorrelated scattering implies that two gain factors  $f_{\nu,\mu}(\tau_n, t)$  and  $f_{\nu',\mu'}(\tau_{n'}, t)$  associated with different discrete delays  $\tau_n$  and  $\tau_{n'}$  are uncorrelated, i.e., the covariances (for a fixed time  $t$ ) are given by

$$\sigma_{f_{\nu,\mu,n,n'}}^2 := \mathbf{E}\{f_{\nu,\mu}(\tau_n, t) f_{\nu',\mu'}^*(\tau_{n'}, t)\} = \sigma_{f_{\nu,\mu,n}}^2 \delta[n - n']. \quad (\text{F.11})$$

This is a reasonable assumption, since different signal delays are typically associated with different scattering objects. Stationarity implies that the statistical properties of the gain factors  $f_{\nu,\mu}(\tau_n, t)$ , such as the spatial covariances

$$\mathbf{E}\{f_{\nu,\mu}(\tau_n, t) f_{\nu',\mu'}^*(\tau_n, t)\} =: \begin{cases} \sigma_{f_{\nu,\mu,\nu',\mu',n}}^2 & \text{for } \mu' \neq \mu \text{ or } \nu' \neq \nu \\ \sigma_{f_{\nu,\mu,n}}^2 & \text{for } \mu' = \mu \text{ and } \nu' = \nu \end{cases} \quad (\text{F.12})$$

(considered below) are time-invariant.<sup>6</sup> Specifically, the auto-correlation function

$$R_{f_{\nu,\mu,n}}(t + \Delta t, t) := \mathbf{E}\{f_{\nu,\mu}(\tau_n, t) f_{\nu,\mu}^*(\tau_n, t + \Delta t)\} / \sigma_{f_{\nu,\mu,n}}^2 \quad (\text{F.13})$$

<sup>5</sup>Given a gain factor  $f_{\nu,\mu}(\tau_0, t)$  with non-zero mean, the subsequent considerations apply only for the scattered components. The LoS component must be considered separately.

<sup>6</sup>Since we have assumed that the gain factors  $f_{\nu,\mu}(\tau_n, t)$  are (circularly symmetric) complex Gaussian random variables, the wireless channel is even strict-sense stationary [Hoe92], i.e., the complete joint PDF of the gain factors does not depend on the absolute time  $t$ .

depends only on the time difference  $\Delta t$ , but not on the absolute time  $t$ .

So far, we have focussed on a single transmit antenna  $\mu$  ( $1 \leq \mu \leq M$ ) and a single receive antenna  $\nu$  ( $1 \leq \nu \leq N$ ). Next, we consider the spatial covariances  $\sigma_{f_{\nu,\mu,\nu',\mu',n}}^2$  between two gain factors  $f_{\nu,\mu}(\tau_n, t)$  and  $f_{\nu',\mu'}(\tau_n, t)$ .

#### Assumption F.4 (Spatio-temporal correlation)

An assumption often made in the literature is that spatial and temporal correlation properties can be modeled independently. Obviously, the joint spatio-temporal statistics of a MIMO channel are not captured by this method, although they may be important for advanced MIMO system designs [XCHV04]. On the other hand, extensive measurement campaigns are necessary, in order to acquire the spatio-temporal statistics of a given wireless scenario in the first place. Within this thesis we will mostly consider quasi-static scenarios, i.e., spatio-temporal channel statistics are beyond scope. Correspondingly, we set the spatio-temporal correlations to

$$\frac{\mathbb{E}\{f_{\nu,\mu}(\tau_n, t) f_{\nu',\mu'}^*(\tau_n, t + \Delta t)\}}{\sqrt{\sigma_{f_{\nu,\mu,n}}^2 \sigma_{f_{\nu',\mu',n}}^2}} =: \rho_{f_{\nu,\mu,\nu',\mu',n}} \cdot R_{f_{\nu,\mu,n}}(t + \Delta t, t), \quad (\text{F.14})$$

where

$$\rho_{f_{\nu,\mu,\nu',\mu',n}} := \frac{\sigma_{f_{\nu,\mu,\nu',\mu',n}}^2}{\sqrt{\sigma_{f_{\nu,\mu,n}}^2 \sigma_{f_{\nu',\mu',n}}^2}}, \quad (\text{F.15})$$

cf. (F.12). Note that the spatio-temporal correlations are in general complex-valued. In a co-located MIMO system, where all transmission links experience (on average) the same physical environment, the auto-correlation function  $R_{f_{\nu,\mu,n}}(t + \Delta t, t)$  does not depend on the indices  $\mu$  and  $\nu$ . The parameters  $\rho_{f_{\nu,\mu,\nu',\mu',n}}$  are called spatial correlations in the sequel. The magnitude of  $\rho_{f_{\nu,\mu,\nu',\mu',n}}$  is always between zero and one, where  $|\rho_{f_{\nu,\mu,\nu',\mu',n}}| = 0$  represents the uncorrelated case and  $|\rho_{f_{\nu,\mu,\nu',\mu',n}}| = 1$  the case of full spatial correlation.

#### The Kronecker Correlation Model

Spatial correlation is caused by a lack of scattering from the physical environment and by insufficient antenna spacings. Correspondingly, given a rich-scattering environment and generous antenna spacings, the spatial correlations are given by  $\rho_{f_{\nu,\mu,\nu',\mu',n}} = \delta[\mu - \mu']$  and  $\rho_{f_{\nu,\mu,\nu',\mu',n}} = \delta[\nu - \nu']$ . In many publications on spatially correlated MIMO channels, e.g. [PBKM00, CTKV02, KSP+02, GBGP02, WJSJ03, XCHV04, XWL+04], the following three assumptions are made:

- (a) The spatial correlations  $\rho_{f_{\nu,\mu,\nu',\mu',n}}$  ( $n = 0, \dots, N_\tau - 1$ ) associated with two transmit antennas  $\mu$  and  $\mu'$  do not depend on the specific receive antenna  $\nu$  under consideration. Correspondingly, the correlations  $\rho_{f_{\nu,\mu,\nu',\mu',n}}$  can be written as  $\rho_{f_{\nu,\mu,\nu',\mu',n}} =: \rho_{f_{\mu,\mu',n}}$  (transmit antenna correlations).
- (b) The spatial correlations  $\rho_{f_{\nu,\mu,\nu',\mu',n}}$  ( $n = 0, \dots, N_\tau - 1$ ) associated with two receive antennas  $\nu$  and  $\nu'$  do not depend on the specific transmit antenna  $\mu$  under consideration. Correspondingly, the correlations  $\rho_{f_{\nu,\mu,\nu',\mu',n}}$  can be written as  $\rho_{f_{\nu,\mu,\nu',\mu',n}} =: \rho_{f_{\nu,\nu',n}}$  (receive antenna correlations).

- (c) The spatial correlations  $\rho_{f_{\nu,\mu,\nu',\mu',n}}$  ( $n=0, \dots, N_\tau-1$ ) associated with transmit antenna pair  $(\mu, \mu')$  and receive antenna pair  $(\nu, \nu')$  can be written as products of the transmit antenna correlations  $\rho_{f_{\mu,\mu',n}}$  and the receive antenna correlations  $\rho_{f_{\nu,\nu',n}}$ .

The above three assumptions are known as the Kronecker correlation model:

**Assumption F.5 (Kronecker correlation model)**

We assume that the spatial correlations  $\rho_{f_{\nu,\mu,\nu',\mu',n}}$  ( $\mu, \mu'=1, \dots, M$ ,  $\nu, \nu'=1, \dots, N$ ,  $n=0, \dots, N_\tau-1$ ) can be written as products

$$\rho_{f_{\nu,\mu,\nu',\mu',n}} = \rho_{f_{\nu,\mu,\nu,\mu',n}} \cdot \rho_{f_{\nu,\mu,\nu',\mu,n}} =: \rho_{f_{\mu,\mu',n}} \cdot \rho_{f_{\nu,\nu',n}} \quad (\text{F.16})$$

of transmit and receive antenna correlations. Specifically, for  $\mu'=\mu$  and  $\nu'=\nu$  we have  $\rho_{f_{\nu,\mu,\nu,\mu,n}} = \rho_{f_{\mu,\mu,n}} = \rho_{f_{\nu,\nu,n}} = 1$ . Since the magnitudes of  $\rho_{f_{\mu,\mu',n}}$  and  $\rho_{f_{\nu,\nu',n}}$  are between zero and one,  $|\rho_{f_{\nu,\mu,\nu',\mu',n}}|$  tends to be comparatively small if  $\mu' \neq \mu$  and  $\nu' \neq \nu$  holds [CTKV02].

**Remark F.4 (Accuracy of the Kronecker correlation model)**

The Kronecker correlation model was shown to be quite accurate, in order to model the spatial correlation properties of practical MIMO channels [XWL+04], at least for co-located systems with a moderate number of transmit and receive antennas [OHW+03]. It should be noted that for systems with distributed transmit antennas and correlated receive antennas (or vice versa), a more advanced correlation model might be necessary, because in this case the receive antenna correlations might depend on the specific transmit antenna under consideration.<sup>7</sup> Nevertheless, we will mainly employ the Kronecker correlation model within this thesis. Possible generalizations are discussed in Section 3.3.

We have now arrived at a statistical multipath signal propagation model for a general MIMO system with  $M$  transmit and  $N$  receive antennas, which includes the effects of spatial and temporal correlations. Altogether, with the above assumptions the correlations of the complex gain factors  $f_{\nu,\mu}(\tau_n, t)$  are given by [XWL+04]

$$\frac{\mathbb{E}\{f_{\nu,\mu}(\tau_n, t) f_{\nu',\mu'}^*(\tau_{n'}, t + \Delta t)\}}{\sqrt{\sigma_{f_{\nu,\mu,n}}^2 \sigma_{f_{\nu',\mu',n'}}^2}} = \rho_{f_{\mu,\mu',n}} \cdot \rho_{f_{\nu,\nu',n}} \cdot R_{f_{\nu,\mu,n}}(t + \Delta t, t) \cdot \delta[n - n'], \quad (\text{F.17})$$

where  $1 < \mu, \mu' < M$ ,  $1 < \nu, \nu' < N$ , and  $0 < n, n' < N_\tau - 1$ .

### F.3 Calculation of Antenna Correlations

The calculation of the transmit antenna correlations  $\rho_{f_{\mu,\mu',n}}$  and the receive antenna correlations  $\rho_{f_{\nu,\nu',n}}$  can be done on the basis of (F.6), where  $N_{P,n} \rightarrow \infty$ . Since we have assumed

<sup>7</sup>An improved correlation model, known as the W-model, was for example proposed in [WHOB06].

that all propagation paths  $i = 1, \dots, N_{P,n}$  are associated with different scatterers, two different gain factors  $a_{\nu,\mu,n,i}(t)$  and  $a_{\nu,\mu,n,i'}(t)$  can be regarded as uncorrelated. Correspondingly, one finds that

$$\begin{aligned} \mathbb{E}\{f_{\nu,\mu}(\tau_n, t) f_{\nu,\mu'}^*(\tau_n, t)\} &= \\ \lim_{N_{P,n} \rightarrow \infty} \sum_{i=1}^{N_{P,n}} \mathbb{E}\{a_{\nu,\mu,n,i}(t) a_{\nu,\mu',n,i}^*(t)\} e^{j(\varphi_{\text{Tx},\mu}(\vartheta_{d,i}) - \varphi_{\text{Tx},\mu'}(\vartheta_{d,i}))} & \quad (\text{F.18}) \end{aligned}$$

$$\begin{aligned} \text{and} \quad \mathbb{E}\{f_{\nu,\mu}(\tau_n, t) f_{\nu',\mu}^*(\tau_n, t)\} &= \\ \lim_{N_{P,n} \rightarrow \infty} \sum_{i=1}^{N_{P,n}} \mathbb{E}\{a_{\nu,\mu,n,i}(t) a_{\nu',\mu,n,i}^*(t)\} e^{j(\varphi_{\text{Rx},\nu}(\vartheta_{a,i}) - \varphi_{\text{Rx},\nu'}(\vartheta_{a,i}))}. & \quad (\text{F.19}) \end{aligned}$$

Since the angles of departure and arrival typically change much more slowly than the complex gain factors  $a_{\nu,\mu,n,i}(t)$ , we have dropped the dependence of  $\vartheta_{d,i}$  and  $\vartheta_{a,i}$  on the absolute time. Let us denote

$$P_{a_i} := \mathbb{E}\{a_{\nu,\mu,n,i}(t) a_{\nu',\mu',n,i}^*(t)\} = \mathbb{E}\{a_{\nu,\mu,n,i}(t) a_{\nu',\mu,n,i}^*(t)\} \quad (\text{F.20})$$

( $i = 1, \dots, N_{P,n}$ ), where<sup>8</sup>

$$\lim_{N_{P,n} \rightarrow \infty} \sum_{i=1}^{N_{P,n}} P_{a_i} =: \sigma_{f_{\nu,\mu,n}}^2. \quad (\text{F.21})$$

Each power term  $P_{a_i}$  is associated with a unique AoD  $\vartheta_{d,i}$  and a unique AoA  $\vartheta_{a,i}$ . Correspondingly, we can rewrite (F.18) and (F.19) as

$$\mathbb{E}\{f_{\nu,\mu}(\tau_n, t) f_{\nu,\mu'}^*(\tau_n, t)\} = \lim_{N_{P,n} \rightarrow \infty} \sum_{i=1}^{N_{P,n}} P_{a_i}(\vartheta_{d,i}) e^{j(\varphi_{\text{Tx},\mu}(\vartheta_{d,i}) - \varphi_{\text{Tx},\mu'}(\vartheta_{d,i}))}, \quad (\text{F.22a})$$

$$\mathbb{E}\{f_{\nu,\mu}(\tau_n, t) f_{\nu',\mu}^*(\tau_n, t)\} = \lim_{N_{P,n} \rightarrow \infty} \sum_{i=1}^{N_{P,n}} P_{a_i}(\vartheta_{a,i}) e^{j(\varphi_{\text{Rx},\nu}(\vartheta_{a,i}) - \varphi_{\text{Rx},\nu'}(\vartheta_{a,i}))}. \quad (\text{F.22b})$$

Recall that the power terms  $P_{a_i}(\vartheta_{d,i})$  and  $P_{a_i}(\vartheta_{a,i})$  also comprise the antenna array gains in the direction of  $\vartheta_{d,i}$  and  $\vartheta_{a,i}$ , since this was assumed earlier for the complex gain factors  $a_{\nu,\mu,n,i}(t)$ .

### Definition F.2 (Power azimuth spectrum)

In the limit, the terms

$$\sum_{i=1}^{N_{P,n}} P_{a_i}(\vartheta_{d,i}) \quad \text{and} \quad \sum_{i=1}^{N_{P,n}} P_{a_i}(\vartheta_{a,i}) \quad (\text{F.23})$$

in (F.22) approach continuous functions  $P_n(\vartheta_d)$  and  $P_n(\vartheta_a)$ , referred to as transmitter- and receiver-sided *power azimuth spectrum (PAS)* [XCHV04]. Note that different discrete

<sup>8</sup>The power terms  $P_{a_i}$  have been assumed to be identical for all indices  $\mu, \mu', \nu, \nu'$ . This is reasonable, since we consider a MIMO system with co-located transmit and receive antennas.

delays  $\tau_n$  may be associated with different power azimuth spectra. Since we have focussed on two-dimensional signal propagation within the azimuth plane (cf. Fig. F.1), we have

$$\int_0^{2\pi} P_n(\vartheta_d) d\vartheta_d = \int_0^{2\pi} P_n(\vartheta_a) d\vartheta_a = \sigma_{f_{\nu,\mu,n}}^2. \quad (\text{F.24})$$

In the case of a three-dimensional multipath propagation model, the power azimuth spectra would additionally depend on the elevation angle under consideration. •

Using the above definition, we finally obtain the following expressions for the transmit antenna correlations  $\rho_{f_{\mu,\mu'},n}$  and the receive antenna correlations  $\rho_{f_{\nu,\nu'},n}$ :

$$\rho_{f_{\mu,\mu'},n} = \frac{1}{\sigma_{f_{\nu,\mu,n}}^2} \int_0^{2\pi} P_n(\vartheta_d) e^{j(\varphi_{\text{Tx},\mu}(\vartheta_d) - \varphi_{\text{Tx},\mu'}(\vartheta_d))} d\vartheta_d, \quad (\text{F.25a})$$

$$\rho_{f_{\nu,\nu'},n} = \frac{1}{\sigma_{f_{\nu,\mu,n}}^2} \int_0^{2\pi} P_n(\vartheta_a) e^{j(\varphi_{\text{Rx},\nu}(\vartheta_a) - \varphi_{\text{Rx},\nu'}(\vartheta_a))} d\vartheta_a, \quad (\text{F.25b})$$

where we have used that  $\sigma_{f_{\nu,\mu',n}}^2 = \sigma_{f_{\nu',\mu,n}}^2 = \sigma_{f_{\nu,\mu,n}}^2$  (co-located MIMO system). Numerical examples for the antenna correlations  $\rho_{f_{\mu,\mu'},n}$  and  $\rho_{f_{\nu,\nu'},n}$  are presented in Section F.4.

#### Remark F.5 (Angular PDFs)

Any PAS  $P_n(\vartheta)$  can be written as

$$P_n(\vartheta) := \sigma_{f_{\nu,\mu,n}}^2 \cdot p_{\vartheta}(\vartheta), \quad (\text{F.26})$$

where  $p_{\vartheta}(\vartheta)$  is an appropriate angular PDF, which depends in general on the discrete delay  $\tau_n$  under consideration. If the transmitter/receiver is surrounded by many local scatterers, like a mobile station in a typical urban or indoor environment, it is reasonable to assume that the PAS is uniform within a certain angular region (and zero elsewhere) [SFGK00]. Consequently, one can choose

$$p_{\vartheta}(\vartheta) = \begin{cases} 1/(2\Delta\vartheta) & \text{for } \vartheta \in [\bar{\vartheta} - \Delta\vartheta, \bar{\vartheta} + \Delta\vartheta] \\ 0 & \text{else} \end{cases}, \quad (\text{F.27})$$

i.e.,  $\vartheta \sim \mathcal{U}([\bar{\vartheta} - \Delta\vartheta, \bar{\vartheta} + \Delta\vartheta])$ , where  $\bar{\vartheta}$  is the mean angle of departure/arrival. Base stations are typically surrounded by comparatively few local scatterers, because they are usually installed at rooftop level. Most of the transmitted/received signal power is thus concentrated within a small angular region comprising the local scatterers around the mobile station. The corresponding PAS is often modeled by means of a (truncated) Gaussian or Laplacian PDF [PMF00, ITE02, ZN03, ZSM+03], i.e.,

$$\vartheta \sim \mathcal{N}(\bar{\vartheta}, \sigma_{\vartheta}^2) \quad \text{or} \quad \vartheta \sim \mathcal{L}(\bar{\vartheta}, \sigma_{\vartheta}^2) \quad (\text{F.28})$$

(cf. Definitions C.7 and C.8 in Appendix C), where the parameter  $\sigma_{\vartheta}^2$  determines the effective width of the PAS.

**Remark F.6 (Uniform power azimuth spectrum)**

In the case of a ULAA and a uniform PAS within  $[-\pi, +\pi]$ , one obtains a particularly simple result for the transmit and receive antenna correlations (cf. [GSS+03]):

$$\rho_{f_{\mu,\mu',n}} = J_0\left(\frac{2\pi d}{\lambda_c}(\mu - \mu')\right), \quad \rho_{f_{\nu,\nu',n}} = J_0\left(\frac{2\pi d}{\lambda_c}(\nu - \nu')\right), \quad (\text{F.29})$$

where the integral representation (C.10) of the Bessel function of the first kind has been used (see Appendix C). Note that  $\rho_{f_{\mu,\mu',n}}$  and  $\rho_{f_{\nu,\nu',n}}$  are real-valued in this case. It should, however, be noted that it might be unrealistic to assume a uniform PAS for all delays  $\tau_n$ , especially for large delays. Generalizations of (F.29) to a uniform PAS within  $[\vartheta_{\min}, \vartheta_{\max}] \subset [-\pi, +\pi]$  can be found in [SFGK00]. Specifically, for some examples approximations are stated that lead to a similar  $J_0(x)$ -representation as (F.29).

**Remark F.7 (Clarke's model)**

The above result is very much related to Clarke's model, which is often employed in the literature, in order to model temporal correlation effects at a mobile terminal. In Clarke's model, it is assumed that

$$R_{f_{\nu,\mu,n}}(t+\Delta t, t) = J_0(2\pi f_{D,\max}\Delta t) \quad (\text{F.30})$$

holds for all indices  $\nu, \mu$  and  $n$  [XWL+04], where  $f_{D,\max} := v/\lambda_c$  denotes the maximum Doppler frequency, with  $v$  being the speed of the mobile terminal. Similar to (F.29), Clarke's model is only valid if the mobile terminal observes a uniform PAS within  $[-\pi, +\pi]$ . For more general scenarios, one can derive an integral expression for  $R_{f_{\nu,\mu,n}}(t+\Delta t, t)$ , which is similar to (F.25) [XCHV04].

## F.4 Numerical Examples

In the following, a couple of numerical examples are provided, which illustrate some of the above definitions as well as certain definitions occurring in the discrete-time MIMO channel model derived in Section 2.2.2. We start with some numerical examples for the transmit and receive antenna correlations  $\rho_{f_{\mu,\mu',n}}$  and  $\rho_{f_{\nu,\nu',n}}$  defined in (F.25).

**Example F.2 (Transmit and receive antenna correlations)**

In the case of a ULAA with antenna spacing  $d$  and broad-side orientation (cf. Fig. F.1), the transmit antenna correlations are given by

$$\rho_{f_{\mu,\mu',n}} = \int_0^{2\pi} p_{\vartheta_d}(\vartheta_d) \exp\left(-j\frac{2\pi d}{\lambda_c}(\mu - \mu') \sin(\vartheta_d)\right) d\vartheta_d \quad (\text{F.31})$$

(cf. [GSS+03]). For the receive antenna correlations, replace  $\mu$  by  $\nu$  and  $\vartheta_d$  by  $\vartheta_a$ . Fig. F.3 shows some numerical results for the correlation between neighboring antenna elements obtained by means of numerical integration. Displayed is the absolute antenna correlation  $|\rho_{f_{\mu,\mu-1,n}}|$  plotted as a function of the relative antenna spacing  $d/\lambda_c$ . As an example, a uniform PAS within  $[-\Delta\vartheta, +\Delta\vartheta]$  is considered for different values for  $\Delta\vartheta$ . As can be seen, if the angular region of the PAS is

small, the resulting correlation tends to be more significant. For example, in the case  $\Delta\vartheta = 0.1\pi$  an antenna spacing of  $d/\lambda_c > 0.95$  is required, in order to obtain a correlation value  $|\rho_{f_{\mu,\mu-1,n}}| < 0.5$ , whereas in the case  $\Delta\vartheta = \pi$  an antenna spacing of  $d/\lambda_c > 0.25$  is already sufficient. However, the antenna correlations do not only depend on the width of the PAS, but also on the mean angle of departure/arrival. This is shown in Fig. F.4, where different uniform PAS within  $[\bar{\vartheta} - \pi/4, \bar{\vartheta} + \pi/4]$  are considered. As can be seen, the resulting correlation becomes more significant when  $\bar{\vartheta}$  approaches  $\pi/2$ , because this reduces the effective antenna spacing seen from the direction of departure/arrival.

In the case of a CAA with radius  $R$  and orientation as shown in Fig. F.2, the (transmit) antenna correlations between the outer antenna elements and the inner antenna element are given by

$$\rho_{f_{\mu,1,n}} = \int_0^{2\pi} p_{\vartheta_d}(\vartheta_d) \exp\left(-j \frac{2\pi R}{\lambda_c} \cos\left(\vartheta_d - \frac{2\pi(\mu-2)}{M-1}\right)\right) d\vartheta_d, \quad (\text{F.32})$$

where  $2 \leq \mu \leq M$ . The correlations between the outer antenna elements result as

$$\begin{aligned} \rho_{f_{\mu,\mu',n}} = \int_0^{2\pi} p_{\vartheta_d}(\vartheta_d) \exp\left(-j \frac{4\pi R}{\lambda_c} \sin\left(\frac{\pi(\mu-\mu')}{M-1}\right) \right. \\ \left. \times \sin\left(\vartheta_d - \frac{\pi(\mu+\mu'-4)}{M-1}\right)\right) d\vartheta_d, \end{aligned} \quad (\text{F.33})$$

where  $2 \leq \mu, \mu' \leq M$ . Fig. F.5 shows some numerical results for the correlations between the outer antenna elements of a CAA with  $M = 6$  elements. Similar curves have also been obtained for the correlations between the outer antenna elements and the inner antenna element. The absolute antenna correlation  $|\rho_{f_{\mu_1,\mu_2,n}}|$  is plotted as a function of the relative antenna radius  $R/\lambda_c$ , where the antenna pairs  $(\mu_1, \mu_2) = (3, 2), (4, 3)$  and  $(5, 4)$  have been taken into account. As an example, a Gaussian PAS (dark color) and a Laplacian PAS (light color) has been considered, with  $\bar{\vartheta} = 0$  and  $\sigma_{\bar{\vartheta}}^2 = 1$  in both cases. As can be seen, the correlations resulting for the individual antenna pairs are quite different, both for the Gaussian PAS and the Laplacian PAS. Similar to the ULAA with uniform PAS, the correlation for a specific antenna pair tends to be more significant when the effective antenna spacing is small (seen from the mean direction of departure/arrival,  $\bar{\vartheta}$ ). In addition to this, we note that the difference between the Gaussian and the Laplacian PAS can be quite significant (at least for specific values of the antenna radius). Fig. F.6 shows corresponding results for a smaller variance  $\sigma_{\bar{\vartheta}}^2$  of 0.1. As can be seen, the resulting correlations tend to be more pronounced than in the case  $\sigma_{\bar{\vartheta}}^2 = 1$ , since the effective width of the PAS is decreased.  $\diamond$

Finally, a numerical example for the discrete-time MIMO channel model is presented, which concerns the channel power profile  $\mathbf{p}_{h_{\nu,\mu}}$ , cf. (2.38), and the spatial correlations  $\rho_{h_{\mu,\mu',l}}$ , cf. (2.43).

### Example F.3 (Discrete-time MIMO channel model)

As an example, we consider a system with two transmit antennas and a single receive antenna. We assume that the two transmission links are characterized



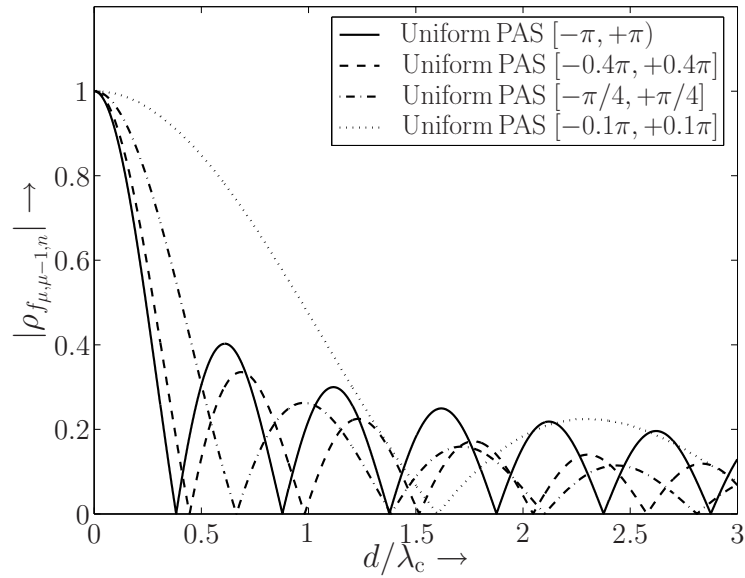


Figure F.3: Absolute correlation between neighboring antenna elements of a ULAA with antenna spacing  $d$  and broad-side orientation: Uniform PAS within  $[-\Delta\vartheta, +\Delta\vartheta]$ , different values for  $\Delta\vartheta$  considered.

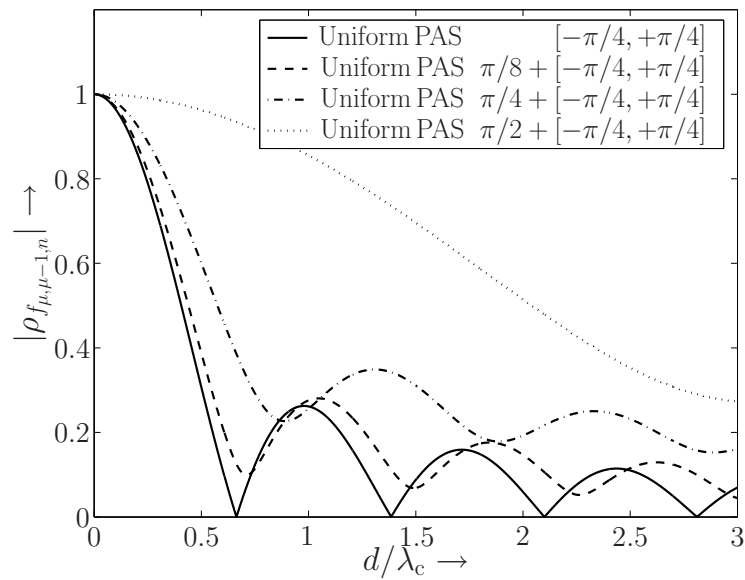


Figure F.4: Absolute correlation between neighboring antenna elements of a ULAA with antenna spacing  $d$  and broad-side orientation: Uniform PAS within  $\bar{\vartheta} + [-\pi/4, +\pi/4]$ , different values for  $\bar{\vartheta}$  considered.

by Rayleigh fading with identical two-tap power delay profile  $\mathbf{p}_{f_{\nu,\mu}} := [1.0, 0.4]^T$  ( $\mu=1, 2, \nu=1$ ), where  $\tau_0 := 0$  and  $\tau_1 := T/2$  ( $N_\tau = 2$ ). The spatial correlations  $\rho_{f_{\mu,\mu',n}}$  ( $\mu=1, \mu'=2, n=0, 1$ ) associated with the two transmit antennas are assumed to be  $\rho_{f_{1,2,0}} = 0.5$  and  $\rho_{f_{1,2,1}} = 0.8$ . For the overall impulse response of transmit and receive filtering,  $g(t)$ , a cosine roll-off impulse with roll-off factor  $r=0.5$  is assumed (cf. Definition C.1 in Appendix C). Sampling is performed with respect to delay  $\tau_0$ , i.e., the sampling phase is chosen as  $\epsilon=0$ . The corresponding channel power profile  $\mathbf{p}_{h_{\nu,\mu}}$  ( $\mu=1, 2, \nu=1$ ) results as

$$\mathbf{p}_{h_{\nu,\mu}} = [1.1442 \quad 0.1440]^T, \quad (L=1), \quad (\text{F.34})$$

cf. (2.37) and (2.38), where variances  $\sigma_{h_{\nu,\mu,l}}^2 < 0.01$  have been neglected. The spatial correlations  $\rho_{h_{\mu,\mu',l}}$  ( $\mu=1, \mu'=2, l=0, 1$ ) result as

$$\rho_{h_{1,2,0}} = 0.5378, \quad \rho_{h_{1,2,1}} = 0.8, \quad (\text{F.35})$$

cf. (2.43a), i.e., they are different for different indices  $l$ .  $\diamond$

## F.5 Further Remarks

In order to conclude this chapter on channel modeling, two further aspects are discussed in the following, namely the issues of antenna coupling and channel reciprocity.

### Remark F.8 (Antenna coupling)

Given a MIMO system with very small antenna spacings, the antenna elements are not only subject to correlation effects, but also to mutual coupling effects [CVOV03, JPv03, Chi03, WKS04, OAA04, WJ04, KR04]. Antenna coupling effects have to be modeled separately on the basis of antenna theory [Bal97] and are not captured by the MIMO channel model derived above. Mutual coupling means that current induced on one antenna element generates a voltage at the terminals of adjacent antenna elements [WJ04]. Consequently, the antenna patterns of the individual antenna elements are not independent anymore [WKS04]. In addition to this, the antenna elements absorb part of each others energy, which reduces the overall power efficiency. In [CVOV03] it was shown that antenna coupling distorts the overall array pattern. In other words, for certain directions the array gain is increased, while for other directions it is reduced. Depending on the physical environment (especially on the observed PAS), antenna coupling can thus either reduce or increase the effective correlation between the individual antenna elements.<sup>9</sup> For simplicity, we will only focus on the aspect of antenna correlations throughout this thesis, i.e., we will always assume that antenna spacings are large enough so that mutual coupling effects can be neglected. However, note that antenna coupling effects can easily be included in the model, by incorporating the resulting effective antenna correlations along with a possible loss concerning the overall transmitted/received signal power.

<sup>9</sup>At the same time, it makes a significant difference whether a user's head or hand is found close to the antenna array [WKS04, KR04], which is of interest for mobile phones equipped with multiple antennas.

**Remark F.9 (Reciprocity)**

When the same carrier frequency is employed both in the forward link and in the reverse link (uplink/downlink), one can often reuse the forward-link MIMO channel model for the reverse link. This might, for example, be the case in a time-division duplex (TDD) system, where forward and reverse link are separated using different (adjacent) time slots. Consider, for example, a TDD system where the forward link is modeled by the discrete-time MIMO channel model (2.26), cf. Section 2.2.2. Assuming strict reciprocity, the corresponding model for the reverse link is then given by

$$\mathbf{y}'[k] = \sum_{l=0}^L \mathbf{H}_l^T[k] \mathbf{x}'[k-l] + \mathbf{n}'[k], \quad (\text{F.36})$$

where  $\mathbf{y}'[k]$  denotes the  $k$ th received vector of size  $(M \times 1)$ ,  $\mathbf{x}'[k]$  the  $k$ th transmitted vector of size  $(N \times 1)$ , and  $\mathbf{n}'[k]$  the  $k$ th noise vector of size  $(M \times 1)$ . However, it should be noted that in many practical systems there are certain pause intervals between forward- and reverse-link transmission, especially in multiuser systems based on time-division multiple access (TDMA). Correspondingly, the channel coefficients  $h_{\nu,\mu,l}[k]$  may evolve between forward- and reverse-link transmission. Moreover, (F.36) implicitly assumes that transmitter and receiver employ identical analog front ends, which might not be the case in practice.

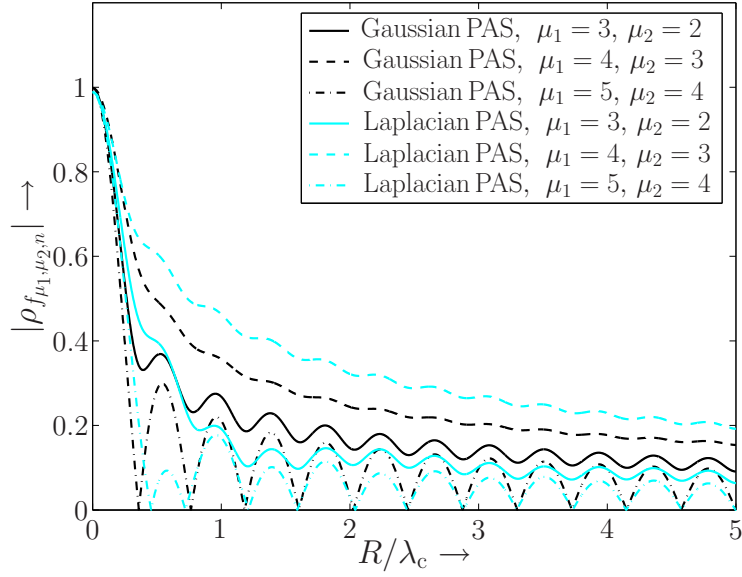


Figure F.5: Absolute correlation between the outer antenna elements of a CAA with  $M=6$  elements, radius  $R$  and orientation as in Fig. F.2: Gaussian PAS (dark color) and Laplacian PAS (light color),  $\bar{v}=0$  and  $\sigma_v^2=1$  in both cases. Different antenna pairs  $(\mu_1, \mu_2)$  have been considered.

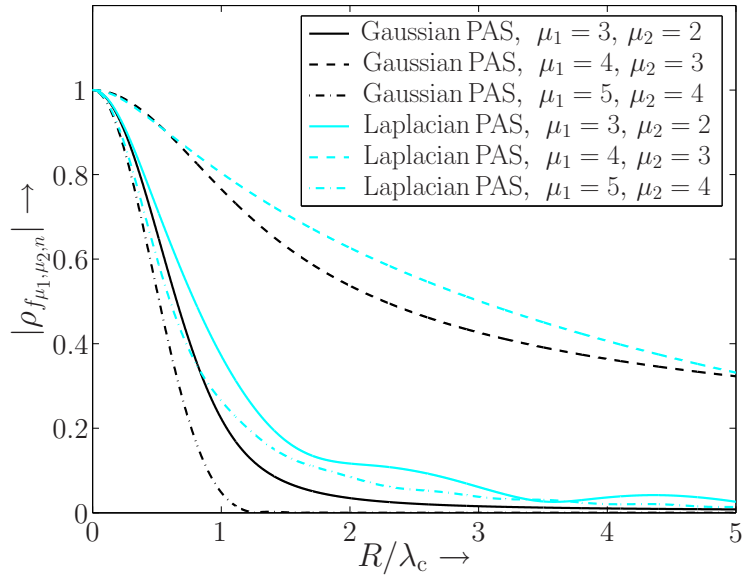


Figure F.6: Absolute correlation between the outer antenna elements of a CAA with  $M=6$  elements, radius  $R$  and orientation as in Fig. F.2: Gaussian PAS (dark color) and Laplacian PAS (light color),  $\bar{v}=0$  and  $\sigma_v^2=0.1$  in both cases. Different antenna pairs  $(\mu_1, \mu_2)$  have been considered.

# Appendix G

## Capacity of Static MIMO Channels

**A**LREADY back in 1948, Claude E. Shannon established a fundamental mathematical definition for the capacity of communication channels [Sha48]. Shannon's definition, which is still state of the art today, is based on the mutual information (cf. Definition C.21 in Appendix C) between random variables. According to this definition, the capacity of a communication channel is the maximum mutual information between channel input and channel output.<sup>1</sup> In this context the channel inputs, i.e., the transmitted data symbols, are regarded as random variables. The degree of freedom, over which the mutual information is maximized, is given by the statistical distribution of the channel input symbols.

Fundamental papers on the capacity of MIMO channels include [BW74, Tel95, FG98, RC98, Tel99, BGP02, ZT02]. In the following, some important capacity results for MIMO channels being of further interest in this thesis are recapitulated.

### G.1 Generic Capacity Result

We consider a point-to-point MIMO communication link between a transmitter equipped with  $M$  antennas and a receiver equipped with  $N$  antennas. To start with, we restrict ourselves to a static MIMO channel model. Moreover, focus is on MIMO systems without intersymbol interference (ISI). The discrete-time matrix-vector transmission model (cf. Section 2.2.2) is thus given by

$$\mathbf{y}[k] = \mathbf{H} \mathbf{x}[k] + \mathbf{n}[k], \quad (\text{G.1})$$

where  $\mathbf{y}[k] \in \mathbb{C}^N$  denotes the  $k$ th received vector,  $\mathbf{H} \in \mathbb{C}^{N \times M}$  an arbitrary fixed channel matrix,  $\mathbf{x}[k] \in \mathbb{C}^M$  the  $k$ th transmitted vector, and  $\mathbf{n}[k] \in \mathbb{C}^N$  the  $k$ th additive noise vector ( $k$  denotes the discrete time index). The entries  $x_\mu[k]$  of the transmitted vector  $\mathbf{x}[k]$  are regarded as random variables with means  $\bar{x}_\mu$  and variances  $\sigma_{x,\mu}^2$  ( $\mu=1, \dots, M$ ). Moreover, in order to have a fixed average transmission power, the means  $\bar{x}_1, \dots, \bar{x}_M$  and the variances

---

<sup>1</sup>Alternatively, one can say that the capacity of a communication channel or system is the highest rate in bits per channel use at which information can be transmitted with an arbitrarily small error probability [CT91, Ch. 8].

$\sigma_{x,1}^2, \dots, \sigma_{x,M}^2$  are subject to (s.t.) the following sum power constraint:

$$\sum_{\mu=1}^M (\bar{x}_\mu^2 + \sigma_{x,\mu}^2) = \text{tr}(\bar{\mathbf{x}}\bar{\mathbf{x}}^H + \mathbf{Q}_{\underline{\mathbf{x}}}) =: \text{tr}(\tilde{\mathbf{Q}}_{\underline{\mathbf{x}}}) \stackrel{!}{\leq} P, \quad (\text{G.2})$$

where  $\bar{\mathbf{x}} := [\bar{x}_1, \dots, \bar{x}_M]^T$  denotes the mean and  $\mathbf{Q}_{\underline{\mathbf{x}}} := \mathbf{E}\{(\mathbf{x}[k] - \bar{\mathbf{x}})(\mathbf{x}[k] - \bar{\mathbf{x}})^H\}$  the covariance matrix of the channel input vector  $\mathbf{x}[k]$ . The entries of the noise vector  $\mathbf{n}[k]$  are assumed to be independent and identically distributed (i.i.d.) samples of a zero-mean spatially and temporally white circularly symmetric complex Gaussian random process (cf. Definition C.9 in Appendix C). The variance of the noise samples is denoted as  $\sigma_n^2$ , i.e.,  $n_\nu[k] \sim \mathcal{CN}(0, \sigma_n^2)$  for all  $\nu=1, \dots, N$  and

$$\mathbf{E}\{n_\nu[k]n_{\nu'}^*[k']\} = \sigma_n^2 \cdot \delta[\nu - \nu'] \cdot \delta[k - k']. \quad (\text{G.3})$$

Finally, it is assumed that the transmitted vector  $\mathbf{x}[k]$  and the noise vector  $\mathbf{n}[k]$  are statistically independent.

For convenience, the time index  $k$  is dropped in the sequel. The capacity of the above discrete-time MIMO system is the maximum mutual information  $I(\mathbf{x}; \mathbf{y})$  between channel input vector  $\mathbf{x}$  and channel output vector  $\mathbf{y}$ :

$$C(\mathbf{H}) := \max_{p_{\underline{\mathbf{x}}}(\mathbf{x}) \text{ s.t. } \text{tr}(\tilde{\mathbf{Q}}_{\underline{\mathbf{x}}}) \leq P} I(\mathbf{x}; \mathbf{y}) \quad \text{bit/channel use}, \quad (\text{G.4})$$

where

$$I(\mathbf{x}; \mathbf{y}) = h(\mathbf{y}) - h(\mathbf{y}|\mathbf{x}) = h(\mathbf{y}) - h(\mathbf{n}) \quad (\text{G.5})$$

(cf. Definition C.21 in Appendix C). Note that the mutual information  $I(\mathbf{x}; \mathbf{y})$  is maximized over the joint PDF  $p_{\underline{\mathbf{x}}}(\mathbf{x})$  of the channel input vector  $\mathbf{x}$ , where the maximization is subject to the sum power constraint (G.2). Since the random noise vector  $\mathbf{n}$  is given (and statistically independent of the channel input vector  $\mathbf{x}$ ), maximizing  $C(\mathbf{H})$  amounts to maximizing the differential entropy  $h(\mathbf{y})$  (cf. Definition C.20) of the channel output vector  $\mathbf{y}$  [Tel99].

It can be shown that the differential entropy of any vector random variable  $\underline{\mathbf{v}} \in \mathbb{C}^m$  with covariance matrix  $\mathbf{Q}_{\underline{\mathbf{v}}} := \mathbf{E}\{(\underline{\mathbf{v}} - \bar{\underline{\mathbf{v}}})(\underline{\mathbf{v}} - \bar{\underline{\mathbf{v}}})^H\}$  is bounded above by [BT04a, App. B.2]

$$h(\underline{\mathbf{v}}) \leq \log_2 \det(e\pi \mathbf{Q}_{\underline{\mathbf{v}}}). \quad (\text{G.6})$$

Moreover, the upper bound is attained if and only if  $\underline{\mathbf{v}}$  is a multivariate complex Gaussian vector random variable (see Definition C.10 in Appendix C), i.e., if the entries of  $\underline{\mathbf{v}}$  are circularly symmetric complex Gaussian random variables:

$$\begin{aligned} h(\underline{\mathbf{v}}) &= -\mathbf{E}\{\log_2 p_{\underline{\mathbf{v}}}(\underline{\mathbf{v}})\} \stackrel{(a)}{=} \mathbf{E}\left\{\log_2(\pi^m \det(\mathbf{Q}_{\underline{\mathbf{v}}})) - \log_2(\exp(-(\underline{\mathbf{v}} - \bar{\underline{\mathbf{v}}})^H \mathbf{Q}_{\underline{\mathbf{v}}}^{-1} (\underline{\mathbf{v}} - \bar{\underline{\mathbf{v}}}))\right\} \\ &= \log_2 \det(\pi \mathbf{Q}_{\underline{\mathbf{v}}}) + \log_2(e) \cdot \mathbf{E}\left\{(\underline{\mathbf{v}} - \bar{\underline{\mathbf{v}}})^H \mathbf{Q}_{\underline{\mathbf{v}}}^{-1} (\underline{\mathbf{v}} - \bar{\underline{\mathbf{v}}})\right\} \\ &\stackrel{(b)}{=} \log_2 \det(\pi \mathbf{Q}_{\underline{\mathbf{v}}}) + \log_2(e) \cdot \mathbf{E}\left\{\text{tr}(\mathbf{Q}_{\underline{\mathbf{v}}}^{-1} (\underline{\mathbf{v}} - \bar{\underline{\mathbf{v}}})(\underline{\mathbf{v}} - \bar{\underline{\mathbf{v}}})^H)\right\} \\ &\stackrel{(c)}{=} \log_2 \det(\pi \mathbf{Q}_{\underline{\mathbf{v}}}) + \log_2(e) \cdot \text{tr}(\mathbf{Q}_{\underline{\mathbf{v}}}^{-1} \mathbf{E}\{(\underline{\mathbf{v}} - \bar{\underline{\mathbf{v}}})(\underline{\mathbf{v}} - \bar{\underline{\mathbf{v}}})^H\}) \\ &= \log_2 \det(\pi \mathbf{Q}_{\underline{\mathbf{v}}}) + \log_2(e) \cdot \text{tr}(\mathbf{Q}_{\underline{\mathbf{v}}}^{-1} \mathbf{Q}_{\underline{\mathbf{v}}}) \\ &= \log_2 \det(\pi \mathbf{Q}_{\underline{\mathbf{v}}}) + m \log_2(e) \\ &= \log_2(e^m \det(\pi \mathbf{Q}_{\underline{\mathbf{v}}})) = \log_2 \det(e\pi \mathbf{Q}_{\underline{\mathbf{v}}}). \end{aligned} \quad (\text{G.7})$$

In step (a), we have plugged in the joint PDF of a multivariate complex Gaussian random vector (see Definition C.10). In step (b), we have used that  $\mathbf{b}^H \mathbf{A} \mathbf{b} = \text{tr}(\mathbf{A} \mathbf{b} \mathbf{b}^H)$  for any  $(m \times 1)$ -vector  $\mathbf{b}$  and any  $(m \times m)$ -matrix  $\mathbf{A}$ . In step (c), we have used that expectation and trace operation may be interchanged. Note that the differential entropy of a multivariate complex Gaussian vector random variable  $\underline{\mathbf{y}}$  depends solely on the covariance matrix  $\mathbf{Q}_{\underline{\mathbf{y}}}$ , but not on the mean  $\bar{\mathbf{v}}$ . Correspondingly, we can restrict ourselves to the case of zero-mean random variables in the sequel.

Obviously, a sufficient condition for maximizing the differential entropy of the channel output vector  $\mathbf{y}$  is to use a (zero-mean) multivariate complex Gaussian random vector  $\mathbf{x} \sim \mathcal{CN}(\mathbf{0}, \mathbf{Q}_{\underline{\mathbf{x}}})$  as channel input vector, because this yields a multivariate complex Gaussian random vector  $\mathbf{y} \sim \mathcal{CN}(\mathbf{0}, \mathbf{Q}_{\underline{\mathbf{y}}})$  at the channel output [BT04a, App. B.2]. Specifically, one obtains

$$\mathbf{Q}_{\underline{\mathbf{y}}} = \mathbb{E}\{\mathbf{y}\mathbf{y}^H\} = \mathbb{E}\{\mathbf{H}\mathbf{x}\mathbf{x}^H\mathbf{H}^H\} + \mathbb{E}\{\mathbf{n}\mathbf{n}^H\} = \mathbf{H}\mathbf{Q}_{\underline{\mathbf{x}}}\mathbf{H}^H + \sigma_n^2\mathbf{I}_N, \quad (\text{G.8})$$

where we have utilized that  $\mathbf{x}$  and  $\mathbf{n}$  are statistically independent. Altogether, we obtain

$$\begin{aligned} C(\mathbf{H}) &= \max_{\mathbf{x} \sim \mathcal{CN}(\mathbf{0}, \mathbf{Q}_{\underline{\mathbf{x}}}) \text{ s.t. } \text{tr}(\mathbf{Q}_{\underline{\mathbf{x}}}) \leq P} \log_2 \det \left( e\pi(\mathbf{H}\mathbf{Q}_{\underline{\mathbf{x}}}\mathbf{H}^H + \sigma_n^2\mathbf{I}_N) \right) - \log_2 \det \left( e\pi\sigma_n^2\mathbf{I}_N \right) \\ &= \max_{\mathbf{x} \sim \mathcal{CN}(\mathbf{0}, \mathbf{Q}_{\underline{\mathbf{x}}}) \text{ s.t. } \text{tr}(\mathbf{Q}_{\underline{\mathbf{x}}}) \leq P} \log_2 \det \left( e\pi(\mathbf{H}\mathbf{Q}_{\underline{\mathbf{x}}}\mathbf{H}^H + \sigma_n^2\mathbf{I}_N)(e\pi\sigma_n^2\mathbf{I}_N)^{-1} \right) \\ &= \max_{\mathbf{x} \sim \mathcal{CN}(\mathbf{0}, \mathbf{Q}_{\underline{\mathbf{x}}}) \text{ s.t. } \text{tr}(\mathbf{Q}_{\underline{\mathbf{x}}}) \leq P} \log_2 \det \left( \mathbf{I}_N + \frac{1}{\sigma_n^2} \mathbf{H}\mathbf{Q}_{\underline{\mathbf{x}}}\mathbf{H}^H \right) \text{ bit/channel use.} \end{aligned} \quad (\text{G.9})$$

Moreover, using the determinant identity  $\det(\mathbf{I}_m + \mathbf{A}\mathbf{B}) = \det(\mathbf{I}_n + \mathbf{B}\mathbf{A})$ , which holds for any  $(m \times n)$ -matrix  $\mathbf{A}$  and any  $(n \times m)$ -matrix  $\mathbf{B}$  [Tel99], we can rewrite (G.9) as

$$C(\mathbf{H}) = \max_{\mathbf{x} \sim \mathcal{CN}(\mathbf{0}, \mathbf{Q}_{\underline{\mathbf{x}}}) \text{ s.t. } \text{tr}(\mathbf{Q}_{\underline{\mathbf{x}}}) \leq P} \log_2 \det \left( \mathbf{I}_M + \frac{1}{\sigma_n^2} \mathbf{Q}_{\underline{\mathbf{x}}}\mathbf{H}^H\mathbf{H} \right) \text{ bit/channel use.} \quad (\text{G.10})$$

As can be seen, the only remaining degree of freedom, over which the mutual information  $I(\mathbf{x}; \mathbf{y})$  has to be maximized, is the covariance matrix  $\mathbf{Q}_{\underline{\mathbf{x}}}$  of the channel input vector  $\mathbf{x}$ , while any Hermitian, non-negative definite  $(M \times M)$ -matrix which meets the sum power constraint constitutes a valid choice for  $\mathbf{Q}_{\underline{\mathbf{x}}}$  (cf. Definition D.13 in Appendix D).

## G.2 Specific Capacity Results

Clearly, the optimal choice of  $\mathbf{Q}_{\underline{\mathbf{x}}}$  depends on how much knowledge the transmitter has about the channel matrix  $\mathbf{H}$ . In the following, we consider two extreme cases: (a) The channel matrix  $\mathbf{H}$  is perfectly known at the transmitter, and (b) the transmitter has no channel knowledge at all. In both cases we assume that the receiver knows the channel matrix  $\mathbf{H}$  perfectly.

### Perfect Channel Knowledge at Transmitter and Receiver

Consider the singular-value decomposition (SVD) of the channel matrix  $\mathbf{H}$ :

$$\mathbf{H} = \mathbf{U}_{\mathbf{H}}\mathbf{\Lambda}_{\mathbf{H}}\mathbf{V}_{\mathbf{H}}^H \quad (\text{G.11})$$



(cf. Definition D.12 in Appendix D), where  $\mathbf{U}_H$  is a unitary  $(N \times N)$ -matrix containing the eigenvectors of  $\mathbf{H}\mathbf{H}^H$ ,  $\mathbf{V}_H$  a unitary  $(M \times M)$ -matrix containing the eigenvectors of  $\mathbf{H}^H\mathbf{H}$ , and  $\mathbf{\Lambda}_H$  an  $(N \times M)$ -diagonal matrix containing the non-negative square-roots  $\lambda_\mu := \sqrt{\chi_\mu}$  of the  $\tilde{M} := \min(M, N)$  eigenvalues  $\chi_1, \dots, \chi_{\tilde{M}}$  of  $\mathbf{H}\mathbf{H}^H$  ( $N \leq M$ ) or  $\mathbf{H}^H\mathbf{H}$  ( $N > M$ ). The combination of (G.9) and (G.11) yields the following result [Tel99]:

$$\begin{aligned} C(\mathbf{H}) &= \max_{\mathbf{x} \sim \mathcal{CN}(\mathbf{0}, \mathbf{Q}_x) \text{ s.t. } \text{tr}(\mathbf{Q}_x) \leq P} \log_2 \det \left( \mathbf{I}_N + \frac{1}{\sigma_n^2} \mathbf{U}_H \mathbf{\Lambda}_H \mathbf{V}_H^H \mathbf{Q}_x \mathbf{V}_H \mathbf{\Lambda}_H^H \mathbf{U}_H^H \right) \\ &= \max_{\mathbf{x} \sim \mathcal{CN}(\mathbf{0}, \mathbf{Q}'_x) \text{ s.t. } \text{tr}(\mathbf{Q}'_x) \leq P} \log_2 \det \left( \mathbf{I}_N + \frac{1}{\sigma_n^2} \mathbf{\Lambda}_H \mathbf{Q}'_x \mathbf{\Lambda}_H^H \right), \end{aligned} \quad (\text{G.12})$$

where we have substituted  $\mathbf{V}_H^H \mathbf{Q}_x \mathbf{V}_H$  by  $\mathbf{Q}'_x$  and utilized that  $\det(\mathbf{U}\mathbf{A}\mathbf{U}^H) = \det(\mathbf{A})$  for any unitary matrix  $\mathbf{U}$  and any Hermitian matrix  $\mathbf{A}$ .<sup>2</sup>

For any non-negative definite  $(m \times m)$ -matrix  $\mathbf{A}$ , the so-called Hadamard inequality holds (cf. Definition D.13, footnote):

$$\det(\mathbf{A}) \leq \prod_{i=1}^m a_{ii}, \quad (\text{G.13})$$

with equality if and only if  $\mathbf{A}$  is diagonal [BT04a, App. B.2]. Since the logarithm is a monotonic function, the logdet-term in (G.12) is maximized if and only if  $\mathbf{Q}'_x$  is a diagonal matrix [Tel99]. Correspondingly, we can rewrite (G.12) as

$$C(\mathbf{H}) = \max_{\mathbf{x} \sim \mathcal{CN}(\mathbf{0}, \mathbf{Q}'_x) \text{ s.t. } \text{tr}(\mathbf{Q}'_x) \leq P, \mathbf{Q}'_x \text{ diagonal}} \sum_{\mu=1}^{\tilde{M}} \log_2 \left( 1 + \frac{\chi_\mu}{\sigma_n^2} [\mathbf{Q}'_x]_{\mu, \mu} \right). \quad (\text{G.14})$$

The optimal choice of the covariance matrix  $\mathbf{Q}'_x$  can now be inferred from earlier capacity results presented in [Gal68, Ch. 7.5], because the expression in (G.14) corresponds to the capacity of  $\tilde{M}$  parallel AWGN channels with SNRs  $\chi_\mu [\mathbf{Q}'_x]_{\mu, \mu} / \sigma_n^2$ . In fact, the maximization in (G.14) constitutes a convex optimization problem (see also Appendix E), which yields the well-known water-filling solution for the diagonal elements of  $\mathbf{Q}'_x$ . One obtains

$$[\mathbf{Q}'_{x, \text{opt}}]_{\mu, \mu} = \left[ \Theta - \frac{\sigma_n^2}{\chi_\mu} \right]_+ \quad (\mu = 1, \dots, \tilde{M}) \quad \text{s.t.} \quad \sum_{\mu=1}^{\tilde{M}} \left[ \Theta - \frac{\sigma_n^2}{\chi_\mu} \right]_+ = P \quad (\text{G.15})$$

( $[x]_+ := \max(0, x)$ ), which can be solved numerically, in order to determine the so-called waterlevel  $\Theta$ .<sup>3</sup> The water-filling solution (G.15) is illustrated in Fig. E.1 in Appendix E ( $\alpha_\mu := 1/\chi_\mu$ ). Altogether the channel capacity  $C(\mathbf{H})$  results as [Tel99]

$$C(\mathbf{H}) = \sum_{\mu=1}^{\tilde{M}} \log_2 \left( 1 + \frac{\chi_\mu}{\sigma_n^2} [\mathbf{Q}'_{x, \text{opt}}]_{\mu, \mu} \right) = \sum_{\mu=1}^{\tilde{M}} \left[ \log_2 \left( \frac{\chi_\mu}{\sigma_n^2} \Theta \right) \right]_+ \quad \text{bit/channel use.} \quad (\text{G.16})$$

<sup>2</sup>Note that  $\mathbf{Q}'_x$  is still a Hermitian, non-negative definite  $(M \times M)$ -matrix. Moreover, we have  $\text{tr}(\mathbf{Q}'_x) = \text{tr}(\mathbf{Q}_x)$ , i.e., the new sum power constraint is identical to the sum power constraint based on  $\mathbf{Q}_x$ .

<sup>3</sup>Since for  $M > N$  the terms  $\mu = (N+1), \dots, M$  do not contribute to the capacity  $C(\mathbf{H})$ , cf. (G.14), the corresponding diagonal elements of  $\mathbf{Q}'_{x, \text{opt}}$  are chosen as zero.

The optimal covariance matrix  $\mathbf{Q}_{\mathbf{x},\text{opt}}$  of the channel input vector  $\mathbf{x}$  is given by

$$\mathbf{Q}_{\mathbf{x},\text{opt}} = \mathbf{V}_{\mathbf{H}} \mathbf{Q}'_{\mathbf{x},\text{opt}} \mathbf{V}_{\mathbf{H}}^{\text{H}}, \quad (\text{G.17})$$

i.e., the channel input vector  $\mathbf{x}$  can be generated as  $\mathbf{x} = \mathbf{V}_{\mathbf{H}} \mathbf{x}'$ , where  $\text{E}\{\mathbf{x}'\mathbf{x}'^{\text{H}}\} =: \mathbf{Q}'_{\mathbf{x},\text{opt}}$ . Note that the optimal choice of  $\mathbf{Q}_{\mathbf{x}}$  according to (G.15) and (G.17) requires perfect channel knowledge at the transmitter (in terms of the eigenvalues  $\chi_{\mu}$  and the eigenvector matrix  $\mathbf{V}_{\mathbf{H}}$ ).

As a final remark it should be noted that the above (optimal) choice of the channel input vector  $\mathbf{x}$  allows for a very simple detection strategy at the receiver. By multiplying the received vector  $\mathbf{y}$  with the unitary matrix  $\mathbf{U}_{\mathbf{H}}^{\text{H}}$  from the SVD (G.11), the channel matrix  $\mathbf{H}$  can be diagonalized, according to

$$\mathbf{y}' := \mathbf{U}_{\mathbf{H}}^{\text{H}} \mathbf{y} = \mathbf{U}_{\mathbf{H}}^{\text{H}} \mathbf{H} \mathbf{V}_{\mathbf{H}} \mathbf{x}' + \mathbf{U}_{\mathbf{H}}^{\text{H}} \mathbf{n} = \mathbf{\Lambda}_{\mathbf{H}} \mathbf{x}' + \mathbf{n}', \quad (\text{G.18})$$

i.e., the spatial interference between the transmitted data symbols is completely canceled, while retaining a spatially and temporally white noise vector  $\mathbf{n}' = \mathbf{U}_{\mathbf{H}}^{\text{H}} \mathbf{n}$  with unaltered variance.

### No Channel Knowledge at the Transmitter

If the transmitter has no channel knowledge at all, the optimal strategy is to divide the available transmit power  $P$  uniformly among the transmit antennas [BT04a, App. B.2]. In order to maximize the logdet-term in (G.12), again a diagonal covariance matrix  $\mathbf{Q}'_{\mathbf{x}}$  is required. Correspondingly, the covariance matrix  $\mathbf{Q}'_{\mathbf{x}}$  is chosen as  $\mathbf{Q}'_{\mathbf{x}} = P/M \cdot \mathbf{I}_M = \mathbf{Q}_{\mathbf{x}}$ , and the capacity results as

$$C(\mathbf{H}) = \log_2 \det \left( \mathbf{I}_N + \frac{P}{M\sigma_{\mathbf{n}}^2} \mathbf{H}\mathbf{H}^{\text{H}} \right) = \log_2 \det \left( \mathbf{I}_M + \frac{P}{M\sigma_{\mathbf{n}}^2} \mathbf{H}^{\text{H}}\mathbf{H} \right) \quad (\text{G.19a})$$

$$= \sum_{\mu=1}^{\tilde{M}} \log_2 \left( 1 + \frac{P\chi_{\mu}}{M\sigma_{\mathbf{n}}^2} \right) \text{ bit/channel use.} \quad (\text{G.19b})$$

Note that if  $M > N$ , a fraction  $(1 - N/M)P$  of the available transmit power  $P$  is wasted, because it does not contribute to the capacity  $C(\mathbf{H})$ .



# Appendix H

## Specific Considerations for Distributed MIMO Systems

**I**N THIS CHAPTER the unitary matrix transforms (3.33) and (3.38) considered in Chapter 3 are illustrated by means of two simple examples. Afterwards, two examples for virtual antenna arrays (VAAs) in cellular mobile radio systems are considered, and specific results are derived concerning the spatial correlation resulting for the equivalent co-located MIMO system.

### H.1 Illustration of the Unitary Matrix Transforms

In the following example, we consider a system with two co-located or distributed transmit antennas and a single receive antenna. Afterwards, a numerical example for a system with four transmit and a single receive antenna is presented. Concerning the system model, the same assumptions as in Section 3.2 are made.

**Example H.1 (MISO system with two transmit antennas)**

Consider first a MISO system with two co-located transmit antennas (assuming equal power allocation) and a single receive antenna, and let

$$\mathbf{R}_{\mathbf{h},\text{Tx}} := \begin{bmatrix} 1 & \rho \\ \rho^* & 1 \end{bmatrix}, \quad \rho = |\rho|e^{j\phi}, \quad (\text{H.1})$$

where  $|\rho| \leq 1$  and  $\phi \in [0, 2\pi)$ . From the eigenvalue decomposition (EVD) of  $\mathbf{R}_{\mathbf{h},\text{Tx}}$ , one obtains

$$\mathbf{U}_{\text{Tx}} = \frac{1}{\sqrt{2}} \begin{bmatrix} -e^{j\phi} & e^{j\phi} \\ 1 & 1 \end{bmatrix}, \quad \mathbf{\Lambda}_{\mathbf{h},\text{Tx}} = \begin{bmatrix} 1-|\rho| & 0 \\ 0 & 1+|\rho| \end{bmatrix}. \quad (\text{H.2})$$

Thus, setting  $\mathbf{\Sigma}_{\mathbf{h},\text{Tx}} := \mathbf{\Lambda}_{\mathbf{h},\text{Tx}}$ , we have found an equivalent MISO system with two distributed transmit antennas and a single receive antenna. Specifically, let  $D$  denote the distance between transmitter and receiver in the co-located system. Assuming that the received power scales with  $D^{-p}$ , where  $p$  denotes the path-loss exponent we obtain  $D'_1 = D(1-|\rho|)^{-1/p}$  and  $D'_2 = D(1+|\rho|)^{-1/p}$  for the distances in

the equivalent distributed system.<sup>1</sup> Typically, the path-loss exponent is between  $p=2$  (free-space propagation) and  $p=4$  (e.g., in rural areas) [Ste94, Ch. 1.2]. For example, given a spatial correlation value of  $\rho=0.8$ , a distance of  $D=100$  meters in the co-located system, and a path-loss exponent of  $p=2$ , we obtain  $D'_1 \approx 223.6$  meters and  $D'_2 \approx 74.5$  meters for the distances in the equivalent distributed system.

Next, consider a MISO system with two distributed transmit antennas and a single receive antenna, and let

$$\mathbf{\Sigma}_{\mathbf{h},\text{Tx}} := \begin{bmatrix} \sigma_1^2 & 0 \\ 0 & \sigma_2^2 \end{bmatrix}, \quad \sigma_1^2, \sigma_2^2 \in \mathbb{R}_{\geq 0}, \quad (\text{H.3})$$

where  $\sigma_1^2 + \sigma_2^2 = M = 2$ . Using the normalized  $(2 \times 2)$ -Hadamard matrix

$$\tilde{\mathbf{U}}_2 := \mathfrak{H}_2 = \frac{1}{\sqrt{2}} \begin{bmatrix} 1 & 1 \\ 1 & -1 \end{bmatrix} \quad (\text{H.4})$$

we find an equivalent MISO system with two co-located transmit antennas, one receive antenna and a transmitter correlation matrix

$$\mathbf{R}_{\mathbf{h},\text{Tx}} := \tilde{\mathbf{U}}_2 \mathbf{\Sigma}_{\mathbf{h},\text{Tx}} \tilde{\mathbf{U}}_2^H = \begin{bmatrix} 1 & \frac{1}{2}(\sigma_1^2 - \sigma_2^2) \\ \frac{1}{2}(\sigma_1^2 - \sigma_2^2) & 1 \end{bmatrix}. \quad (\text{H.5})$$

Specifically, let  $D_1$  and  $D_2$  denote the distances between the distributed transmit antennas and the receive antenna. Then, the corresponding distance  $D'$  in the equivalent co-located system is given by  $D' = D_1 \cdot (\sigma_1^2)^{-1/p} = D_2 \cdot (\sigma_2^2)^{-1/p}$ .

The relation between the system with co-located transmit antennas and the system with distributed transmit antennas can best be illustrated by considering the joint PDF of the corresponding channel coefficients. For simplicity, we restrict ourselves to the case of real-valued channel coefficients. In the following, let

$$\mathbf{h}_c := [h_{c,1,1}, h_{c,1,2}]^T \quad \text{and} \quad \mathbf{h}_d := [h_{d,1,1}, h_{d,1,2}]^T \quad (\text{H.6})$$

denote the channel coefficients in the co-located MISO system and in the equivalent distributed MISO system, respectively. To this end, we set

$$\mathbf{h}_c := \mathbf{R}_{\mathbf{h},\text{Tx}}^{1/2} \mathbf{h}' \quad \text{and} \quad \mathbf{h}_d := \mathbf{\Sigma}_{\mathbf{h},\text{Tx}}^{1/2} \mathbf{h}', \quad (\text{H.7})$$

where  $\mathbf{h}' := [h'_{1,1}, h'_{1,2}]^T$  with  $h'_{1,\mu} \sim \mathcal{N}(0, 1)$  ( $\mu = 1, 2$ ) and  $\mathbf{E}\{\mathbf{h}'\mathbf{h}'^H\} = \mathbf{I}_2$ . In the case of the co-located MISO system we assume a real-valued correlation parameter  $0 \leq \rho < 1$ , i.e.,  $\phi = 0$  (cf. (H.1)). The PDF of the channel vector  $\mathbf{h}_c$  is thus given by

$$p_{\mathbf{h}_c}(\mathbf{h}_c) = \frac{1}{2\pi\sqrt{1-\rho^2}} \cdot \exp\left(-\frac{h_{c,1,1}^2 + h_{c,1,2}^2 - 2\rho h_{c,1,1} h_{c,1,2}}{2(1-\rho^2)}\right), \quad (\text{H.8})$$

and the PDF of the channel vector  $\mathbf{h}_d$  is given by

$$p_{\mathbf{h}_d}(\mathbf{h}_d) = \frac{1}{2\pi\sqrt{\sigma_1^2\sigma_2^2}} \cdot \exp\left(-\frac{\sigma_1^2 h_{d,1,2}^2 + \sigma_2^2 h_{d,1,1}^2}{2\sigma_1^2\sigma_2^2}\right) \quad (\text{H.9a})$$

$$= \frac{1}{2\pi\sqrt{1-\rho^2}} \cdot \exp\left(-\frac{h_{d,1,1}^2 + h_{d,1,2}^2 + \rho(h_{d,1,1}^2 - h_{d,1,2}^2)}{2(1-\rho^2)}\right). \quad (\text{H.9b})$$

<sup>1</sup>For simplicity, we have assumed that congenerous omni-directional antennas are used in the equivalent distributed system. Moreover, shadowing effects have not been taken into account.

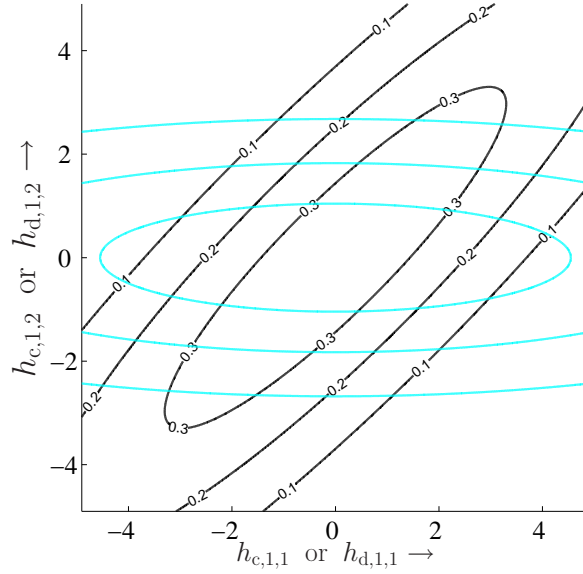


Figure H.1: Contour plots of the PDFs  $p_{\mathbf{h}_c}(\mathbf{h}_c)$  and  $p_{\mathbf{h}_d}(\mathbf{h}_d)$  for  $\rho=0.9$ .

In Fig. H.1, the contour plots of the PDFs  $p_{\mathbf{h}_c}(\mathbf{h}_c)$  and  $p_{\mathbf{h}_d}(\mathbf{h}_d)$  are displayed, for the example  $\rho = 0.9$ . As can be seen both PDFs are identical, apart from a  $45^\circ$ -rotation within the  $(x, y)$ -plane.<sup>2</sup> Obviously, in the co-located system a large amplitude of channel coefficient  $h_{c,1,1}$  implies a high probability that the amplitude of  $h_{c,1,2}$  is also large (due to the strong correlation). In contrast to this, the channel coefficients  $h_{d,1,1}$  and  $h_{d,1,2}$  in the distributed system are uncorrelated, but their average amplitudes are different.  $\diamond$

### Example H.2 (Numerical example for four transmit antennas)

Consider a distributed MISO system with four transmit antennas and a single receive antenna, and let

$$\Sigma_{\mathbf{h},\text{Tx}} = \text{diag}([0.2 \ 0.3 \ 1.0 \ 2.5]). \quad (\text{H.10})$$

Using the normalized Hadamard matrix

$$\tilde{\mathbf{U}}_4 := \mathfrak{H}_4 = \frac{1}{\sqrt{2}} \begin{bmatrix} \mathfrak{H}_2 & \mathfrak{H}_2 \\ \mathfrak{H}_2 & -\mathfrak{H}_2 \end{bmatrix}, \quad (\text{H.11})$$

we find the following transmitter correlation matrix for the equivalent co-located MISO system:

$$\mathbf{R}_{\mathbf{h},\text{Tx}} := \tilde{\mathbf{U}}_4 \Sigma_{\mathbf{h},\text{Tx}} \tilde{\mathbf{U}}_4^H = \begin{bmatrix} 1 & -0.4 & -0.75 & 0.35 \\ -0.4 & 1 & 0.35 & -0.75 \\ -0.75 & 0.35 & 1 & -0.4 \\ 0.35 & -0.75 & -0.4 & 1 \end{bmatrix}. \quad (\text{H.12})$$

The above transform  $\Sigma_{\mathbf{h},\text{Tx}} \rightarrow \mathbf{R}_{\mathbf{h},\text{Tx}}$  is illustrated in Fig. H.2.

<sup>2</sup>Correspondingly, the unitary transforms  $\mathbf{R}_{\mathbf{h},\text{Tx}} \leftrightarrow \Sigma_{\mathbf{h},\text{Tx}}$  can be interpreted as a rotation of the coordinate system [Boe03].

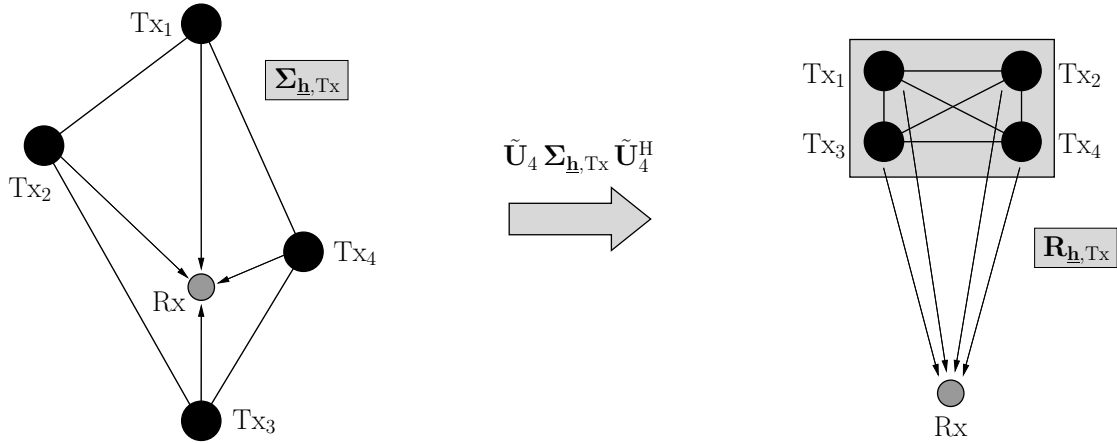


Figure H.2: Illustration of the transform  $\Sigma_{\mathbf{h},\text{Tx}} \rightarrow \mathbf{R}_{\mathbf{h},\text{Tx}}$ . Left: Distributed MISO system with four transmit antennas and a single receive antenna. Right: Equivalent co-located MISO system with correlated transmit antennas.

Using, for example, the  $(4 \times 4)$ -Fourier matrix  $\mathfrak{F}_4$  instead of the normalized  $(4 \times 4)$ -Hadamard matrix, we can find another equivalent co-located MISO system with a different correlation matrix  $\mathbf{R}'_{\mathbf{h},\text{Tx}} \neq \mathbf{R}_{\mathbf{h},\text{Tx}}$ . Correspondingly, the transform  $\Sigma_{\mathbf{h},\text{Tx}} \rightarrow \mathbf{R}_{\mathbf{h},\text{Tx}}$  is not unique. In contrast to this, the transform  $\mathbf{R}_{\mathbf{h},\text{Tx}} \rightarrow \Sigma_{\mathbf{h},\text{Tx}}$  according to (3.33) is always unique (up to an arbitrary permutation of the eigenvalues).  $\diamond$

## H.2 Virtual Antenna Arrays for Cellular Systems

Next, we focus on cellular mobile radio systems and consider two examples of distributed MIMO systems taking geometrical parameters into account. In the first example, a virtual antenna array is considered that is established by two cooperating mobile stations. In the second example two cooperating base stations are considered.

### Example H.3 (Virtual antenna array established by two mobile stations)

We consider a virtual antenna array (VAA) established by two cooperating mobile stations, as depicted in Fig. H.3. For simplicity we assume that the base station BS and the two mobile stations MS<sub>1</sub> and MS<sub>2</sub> are each equipped with a single antenna. In [KDA03] it was proposed to use such a VAA in the downlink of cellular systems, so as to provide spatial diversity at the receiver. It was argued that due to space limitations at the mobile receiver, multiple co-located antennas are typically characterized by strong spatial correlations and might therefore often be not practicable. In order to circumvent the problem of spatial correlation, it was therefore proposed in [KDA03] to establish VAAs by means of multiple adjacent single-antenna receivers that mutually relay their received signals. However, according to the results presented in Chapter 3 the use of VAAs merely trades one form of correlation for another.

For example, let  $D$  denote the distance between the base station (BS) and the first mobile station (MS<sub>1</sub>), and let  $d$  denote the antenna spacing of the VAA (cf. Fig. H.3),



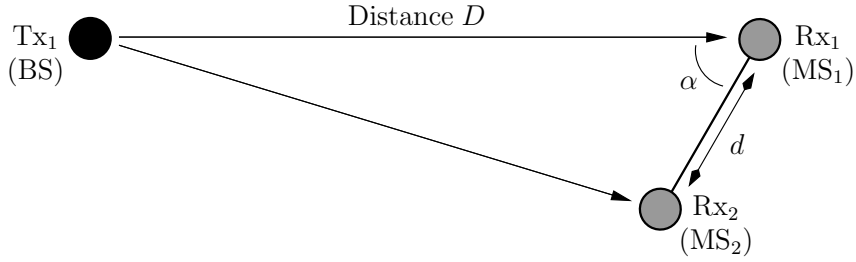


Figure H.3: Virtual antenna array (VAA) established by two mobile stations.

where we denote  $\xi := d/D$  ( $\xi < 1$ ). Moreover, let  $\alpha$  denote the angle between the link  $\text{BS} \rightarrow \text{MS}_1$  and the VAA, where  $\alpha = \pi/2$  represents the case of broad-side orientation. Using the normalization introduced in Section 3.2.2, and assuming that congenerous omni-directional antennas are used at the two mobile stations, one obtains the following receiver covariance matrix:

$$\Sigma_{\mathbf{h},\text{Rx}} = \begin{bmatrix} \sigma_1^2 & 0 \\ 0 & \sigma_2^2 \end{bmatrix}, \quad \sigma_1^2 = \frac{2(f(\alpha))^p}{1 + (f(\alpha))^p}, \quad \sigma_2^2 = \frac{2}{1 + (f(\alpha))^p}, \quad (\text{H.13})$$

where

$$f(\alpha) := 1 + \xi^2 - 2\xi \cos \alpha. \quad (\text{H.14})$$

(The parameter  $p$  again denotes the path-loss exponent, cf. Example H.1. As earlier, shadowing effects have not been taken into account.) This corresponds to an equivalent co-located SIMO system with correlated receive antennas and a receiver correlation matrix<sup>3</sup>

$$\mathbf{R}_{\mathbf{h},\text{Rx}} = \begin{bmatrix} 1 & \rho \\ \rho & 1 \end{bmatrix}, \quad \rho := -\frac{1 - (f(\alpha))^p}{1 + (f(\alpha))^p}. \quad (\text{H.15})$$

In Fig. H.4, the magnitude of the correlation coefficient  $\rho$  in the equivalent co-located SIMO system is plotted as a function of the angle  $\alpha$ , for path-loss exponents  $p=2$ ,  $p=3$ ,  $p=4$  and ratios  $\xi=0.1$ ,  $\xi=0.3$ . As can be seen, depending on the scenario under consideration the magnitude of  $\rho$  can be quite significant. Specifically,  $|\rho|$  is particularly large when  $p$  and  $\xi$  are large, and when the angle  $\alpha$  is small, as expected, since in these cases a significant difference in the average received powers at the two mobile stations results.

In the following, we assume that the two mobile stations  $\text{MS}_1$  and  $\text{MS}_2$  do only cooperate if mobile station  $\text{MS}_2$  is located anywhere within a disk of radius  $R$  around mobile station  $\text{MS}_1$  ( $R < D$ ). If the radius  $R$  is chosen properly, this constraint guarantees a sufficient quality of the link between the two mobile stations, which limits effects of error propagation caused by the mutual relaying process.<sup>4</sup> As an

<sup>3</sup>It should be noted that also the overall average received power depends on the angle  $\alpha$  and the ratio  $\xi$ . However, since we only consider the spatial correlations resulting for the equivalent co-located SIMO system, the variation of the average received power has not been taken into account.

<sup>4</sup>The actual distance  $d$  between  $\text{MS}_1$  and  $\text{MS}_2$  can, for example, be estimated by measuring the average received SNR offered by the link between the two mobile stations.

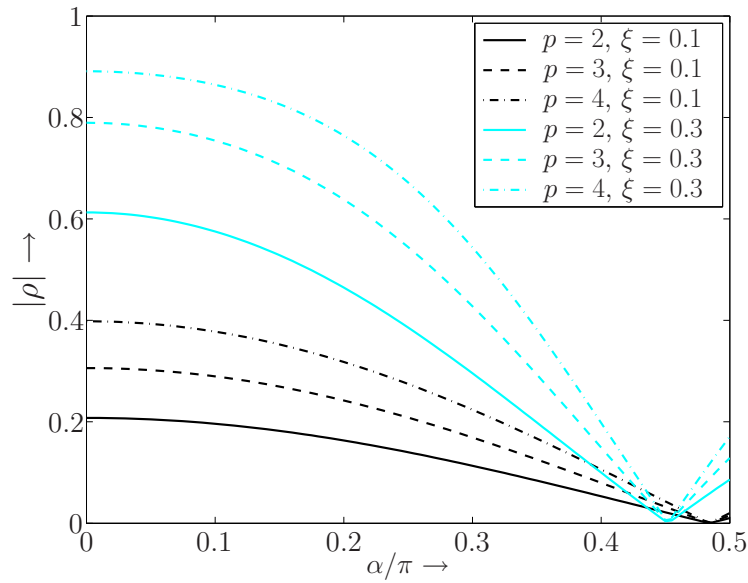


Figure H.4: Virtual antenna array (VAA) established by two mobile stations: Correlation coefficient  $\rho$  in the equivalent co-located SIMO system as a function of the angle  $\alpha$  (analytical results).

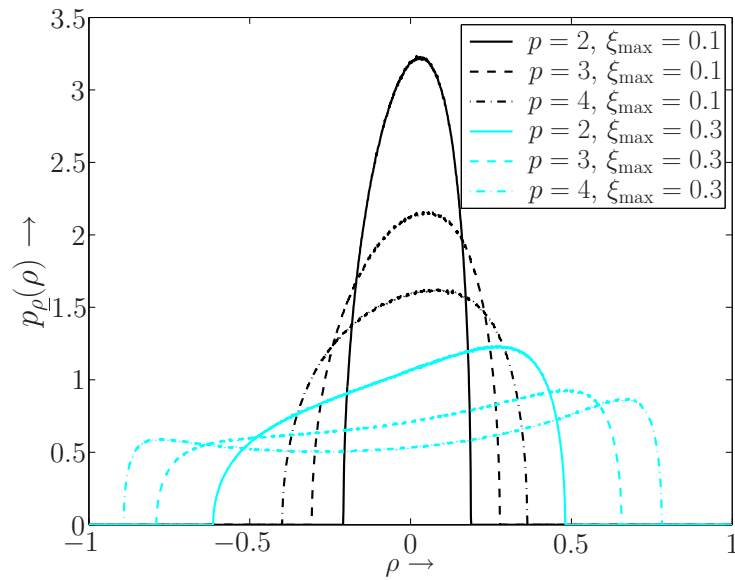


Figure H.5: Virtual antenna array (VAA) established by two mobile stations: PDF of the correlation coefficient  $\rho$  in the equivalent co-located SIMO system (obtained by means of Monte-Carlo simulations).

example, we assume that the distance  $D$  between the base station and mobile station  $\text{MS}_1$  is fixed, and that mobile station  $\text{MS}_2$  has a random position within the disk around mobile station  $\text{MS}_1$ , according to a uniform distribution.<sup>5</sup> Correspondingly, the correlation coefficient  $\rho$  according to (H.15) is now a random variable, while the angle  $\alpha$  is uniformly distributed on  $[0, 2\pi)$ , i.e.,  $\alpha \sim \mathcal{U}([0, 2\pi))$ , and the PDF of the ratio  $\xi = d/D$  is given by

$$p_{\xi}(\xi) = \frac{2D^2}{R^2} \xi \quad (0 \leq \xi \leq R/D). \quad (\text{H.16})$$

The PDF of the correlation parameter  $\rho$ , resulting for path-loss exponents  $p=2$ ,  $p=3$ ,  $p=4$  and ratios  $\xi_{\max} := R/D=0.1$  and  $\xi_{\max}=0.3$ , is depicted in Fig. H.5. The PDFs of  $\rho$  were obtained by means of Monte-Carlo simulations over a large number of random positions of mobile station  $\text{MS}_2$ . As can be seen, if the radius  $R$  is small compared to the distance  $D$  ( $\xi_{\max} \ll 1$ ) the PDF of  $\rho$  is rather narrow, i.e., large magnitudes of  $\rho$  do not occur. However, if the radius  $R$  becomes larger (e.g.,  $\xi_{\max}=0.3$ ) the PDF of  $\rho$  becomes quite broad, especially for large path-loss exponents  $p$ . Correspondingly, the radius  $R$  should not be chosen too large, so as to keep the resulting correlation parameter small and at the same time limit the effects of error propagation caused by mutual relaying.  $\diamond$

#### Example H.4 (Virtual antenna array established by two base stations)

Finally, we consider a VAA established by two cooperating base stations, as depicted in Fig. H.6. For simplicity, we again assume that the base stations  $\text{BS}_1$ ,  $\text{BS}_2$  and the mobile station  $\text{MS}$  are each equipped with a single antenna. The two base stations may, for example, be part of a simulcast network serving mobile users located within the shaded area (i.e., within the intersection of the coverage areas of base station  $\text{BS}_1$  and  $\text{BS}_2$ ).

In the following, we assume that both base stations have the same coverage radius  $R$ . Moreover, the distance between the two base stations  $\text{BS}_1$  and  $\text{BS}_2$  is denoted as  $d$  ( $d < 2R$ ). As earlier, let

$$\Sigma_{\mathbf{h}, \text{Tx}} = \begin{bmatrix} \sigma_1^2 & 0 \\ 0 & \sigma_2^2 \end{bmatrix}, \quad \sigma_1^2, \sigma_2^2 \in \mathbb{R}_{\geq 0} \quad (\text{H.17})$$

denote the transmitter covariance matrix associated with the distributed transmit antennas. Employing the normalization introduced in Section 3.2.2, and assuming that both base stations use congenerous omni-directional transmit antennas and the same average transmission power, one finds the following transmitter correlation matrix for the equivalent co-located MISO system:

$$\mathbf{R}_{\mathbf{h}, \text{Tx}} = \begin{bmatrix} 1 & \rho \\ \rho & 1 \end{bmatrix}, \quad \rho := -\frac{D_1^p - D_2^p}{D_1^p + D_2^p}, \quad (\text{H.18})$$

where  $D_1$  and  $D_2$  denotes the distance between the mobile station and base station  $\text{BS}_1$  and  $\text{BS}_2$ , respectively. As earlier,  $p$  denotes the path-loss exponent. Shadowing effects have not been taken into account.

<sup>5</sup>Similar considerations concerning the spatial distribution of wireless network nodes were, for example, made in [BHP04].

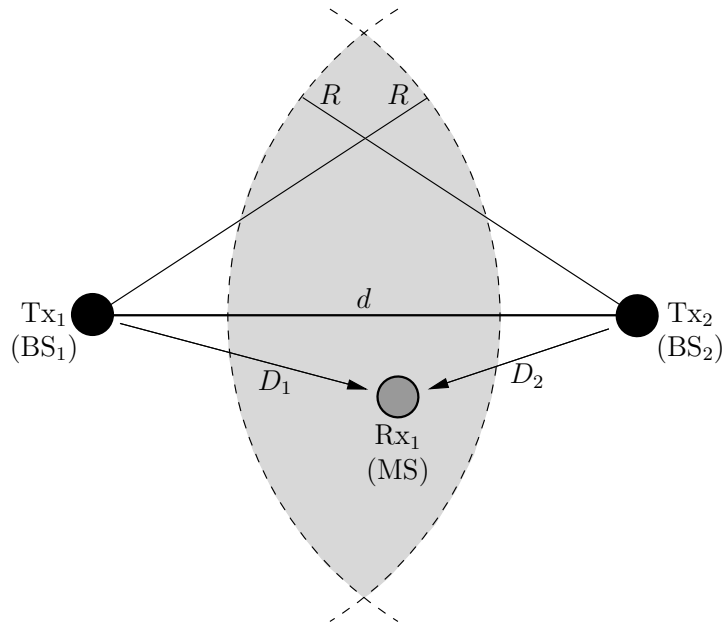


Figure H.6: Virtual antenna array (VAA) established by two base stations.

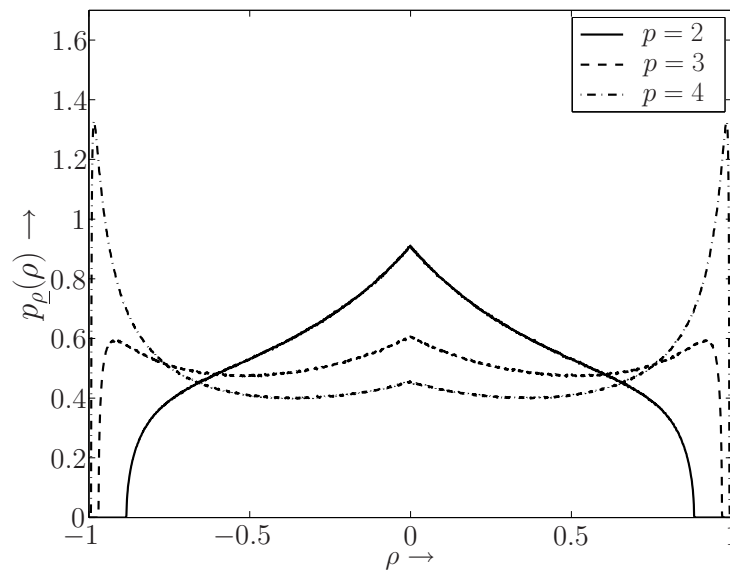


Figure H.7: Virtual antenna array (VAA) established by two base stations: PDF of the correlation coefficient  $\rho$  in the equivalent co-located MISO system (Monte-Carlo simulations).

Similar to Example H.3, we assume that the mobile station MS has a random position within the intersection of the coverage areas of base station BS<sub>1</sub> and BS<sub>2</sub>, according to a uniform distribution. Correspondingly, the correlation coefficient  $\rho$  according to (H.18) is again a random variable. The PDF of the correlation parameter  $\rho$ , resulting for path-loss exponents  $p=2$ ,  $p=3$ ,  $p=4$  and a ratio  $R/d=0.8$ , is depicted in Fig. H.7. As can be seen, the PDF of  $\rho$  is quite broad, already for a small path-loss exponent of  $p=2$ .  $\diamond$



# Appendix I

## Error Performance of Maximum-Ratio-Combining Systems

**T**HE IDEA to exploit multiple receive antennas, in order to accomplish (microscopic) diversity gains, dates already back to the 1950's. Given a wireless system with a single transmit antenna and multiple receive antennas, the optimal linear combining strategy in terms of maximizing the signal-to-noise ratio (SNR) at the combiner output is maximum ratio combining (MRC) [Bre59], which requires perfect channel knowledge at the receiver. Since the advent of orthogonal space-time block codes (OSTBCs) [Ala98, TJC99a, TJC99b], the topic of performance evaluation for MRC systems has received renewed interest, because any OSTBC system with  $M$  transmit and  $N$  receive antennas can be transformed into an equivalent MRC system with a single transmit antenna and  $MN$  receive antennas (cf. Section 2.3.1). Moreover, Craig's alternative representation of the Gaussian Q-function [Cra91] enabled novel advances in assessing the performance of MRC systems, given (nearly) arbitrary fading statistics [AG99, SA00] and signal constellations. In the following, the most important performance results for MRC systems are briefly summarized. These results are then utilized in Chapter 3 and 4, in order to assess the performance of OSTBCs in co-located and distributed MIMO systems.

To start with, we consider the PDF of the instantaneous SNR at the maximum ratio combiner output.

### I.1 PDF of the Instantaneous Signal-to-Noise Ratio

We consider a point-to-point link in a wireless system equipped with a single transmit antenna and  $N$  receive antennas, as depicted in Fig. I.1. Assuming quasi-static frequency-flat fading, the discrete-time channel model (without MRC) is given by

$$\mathbf{y}[k] = \mathbf{h} a[k] + \mathbf{n}[k] \quad (\text{I.1})$$

where  $\mathbf{y}[k] := [y_1[k], \dots, y_N[k]] \in \mathbb{C}^N$  denotes the  $k$ th received vector,  $k$  the discrete time index,  $\mathbf{h} := [h_1, \dots, h_N] \in \mathbb{C}^N$  the channel coefficient vector,  $a[k]$  the  $k$ th transmitted in-



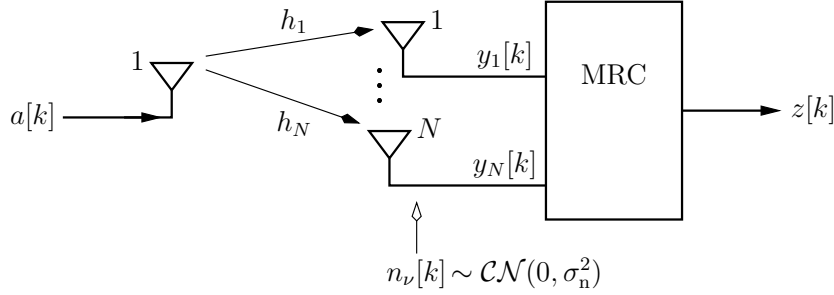


Figure I.1: Maximum-ratio-combining (MRC) system with a single transmit antenna and  $N$  receive antennas.

formation symbol, and  $\mathbf{n}[k] := [n_1[k], \dots, n_N[k]] \in \mathbb{C}^N$  the  $k$ th additive noise vector. The entries of  $\mathbf{h}$  are modeled as statistically independent random variables with average power

$$\Omega_{h_\nu} := \mathbf{E}\{|h_\nu|^2\} = \bar{h}_\nu^2 + \sigma_{h_\nu}^2 \quad (\nu = 1, \dots, N). \quad (\text{I.2})$$

The information symbols are assumed to be randomly drawn from a  $Q$ -ary symbol alphabet  $\mathbb{A}$ , such as a phase-shift keying (PSK) or a quadrature amplitude modulation (QAM) constellation, where we assume  $\mathbf{E}\{a[k]\} := 0$  and  $\mathbf{E}\{|a[k]|^2\} := \sigma_a^2$ . Finally, the noise samples  $n_\nu[k]$  are assumed to be temporally and spatially white zero-mean complex Gaussian random variables with variance  $\sigma_n^2$ , i.e.,  $n_\nu[k] \sim \mathcal{CN}(0, \sigma_n^2)$  ( $\nu = 1, \dots, N$ ) and  $\mathbf{E}\{\mathbf{n}[k]\mathbf{n}^H[k']\} = \sigma_n^2 \cdot \delta[k' - k] \cdot \mathbf{I}_N$ . Moreover, it is assumed that  $\mathbf{h}$ ,  $a[k]$  and  $\mathbf{n}[k]$  are statistically independent.

The  $k$ th output sample of the maximum ratio combiner is given by

$$z[k] := c \sum_{\nu=1}^N h_\nu^* y_\nu[k] = c \|\mathbf{h}\|_2^2 a[k] + \eta[k], \quad (\text{I.3})$$

where  $\eta[k] \sim \mathcal{CN}(0, c^2 \|\mathbf{h}\|_2^2 \sigma_n^2)$  and  $c$  is an arbitrary constant. In the following, we set  $c := 1/\|\mathbf{h}\|_2$ , so that the variance of the noise term  $\eta[k]$  does not depend on the channel vector  $\mathbf{h}$ . The metric for maximum-likelihood (ML) detection of the information symbols  $a[k]$  is thus given by

$$\mu_{\text{ML}}(z[k], \tilde{a}[k]) := |z[k] - \|\mathbf{h}\|_2 \tilde{a}[k]|^2, \quad (\text{I.4})$$

where  $\tilde{a}[k]$  denotes a hypothesis for  $a[k]$ .

The instantaneous received SNR (given a fixed channel realization) per information symbol at the  $\nu$ th receive antenna is given by

$$\gamma_{s,\nu} := \frac{|h_\nu|^2 \sigma_a^2}{\sigma_n^2}. \quad (\text{I.5})$$

Note that the instantaneous received SNRs  $\gamma_{s,\nu}$  are statistically independent random variables. Similarly, the instantaneous SNR at the maximum ratio combiner output results as

$$\gamma_s := \frac{\|\mathbf{h}\|_2^2 \sigma_a^2}{\sigma_n^2} = \sum_{\nu=1}^N \gamma_{s,\nu}. \quad (\text{I.6})$$

In the following, let  $\bar{\gamma}_{s,\nu}$  ( $\nu = 1, \dots, N$ ) and  $\bar{\gamma}_s$  denote the corresponding average SNRs. Moreover, let  $p_{\gamma_{s,\nu}}(\gamma_{s,\nu})$  and  $p_{\gamma_s}(\gamma_s)$  denote the PDF of the instantaneous SNRs  $\gamma_{s,\nu}$  and  $\gamma_s$ , respectively.

The PDF of a sum of statistically independent random variables is given by the convolution of the individual PDFs [BS91, p. 674]. For the PDF of the instantaneous SNR at the maximum ratio combiner output, one therefore obtains

$$p_{\gamma_s}(\gamma_s) = p_{\gamma_{s,1}}(\gamma_s) * \dots * p_{\gamma_{s,N}}(\gamma_s). \quad (\text{I.7})$$

Equivalently, the PDF  $p_{\gamma_s}(\gamma_s)$  can be expressed in terms of the characteristic function of the instantaneous SNR  $\gamma_s$  (cf. Definition C.17 in Appendix C), according to

$$p_{\gamma_s}(\gamma_s) = \frac{1}{2\pi} \int_{-\infty}^{+\infty} \mathbf{C}\{\gamma_s\}(j\omega) e^{-j\omega\gamma_s} d\omega, \quad (\text{I.8})$$

where  $\mathbf{C}\{\gamma_s\}(j\omega) = \mathbf{F}\{p_{\gamma_s}(\gamma_s)\}(-j\omega)$ . Alternatively, the moment-generating function  $\mathbf{M}\{\gamma_s\}(s) = \mathbf{L}\{p_{\gamma_s}(\gamma_s)\}(-s)$  can be used. The characteristic function  $\mathbf{C}\{\gamma_s\}(j\omega)$  can in turn be expressed as the product of the characteristic functions of the instantaneous SNRs  $\gamma_{s,\nu}$ , i.e.,

$$\mathbf{C}\{\gamma_s\}(j\omega) = \prod_{\nu=1}^N \mathbf{C}\{\gamma_{s,\nu}\}(j\omega) = \prod_{\nu=1}^N \mathbf{F}\{p_{\gamma_{s,\nu}}(\gamma_{s,\nu})\}(-j\omega). \quad (\text{I.9})$$

Similarly, we have  $\mathbf{M}\{\gamma_s\}(s) = \prod_{\nu=1}^N \mathbf{M}\{\gamma_{s,\nu}\}(s)$ . As will be seen in the sequel, the above properties of  $p_{\gamma_s}(\gamma_s)$  allow for an analytical evaluation of the resulting average symbol error probability provided by MRC with subsequent ML detection.

## I.2 Symbol and Bit Error Probability

To start with, we focus on the case of binary transmission. Afterwards, generalizations to higher-order modulation schemes are discussed.

### Binary Transmission

In the case of binary (antipodal) transmission, i.e.,  $a[k] \in \{\pm\sqrt{\sigma_a^2}\}$ , the instantaneous bit error probability is given by

$$P_b(\gamma_s) = \mathbf{Q}\left(\sqrt{2\gamma_s}\right), \quad (\text{I.10})$$

where  $\mathbf{Q}(x)$  denotes the Gaussian Q-function, cf. Definition C.2 in Appendix C. Correspondingly, the average bit error probability can be calculated as

$$\bar{P}_b = \int_0^{\infty} \mathbf{Q}\left(\sqrt{2\gamma_s}\right) p_{\gamma_s}(\gamma_s) d\gamma_s. \quad (\text{I.11})$$

The traditional definition of the Gaussian Q-function is given by

$$\mathbf{Q}(x) := \frac{1}{\sqrt{2\pi}} \int_x^{\infty} e^{-t^2/2} dt. \quad (\text{I.12})$$

However, this definition of  $Q(x)$  renders a further evaluation of (I.11) difficult, because the integration variable of the outer integral,  $\gamma_s$ , is found in the (lower) limit of the inner integral [AG99, SA00]. Another difficulty arises from the fact, that a closed-form expression of the PDF  $p_{\gamma_s}(\gamma_s)$  must be known. In general, this might be difficult to obtain, especially when the individual transmission links are characterized by different fading statistics.<sup>1</sup>

An alternative representation of the Gaussian Q-function, which significantly simplifies the evaluation of (I.11), was presented in [Cra91]. It is given by

$$Q(x) = \frac{1}{\pi} \int_0^{\pi/2} \exp\left(-\frac{x^2}{2 \sin^2 \phi}\right) d\phi \quad (x \geq 0). \quad (\text{I.13})$$

Plugging (I.13) into (I.11) yields [AG99, SA00]

$$\bar{P}_b = \frac{1}{\pi} \int_0^\infty \int_0^{\pi/2} p_{\gamma_s}(\gamma_s) \cdot \exp\left(-\frac{\gamma_s}{\sin^2 \phi}\right) d\phi d\gamma_s \quad (\text{I.14a})$$

$$= \frac{1}{\pi} \int_0^{\pi/2} \mathbf{M}\{\gamma_s\}(s=\zeta(\phi)) d\phi, \quad (\text{I.14b})$$

where

$$\zeta(\phi) := -\frac{1}{\sin^2 \phi}. \quad (\text{I.15})$$

Furthermore, since the instantaneous received SNRs  $\gamma_{s,\nu}$  are statistically independent random variables, we can further simplify (I.14b) according to

$$\bar{P}_b = \frac{1}{\pi} \int_0^{\pi/2} \prod_{\nu=1}^N \mathbf{M}\{\gamma_{s,\nu}\}(s=\zeta(\phi)) d\phi =: \frac{1}{\pi} \int_0^{\pi/2} f(\phi) d\phi. \quad (\text{I.16})$$

In many cases, closed-form expressions are known for the moment-generating functions  $\mathbf{M}\{\gamma_{s,\nu}\}(s)$  (cf. Definition C.17 in Appendix C, Table C.1). Correspondingly, the problem of calculating the average bit error probability of MRC with subsequent ML detection amounts to evaluating a single finite-range integral over a known function  $f(\phi)$ , which can for example be done by means of numerical integration. For example, in the case of Rayleigh fading we have

$$\mathbf{M}\{\gamma_{s,\nu}\}(s) = \frac{1}{1 - s\bar{\gamma}_{s,\nu}}, \quad (\text{I.17})$$

i.e.,

$$\bar{P}_b = \frac{1}{\pi} \int_0^{\pi/2} \prod_{\nu=1}^N \frac{\sin^2 \phi}{\sin^2 \phi + \bar{\gamma}_{s,\nu}} d\phi. \quad (\text{I.18})$$

In this specific case, even closed-form expressions are known for the integral (I.18) [Pro01, Ch. 14]. Given equal average received SNRs  $\bar{\gamma}_{s,1} = \dots = \bar{\gamma}_{s,N} = \bar{\gamma}_s/N$  one obtains:

$$\bar{P}_b = \frac{1}{2^N} (1 - \mu(\bar{\gamma}_s))^N \sum_{i=0}^{N-1} \binom{N-1+i}{i} \frac{1}{2^i} (1 + \mu(\bar{\gamma}_s))^i, \quad (\text{I.19})$$

<sup>1</sup>In a system with distributed antennas, for example, the average received SNRs on the individual transmission links are typically different. Moreover, single links may contain a line-of sight component.

where

$$\mu(\bar{\gamma}_s) := \sqrt{\frac{\bar{\gamma}_s}{N + \bar{\gamma}_s}}. \quad (\text{I.20})$$

In the case of unequal average received SNRs  $\bar{\gamma}_{s,\nu}$ , one obtains<sup>2</sup>

$$\bar{P}_b = \frac{1}{2} \sum_{\nu=1}^N \left( \prod_{\substack{\nu'=1 \\ \nu' \neq \nu}}^N \frac{\bar{\gamma}_{s,\nu}}{\bar{\gamma}_{s,\nu} - \bar{\gamma}_{s,\nu'}} \right) \left( 1 - \sqrt{\frac{\bar{\gamma}_{s,\nu}}{1 + \bar{\gamma}_{s,\nu}}} \right). \quad (\text{I.21})$$

It should be noted that the derivation of (I.19) and (I.21) in [Pro01, Ch. 14] is not based on (I.16), but on explicit expressions for the PDF  $p_{\bar{\gamma}_s}(\gamma_s)$  obtained via the corresponding characteristic function  $\mathcal{C}\{\gamma_s\}(j\omega)$ .

### Higher-Order Modulation Schemes

So far, we have focused on the case of binary transmission. However, the derivation of (I.16) can be generalized to higher-order modulation schemes, so as to find similar integral expressions for the average symbol error probability provided by MRC with subsequent ML detection [AG99,SA00]. For example, for  $Q$ -ary phase-shift keying (PSK) modulation, one obtains

$$\bar{P}_s = \frac{1}{\pi} \int_0^{\frac{(Q-1)\pi}{Q}} \prod_{\nu=1}^N \mathcal{M}\{\gamma_{s,\nu}\}(s = \varsigma_{\text{PSK}}(\phi)) \, d\phi, \quad (\text{I.22})$$

where

$$\varsigma_{\text{PSK}}(\phi) := -\frac{g_{\text{PSK}}}{\sin^2 \phi}, \quad g_{\text{PSK}} := \sin^2(\pi/Q). \quad (\text{I.23})$$

Similarly, for  $Q$ -ary amplitude-shift keying (ASK) modulation, one obtains

$$\bar{P}_s = \frac{2(Q-1)}{Q\pi} \int_0^{\pi/2} \prod_{\nu=1}^N \mathcal{M}\{\gamma_{s,\nu}\}(s = \varsigma_{\text{ASK}}(\phi)) \, d\phi, \quad (\text{I.24})$$

where

$$\varsigma_{\text{ASK}}(\phi) := -\frac{g_{\text{ASK}}}{\sin^2 \phi}, \quad g_{\text{ASK}} := \frac{3}{Q^2 - 1}, \quad (\text{I.25})$$

and for a square  $Q$ -ary quadrature amplitude modulation (QAM) constellation, one obtains

$$\begin{aligned} \bar{P}_s &= \frac{4}{\pi} \left( 1 - \frac{1}{\sqrt{Q}} \right) \int_0^{\pi/2} \prod_{\nu=1}^N \mathcal{M}\{\gamma_{s,\nu}\}(s = \varsigma_{\text{QAM}}(\phi)) \, d\phi \\ &\quad - \frac{4}{\pi} \left( 1 - \frac{1}{\sqrt{Q}} \right)^2 \int_0^{\pi/4} \prod_{\nu=1}^N \mathcal{M}\{\gamma_{s,\nu}\}(s = \varsigma_{\text{QAM}}(\phi)) \, d\phi, \end{aligned} \quad (\text{I.26})$$

<sup>2</sup>If some of the average SNRs  $\bar{\gamma}_{s,\nu}$  are equal, the corresponding average bit error probability can be obtained as a limiting case of (I.21).

where

$$\varsigma_{\text{QAM}}(\phi) := -\frac{g_{\text{QAM}}}{\sin^2 \phi}, \quad g_{\text{QAM}} := \frac{3}{2(Q-1)}. \quad (\text{I.27})$$

For the case of a  $Q$ -ary QAM signal constellation and Rayleigh fading, there are also closed-form expressions for  $\bar{P}_s$  [AG99], both for equal and unequal average received SNRs  $\bar{\gamma}_{s,\nu}$  (similar to the case of binary antipodal transmission).

An interesting unifying upper bound on the average symbol error probability  $\bar{P}_s$  (for an arbitrary  $Q$ -ary PSK/ASK/QAM signal constellation) was presented in [ZG03a]. The result is

$$\bar{P}_s \leq \frac{Q-1}{Q} \prod_{\nu=1}^N \text{M}\{\gamma_{s,\nu}\}(s=-g), \quad (\text{I.28})$$

where  $g$  is equal to  $g_{\text{PSK}}$ ,  $g_{\text{ASK}}$ , or  $g_{\text{QAM}}$ .

So far, we have focussed on the calculation of the average symbol error probability. In [XD05], the above results were extended such that the corresponding average bit error probabilities can be calculated (given an arbitrary two-dimensional signal constellation with polygonal decision regions and an arbitrary bit mapping). Alternatively, the analytical results for binary antipodal transmission can be reused, in order to find bounds on the average bit error probability. Let  $\mathbb{A} := \{a_0, \dots, a_{Q-1}\}$  denote the signal constellation under consideration, and let  $d_{i,j} := |a_i - a_j|$  denote the distance between the constellation points  $a_i$  and  $a_j$  within the complex plane ( $j \neq i$ ). The average probability that an ML detector decides in favor of the constellation point  $a_j$ , although the constellation point  $a[k] = a_i$  has been transmitted, is given by [Pro01, Ch. 5.2]

$$P(a_i \rightarrow a_j) = \int_0^\infty \text{Q}\left(\sqrt{d_{i,j}^2 \gamma_s / (2\sigma_a^2)}\right) p_{\gamma_s}(\gamma_s) d\gamma_s \quad (\text{I.29a})$$

$$= \frac{1}{\pi} \int_0^{\pi/2} \prod_{\nu=1}^N \text{M}\{d_{i,j}^2 \gamma_{s,\nu} / (4\sigma_a^2)\}(s=\varsigma(\phi)) d\phi, \quad (\text{I.29b})$$

cf. (I.11) and (I.16). Let  $e_{i,j}$  denote the number of bit errors associated with an erroneous symbol decision  $a_i \rightarrow a_j$ , and let  $a_{i_{\min}}$  denote the constellation point that is closest to  $a_i$ .<sup>3</sup> A simple lower bound on the average bit error probability is then given by

$$\bar{P}_b \geq \frac{1}{Q \log_2(Q)} \sum_{i=0}^{Q-1} e_{i,i_{\min}} \cdot P(a_i \rightarrow a_{i_{\min}}). \quad (\text{I.30})$$

The above lower bound is asymptotically tight (i.e., for  $\gamma_s \rightarrow \infty$ ). Similarly, a simple upper bound on the average bit error probability is given by the union bound [Hub92, Ch. 2.8.4]

$$\bar{P}_b \leq \frac{1}{Q \log_2(Q)} \sum_{i=0}^{Q-1} \sum_{\substack{j=0 \\ j \neq i}}^{Q-1} e_{i,j} \cdot P(a_i \rightarrow a_j). \quad (\text{I.31})$$

<sup>3</sup>For simplicity we assume that if there are multiple closest points, all corresponding decision errors are associated with the same number of bit errors [Sch06].

# Appendix J

## Space-Time Coding in the Presence of Intersymbol Interference

**M**OST SPACE-TIME coding techniques proposed in the literature were designed for MIMO channels without intersymbol interference (ISI). However, as discussed in Chapter 2, this assumption might not be valid in a practical system. If no counter measures are taken, ISI can cause substantial performance losses that compromise the achieved diversity gains. Basically, there are three different options to design a space-time coding scheme for MIMO channels with ISI. First, one might refine or generalize existing space-time codes such that they are suited for ISI channels (see, for example, the time-reversal STBC scheme discussed in Section 2.3.3). Second, one might employ a space-time code originally designed for channels without ISI, and mitigate the impact of ISI by means of appropriate equalization techniques at the receiver. Finally, one might employ a multi-carrier transmission scheme, so as to circumvent the problem of ISI.

In this section we consider the second option, while we focus on trellis-based equalization and detection<sup>1</sup> at the receiver, e.g., maximum-likelihood sequence estimation (MLSE) by means of the Viterbi algorithm [For72] or symbol-by-symbol maximum-a-posteriori (MAP) detection by means of the BCJR algorithm [BCJR74]. First, the topic of training-based channel estimation for MIMO systems with ISI is briefly discussed. Then, the trellis structure resulting for a general non-differential STBC in the presence of ISI is described (given arbitrary training sequences). Finally, the topic of performance evaluation based on distance spectra is addressed.

### J.1 Channel Estimation for MIMO Systems

Consider again the discrete-time MIMO channel model for frequency-selective fading introduced in Section 2.2.2:

$$\mathbf{y}[k] = \sum_{l=0}^L \mathbf{H}_l[k] \mathbf{x}[k-l] + \mathbf{n}[k], \quad (\text{J.1})$$

---

<sup>1</sup>Equalization of the ISI channel and detection of the transmitted information symbols is typically performed in a single step. Therefore, we use the notion equalization/detection in the sequel.

cf. (2.26). As earlier, let  $M$  denote the number of transmit antennas,  $N$  the number of receive antennas, and  $L$  the effective memory length of the channel. It is again assumed that the physical channel is slowly time-varying, i.e., the channel matrices  $\mathbf{H}_l[k]$  can be regarded as constant over  $(L+1)$  consecutive time indices. For the time being, we therefore drop the time index  $k$  for the channel coefficients.

In the following, we assume that coherent detection is performed at the receiver. In order to enable channel estimation, the transmitter is assumed to send a block of  $p_t$  known training vectors  $\mathbf{x}_t[k], \dots, \mathbf{x}_t[k+p_t-1]$ . Let  $x_{t,\mu}[k]$  denote the training symbol transmitted at time index  $k$  via the  $\mu$ th antenna ( $1 \leq \mu \leq M$ ). Moreover, let us define the matrices

$$\mathbf{X}_{t,\mu}[k] := \begin{bmatrix} x_{t,\mu}[k+L] & \dots & x_{t,\mu}[k+1] & x_{t,\mu}[k] \\ x_{t,\mu}[k+L+1] & \dots & x_{t,\mu}[k+2] & x_{t,\mu}[k+1] \\ \vdots & \ddots & \vdots & \vdots \\ x_{t,\mu}[k+p_t-1] & \dots & x_{t,\mu}[k+p_t-L] & x_{t,\mu}[k+p_t-(L+1)] \end{bmatrix}, \quad (\text{J.2})$$

$\mu = 1, \dots, M$  [Sch06]. The received samples of the  $\nu$ th receive antenna are collected in a vector  $\mathbf{y}_\nu[k]$ , according to

$$\mathbf{y}_\nu[k] := [y_\nu[k+L], \dots, y_\nu[k+p_t-1]]^T. \quad (\text{J.3})$$

We can then write

$$\mathbf{y}_\nu[k] = \sum_{\mu=1}^M \mathbf{X}_{t,\mu}[k] \mathbf{h}_{\nu,\mu} + \mathbf{n}_\nu[k] =: \mathbf{X}_t[k] \mathbf{h}_\nu + \mathbf{n}_\nu[k], \quad (\text{J.4})$$

where

$$\mathbf{h}_{\nu,\mu} := [h_{\nu,\mu,0}, \dots, h_{\nu,\mu,L}]^T, \quad (\text{J.5})$$

$$\mathbf{n}_\nu[k] := [n_\nu[k+L], \dots, n_\nu[k+p_t-1]]^T, \quad (\text{J.6})$$

$$\mathbf{X}_t[k] := [\mathbf{X}_{t,1}[k], \dots, \mathbf{X}_{t,\mu}[k], \dots, \mathbf{X}_{t,M}[k]], \quad (\text{J.7})$$

and

$$\mathbf{h}_\nu := [\mathbf{h}_{\nu,1}^T, \dots, \mathbf{h}_{\nu,\mu}^T, \dots, \mathbf{h}_{\nu,M}^T]^T. \quad (\text{J.8})$$

If no ISI is present ( $L=0$ ), the matrix  $\mathbf{X}_t[k]$  simplifies to

$$\mathbf{X}_t[k] = [\mathbf{x}_t[k+L], \dots, \mathbf{x}_t[k+p_t-1]]^T \quad (\text{J.9})$$

and the vector  $\mathbf{h}_\nu$  to

$$\mathbf{h}_\nu = [h_{\nu,1}, \dots, h_{\nu,\mu}, \dots, h_{\nu,M}]^T. \quad (\text{J.10})$$

The maximum-likelihood (ML) estimate for the channel coefficient vector  $\mathbf{h}_\nu$ , given the received vector  $\mathbf{y}_\nu[k]$  and the training vectors  $\mathbf{x}_t[k], \dots, \mathbf{x}_t[k+p_t-1]$ , results from maximizing the conditional PDF  $p(\mathbf{y}_\nu[k] | \tilde{\mathbf{h}}_\nu, \mathbf{x}_t[k], \dots, \mathbf{x}_t[k+p_t-1])$  with respect to  $\tilde{\mathbf{h}}_\nu$  [Che05, Ch. 3.1]:

$$\hat{\mathbf{h}}_{\nu,\text{ML}} = \underset{\tilde{\mathbf{h}}_\nu}{\operatorname{argmax}} \left\{ p(\mathbf{y}_\nu[k] | \tilde{\mathbf{h}}_\nu, \mathbf{x}_t[k], \dots, \mathbf{x}_t[k+p_t-1]) \right\}. \quad (\text{J.11})$$



Note that the task of ML channel estimation given known data symbols is dual to the task of MLSE given known channel coefficients. Assuming white Gaussian noise (with variance  $\sigma_n^2$ ) and a training length  $p_t \geq 2L + 1$ , the ML estimate  $\hat{\mathbf{h}}_{\nu, \text{ML}}$  can explicitly be calculated according to [RHH95]

$$\hat{\mathbf{h}}_{\nu, \text{ML}} = \underset{\tilde{\mathbf{h}}_{\nu}}{\operatorname{argmin}} \left\{ \|\mathbf{y}_{\nu}[k] - \mathbf{X}_t[k] \tilde{\mathbf{h}}_{\nu}\|^2 \right\} = \mathbf{X}_t^{\dagger}[k] \mathbf{y}_{\nu}[k] = \mathbf{h}_{\nu} + \mathbf{n}'_{\nu}[k], \quad (\text{J.12})$$

where  $\mathbf{X}_t^{\dagger}[k] := (\mathbf{X}_t^{\text{H}}[k] \mathbf{X}_t[k])^{-1} \mathbf{X}_t^{\text{H}}[k]$  denotes the Moore-Penrose left-hand pseudoinverse of  $\mathbf{X}_t[k]$ . The solution (J.12) is also known as the joint least-squares channel-estimation (JLSCE) solution.<sup>2</sup> The covariance matrix of the resulting noise vector  $\mathbf{n}'_{\nu}[k] := \mathbf{X}_t^{\dagger}[k] \mathbf{n}_{\nu}[k]$  is equal to  $\mathbf{E}\{\mathbf{n}'_{\nu}[k] \mathbf{n}'_{\nu}{}^{\text{H}}[k]\} = \sigma_n^2 (\mathbf{X}_t^{\text{H}}[k] \mathbf{X}_t[k])^{-1}$ . The mean power of the noise vector  $\mathbf{n}'_{\nu}[k]$  represents the mean squared channel estimation error. It is minimized if and only if the matrix  $\mathbf{X}_t[k]$  is orthogonal [CM98], i.e.,  $\mathbf{X}_t^{\text{H}}[k] \mathbf{X}_t[k] = \alpha[k] \mathbf{I}_{L+1}$  with some constant factor  $\alpha[k]$ . In other words, the optimal estimation result is obtained if the training sequences transmitted via the  $M$  antennas have perfect auto- and cross-correlation properties.

In the case of coherent detection at the receiver, the choice of ‘good’ training sequences is typically crucial for the overall resulting error performance. However, for a given training length and number of transmit antennas, it is often a demanding task to find sets of training sequences with (near-) perfect auto- and cross-correlation properties [MHS03a]. This is especially true if the training symbols are supposed to be taken from a certain, pre-defined symbol alphabet. For example, so-called perfect roots-of-unity sequences (PRUS) have perfect auto- and cross-correlation properties and exist for any number of transmit antennas [CM98]. However, the training symbols are taken from the  $Q$ -ary roots-of-unity alphabet

$$\mathbb{A} := \{e^{j2\pi i/Q} \mid i = 0, \dots, Q-1\}. \quad (\text{J.13})$$

Since the cardinality  $Q$  of the alphabet  $\mathbb{A}$  is not necessarily equal to  $2^m$  ( $m$  integer),  $\mathbb{A}$  is in general not a standard phase-shift keying (PSK) signal constellation. Moreover, the smallest possible cardinality  $Q$  depends on the desired training length  $p_t$  [FAT03].

In the case of frequency-flat fading ( $L=0$ ), only the cross-correlation properties of the employed training sequences are of interest. In fact, orthogonal training sequences can easily be found [FAT03]. In particular, if an OSTBC is employed, a specific training sequence design is not required at all, due to the intrinsic orthogonality of the transmission scheme. One can simply take a single (arbitrary) training sequence of length  $np_i$  and encode it by means of the OSTBC encoder, where  $n$  denotes an arbitrary integer number and  $p_i$  the number of (information) symbols per OSTBC code matrix (cf. Section 2.3.1). This enables ML channel estimation at the receiver by means of simple widely linear processing, in terms of matrix-vector products  $\hat{\mathbf{h}}_{\nu, \text{ML}} := \mathbf{X}_t^{\dagger}[k] \mathbf{y}_{\nu}[k] \propto \mathbf{X}_t^{\text{H}}[k] \mathbf{y}_{\nu}[k]$  ( $\nu = 1, \dots, N$ ).<sup>3</sup> A similar idea was presented in [FAT03], where quasi-optimal sets of training sequences

<sup>2</sup>The JLSCE solution constitutes a zero-forcing (ZF) solution. It should therefore be noted that the quality of the channel estimates can usually be improved by employing a minimum-mean-squared-error (MMSE) solution instead.

<sup>3</sup>This is dual to the OSTBC decoding step performed in the case of perfect channel knowledge at the receiver, cf. Section 2.3.1. Here the duality between channel estimation and data detection again becomes obvious.

were derived for MIMO channels with ISI, by optimizing a single training sequence which was then encoded by means of an appropriate space-time encoder (not necessarily the same as employed for the information symbols).

## J.2 Trellis-Based Equalization for STBCs

In this section, the trellis structure resulting for a general non-differential STBC in the presence of ISI is described, which builds the basis for trellis-based equalization/detection by means of the Viterbi algorithm [For72], the BCJR algorithm [BCJR74] or the MaxLogMAP algorithm [RHV97].<sup>4</sup> In particular, we assume the general case that an arbitrary set of training sequences is employed that is not necessarily generated by the STBC encoder used for the information symbols. To this end, we consider a frame structure as depicted in Fig. J.1, where the transmitter periodically switches between blocks of space-time encoded information symbols ('info blocks') and blocks of training symbols ('training blocks'). As will be seen, this leads to an irregular (i.e., time-varying) trellis structure.

The transmitter structure under consideration is depicted in Fig. J.2. At the transmitter, the information symbols  $a[\kappa]$  are partitioned into groups

$$\mathbf{a}[\kappa] := [a[\kappa], \dots, a[\kappa+p_i-1]]^T$$

of  $p_i$  complex-valued  $Q$ -ary information symbols (cf. Section 2.3.1), which are subsequently mapped onto STBC code matrices  $\mathbf{X}[k]$  of size  $(p \times M)$ , according to

$$\mathcal{S}: \mathbb{C}^{p_i} \rightarrow \mathbb{C}^{p \times M}, \quad \mathbf{a}[\kappa] \mapsto \mathbf{X}[k] = \begin{bmatrix} x_{1,1}(\mathbf{a}[\kappa]) & \cdots & x_{1,M}(\mathbf{a}[\kappa]) \\ \vdots & \ddots & \vdots \\ x_{p,1}(\mathbf{a}[\kappa]) & \cdots & x_{p,M}(\mathbf{a}[\kappa]) \end{bmatrix}. \quad (\text{J.14})$$

Note that  $\kappa$  denotes the time index before the STBC encoder and  $k$  the time index after the STBC encoder. Moreover,  $p$  denotes the number of time indices  $k, k+1, \dots, k+p-1$  used for the transmission of a single STBC code matrix. In particular, the complex-valued symbol  $x_{\xi,\mu}(\mathbf{a}[\kappa])$  ( $1 \leq \xi \leq p, 1 \leq \mu \leq M$ ) is transmitted at time index  $k+\xi-1$  via the  $\mu$ th transmit antenna. Since the STBC code matrix  $\mathbf{X}[k]$  comprises  $p$  consecutive time indices, the preceding code matrix is in the sequel denoted as  $\mathbf{X}[k-p]$ , and the subsequent code matrix as  $\mathbf{X}[k+p]$ . Similarly, the corresponding information symbol vectors are denoted as  $\mathbf{a}[\kappa-p_i]$  and  $\mathbf{a}[\kappa+p_i]$ , respectively.

In the following, a single info block is assumed to span  $N_i$  successive STBC code matrices  $\mathbf{X}[k]$ , cf. Fig. J.1. After  $N_i$  STBC code matrices have been transmitted, the transmitter switches to  $p_t$  subsequent training vectors  $\mathbf{x}_t[k], \dots, \mathbf{x}_t[k+p_t-1] \in \mathbb{C}^{M \times 1}$ , cf. Fig. J.2. At the receiver, first the task of channel estimation is performed (based

<sup>4</sup>The Viterbi algorithm is optimal in the sense of maximum-likelihood sequence estimation (MLSE) and the BCJR algorithm in the sense of maximum a-posteriori (MAP) symbol-by-symbol estimation. The MaxLogMAP algorithm is a suboptimal algorithm which (closely) approximates the a-posteriori probability values provided by the BCJR algorithm. All three algorithms operate on the same trellis diagram. In particular, identical branch metrics are computed by all three algorithms.

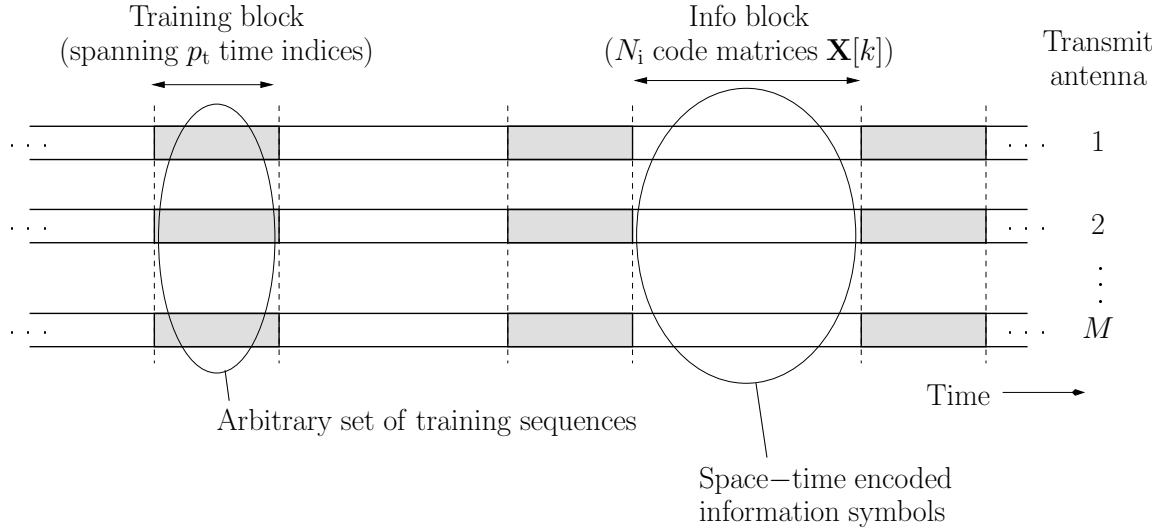


Figure J.1: Frame structure under consideration.

on the training blocks). Then, a trellis-based equalizer/detector algorithm is employed, which delivers estimates  $\hat{a}[\kappa]$  of the transmitted information symbols.

### Trellis Structure Without Embedded Training Symbols

First, the general trellis structure without embedded training symbols is described. Consider again the discrete-time MIMO channel model (J.1) for frequency-selective fading. As earlier, let  $L$  denote the effective channel memory length, where

$$L := np + l \tag{J.15}$$

( $n, l$  integer and  $l < p$ ). In order to obtain a trellis-based equalizer/detector algorithm with a preferably small number of trellis states, a single trellis segment is associated with a complete STBC code matrix  $\mathbf{X}[k] := [\mathbf{x}[k], \dots, \mathbf{x}[k+p-1]]^T$  (and thus with  $p_i$  information symbols), i.e., a transition from one trellis state to a subsequent state spans  $p$  consecutive time indices  $k, \dots, k+p-1$  [Bau00, BHS01]. Since the individual trellis branches are associated with  $p_i$  information symbol hypotheses, altogether  $Q^{p_i}$  branches start from each trellis state.

The channel memory comprises  $n$  complete STBC code matrices  $\mathbf{X}[k-p], \dots, \mathbf{X}[k-np]$ , which correspond to the information symbols  $\mathbf{a}[\kappa-p_i], \dots, \mathbf{a}[\kappa-np_i]$ , respectively. In addition, the channel memory comprises the first  $l$  rows of code matrix  $\mathbf{X}[k-(n+1)p]$ , which correspond to another  $\zeta(l)$  information symbols. The value of  $\zeta(l)$  depends on the particular structure of the STBC code matrix under consideration ( $1 \leq \zeta(l) \leq p_i$ ). Correspondingly, the starting states of the trellis segment for code matrix  $\mathbf{X}[k]$  are defined by the  $np_i$  hypotheses for the information symbols  $\mathbf{a}[\kappa-p_i], \dots, \mathbf{a}[\kappa-np_i]$  and by the  $\zeta(l)$  hypotheses for the information symbols associated with the first  $l$  rows of code matrix  $\mathbf{X}[k-(n+1)p]$ . Similarly, the target states are defined by the hypotheses for the information symbols  $\mathbf{a}[\kappa], \dots, \mathbf{a}[\kappa-(n-1)p_i]$  and by the symbol hypotheses associated with the

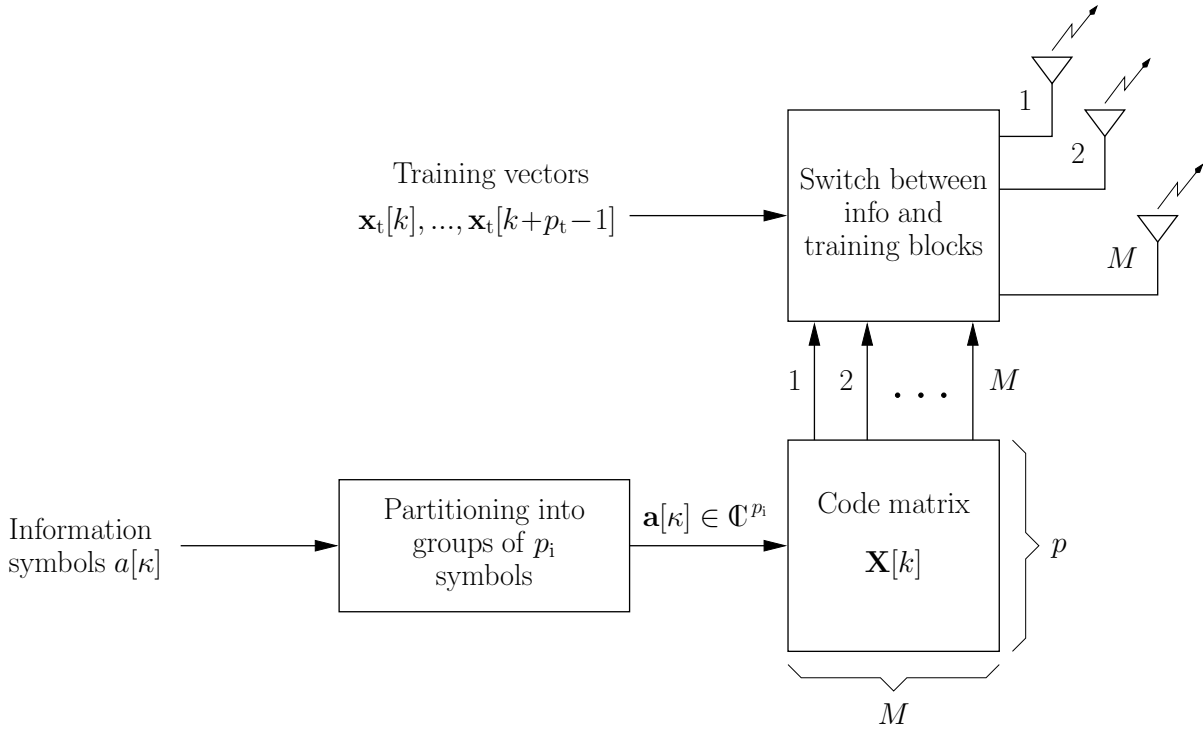


Figure J.2: Transmitter structure of a general non-differential STBC scheme with embedded training symbols.

first  $l$  rows of code matrix  $\mathbf{X}[k-np]$ . As a result, the number of trellis states is equal to  $Q^{np_i+\varsigma(l)}$ . Specifically, for  $l=0$  we have  $\varsigma(l)=0$ , i.e., the number of trellis states is  $Q^{p_i L/p} = Q^{R_t L}$ , where  $R_t$  denotes the temporal rate of the STBC (cf. Section 2.3.1). Obviously, for STBCs with a temporal rate of one (such as Alamouti's transmit diversity scheme), the number of required trellis states is the same as in a single-antenna system.

Assuming  $N$  receive antennas and additive white Gaussian noise, metric increments of form

$$\Gamma_b[k] := \sum_{\nu=1}^N \sum_{\xi=1}^p |y_\nu[k+\xi-1] - \tilde{y}_\nu[k+\xi-1]|^2 \quad (\text{J.16})$$

are computed for each trellis branch ( $b=1, \dots, Q^{p_i}$ ), where  $\tilde{y}_\nu[k]$  denotes a replica of the  $k$ th received sample at receive antenna  $\nu$ , which is based on the information symbol hypotheses associated with the trellis branch under consideration. Note that only  $(n+1)p_i + \varsigma(l)$  symbol hypotheses are required, in order to construct the replicas  $\tilde{y}_\nu[k], \dots, \tilde{y}_\nu[k+p-1]$ , although altogether  $(n+1)pM + lM$  transmitted symbols  $x_{\xi,\mu}(\mathbf{a}[k])$  contribute to the received samples  $y_\nu[k], \dots, y_\nu[k+p-1]$ .

In the sequel, the term  $\varsigma(l)$  is specified more precisely. The entries  $x_{\xi,\mu}(\mathbf{a}[k])$  of the STBC code matrix  $\mathbf{X}[k]$  do not necessarily depend on the complete information symbol vector  $\mathbf{a}[k]$ , but rather on a subvector or only a single element of  $\mathbf{a}[k]$ . To this end, let  $\mathbf{a}_\mathbb{I}[k]$  denote a subvector of  $\mathbf{a}[k]$  which corresponds to an index set  $\mathbb{I} \subseteq \{1, \dots, p_i\}$ , i.e., all elements  $a[k+\lambda-1]$  of  $\mathbf{a}[k]$  with  $\lambda \notin \mathbb{I}$  are discarded. Each entry  $x_{\xi,\mu}(\mathbf{a}[k])$  of  $\mathbf{X}[k]$  can

thus be associated with a dedicated index set  $\mathbb{I}_{\xi,\mu}$ . By this means, (J.14) can be rewritten as [Lan02a]

$$\mathcal{S} : \mathbb{C}^{p_i} \longrightarrow \mathbb{C}^{p \times M}, \quad \mathbf{a}[\kappa] \longmapsto \mathbf{X}[k] = \begin{bmatrix} x_{1,1}(\mathbf{a}_{\mathbb{I}_{1,1}}[\kappa]) & \cdots & x_{1,M}(\mathbf{a}_{\mathbb{I}_{1,M}}[\kappa]) \\ \vdots & \ddots & \vdots \\ x_{p,1}(\mathbf{a}_{\mathbb{I}_{p,1}}[\kappa]) & \cdots & x_{p,M}(\mathbf{a}_{\mathbb{I}_{p,M}}[\kappa]) \end{bmatrix}, \quad (\text{J.17})$$

where

$$\bigcup_{\substack{1 \leq \xi \leq p \\ 1 \leq \mu \leq M}} \mathbb{I}_{\xi,\mu} = \{1, \dots, p_i\}. \quad (\text{J.18})$$

Using the above definitions,  $\varsigma(l)$  can be expressed as

$$\varsigma(l) = |\mathbb{I}_{11} \cup \cdots \cup \mathbb{I}_{1M} \cup \mathbb{I}_{21} \cup \cdots \cup \mathbb{I}_{2M} \cup \cdots \cup \mathbb{I}_{l1} \cup \cdots \cup \mathbb{I}_{lM}|. \quad (\text{J.19})$$

It is now simple to extend the above framework to the case of general embedded training symbols.

### Trellis Structure With Embedded Training Symbols

For simplicity, we assume in the sequel that  $l=0$ , i.e.,  $L$  is a multiple of  $p$ . At the edges of the info blocks, the transmitted symbols  $x_{\xi,\mu}(\mathbf{a}_{\mathbb{I}_{\xi,\mu}}[\kappa - np_i]), \dots, x_{\xi,\mu}(\mathbf{a}_{\mathbb{I}_{\xi,\mu}}[\kappa]), \mu = 1, \dots, M, \xi = 1, \dots, p$ , which contribute to the current received samples  $y_\nu[k + \xi - 1], \nu = 1, \dots, N, \xi = 1, \dots, p$ , are partially replaced by known training symbols. This has to be taken into account, when constructing the replicas  $\tilde{y}_\nu[k + \xi - 1]$  required for the metric increments  $\Gamma_b[k]$  in (J.16). The construction rule for the replicas  $\tilde{y}_\nu[k + \xi - 1]$  is therefore time-varying, i.e., it depends on the current position within the trellis diagram. In particular, some of the  $(n+1)p_i$  information symbol hypotheses  $\tilde{\mathbf{a}}[\kappa - np_i], \dots, \tilde{\mathbf{a}}[\kappa]$  become dispensable, which leads to a time-varying trellis structure.<sup>5</sup>

Consider first the left edge of an info block. In the first trellis segment following the training block (starting at time index  $k_0$ ), the channel memory is completely filled with known symbols, provided that the training block length,  $p_t$ , is greater than or equal to the channel memory length  $L$ . Accordingly, in order to calculate the metric increments  $\Gamma_b[k_0]$  ( $1 \leq b \leq Q^{p_i}$ ), only the hypotheses for the current information symbols,  $\tilde{\mathbf{a}}[\kappa_0]$ , are required. Correspondingly, only a single starting state exists in the first trellis segment, which does not contain any information symbol hypotheses ('void' state).

If the training block length  $p_t$  is smaller than  $L$ , also information symbols from the previous info block contribute to the current received samples  $y_\nu[k_0 + \xi - 1], \nu = 1, \dots, N, \xi = 1, \dots, p$ . Let the difference  $\Delta := L - p_t$  be given by  $\Delta := n'p + l'$ , with  $n', l'$  integer and  $l' < p$ . Then, only the code matrices  $\mathbf{X}[k_0 - p], \dots, \mathbf{X}[k_0 - (n - n' - 1)p]$  are filled with known symbols as well as the upper  $(p - l')$  rows of the matrix  $\mathbf{X}[k_0 - (n - n')p]$ . The information symbols from the previous info block, which contribute to the received

<sup>5</sup>In a single-antenna system, where each trellis segment is associated with only a single time index  $k$ , the information symbols  $a[k]$  are directly replaced by training symbols  $x_t[k]$ , according to a one-to-one correspondence. Therefore, those trellis branches associated with symbol hypotheses  $\tilde{a}[k] \neq x_t[k]$  can simply be eliminated from the trellis diagram, provided that the information and training symbols are taken from the same symbol alphabet.

samples  $y_\nu[k_0 + \xi - 1]$ , are therefore given by  $\mathbf{a}[\kappa_0 - (n - n' + 1)p_i], \dots, \mathbf{a}[\kappa_0 - np_i]$  and by  $\mathbf{a}_{\mathbb{I}'}[\kappa_0 - (n - n')p_i]$ , where  $\mathbb{I}' := \mathbb{I}_{(p-l'+1),1} \cup \dots \cup \mathbb{I}_{(p-l'+1),M} \cup \dots \cup \mathbb{I}_{p,1} \cup \dots \cup \mathbb{I}_{p,M}$ . Therefore, altogether  $Q^{n'p_i + \zeta'(l')}$  starting states exist in the first trellis segment, where  $\zeta'(l') := |\mathbb{I}'|$ . Note that the a-priori probability of each starting state is influenced by the previous info block and is, in general, different from one state to another.

In the sequel, we focus on the case  $p_t \geq L$  for simplicity, i.e., the first trellis segment has only a single starting state. As a short-hand notation, we denote the time index  $k_0 + m$  as  $k_m$ , and the time index  $\kappa_0 + m$  as  $\kappa_m$ , for a given integer  $m$ . In the second trellis segment following the training block (starting at time index  $k_p$ ), the branches are associated with new symbol hypotheses  $\tilde{a}[\kappa_{p_i}], \dots, \tilde{a}[\kappa_{p_i} + p_i - 1]$ . The starting states now comprise the symbol hypotheses  $\tilde{a}[\kappa_0], \dots, \tilde{a}[\kappa_0 + p_i - 1]$ , i.e., there are altogether  $Q^{p_i}$  starting states. The branches in the third trellis segment (starting at time index  $k_{2p}$ ) are associated with symbol hypotheses  $\tilde{a}[\kappa_{2p_i}], \dots, \tilde{a}[\kappa_{2p_i} + p_i - 1]$ , and the starting states comprise the symbol hypotheses  $\tilde{a}[\kappa_0], \dots, \tilde{a}[\kappa_0 + p_i - 1], \tilde{a}[\kappa_{p_i}], \dots, \tilde{a}[\kappa_{p_i} + p_i - 1]$ . Correspondingly, there are now  $Q^{2p_i}$  starting states, provided that the channel memory length  $L$  is sufficiently large, i.e.,  $L \geq 2p$ . Thus, the channel memory is subsequently filled with information symbols, and the complexity in terms of trellis states inflates, until the complexity of the full-state trellis diagram is reached ( $Q^{R_t L}$  trellis states).

Finally, consider the right edge of an info block. The number of starting states of the first trellis segment within the subsequent training block (starting at time index  $k_{N_i p}$ ) corresponds to that of the full-state trellis. The branches are now associated with known symbols, i.e., they do not contain any information symbol hypotheses ('void' branch). Correspondingly, only a single branch starts from each trellis state. In the subsequent trellis segment (starting at time index  $k_{(N_i+1)p}$ ), the known training symbols enter the channel memory. This reduces the number of required starting states by a factor of  $1/Q^{p_i}$ . Thus, the channel memory is subsequently filled with known symbols, and the complexity in terms of trellis states deflates, until there is only a single trellis state left. The trellis branches remain void, until a new info block begins.

### Example J.1 (Trellis structure resulting for Alamouti's scheme)

In the following, the above trellis structure is illustrated for the example of Alamouti's transmit diversity scheme [Ala98] ( $M = p = p_i = 2$ ,  $R_t = 1$ ), cf. Section 2.3.1. Since  $p = p_i = 2$  holds, a single trellis segment spans two consecutive time indices  $k$ ,  $k+1$  and is associated with  $p_i = 2$  information symbols  $a[\kappa]$ ,  $a[\kappa+1]$ . Correspondingly,  $Q^2$  branches start from each trellis state. If the channel memory length  $L$  is an even number, the full-state trellis has  $Q^L$  states (just as in a single-antenna system), otherwise the number of trellis states is  $Q^{L+1}$  [MHS03a]. For simplicity, we assume in the sequel that a single antenna is employed at the receiver ( $N = 1$ ). In this case, the branch metrics  $\Gamma_b[k]$  according to (J.16) read

$$\Gamma_b[k] = |y[k] - \tilde{y}[k]|^2 + |y[k+1] - \tilde{y}[k+1]|^2. \quad (\text{J.20})$$

The receive antenna index  $\nu = 1$  has been dropped for convenience. The replicas  $\tilde{y}[k]$  and  $\tilde{y}[k+1]$  in (J.20) are calculated as

$$\tilde{y}[k] = \sum_{\substack{l=0 \\ l \text{ even}}}^L \left[ \hat{h}_{1,1,l}[k] \tilde{a}[\kappa - l] + \hat{h}_{1,2,l}[k] \tilde{a}[\kappa + 1 - l] \right] \quad (\text{J.21})$$



$$+ \sum_{\substack{l=1 \\ l \text{ odd}}}^L \left[ \hat{h}_{1,2,l}[k] \tilde{a}^*[\kappa-1-l] - \hat{h}_{1,1,l}[k] \tilde{a}^*[\kappa-l] \right]$$

and

$$\begin{aligned} \tilde{y}[k+1] &= \sum_{\substack{l=0 \\ l \text{ even}}}^L \left[ \hat{h}_{1,2,l}[k+1] \tilde{a}^*[\kappa-l] - \hat{h}_{1,1,l}[k+1] \tilde{a}^*[\kappa+1-l] \right] \\ &+ \sum_{\substack{l=1 \\ l \text{ odd}}}^L \left[ \hat{h}_{1,1,l}[k+1] \tilde{a}[\kappa+1-l] + \hat{h}_{1,2,l}[k+1] \tilde{a}[\kappa+2-l] \right], \end{aligned} \quad (\text{J.22})$$

where  $\hat{h}_{1,\mu,l}[k]$  denotes an estimate of the channel coefficient  $h_{1,\mu,l}[k]$ . As an example, we focus on the case  $L=4$  in the sequel. Consider a full-state trellis segment associated with the time indices  $k$  and  $k+1$ . The channel memory comprises the code matrices  $\mathbf{X}[k-2]$  and  $\mathbf{X}[k-4]$ , i.e., the starting states of the trellis segment are defined by the symbol hypotheses  $\tilde{a}[\kappa-4], \tilde{a}[\kappa-3]$  (code matrix  $\mathbf{X}[k-4]$ ) and  $\tilde{a}[\kappa-2], \tilde{a}[\kappa-1]$  (code matrix  $\mathbf{X}[k-2]$ ). The target states are defined by the symbol hypotheses  $\tilde{a}[\kappa-2], \tilde{a}[\kappa-1], \tilde{a}[\kappa], \tilde{a}[\kappa+1]$ . Consider, for example, the first trellis segment within a training block. Here, the current code matrix  $\mathbf{X}[k]$  is replaced by training symbols  $x_{t,1}[k], x_{t,1}[k+1]$  (first transmit antenna) and  $x_{t,2}[k], x_{t,2}[k+1]$  (second transmit antenna). Correspondingly, the computation of the branch metrics according to (J.20)-(J.22) has to be modified, by replacing  $\tilde{a}[\kappa], -\tilde{a}^*[\kappa+1], \tilde{a}[\kappa+1], \tilde{a}^*[\kappa]$  by  $x_{t,1}[k], x_{t,1}[k+1], x_{t,2}[k], x_{t,2}[k+1]$ , respectively.

For the example of binary transmission ( $Q=2$ ), the complete trellis structure resulting for Alamouti's transmit diversity scheme is depicted in Fig. J.3 ( $p_t \geq L$  assumed). As can be seen, during the first two trellis segments within the info block, the trellis complexity inflates from one to  $Q^L=16$  trellis states, which corresponds to the complexity of the full-state trellis. During the first two trellis segments within the training block, the trellis complexity deflates again to a single state.  $\diamond$

### J.3 Performance Analysis Based on Distance Spectra

In order to conclude this chapter, the topic of performance evaluation for STBCs in the presence of ISI is briefly addressed. We focus on MLSE equalization/detection and assume perfect channel knowledge at the receiver. Moreover, for simplicity we restrict ourselves to a frame structure without embedded training symbols.

The performance of a (trellis-based) MLSE equalizer can be assessed on the basis of distance spectra. Consider a certain sequence  $\mathbf{a} := [\dots, a[\kappa-1], a[\kappa], a[\kappa+1], \dots]$  of information symbols, while we focus on binary antipodal transmission for simplicity, i.e.,  $a[\kappa] \in \{\pm 1\}$ . As earlier, we assume that an STBC with  $M$  transmit antennas is employed, while the average transmit power per antenna is equal to  $P/M$ . In this case, the pairwise error probability (PEP) that an MLSE equalizer decides in favor of an erroneous sequence  $\mathbf{a}' \neq \mathbf{a}$  although sequence  $\mathbf{a}$  has been transmitted, is given by [Pro01, Ch. 5.2]

$$P(\mathbf{a} \rightarrow \mathbf{a}') = Q \left( \sqrt{\frac{P}{2M\sigma_n^2} d_E^2(\mathbf{a}, \mathbf{a}')} \right), \quad (\text{J.23})$$



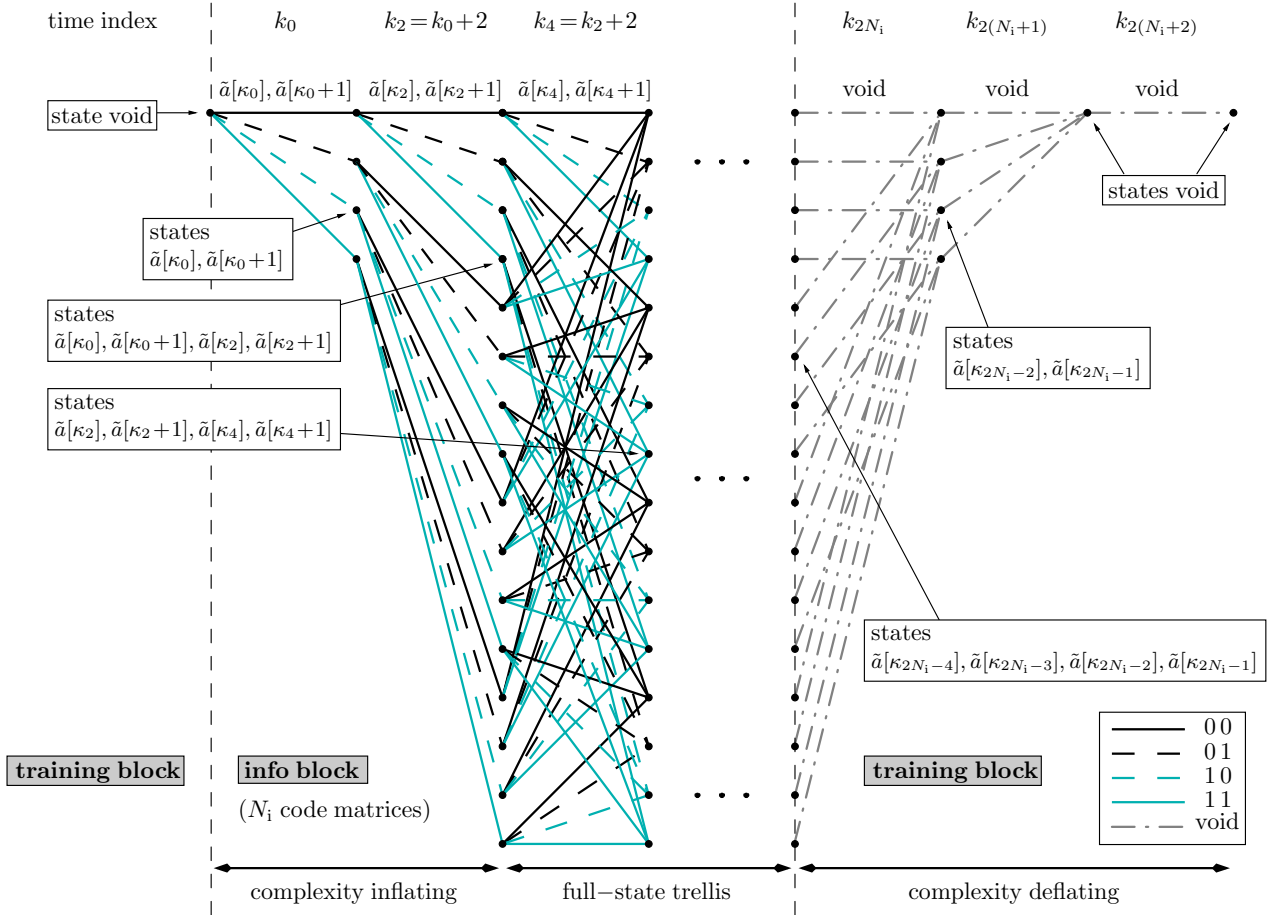


Figure J.3: Trellis-structure resulting for Alamouti's transmit diversity scheme, for the example of binary transmission ( $Q=2$ ) and a channel memory length of  $L=4$ . The trellis states from top to bottom are given by the binary representations of 0, 1, 2, 3 and 0, 1, 2, ..., 15, respectively.

where  $Q(x)$  denotes the Gaussian Q-function (cf. Definition C.2 in Appendix C) and  $d_E^2(\mathbf{a}, \mathbf{a}')$  denotes the squared Euclidean distance between  $\mathbf{a}$  and  $\mathbf{a}'$  after the STBC encoder and the ISI channel, cf. Fig. J.4.<sup>6</sup>

According to the ML criterion, we assume in the following that all information sequences  $\mathbf{a}$  are equiprobable. In the sequel, we consider the so-called error event probability  $\Pr\{\mathcal{E}_{\text{error}, k_0}\}$ , i.e., the probability that at a certain time index  $k_0$  the MLSE equalizer diverts from the correct trellis path representing the transmitted information sequence  $\mathbf{a}$ . To this end, we introduce error symbols  $\epsilon[\kappa]$ , according to

$$\epsilon[\kappa] := a[\kappa] - a'[\kappa] = \begin{cases} 0 & \text{if } a'[\kappa] = a[\kappa] \\ +2 & \text{if } a'[\kappa] \neq a[\kappa] \text{ and } a[\kappa] = +1 \\ -2 & \text{if } a'[\kappa] \neq a[\kappa] \text{ and } a[\kappa] = -1 \end{cases} . \quad (\text{J.24})$$

<sup>6</sup>This is similar to the PEP of space-time codes in the presence of frequency-flat fading, cf. Section 2.3.4 and Section 3.2.4.

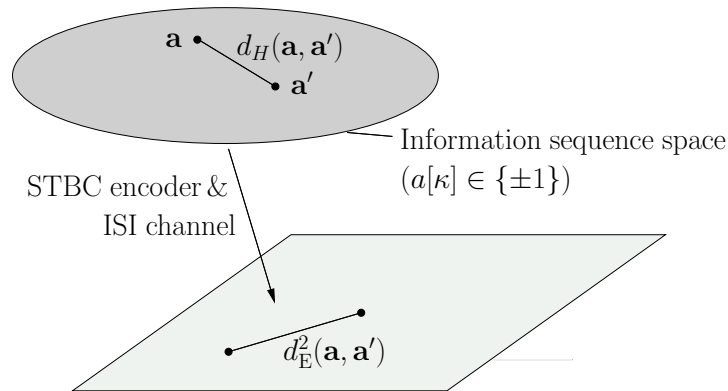


Figure J.4: Illustration of the PEP between two information sequences  $\mathbf{a}$  and  $\mathbf{a}'$  ( $d_E^2$ : squared Euclidean distance,  $d_H$ : Hamming distance).

Note that different sequence pairs  $(\mathbf{a}, \mathbf{a}')$  can lead to the same error sequence

$$\boldsymbol{\epsilon} := [\dots, \epsilon[\kappa-1], \epsilon[\kappa], \epsilon[\kappa+1], \dots]. \tag{J.25}$$

Based on the error symbols  $\epsilon[\kappa]$ , a difference trellis diagram can be constructed [Hub92, Ch. 5.1.2], along the same lines as for the information symbols  $a[\kappa]$  (cf. Section J.2). In the following, let  $\mathbb{E}_{k_0}$  denote the set of all error sequences  $\boldsymbol{\epsilon}$  that divert at time index  $k_0$  from the all-zeros path within the difference trellis (representing error-free transmission). The error event probability  $\Pr\{\mathcal{E}_{\text{error}, k_0}\}$  can then be bounded above as

$$\Pr\{\mathcal{E}_{\text{error}, k_0}\} \leq \sum_{\boldsymbol{\epsilon} \in \mathbb{E}_{k_0}} p_{\boldsymbol{\epsilon}} \cdot Q\left(\sqrt{\frac{P}{2M\sigma_n^2}} d_E^2(\boldsymbol{\epsilon})\right) \tag{J.26}$$

(union bound [Hub92, Ch. 3.3.2]), where  $d_E^2(\boldsymbol{\epsilon})$  denotes the squared Euclidean distance associated with error sequence  $\boldsymbol{\epsilon}$ . The factors  $p_{\boldsymbol{\epsilon}}$  are appropriate constants, which represent the a-priori probabilities of the individual error sequences  $\boldsymbol{\epsilon}$ .<sup>7</sup>

The squared Euclidean distances  $d_E^2(\boldsymbol{\epsilon})$  as well as the constants  $p_{\boldsymbol{\epsilon}}$  can, for example, be determined by means of state transition matrices. Alternatively, the squared Euclidean distances  $d_E^2(\boldsymbol{\epsilon})$  can be determined via the difference trellis diagram, e.g., by means of a list Viterbi algorithm [BH00]. One can thus compute so-called distance spectra, which comprise the occurring squared Euclidean distances along with their relative frequencies (including the factors  $p_{\boldsymbol{\epsilon}}$ ). If there are relatively few squared Euclidean distances  $d_E^2(\boldsymbol{\epsilon})$  with a value close to zero, the upper bound (J.26) will be comparatively small, implying a good resulting error performance.<sup>8</sup>

<sup>7</sup>Since the information symbols  $a[\kappa]$  are assumed to be equally likely  $+1$  or  $-1$ , the error symbols  $\epsilon[\kappa] = +2$  and  $\epsilon[\kappa] = -2$  can only occur in one half of all cases, whereas  $\epsilon[\kappa] = 0$  can always occur, irrespective of the value of  $a[\kappa]$ .

<sup>8</sup>State transition matrices are also useful, in order to determine the Hamming distances  $d_H(\boldsymbol{\epsilon})$ , i.e., the number of information bit errors, associated with the individual error sequences  $\boldsymbol{\epsilon}$ .

The concept of state transition matrices, along with the calculation of the squared Euclidean distances  $d_E^2(\boldsymbol{\epsilon})$  and the factors  $p_\epsilon$ , is in the following illustrated for Alamouti's transmit diversity scheme [Ala98] in the presence of ISI.

**Example J.2 (State transition matrix for Alamouti's scheme)**

For simplicity, we focus on the case of a single receive antenna ( $N=1$ ) and a channel model with memory length  $L=1$ . Generalizations to multiple receive antennas or larger channel memory lengths are, however, straightforward. In the sequel, let  $\mathbf{h} := [h_0, h_1]^T$  and  $\mathbf{g} := [g_0, g_1]^T$  denote the channel coefficient vector associated with the first and the second transmit antenna, respectively. The noiseless received samples at time index  $k$  and  $k+1$  are thus given by

$$y[k] = h_0 a[\kappa] - h_1 a^*[\kappa-1] + g_0 a[\kappa+1] + g_1 a^*[\kappa-2] \quad (\text{J.27a})$$

$$y[k+1] = -h_0 a^*[\kappa+1] + h_1 a[\kappa] + g_0 a^*[\kappa] + g_1 a[\kappa+1]. \quad (\text{J.27b})$$

Therefore, the starting states of the corresponding trellis segment are given by  $\tilde{a}[\kappa-2], \tilde{a}[\kappa-1]$ , and the target states are given by  $\tilde{a}[\kappa], \tilde{a}[\kappa+1]$  (cf. Section J.2). Accordingly, the starting states of the corresponding trellis segment within the difference trellis diagram are defined by the error symbols  $\epsilon[\kappa-2], \epsilon[\kappa-1]$  and the target states by the error symbols  $\epsilon[\kappa], \epsilon[\kappa+1]$ . Thus, there are altogether  $3^2=9$  trellis states ( $a[\kappa] \in \{\pm 1\}$  assumed). Moreover, each starting state is connected with each target state, i.e., there are altogether 81 branches within each trellis segment. Each trellis branch within the difference trellis is associated with a certain squared Euclidean distance

$$\begin{aligned} d_{E,k}^2 &:= |y[k] - y'[k]|^2 + |y[k+1] - y'[k+1]|^2 \\ &= |h_0 \epsilon[\kappa] - h_1 \epsilon[\kappa-1] + g_0 \epsilon[\kappa+1] + g_1 \epsilon[\kappa-2]|^2 \\ &\quad + |h_0 \epsilon[\kappa+1] - h_1 \epsilon[\kappa] - g_0 \epsilon[\kappa] - g_1 \epsilon[\kappa+1]|^2, \end{aligned} \quad (\text{J.28})$$

a certain Hamming distance

$$d_{H,k} := \begin{cases} 0 & \text{if } \epsilon[\kappa]=0 \quad \text{and} \quad \epsilon[\kappa+1]=0 \\ 1 & \text{if } \epsilon[\kappa] \neq 0 \quad \text{or} \quad \epsilon[\kappa+1] \neq 0, \\ 2 & \text{if } \epsilon[\kappa] \neq 0 \quad \text{and} \quad \epsilon[\kappa+1] \neq 0 \end{cases}, \quad (\text{J.29})$$

and an a-priori probability factor

$$p_k := \begin{cases} 1 & \text{if } \epsilon[\kappa]=0 \quad \text{and} \quad \epsilon[\kappa+1]=0 \\ \frac{1}{2} & \text{if } \epsilon[\kappa] \neq 0 \quad \text{or} \quad \epsilon[\kappa+1] \neq 0 \\ \frac{1}{4} & \text{if } \epsilon[\kappa] \neq 0 \quad \text{and} \quad \epsilon[\kappa+1] \neq 0 \end{cases}. \quad (\text{J.30})$$

For a given error sequence  $\boldsymbol{\epsilon}$ , the squared Euclidean distance  $d_E^2(\boldsymbol{\epsilon})$ , the Hamming distance  $d_H(\boldsymbol{\epsilon})$ , and the factor  $p_\epsilon$  can thus be calculated as

$$d_E^2(\boldsymbol{\epsilon}) = \sum_k d_{E,k}^2, \quad d_H(\boldsymbol{\epsilon}) = \sum_k d_{H,k}, \quad p_\epsilon = \prod_k p_k. \quad (\text{J.31})$$

An elegant way to calculate the distances  $d_E^2(\epsilon)$ ,  $d_H(\epsilon)$  and the factor  $p_\epsilon$  can be adopted from the theory of convolutional codes (see e.g. [RWM93]). To this end, each state transition  $\epsilon[\kappa-2], \epsilon[\kappa-1] \rightarrow \epsilon[\kappa], \epsilon[\kappa+1]$  within the difference trellis diagram is associated with a symbolic branch label [Hub92, Ch. 5.1.2]

$$\Lambda_k(D, E, J) := p_k D^{d_{E,k}^2} E^{d_{H,k}} J, \quad (\text{J.32})$$

where  $D$ ,  $E$  and  $J$  are symbolic bases. Considering a single error path  $\epsilon$  spanning  $S$  trellis segments within the difference trellis diagram, the associated quantities  $d_E^2(\epsilon)$ ,  $d_H(\epsilon)$  and  $p_\epsilon$  can thus be computed by multiplying the corresponding symbolic branch labels  $\Lambda_k(D, E, J)$ , according to

$$\Lambda_\epsilon(D, E, J) := \prod_k \Lambda_k(D, E, J) = p_\epsilon D^{d_E^2(\epsilon)} E^{d_H(\epsilon)} J^S. \quad (\text{J.33})$$

The exponent of  $J$  counts the number of considered trellis segments.

For convenience, the symbolic branch labels  $\Lambda_k(D, E, J)$  are aligned in a  $(9 \times 9)$ -state transition matrix  $\mathbf{T}(D, E, J)$ , where the rows of  $\mathbf{T}(D, E, J)$  represent the possible starting states  $\epsilon[\kappa-2], \epsilon[\kappa-1]$  and the columns the possible target states  $\epsilon[\kappa], \epsilon[\kappa+1]$ . In the sequel, the following order of the starting states (from top to bottom) and target states (from left to right) is used:

$$+2, +2 \quad +2, 0 \quad +2, -2 \quad 0, +2 \quad 0, 0 \quad 0, -2 \quad -2, +2 \quad -2, 0 \quad -2, -2.$$

In this case, one obtains a state transition matrix of form

$$\mathbf{T}(D, E, J) := \quad (\text{J.34})$$

$$\begin{bmatrix} \frac{1}{4} D^{\alpha_1} E^2 & \frac{1}{2} D^{\beta_1} E & \frac{1}{4} D^{\gamma_1} E^2 & \frac{1}{2} D^{\delta_1} E & D^{\zeta_1} & \frac{1}{2} D^{\delta_9} E & \frac{1}{4} D^{\gamma_9} E^2 & \frac{1}{2} D^{\beta_9} E & \frac{1}{4} D^{\alpha_9} E^2 \\ \frac{1}{4} D^{\alpha_2} E^2 & \frac{1}{2} D^{\beta_2} E & \frac{1}{4} D^{\gamma_2} E^2 & \frac{1}{2} D^{\delta_2} E & D^{\zeta_2} & \frac{1}{2} D^{\delta_8} E & \frac{1}{4} D^{\gamma_8} E^2 & \frac{1}{2} D^{\beta_8} E & \frac{1}{4} D^{\alpha_8} E^2 \\ \frac{1}{4} D^{\alpha_3} E^2 & \frac{1}{2} D^{\beta_3} E & \frac{1}{4} D^{\gamma_3} E^2 & \frac{1}{2} D^{\delta_3} E & D^{\zeta_3} & \frac{1}{2} D^{\delta_7} E & \frac{1}{4} D^{\gamma_7} E^2 & \frac{1}{2} D^{\beta_7} E & \frac{1}{4} D^{\alpha_7} E^2 \\ \frac{1}{4} D^{\alpha_4} E^2 & \frac{1}{2} D^{\beta_4} E & \frac{1}{4} D^{\gamma_4} E^2 & \frac{1}{2} D^{\delta_4} E & D^{\zeta_4} & \frac{1}{2} D^{\delta_6} E & \frac{1}{4} D^{\gamma_6} E^2 & \frac{1}{2} D^{\beta_6} E & \frac{1}{4} D^{\alpha_6} E^2 \\ \frac{1}{4} D^{\alpha_5} E^2 & \frac{1}{2} D^{\beta_5} E & \frac{1}{4} D^{\gamma_5} E^2 & \frac{1}{2} D^{\delta_5} E & 1 & \frac{1}{2} D^{\delta_5} E & \frac{1}{4} D^{\gamma_5} E^2 & \frac{1}{2} D^{\beta_5} E & \frac{1}{4} D^{\alpha_5} E^2 \\ \frac{1}{4} D^{\alpha_6} E^2 & \frac{1}{2} D^{\beta_6} E & \frac{1}{4} D^{\gamma_6} E^2 & \frac{1}{2} D^{\delta_6} E & D^{\zeta_4} & \frac{1}{2} D^{\delta_4} E & \frac{1}{4} D^{\gamma_4} E^2 & \frac{1}{2} D^{\beta_4} E & \frac{1}{4} D^{\alpha_4} E^2 \\ \frac{1}{4} D^{\alpha_7} E^2 & \frac{1}{2} D^{\beta_7} E & \frac{1}{4} D^{\gamma_7} E^2 & \frac{1}{2} D^{\delta_7} E & D^{\zeta_3} & \frac{1}{2} D^{\delta_3} E & \frac{1}{4} D^{\gamma_3} E^2 & \frac{1}{2} D^{\beta_3} E & \frac{1}{4} D^{\alpha_3} E^2 \\ \frac{1}{4} D^{\alpha_8} E^2 & \frac{1}{2} D^{\beta_8} E & \frac{1}{4} D^{\gamma_8} E^2 & \frac{1}{2} D^{\delta_8} E & D^{\zeta_2} & \frac{1}{2} D^{\delta_2} E & \frac{1}{4} D^{\gamma_2} E^2 & \frac{1}{2} D^{\beta_2} E & \frac{1}{4} D^{\alpha_2} E^2 \\ \frac{1}{4} D^{\alpha_9} E^2 & \frac{1}{2} D^{\beta_9} E & \frac{1}{4} D^{\gamma_9} E^2 & \frac{1}{2} D^{\delta_9} E & D^{\zeta_1} & \frac{1}{2} D^{\delta_1} E & \frac{1}{4} D^{\gamma_1} E^2 & \frac{1}{2} D^{\beta_1} E & \frac{1}{4} D^{\alpha_1} E^2 \end{bmatrix} \cdot J.$$

A complete list of the exponents  $\alpha_i, \beta_i, \gamma_i, \delta_i$  ( $i = 1, \dots, 9$ ) and  $\zeta_j$  ( $j = 1, \dots, 4$ ) resulting for Alamouti's transmit diversity scheme in the case  $L = 1$  is stated in Table J.1.

Adopting an idea evaluated for (terminated) convolutional codes [WV96], the squared Euclidean distances  $d_E^2(\epsilon)$  and the factors  $p_\epsilon$  required for the union bound (J.26) can theoretically be determined by computing [Lan02b]

$$P(D, E, J) := \lim_{n \rightarrow \infty} \mathbf{t}_i(D, E, J) \cdot [\mathbf{T}(D, E, J)]^{n-2} \cdot \mathbf{t}_t(D, E, J) - J^n \quad (\text{J.35a})$$

$$= \lim_{S \rightarrow \infty} \sum_{\epsilon \in \mathbb{E}_{k_0}} \Lambda_\epsilon(D, E, J), \quad (\text{J.35b})$$

where the vectors  $\mathbf{t}_i(D, E, J)$  and  $\mathbf{t}_t(D, E, J)$  denote the row and the column vector of  $\mathbf{T}(D, E, J)$  corresponding to the starting state  $0, 0$  and the target state  $0, 0$  respectively:

$$\mathbf{t}_i(D, E, J) := \tag{J.36a}$$

$$\left[ \frac{1}{4}D^{\alpha_5}E^2 \quad \frac{1}{2}D^{\beta_5}E \quad \frac{1}{4}D^{\gamma_5}E^2 \quad \frac{1}{2}D^{\delta_5}E \quad 1 \quad \frac{1}{2}D^{\delta_5}E \quad \frac{1}{4}D^{\gamma_5}E^2 \quad \frac{1}{2}D^{\beta_5}E \quad \frac{1}{4}D^{\alpha_5}E^2 \right] \cdot J,$$

$$\mathbf{t}_t(D, E, J) := \left[ D^{\zeta_1} \quad D^{\zeta_2} \quad D^{\zeta_3} \quad D^{\zeta_4} \quad 1 \quad D^{\zeta_4} \quad D^{\zeta_3} \quad D^{\zeta_2} \quad D^{\zeta_1} \right]^T \cdot J. \tag{J.36b}$$

The result is a polynomial  $P(D, E, J)$  with symbolic bases  $D, E, J$ , which contains the occurring distances  $d_E^2(\epsilon)$ ,  $d_H(\epsilon)$  as well as the factors  $p_\epsilon$ . The term  $-J^n$  in (J.35a) is required, in order to exclude the all-zeros path  $\epsilon = \mathbf{0}$ .

In practice one typically has to resort to a finite error path length ( $S < \infty$ ), which yields a polynomial of degree  $S$  in  $J$ :

$$P_S(D, E, J) := \mathbf{t}_i(D, E, J) \cdot [\mathbf{T}(D, E, J)]^{S-2} \cdot \mathbf{t}_t(D, E, J). \tag{J.37}$$

(Again, the term  $-J^S$  should be subtracted, so as to exclude the all-zeros path.) The polynomial  $P_S(D, E, J)$  can, for example, be determined by means of symbolic math computer software, such as Maple<sup>®</sup> or the Symbolic Math Toolbox provided by MATLAB<sup>®</sup>. In order to speed up calculations,  $D$  or  $E$  can be set to one if only the Hamming distances  $d_H(\epsilon)$  or the squared Euclidean distances  $d_E^2(\epsilon)$  are required, respectively.

Within this thesis, the above framework is employed in Chapter 5 (Section 5.2.2), so as to analyze the performance of Alamouti's transmit diversity scheme in the case of distributed transmit antennas with imperfect timing synchronization.  $\diamond$

|  |
|--|
| $\alpha_1 = 4 ( h_0 - h_1 + g_0 + g_1 ^2 +  h_0 - h_1 - g_0 - g_1 ^2)$<br>$\alpha_2 = 4 ( h_0 + g_0 + g_1 ^2 +  h_0 - h_1 - g_0 - g_1 ^2)$<br>$\alpha_3 = 4 ( h_0 + h_1 + g_0 + g_1 ^2 +  h_0 - h_1 - g_0 - g_1 ^2)$<br>$\alpha_4 = 4 ( h_0 - h_1 + g_0 ^2 +  h_0 - h_1 - g_0 - g_1 ^2)$<br>$\alpha_5 = 4 ( h_0 + g_0 ^2 +  h_0 - h_1 - g_0 - g_1 ^2)$<br>$\alpha_6 = 4 ( h_0 + h_1 + g_0 ^2 +  h_0 - h_1 - g_0 - g_1 ^2)$<br>$\alpha_7 = 4 ( h_0 - h_1 + g_0 - g_1 ^2 +  h_0 - h_1 - g_0 - g_1 ^2)$<br>$\alpha_8 = 4 ( h_0 + g_0 - g_1 ^2 +  h_0 - h_1 - g_0 - g_1 ^2)$<br>$\alpha_9 = 4 ( h_0 + h_1 + g_0 - g_1 ^2 +  h_0 - h_1 - g_0 - g_1 ^2)$ |
| $\beta_1 = 4 ( h_0 - h_1 + g_1 ^2 +  h_1 + g_0 ^2)$<br>$\beta_2 = 4 ( h_0 + g_1 ^2 +  h_1 + g_0 ^2)$<br>$\beta_3 = 4 ( h_0 + h_1 + g_1 ^2 +  h_1 + g_0 ^2)$<br>$\beta_4 = 4 ( h_0 - h_1 ^2 +  h_1 + g_0 ^2)$<br>$\beta_5 = 4 ( h_0 ^2 +  h_1 + g_0 ^2)$<br>$\beta_6 = 4 ( h_0 + h_1 ^2 +  h_1 + g_0 ^2)$<br>$\beta_7 = 4 ( h_0 - h_1 - g_1 ^2 +  h_1 + g_0 ^2)$<br>$\beta_8 = 4 ( h_0 - g_1 ^2 +  h_1 + g_0 ^2)$<br>$\beta_9 = 4 ( h_0 + h_1 - g_1 ^2 +  h_1 + g_0 ^2)$  |
| $\gamma_1 = 4 ( h_0 - h_1 - g_0 + g_1 ^2 +  h_0 + h_1 + g_0 - g_1 ^2)$<br>$\gamma_2 = 4 ( h_0 - g_0 + g_1 ^2 +  h_0 + h_1 + g_0 - g_1 ^2)$<br>$\gamma_3 = 4 ( h_0 + h_1 - g_0 + g_1 ^2 +  h_0 + h_1 + g_0 - g_1 ^2)$<br>$\gamma_4 = 4 ( h_0 - h_1 - g_0 ^2 +  h_0 + h_1 + g_0 - g_1 ^2)$<br>$\gamma_5 = 4 ( h_0 - g_0 ^2 +  h_0 + h_1 + g_0 - g_1 ^2)$<br>$\gamma_6 = 4 ( h_0 + h_1 - g_0 ^2 +  h_0 + h_1 + g_0 - g_1 ^2)$<br>$\gamma_7 = 4 ( h_0 - h_1 - g_0 - g_1 ^2 +  h_0 + h_1 + g_0 - g_1 ^2)$<br>$\gamma_8 = 4 ( h_0 - g_0 - g_1 ^2 +  h_0 + h_1 + g_0 - g_1 ^2)$<br>$\gamma_9 = 4 ( h_0 + h_1 - g_0 - g_1 ^2 +  h_0 + h_1 + g_0 - g_1 ^2)$ |
| $\delta_1 = 4 ( h_1 - g_0 - g_1 ^2 +  h_0 - g_1 ^2)$<br>$\delta_2 = 4 ( g_0 + g_1 ^2 +  h_0 - g_1 ^2)$<br>$\delta_3 = 4 ( h_1 + g_0 + g_1 ^2 +  h_0 - g_1 ^2)$<br>$\delta_4 = 4 ( h_1 - g_0 ^2 +  h_0 - g_1 ^2)$<br>$\delta_5 = 4 ( g_0 ^2 +  h_0 - g_1 ^2)$<br>$\delta_6 = 4 ( h_1 + g_0 ^2 +  h_0 - g_1 ^2)$<br>$\delta_7 = 4 ( h_1 - g_0 + g_1 ^2 +  h_0 - g_1 ^2)$<br>$\delta_8 = 4 ( g_0 - g_1 ^2 +  h_0 - g_1 ^2)$<br>$\delta_9 = 4 ( h_1 + g_0 - g_1 ^2 +  h_0 - g_1 ^2)$   |
| $\zeta_1 = 4 ( h_1 - g_1 ^2)$<br>$\zeta_2 = 4  g_1 ^2$<br>$\zeta_3 = 4 ( h_1 + g_1 ^2)$<br>$\zeta_4 = 4  h_1 ^2$   |

Table J.1: Exponents  $\alpha_i$ ,  $\beta_i$ ,  $\gamma_i$ ,  $\delta_i$  ( $i=1, \dots, 9$ ) and  $\zeta_j$  ( $j=1, \dots, 4$ ) resulting for Alamouti's transmit diversity scheme in the case  $L=1$ .





# Appendix K

## Own Publications Related to Thesis

### Journal Papers and Letters

- J. Mietzner and P. A. Hoeher, “Improving the performance of mobile broadcasting systems using multiple base stations and distributed space-time codes,” *IEE Proc. Commun.*, accepted for publication, Nov. 2006.
- J. Mietzner, S. Badri-Hoeher, I. Land, and P. A. Hoeher, “Equalization of sparse intersymbol-interference channels revisited,” *EURASIP J. Wireless Commun. and Networking*, vol. 2006, Article ID 29075, 13 pages, 2006.
- J. Ch. Fricke, M. Sandell, J. Mietzner, and P. A. Hoeher, “Impact of the Gaussian approximation on the performance of the probabilistic data association MIMO decoder,” *EURASIP J. Wireless Commun. and Networking*, vol. 2005, no. 5, pp. 796-800, Dec. 2005.
- J. Mietzner and P. A. Hoeher, “Boosting the performance of wireless communication systems – Theory and practice of multiple antenna techniques,” *IEEE Commun. Mag.*, vol. 42, no. 10, pp. 40-47, Oct. 2004.
- J. Mietzner, P. A. Hoeher, and M. Sandell, “Compatible improvement of the GSM/EDGE system by means of space-time coding techniques,” *IEEE Trans. Wireless Commun.*, vol. 2, no. 4, pp. 690-702, Jul. 2003.
- J. Mietzner, M. Kautza, and P. A. Hoeher, “Application of the Alamouti scheme in resilient microwave radio links,” *IEE Electron. Lett.*, vol. 39, no. 12, pp. 927-928, June 2003.

### Conference Papers

- J. Mietzner, P. A. Hoeher, C. Krakowski, and W. Xu, “A statistical transmit power allocation scheme for spatially correlated MIMO systems and its robustness to estimation errors,” in *Proc. World Wireless Congress (WWC)*, San Francisco, California, USA, May 2006.

- J. Mietzner, P. A. Hoeher, C. Krakowski, and W. Xu, “A robust receive diversity scheme for spatially correlated multiple-antenna systems using second-order channel statistics,” in *Proc. 4th Int. Symp. on Turbo Codes & Rel. Topics/ 6th Int. ITG Conf. on Source and Channel Coding (SCC)*, Munich, Germany, Apr. 2006.
- J. Mietzner and P. A. Hoeher, “Equivalence of spatially correlated and distributed MIMO systems,” in *Proc. Int. ITG-IEEE Workshop on Smart Antennas (WSA 2006)*, Castle Reisenburg, Günzburg, Germany, Mar. 2006.
- J. Mietzner, S. Badri-Hoeher, I. Land, and P. A. Hoeher, “Trellis-based equalization for sparse ISI channels revisited,” in *Proc. IEEE Int. Symp. Inform. Theory (ISIT’05)*, Adelaide, Australia, Sept. 2005, pp. 229-233.
- J. Mietzner and P. A. Hoeher, “On the duality of wireless systems with multiple cooperating transmitters and wireless systems with correlated antennas,” in *Proc. 14th IST Mobile & Wireless Commun. Summit*, Dresden, Germany, June 2005, paper no. 245.
- J. Mietzner, S. Badri-Hoeher, and P. A. Hoeher, “Prefiltering and trellis-based equalization for sparse ISI channels,” in *Proc. 14th IST Mobile & Wireless Commun. Summit*, Dresden, Germany, June 2005, paper no. 247.
- J. Ch. Fricke, M. Sandell, J. Mietzner, and P. A. Hoeher, “On the soft outputs provided by the probabilistic data association MIMO decoder,” in *Proc. Winter School on Coding and Information Theory*, Bratislava, Slovakia, Feb. 2005.
- J. Mietzner, R. Thobaben, and P. A. Hoeher, “Analysis of the expected error performance of cooperative wireless networks employing distributed space-time codes,” in *Proc. IEEE Global Telecommun. Conf. (Globecom 2004)*, Dallas, Texas, USA, Nov./Dec., 2004, pp. 2854-2858.
- J. Mietzner and P. A. Hoeher, “Distributed space-time codes for cooperative wireless networks in the presence of different propagation delays and path losses,” in *Proc. 3rd IEEE Sensor Array and Multichannel Signal Processing Workshop (SAM 2004)*, Sitges, Barcelona, Spain, Jul. 2004, paper no. S5\_5.
- J. Mietzner, J. Eick, and P. A. Hoeher, “On distributed space-time coding techniques for cooperative wireless networks and their sensitivity to frequency offsets,” in *Proc. ITG Workshop on Smart Antennas (WSA 2004)*, Munich, Germany, Mar. 2004, paper no. 15.
- J. Mietzner, J. Eick, and P. A. Hoeher, “Frequency-offset sensitivity of resilient microwave links applying the Alamouti scheme,” in *Proc. 5th Int. ITG Conf. on Source and Channel Coding (SCC)*, Erlangen-Nuremberg, Germany, Jan. 2004, pp. 165-172.
- J. Mietzner, P. A. Hoeher, and M. Sandell, “Compatible improvement of the GSM/GPRS system by means of space-time block codes,” in *Proc. IV IEEE Signal Processing Workshop on Signal Processing Adv. Wireless Commun. (SPAWC’03)*, Rome, Italy, June 2003, pp. 412-416.

- J. Mietzner, P. A. Hoeher, and M. Sandell, “Compatible improvement of the GSM/GPRS system by means of delay diversity,” in *Proc. IEEE Int. Conf. Commun. (ICC'03)*, Anchorage, Alaska, USA, May 2003, pp. 1983-1987.
- J. Mietzner and P. A. Hoeher, “Compatible improvement of the GSM/EDGE system by means of space-time coding techniques,” in *Proc. Winter School on Coding and Information Theory*, Monte Verità, Ascona, Switzerland, Feb. 2003, p. 13.





# Bibliography

- [AA06] E. Akay and E. Ayanoglu, "Achieving full frequency and space diversity in wireless systems via BICM, OFDM, STBC, and Viterbi decoding," *IEEE Trans. Commun.*, vol. 54, no. 12, pp. 2164–2172, Dec. 2006.
- [AB03] K. S. Ahn and H. K. Baik, "Decision feedback detection for space-time block coding over time-selective fading channels," in *Proc. IEEE Int. Symp. on Pers., Indoor, and Mobile Radio Commun. (PIMRC)*, Beijing, China, Sept. 2003, pp. 1983–1987.
- [Ada79] F. Adachi, "Transmitter diversity for a digital FM paging system," *IEEE Trans. Veh. Technol.*, vol. VT-28, no. 4, pp. 333–338, Nov. 1979.
- [AEVZ02] E. Agrell, T. Eriksson, A. Vardy, and K. Zeger, "Closest point search in lattices," *IEEE Trans. Inform. Theory*, vol. 48, no. 8, pp. 2201–2214, Aug. 2002.
- [AFLP03] D. Avidor, D. Furman, J. Ling, and C. Papadias, "On the financial impact of capacity-enhancing technologies to wireless operators," *IEEE Wireless Commun.*, vol. 10, no. 4, pp. 62–65, Apr. 2003.
- [AFS+02] N. Al-Dhahir, C. Fragouli, A. Stamoulis, W. Younis, and R. Calderbank, "Space-time processing for broadband wireless access," *IEEE Commun. Mag.*, vol. 40, no. 9, pp. 136–142, Sept. 2002.
- [AG99] M.-S. Alouini and A. J. Goldsmith, "A unified approach for calculating error rates of linearly modulated signals over generalized fading channels," *IEEE Trans. Commun.*, vol. 47, no. 9, pp. 1324–1334, Sept. 1999.
- [AG05] J. Akhtar and D. Gesbert, "Spatial multiplexing over correlated MIMO channels with a closed-form precoder," *IEEE Trans. Wireless Commun.*, vol. 4, no. 5, pp. 2400–2409, Sept. 2005.
- [AH04] A. Alexiou and M. Haardt, "Smart antenna technologies for future wireless systems: Trends and challenges," *IEEE Commun. Mag.*, vol. 42, no. 9, pp. 90–97, Sept. 2004.
- [AHR+03] B. Abdool-Rassool, F. Heliot, L. Revely, R. Nakhai, and H. Aghvami, "4-PSK space-time trellis codes with five and six transmit antennas for slow Rayleigh fading channels," *Electron. Letters*, vol. 39, no. 3, pp. 297–299, Feb. 2003.
- [AK04] P. A. Anghel and M. Kaveh, "Exact symbol error probability of a cooperative network in a Rayleigh-fading environment," *IEEE Trans. Wireless Commun.*, vol. 3, no. 5, pp. 1416–1421, Sept. 2004.

- [AK06] ———, “On the performance of distributed space-time coding systems with one and two non-regenerative relays,” *IEEE Trans. Wireless Commun.*, vol. 5, no. 3, pp. 682–692, Mar. 2006.
- [AKB05] K. S. Ahn, J.-Y. Kim, and H. K. Baik, “Bit error rate performance of decision feedback detection for space-time block coded systems over time-selective fading channels,” in *Proc. IEEE Int. Conf. Acoustics, Speech and Signal Processing (ICASSP)*, Philadelphia, Pennsylvania, USA, Mar. 2005, pp. 869–872.
- [Al-01a] N. Al-Dhahir, “FIR channel-shortening equalizers for MIMO ISI channels,” *IEEE Trans. Commun.*, vol. 49, no. 2, pp. 213–218, Feb. 2001.
- [Al-01b] ———, “Single-carrier frequency-domain equalization for space-time block-coded transmissions over frequency-selective fading channels,” *IEEE Commun. Lett.*, vol. 5, no. 7, pp. 304–306, July 2001.
- [Al-02] ———, “Overview and comparison of equalization schemes for space-time-coded signals with application to EDGE,” *IEEE Trans. Signal Processing*, vol. 50, no. 10, pp. 2477–2488, Oct. 2002.
- [Al-03] ———, “A new high-rate differential space-time block coding scheme,” *IEEE Commun. Lett.*, vol. 7, no. 11, pp. 540–542, Nov. 2003.
- [Ala98] S. M. Alamouti, “A simple transmit diversity technique for wireless communications,” *IEEE J. Select. Areas Commun.*, vol. 16, no. 8, pp. 1451–1458, Oct. 1998.
- [Ale01] A. Alexiou, “Comparison of multiple antenna techniques for UMTS downlink capacity enhancement,” in *Proc. IEEE Veh. Technol. Conf. (VTC-Spring)*, Rhodes, Greece, May 2001, pp. 3–7.
- [Ale04] ———, “Re-configurability to channel state information reliability in space-time block coded systems,” in *Proc. IEEE Int. Conf. on 3G Mobile Commun. Technol. (3G)*, London, UK, Oct. 2004, pp. 158–162.
- [ALK03] P. A. Anghel, G. Leus, and M. Kaveh, “Multi-user space-time coding in cooperative networks,” in *Proc. IEEE Int. Conf. Acoustics, Speech and Signal Processing (ICASSP)*, Hong Kong, China, Apr. 2003, pp. 73–76.
- [AN02] W. C. Ang and C. S. Ng, “Analysis of a transmit diversity scheme in fading channels and imperfect channel estimation,” in *Proc. IEEE Int. Conf. Commun. Systems (ICCS)*, Singapore, Nov. 2002.
- [ANC01] N. Al-Dhahir, A. F. Naguib, and A. R. Calderbank, “Finite-length MIMO decision feedback equalization for space-time block-coded signals over multipath-fading channels,” *IEEE Trans. Veh. Technol.*, vol. 50, no. 4, pp. 1176–1182, July 2001.
- [ANH+04] B. Abdool-Rassool, M. R. Nakhai, F. Heliot, L. Revelly, and H. Aghvami, “Search for space-time trellis codes: Novel codes for Rayleigh fading channels,” *IEE Proc. Commun.*, vol. 151, no. 1, pp. 25–31, Feb. 2004.
- [App76] S. P. Applebaum, “Adaptive arrays,” *IEEE Trans. Antennas Propagat.*, vol. 24, no. 5, pp. 585–598, Sept. 1976.

- [AQ04] A. Alexiou and M. Qaddi, "Re-configurable linear precoders to compensate for antenna correlation in orthogonal and quasi-orthogonal space-time block coded systems," in *Proc. IEEE Veh. Technol. Conf. (VTC-Spring)*, Genoa, Italy, May 2004, pp. 665–669.
- [AR06] A. R. Ahmadi and R. K. Rao, "Space-time trellis code design with binary CPM," *Electron. Letters*, vol. 42, no. 3, pp. 168–170, Feb. 2006.
- [AS00] N. Al-Dhahir and A. H. Sayed, "The finite-length multi-input multi-output MMSE-DFE," *IEEE Trans. Signal Processing*, vol. 48, no. 10, pp. 2921–2936, Oct. 2000.
- [AS02] M.-S. Alouini and M. K. Simon, "Dual diversity over correlated log-normal fading channels," *IEEE Trans. Commun.*, vol. 50, no. 12, pp. 1946–1959, Dec. 2002.
- [ASB+05] B. Allen, F. Said, G. Bauch, G. Auer, and A. H. Aghvami, "Spectrally efficient transmit diversity scheme for differentially modulated multicarrier transmissions," *IEE Proc. Commun.*, vol. 152, no. 4, pp. 457–462, Aug. 2005.
- [ASC97] N. Al-Dhahir, A. H. Sayed, and J. M. Cioffi, "Stable pole-zero modeling of long FIR filters with application to the MMSE-DFE," *IEEE Trans. Commun.*, vol. 45, no. 5, pp. 508–513, May 1997.
- [ATNS98] D. Agrawal, V. Tarokh, A. Naguib, and N. Seshadri, "Space-time coded OFDM for high data-rate wireless communication over wideband channels," in *Proc. IEEE Veh. Technol. Conf. (VTC)*, Ottawa, Ontario, Canada, May 1998, pp. 2232–2236.
- [ATP98] S. M. Alamouti, V. Tarokh, and P. Poon, "Trellis-coded modulation and transmit diversity: Design criteria and performance evaluation," in *Proc. IEEE Int. Conf. Univ. Pers. Commun. (ICUPC)*, Florence, Italy, Oct. 1998, pp. 703–707.
- [AWS03] S. Alkhaldeh, X. Wang, and Y. Shayan, "A new diversity scheme for frequency selective MIMO channels," in *Proc. IEEE Int. Symp. on Pers., Indoor, and Mobile Radio Commun. (PIMRC)*, Beijing, China, Sept. 2003, pp. 1410–1414.
- [BA02] G. Bauch and N. Al-Dhahir, "Reduced-complexity space-time turbo-equalization for frequency-selective MIMO channels," *IEEE Trans. Wireless Commun.*, vol. 1, no. 4, pp. 819–828, Oct. 2002.
- [BA05a] D. Bokolamulla and T. M. Aulin, "Optimum symbol-by-symbol detection of space-time coded continuous phase modulated signals," in *Proc. IEEE Int. Conf. Commun. (ICC)*, Seoul, Korea, May 2005, pp. 805–809.
- [BA05b] —, "Performance of space-time coded continuous phase modulated signals over different fading environments," in *Proc. IEEE Int. Symp. Inform. Theory (ISIT)*, Adelaide, Australia, Sept. 2005, pp. 1048–1052.
- [Bad01] S. Badri-Hoehner, "Digitale Empfänger Algorithmen für TDMA-Mobilfunksysteme mit besonderer Berücksichtigung des EDGE-Systems," Ph.D. dissertation, University of Erlangen-Nuremberg, Germany, 2001.
- [Bal97] C. A. Balanis, *Antenna Theory: Analysis and Design*, 2nd ed. New York: John Wiley & Sons, 1997.



- [Bau00] G. Bauch, "Turbo-Entzerrung und Sendeantennen-Diversity mit Space-Time-Codes im Mobilfunk," Ph.D. dissertation, Munich University of Technology, Germany, 2000.
- [Bau03] —, "Space-time block codes versus space-frequency block codes," in *Proc. IEEE Veh. Technol. Conf. (VTC-Spring)*, Jeju, Korea, Apr. 2003, pp. 567–571.
- [Bau04] —, "Differential amplitude and unitary space-time modulation," in *Proc. Int. ITG Conf. on Source and Channel Coding (SCC)*, Erlangen-Nuremberg, Germany, Jan. 2004, pp. 135–142.
- [Bau06] —, "Differential modulation and cyclic delay diversity in orthogonal frequency-division multiplex," *IEEE Trans. Commun.*, vol. 54, no. 5, pp. 798–801, May 2006.
- [BB99] S. Benedetto and E. Biglieri, *Principles of Digital Transmission*. Boston: Kluwer Academic / Plenum Publishers, 1999.
- [BB05] M. Borgmann and H. Boelcskei, "Noncoherent space-frequency coded MIMO-OFDM," *IEEE J. Select. Areas Commun.*, vol. 23, no. 9, pp. 1799–1810, Sept. 2005.
- [BBH00] S. Baero, G. Bauch, and A. Hansmann, "Improved codes for space-time trellis-coded modulation," *IEEE Commun. Lett.*, vol. 4, no. 1, pp. 20–22, Jan. 2000.
- [BBP03] H. Boelcskei, M. Borgmann, and A. J. Paulraj, "Impact of the propagation environment on the performance of space-frequency coded MIMO-OFDM," *IEEE J. Select. Areas Commun.*, vol. 21, no. 3, pp. 427–439, Apr. 2003.
- [BBPS00] S. Baero, G. Bauch, A. Pavlic, and A. Semmler, "Improving BLAST performance using space-time block codes and turbo decoding," in *Proc. IEEE Global Telecommun. Conf. (Globecom)*, San Francisco, California, USA, Nov./Dec. 2000, pp. 1067–1071.
- [BCBR01] O. Berder, L. Collin, G. Burel, and P. Rostaing, "Digital transmission combining BLAST and OFDM concepts: Experimentation on the UHF COST 207 channel," in *Proc. IEEE Global Telecommun. Conf. (Globecom)*, San Antonio, Texas, USA, Nov. 2001, pp. 141–145.
- [BCJR74] L. Bahl, J. Cocke, F. Jelinek, and J. Raviv, "Optimal decoding of linear codes for minimizing symbol error rate," *IEEE Trans. Inform. Theory*, vol. 20, no. 2, pp. 284–287, Mar. 1974.
- [BdE01] A. Bhargave, R. J. P. de Figueiredo, and T. Eltoft, "A detection algorithm for the V-BLAST system," in *Proc. IEEE Global Telecommun. Conf. (Globecom)*, San Antonio, Texas, USA, Nov. 2001, pp. 494–498.
- [BE04] M.-H. Bourles-Hamon and H. El Gamal, "On the design of adaptive space-time codes," *IEEE Trans. Commun.*, vol. 52, no. 10, pp. 1670–1674, Oct. 2004.
- [Bel63] P. Bello, "Characterization of randomly time-variant linear channels," *IEEE Trans. Commun.*, vol. 11, no. 4, pp. 360–393, Dec. 1963.

- [BFY04] J. Boyer, D. D. Falconer, and H. Yanikomeroglu, "Multihop diversity in wireless relaying channels," *IEEE Trans. Commun.*, vol. 52, no. 10, pp. 1820–1830, Oct. 2004.
- [BGP02] H. Boelcskei, D. Gesbert, and A. J. Paulraj, "On the capacity of OFDM-based spatial multiplexing systems," *IEEE Trans. Commun.*, vol. 50, no. 2, pp. 225–234, Feb. 2002.
- [BGT93] C. Berrou, A. Glavieux, and P. Thitimajshima, "Near Shannon limit error-correcting coding and decoding: Turbo-codes," in *Proc. IEEE Int. Conf. Commun. (ICC)*, Geneva, Switzerland, May 1993, pp. 1064–1070.
- [BH00] S. Badri-Hoehner and P. Hoehner, "Use of the list Viterbi algorithm to compute the distance spectrum of trellis codes and ISI channels," in *Proc. IEEE Int. Symp. Inform. Theory (ISIT)*, Sorrento, Italy, June 2000, p. 101.
- [BH04] S. Badri-Hoehner and P. A. Hoehner, "Fast computation of a discrete-time whitened matched filter based on Kalman filtering," *IEEE Trans. Wireless Commun.*, vol. 3, no. 6, pp. 2417–2424, Nov. 2004.
- [BHC03] J. Benesty, Y. Huang, and J. Chen, "A fast recursive algorithm for optimum sequential signal detection in a BLAST system," *IEEE Trans. Signal Processing*, vol. 51, no. 7, pp. 1722–1730, July 2003.
- [BHKX05] S. Badri-Hoehner, P. A. Hoehner, C. Krakowski, and W. Xu, "Impulse response shortening for multiple co-channels," in *Proc. IEEE Int. Conf. Commun. (ICC)*, Seoul, Korea, May 2005, pp. 1896–1900.
- [BHP04] C. Bettstetter, H. Hartenstein, and X. Perez-Costa, "Stochastic properties of the random waypoint mobility model," *ACM/Kluwer Wireless Networks*, vol. 10, no. 5, pp. 555–567, Sept. 2004.
- [BHS01] G. Bauch, J. Hagenauer, and N. Seshadri, "Turbo processing in transmit antenna diversity systems," *Ann. Telecommun.*, vol. 56, no. 7-8, pp. 455–471, Aug. 2001.
- [BI03] A. Boariu and D. M. Ionescu, "A class of nonorthogonal rate-one space-time block codes with controlled interference," *IEEE Trans. Wireless Commun.*, vol. 2, no. 2, pp. 270–276, Mar. 2003.
- [BKRL06] A. Bletsas, A. Khisti, D. P. Reed, and A. Lippman, "A simple cooperative diversity method based on network path selection," *IEEE J. Select. Areas Commun.*, vol. 24, no. 3, pp. 659–672, Mar. 2006.
- [BLM01] N. Boubaker, K. B. Letaief, and R. D. Murch, "A layered space-time coded wideband OFDM architecture for dispersive wireless links," in *Proc. IEEE Symp. on Comput. and Commun. (ISCC)*, Hammamet, Tunisia, July 2001, pp. 518–523.
- [BLM02] —, "Performance of BLAST over frequency-selective wireless communication channels," *IEEE Trans. Commun.*, vol. 50, no. 2, pp. 196–199, Feb. 2002.
- [BLS06] S. Buzzi, M. Lops, and S. Sardellitti, "Widely linear reception strategies for layered space-time wireless communications," *IEEE Trans. Signal Processing*, vol. 54, no. 6, pp. 2252–2262, June 2006.

- [Blu02] R. S. Blum, "Some analytical tools for the design of space-time convolutional codes," *IEEE Trans. Commun.*, vol. 50, no. 10, pp. 1593–1599, Oct. 2002.
- [Blu03] ———, "MIMO with limited feedback of channel state information," in *Proc. IEEE Int. Conf. Acoustics, Speech and Signal Processing (ICASSP)*, Hong Kong, China, Apr. 2003, pp. 89–92.
- [BLWY01] R. S. Blum, Y. Li, J. H. Winters, and Q. Yan, "Improved space-time coding for MIMO-OFDM wireless communications," *IEEE Trans. Commun.*, vol. 49, no. 11, pp. 1873–1878, Nov. 2001.
- [BM96] N. Benvenuto and R. Marchesani, "The Viterbi algorithm for sparse channels," *IEEE Trans. Commun.*, vol. 44, no. 3, pp. 287–289, Mar. 1996.
- [BMY01a] A. Benjebbour, H. Murata, and S. Yoshida, "Comparison of ordered successive receivers for space-time transmission," in *Proc. IEEE Veh. Technol. Conf. (VTC-Fall)*, Atlantic City, New Jersey, USA, Oct. 2001, pp. 2053–2057.
- [BMY01b] ———, "Performance of iterative successive detection algorithm with space-time transmission," in *Proc. IEEE Veh. Technol. Conf. (VTC-Spring)*, Rhodes, Greece, May 2001, pp. 1287–1291.
- [BN99] G. Bauch and A. F. Naguib, "MAP equalization of space-time coded signals over frequency selective channels," in *Proc. IEEE Wireless Commun. and Networking Conf. (WCNC)*, New Orleans, Louisiana, USA, Sept. 1999, pp. 261–265.
- [Boe03] R. Boehnke, personal communication, University of Bremen, Germany, Sept. 2003.
- [Boe05] ———, personal communication, Digital Communications Workshop "Kommunikation im Kleinwalsertal (KiK)", Hirschegg, Austria, July 2005.
- [Bos99] M. Bossert, *Channel Coding for Telecommunications*. New York: John Wiley & Sons, 1999.
- [BP00a] H. Boelcskei and A. J. Paulraj, "Performance of space-time codes in the presence of spatial fading correlation," in *Proc. Asilomar Conf. on Signals, Systems and Comput.*, Pacific Grove, California, USA, Oct./Nov. 2000, pp. 687–693.
- [BP00b] ———, "Space-frequency coded broadband OFDM systems," in *Proc. IEEE Wireless Commun. and Networking Conf. (WCNC)*, Chicago, Illinois, USA, Sept. 2000, pp. 1–6.
- [Bre59] D. G. Brennan, "Linear diversity combining techniques," *Proc. IRE*, vol. 47, pp. 1075–1102, June 1959. Reprint: *Proc. IEEE*, vol. 91, no. 2, pp. 331–356, Feb. 2003.
- [BRV05] J.-C. Belfiore, G. Rekaya, and E. Viterbo, "The Golden code: A  $2 \times 2$  full-rate space-time code with nonvanishing determinants," *IEEE Trans. Inform. Theory*, vol. 51, no. 4, pp. 1432–1436, Apr. 2005.
- [BRW04] B. Badic, M. Rupp, and H. Weinrichter, "Extended Alamouti codes in correlated channels using partial feedback," in *Proc. IEEE Int. Conf. Commun. (ICC)*, Paris, France, June 2004, pp. 896–900.

- [BS91] I. N. Bronstein and K. A. Semendjajew, *Taschenbuch der Mathematik*, 25th ed. Stuttgart - Leipzig / Moscow: B. G. Teubner/Nauka, 1991.
- [BS92] P. Balaban and J. Salz, "Optimum diversity combining and equalization in digital data transmission with applications to cellular mobile radio – Part I: Theoretical considerations; Part II: Numerical results," *IEEE Trans. Commun.*, vol. 40, no. 5, pp. 885–894, 895–907, May 1992.
- [BS03a] S. Barbarossa and G. Scutari, "Cooperative diversity through virtual arrays in multihop networks," in *Proc. IEEE Int. Conf. Acoustics, Speech and Signal Processing (ICASSP)*, Hong Kong, China, Apr. 2003, pp. 209–212.
- [BS03b] O. Besson and P. Stoica, "On parameter estimation of MIMO flat-fading channels with frequency offsets," *IEEE Trans. Signal Processing*, vol. 51, no. 3, pp. 602–613, Mar. 2003.
- [BT04a] E. Biglieri and G. Taricco, *Transmission and Reception with Multiple Antennas: Theoretical Foundations*. Hanover (MA) - Delft: now Publishers Inc., 2004.
- [BT04b] G. J. Byers and F. Takawira, "Spatially and temporally correlated MIMO channels: Modeling and capacity analysis," *IEEE Trans. Veh. Technol.*, vol. 53, no. 3, pp. 634–643, May 2004.
- [BTT02] E. Biglieri, G. Taricco, and A. Tulino, "Performance of space-time codes for a large number of antennas," *IEEE Trans. Inform. Theory*, vol. 48, no. 7, pp. 1794–1803, July 2002.
- [BV04] S. Boyd and L. Vandenberghe, *Convex Optimization*. Cambridge University Press, 2004.
- [BW74] L. H. Brandenburg and A. D. Wyner, "Capacity of the Gaussian channel with memory: The multivariate case," *Bell Syst. Tech. J.*, vol. 53, no. 5, pp. 745–778, May/June 1974.
- [Cap69] J. Capon, "High-resolution frequency-wavenumber spectrum analysis," *Proc. IEEE*, vol. 57, no. 8, pp. 1408–1418, Aug. 1969.
- [Cav99] J. K. Cavers, "Optimized use of diversity modes in transmitter diversity systems," in *Proc. IEEE Veh. Technol. Conf. (VTC)*, Houston, Texas, USA, May 1999, pp. 1768–1773.
- [Cav05] —, "Space-time coding using MSK," *IEEE Trans. Wireless Commun.*, vol. 4, no. 1, pp. 185–191, Jan. 2005.
- [CB00] M. Coupechoux and V. Braun, "Space-time coding for the EDGE mobile radio system," in *Proc. IEEE Int. Conf. Pers. Wireless Commun. (ICPWC)*, Hyderabad, India, Dec. 2000, pp. 28–32.
- [CBRB04] L. Collin, O. Berder, P. Rostaing, and G. Burel, "Optimal minimum distance-based precoder for MIMO spatial multiplexing systems," *IEEE Trans. Signal Processing*, vol. 52, no. 3, pp. 617–627, Mar. 2004.

- [CC99] W.-J. Choi and J. M. Cioffi, "Multiple input/ multiple output (MIMO) equalization for space-time block coding," in *Proc. IEEE Pacific Rim Conf. on Commun., Comput., and Signal Processing (PACRIM)*, Victoria, British Columbia, Canada, Aug. 1999, pp. 341–344.
- [CC03] J. Choi and S. Choi, "Diversity gain for CDMA systems equipped with antenna arrays," *IEEE Trans. Veh. Technol.*, vol. 52, no. 3, pp. 720–724, May 2003.
- [CCC00] W.-J. Choi, K.-W. Cheong, and J. M. Cioffi, "Iterative soft interference cancellation for multiple antenna systems," in *Proc. IEEE Wireless Commun. and Networking Conf. (WCNC)*, Chicago, Illinois, USA, Sept. 2000, pp. 304–309.
- [CEGH02] S. Catreux, V. Erceg, D. Gesbert, and R. W. Heath, Jr., "Adaptive modulation and MIMO coding for broadband wireless data networks," *IEEE Commun. Mag.*, vol. 40, no. 6, pp. 108–115, June 2002.
- [CFK+00] T. A. Chen, M. P. Fitz, W.-Y. Kuo, M. D. Zoltowski, and J. H. Grimm, "A space-time model for frequency nonselective Rayleigh fading channels with applications to space-time modems," *IEEE J. Select. Areas Commun.*, vol. 18, no. 7, pp. 1175–1190, July 2000.
- [CG05] G. Colavolpe and G. Geremi, "On the application of factor graphs and the sum-product algorithm to ISI channels," *IEEE Trans. Commun.*, vol. 53, no. 5, pp. 818–825, May 2005.
- [CG06] X. Cai and G. B. Giannakis, "Differential space-time modulation with eigenbeamforming for correlated MIMO fading channels," *IEEE Trans. Signal Processing*, vol. 54, no. 4, pp. 1279–1288, Apr. 2006.
- [CGB04] S. Cui, A. J. Goldsmith, and A. Bahai, "Energy-efficiency of MIMO and cooperative MIMO techniques in sensor networks," *IEEE J. Select. Areas Commun.*, vol. 22, no. 6, pp. 1089–1098, Aug. 2004.
- [CGZ05] X. Cai, G. B. Giannakis, and M. D. Zoltowski, "Space-time spreading and block coding for correlated fading channels in the presence of interference," *IEEE Trans. Commun.*, vol. 53, no. 3, pp. 515–525, Mar. 2005.
- [CH99] C. Cozzo and B. L. Hughes, "Space diversity in the presence of discrete multipath," in *Proc. IEEE Veh. Technol. Conf. (VTC)*, Houston, Texas, USA, May 1999, pp. 1286–1290.
- [CH04] X.-M. Chen and P. A. Hoehner, "Receiver concepts for differential space-time modulation schemes over flat time-varying channels," in *Proc. Nordic Signal Processing Symp. (NORSIG)*, Meripuisto, Finland, June 2004, pp. 169–172.
- [CH05] J. Choi and R. W. Heath, Jr., "Interpolation based transmit beamforming for MIMO-OFDM with limited feedback," *IEEE Trans. Signal Processing*, vol. 53, no. 11, pp. 4125–4135, Nov. 2005.
- [Che05] X.-M. Chen, "Trellis-based joint data/channel estimation for differentially encoded SISO and MIMO systems," Ph.D. dissertation, University of Kiel, Germany, 2005.

- [Chi03] N. Chiurtu, "Multiple antenna systems for mobile communications," Ph.D. dissertation, Swiss Federal Institute of Technology Lausanne (EPFL), Switzerland, 2003.
- [Cho04a] J. Choi, "A bi-directional zero-forcing BLAST receiver," *IEEE Trans. Signal Processing*, vol. 52, no. 9, pp. 2670–2673, Sept. 2004.
- [Cho04b] —, "Equalization and semi-blind channel estimation for space-time block-coded signals over a frequency-selective fading channel," *IEEE Trans. Signal Processing*, vol. 52, no. 3, pp. 774–785, Mar. 2004.
- [Chr00] M. Chryssomallis, "Smart antennas," *IEEE Antennas Propagat. Mag.*, vol. 42, no. 3, pp. 129–136, June 2000.
- [CKLL05] J. Cha, J. Kang, H. Lee, and H. Lee, "Reduced complexity sequential sequence detection using modified Fano algorithm for V-BLAST systems," in *Proc. IEEE Veh. Technol. Conf. (VTC-Fall)*, Dallas, Texas, USA, Sept. 2005, pp. 11–15.
- [CL05] C.-C. Cheng and C.-C. Lu, "Space-time code design for CPFSK modulation over frequency-nonselctive fading channels," *IEEE Trans. Commun.*, vol. 53, no. 9, pp. 1477–1489, Sept. 2005.
- [CLP05] M.-Y. Chen, H.-C. Li, and S.-C. Pei, "Algebraic identification for optimal nonorthogonality  $4 \times 4$  complex space-time block codes using tensor product on quaternions," *IEEE Trans. Inform. Theory*, vol. 51, no. 1, pp. 324–330, Jan. 2005.
- [CLW+03] D. Chizhik, J. Ling, P. W. Wolniansky, R. A. Valenzuela, N. Costa, and K. Huber, "Multiple-input-multiple-output measurements and modeling in Manhattan," *IEEE J. Select. Areas Commun.*, vol. 21, no. 3, pp. 321–331, Apr. 2003.
- [CM98] G. Caire and U. Mitra, "Training sequence design for adaptive equalization of multi-user systems," in *Proc. Asilomar Conf. on Signals, Systems and Comput.*, Pacific Grove, California, USA, Nov. 1998, pp. 1479–1483.
- [CM99] R. Cusani and J. Mattila, "Equalization of digital radio channels with large multipath delay for cellular land mobile applications," *IEEE Trans. Commun.*, vol. 47, no. 3, pp. 348–351, Mar. 1999.
- [CM04] L.-U. Choi and R. D. Murch, "A pre-BLAST-DFE technique for the downlink of frequency-selective fading MIMO channels," *IEEE Trans. Commun.*, vol. 52, no. 5, pp. 737–743, May 2004.
- [Com88] R. T. Compton, *Adaptive Antennas: Concepts and Performance*. Englewood Cliffs (NJ): Prentice-Hall, 1988.
- [CPD06] H. A. Cirpan, E. Panayirci, and H. Dogan, "Nondata-aided channel estimation for OFDM systems with space-frequency transmit diversity," *IEEE Trans. Veh. Technol.*, vol. 55, no. 2, pp. 449–457, Mar. 2006.
- [CR00] S. F. Cotter and B. D. Rao, "The adaptive matching pursuit algorithm for estimation and equalization of sparse time-varying channels," in *Proc. Asilomar Conf. on Signals, Systems and Comput.*, Pacific Grove, California, USA, Oct./Nov. 2000, pp. 1772–1776.



- [Cra91] J. W. Craig, "A new, simple, and exact result for calculating the probability of error for two-dimensional signal constellations," in *Proc. IEEE Military Commun. Conf. (MILCOM)*, McLean, Virginia, USA, Nov. 1991, pp. 571–575.
- [CS06] S. K. Cheung and R. Schober, "Differential spatial multiplexing," *IEEE Trans. Wireless Commun.*, vol. 5, no. 8, pp. 2127–2135, Aug. 2006.
- [CT91] T. M. Cover and J. A. Thomas, *Elements of Information Theory*. New York: John Wiley & Sons, 1991.
- [CTKV02] C.-N. Chuah, D. N. C. Tse, J. M. Kahn, and R. A. Valenzuela, "Capacity scaling in MIMO wireless systems under correlated fading," *IEEE Trans. Inform. Theory*, vol. 48, no. 3, pp. 637–650, Mar. 2002.
- [CV03] E. Chiavaccini and G. M. Vitetta, "Further results on differential space-time modulations," *IEEE Trans. Commun.*, vol. 51, no. 7, pp. 1093–1101, July 2003.
- [CVOV03] B. Clerckx, D. Vanhoenacker-Janvier, C. Oestges, and L. Vandendorpe, "Mutual coupling effects on the channel capacity and the space-time processing of MIMO communication systems," in *Proc. IEEE Int. Conf. Commun. (ICC)*, Anchorage, Alaska, USA, May 2003, pp. 2638–2642.
- [CVYL02] Z. Chen, B. S. Vucetic, J. Yuan, and K. Leong Lo, "Space-time trellis codes for 4-PSK with three and four transmit antennas in quasi-static flat fading channels," *IEEE Commun. Lett.*, vol. 6, no. 2, pp. 67–69, Feb. 2002.
- [CWZ03] M. Chiani, M. Z. Win, and A. Zanella, "The distribution of eigenvalues of a Wishart matrix with correlation and application to MIMO capacity," in *Proc. IEEE Global Telecommun. Conf. (Globecom)*, San Francisco, California, USA, Dec. 2003, pp. 1802–1805.
- [CYV01] Z. Chen, J. Yuan, and B. Vucetic, "Improved space-time trellis coded modulation scheme on slow Rayleigh fading channels," *Electron. Letters*, vol. 37, no. 7, pp. 440–441, Mar. 2001.
- [CZA06] X. Chen, K. Zhou, and J. L. Aravena, "A new family of unitary space-time codes with a fast parallel sphere decoder algorithm," *IEEE Trans. Inform. Theory*, vol. 52, no. 1, pp. 115–140, Jan. 2006.
- [DAB02] M. O. Damen, K. Abed-Meraim, and J.-C. Belfiore, "Diagonal algebraic space-time block codes," *IEEE Trans. Inform. Theory*, vol. 48, no. 3, pp. 628–636, Mar. 2002.
- [DASC02] S. N. Diggavi, N. Al-Dhahir, A. Stamoulis, and A. R. Calderbank, "Differential space-time coding for frequency-selective channels," *IEEE Commun. Lett.*, vol. 6, no. 6, pp. 253–255, June 2002.
- [DASC04] —, "Great expectations: The value of spatial diversity in wireless networks," *Proc. IEEE*, vol. 92, no. 2, pp. 219–270, Feb. 2004.
- [DB02] X. Dong and N. C. Beaulieu, "Optimal maximal ratio combining with correlated diversity branches," *IEEE Commun. Lett.*, vol. 6, no. 1, pp. 22–24, Jan. 2002.



- [DB03] M. O. Damen and N. C. Beaulieu, "On diagonal algebraic space-time block codes," *IEEE Trans. Commun.*, vol. 51, no. 6, pp. 911–919, June 2003.
- [DB06] Z. Du and N. C. Beaulieu, "Decision-feedback detection for block differential space-time modulation," *IEEE Trans. Commun.*, vol. 54, no. 5, pp. 900–910, May 2006.
- [DC04] Y. Du and K. T. Chan, "Enhanced space-time block coded systems by concatenating turbo product codes," *IEEE Commun. Lett.*, vol. 8, no. 6, pp. 388–390, June 2004.
- [DCB00] O. Damen, A. Chkeif, and J.-C. Belfiore, "Lattice code decoder for space-time codes," *IEEE Commun. Lett.*, vol. 4, no. 5, pp. 161–163, May 2000.
- [DG05] L. A. Dalton and C. N. Georghiadis, "A full-rate, full-diversity four-antenna quasi-orthogonal space-time block code," *IEEE Trans. Wireless Commun.*, vol. 4, no. 2, pp. 363–366, Mar. 2005.
- [DGI+02] R. T. Derryberry, S. D. Gray, D. M. Ionescu, G. Mandyam, and B. Raghothaman, "Transmit diversity in 3G CDMA systems," *IEEE Commun. Mag.*, vol. 40, no. 4, pp. 68–75, Apr. 2002.
- [DH89] A. Duel-Hallen and C. Heegard, "Delayed decision-feedback sequence estimation," *IEEE Trans. Commun.*, vol. 37, no. 5, pp. 428–436, May 1989.
- [DH05] X. Deng and A. M. Haimovich, "Power allocation for cooperative relaying in wireless networks," *IEEE Commun. Lett.*, vol. 9, no. 11, pp. 994–996, Nov. 2005.
- [DHDA04] M. Dohler, M. Hussain, A. Desai, and H. Aghvami, "Performance of distributed space-time block codes," in *Proc. IEEE Veh. Technol. Conf. (VTC-Spring)*, Genoa, Italy, May 2004, pp. 742–746.
- [DIU06] F. A. Dietrich, T. Ivanov, and W. Utschick, "Estimation of channel and noise correlations for MIMO channel estimation," in *Proc. Int. ITG-IEEE Workshop on Smart Antennas (WSA)*, Castle Reizensburg, Günzburg, Germany, Mar. 2006.
- [DJB+95] C. Douillard, M. Jezequel, C. Berrou, A. Picart, P. Didier, and A. Glavieux, "Iterative correction of intersymbol interference: Turbo-equalization," *Europ. Trans. Telecommun.*, vol. 6, no. 5, pp. 507–511, Sept./Oct. 1995.
- [DJM98] D. Divsalar, H. Jin, and R. J. McEliece, "Coding theorems for 'turbo-like' codes," in *Proc. Allerton Conf. on Commun., Control, and Comput.*, Monticello, Illinois, USA, Sept. 1998, pp. 201–210.
- [DKZ+03] P. M. Djuric, J. H. Kotecha, J. Zhang, Y. Huang, T. Ghirmai, M. F. Bugallo, and J. Miguez, "Particle filtering," *IEEE Signal Processing Mag.*, vol. 20, no. 5, pp. 19–38, Sept. 2003.
- [DLWZ06] P. Ding, D. J. Love, J. Wang, and M. D. Zoltowski, "Low complexity adaptive design for full-diversity full-rate space-time codes," *IEEE Trans. Signal Processing*, vol. 54, no. 8, pp. 3180–3189, Aug. 2006.
- [Doh03] M. Dohler, "Virtual antenna arrays," Ph.D. dissertation, King's College London, University of London, UK, 2003.

- [DR05] P. Dharmawansa and N. Rajatheva, "Pairwise error probability of space-time codes in frequency selective Rician channels," *IEEE Commun. Lett.*, vol. 9, no. 10, pp. 894–896, Oct. 2005.
- [DS97] V. M. DaSilva and E. S. Sousa, "Fading-resistant modulation using several transmitter antennas," *IEEE Trans. Commun.*, vol. 45, no. 10, pp. 1236–1244, Oct. 1997.
- [DSL04] Z. Diao, D. Shen, and V. O. K. Li, "Performance analysis of space-time codes with channel information errors," in *Proc. IEEE Veh. Technol. Conf. (VTC-Fall)*, Los Angeles, California, USA, Sept. 2004, pp. 2399–2403.
- [DT05] D. N. Dao and C. Tellambura, "Intercarrier interference self-cancellation space-frequency codes for MIMO-OFDM," *IEEE Trans. Veh. Technol.*, vol. 54, no. 5, pp. 1729–1738, Sept. 2005.
- [DTB02] M. O. Damen, A. Tewfik, and J.-C. Belfiore, "A construction of a space-time code based on number theory," *IEEE Trans. Inform. Theory*, vol. 48, no. 3, pp. 753–760, Mar. 2002.
- [DTN+03] A. Doufexi, E. Tameh, A. Nix, S. Armour, and A. Molina, "Hotspot wireless LANs to enhance the performance of 3G and beyond cellular networks," *IEEE Commun. Mag.*, vol. 41, no. 7, pp. 58–65, July 2003.
- [DU05] F. A. Dietrich and W. Utschick, "Impact of imperfect channel knowledge on transmit processing concepts," in *Proc. IEEE Int. Conf. Commun. (ICC)*, Seoul, Korea, May 2005, pp. 1916–1921.
- [DV05a] P. Dayal and M. K. Varanasi, "Maximal diversity algebraic space-time codes with low peak-to-mean power ratio," *IEEE Trans. Inform. Theory*, vol. 51, no. 5, pp. 1691–1708, May 2005.
- [DV05b] ———, "An optimal two transmit antenna space-time code and its stacked extensions," *IEEE Trans. Inform. Theory*, vol. 51, no. 12, pp. 4348–4355, Dec. 2005.
- [DW05] Z. Ding and D. B. Ward, "Direct semi-blind MMSE equalization for STBC," *IEEE Signal Processing Lett.*, vol. 12, no. 5, pp. 380–383, May 2005.
- [DWC06] Z. Ding, D. B. Ward, and W. H. Chin, "A general scheme for equalization of space-time block-coded systems with unknown CSI," *IEEE Trans. Signal Processing*, vol. 54, no. 7, pp. 2737–2746, July 2006.
- [DWLR01] C. M. Degen, C. M. Walke, A. Lecomte, and B. Rembold, "Adaptive MIMO techniques for the UTRA-TDD mode," in *Proc. IEEE Veh. Technol. Conf. (VTC-Spring)*, Rhodes, Greece, May 2001, pp. 108–112.
- [E03] "Universal mobile telecommunications systems (UMTS); Physical layer – general description," ETSI/3GPP, Technical Specifications 3GPP TS 25.201 version 6.0.0 Release 6, Dec. 2003.
- [ECD04] H. El Gamal, G. Caire, and M. O. Damen, "Lattice coding and decoding achieve the optimal diversity-multiplexing tradeoff of MIMO channels," *IEEE Trans. Inform. Theory*, vol. 50, no. 6, pp. 968–985, June 2004.

- [ECS+98] R. B. Ertel, P. Cardieri, K. W. Sowerby, T. S. Rappaport, and J. H. Reed, "Overview of spatial channel models for antenna array communication systems," *IEEE Pers. Commun.*, vol. 5, no. 1, pp. 10–22, Feb. 1998.
- [ED03] H. El Gamal and M. O. Damen, "Universal space-time coding," *IEEE Trans. Inform. Theory*, vol. 49, no. 5, pp. 1097–1119, May 2003.
- [ED06] C. Esli and H. Delic, "Antijamming performance of space-frequency coding in partial-band noise," *IEEE Trans. Veh. Technol.*, vol. 55, no. 2, pp. 466–476, Mar. 2006.
- [EH01] H. El Gamal and A. R. Hammons, Jr., "A new approach to layered space-time coding and signal processing," *IEEE Trans. Inform. Theory*, vol. 47, no. 6, pp. 2321–2334, Sept. 2001.
- [EHL+03] H. El Gamal, A. R. Hammons, Jr., Y. Liu, M. P. Fitz, and O. Y. Takeshita, "On the design of space-time and space-frequency codes for MIMO frequency-selective fading channels," *IEEE Trans. Inform. Theory*, vol. 49, no. 9, pp. 2277–2292, Sept. 2003.
- [EI99] S. C. Eisenstat and I. C. F. Ipsen, "Three absolute perturbation bounds for matrix eigenvalues imply relative bounds," *SIAM J. Matrix Analysis and Applications*, vol. 20, no. 1, pp. 149–158, 1999.
- [EKA02] V. Emamian, M. Kaveh, and M.-S. Alouini, "Outage probability with transmit and receive diversity in a shadowing environment," in *Proc. IEEE Wireless Commun. and Networking Conf. (WCNC)*, Orlando, Florida, USA, Mar. 2002, pp. 54–57.
- [EKL05] P. Elia, K. R. Kumar, and H.-F. Lu, "Explicit space-time codes that achieve the diversity-multiplexing gain tradeoff," in *Proc. IEEE Int. Symp. Inform. Theory (ISIT)*, Adelaide, Australia, Sept. 2005, pp. 896–900.
- [EKM96] T. Eng, N. Kong, and L. B. Milstein, "Comparison of diversity combining techniques for Rayleigh-fading channels," *IEEE Trans. Commun.*, vol. 44, no. 9, pp. 1117–1129, Sept. 1996.
- [El 02a] H. El Gamal, "On the design of layered space-time systems for autocoding," *IEEE Trans. Commun.*, vol. 50, no. 9, pp. 1451–1461, Sept. 2002.
- [El 02b] —, "On the robustness of space-time coding," *IEEE Trans. Signal Processing*, vol. 50, no. 10, pp. 2417–2428, Oct. 2002.
- [Eli55] P. Elias, "Coding for noisy channels," in *IRE Nat. Conv. Rec.*, 1955, pp. 37–47.
- [EPP06] A. Elkhazin, K. N. Plataniotis, and S. Pasupathy, "Reduced-dimension MAP turbo-BLAST detection," *IEEE Trans. Commun.*, vol. 54, no. 1, pp. 108–118, Jan. 2006.
- [EQ88] M. V. Eyuboglu and S. U. H. Qureshi, "Reduced-state sequence estimation with set partitioning and decision feedback," *IEEE Trans. Commun.*, vol. 36, no. 1, pp. 13–20, Jan. 1988.

- [FABE02] D. Falconer, S. L. Ariyavisitakul, A. Benyamin-Seeyar, and B. Eidson, "Frequency domain equalization for single-carrier broadband wireless systems," *IEEE Commun. Mag.*, vol. 40, no. 4, pp. 58–66, Apr. 2002.
- [FAT03] C. Fragouli, N. Al-Dhahir, and W. Turin, "Training-based channel estimation for multiple-antenna broadband transmissions," *IEEE Trans. Wireless Commun.*, vol. 2, no. 2, pp. 384–391, Mar. 2003.
- [FCG+03] G. J. Foschini, D. Chizhik, M. J. Gans, C. Papadias, and R. A. Valenzuela, "Analysis and performance of some basic space-time architectures," *IEEE J. Select. Areas Commun.*, vol. 21, no. 3, pp. 303–320, Apr. 2003.
- [FG98] G. J. Foschini and M. J. Gans, "On limits of wireless communications in a fading environment when using multiple antennas," *Kluwer Wireless Pers. Commun.*, vol. 6, pp. 311–335, Mar. 1998.
- [FGF99] I. J. Fevrier, S. B. Gelfand, and M. P. Fitz, "Reduced complexity decision feedback equalization for multipath channels with large delay spreads," *IEEE Trans. Commun.*, vol. 47, no. 6, pp. 927–937, June 1999.
- [FGVW99] G. J. Foschini, G. D. Golden, R. A. Valenzuela, and P. W. Wolniansky, "Simplified processing for high spectral efficiency wireless communication employing multi-element arrays," *IEEE J. Select. Areas Commun.*, vol. 17, no. 11, pp. 1841–1852, Nov. 1999.
- [FMS05] M. Fozunbal, S. W. McLaughlin, and R. W. Schafer, "On space-time-frequency coding over MIMO-OFDM systems," *IEEE Trans. Wireless Commun.*, vol. 4, no. 1, pp. 320–331, Jan. 2005.
- [FMSL04] M. Fozunbal, S. W. McLaughlin, R. W. Schafer, and J. M. Landsberg, "On space-time coding in the presence of spatio-temporal correlation," *IEEE Trans. Inform. Theory*, vol. 50, no. 9, pp. 1910–1926, Sept. 2004.
- [For72] G. Forney, Jr., "Maximum-likelihood sequence estimation of digital sequences in the presence of intersymbol interference," *IEEE Trans. Inform. Theory*, vol. 18, no. 3, pp. 363–378, May 1972.
- [Fos96] G. J. Foschini, "Layered space-time architecture for wireless communication in a fading environment when using multi-element antennas," *Bell Syst. Tech. J.*, pp. 41–59, Autumn 1996.
- [FP85] U. Fincke and M. Pohst, "Improved methods for calculating vectors of short length in a lattice, including a complexity analysis," *Math. Comput.*, vol. 44, no. 170, pp. 463–471, Apr. 1985.
- [FPKH05] A. Forenza, A. Pandharipande, H. Kim, and R. W. Heath, Jr., "Adaptive MIMO transmission scheme: Exploiting the spatial selectivity of wireless channels," in *Proc. IEEE Veh. Technol. Conf. (VTC-Spring)*, Stockholm, Sweden, May/June 2005, pp. 3188–3192.
- [FSH04] R. F. H. Fischer, C. Stierstorfer, and J. B. Huber, "Precoding for point-to-multipoint transmission over MIMO ISI channels," in *Proc. Int. Zurich Seminar on Commun. (IZS)*, Zurich, Switzerland, Feb. 2004, pp. 208–211.

- [FSMH05] J. Ch. Fricke, M. Sandell, J. Mietzner, and P. A. Hoeher, "Impact of the Gaussian approximation on the performance of the probabilistic data association MIMO decoder," *EURASIP J. Wireless Commun. and Networking*, vol. 2005, no. 5, pp. 796–800, Dec. 2005.
- [FVY01] W. Firmanto, B. S. Vucetic, and J. Yuan, "Space-time TCM with improved performance on fast fading channels," *IEEE Commun. Lett.*, vol. 5, no. 4, pp. 154–156, Apr. 2001.
- [FW03] R. F. H. Fischer and C. Windpassinger, "Real versus complex-valued equalisation in V-BLAST systems," *Electron. Letters*, vol. 39, no. 5, pp. 470–471, Mar. 2003.
- [FWLH02] R. F. H. Fischer, C. Windpassinger, A. Lampe, and J. B. Huber, "Tomlinson-Harashima precoding in space-time transmission for low-rate backward channel," in *Proc. Int. Zurich Seminar on Broadband Commun. (IZS)*, Zurich, Switzerland, Feb. 2002.
- [Gab92] W. F. Gabriel, "Adaptive processing array systems," *Proc. IEEE*, vol. 80, no. 1, pp. 152–162, Jan. 1992.
- [Gal62] R. G. Gallager, "Low-density parity-check codes," *IRE Trans. Inform. Theory*, vol. IT-8, pp. 21–28, Jan. 1962.
- [Gal68] ———, *Information Theory and Reliable Communication*. New York: John Wiley & Sons, 1968.
- [GBGP02] D. Gesbert, H. Boelcskei, D. A. Gore, and A. J. Paulraj, "Outdoor MIMO wireless channels: Models and performance prediction," *IEEE Trans. Commun.*, vol. 50, no. 12, pp. 1926–1934, Dec. 2002.
- [GCSS03] A. Giorgetti, M. Chiani, M. Shafi, and P. J. Smith, "Level crossing rates and MIMO capacity fades: Impacts of spatial/temporal channel correlation," in *Proc. IEEE Int. Conf. Commun. (ICC)*, Anchorage, Alaska, USA, May 2003, pp. 3046–3050.
- [GFVW99] G. D. Golden, G. J. Foschini, R. A. Valenzuela, and P. W. Wolniansky, "Detection algorithm and initial laboratory results using V-BLAST space-time communication architecture," *Electron. Letters*, vol. 35, no. 1, pp. 14–16, Jan. 1999.
- [GG05] M. Gharavi-Alkhansari and A. B. Gershman, "On diversity and coding gains and optimal matrix constellations for space-time block codes," *IEEE Trans. Signal Processing*, vol. 53, no. 10, pp. 3703–3717, Oct. 2005.
- [GHL06] C. Gao, A. M. Haimovich, and D. Lao, "Multiple-symbol differential detection for MPSK space-time block codes: Decision metric and performance analysis," *IEEE Trans. Commun.*, vol. 54, no. 8, pp. 1502–1510, Aug. 2006.
- [GHW92] R. D. Gitlin, J. F. Hayes, and S. B. Weinstein, *Data Communications Principles*. New York: Plenum Press, 1992.
- [GJJV03] A. Goldsmith, S. A. Jafar, N. Jindal, and S. Vishwanath, "Capacity limits of MIMO channels," *IEEE J. Select. Areas Commun.*, vol. 21, no. 5, pp. 684–701, June 2003.

- [GL00] Y. Gong and K. B. Letaief, "Performance evaluation and analysis of space-time coding in unequalized multipath fading links," *IEEE Trans. Commun.*, vol. 48, no. 11, pp. 1778–1782, Nov. 2000.
- [GL02] ———, "Concatenated space-time block coding with trellis coded modulation in fading channels," *IEEE Trans. Wireless Commun.*, vol. 1, no. 4, pp. 580–590, Oct. 2002.
- [GL03a] ———, "An efficient space-frequency coded OFDM system for broadband wireless communications," *IEEE Trans. Commun.*, vol. 51, no. 12, pp. 2019–2029, Dec. 2003.
- [GL03b] D. Gu and C. Leung, "Performance analysis of a transmit diversity scheme in spatially correlated fading with imperfect channel estimation," in *Proc. IEEE Pacific Rim Conf. on Commun., Comput., and Signal Processing (PACRIM)*, Victoria, British Columbia, Canada, Aug. 2003, pp. 111–114.
- [GL03c] ———, "Performance analysis of transmit diversity scheme with imperfect channel estimation," *Electron. Letters*, vol. 39, no. 4, pp. 402–403, Feb. 2003.
- [GN03] V. Gulati and K. R. Narayanan, "Concatenated codes for fading channels based on recursive space-time trellis codes," *IEEE Trans. Wireless Commun.*, vol. 2, no. 1, pp. 118–128, Jan. 2003.
- [God97] L. C. Godara, "Application of antenna arrays to mobile communications – Part I: Performance improvement, feasibility, and system considerations; Part II: Beam-forming and direction-of-arrival considerations," *Proc. IEEE*, vol. 85, no. 7/8, pp. 1031–1060, 1195–1245, July/Aug. 1997.
- [GOMH02] W. H. Gerstacker, F. Obernosterer, R. Meyer, and J. B. Huber, "On prefilter computation for reduced-state equalization," *IEEE Trans. Wireless Commun.*, vol. 1, no. 4, pp. 793–800, Oct. 2002.
- [Goo00] D. J. Goodman, "The wireless Internet: Promises and challenges," *Computer*, vol. 33, no. 7, pp. 36–41, July 2000.
- [Gor03] A. Gorokhov, "Bit sharing for layered space-time architectures with ordered signal retrieval," *IEEE Trans. Commun.*, vol. 51, no. 11, pp. 1809–1819, Nov. 2003.
- [GOS+04] W. H. Gerstacker, F. Obernosterer, R. Schober, A. T. Lehmann, A. Lampe, and P. Gunreben, "Equalization concepts for Alamouti's space-time block code," *IEEE Trans. Commun.*, vol. 52, no. 7, pp. 1178–1190, July 2004.
- [GPPF05] L. Garcia-Ordóñez, D. P. Palomar, A. Pages-Zamora, and J. R. Fonollosa, "Analytical BER performance in spatial multiplexing MIMO systems," in *Proc. IEEE Workshop on Signal Processing Adv. Wireless Commun. (SPAWC)*, New York City, New York, USA, June 2005, pp. 460–464.
- [Gra79] G. D. Gray, "The simulcasting technique: An approach to total-area radio coverage," *IEEE Trans. Veh. Technol.*, vol. VT-28, no. 2, pp. 117–125, May 1979.
- [Gra83] F. A. Graybill, *Matrices with Applications in Statistics*, 2nd ed. Pacific Grove (CA): Wadsworth, Inc., 1983.



- [GS01] G. Ganesan and P. Stoica, "Space-time block codes: A maximum SNR approach," *IEEE Trans. Inform. Theory*, vol. 47, no. 4, pp. 1650–1656, May 2001.
- [GSP01] D. Gore, S. Sandhu, and A. Paulraj, "Delay diversity code for frequency-selective channels," *Electron. Letters*, vol. 37, no. 20, pp. 1230–1231, Sept. 2001.
- [GSS+03] D. Gesbert, M. Shafi, D. Shiu, P. J. Smith, and A. Naguib, "From theory to practice: An overview of MIMO space-time coded wireless systems," *IEEE J. Select. Areas Commun.*, vol. 21, no. 3, pp. 281–302, Apr. 2003.
- [GT04] W. H. Gerstacker and D. P. Taylor, "On prefiltering for reduced-state equalization of MIMO channels," in *Proc. Int. ITG Conf. on Source and Channel Coding (SCC)*, Erlangen-Nuremberg, Germany, Jan. 2004, pp. 25–30.
- [Gv96] G. H. Golub and C. F. van Loan, *Matrix Computations*, 3rd ed. Baltimore - London: The Johns Hopkins University Press, 1996.
- [GW02a] R. Gozali and B. D. Woerner, "The impact of channel estimation errors on space-time trellis codes paired with iterative equalization/decoding," in *Proc. IEEE Veh. Technol. Conf. (VTC-Spring)*, Birmingham, Alabama, USA, May 2002, pp. 826–831.
- [GW02b] ———, "On the robustness of space-time block codes to spatial correlation," in *Proc. IEEE Veh. Technol. Conf. (VTC-Spring)*, Birmingham, Alabama, USA, May 2002, pp. 832–836.
- [HA02] M. O. Hasna and M.-S. Alouini, "Optimum power allocation for selective transmit-diversity systems over Nakagami fading channels," in *Proc. IEEE Int. Conf. Acoustics, Speech and Signal Processing (ICASSP)*, Orlando, Florida, USA, May 2002, pp. 2193–2196.
- [HA03] ———, "End-to-end performance of transmission systems with relays over Rayleigh-fading channels," *IEEE Trans. Wireless Commun.*, vol. 2, no. 6, pp. 1126–1131, Nov. 2003.
- [Hag03] J. Hagenauer, "A soft-in/soft-out list sequential (LISS) decoder for turbo schemes," in *Proc. IEEE Int. Symp. Inform. Theory (ISIT)*, Yokohama, Japan, June/July 2003, p. 382.
- [Has00] B. Hassibi, "An efficient square-root algorithm for BLAST," in *Proc. IEEE Int. Conf. Acoustics, Speech and Signal Processing (ICASSP)*, Istanbul, Turkey, June 2000, pp. 737–740.
- [Hay85] S. Haykin, Ed., *Array Signal Processing*. Englewood Cliffs (NJ): Prentice-Hall, 1985.
- [HB98] P. Hoeher and S. Badri, "On the timing sensitivity of symbol-spaced trellis-based equalizers applied to frequency-selective fading channels," in *Proc. Seventh Communication Theory Mini-Conference in conjunction with IEEE Global Telecommun. Conf. (Globecom'98)*, Sydney, Australia, Nov. 1998, pp. 88–93.



- [HB03] S. Hirst and A. Burr, "Design of low density parity check codes for space-time coding," in *Proc. Int. Symp. on Turbo Codes & Rel. Topics*, Brest, France, Sept. 2003, pp. 315–318.
- [HBA00] E. F. Haratsch, A. J. Blanksby, and K. Azadet, "Reduced-state sequence estimation with tap-selectable decision-feedback," in *Proc. IEEE Int. Conf. Commun. (ICC)*, New Orleans, Louisiana, USA, June 2000, pp. 372–376.
- [HBXK05] P. A. Hoeher, S. Badri-Hoeher, W. Xu, and C. Krakowski, "Single-antenna co-channel interference cancellation for TDMA cellular radio systems," *IEEE Wireless Commun.*, vol. 12, no. 2, pp. 30–37, Apr. 2005.
- [HC04] X. Hu and Y. H. Chew, "On the performance and capacity of an asynchronous space-time block-coded MC-CDMA system in the presence of carrier frequency offset," *IEEE Trans. Veh. Technol.*, vol. 53, no. 5, pp. 1327–1340, Sept. 2004.
- [HC06] S. K. Hong and J.-M. Chung, "Space time codes for CPFSK with arbitrary number of receive antennas," *IEEE Trans. Wireless Commun.*, vol. 5, no. 11, pp. 2988–2991, Nov. 2006.
- [HE95] J. Hartung and B. Elpelt, *Multivariate Statistik*. München - Wien: Oldenbourg Verlag, 1995.
- [HF03a] L. W. Hanlen and M. Fu, "Capacity of MIMO channels: A volumetric approach," in *Proc. IEEE Int. Conf. Commun. (ICC)*, Anchorage, Alaska, USA, May 2003, pp. 3001–3005.
- [HF03b] C. K. Ho and B. Farhang-Boroujeny, "On channel estimation effects in space-time orthogonal block coded system," in *Proc. IEEE Signal Processing Workshop on Signal Processing Adv. Wireless Commun. (SPAWC)*, Rome, Italy, June 2003, pp. 472–476.
- [HG04] A. Hjørungnes and D. Gesbert, "Minimum exact SER precoding of orthogonal space-time block codes for correlated MIMO channels," in *Proc. IEEE Global Telecommun. Conf. (Globecom)*, Dallas, Texas, USA, Nov./Dec. 2004, pp. 111–115.
- [HG05] L. W. Hanlen and A. J. Grant, "Optimal transmit covariance for MIMO channels with statistical transmitter side information," in *Proc. IEEE Int. Symp. Inform. Theory (ISIT)*, Adelaide, Australia, Sept. 2005, pp. 1818–1822.
- [HH02a] B. Hassibi and B. M. Hochwald, "Cayley differential unitary space-time codes," *IEEE Trans. Inform. Theory*, vol. 48, no. 6, pp. 1485–1503, June 2002.
- [HH02b] —, "High-rate codes that are linear in space and time," *IEEE Trans. Inform. Theory*, vol. 48, no. 7, pp. 1804–1824, July 2002.
- [HH04] Z. Hong and B. L. Hughes, "Bit-interleaved space-time coded modulation with iterative decoding," *IEEE Trans. Wireless Commun.*, vol. 3, no. 6, pp. 1912–1917, Nov. 2004.
- [HJ85] R. A. Horn and C. R. Johnson, *Matrix analysis*. Cambridge University Press, 1985.

- [HL05] R. W. Heath, Jr. and D. J. Love, "Multimode antenna selection for spatial multiplexing systems with linear receivers," *IEEE Trans. Signal Processing*, vol. 53, no. 8, pp. 3042–3056, Aug. 2005.
- [HLHS03] Z. Hong, K. Liu, R. W. Heath, Jr., and A. M. Sayeed, "Spatial multiplexing in correlated fading via the virtual channel representation," *IEEE J. Select. Areas Commun.*, vol. 21, no. 5, pp. 856–866, June 2003.
- [HLY02] L. Hanzo, T. H. Liew, and B. L. Yeap, *Turbo Coding, Turbo Equalisation and Space-Time Coding for Transmission over Fading Channels*. John Wiley & Sons, 2002.
- [HM00] B. M. Hochwald and T. L. Marzetta, "Unitary space-time modulation for multiple-antenna communications in Rayleigh flat fading," *IEEE Trans. Inform. Theory*, vol. 46, no. 2, pp. 543–564, Mar. 2000.
- [HMCK03] L. Hanzo, M. Muenster, B. J. Choi, and T. Keller, *OFDM and MC-CDMA for Broadband Multi-User Communications, WLANs and Broadcasting*. Chichester: John Wiley & Sons / IEEE Press, 2003.
- [HMR+00] B. M. Hochwald, T. L. Marzetta, T. J. Richardson, W. Sweldens, and R. Urbanke, "Systematic design of unitary space-time constellations," *IEEE Trans. Inform. Theory*, vol. 46, no. 6, pp. 1962–1973, Sept. 2000.
- [HO80] T. Hattori and S. Ogose, "A new modulation scheme for multitransmitter simulcast digital mobile radio communication," *IEEE Trans. Veh. Technol.*, vol. VT-29, no. 2, pp. 260–270, May 1980.
- [Hoe92] P. Hoeher, "A statistical discrete-time model for the WSSUS multipath channel," *IEEE Trans. Veh. Technol.*, vol. 41, no. 4, pp. 461–468, Nov. 1992.
- [How65] P. Howells, *Intermediate frequency side-lobe canceller*, Aug. 1965, U.S. Patent 3 202 990.
- [HP97] S. Hara and R. Prasad, "Overview of multicarrier CDMA," *IEEE Commun. Mag.*, vol. 35, no. 12, pp. 126–133, Dec. 1997.
- [HS93] M.-J. Ho and G. L. Stueber, "Co-channel interference of microcellular systems on shadowed Nakagami fading channels," in *Proc. IEEE Veh. Technol. Conf. (VTC)*, Secaucus, New Jersey, USA, May 1993, pp. 568–571.
- [HS00] B. M. Hochwald and W. Sweldens, "Differential unitary space-time modulation," *IEEE Trans. Commun.*, vol. 48, no. 12, pp. 2041–2052, Dec. 2000.
- [HSA04] T. S. Ho, K. Sakaguchi, and K. Araki, "Performance analysis of MIMO eigenmode transmission system under realistic channel and system conditions," in *Proc. IEEE Veh. Technol. Conf. (VTC-Spring)*, Genoa, Italy, May 2004, pp. 708–712.
- [HSdW04] S. Haykin, M. Sellathurai, Y. de Jong, and T. Willink, "Turbo-MIMO for wireless communications," *IEEE Commun. Mag.*, vol. 42, no. 10, pp. 48–53, Oct. 2004.

- [HSG05] T. Hehn, R. Schober, and W. H. Gerstacker, "Optimized delay diversity for frequency-selective fading channels," *IEEE Trans. Wireless Commun.*, vol. 4, no. 5, pp. 2289–2298, Sept. 2005.
- [HSL05] T. Himsoon, W. Su, and K. J. R. Liu, "Differential unitary space-time signal design using matrix rotation structure," *IEEE Signal Processing Lett.*, vol. 12, no. 1, pp. 45–48, Jan. 2005.
- [HSL06] ———, "Single-block differential transmit scheme for broadband wireless MIMO-OFDM systems," *IEEE Trans. Signal Processing*, vol. 54, no. 9, pp. 3305–3314, Sept. 2006.
- [HSM05] J. Hou, P. H. Siegel, and L. B. Milstein, "Design of multi-input multi-output systems based on low-density parity-check codes," *IEEE Trans. Commun.*, vol. 53, no. 4, pp. 601–611, Apr. 2005.
- [HSN05] A. Hedayat, H. Shah, and A. Nosratinia, "Analysis of space-time coding in correlated fading channels," *IEEE Trans. Wireless Commun.*, vol. 4, no. 6, pp. 2882–2891, Nov. 2005.
- [HSN06] T. E. Hunter, S. Sanayei, and A. Nosratinia, "Outage analysis of coded cooperation," *IEEE Trans. Inform. Theory*, vol. 52, no. 2, pp. 375–391, Feb. 2006.
- [Hub92] J. Huber, *Trelliscodierung*. Springer-Verlag, 1992.
- [Hug00] B. L. Hughes, "Differential space-time modulation," *IEEE Trans. Inform. Theory*, vol. 46, no. 7, pp. 2567–2578, Nov. 2000.
- [Hur98] A. Hurwitz, "Über die Komposition der quadratischen Formen von beliebig vielen Variablen," *Nachr. Gesell. d. Wiss. Göttingen*, pp. 309–316, 1898.
- [HYFP04] H. Hu, H. Yanikomeroglu, D. D. Falconer, and S. Periyalvar, "Range extension without capacity penalty in cellular networks with digital fixed relays," in *Proc. IEEE Global Telecommun. Conf. (Globecom)*, Dallas, Texas, USA, Nov./Dec. 2004, pp. 3053–3057.
- [HYVC02] Y. Hong, J. Yuan, B. Vucetic, and Z. Chen, "Design of space-time turbo trellis codes for two, three and four transmit antennas," in *Proc. IEEE Int. Conf. Commun. Systems (ICCS)*, Singapore, Nov. 2002.
- [HZD05] Y. Huang, J. Zhang, and P. M. Djuric, "Bayesian detection for BLAST," *IEEE Trans. Signal Processing*, vol. 53, no. 3, pp. 1086–1096, Mar. 2005.
- [I04a] "Network-Centric Military Communications," Guest Editorial, *IEEE Commun. Mag.*, vol. 42, no. 11, pp. 77–79, Nov. 2004.
- [I04b] "System requirements for IEEE 802.20 mobile broadband wireless access systems," IEEE, Draft IEEE 802.20-PD-06 version 14, July 2004.
- [I05a] "Network-Centric Military Communications," Guest Editorial, *IEEE Commun. Mag.*, vol. 43, no. 11, pp. 102–106, Nov. 2005.

- [I05b] “Topics in Ad Hoc and Sensor Networks,” Guest Editorial, *IEEE Commun. Mag.*, vol. 43, no. 10, p. 92, Oct. 2005.
- [I06] “Public Safety Communications,” Guest Editorial, *IEEE Commun. Mag.*, vol. 44, no. 1, pp. 28-29, Jan. 2006.
- [IMYL01] D. M. Ionescu, K. K. Mukkavilli, Z. Yan, and J. Lilleberg, “Improved 8- and 16-state space-time codes for 4-PSK with two transmit antennas,” *IEEE Commun. Lett.*, vol. 5, no. 7, pp. 301–303, July 2001.
- [IN03] M. T. Ivrlac and J. A. Nossek, “Quantifying diversity and correlation in Rayleigh fading MIMO communication systems,” in *Proc. IEEE Int. Symp. Signal Processing and Inform. Theory (ISSPIT)*, Darmstadt, Germany, Dec. 2003, pp. 158–161.
- [IN04] ———, “Cross layer optimization – An equivalence class approach,” in *Proc. ITG Workshop on Smart Antennas (WSA)*, Munich, Germany, Mar. 2004, paper no. 9.
- [Ion03] D. M. Ionescu, “On space-time code design,” *IEEE Trans. Wireless Commun.*, vol. 2, no. 1, pp. 20–28, Jan. 2003.
- [ITE02] S. Ichitsubo, K. Tsunekawa, and Y. Ebine, “Multipath propagation model of spatio-temporal dispersion observed at base station in urban areas,” *IEEE J. Select. Areas Commun.*, vol. 20, no. 6, pp. 1204–1210, Aug. 2002.
- [IUN03] M. T. Ivrlac, W. Utschick, and J. A. Nossek, “Fading correlations in wireless MIMO communication systems,” *IEEE J. Select. Areas Commun.*, vol. 21, no. 5, pp. 819–827, June 2003.
- [Jaf01] H. Jafarkhani, “A quasi-orthogonal space-time block code,” *IEEE Trans. Commun.*, vol. 49, no. 1, pp. 1–4, Jan. 2001.
- [Jaf05] ———, *Space-Time Coding – Theory and Practice*. Cambridge University Press, 2005.
- [Jak74] W. C. Jakes, Ed., *Microwave Mobile Communications*. New York: John Wiley & Sons, 1974.
- [JB04a] E. A. Jorswieck and H. Boche, “Average mutual information in spatial correlated MIMO systems with uninformed transmitter,” in *Proc. Conf. Inform. Sciences and Systems (CISS)*, Princeton, New Jersey, USA, Mar. 2004.
- [JB04b] E. A. Jorswieck and H. Boche, “Channel capacity and capacity-range of beamforming in MIMO wireless systems under correlated fading with covariance feedback,” *IEEE Trans. Wireless Commun.*, vol. 3, no. 5, pp. 1543–1553, Sept. 2004.
- [JB04c] ———, “Optimal transmission strategies and impact of correlation in multiantenna systems with different types of channel state information,” *IEEE Trans. Signal Processing*, vol. 52, no. 12, pp. 3440–3453, Dec. 2004.
- [JBM+02] C. A. Jotten, P. W. Baier, M. Meurer, T. Weber, and M. Haardt, “Efficient representation and feedback signaling of channel state information in frequency division duplexing MIMO systems,” in *Proc. IEEE Int. Symp. Wireless Pers. Multimedia Commun. (WPMC)*, Honolulu, Hawaii, USA, Oct. 2002, pp. 444–448.

- [Jel01] J. Jelitto, "Dimensionsreduktion des Empfangsraums von Systemen mit mehreren Empfangsantennen und deren Anwendung in der Raum-Zeit-Verarbeitung," Ph.D. dissertation, TU Dresden, Germany, 2001.
- [JF02] J. Jelitto and G. Fettweis, "Reduced dimension space-time processing for multi-antenna wireless systems," *IEEE Wireless Commun.*, vol. 9, no. 6, pp. 18–25, Dec. 2002.
- [JGS06] C. Jonietz, W. H. Gerstacker, and R. Schober, "Transmission and reception concepts for WLAN IEEE 802.11b," *IEEE Trans. Wireless Commun.*, vol. 5, no. 12, pp. 3375–3381, Dec. 2006.
- [JH05a] H. Jafarkhani and N. Hassanpour, "Super-quasi-orthogonal space-time trellis codes for four transmit antennas," *IEEE Trans. Wireless Commun.*, vol. 4, no. 1, pp. 215–227, Jan. 2005.
- [JH05b] Y. Jing and B. Hassibi, "Cooperative diversity in wireless relay networks with multiple-antenna nodes," in *Proc. IEEE Int. Symp. Inform. Theory (ISIT)*, Adelaide, Australia, Sept. 2005, pp. 815–819.
- [JH05c] —, "Three-transmit-antenna space-time codes based on  $SU(3)$ ," *IEEE Trans. Signal Processing*, vol. 53, no. 10, pp. 3688–3702, Oct. 2005.
- [JH06] —, "Distributed space-time coding in wireless relay networks," *IEEE Trans. Wireless Commun.*, vol. 5, no. 12, pp. 3524–3536, Dec. 2006.
- [JHHN04] M. Janani, A. Hedayat, T. E. Hunter, and A. Nosratinia, "Coded cooperation in wireless communications: Space-time transmission and iterative decoding," *IEEE Trans. Signal Processing*, vol. 52, no. 2, pp. 362–371, Feb. 2004.
- [JPv03] V. Jungnickel, V. Pohl, and C. von Helmolt, "Capacity of MIMO systems with closely spaced antennas," *IEEE Commun. Lett.*, vol. 7, no. 8, pp. 361–363, Aug. 2003.
- [JS03] H. Jafarkhani and N. Seshadri, "Super-orthogonal space-time trellis codes," *IEEE Trans. Inform. Theory*, vol. 49, no. 4, pp. 937–950, Apr. 2003.
- [JS04a] G. Jongren and M. Skoglund, "Quantized feedback information in orthogonal space-time block coding," *IEEE Trans. Inform. Theory*, vol. 50, no. 10, pp. 2473–2486, Oct. 2004.
- [JS04b] E. A. Jorswieck and A. Sezgin, "Impact of spatial correlation on the performance of orthogonal space-time block codes," *IEEE Commun. Lett.*, vol. 8, no. 1, pp. 21–23, Jan. 2004.
- [JSO02] G. Jongren, M. Skoglund, and B. Ottersten, "Combining beamforming and orthogonal space-time block coding," *IEEE Trans. Inform. Theory*, vol. 48, no. 3, pp. 611–627, Mar. 2002.
- [JWMC03] X. Jing, H. Wang, C. Ming, and S. Cheng, "A novel BLAST detection algorithm based instantaneous error ordering," in *Proc. IEEE Int. Conf. Commun. (ICC)*, Anchorage, Alaska, USA, May 2003, pp. 3056–3060.

- [JZP05] J. Jootar, J. R. Zeidler, and J. G. Proakis, "Performance of Alamouti space-time code in time-varying channels with noisy channel estimates," in *Proc. IEEE Wireless Commun. and Networking Conf. (WCNC)*, New Orleans, Louisiana, USA, Mar. 2005, pp. 498–503.
- [KA03] Y.-C. Ko and M.-S. Alouini, "Estimation of Nakagami- $m$  fading channel parameters with application to optimized transmitter diversity systems," *IEEE Trans. Wireless Commun.*, vol. 2, no. 2, pp. 250–259, Mar. 2003.
- [KA06] M. Kang and M.-S. Alouini, "Capacity of correlated MIMO Rayleigh channels," *IEEE Trans. Wireless Commun.*, vol. 5, no. 1, pp. 143–155, Jan. 2006.
- [Kad03] T. Kadous, "Ordered H-BLAST for MIMO/OFDM systems over multipath channels," in *Proc. IEEE Symp. on Comput. and Commun. (ISCC)*, Kemer, Antalya, Turkey, June/July 2003, pp. 481–485.
- [Kam94] K. D. Kammeyer, "Time truncation of channel impulse responses by linear filtering: A method to reduce the complexity of Viterbi equalization," *AEÜ Int. J. Electron. Commun.*, vol. 48, no. 5, pp. 237–243, 1994.
- [Kam96] ———, *Nachrichtenübertragung*, 2nd ed. Stuttgart: B. G. Teubner, 1996.
- [KBB+04] T. Kaiser, A. Bourdoux, H. Boche, J. R. Fonollosa, J. Bach Andersen, and W. Utschick, Eds., *Smart Antennas – State of the Art*. New York: Hindawi Publishing Corp., 2004.
- [KBJP04] J. Kim, K. T. Bae, W. G. Jeon, and E. J. Powers, "Orthogonal space-time block coding in fast flat fading channels," in *Proc. IEEE Veh. Technol. Conf. (VTC-Fall)*, Los Angeles, California, USA, Sept. 2004, pp. 2473–2476.
- [KC02] R. Knopp and G. Caire, "Power control and beamforming for systems with multiple transmit and receive antennas," *IEEE Trans. Wireless Commun.*, vol. 1, no. 4, pp. 638–648, Oct. 2002.
- [KC04] H. Kim and J. Chun, "MIMO structure which combines the spatial multiplexing and beamforming," in *Proc. IEEE Veh. Technol. Conf. (VTC-Spring)*, Genoa, Italy, May 2004, pp. 108–112.
- [KCVW03] P. Kyritsi, D. C. Cox, R. A. Valenzuela, and P. W. Wolniansky, "Correlation analysis based on MIMO channel measurements in an indoor environment," *IEEE J. Select. Areas Commun.*, vol. 21, no. 5, pp. 713–719, June 2003.
- [KDA03] A. Kastrisios, M. Dohler, and H. Aghvami, "Influence of channel characteristics on the performance of VAA with deployed STBCs," in *Proc. IEEE Veh. Technol. Conf. (VTC-Spring)*, Jeju, Korea, Apr. 2003, pp. 1138–1142.
- [KDFB04] R. Kalbasi, R. Dinis, D. D. Falconer, and A. H. Banihashemi, "Layered space-time receivers for single-carrier transmission with iterative frequency-domain equalization," in *Proc. IEEE Veh. Technol. Conf. (VTC-Spring)*, Genoa, Italy, May 2004, pp. 575–579.



- [KF97] W.-Y. Kuo and M. P. Fitz, "Design and analysis of transmitter diversity using intentional frequency offset for wireless communications," *IEEE Trans. Veh. Technol.*, vol. 46, no. 4, pp. 871–881, Nov. 1997.
- [KGK05] L. G. Krasny, J.-C. Guey, and A. Khayrallah, "Transmit diversity with constrained feedback," in *Proc. IST Mobile & Wireless Commun. Summit*, Dresden, Germany, June 2005, paper no. 63.
- [KHP05] J. Kim, R. W. Heath, Jr., and E. J. Powers, "Receiver designs for Alamouti coded OFDM systems in fast fading channels," *IEEE Trans. Wireless Commun.*, vol. 4, no. 2, pp. 550–559, Mar. 2005.
- [Kie04] M. Kiessling, "Statistical analysis and transmit prefiltering for MIMO wireless systems in correlated fading environments," Ph.D. dissertation, University of Stuttgart, Germany, 2004.
- [Kie05] —, "Unifying analysis of ergodic MIMO capacity in correlated Rayleigh fading environments," *Europ. Trans. Telecommun.*, vol. 16, no. 1, pp. 17–35, Jan. 2005.
- [Koh98] R. Kohno, "Spatial and temporal communication theory using adaptive antenna arrays," *IEEE Pers. Commun.*, vol. 5, no. 1, pp. 28–35, Feb. 1998.
- [KR04] P.-S. Kildal and K. Rosengren, "Correlation and capacity of MIMO systems and mutual coupling, radiation efficiency, and diversity gain of their antennas: Simulations and measurements in a reverberation chamber," *IEEE Commun. Mag.*, vol. 42, no. 12, pp. 104–112, Dec. 2004.
- [KR05] T. Kiran and B. S. Rajan, "STBC-schemes with nonvanishing determinant for certain number of transmit antennas," *IEEE Trans. Inform. Theory*, vol. 51, no. 8, pp. 2984–2992, Aug. 2005.
- [KSB04] M. Kiessling, J. Speidel, and A. Boronka, "Asymptotics of ergodic MIMO capacity in correlated Rayleigh fading environments," in *Proc. IEEE Veh. Technol. Conf. (VTC-Spring)*, Genoa, Italy, May 2004, pp. 843–847.
- [KSH97] D. Kim, G. L. Stueber, and N. Hightower, "Performance of simulcast systems in mobile radio environments," in *Proc. IEEE Veh. Technol. Conf. (VTC)*, Phoenix, Arizona, USA, May 1997, pp. 495–499.
- [KSP+02] J. P. Kermoal, L. Schumacher, K. I. Pedersen, P. E. Mogensen, and F. Frederiksen, "A stochastic MIMO radio channel model with experimental validation," *IEEE J. Select. Areas Commun.*, vol. 20, no. 6, pp. 1211–1226, Aug. 2002.
- [KT04] Y. Ko and C. Tepedelenlioglu, "Optimal switching thresholds for space-time block coded rate-adaptive M-QAM," in *Proc. IEEE Int. Conf. Acoustics, Speech and Signal Processing (ICASSP)*, Montréal, Quebec, Canada, May 2004, pp. 477–480.
- [Kuh05] C. Kuhn, "A bidirectional list-sequential (BI-LISS) equalizer for turbo schemes," in *Proc. IST Mobile & Wireless Commun. Summit*, Dresden, Germany, June 2005, paper no. 306.
- [Kuh06] —, "Detection, decoding and estimation with a list-sequential (LISS) algorithm," Ph.D. dissertation, Munich University of Technology, Germany, 2006.



- [KW03] C. Koese and R. D. Wesel, "Universal space-time trellis codes," *IEEE Trans. Inform. Theory*, vol. 49, no. 10, pp. 2717–2727, Oct. 2003.
- [KW06] ———, "Universal space-time codes from demultiplexed trellis codes," *IEEE Trans. Commun.*, vol. 54, no. 7, pp. 1243–1250, July 2006.
- [KWBR04] T. Kaiser, A. Wilzeck, M. Berentsen, and M. Rupp, "Prototyping for MIMO systems – An overview," in *Proc. Europ. Signal Processing Conf. (EUSIPCO)*, Vienna, Austria, Sept. 2004, pp. 681–688.
- [KWZ02] S.-Y. Kung, Y. Wu, and X. Zhang, "Bezout space-time precoders and equalizers for MIMO channels," *IEEE Trans. Signal Processing*, vol. 50, no. 10, pp. 2499–2514, Oct. 2002.
- [KYIG05] K. J. Kim, J. Yue, R. A. Iltis, and J. D. Gibson, "A QRD-M/Kalman filter-based detection and channel estimation algorithm for MIMO-OFDM systems," *IEEE Trans. Wireless Commun.*, vol. 4, no. 2, pp. 710–721, Mar. 2005.
- [LAK04] T. A. Lamahewa, T. D. Abhayapala, and R. A. Kennedy, "Fading resistance of orthogonal space-time block codes under correlation," in *Proc. IEEE Signal Processing Workshop on Signal Processing Adv. Wireless Commun. (SPAWC)*, Lisbon, Portugal, July 2004, pp. 278–282.
- [Lan02a] I. Land, personal communication, University of Kiel, Germany, Sept. 2002.
- [Lan02b] ———, personal communication, University of Kiel, Germany, Dec. 2002.
- [Lan04] ———, "Reliability information in channel decoding – Practical aspects and information theoretical bounds," Ph.D. dissertation, University of Kiel, Germany, 2004.
- [LC83] S. Lin and D. J. Costello, *Error Control Coding: Fundamentals and Applications*. Englewood Cliffs (NJ): Prentice-Hall, 1983.
- [LC04] S. Liu and J.-W. Chong, "Improved design criterion for space-time trellis codes over time-correlated Rayleigh fading channels," in *Proc. IEEE Veh. Technol. Conf. (VTC-Fall)*, Los Angeles, California, USA, Sept. 2004, pp. 4711–4715.
- [LC05] X. Li and X. Cao, "Low complexity signal detection algorithm for MIMO-OFDM systems," *Electron. Letters*, vol. 41, no. 2, pp. 83–85, Jan. 2005.
- [LCL05a] Z. Lei, F. P. S. Chin, and Y.-C. Liang, "Orthogonal switched beams for downlink diversity transmission," *IEEE Trans. Antennas Propagat.*, vol. 53, no. 7, pp. 2169–2177, July 2005.
- [LCL05b] X. Li, M. Chen, and W. Liu, "Application of STBC-encoded cooperative transmissions in wireless sensor networks," *IEEE Signal Processing Lett.*, vol. 12, no. 2, pp. 134–137, Feb. 2005.
- [LCL05c] D.-B. Lin, P.-H. Chiang, and H.-J. Li, "Performance analysis of two-branch transmit diversity block-coded OFDM systems in time-varying multipath Rayleigh-fading channels," *IEEE Trans. Veh. Technol.*, vol. 54, no. 1, pp. 136–148, Jan. 2005.

- [LFT01] Y. Liu, M. P. Fitz, and O. Y. Takeshita, "Space-time codes performance criteria and design for frequency-selective fading channels," in *Proc. IEEE Int. Conf. Commun. (ICC)*, Helsinki, Finland, June 2001, pp. 2800–2804.
- [LFV01] A. Lozano, F. R. Farrokhi, and R. A. Valenzuela, "Lifting the limits on high-speed wireless data access using antenna arrays," *IEEE Commun. Mag.*, vol. 39, no. 9, pp. 156–162, Sept. 2001.
- [LFWS04] Y. Li, P. H. W. Fung, Y. Wu, and S. Sun, "Bit-interleaved coded modulation in linear dispersion coded MIMO system over spatially correlated Rician fading channel," in *Proc. IEEE Global Telecommun. Conf. (Globecom)*, Dallas, Texas, USA, Nov./Dec. 2004, pp. 5–9.
- [LFX05] K. Lu, S. Fu, and X.-G. Xia, "Closed-form designs of complex orthogonal space-time block codes of rates  $(k+1)/(2k)$  for  $2k-1$  or  $2k$  transmit antennas," *IEEE Trans. Inform. Theory*, vol. 51, no. 12, pp. 4340–4347, Dec. 2005.
- [LG01] L. Li and A. J. Goldsmith, "Capacity and optimal resource allocation for fading broadcast channels – Part II: Outage capacity," *IEEE Trans. Inform. Theory*, vol. 47, no. 3, pp. 1103–1127, Mar. 2001.
- [LG04] S. Loyka and F. Gagnon, "Performance analysis of the V-BLAST algorithm: An analytical approach," *IEEE Trans. Wireless Commun.*, vol. 3, no. 4, pp. 1326–1337, July 2004.
- [LGB03] P. Lusina, E. Gabidulin, and M. Bossert, "Maximum rank distance codes as space-time codes," *IEEE Trans. Inform. Theory*, vol. 49, no. 10, pp. 2757–2760, Oct. 2003.
- [LGBS01] Z. Liu, G. B. Giannakis, S. Barbarossa, and A. Scaglione, "Transmit antennae space-time block coding for generalized OFDM in the presence of unknown multipath," *IEEE J. Select. Areas Commun.*, vol. 19, no. 7, pp. 1352–1364, July 2001.
- [LGW05] Y. Li, X. Guo, and X. Wang, "Design of recursive convolutional space-time codes with an arbitrary number of transmit antennas," *IEEE Commun. Lett.*, vol. 9, no. 7, pp. 637–639, July 2005.
- [LH02] T. H. Liew and L. Hanzo, "Space-time codes and concatenated channel codes for wireless communications," *Proc. IEEE*, vol. 90, no. 2, pp. 187–219, Feb. 2002.
- [LH03a] Z.-Q. Li and G.-R. Hu, "Space-time block codes based on coordinate symmetric orthogonal designs," *Electron. Letters*, vol. 39, no. 8, pp. 670–671, Apr. 2003.
- [LH03b] D. J. Love and R. W. Heath, Jr., "Equal gain transmission in multiple-input multiple-output wireless systems," *IEEE Trans. Commun.*, vol. 51, no. 7, pp. 1102–1110, July 2003.
- [LH04a] —, "Diversity performance of precoded orthogonal space-time block codes using limited feedback," *IEEE Commun. Lett.*, vol. 8, no. 5, pp. 305–307, May 2004.
- [LH04b] —, "What is the value of limited feedback for MIMO channels?" *IEEE Commun. Mag.*, vol. 42, no. 10, pp. 54–59, Oct. 2004.

- [LH05a] ———, “Limited feedback unitary precoding for orthogonal space-time block codes,” *IEEE Trans. Signal Processing*, vol. 53, no. 1, pp. 64–73, Jan. 2005.
- [LH05b] ———, “Limited feedback unitary precoding for spatial multiplexing systems,” *IEEE Trans. Inform. Theory*, vol. 51, no. 8, pp. 2967–2976, Aug. 2005.
- [LH05c] ———, “Multimode precoding for MIMO wireless systems,” *IEEE Trans. Signal Processing*, vol. 53, no. 10, pp. 3674–3687, Oct. 2005.
- [LH05d] ———, “Necessary and sufficient conditions for full diversity order in correlated Rayleigh fading beamforming and combining systems,” *IEEE Trans. Wireless Commun.*, vol. 4, no. 1, pp. 20–23, Jan. 2005.
- [LH06] ———, “Limited feedback diversity techniques for correlated channels,” *IEEE Trans. Veh. Technol.*, vol. 55, no. 2, pp. 718–722, Mar. 2006.
- [LHS03] D. J. Love, R. W. Heath, Jr., and T. Strohmer, “Grassmanian beamforming for multiple-input multiple-output wireless systems,” *IEEE Trans. Inform. Theory*, vol. 49, no. 10, pp. 2735–2747, Oct. 2003.
- [LI02] K.-H. Li and M. A. Ingram, “Space-time block-coded OFDM systems with RF beamformers for high-speed indoor wireless communications,” *IEEE Trans. Commun.*, vol. 50, no. 12, pp. 1899–1901, Dec. 2002.
- [Li03a] H. Li, “Differential space-time-frequency modulation over frequency-selective fading channels,” *IEEE Commun. Lett.*, vol. 7, no. 8, pp. 349–351, Aug. 2003.
- [Li03b] X. Li, “Energy efficient wireless sensor networks with transmission diversity,” *Electron. Letters*, vol. 39, no. 24, pp. 1753–1755, Nov. 2003.
- [Li04] ———, “Space-time coded multi-transmission among distributed transmitters without perfect synchronization,” *IEEE Signal Processing Lett.*, vol. 11, no. 12, pp. 948–951, Dec. 2004.
- [Li05] H. Li, “Differential space-time modulation over frequency-selective channels,” *IEEE Trans. Signal Processing*, vol. 53, no. 6, pp. 2228–2242, June 2005.
- [Lia03a] X.-B. Liang, “A high-rate orthogonal space-time block code,” *IEEE Commun. Lett.*, vol. 7, no. 5, pp. 222–223, May 2003.
- [Lia03b] ———, “Orthogonal designs with maximal rates,” *IEEE Trans. Inform. Theory*, vol. 49, no. 10, pp. 2468–2503, Oct. 2003.
- [LJ05] L. Liu and H. Jafarkhani, “Application of quasi-orthogonal space-time block codes in beamforming,” *IEEE Trans. Signal Processing*, vol. 53, no. 1, pp. 54–63, Jan. 2005.
- [LK05] H.-F. F. Lu and P. V. Kumar, “A unified construction of space-time codes with optimal rate-diversity tradeoff,” *IEEE Trans. Inform. Theory*, vol. 51, no. 5, pp. 1709–1730, May 2005.
- [LK06] J.-H. Lee and S.-C. Kim, “Efficient ISI cancellation for STBC OFDM systems using successive interference cancellation,” *IEEE Commun. Lett.*, vol. 10, no. 8, pp. 629–631, Aug. 2006.

- [LL05a] W. S. Leon and Y.-C. Liang, "Statistical pre-filtering for MIMO-OFDM systems," in *Proc. IEEE Veh. Technol. Conf. (VTC-Spring)*, Stockholm, Sweden, May/June 2005, pp. 1012–1016.
- [LL05b] P. Luo and H. Leib, "Full-rate full-diversity space-time code for four-transmit-antenna systems," *IEEE Trans. Wireless Commun.*, vol. 4, no. 5, pp. 1974–1979, Sept. 2005.
- [LL06] H. Li and T. Li, "A new differential modulation for coded OFDM with multiple transmit antennas," *IEEE Signal Processing Lett.*, vol. 13, no. 6, pp. 317–320, June 2006.
- [LLC03] J. Li, K. B. Letaief, and Z. Cao, "Co-channel interference cancellation for space-time coded OFDM systems," *IEEE Trans. Wireless Commun.*, vol. 2, no. 1, pp. 41–49, Jan. 2003.
- [LLK03] C. Ling, K. H. Li, and A. C. Kot, "Noncoherent sequence detection of differential space-time modulation," *IEEE Trans. Inform. Theory*, vol. 49, no. 10, pp. 2727–2734, Oct. 2003.
- [LLK04] ———, "On decision-feedback detection of differential space-time modulation in continuous fading," *IEEE Trans. Commun.*, vol. 52, no. 10, pp. 1613–1617, Oct. 2004.
- [LLKZ03] C. Ling, K. H. Li, A. C. Kot, and Q. T. Zhang, "Multisampling decision-feedback linear prediction receivers for differential space-time modulation over Rayleigh fast fading channels," *IEEE Trans. Commun.*, vol. 51, no. 7, pp. 1214–1223, July 2003.
- [LLL82] A. K. Lenstra, H. W. Lenstra, and L. Lovasz, "Factoring polynomials with rational coefficients," *Math. Ann.*, vol. 261, pp. 515–534, 1982.
- [LLL06] H. Lee, B. Lee, and I. Lee, "Iterative detection and decoding with an improved V-BLAST for MIMO-OFDM systems," *IEEE J. Select. Areas Commun.*, vol. 24, no. 3, pp. 504–513, Mar. 2006.
- [LM02] F. K. H. Lee and P. J. McLane, "Iterative parallel-trellis MAP equalizers with nonuniformly-spaced prefilters for sparse multipath channels," in *Proc. IEEE Veh. Technol. Conf. (VTC-Fall)*, Vancouver, British Columbia, Canada, Sept. 2002, pp. 2201–2205.
- [LM03] G. Leus and M. Moonen, "Per-tone equalization for MIMO OFDM systems," *IEEE Trans. Signal Processing*, vol. 51, no. 11, pp. 2965–2975, Nov. 2003.
- [LM04] F. K. H. Lee and P. J. McLane, "Design of nonuniformly spaced tapped-delay-line equalizers for sparse multipath channels," *IEEE Trans. Commun.*, vol. 52, no. 4, pp. 530–535, Apr. 2004.
- [LM06] Y. Li and J. Moon, "Bit-interleaved space-time trellis coding for frequency-selective block fading channels," *IEEE Commun. Lett.*, vol. 10, no. 1, pp. 40–42, Jan. 2006.
- [LMG02] Z. Liu, X. Ma, and G. B. Giannakis, "Space-time coding and Kalman filtering for time-selective fading channels," *IEEE Trans. Commun.*, vol. 50, no. 2, pp. 183–186, Feb. 2002.

- [Lo04] T. Lo, "Adaptive space-time transmission with side information," *IEEE Trans. Wireless Commun.*, vol. 3, no. 5, pp. 1496–1501, Sept. 2004.
- [Loe04] H.-A. Loeliger, "An introduction to factor graphs," *IEEE Signal Processing Mag.*, vol. 21, no. 1, pp. 28–41, Jan. 2004.
- [LP99] P. H. Lehne and M. Pettersen, "An overview of smart antenna technology for mobile communications systems," *IEEE Commun. Surveys and Tutorials*, vol. 2, no. 4, pp. 2–13, Fourth Quarter 1999.
- [LP00] E. Lindskog and A. Paulraj, "A transmit diversity scheme for channels with intersymbol interference," in *Proc. IEEE Int. Conf. Commun. (ICC)*, New Orleans, Louisiana, USA, June 2000, pp. 307–311.
- [LP02] A. Lozano and C. Papadias, "Layered space-time receivers for frequency-selective wireless channels," *IEEE Trans. Commun.*, vol. 50, no. 1, pp. 65–73, Jan. 2002.
- [LPWH01] J. Luo, K. R. Pattipati, P. K. Willett, and F. Hasegawa, "Near-optimal multiuser detection in synchronous CDMA using probabilistic data association," *IEEE Commun. Lett.*, vol. 5, no. 9, pp. 361–363, Sept. 2001.
- [LS02] L. H.-J. Lampe and R. Schober, "Bit-interleaved coded differential space-time modulation," *IEEE Trans. Commun.*, vol. 50, no. 9, pp. 1429–1439, Sept. 2002.
- [LS03] E. G. Larsson and P. Stoica, *Space-Time Block Coding for Wireless Communications*. John Wiley & Sons, 2003.
- [LSB04] P. Lusina, S. Shavgulidze, and M. Bossert, "Space-time block factorisation codes over Gaussian integers," *IEE Proc. Commun.*, vol. 151, no. 5, pp. 415–421, Oct. 2004.
- [LSF03] L. H.-J. Lampe, R. Schober, and R. F. H. Fischer, "Coded differential space-time modulation for flat fading channels," *IEEE Trans. Wireless Commun.*, vol. 2, no. 3, pp. 582–590, May 2003.
- [LSG06] Y.-W. Liang, R. Schober, and W. Gerstacker, "Transmit beamforming with finite-rate feedback for frequency-selective channels," in *Proc. IEEE Global Telecommun. Conf. (Globecom)*, San Francisco, California, USA, Nov./Dec. 2006.
- [LT85] P. Lancaster and M. Tismenetsky, *The Theory of Matrices*, 2nd ed. New York: Academic Press, 1985.
- [LT04] S. Liu and Z. Tian, "Near-optimum soft decision equalization for frequency selective MIMO channels," *IEEE Trans. Signal Processing*, vol. 52, no. 3, pp. 721–733, Mar. 2004.
- [LT05] S. Lambbotharan and C. Toker, "Closed-loop space time block coding techniques for OFDM broadband wireless access systems," *IEEE Trans. Consumer Electron.*, vol. 51, no. 3, pp. 765–769, Aug. 2005.
- [LTW04] J. N. Laneman, D. N. C. Tse, and G. W. Wornell, "Cooperative diversity in wireless networks: Efficient protocols and outage behavior," *IEEE Trans. Inform. Theory*, vol. 50, no. 12, pp. 3062–3080, Dec. 2004.

- [Lu05] H.-F. Lu, "Space-time codes with AM-PSK constellations," *IEEE Trans. Inform. Theory*, vol. 51, no. 12, pp. 4355–4358, Dec. 2005.
- [Lu06] ———, "On constructions of algebraic space-time codes with AM-PSK constellations satisfying rate-diversity tradeoff," *IEEE Trans. Inform. Theory*, vol. 52, no. 7, pp. 3198–3209, July 2006.
- [LV05a] E. G. Larsson and B. R. Vojcic, "Cooperative transmit diversity based on superposition modulation," *IEEE Commun. Lett.*, vol. 9, no. 9, pp. 778–780, Sept. 2005.
- [LV05b] Y. Li and B. Vucetic, "Optimization of space-time block codes based on multidimensional super-set partitioning," *IEEE Signal Processing Lett.*, vol. 12, no. 4, pp. 317–320, Apr. 2005.
- [LVTZ04] Y. Li, B. Vucetic, Y. Tang, and Q. Zhang, "Space-time trellis codes with linear transformation for fast fading channels," *IEEE Signal Processing Lett.*, vol. 11, no. 11, pp. 895–898, Nov. 2004.
- [LVZT06] Y. Li, B. Vucetic, Z. Zhou, and Y. Tang, "Novel full diversity space time codes," *IEEE Trans. Wireless Commun.*, vol. 5, no. 2, pp. 296–300, Feb. 2006.
- [LW00] K. F. Lee and D. B. Williams, "A space-frequency transmitter diversity technique for OFDM systems," in *Proc. IEEE Global Telecommun. Conf. (Globecom)*, San Francisco, California, USA, Nov./Dec. 2000, pp. 1473–1477.
- [LW03] J. N. Laneman and G. W. Wornell, "Distributed space-time-coded protocols for exploiting cooperative diversity in wireless networks," *IEEE Trans. Inform. Theory*, vol. 49, no. 10, pp. 2415–2425, Oct. 2003.
- [LWL02] B. Lu, X. Wang, and Y. Li, "Iterative receivers for space-time block-coded OFDM systems in dispersive fading channels," *IEEE Trans. Wireless Commun.*, vol. 1, no. 2, pp. 213–225, Apr. 2002.
- [LX02] X.-B. Liang and X.-G. Xia, "Unitary signal constellations for differential space-time modulation with two transmit antennas: Parametric codes, optimal designs, and bounds," *IEEE Trans. Inform. Theory*, vol. 48, no. 8, pp. 2291–2322, Aug. 2002.
- [LX03] ———, "On the nonexistence of rate-one generalized complex orthogonal designs," *IEEE Trans. Inform. Theory*, vol. 49, no. 11, pp. 2984–2989, Nov. 2003.
- [LX05a] Y. Li and X.-G. Xia, "Full diversity distributed space-time trellis codes for asynchronous cooperative communications," in *Proc. IEEE Int. Symp. Inform. Theory (ISIT)*, Adelaide, Australia, Sept. 2005, pp. 911–915.
- [LX05b] X.-B. Liang and X.-G. Xia, "Fast differential unitary space-time demodulation via square orthogonal designs," *IEEE Trans. Wireless Commun.*, vol. 4, no. 4, pp. 1331–1336, July 2005.
- [LXG02] Z. Liu, Y. Xin, and G. B. Giannakis, "Space-time-frequency coded OFDM over frequency-selective fading channels," *IEEE Trans. Signal Processing*, vol. 50, no. 10, pp. 2465–2476, Oct. 2002.



- [LY05] Y. Li and Z. Ye, "On optimum transmission power strategy in MIMO systems with covariance feedback," *IEEE Commun. Lett.*, vol. 9, no. 5, pp. 444–446, May 2005.
- [LY06] Z.-Q. Luo and W. Yu, "An introduction to convex optimization for communications and signal processing," *IEEE J. Select. Areas Commun.*, vol. 24, no. 8, pp. 1426–1438, Aug. 2006.
- [LYL01] L. Li, Y. D. Yao, and H. Li, "Intersymbol/cochannel interference cancellation for transmit diversity systems in frequency selective fading channels," in *Proc. IEEE Veh. Technol. Conf. (VTC-Fall)*, Atlantic City, New Jersey, USA, Oct. 2001, pp. 678–682.
- [LYW04] B. Lu, G. Yue, and X. Wang, "Performance analysis and design optimization of LDPC-coded MIMO OFDM systems," *IEEE Trans. Signal Processing*, vol. 52, no. 2, pp. 348–361, Feb. 2004.
- [LZC04] D. P. Liu, Q. T. Zhang, and Q. Chen, "Structures and performance of noncoherent receivers for unitary space-time modulation on correlated fast-fading channels," *IEEE Trans. Veh. Technol.*, vol. 53, no. 4, pp. 1116–1125, July 2004.
- [MA04] A. Maaref and S. Aissa, "On the capacity of space-time block codes in MIMO Rayleigh fading channels," in *Proc. IEEE Global Telecommun. Conf. (Globecom)*, Dallas, Texas, USA, Nov./Dec. 2004, pp. 2936–2940.
- [Mac03] D. J. C. MacKay, *Information Theory, Inference and Learning Algorithms*. Cambridge University Press, 2003.
- [MBH05] J. Mietzner, S. Badri-Hoehner, and P. A. Hoehner, "Prefiltering and trellis-based equalization for sparse ISI channels," in *Proc. IST Mobile & Wireless Commun. Summit*, Dresden, Germany, June 2005, paper no. 247.
- [MBLH05] J. Mietzner, S. Badri-Hoehner, I. Land, and P. A. Hoehner, "Trellis-based equalization for sparse ISI channels revisited," in *Proc. IEEE Int. Symp. Inform. Theory (ISIT)*, Adelaide, Australia, Sept. 2005, pp. 229–233.
- [MBLH06] —, "Equalization of sparse intersymbol-interference channels revisited," *EURASIP J. Wireless Commun. and Networking*, vol. 2006, Article ID 29075, 13 pages, 2006.
- [McG98] N. C. McGinty, "Reduced complexity equalization for data communication," Ph.D. dissertation, The Australian National University, Canberra, Australia, 1998.
- [MEH04a] J. Mietzner, J. Eick, and P. A. Hoehner, "Frequency-offset sensitivity of resilient microwave links applying the Alamouti scheme," in *Proc. Int. ITG Conf. on Source and Channel Coding (SCC)*, Erlangen-Nuremberg, Germany, Jan. 2004, pp. 165–172.
- [MEH04b] —, "On distributed space-time coding techniques for cooperative wireless networks and their sensitivity to frequency offsets," in *Proc. ITG Workshop on Smart Antennas (WSA)*, Munich, Germany, Mar. 2004, paper no. 15.



- [MFP03] X. Mestre, J. R. Fonollosa, and A. Pages-Zamora, "Capacity of MIMO channels: Asymptotic evaluation under correlated fading," *IEEE J. Select. Areas Commun.*, vol. 21, no. 5, pp. 829–838, June 2003.
- [MGJ05] J. K. Milleth, K. Giridhar, and D. Jaliha, "Closed-loop transmit diversity schemes for five and six transmit antennas," *IEEE Signal Processing Lett.*, vol. 12, no. 2, pp. 130–133, Feb. 2005.
- [MGJ06] —, "On channel orthogonalization using space-time block coding with partial feedback," *IEEE Trans. Commun.*, vol. 54, no. 6, pp. 1121–1130, June 2006.
- [MH04a] J. Mietzner and P. A. Hoeher, "Boosting the performance of wireless communication systems – Theory and practice of multiple-antenna techniques," *IEEE Commun. Mag.*, vol. 42, no. 10, pp. 40–47, Oct. 2004.
- [MH04b] —, "Distributed space-time codes for cooperative wireless networks in the presence of different propagation delays and path losses," in *Proc. IEEE Sensor Array and Multichannel Signal Processing Workshop (SAM)*, Sitges, Barcelona, Spain, July 2004, paper no. S5.5.
- [MH05] —, "On the duality of wireless systems with multiple cooperating transmitters and wireless systems with correlated antennas," in *Proc. IST Mobile & Wireless Commun. Summit*, Dresden, Germany, June 2005, paper no. 245.
- [MH06a] —, "Why linear MMSE detection is not necessarily superior to linear ZF detection," Mar. 2006, University of Kiel, unpublished.
- [MH06b] —, "Equivalence of spatially correlated and distributed MIMO systems," in *Proc. Int. ITG-IEEE Workshop on Smart Antennas (WSA)*, Castle Reinsburg, Günzburg, Germany, Mar. 2006.
- [MH06c] —, "Improving the performance of mobile broadcasting systems using multiple base stations and distributed space-time codes," *IEE Proc. Commun.*, accepted for publication, Nov. 2006.
- [MHKX06a] J. Mietzner, P. A. Hoeher, C. Krakowski, and W. Xu, "A robust receive diversity scheme for spatially correlated multiple-antenna systems using second-order channel statistics," in *Proc. Int. Symp. on Turbo Codes & Rel. Topics/ Int. ITG Conf. on Source and Channel Coding (SCC)*, Munich, Germany, Apr. 2006.
- [MHKX06b] —, "A statistical transmit power allocation scheme for spatially correlated MIMO systems and its robustness to estimation errors," in *Proc. World Wireless Congress (WWC)*, San Francisco, California, USA, May 2006.
- [MHS03a] J. Mietzner, P. A. Hoeher, and M. Sandell, "Compatible improvement of the GSM/EDGE system by means of space-time coding techniques," *IEEE Trans. Wireless Commun.*, vol. 2, no. 4, pp. 690–702, July 2003.
- [MHS03b] —, "Compatible improvement of the GSM/GPRS system by means of delay diversity," in *Proc. IEEE Int. Conf. Commun. (ICC)*, Anchorage, Alaska, USA, May 2003, pp. 1983–1987.

- [MHS03c] ———, “Compatible improvement of the GSM/GPRS system by means of space-time block codes,” in *Proc. IEEE Signal Processing Workshop on Signal Processing Adv. Wireless Commun. (SPAWC)*, Rome, Italy, June 2003, pp. 412–416.
- [MHSD05] Y. Mei, Y. Hua, A. Swami, and B. Daneshrad, “Combating synchronization errors in cooperative relays,” in *Proc. IEEE Int. Conf. Acoustics, Speech and Signal Processing (ICASSP)*, Philadelphia, Pennsylvania, USA, Mar. 2005, pp. 369–372.
- [MJSW02] J.-S. Maeng, I. S. Jin, W. Sung, and K.-C. Whang, “Modified performance criterion for space-time codes on fast fading channels,” *Electron. Letters*, vol. 38, no. 16, pp. 889–890, Aug. 2002.
- [MK06] M. A. Maddah-Ali and A. K. Khandani, “A new non-orthogonal space-time code with low decoding complexity,” *IEEE Trans. Wireless Commun.*, vol. 5, no. 5, pp. 1115–1121, May 2006.
- [MKH98] N. C. McGinty, R. A. Kennedy, and P. Hoeher, “Parallel trellis Viterbi algorithm for sparse channels,” *IEEE Commun. Lett.*, vol. 2, no. 5, pp. 143–145, May 1998.
- [MKH03] J. Mietzner, M. Kautza, and P. A. Hoeher, “Application of the Alamouti scheme in resilient microwave radio links,” *Electron. Letters*, vol. 39, no. 12, pp. 927–928, June 2003.
- [ML02] R. D. Murch and K. B. Letaief, “Antenna systems for broadband wireless access,” *IEEE Commun. Mag.*, vol. 40, no. 4, pp. 76–83, Apr. 2002.
- [ML03] P. Malm and B. Lindoff, “Theoretical analysis of a simple transmit diversity scheme,” in *Proc. IEEE Signal Processing Workshop on Signal Processing Adv. Wireless Commun. (SPAWC)*, Rome, Italy, June 2003, pp. 26–30.
- [MLTS97] J. G. Markoulidakis, G. L. Lyberopoulos, D. F. Tsirkas, and E. D. Sykas, “Mobility modeling in third-generation mobile telecommunications systems,” *IEEE Pers. Commun.*, vol. 4, no. 4, pp. 41–56, Aug. 1997.
- [MMA04] T. Miyano, H. Murata, and K. Araki, “Cooperative relaying scheme with space-time code for multihop communications among single antenna terminals,” in *Proc. IEEE Global Telecommun. Conf. (Globecom)*, Dallas, Texas, USA, Nov./Dec. 2004, pp. 3763–3767.
- [MMPL03] T. M. Minggiani, A. S. Madhukumar, A. B. Premkumar, and E. M.-K. Lai, “Frequency offset correction for space-time block coded OFDM systems based on maximum likelihood estimation,” in *Proc. Int. Conf. on Inform., Commun., and Signal Processing (ICICS)/ IEEE Pacific Rim Conf. on Multimedia (PCM)*, Singapore, Dec. 2003, pp. 926–929.
- [MO04] C. Martin and B. Ottersten, “Asymptotic eigenvalue distributions and capacity for MIMO channels under correlated fading,” *IEEE Trans. Wireless Commun.*, vol. 3, no. 4, pp. 1350–1359, July 2004.
- [MOP94] H. Meyr, M. Oerder, and A. Polydoros, “On sampling rate, analog prefiltering, and sufficient statistics for digital receivers,” *IEEE Trans. Commun.*, vol. 42, no. 12, pp. 3208–3213, Dec. 1994.

- [MP00a] S. Mudulodu and A. J. Paulraj, "A simple multiplexing scheme for MIMO systems using multiple spreading codes," in *Proc. Asilomar Conf. on Signals, Systems and Comput.*, Pacific Grove, California, USA, Oct./Nov. 2000, pp. 769–774.
- [MP00b] —, "A transmit diversity scheme for frequency selective fading channels," in *Proc. IEEE Global Telecommun. Conf. (Globecom)*, San Francisco, California, USA, Nov./Dec. 2000, pp. 1089–1093.
- [MPM04] T. M. Minggiani, A. B. Premkumar, and A. S. Madhukumar, "Performance investigation of STBC-OFDM systems with frequency offset and a semi-blind approach for the correction," in *Proc. IEEE Veh. Technol. Conf. (VTC-Spring)*, Genoa, Italy, May 2004, pp. 1836–1839.
- [MS05] A. Medles and D. T. Slock, "Linear precoding and DFE equalization achieve the diversity vs. multiplexing optimal tradeoff," in *Proc. IEEE Int. Conf. Acoustics, Speech and Signal Processing (ICASSP)*, Philadelphia, Pennsylvania, USA, Mar. 2005, pp. 421–424.
- [MSEA03] K. K. Mukkavilli, A. Sabharwal, E. Erkip, and B. Aazhang, "On beamforming with finite rate feedback in multiple-antenna systems," *IEEE Trans. Inform. Theory*, vol. 49, no. 10, pp. 2562–2579, Oct. 2003.
- [MTH04] J. Mietzner, R. Thobaben, and P. A. Hoeher, "Analysis of the expected error performance of cooperative wireless networks employing distributed space-time codes," in *Proc. IEEE Global Telecommun. Conf. (Globecom)*, Dallas, Texas, USA, Nov./Dec., 2004, pp. 2854–2858.
- [MTL05] Q. Ma, C. Tepedelenlioglu, and Z. Liu, "Differential space-time-frequency coded OFDM with maximum multipath diversity," *IEEE Trans. Wireless Commun.*, vol. 4, no. 5, pp. 2232–2243, Sept. 2005.
- [Mue02a] R. R. Mueller, "A random matrix model of communication via antenna arrays," *IEEE Trans. Inform. Theory*, vol. 48, no. 9, pp. 2495–2506, Sept. 2002.
- [Mue02b] S. H. Mueller-Weinfurtner, "Coding approaches for multiple antenna transmission in fast fading and OFDM," *IEEE Trans. Signal Processing*, vol. 50, no. 10, pp. 2442–2450, Oct. 2002.
- [MW03] A. Matache and R. D. Wesel, "Universal trellis codes for diagonally layered space-time systems," *IEEE Trans. Signal Processing*, vol. 51, no. 11, pp. 2773–2783, Nov. 2003.
- [MWC03] C.-S. Maa, Y.-C. Wang, and J.-T. Chen, "New design criteria of space-time codes for frequency-selective multipath wireless channels," in *Proc. IEEE Veh. Technol. Conf. (VTC-Spring)*, Jeju, Korea, Apr. 2003, pp. 1114–1118.
- [MWC04] —, "Structure-based water-filling algorithm in multipath MIMO channels," in *Proc. IEEE Int. Conf. Acoustics, Speech and Signal Processing (ICASSP)*, Montréal, Quebec, Canada, May 2004, pp. 317–320.
- [MWW02] A. F. Molisch, M. Z. Win, and J. H. Winters, "Space-time-frequency (STF) coding for MIMO-OFDM systems," *IEEE Commun. Lett.*, vol. 6, no. 9, pp. 370–372, Sept. 2002.

- [N00] “Nokia FlexiHopper microwave radio,” Nokia Networks, Product Overview C33513.21 H0, 2000.
- [Nak60] M. Nakagami, “The  $m$ -distribution – A general formula of intensity distribution of rapid fading,” in *Statistical Methods in Radio Wave Propagation*, New York: Pergamon, 1960, pp. 3–36.
- [NAP04] H. T. Nguyen, J. B. Andersen, and G. F. Pedersen, “Capacity and performance of MIMO systems under the impact of feedback delay,” in *Proc. IEEE Int. Symp. on Pers., Indoor, and Mobile Radio Commun. (PIMRC)*, Barcelona, Spain, Sept. 2004, pp. 53–57.
- [NBK04] R. U. Nabar, H. Boelcskei, and F. W. Kneubuehler, “Fading relay channels: Performance limits and space-time signal design,” *IEEE J. Select. Areas Commun.*, vol. 22, no. 6, pp. 1099–1109, Aug. 2004.
- [NBP01] R. U. Nabar, H. Boelcskei, and A. J. Paulraj, “Transmit optimization for spatial multiplexing in the presence of spatial fading correlation,” in *Proc. IEEE Global Telecommun. Conf. (Globecom)*, San Antonio, Texas, USA, Nov. 2001, pp. 131–135.
- [Ngu07] V. K. Nguyen, “A differential space-time modulation scheme for correlated Rayleigh fading channels: Performance analysis and design,” *IEEE Trans. Signal Processing*, vol. 55, no. 1, pp. 299–312, Jan. 2007.
- [NHH04] A. Nosratinia, T. E. Hunter, and A. Hedayat, “Cooperative communication in wireless networks,” *IEEE Commun. Mag.*, vol. 42, no. 10, pp. 74–80, Oct. 2004.
- [NM02] N. Nefedov and G. P. Mattellini, “Evaluation of potential transmit diversity schemes with iterative receivers in EDGE,” in *Proc. IEEE Int. Symp. on Pers., Indoor, and Mobile Radio Commun. (PIMRC)*, Pavilhao Atlantico, Lisboa, Portugal, Sept. 2002, pp. 2087–2091.
- [NMN06] T. Niyomsataya, A. Miri, and M. Nevins, “A new unitary space-time code with high diversity product,” *IEEE Trans. Wireless Commun.*, vol. 5, no. 11, pp. 3045–3049, Nov. 2006.
- [NS00] A. F. Naguib and N. Seshadri, “MLSE and equalization of space-time coded signals,” in *Proc. IEEE Veh. Technol. Conf. (VTC-Spring)*, Tokyo, Japan, May 2000, pp. 1688–1693.
- [NSC00] A. F. Naguib, N. Seshadri, and A. R. Calderbank, “Increasing data rate over wireless channels,” *IEEE Signal Processing Mag.*, vol. 17, no. 3, pp. 76–92, May 2000.
- [NSL04] S. H. Nam, O.-S. Shin, and K. B. Lee, “Transmit power allocation for a modified V-BLAST system,” *IEEE Trans. Commun.*, vol. 52, no. 7, pp. 1074–1079, July 2004.
- [NTC02] R. Negi, A. M. Tehrani, and J. M. Cioffi, “Adaptive antennas for space-time codes in outdoor channels,” *IEEE Trans. Commun.*, vol. 50, no. 12, pp. 1918–1925, Dec. 2002.

- [NTSC98] A. F. Naguib, V. Tarokh, N. Seshadri, and A. R. Calderbank, "A space-time coding modem for high-data-rate wireless communications," *IEEE J. Select. Areas Commun.*, vol. 16, no. 8, pp. 1459–1478, Oct. 1998.
- [OAA04] M. K. Oezdemir, E. Arvas, and H. Arslan, "Dynamics of spatial correlation and implications on MIMO systems," *IEEE Radio Commun.*, vol. 1, no. 2, pp. S14–S19, June 2004, supplement within the *IEEE Commun. Mag.*
- [OANA02] F. S. Ostuni, B. Abdool-Rassool, M. R. Nakhai, and H. Aghvami, "Layered space-time codes with iterative receiver and space-time soft-output decoding in a Rayleigh fading environment," in *Proc. IEEE Int. Symp. on Pers., Indoor, and Mobile Radio Commun. (PIMRC)*, Pavilhao Atlantico, Lisboa, Portugal, Sept. 2002, pp. 418–422.
- [OD02] E. N. Onggosanusi and A. G. Dabak, "A feedback-based adaptive multi-input multi-output signaling scheme," in *Proc. Asilomar Conf. on Signals, Systems and Comput.*, Pacific Grove, California, USA, Nov. 2002, pp. 1694–1698.
- [Ohn04] S. Ohno, "Impact of time-selective fading on orthogonal space-time block coding," in *Proc. IEEE Global Telecommun. Conf. (Globecom)*, Dallas, Texas, USA, Nov./Dec. 2004, pp. 2620–2624.
- [OHW+03] H. Oezcelik, M. Herdin, W. Weichselberger, J. Wallace, and E. Bonek, "Deficiencies of 'Kronecker' MIMO radio channel model," *Electron. Letters*, vol. 39, no. 16, pp. 1209–1210, Aug. 2003.
- [Oli99] M. W. Oliphant, "The mobile phone meets the Internet," *IEEE Spectrum*, vol. 36, no. 8, pp. 20–28, Aug. 1999.
- [OMH84] S. Ogose, K. Murota, and K. Hirade, "A transmitter diversity for MSK with two-bit differential detection," *IEEE Trans. Veh. Technol.*, vol. VT-33, no. 1, pp. 37–43, Feb. 1984.
- [PAK03] T. S. Pollock, T. D. Abhayapala, and R. A. Kennedy, "Antenna saturation effects on MIMO capacity," in *Proc. IEEE Int. Conf. Commun. (ICC)*, Anchorage, Alaska, USA, May 2003, pp. 2301–2305.
- [PBKM00] K. I. Pedersen, J. Bach Andersen, J. P. Kermoal, and P. E. Mogensen, "A stochastic multiple-input multiple-output radio channel model for evaluation of space-time coding algorithms," in *Proc. IEEE Veh. Technol. Conf. (VTC-Fall)*, Boston, Massachusetts, USA, Sept. 2000, pp. 893–897.
- [PF03] C. B. Papadias and G. J. Foschini, "Capacity-approaching space-time codes for systems employing four transmitter antennas," *IEEE Trans. Inform. Theory*, vol. 49, no. 3, pp. 726–732, Mar. 2003.
- [PFN+01] R. J. Piechocki, P. N. Fletcher, A. R. Nix, C. N. Canagarajah, and J. P. McGeehan, "Performance evaluation of BLAST-OFDM enhanced Hiperlan/2 using simulated and measured channel data," *Electron. Letters*, vol. 37, no. 18, pp. 1137–1139, Aug. 2001.

- [PG04] J. Park and S. B. Gelfand, "Turbo equalizations for sparse channels," in *Proc. IEEE Wireless Commun. and Networking Conf. (WCNC)*, Atlanta, Georgia, USA, Mar. 2004, pp. 2301–2306.
- [PGNB04] A. J. Paulraj, D. A. Gore, R. U. Nabar, and H. Boelcskei, "An overview of MIMO communications – A key to gigabit wireless," *Proc. IEEE*, vol. 92, no. 2, pp. 198–218, Feb. 2004.
- [PHK05] T. Pande, H. Huh, and J. V. Krogmeier, "Non-coherent demodulation for orthogonal space-time coded CPM," in *Proc. IEEE Veh. Technol. Conf. (VTC-Spring)*, Stockholm, Sweden, June 2005, pp. 1206–1209.
- [PJ05] O. Piirainen and M. Juntti, "Achievable data rates of frequency selective Rayleigh fading MIMO burst channels," in *Proc. IEEE Int. Symp. Inform. Theory (ISIT)*, Adelaide, Australia, Sept. 2005, pp. 775–779.
- [PK92] A. Paulraj and T. Kailath, *Increasing capacity in wireless broadcast systems using distributed transmission/directional reception*, Feb. 21, 1992, U.S. Patent 5 345 599.
- [PKB99] M. Precht, R. Kraft, and M. Bachmaier, *Angewandte Statistik 1*, 6th ed. München - Wien: Oldenbourg Verlag, 1999.
- [PL03] D. P. Palomar and M. A. Lagunas, "Joint transmit-receive space-time equalization in spatially correlated MIMO channels: A beamforming approach," *IEEE J. Select. Areas Commun.*, vol. 21, no. 5, pp. 730–743, June 2003.
- [PLWL06] L. Ping, L. Liu, K. Wu, and W. K. Leung, "Interleave division multiple-access," *IEEE Trans. Wireless Commun.*, vol. 5, no. 4, pp. 938–947, Apr. 2006.
- [PMF00] K. I. Pedersen, P. E. Mogensen, and B. H. Fleury, "A stochastic model of the temporal and azimuthal dispersion seen at the base station in outdoor propagation environments," *IEEE Trans. Veh. Technol.*, vol. 49, no. 2, pp. 437–447, Mar. 2000.
- [PMT01] R. J. Piechocki, J. P. McGeehan, and G. V. Tsoulos, "A new stochastic spatio-temporal propagation model (SSTPM) for mobile communications with antenna arrays," *IEEE Trans. Commun.*, vol. 49, no. 5, pp. 855–862, May 2001.
- [PN98] A. J. Paulraj and B. C. Ng, "Space-time modems for wireless personal communications," *IEEE Pers. Commun.*, vol. 5, no. 1, pp. 36–48, Feb. 1998.
- [PNG03] A. Paulraj, R. Nabar, and D. Gore, *Introduction to Space-Time Wireless Communications*. Cambridge University Press, 2003.
- [Pon99] S. Ponnekanti, "An overview of smart antenna technology for heterogeneous networks," *IEEE Commun. Surveys and Tutorials*, vol. 2, no. 4, pp. 14–23, Fourth Quarter 1999.
- [PP97] A. J. Paulraj and C. B. Papadias, "Space-time processing for wireless communications," *IEEE Signal Processing Mag.*, vol. 14, no. 6, pp. 49–83, Nov. 1997.
- [PPPL06] A. Pascual-Iserte, D. P. Palomar, A. I. Perez-Neira, and M. A. Lagunas, "A robust maximin approach for MIMO communications with imperfect channel state information based on convex optimization," *IEEE Trans. Signal Processing*, vol. 54, no. 1, pp. 346–360, Jan. 2006.



- [PPWL04] D. Pham, K. R. Pattipati, P. K. Willett, and J. Luo, "A generalized probabilistic data association detector for multiple antenna systems," *IEEE Commun. Lett.*, vol. 8, no. 4, pp. 205–207, Apr. 2004.
- [Pro01] J. G. Proakis, *Digital Communications*, 4th ed. New York: McGraw-Hill, 2001.
- [PSL03] S. Parker, M. Sandell, and M. Lee, "The performance of space-time codes in office environments," in *Proc. IEEE Veh. Technol. Conf. (VTC-Spring)*, Jeju, Korea, Apr. 2003, pp. 741–745.
- [PSL04] S. Park, H. Shin, and J. H. Lee, "Capacity statistics and scheduling gain for MIMO systems in correlated Rayleigh fading," in *Proc. IEEE Veh. Technol. Conf. (VTC-Fall)*, Los Angeles, California, USA, Sept. 2004, pp. 1508–1512.
- [PSY+04] S. Parker, M. Sandell, M. S. Yee, Y. Sun, M. Ismail, P. Strauch, and J. McGeehan, "Space-time codes for future WLANs: Principles, practice, and performance," *IEEE Commun. Mag.*, vol. 42, no. 12, pp. 96–103, Dec. 2004.
- [PV01] N. Prasad and M. K. Varanasi, "Optimum efficiently decodable layered space-time block codes," in *Proc. Asilomar Conf. on Signals, Systems and Comput.*, Pacific Grove, California, USA, Nov. 2001, pp. 227–231.
- [PV05a] F. Pancaldi and G. M. Vitetta, "Frequency-domain equalization for space-time block coded systems," *IEEE Trans. Wireless Commun.*, vol. 4, no. 6, pp. 2907–2916, Nov. 2005.
- [PV05b] ———, "Space-time block codes for noncoherent CPFSK," in *Proc. IEEE Global Telecommun. Conf. (Globecom)*, St. Louis, Missouri, USA, Nov./Dec. 2005, pp. 3043–3047.
- [PWS+04] R. Pabst, B. H. Walke, D. C. Schultz, P. Herhold, H. Yanikomeroglu, S. Mukherjee, H. Viswanathan, M. Lott, W. Zirwas, M. Dohler, H. Aghvami, D. D. Falconer, and G. P. Fettweis, "Relay-based deployment concepts for wireless and mobile broadband radio," *IEEE Commun. Mag.*, vol. 42, no. 9, pp. 80–89, Sept. 2004.
- [PZS04] L. Ping, L. Zhang, and H. C. So, "On a hybrid beamforming/space-time coding scheme," *IEEE Commun. Lett.*, vol. 8, no. 1, pp. 15–17, Jan. 2004.
- [QB04] M. Qin and R. S. Blum, "Properties of space-time codes for frequency-selective channels," *IEEE Trans. Signal Processing*, vol. 52, no. 3, pp. 694–702, Mar. 2004.
- [RABT02] T. S. Rappaport, A. Annamalai, R. M. Buehrer, and W. H. Tranter, "Wireless communications: Past events and a future perspective," *IEEE Commun. Mag. – 50th Anniversary Commemorative Issue*, pp. 148–161, May 2002.
- [Rad22] J. Radon, "Lineare Scharen orthogonaler Matrizen," *Abh. Mathem. Sem. d. Hamburgischen Universität*, vol. I, pp. 1–14, 1922.
- [Rap96] T. S. Rappaport, *Wireless Communications – Principles and Practice*. Upper Saddle River (NJ): Prentice-Hall, 1996.



- [RB03] A. A. Rontogiannis and K. Berberidis, "Efficient decision feedback equalization for sparse wireless channels," *IEEE Trans. Wireless Commun.*, vol. 2, no. 3, pp. 570–581, May 2003.
- [RC98] G. G. Raleigh and J. M. Cioffi, "Spatio-temporal coding for wireless communication," *IEEE Trans. Commun.*, vol. 46, no. 3, pp. 357–366, Mar. 1998.
- [RCG05] A. Ribeiro, X. Cai, and G. B. Giannakis, "Symbol error probabilities for general cooperative links," *IEEE Trans. Wireless Commun.*, vol. 4, no. 3, pp. 1264–1273, May 2005.
- [RG02] S. Rouquette-Leveil and K. Gosse, "Space-time coding options for OFDM-based WLANs," in *Proc. IEEE Veh. Technol. Conf. (VTC-Spring)*, Birmingham, Alabama, USA, May 2002, pp. 904–908.
- [RHH95] P. A. Ranta, A. Hottinen, and Z.-C. Honkasalo, "Co-channel interference cancelling receiver for TDMA mobile systems," in *Proc. IEEE Int. Conf. Commun. (ICC)*, Seattle, Washington, USA, June 1995, pp. 17–21.
- [RHV97] P. Robertson, P. Hoeher, and E. Villebrun, "Optimal and sub-optimal maximum a posteriori algorithms suitable for turbo decoding," *Europ. Trans. Telecommun.*, vol. 8, no. 2, pp. 119–125, Mar./Apr 1997.
- [Ric48] S. O. Rice, "Statistical properties of a sine wave plus random noise," *Bell Syst. Tech. J.*, vol. 27, pp. 109–157, Jan. 1948.
- [RJ99] G. G. Raleigh and V. K. Jones, "Multivariate modulation and coding for wireless communication," *IEEE J. Select. Areas Commun.*, vol. 17, no. 5, pp. 851–866, May 1999.
- [RK89] R. Roy and T. Kailath, "ESPRIT – Estimation of signal parameters via rotational invariance techniques," *IEEE Trans. Acoustics, Speech and Signal Processing*, vol. 37, no. 7, pp. 984–995, July 1989.
- [RR04] J. C. Roh and B. D. Rao, "Multiple antenna channels with partial channel state information at the transmitter," *IEEE Trans. Wireless Commun.*, vol. 3, no. 2, pp. 677–688, Mar. 2004.
- [RR06a] —, "Design and analysis of MIMO spatial multiplexing systems with quantized feedback," *IEEE Trans. Signal Processing*, vol. 54, no. 8, pp. 2874–2886, Aug. 2006.
- [RR06b] —, "Transmit beamforming in multiple-antenna systems with finite rate feedback: A VQ-based approach," *IEEE Trans. Inform. Theory*, vol. 52, no. 3, pp. 1101–1112, Mar. 2006.
- [RS03] V. Raghavan and A. M. Sayeed, "MIMO capacity scaling and saturation in correlated environments," in *Proc. IEEE Int. Conf. Commun. (ICC)*, Anchorage, Alaska, USA, May 2003, pp. 3006–3010.
- [RSB05] V. Raghavan, A. M. Sayeed, and N. Boston, "When is limited feedback for transmit beamforming beneficial?" in *Proc. IEEE Int. Symp. Inform. Theory (ISIT)*, Adelaide, Australia, Sept. 2005, pp. 1544–1548.

- [RV05] T. Ratnarajah and R. Vaillancourt, "Quadratic forms on complex random matrices and multiple-antenna systems," *IEEE Trans. Inform. Theory*, vol. 51, no. 8, pp. 2976–2984, Aug. 2005.
- [RVA03] T. Ratnarajah, R. Vaillancourt, and M. Alvo, "Complex random matrices and Rayleigh channel capacity," *Communications in Information and Systems*, vol. 3, no. 2, pp. 119–138, Oct. 2003.
- [RW05] D. Rende and T. F. Wong, "Bit-interleaved space-frequency coded modulation for OFDM systems," *IEEE Trans. Wireless Commun.*, vol. 4, no. 5, pp. 2256–2266, Sept. 2005.
- [RWM93] S. A. Raghavan, J. K. Wolf, and L. B. Milstein, "On the performance evaluation of ISI channels," *IEEE Trans. Inform. Theory*, vol. 39, no. 3, pp. 957–965, May 1993.
- [RZC04] G. Ren, H. Zhang, and Y. Chang, "A novel scheme for space-time block coding with a variable transmit diversity gain in OFDM systems," *IEEE Trans. Consumer Electron.*, vol. 50, no. 2, pp. 478–483, May 2004.
- [SA00] M. K. Simon and M.-S. Alouini, *Digital Communication over Fading Channels: A Unified Approach to Performance Analysis*. John Wiley & Sons, 2000.
- [SAB06] M. Shamsi, M. Ardakani, and I. F. Blake, "Mixed-Q linear space-time codes," *IEEE Trans. Commun.*, vol. 54, no. 5, pp. 849–857, May 2006.
- [San03] M. Sandell, "Nonlinear space-time block codes designed for iterative decoding," *Electron. Letters*, vol. 39, no. 20, pp. 1453–1455, Oct. 2003.
- [Say02] A. M. Sayeed, "Deconstructing multiantenna fading channels," *IEEE Trans. Signal Processing*, vol. 50, no. 10, pp. 2563–2579, Oct. 2002.
- [SB02] N. D. Sidiropoulos and R. S. Budampati, "Khatri-Rao space-time codes," *IEEE Trans. Signal Processing*, vol. 50, no. 10, pp. 2396–2407, Oct. 2002.
- [SB05] G. Scutari and S. Barbarossa, "Distributed space-time-coding for regenerative relay networks," *IEEE Trans. Wireless Commun.*, vol. 4, no. 5, pp. 2387–2399, Sept. 2005.
- [SBEM90] S. C. Swales, M. A. Beach, D. J. Edwards, and J. P. McGeehan, "The performance enhancement of multibeam adaptive base-station antennas for cellular land mobile radio systems," *IEEE Trans. Veh. Technol.*, vol. 39, no. 1, pp. 56–67, Feb. 1990.
- [SBF01] M. Stege, M. Bronzel, and G. Fettweis, "On the performance of space-time block codes," in *Proc. IEEE Veh. Technol. Conf. (VTC-Spring)*, Rhodes, Greece, May 2001, pp. 2282–2286.
- [SBM+04] G. L. Stuber, J. R. Barry, S. W. McLaughlin, Y. Li, M. A. Ingram, and T. G. Pratt, "Broadband MIMO-OFDM wireless communications," *Proc. IEEE*, vol. 92, no. 2, pp. 271–294, Feb. 2004.

- [SBV02] P. J. Sartori, K. L. Baum, and F. W. Vook, "Impact of spatial correlation on the spectral efficiency of wireless OFDM systems using multiple antenna techniques," in *Proc. IEEE Veh. Technol. Conf. (VTC-Spring)*, Birmingham, Alabama, USA, May 2002, pp. 1150–1154.
- [SC06] D. K. C. So and R. S. Cheng, "Achievable diversity order by space-time trellis coding combined with MLED and OFDM over frequency selective fading channels," *IEEE Trans. Wireless Commun.*, vol. 5, no. 6, pp. 1217–1222, June 2006.
- [SCG04] R. Schober, H. Z. B. Chen, and W. H. Gerstacker, "Decision-feedback sequence estimation for time-reversal space-time block-coded transmission," *IEEE Trans. Veh. Technol.*, vol. 53, no. 4, pp. 1273–1278, July 2004.
- [Sch86] R. Schmidt, "Multiple emitter location and signal parameter estimation," *IEEE Trans. Antennas Propagat.*, vol. 34, no. 3, pp. 276–280, Mar. 1986.
- [Sch06] H. Schoeneich, personal communication, University of Kiel, Germany, Feb. 2006.
- [SD03] A. Stefanov and T. M. Duman, "Performance bounds for space-time trellis codes," *IEEE Trans. Inform. Theory*, vol. 49, no. 9, pp. 2134–2140, Sept. 2003.
- [SDL05] S. Sfar, L. Dai, and K. B. Letaief, "Optimal diversity-multiplexing tradeoff with group detection for MIMO systems," *IEEE Trans. Commun.*, vol. 53, no. 7, pp. 1178–1190, July 2005.
- [SE94] C. P. Schnorr and M. Euchner, "Lattice basis reduction: Improved practical algorithms and solving subset sum problems," *Math. Programm.*, vol. 66, pp. 181–191, 1994.
- [SE04] A. Stefanov and E. Erkip, "Cooperative coding for wireless networks," *IEEE Trans. Commun.*, vol. 52, no. 9, pp. 1470–1476, Sept. 2004.
- [SE05] ———, "Cooperative space-time coding for wireless networks," *IEEE Trans. Commun.*, vol. 53, no. 11, pp. 1804–1809, Nov. 2005.
- [SEA03] A. Sendonaris, E. Erkip, and B. Aazhang, "User cooperation diversity – Part I: System description; Part II: Implementation aspects and performance analysis," *IEEE Trans. Commun.*, vol. 51, no. 11, pp. 1927–1938, 1939–1948, Nov. 2003.
- [See03] R. Seeger, personal communication, University of Bremen, Germany, Sept. 2003.
- [SF03a] M. Sellathurai and G. J. Foschini, "Stratified diagonal layered space-time architectures: Signal processing and information theoretic aspects," *IEEE Trans. Signal Processing*, vol. 51, no. 11, pp. 2943–2954, Nov. 2003.
- [SF03b] M. Stege and G. Fettweis, "Multistratum-permutation codes for MIMO communication," *IEEE J. Select. Areas Commun.*, vol. 21, no. 5, pp. 774–782, June 2003.
- [SFGK00] D.-S. Shiu, G. J. Foschini, M. J. Gans, and J. M. Kahn, "Fading correlation and its effect on the capacity of multielement antenna systems," *IEEE Trans. Commun.*, vol. 48, no. 3, pp. 502–512, Mar. 2000.

- [SG03] C. Schlegel and A. Grant, "Differential space-time turbo codes," *IEEE Trans. Inform. Theory*, vol. 49, no. 9, pp. 2298–2306, Sept. 2003.
- [SGG05] S. Shahbazpanahi, A. B. Gershman, and G. B. Giannakis, "Joint blind channel and carrier frequency offset estimation in orthogonally space-time block coded MIMO systems," in *Proc. IEEE Workshop on Signal Processing Adv. Wireless Commun. (SPAWC)*, New York City, New York, USA, June 2005, pp. 363–367.
- [SGGP99] K. Sheikh, D. Gesbert, D. Gore, and A. Paulraj, "Smart antennas for broadband wireless access networks," *IEEE Commun. Mag.*, vol. 37, no. 11, pp. 100–105, Nov. 1999.
- [SGL04] R. Schober, W. H. Gerstacker, and L. H.-J. Lampe, "Performance analysis and design of STBCs for frequency-selective fading channels," *IEEE Trans. Wireless Commun.*, vol. 3, no. 3, pp. 734–744, May 2004.
- [SH02] M. Sellathurai and S. Haykin, "TURBO-BLAST for wireless communications: Theory and experiments," *IEEE Trans. Signal Processing*, vol. 50, no. 10, pp. 2538–2546, Oct. 2002.
- [SH03a] W. Santipach and M. L. Honig, "Asymptotic performance of MIMO wireless channels with limited feedback," in *Proc. IEEE Military Commun. Conf. (MILCOM)*, Monterey, California, USA, Oct. 2003, pp. 141–146.
- [SH03b] M. Sellathurai and S. Haykin, "T-BLAST for wireless communications: First experimental results," *IEEE Trans. Veh. Technol.*, vol. 52, no. 3, pp. 530–535, May 2003.
- [Sha48] C. E. Shannon, "A mathematical theory of communication – Part I & II," *Bell Syst. Tech. J.*, vol. 27, pp. 379–423, 623–656, July/Oct. 1948.
- [SHHS01] A. Shokrollahi, B. Hassibi, B. M. Hochwald, and W. Sweldens, "Representation theory for high-rate multiple-antenna code design," *IEEE Trans. Inform. Theory*, vol. 47, no. 6, pp. 2335–2367, Sept. 2001.
- [SHP01] R. Srinivasan, M. J. Heikkila, and R. Pirhonen, "Performance evaluation of space-time coding for EDGE," in *Proc. IEEE Int. Conf. Commun. (ICC)*, Helsinki, Finland, June 2001, pp. 3056–3060.
- [Sik05] T. Sikora, "Trends and perspectives in image and video coding," *Proc. IEEE*, vol. 93, no. 1, pp. 6–17, Jan. 2005.
- [SJ05] A. Sezgin and E. A. Jorswieck, "Capacity achieving high rate space-time block codes," *IEEE Commun. Lett.*, vol. 9, no. 5, pp. 435–437, May 2005.
- [SKKY04] H.-K. Song, S.-J. Kang, M.-J. Kim, and Y.-H. You, "Error performance analysis of STBC-OFDM systems with parameter imbalances," *IEEE Trans. Broadcasting*, vol. 50, no. 1, pp. 76–82, Mar. 2004.
- [SKL04] M. A. Sadrabadi, A. K. Khandani, and F. Lahouti, "A new method of channel feedback quantization for high data rate MIMO systems," in *Proc. IEEE Global Telecommun. Conf. (Globecom)*, Dallas, Texas, USA, Nov./Dec. 2004, pp. 91–95.

- [SL01] P. Stoica and E. Lindskog, "Space-time block coding for channels with intersymbol interference," in *Proc. Asilomar Conf. on Signals, Systems and Comput.*, Pacific Grove, California, USA, Nov. 2001, pp. 252–256.
- [SL02a] Z. Safar and K. J. R. Liu, "Space-time trellis code construction for fast fading channels," in *Proc. IEEE Int. Conf. Commun. (ICC)*, New York City, New York, USA, May 2002, pp. 563–567.
- [SL02b] R. Schober and L. H.-J. Lampe, "Differential modulation diversity," *IEEE Trans. Veh. Technol.*, vol. 51, no. 6, pp. 1431–1444, Nov. 2002.
- [SL02c] —, "Noncoherent receivers for differential space-time modulation," *IEEE Trans. Commun.*, vol. 50, no. 5, pp. 768–777, May 2002.
- [SL02d] H. Shin and J. H. Lee, "Exact symbol error probability of orthogonal space-time block codes," in *Proc. IEEE Global Telecommun. Conf. (Globecom)*, Taipei, Taiwan, R.O.C., Nov. 2002, pp. 1197–1201.
- [SL02e] —, "Upper bound on the error probability for space-time codes in fast fading," in *Proc. IEEE Veh. Technol. Conf. (VTC-Fall)*, Vancouver, British Columbia, Canada, Sept. 2002, pp. 243–246.
- [SL03] —, "Capacity of multiple-antenna fading channels: Spatial fading correlation, double scattering, and keyhole," *IEEE Trans. Inform. Theory*, vol. 49, no. 10, pp. 2636–2647, Oct. 2003.
- [SLSL05] C. K. Sung, H. Lee, H. Song, and I. Lee, "Decision feedback detection with error compensation for hybrid space-time block codes," *IEEE Commun. Lett.*, vol. 9, no. 10, pp. 882–884, Oct. 2005.
- [SN04] S. Sanayei and A. Nosratinia, "Antenna selection in MIMO systems," *IEEE Commun. Mag.*, vol. 42, no. 10, pp. 68–73, Oct. 2004.
- [SNK04] C. Shan, A. Nallanathan, and P. Y. Kam, "A new class of signal constellations for differential unitary space-time modulation (DUSTM)," *IEEE Commun. Lett.*, vol. 8, no. 1, pp. 1–3, Jan. 2004.
- [SNK05] T. P. Soh, C. S. Ng, and P. Y. Kam, "Improved signal constellations for differential unitary space-time modulations with more than two antennas," *IEEE Commun. Lett.*, vol. 9, no. 1, pp. 7–9, Jan. 2005.
- [SO02a] Y. Sasazaki and T. Ohtsuki, "Improved design criteria and new trellis codes on space-time trellis coded modulation in fast fading channels," in *Proc. IEEE Global Telecommun. Conf. (Globecom)*, Taipei, Taiwan, R.O.C., Nov. 2002, pp. 1103–1107.
- [SO02b] K. Suto and T. Ohtsuki, "Performance evaluation of space-time-frequency block codes over frequency selective fading channels," in *Proc. IEEE Veh. Technol. Conf. (VTC-Fall)*, Vancouver, British Columbia, Canada, Sept. 2002, pp. 1466–1470.
- [Soh03] I. Sohn, "Space frequency block coded turbo-BLAST detection for MIMO-OFDM systems," *Electron. Letters*, vol. 39, no. 21, pp. 1557–1558, Oct. 2003.

- [SP00] S. Sandhu and A. Paulraj, "Space-time block codes: A capacity perspective," *IEEE Commun. Lett.*, vol. 4, no. 12, pp. 384–386, Dec. 2000.
- [SP02] H. Sampath and A. Paulraj, "Linear precoding for space-time coded systems with known fading correlations," *IEEE Commun. Lett.*, vol. 6, no. 6, pp. 239–241, June 2002.
- [SP03] N. Sharma and C. B. Papadias, "Improved quasi-orthogonal codes through constellation rotation," *IEEE Trans. Commun.*, vol. 51, no. 3, pp. 332–335, Mar. 2003.
- [SP04] —, "Full-rate full-diversity linear quasi-orthogonal space-time codes for any number of transmit antennas," *EURASIP J. Applied Signal Processing*, vol. 2004, no. 9, pp. 1246–1256, Aug. 2004.
- [Spa94] A. S. Spanias, "Speech coding: A tutorial review," *Proc. IEEE*, vol. 82, no. 10, pp. 1541–1582, Oct. 1994.
- [SPS02] A. Steiner, M. Peleg, and S. Shamai, "Iterative decoding of space-time differentially coded unitary matrix modulation," *IEEE Trans. Signal Processing*, vol. 50, no. 10, pp. 2385–2395, Oct. 2002.
- [SPS03a] —, "SVD iterative decision feedback demodulation and detection of coded space-time unitary differential modulation," *IEEE Trans. Inform. Theory*, vol. 49, no. 10, pp. 2648–2657, Oct. 2003.
- [SPS03b] —, "SVD iterative detection of turbo-coded multiantenna unitary differential modulation," *IEEE Trans. Commun.*, vol. 51, no. 3, pp. 441–452, Mar. 2003.
- [SPSH04] Q. H. Spencer, C. B. Peel, A. L. Swindlehurst, and M. Haardt, "An introduction to the multi-user MIMO downlink," *IEEE Commun. Mag.*, vol. 42, no. 10, pp. 60–67, Oct. 2004.
- [SR05] L. Shao and S. Roy, "Rate-one space-frequency block codes with maximum diversity for MIMO-OFDM," *IEEE Trans. Wireless Commun.*, vol. 4, no. 4, pp. 1674–1687, July 2005.
- [SRK04a] V. Shashidhar, B. S. Rajan, and P. V. Kumar, "Asymptotic-information-lossless designs and diversity-multiplexing tradeoff," in *Proc. IEEE Global Telecommun. Conf. (Globecom)*, Dallas, Texas, USA, Nov./Dec. 2004, pp. 366–370.
- [SRK04b] —, "STBCs with optimal diversity-multiplexing tradeoff for 2, 3 and 4 transmit antennas," in *Proc. IEEE Int. Symp. Inform. Theory (ISIT)*, Chicago, Illinois, USA, June/July 2004, p. 125.
- [SRS03] B. A. Sethuraman, B. S. Rajan, and V. Shashidhar, "Full-diversity, high-rate space-time block codes from division algebras," *IEEE Trans. Inform. Theory*, vol. 49, no. 10, pp. 2596–2616, Oct. 2003.
- [SS03] O. Simeone and U. Spagnolini, "Combined linear pre-equalization and BLAST equalization with channel correlation feedback," *IEEE Commun. Lett.*, vol. 7, no. 10, pp. 487–489, Oct. 2003.



- [SS06] A. Slaney and Y. Sun, "Space-time coding for wireless communications: An overview," *IEE Proc. Commun.*, vol. 153, no. 4, pp. 509–518, Aug. 2006.
- [SSL04] W. Su, Z. Safar, and K. J. R. Liu, "Diversity analysis of space-time modulation over time-correlated Rayleigh-fading channels," *IEEE Trans. Inform. Theory*, vol. 50, no. 8, pp. 1832–1840, Aug. 2004.
- [SSL05a] A.-M. Silvester, R. Schober, and L. Lampe, "Burst-based orthogonal ST block coding for CPM," in *Proc. IEEE Global Telecommun. Conf. (Globecom)*, St. Louis, Missouri, USA, Nov./Dec. 2005, pp. 3159–3163.
- [SSL05b] W. Su, Z. Safar, and K. J. R. Liu, "Full-rate full-diversity space-frequency codes with optimum coding advantage," *IEEE Trans. Inform. Theory*, vol. 51, no. 1, pp. 229–249, Jan. 2005.
- [SSL05c] ———, "Towards maximum achievable diversity in space, time, and frequency: Performance analysis and code design," *IEEE Trans. Wireless Commun.*, vol. 4, no. 4, pp. 1847–1857, July 2005.
- [SSL06] A. K. Sadek, W. Su, and K. J. R. Liu, "Diversity analysis for frequency-selective MIMO-OFDM systems with general spatial and temporal correlation model," *IEEE Trans. Commun.*, vol. 54, no. 5, pp. 878–888, May 2006.
- [SSOL03] W. Su, Z. Safar, M. Olfat, and K. J. R. Liu, "Obtaining full-diversity space-frequency codes from space-time codes via mapping," *IEEE Trans. Signal Processing*, vol. 51, no. 11, pp. 2905–2916, Nov. 2003.
- [SSOL06] W. P. Siritwongpairat, W. Su, M. Olfat, and K. J. R. Liu, "Multiband-OFDM MIMO coding framework for UWB communication systems," *IEEE Trans. Signal Processing*, vol. 54, no. 1, pp. 214–224, Jan. 2006.
- [SSP01] H. Sampath, P. Stoica, and A. Paulraj, "Generalized linear precoder and decoder design for MIMO channels using the weighted MMSE criterion," *IEEE Trans. Commun.*, vol. 49, no. 12, pp. 2198–2206, Dec. 2001.
- [SSPH06] C. E. D. Sterian, H. Singh, M. Patzold, and B. O. Hogstad, "Super-orthogonal space-time codes with rectangular constellations and two transmit antennas for high data rate wireless communications," *IEEE Trans. Wireless Commun.*, vol. 5, no. 7, pp. 1857–1865, July 2006.
- [SSX99] S. Souissi, S. Sek, and H. Xie, "The effect of frequency offsets on the performance of FLEX<sup>®</sup> simulcast systems," in *Proc. IEEE Veh. Technol. Conf. (VTC)*, Houston, Texas, USA, May 1999, pp. 2348 – 2352.
- [Ste94] R. Steele, Ed., *Mobile Radio Communications*. New York: IEEE Press, 1994.
- [STT+02] H. Sampath, S. Talwar, J. Tellado, V. Erceg, and A. Paulraj, "A fourth-generation MIMO-OFDM broadband wireless system: Design, performance, and field trial results," *IEEE Commun. Mag.*, vol. 40, no. 9, pp. 143–149, Sept. 2002.
- [Stu96] G. L. Stueber, *Principles of Mobile Communications*. Norwell (MA): Kluwer Academic Publishers, 1996.



- [Suz77] H. Suzuki, "A statistical model for urban radio propagation," *IEEE Trans. Commun.*, vol. COM-25, no. 7, pp. 673–680, July 1977.
- [SW93] N. Seshadri and J. H. Winters, "Two signaling schemes for improving the error performance of frequency-division-duplex (FDD) transmission systems using transmitter antenna diversity," in *Proc. IEEE Veh. Technol. Conf. (VTC)*, Secaucus, New Jersey, USA, May 1993, pp. 508–511.
- [SW02] H. Stark and J. W. Woods, *Probability and Random Processes with Applications to Signal Processing*, 3rd ed. Upper Saddle River (NJ): Prentice-Hall, 2002.
- [SWSX04] A. Song, G. Wang, W. Su, and X.-G. Xia, "Unitary space-time codes from Alamouti's scheme with APSK signals," *IEEE Trans. Wireless Commun.*, vol. 3, no. 6, pp. 2374–2384, Nov. 2004.
- [SWX05] A. Song, G. Wang, and X.-G. Xia, "Some super-orthogonal space-time trellis codes based on non-PSK MTCM," *IEEE Trans. Wireless Commun.*, vol. 4, no. 3, pp. 1214–1221, May 2005.
- [SX03] W. Su and X.-G. Xia, "Two generalized complex orthogonal space-time block codes of rates 7/11 and 3/5 for 5 and 6 transmit antennas," *IEEE Trans. Inform. Theory*, vol. 49, no. 1, pp. 313–316, Jan. 2003.
- [SX04a] A. Song and X.-G. Xia, "Decision feedback differential detection for differential orthogonal space-time modulation with APSK signals over flat-fading channels," *IEEE Trans. Wireless Commun.*, vol. 3, no. 6, pp. 1873–1878, Nov. 2004.
- [SX04b] W. Su and X.-G. Xia, "Signal constellations for quasi-orthogonal space-time block codes with full diversity," *IEEE Trans. Inform. Theory*, vol. 50, no. 10, pp. 2331–2347, Oct. 2004.
- [SXL04] W. Su, X.-G. Xia, and K. J. R. Liu, "A systematic design of high-rate complex orthogonal space-time block codes," *IEEE Commun. Lett.*, vol. 8, no. 6, pp. 380–382, June 2004.
- [SZDZ03] C. Shen, H. Zhuang, L. Dai, and S. Zhou, "Detection algorithm improving V-BLAST performance over error propagation," *Electron. Letters*, vol. 39, no. 13, pp. 1007–1008, June 2003.
- [SZG02] A. Stamoulis, L. Zhigiang, and G. B. Giannakis, "Space-time block-coded OFDMA with linear precoding for multirate services," *IEEE Trans. Signal Processing*, vol. 50, no. 1, pp. 119–129, Jan. 2002.
- [Tao06] M. Tao, "High rate trellis coded differential unitary space-time modulation via super unitarity," *IEEE Trans. Wireless Commun.*, vol. 5, no. 12, pp. 3350–3354, Dec. 2006.
- [TC01] M. Tao and R. S. Cheng, "Improved design criteria and new trellis codes for space-time coded modulation in slow flat fading channels," *IEEE Commun. Lett.*, vol. 5, no. 7, pp. 313–315, July 2001.
- [TC03] —, "Trellis-coded differential unitary space-time modulation over flat fading channels," *IEEE Trans. Commun.*, vol. 51, no. 4, pp. 587–596, Apr. 2003.

- [TC04a] ———, “Diagonal block space-time code design for diversity and coding advantage,” *IEEE Trans. Signal Processing*, vol. 52, no. 4, pp. 1012–1020, Apr. 2004.
- [TC04b] ———, “Generalized layered space-time codes for high data rate wireless communications,” *IEEE Trans. Wireless Commun.*, vol. 3, no. 4, pp. 1067–1075, July 2004.
- [Tel95] E. Telatar, “Capacity of multi-antenna Gaussian channels,” Oct. 1995, Technical memorandum, Bell Labs.
- [Tel99] ———, “Capacity of multi-antenna Gaussian channels,” *Europ. Trans. Telecommun.*, vol. 10, no. 6, pp. 585–595, Nov./Dec. 1999.
- [ten01] S. ten Brink, “Convergence behavior of iteratively decoded parallel concatenated codes,” *IEEE Trans. Commun.*, vol. 49, no. 10, pp. 1727–1737, Oct. 2001.
- [TH00] O. Tirkkonen and A. Hottinen, “Complex space-time block codes for four Tx antennas,” in *Proc. IEEE Global Telecommun. Conf. (Globecom)*, San Francisco, California, USA, Nov./Dec. 2000, pp. 1005–1009.
- [TH02] ———, “Square-matrix embeddable space-time block codes for complex signal constellations,” *IEEE Trans. Inform. Theory*, vol. 48, no. 2, pp. 384–395, Feb. 2002.
- [TJ00] V. Tarokh and H. Jafarkhani, “A differential detection scheme for transmit diversity,” *IEEE J. Select. Areas Commun.*, vol. 18, no. 7, pp. 1169–1174, July 2000.
- [TJC99a] V. Tarokh, H. Jafarkhani, and A. R. Calderbank, “Space-time block codes from orthogonal designs,” *IEEE Trans. Inform. Theory*, vol. 45, no. 5, pp. 1456–1467, July 1999.
- [TJC99b] ———, “Space-time block coding for wireless communications: Performance results,” *IEEE J. Select. Areas Commun.*, vol. 17, no. 3, pp. 451–460, Mar. 1999.
- [TJJG03] L. Tao, L. Jianfeng, H. Jianjun, and Y. Guangxin, “Performance analysis for orthogonal space-time block codes in the absence of perfect channel state information,” in *Proc. IEEE Int. Symp. on Pers., Indoor, and Mobile Radio Commun. (PIMRC)*, Beijing, China, Sept. 2003, pp. 1012–1016.
- [TJL01] D. Tujkovic, M. Juntti, and M. Latva-Aho, “Space-frequency-time turbo coded modulation,” *IEEE Commun. Lett.*, vol. 5, no. 12, pp. 480–482, Dec. 2001.
- [tK03] S. ten Brink and G. Kramer, “Design of repeat-accumulate codes for iterative detection and decoding,” *IEEE Trans. Signal Processing*, vol. 51, no. 11, pp. 2764–2772, Nov. 2003.
- [tKA04] S. ten Brink, G. Kramer, and A. Ashikhmin, “Design of low-density parity-check codes for modulation and detection,” *IEEE Trans. Commun.*, vol. 52, no. 4, pp. 670–678, Apr. 2004.
- [TLB05] M. Tan, Z. Latinovic, and Y. Bar-Ness, “STBC MIMO-OFDM peak-to-average power ratio reduction by cross-antenna rotation and inversion,” *IEEE Commun. Lett.*, vol. 9, no. 7, pp. 592–594, July 2005.

- [TNSC99a] V. Tarokh, A. Naguib, N. Seshadri, and A. R. Calderbank, "Combined array processing and space-time coding," *IEEE Trans. Inform. Theory*, vol. 45, no. 4, pp. 1121–1128, May 1999.
- [TNSC99b] —, "Space-time codes for high data rate wireless communication: Performance criteria in the presence of channel estimation errors, mobility, and multiple paths," *IEEE Trans. Commun.*, vol. 47, no. 2, pp. 199–207, Feb. 1999.
- [Ton00] A. M. Tonello, "Space-time bit-interleaved coded modulation with an iterative decoding strategy," in *Proc. IEEE Veh. Technol. Conf. (VTC-Fall)*, Boston, Massachusetts, USA, Sept. 2000, pp. 473–478.
- [TSC98] V. Tarokh, N. Seshadri, and A. R. Calderbank, "Space-time codes for high data rate wireless communication: Performance criterion and code construction," *IEEE Trans. Inform. Theory*, vol. 44, no. 2, pp. 744–765, Mar. 1998.
- [TSW+04] L. C. Tran, J. Seberry, Y. Wang, B. J. Wysocki, T. A. Wysocki, T. Xia, and Y. Zhao, "Two complex orthogonal space-time codes for eight transmit antennas," *Electron. Letters*, vol. 40, no. 1, pp. 55–57, Jan. 2004.
- [TV04a] S. Tavildar and P. Viswanath, "Permutation codes: Achieving the diversity-multiplexing tradeoff," in *Proc. IEEE Int. Symp. Inform. Theory (ISIT)*, Chicago, Illinois, USA, June/July 2004, p. 616.
- [TV04b] A. M. Tulino and S. Verdu, *Random Matrix Theory and Wireless Communications*. Hanover (MA) - Delft: now Publishers Inc., 2004.
- [TV05] D. Tse and P. Viswanath, *Fundamentals of Wireless Communication*. Cambridge University Press, 2005.
- [TV06] S. Tavildar and P. Viswanath, "Approximately universal codes over slow-fading channels," *IEEE Trans. Inform. Theory*, vol. 52, no. 7, pp. 3233–3258, July 2006.
- [UCF06] M. Uysal, O. Canpolat, and M. M. Fareed, "Asymptotic performance analysis of distributed space-time codes," *IEEE Commun. Lett.*, vol. 10, no. 11, pp. 775–777, Nov. 2006.
- [UG04] M. Uysal and C. N. Georghiades, "On the error performance analysis of space-time trellis codes," *IEEE Trans. Wireless Commun.*, vol. 3, no. 4, pp. 1118–1123, July 2004.
- [UK06] T. Unger and A. Klein, "Cooperative MIMO relaying with distributed space-time block codes," in *Proc. IEEE Int. Symp. on Pers., Indoor, and Mobile Radio Commun. (PIMRC)*, Helsinki, Finland, Sept. 2006.
- [Ung74] G. Ungerboeck, "Adaptive maximum-likelihood receiver for carrier-modulated data-transmission systems," *IEEE Trans. Commun.*, vol. 22, no. 5, pp. 624–636, May 1974.
- [Ung82] —, "Channel coding with multilevel/phase signals," *IEEE Trans. Inform. Theory*, vol. 28, no. 1, pp. 55–67, Jan. 1982.

- [Ung87] ———, “Trellis-coded modulation with redundant signal sets – Part I: Introduction; Part II: State of the art,” *IEEE Commun. Mag.*, vol. 25, no. 2, pp. 5–11, 12–21, Feb. 1987.
- [Uts06a] W. Utschick, personal communication, Int. ITG-IEEE Workshop on Smart Antennas (WSA), Castle Reisensburg, Günzburg, Germany, Mar. 2006.
- [Uts06b] ———, personal communication, Int. Symp. on Turbo Codes & Rel. Topics/ Int. ITG Conf. on Source and Channel Coding (SCC), Munich, Germany, Apr. 2006.
- [VA03] K. Vanganuru and A. Annamalai, “Analysis of transmit diversity schemes: Impact of fade distribution, spatial correlation and channel estimation errors,” in *Proc. IEEE Wireless Commun. and Networking Conf. (WCNC)*, New Orleans, Louisiana, USA, Mar. 2003, pp. 247–251.
- [van76] W. van Etten, “Maximum likelihood receiver for multiple channel transmission systems,” *IEEE Trans. Commun.*, vol. 24, no. 2, pp. 276–283, Feb. 1976.
- [VB99] E. Viterbo and J. Boutros, “A universal lattice code decoder for fading channels,” *IEEE Trans. Inform. Theory*, vol. 45, no. 5, pp. 1639–1642, July 1999.
- [VB02] H. Viswanathan and J. Balakrishnan, “Space-time signaling for high data rates in EDGE,” *IEEE Trans. Veh. Technol.*, vol. 51, no. 6, pp. 1522–1533, Nov. 2002.
- [Ver93] S. Verdu, “Multiuser detection,” in *Advances in Statistical Signal Processing*, V. Poor, Ed., vol. 2: Signal Detection, Greenwich, Connecticut, USA: JAI Press, 1993, pp. 369–409.
- [vF04] C. van Rensburg and B. Friedlander, “Transmit diversity for arrays in correlated fading,” *IEEE Trans. Veh. Technol.*, vol. 53, no. 6, pp. 1726–1734, Nov. 2004.
- [vH02a] A. van Zelst and J. S. Hammerschmidt, “A single coefficient spatial correlation model for multiple-input multiple-output (MIMO) radio channels,” in *Proc. General Assembly of the Int. Union of Radio Science (URSI)*, Maastricht, The Netherlands, Aug. 2002.
- [vH02b] H. Vikalo and B. Hassibi, “Maximum-likelihood sequence detection of multiple antenna systems over dispersive channels via sphere decoding,” *EURASIP J. Applied Signal Processing*, vol. 2002, no. 5, pp. 525–531, May 2002.
- [VJU03] A. Voulgarelis, M. Joham, and W. Utschick, “Space-time equalization based on V-BLAST and DFE for frequency-selective MIMO channels,” in *Proc. IEEE Int. Conf. Acoustics, Speech and Signal Processing (ICASSP)*, Hong Kong, China, Apr. 2003, pp. 381–384.
- [VLB04] A. Vielmon, Y. Li, and J. R. Barry, “Performance of Alamouti transmit diversity over time-varying Rayleigh-fading channels,” *IEEE Trans. Wireless Commun.*, vol. 3, no. 5, pp. 1369–1373, Sept. 2004.
- [VR06] R. Vaze and B. S. Rajan, “On space-time trellis codes achieving optimal diversity multiplexing tradeoff,” *IEEE Trans. Inform. Theory*, vol. 52, no. 11, pp. 5060–5067, Nov. 2006.

- [VVL03] J. Villares, G. Vazques, and M. Lamarca, "Maximum likelihood blind carrier synchronization in space-time coded OFDM systems," in *Proc. IEEE Signal Processing Workshop on Signal Processing Adv. Wireless Commun. (SPAWC)*, Rome, Italy, June 2003, pp. 610–614.
- [VY03] B. Vucetic and J. Yuan, *Space-Time Coding*. John Wiley & Sons, 2003.
- [WB05] D. W. Waters and J. R. Barry, "Noise-predictive decision-feedback detection for multiple-input multiple-output channels," *IEEE Trans. Signal Processing*, vol. 53, no. 5, pp. 1852–1859, May 2005.
- [WBKK03] D. Wuebben, R. Boehnke, V. Kuehn, and K.-D. Kammeyer, "MMSE extension of V-BLAST based on sorted QR decomposition," in *Proc. IEEE Veh. Technol. Conf. (VTC-Fall)*, Orlando, Florida, USA, Oct. 2003, pp. 508–512.
- [WBKK04] ———, "Near-maximum-likelihood detection of MIMO systems using MMSE-based lattice-reduction," in *Proc. IEEE Int. Conf. Commun. (ICC)*, Paris, France, June 2004, pp. 798–802.
- [WBR+01] D. Wuebben, R. Boehnke, J. Rinas, V. Kuehn, and K.-D. Kammeyer, "Efficient algorithm for decoding layered space-time codes," *Electron. Letters*, vol. 37, no. 22, pp. 1348–1350, Oct. 2001.
- [WCWC01] G. Wu, M. Chen, H. Wang, and S. Cheng, "Improved smart greedy space-time codes for both slow and fast fading," in *Proc. IEEE Military Commun. Conf. (MILCOM)*, Vienna, Virginia, USA, Oct. 2001, pp. 1315–1319.
- [WFGV98] P. W. Wolniansky, G. J. Foschini, G. D. Golden, and R. A. Valenzuela, "V-BLAST: An architecture for realizing very high data rates over the rich-scattering wireless channel," in *Proc. URSI/IEEE Int. Symp. Signals, Systems, and Electronics (ISSSE)*, Pisa, Italy, Sept./Oct. 1998, pp. 295–300.
- [WGJ03] S. Wei, D. L. Goeckel, and R. Janaswamy, "On the asymptotic capacity of MIMO systems with fixed length linear antenna arrays," in *Proc. IEEE Int. Conf. Commun. (ICC)*, Anchorage, Alaska, USA, May 2003, pp. 2633–2637.
- [WHOB06] W. Weichselberger, M. Herdin, H. Oezcelik, and E. Bonek, "A stochastic MIMO channel model with joint correlation of both link ends," *IEEE Trans. Wireless Commun.*, vol. 5, no. 1, pp. 90–100, Jan. 2006.
- [WI05] H.-C. Won and G.-H. Im, "Iterative cyclic prefix reconstruction and channel estimation for a STBC OFDM system," *IEEE Commun. Lett.*, vol. 9, no. 4, pp. 307–309, Apr. 2005.
- [Win98] J. H. Winters, "Smart antennas for wireless systems," *IEEE Pers. Commun.*, vol. 5, no. 1, pp. 23–27, Feb. 1998.
- [Wit91] A. Wittneben, "Basestation modulation diversity for digital simulcast," in *Proc. IEEE Veh. Technol. Conf. (VTC)*, St. Louis, Missouri, USA, May 1991, pp. 848–853.

- [Wit93] ———, “A new bandwidth efficient transmit antenna modulation diversity scheme for linear digital modulation,” in *Proc. IEEE Int. Conf. Commun. (ICC)*, Geneva, Switzerland, May 1993, pp. 1630–1634.
- [WJ02] J. W. Wallace and M. A. Jensen, “Modeling the indoor MIMO wireless channel,” *IEEE Trans. Antennas Propagat.*, vol. 50, no. 5, pp. 591–599, May 2002.
- [WJ04] ———, “Mutual coupling in MIMO wireless systems: A rigorous network theory analysis,” *IEEE Trans. Wireless Commun.*, vol. 3, no. 4, pp. 1317–1325, July 2004.
- [WJSJ03] J. W. Wallace, M. A. Jensen, A. L. Swindlehurst, and B. D. Jeffs, “Experimental characterization of the MIMO wireless channel: Data acquisition and analysis,” *IEEE Trans. Wireless Commun.*, vol. 2, no. 2, pp. 335–343, Mar. 2003.
- [WK03] D. Wuebben and K.-D. Kammeyer, “Impulse shortening and equalization of frequency-selective MIMO channels with respect to layered space-time architectures,” *EURASIP Signal Processing*, vol. 83, no. 8 – Special Section: Hans Wilhelm Schuessler celebrates his 75th birthday, pp. 1643–1659, Aug. 2003.
- [WK06] ———, “Low complexity successive interference cancellation for per-antenna-coded MIMO-OFDM schemes by applying parallel-SQRD,” in *Proc. IEEE Veh. Technol. Conf. (VTC-Spring)*, Melbourne, Australia, May 2006, pp. 2183–2187.
- [WKSJ04] C. Waldschmidt, C. Kuhnert, S. Schulteis, and W. Wiesbeck, “On the integration of MIMO systems into handheld devices,” in *Proc. ITG Workshop on Smart Antennas (WSA)*, Munich, Germany, Mar. 2004, paper no. 25.
- [WL04] J. Wu and H.-N. Lee, “Best mapping for LDPC coded modulation on SISO, MIMO and MAC channels,” in *Proc. IEEE Wireless Commun. and Networking Conf. (WCNC)*, Atlanta, Georgia, USA, Mar. 2004, pp. 2428–2431.
- [WLP03] K. Y. Wu, W. K. Leung, and L. Ping, “A simple approach to near-optimal multiple transmit antenna space-time codes,” in *Proc. IEEE Int. Conf. Commun. (ICC)*, Anchorage, Alaska, USA, May 2003, pp. 2603 – 2607.
- [WLWX04] G. Wang, H. Liao, H. Wang, and X.-G. Xia, “Systematic and optimal cyclotomic lattices and diagonal space-time block code designs,” *IEEE Trans. Inform. Theory*, vol. 50, no. 12, pp. 3348–3360, Dec. 2004.
- [WM02] D. Warrier and U. Madhow, “Spectrally efficient noncoherent communication,” *IEEE Trans. Inform. Theory*, vol. 48, no. 3, pp. 651–668, Mar. 2002.
- [WOCV04] Y. Wang, R. Omrani, K. M. Chugg, and P. Vijay Kumar, “Low-density parity-check space-time codes: Performance analysis and code construction,” in *Proc. IEEE Int. Symp. Inform. Theory (ISIT)*, Chicago, Illinois, USA, June/July 2004, p. 156.
- [WP06] K. Wu and L. Ping, “Multilayer turbo space-time codes,” *IEEE Commun. Lett.*, vol. 9, no. 1, pp. 55–57, Jan. 2006.



- [WSFY04] J. Wang, M. K. Simon, M. P. Fitz, and K. Yao, "On the performance of space-time codes over spatially correlated Rayleigh fading channels," *IEEE Trans. Commun.*, vol. 52, no. 6, pp. 877–881, June 2004.
- [WSG94] J. H. Winters, J. Salz, and R. D. Gitlin, "The impact of antenna diversity on the capacity of wireless communication systems," *IEEE Trans. Commun.*, vol. 42, no. 2/3/4, pp. 1740–1751, Feb./Mar./Apr. 1994.
- [WSLW03] T. Weber, A. Sklavos, Y. Liu, and M. Weckerle, "The air interface concept JOINT for beyond 3G mobile radio networks," in *Proc. Int. Conf. on Wireless Commun. (WIRELESS)*, Calgary, British Columbia, Canada, July 2003, pp. 25–33.
- [WSW+06] J.-T. Wang, J. Song, J. Wang, C.-Y. Pan, Z.-X. Yang, and L. Yang, "A general SFN structure with transmit diversity for TDS-OFDM system," *IEEE Trans. Broadcasting*, vol. 52, no. 2, pp. 245–251, June 2006.
- [WSX03] G. Wang, W. Su, and X.-G. Xia, "Orthogonal-like space-time coded CPM with fast demodulation for three and four transmit antennas," in *Proc. IEEE Global Telecommun. Conf. (Globecom)*, San Francisco, California, USA, Dec. 2003, pp. 3321–3325.
- [WTS01] U. Wachsmann, J. Thielecke, and H. Schotten, "Exploiting the data-rate potential of MIMO channels: Multi-stratum space-time coding," in *Proc. IEEE Veh. Technol. Conf. (VTC-Spring)*, Rhodes, Greece, May 2001, pp. 199–203.
- [Wue05] D. Wuebben, "Effiziente Detektionsverfahren für Multilayer-MIMO-Systeme," Ph.D. dissertation, University of Bremen, Germany, 2005.
- [WV96] J. K. Wolf and A. J. Viterbi, "On the weight distribution of linear block codes formed from convolutional codes," *IEEE Trans. Commun.*, vol. 44, no. 9, pp. 1049–1051, Sept. 1996.
- [WVF03] C. Windpassinger, T. Vencel, and R. F. H. Fischer, "Precoding and loading for BLAST-like systems," in *Proc. IEEE Int. Conf. Commun. (ICC)*, Anchorage, Alaska, USA, May 2003, pp. 3061–3065.
- [WW04] X. Wang and J. Wang, "Effect of imperfect channel estimation on transmit diversity in CDMA systems," *IEEE Trans. Veh. Technol.*, vol. 53, no. 5, pp. 1400–1412, Sept. 2004.
- [WW06] J. Wang and X. Wang, "Optimum design of noncoherent Cayley unitary space-time codes," *IEEE Trans. Wireless Commun.*, vol. 5, no. 7, pp. 1942–1951, July 2006.
- [WWM05] J. Wang, X. Wang, and M. Madhian, "Design of minimum error-rate Cayley differential unitary space-time codes," *IEEE J. Select. Areas Commun.*, vol. 23, no. 9, pp. 1779–1787, Sept. 2005.
- [WWX04] H. Wang, G. Wang, and X.-G. Xia, "Some  $2 \times 2$  unitary space-time codes from sphere packing theory with optimal diversity product of code size 6," *IEEE Trans. Inform. Theory*, vol. 50, no. 12, pp. 3361–3368, Dec. 2004.



- [WWX05] D. Wang, G. Wang, and X.-G. Xia, "An orthogonal space-time coded partial response CPM system with fast decoding for two transmit antennas," *IEEE Trans. Wireless Commun.*, vol. 4, no. 5, pp. 2410–2422, Sept. 2005.
- [WX04] G. Wang and X.-G. Xia, "An orthogonal space-time coded CPM system with fast decoding for two transmit antennas," *IEEE Trans. Inform. Theory*, vol. 50, no. 3, pp. 486–493, Mar. 2004.
- [WX05] ———, "On optimal multilayer cyclotomic space-time code designs," *IEEE Trans. Inform. Theory*, vol. 51, no. 3, pp. 1102–1135, Mar. 2005.
- [WYG06] T. Wang, Y. Yao, and G. B. Giannakis, "Non-coherent distributed space-time processing for multiuser cooperative transmissions," *IEEE Trans. Wireless Commun.*, vol. 5, no. 12, pp. 3339–3343, Dec. 2006.
- [WYL02] Y. Wu, Y. Yang, and X. Luo, "Improving the performance of V-BLAST with STTC," in *Proc. IEEE Int. Conf. Commun. Systems (ICCS)*, Singapore, Nov. 2002, pp. 174–177.
- [WYP+05] J.-T. Wang, Z.-X. Yang, C.-Y. Pan, J. Song, and L. Yang, "Design of space-time-frequency transmitter diversity scheme for TDS-OFDM system," *IEEE Trans. Consumer Electron.*, vol. 51, no. 3, pp. 759–764, Aug. 2005.
- [WZA06] G. Wang, Y. Zhang, and M. Amin, "Differential distributed space-time modulation for cooperative networks," *IEEE Trans. Wireless Commun.*, vol. 5, no. 11, pp. 3097–3108, Nov. 2006.
- [XCHV04] H. Xu, D. Chizhik, H. Huang, and R. Valenzuela, "A generalized space-time multiple-input multiple-output (MIMO) channel model," *IEEE Trans. Wireless Commun.*, vol. 3, no. 3, pp. 966–975, May 2004.
- [XD05] L. Xiao and X. Dong, "The exact transition probability and bit error probability of two-dimensional signaling," *IEEE Trans. Wireless Commun.*, vol. 4, no. 5, pp. 2600–2609, Sept. 2005.
- [XG04] P. Xia and G. B. Giannakis, "Design and analysis of transmit-beamforming based on limited-rate feedback," in *Proc. IEEE Veh. Technol. Conf. (VTC-Fall)*, Los Angeles, California, USA, Sept. 2004, pp. 1653–1657.
- [Xia02] X.-G. Xia, "Differentially en/decoded orthogonal space-time block codes with APSK signals," *IEEE Commun. Lett.*, vol. 6, no. 4, pp. 150–152, Apr. 2002.
- [XK05] C. Xu and K. S. Kwak, "On decoding algorithm and performance of space-time block codes," *IEEE Trans. Wireless Commun.*, vol. 4, no. 3, pp. 825–829, May 2005.
- [XL05] L. Xian and H. Liu, "Space-time block codes from cyclic design," *IEEE Commun. Lett.*, vol. 9, no. 3, pp. 231–233, Mar. 2005.
- [XLRP05] H. Xu, J. Liu, F. Rubio, and A. I. Perez-Neira, "Analysis of orthogonal transmit beamforming using statistical channel information," in *Proc. IST Mobile & Wireless Commun. Summit*, Dresden, Germany, June 2005, paper no. 477.

- [XPL06] L. Xian, R. Punnoose, and H. Liu, "Space-time block coded GMSK with low-complexity linear receiver," in *Proc. IEEE Int. Conf. Commun. (ICC)*, Istanbul, Turkey, June 2006, pp. 4876–4881.
- [XWG03] Y. Xia, Z. Wang, and G. B. Giannakis, "Space-time diversity systems based on linear constellation precoding," *IEEE Trans. Wireless Commun.*, vol. 2, no. 2, pp. 294–309, Mar. 2003.
- [XWL+04] C. Xiao, J. Wu, S.-Y. Leong, Y. R. Zheng, and K. B. Letaief, "A discrete-time model for triply selective MIMO Rayleigh fading channels," *IEEE Trans. Wireless Commun.*, vol. 3, no. 5, pp. 1678–1688, Sept. 2004.
- [XZ04] C. Xiao and Y. R. Zheng, "Ergodic capacity of MIMO triply selective Rayleigh fading channels," in *Proc. IEEE Global Telecommun. Conf. (Globecom)*, Dallas, Texas, USA, Nov./Dec. 2004, pp. 3133–3137.
- [XZH+02] T. Xiaofeng, Y. Zhuizhuan, Q. Haiyan, Z. Ping, H. Haas, and E. Costa, "New sub-optimal detection algorithm of layered space-time code," in *Proc. IEEE Veh. Technol. Conf. (VTC-Spring)*, Birmingham, Alabama, USA, May 2002, pp. 1791–1794.
- [YA02] W. Younis and N. Al-Dhahir, "Joint prefiltering and MLSE equalization of space-time-coded transmissions over frequency-selective channels," *IEEE Trans. Veh. Technol.*, vol. 51, no. 1, pp. 144–154, Jan. 2002.
- [Yan05] H. Yang, "A road to future broadband wireless access: MIMO-OFDM-based air interface," *IEEE Commun. Mag.*, vol. 43, no. 1, pp. 53–60, Jan. 2005.
- [YB07] S. Yang and J.-C. Belfiore, "Optimal space-time codes for the MIMO amplify-and-forward cooperative channel," *IEEE Trans. Inform. Theory*, vol. 53, no. 2, pp. 647–663, Feb. 2007.
- [YC04] J. Yang and K. Cheun, "Low complexity implementation of Alamouti space-time coded OFDM transmitters," *IEEE Commun. Lett.*, vol. 8, no. 4, pp. 229–231, Apr. 2004.
- [YCVF03] J. Yuan, Z. Chen, B. Vucetic, and W. Firmanto, "Performance and design of space-time coding in fading channels," *IEEE Trans. Commun.*, vol. 51, no. 12, pp. 1991–1996, Dec. 2003.
- [YGT05] C. Yuen, Y. L. Guan, and T. T. Tjhung, "Quasi-orthogonal STBC with minimum decoding complexity," *IEEE Trans. Wireless Commun.*, vol. 4, no. 5, pp. 2089–2094, Sept. 2005.
- [YGT06] ———, "Single-symbol-decodable differential space-time modulation based on QO-STBC," *IEEE Trans. Wireless Commun.*, vol. 5, no. 12, pp. 3329–3334, Dec. 2006.
- [YJP+05] Y.-H. You, W.-G. Jeon, J.-H. Paik, M.-J. Kim, D.-S. Kim, and H.-K. Song, "Performance evaluation of OFDM-CDMA with multiple antennas for broadband wireless access networks," *IEEE Trans. Veh. Technol.*, vol. 54, no. 1, pp. 385–398, Jan. 2005.

- [YKH+04] Y.-H. You, M.-J. Kim, S.-K. Hong, I. Hwang, and H.-K. Song, "Performance investigation of STBC-OFDM with code-division multiplexing in time-varying channels," *IEEE Trans. Broadcasting*, vol. 50, no. 4, pp. 408–413, Dec. 2004.
- [YKY06] Y. Yu, S. Kerouedan, and J. Yuan, "Transmit antenna shuffling for quasi-orthogonal space-time block codes with linear receivers," *IEEE Commun. Lett.*, vol. 10, no. 8, pp. 596–598, Aug. 2006.
- [YPW05] G. Yue, L. Ping, and X. Wang, "Low-rate generalized low-density parity-check codes with Hadamard constraints," in *Proc. IEEE Int. Symp. Inform. Theory (ISIT)*, Adelaide, Australia, Sept. 2005, pp. 1377–1381.
- [YS99] A. Yongacoglu and M. Siala, "Space-time codes for fading channels," in *Proc. IEEE Veh. Technol. Conf. (VTC-Fall)*, Amsterdam, The Netherlands, Sept. 1999, pp. 2495–2499.
- [YS06] S. Yiu and R. Schober, "Optimized distributed space-time filtering," *IEEE Trans. Wireless Commun.*, accepted for publication, 2006.
- [YSG06] S. Yiu, R. Schober, and W. H. Gerstacker, "Optimized delay diversity for suboptimum equalization," *IEEE Trans. Veh. Technol.*, vol. 55, no. 5, pp. 1535–1543, Sept. 2006.
- [YSL04] L. T. Younkings, W. Su, and K. J. R. Liu, "On the robustness of space-time coding for spatially and temporally correlated wireless channels," in *Proc. IEEE Wireless Commun. and Networking Conf. (WCNC)*, Atlanta, Georgia, USA, Mar. 2004, pp. 587–592.
- [YSL06a] S. Yiu, R. Schober, and L. Lampe, "Distributed space-time block coding," *IEEE Trans. Commun.*, vol. 54, no. 7, pp. 1195–1206, July 2006.
- [YSL06b] —, "Decentralized distributed space-time trellis coding," *IEEE Trans. Wireless Commun.*, accepted for publication, 2006.
- [YW02] H. Yao and G. Wornell, "Lattice-reduction-aided detectors for MIMO communication systems," in *Proc. IEEE Global Telecommun. Conf. (Globecom)*, Taipei, Taiwan, R.O.C., Nov. 2002, pp. 424–428.
- [YW03] —, "Structured space-time block codes with optimal diversity-multiplexing tradeoff and minimum delay," in *Proc. IEEE Global Telecommun. Conf. (Globecom)*, San Francisco, California, USA, Dec. 2003, pp. 1941–1945.
- [YW05a] J. Yang and D. B. Williams, "MIMO transmission subspace tracking with low rate feedback," in *Proc. IEEE Int. Conf. Acoustics, Speech and Signal Processing (ICASSP)*, Philadelphia, Pennsylvania, USA, Mar. 2005, pp. 405–408.
- [YW05b] G. Yue and X. Wang, "Optimization of irregular repeat accumulate codes for MIMO systems with iterative receivers," *IEEE Trans. Wireless Commun.*, vol. 4, no. 6, pp. 2843–2855, Nov. 2005.
- [YYH01] M. S. Yee, B. L. Yeap, and L. Hanzo, "RBF-based decision feedback aided turbo equalisation of convolutional and space-time trellis-coded systems," *Electron. Letters*, vol. 37, no. 21, pp. 1298–1299, Oct. 2001.

- [ZB02] W. Zha and S. D. Blostein, "Modified decorrelating decision-feedback detection of BLAST space-time system," in *Proc. IEEE Int. Conf. Commun. (ICC)*, New York City, New York, USA, Apr./May 2002, pp. 335–339.
- [ZD05] L. Zhao and V. K. Dubey, "Detection schemes for space-time block code and spatial multiplexing combined system," *IEEE Commun. Lett.*, vol. 9, no. 1, pp. 49–51, Jan. 2005.
- [ZDZY03] H. Zhuang, L. Dai, S. Zhou, and Y. Yao, "Low complexity per-antenna rate and power control approach for closed-loop V-BLAST," *IEEE Trans. Commun.*, vol. 51, no. 11, pp. 1783–1787, Nov. 2003.
- [ZF02] X. Zhang and M. P. Fitz, "Soft-output demodulator in space-time-coded continuous phase modulation," *IEEE Trans. Signal Processing*, vol. 50, no. 10, pp. 2589–2598, Oct. 2002.
- [ZF03] —, "Space-time code design with continuous phase modulation," *IEEE J. Select. Areas Commun.*, vol. 21, no. 5, pp. 783–792, June 2003.
- [ZFW02] T. Zwick, C. Fischer, and W. Wiesbeck, "A stochastic multipath channel model including path directions for indoor environments," *IEEE J. Select. Areas Commun.*, vol. 20, no. 6, pp. 1178–1192, Aug. 2002.
- [ZG01] S. Zhou and G. B. Giannakis, "Space-time coding with maximum diversity gains over frequency-selective fading channels," *IEEE Signal Processing Lett.*, vol. 8, no. 10, pp. 269–272, Oct. 2001.
- [ZG02] —, "Optimal transmitter eigen-beamforming and space-time block coding based on channel mean feedback," *IEEE Trans. Commun.*, vol. 50, no. 10, pp. 2599–2613, Oct. 2002.
- [ZG03a] —, "Optimal transmitter eigen-beamforming and space-time block coding based on channel correlations," *IEEE Trans. Inform. Theory*, vol. 49, no. 7, pp. 1673–1690, July 2003.
- [ZG03b] —, "Single-carrier space-time block-coded transmissions over frequency-selective fading channels," *IEEE Trans. Inform. Theory*, vol. 49, no. 1, pp. 164–179, Jan. 2003.
- [ZHC01] K. Zangi, D. Hui, and J.-F. Cheng, "Physical-layer issues for deploying transmit diversity in GPRS/EGPRS networks," in *Proc. IEEE Veh. Technol. Conf. (VTC-Fall)*, Atlantic City, New Jersey, USA, Oct. 2001, pp. 538–542.
- [ZHF04] E. Zimmermann, P. Herhold, and G. Fettweis, "The impact of cooperation on diversity-exploiting protocols," in *Proc. IEEE Veh. Technol. Conf. (VTC-Spring)*, Genoa, Italy, May 2004, pp. 410–414.
- [ZI03] Z. Zhang and J. Ilow, "A differential space-time transceiver for unknown time-dispersive multipath channels," in *Proc. IEEE Int. Symp. Signal Processing and Inform. Theory (ISSPIT)*, Darmstadt, Germany, Dec. 2003, pp. 90–93.
- [ZJ06] Y. Zhu and H. Jafarkhani, "Differential super-orthogonal space-time trellis codes," *IEEE Trans. Wireless Commun.*, vol. 5, no. 12, pp. 3634–3643, Dec. 2006.

- [ZLC04] H. Zhu, Z. Lei, and F. P. S. Chin, "An improved square-root algorithm for BLAST," *IEEE Signal Processing Lett.*, vol. 11, no. 9, pp. 772–775, Sept. 2004.
- [ZLW05] J.-K. Zhang, J. Liu, and K. M. Wong, "Linear Toeplitz space-time block codes," in *Proc. IEEE Int. Symp. Inform. Theory (ISIT)*, Adelaide, Australia, Sept. 2005, pp. 1942–1946.
- [ZLW06] S. Zhou, B. Li, and P. Willett, "Recursive and trellis-based feedback reduction for MIMO-OFDM with rate-limited feedback," *IEEE Trans. Wireless Commun.*, vol. 5, no. 12, pp. 3400–3405, Dec. 2006.
- [ZLZ+05] S. Zhou, Y. Li, M. Zhao, X. Xu, J. Wang, and Y. Yao, "Novel techniques to improve downlink multiple access capacity for beyond 3G," *IEEE Commun. Mag.*, vol. 43, no. 1, pp. 61–69, Jan. 2005.
- [ZM03] X. Zhu and R. D. Murch, "Layered space-time equalization for wireless MIMO systems," *IEEE Trans. Wireless Commun.*, vol. 2, no. 6, pp. 1189–1203, Nov. 2003.
- [ZN03] S. A. Zekavat and C. R. Nassar, "Power-azimuth-spectrum modeling for antenna array systems: A geometric-based approach," *IEEE Trans. Antennas Propagat.*, vol. 51, no. 12, pp. 3292–3294, Dec. 2003.
- [ZSM+03] J. Zhou, S. Sasaki, S. Muramatsu, H. Kikuchi, and Y. Onozato, "Spatial correlation for a circular antenna array and its applications in wireless communications," in *Proc. IEEE Global Telecommun. Conf. (Globecom)*, San Francisco, California, USA, Dec. 2003, pp. 1108–1113.
- [ZT02] L. Zheng and D. N. C. Tse, "Communication on the Grassmann manifold: A geometric approach to the noncoherent multiple-antenna channel," *IEEE Trans. Inform. Theory*, vol. 48, no. 2, pp. 359–383, Feb. 2002.
- [ZT03] ———, "Diversity and multiplexing: A fundamental tradeoff in multiple-antenna channels," *IEEE Trans. Inform. Theory*, vol. 49, no. 5, pp. 1073–1096, May 2003.
- [ZXC07] W. Zhang, X.-G. Xia, and P. C. Ching, "High-rate full-diversity space-time-frequency codes for broadband MIMO block-fading channels," *IEEE Trans. Commun.*, vol. 55, no. 1, pp. 25–34, Jan. 2007.
- [ZZX+03] S. Zhou, M. Zhao, X. Xu, J. Wang, and Y. Yao, "Distributed wireless communication system: A new architecture for future public wireless access," *IEEE Commun. Mag.*, vol. 41, no. 3, pp. 108–113, Mar. 2003.



# Author's Biography

Jan Mietzner was born in Rendsburg, Germany, on March 6, 1975. He studied electrical engineering and information engineering at the Faculty of Engineering, Christian-Albrechts University (CAU) of Kiel, Germany, with focus on digital communications. During his studies, he spent six months in 2000 with the Global Wireless Systems Research Group, Lucent Technologies, Bell Labs U.K., in Swindon, England. He received the Dipl.-Ing. degree from the CAU Kiel in July 2001. For his diploma thesis on space-time coding techniques he received the Prof.-Dr.-Werner-Petersen Award in December 2001.

From August 2001 to October 2006 he was working toward his Ph.D. degree as a research and teaching assistant at the Information and Coding Theory Lab (ICT), Faculty of Engineering, CAU Kiel, and received his Ph.D. degree in December 2006. His research interests concern physical layer aspects of future wireless communication systems, especially multiple-input multiple-output (MIMO) systems, space-time coding techniques, and cooperative diversity schemes. During his time with the ICT, he has co-authored 20 technical papers published in international journals and conference proceedings.

Since January 2007 he is with the Communication Theory Group, Department of Electrical and Computer Engineering, The University of British Columbia, Vancouver, Canada, as a post-doctoral research fellow. ★